# INFORMATION TO USERS

This manuscript has been reproduced from the microfilm master. UMI films the text directly from the original or copy submitted. Thus, some thesis and dissertation copies are in typewriter face, while others may be from any type of computer printer.

**The quality of this reproduction is dependent upon the quality of the copy submitted.** Broken or indistinct print, colored or poor quality illustrations and photographs, print bleedthrough, substandard margins, and improper alignment can adversely affect reproduction.

In the unlikely event that the author did not send UMI a complete manuscript and there are missing pages, these will be noted. Also, if unauthorized copyright material had to be removed, a note will indicate the deletion.

Oversize materials (e.g., maps, drawings, charts) are reproduced by sectioning the original, beginning at the upper left-hand corner and continuing from left to right in equal sections with small overlaps. Each original is also photographed in one exposure and is included in reduced form at the back of the book.

Photographs included in the original manuscript have been reproduced xerographically in this copy. Higher quality 6" x 9" black and white photographic prints are available for any photographs or illustrations appearing in this copy for an additional charge. Contact UMI directly to order.

**UMI**

A Bell & Howell Information Company
300 North Zeeb Road, Ann Arbor MI 48106-1346 USA
313/761-4700 800/521-0600

Reproduced with permission of the copyright owner. Further reproduction prohibited without permission.

Reproduced with permission of the copyright owner. Further reproduction prohibited without permission.

# CHARACTERISTICS OF DAYSIDE AURORAL DISPLAYS IN RELATION TO MAGNETOSPHERIC PROCESSES

A

THESIS

Presented to the Faculty

of the University of Alaska Fairbanks

in Partial Fulfillment of the Requirements

for the Degree of

DOCTOR OF PHILOSOPHY

By

Joseph I. Minow, B.A., M.S.

Fairbanks, Alaska

May 1997

Reproduced with permission of the copyright owner. Further reproduction prohibited without permission.

UMI Number: 9725097

UMI Microform 9725097
Copyright 1997, by UMI Company. All rights reserved.

This microform edition is protected against unauthorized copying under Title 17, United States Code.

UMI
300 North Zeeb Road
Ann Arbor, MI 48103

Reproduced with permission of the copyright owner. Further reproduction prohibited without permission.

CHARACTERISTICS OF DAYSIDE AURORAL DISPLAYS IN

RELATION TO MAGNETOSPHERIC PROCESSES

by

Joseph I. Minow

RECOMMENDED:

Chairman, Advisory Committee

Head, Physics Department

APPROVED:

Dean, College of Natural Sciences

Dean of the Graduate School

4-7-97

Date

Reproduced with permission of the copyright owner. Further reproduction prohibited without permission.

## Abstract

The use of dayside aurorae as a ground based monitor of magnetopause activity is explored in this thesis. The origin of diffuse [OI] 630.0 nm emissions in the midday auroral oval is considered first. Analysis of low altitude satellite records of precipitating charged particles within the cusp show an unstructured electron component that will produce a 0.5-1 kR 630.0 nm emission throughout the cusp. Distribution of the electrons is controlled by the requirement of charge neutrality in the cusp, predicting a diffuse 630.0 nm background even if the magnetosheath plasma is introduced into the magnetosphere in discrete merging events. Cusp electron fluxes also contain a structured component characterized by enhancements in the electron energy and energy flux over background values in narrow regions a few 10's of kilometers in width. These structured features are identified as the source of the transient midday arcs. An auroral model is developed to study the morphology of [OI] 630.0 nm auroral emissions produced by the transient arcs. The model demonstrates that a diffuse 630.0 nm background emission is produced by transient arcs due to the long lifetime of the $O(^1D)$ state. Two sources of diffuse 630.0 nm background emissions exist in the cusp which may originate in discrete merging events. The conclusion is that persistent 630.0 nm emissions cannot be interpreted as prima facie evidence for continuous particle transport from the magnetosheath across the magnetopause boundary and into the polar cusp

The second subject that is considered is the analysis of temporal and spatial variations of the diffuse 557.7 nm pulsating aurora in relation to the 630.0 nm dominated transient aurora. Temporal variations at the poleward boundary of the diffuse 557.7 nm aurora correlate with the formation of the 630.0 nm transient aurorae suggesting that the two events are related. The character of the auroral variations is consistent with the behavior of particle populations reported during satellite observations of flux transfer events near the dayside magnetopause. An interpretation of the events in terms of impulsive magnetic reconnection yields a new observation that relates the poleward moving transient auroral arcs in the midday sector to the flux transfer events.


Reproduced with permission of the copyright owner. Further reproduction prohibited without permission.

## Table of Contents



Reproduced with permission of the copyright owner. Further reproduction prohibited without permission.

Reproduced with permission of the copyright owner. Further reproduction prohibited without permission.

Reproduced with permission of the copyright owner. Further reproduction prohibited without permission.

Reproduced with permission of the copyright owner. Further reproduction prohibited without permission.

## Appendix A
## The Meridian Scanning Photometer



## Appendix B
## The Television Camera



## Appendix C
## Color Figures



## Appendix D
## Charged Particle Flux Relations



Reproduced with permission of the copyright owner. Further reproduction prohibited without permission.

## Appendix E
## Spectra of Dayside Aurora



Reproduced with permission of the copyright owner. Further reproduction prohibited without permission.

## List of Figures



Reproduced with permission of the copyright owner. Further reproduction prohibited without permission.

Reproduced with permission of the copyright owner. Further reproduction prohibited without permission.

Reproduced with permission of the copyright owner. Further reproduction prohibited without permission.

# List of Tables



Reproduced with permission of the copyright owner. Further reproduction prohibited without permission.

Reproduced with permission of the copyright owner. Further reproduction prohibited without permission.

**Acknowledgements**

There are many people who have contributed in many ways to the completion of this thesis. I will never remember them all but I hope this is a good start.

A number of data sets and models were used directly in the thesis or examined as part of the development work. They were an invaluable resource and the many people in the space science community who willingly provided data must be thanked. Dr. R.P. Lepping provided the IMP-8 interplanetary magnetic field data through the National Space Science Data Center and Dr. A. Lazarus the IMP-8 plasma data. DMSP driftmeter data was obtained both from Dr. W.F. Denig (Philips Laboratory, Hanscom Air Force Base) and Dr. R. Heelis (University of Texas in Dallas). Dr. P.T. Newell (Applied Physics Laboratory, Johns Hopkins University) provided DMSP SSJ/4 particle data in response to numerous requests through the mail and also by sponsoring a visit to JHU/APL where I was allowed to roam freely through their archive of DMSP particle data. Dr. Stanley Solomon, University of Colorado, provided the computer code for his GLOW airglow and aurora model.

The operations of the field station and activities in Longyearbyen are possible due to the support of Store Norske Spitzbergen Kuhlkompani, the office of the Syssellmann of Svalbard, the townspeople of Longyearbyen, and the University of Tromsø. I regret that I must thank Kjell Henriksen posthumously since it was largely through his tireless effort that the field station was established and continued to grow in Adventdalen. Kjell was a good friend and will be missed.

The faculty and staff of the Geophysical Institute were a tremendous resource and constant source of support. Dr. S.-I. Akasofu deserves a special thanks for his continued willingness to take the time out of his busy schedule to discuss dayside aurora. Jim Desroacher, Dan Osborne, and Jim Baldridge of the Geophysical Institute provided valuable information on the CCD camera equipment used during the 1992/1993 field season, the proper adjustment of the MSP filter tilting apparatus, and the details of the MSP data logging formats, respectively. Dr. Antonius Otto and Dr. Dirk Lummerzheim were always willing to discuss flux transfer events, magnetic reconnection, and auroral models. Their help and insight was invaluable. Dr. Dave Covey and Celia Rohwer of the computer resource center made sure our computers always worked. Thanks are also deserved to members of my thesis committee who read through the thesis and who have offered helpful comments. Special thanks to Drs. Chuck Deehr, Thomas Hallinan, Hans Nielsen, and John Olson for their interest in aurora and insights on television cameras, photometers, and magnetometers. Thanks to Dr. Dan Jaffe, a chemist who served on my physics thesis committee, for forcing me to think about the basics of physics. Judy Triplehorn of the GI library provided invaluable help in locating references.

A special word of thanks must go to those from Fairbanks, Tromso, and Apatity, with whom I shared the unique and memorable experience of Svalbard's long polar night: Drs. Jim Conner, Don Hampton, Fred Sigernes, Gina Price, Ilya Kornilov, and Mr. Dag Lorentzen. A special word of thanks is due to Dr. Gerard Fasel for the never ending arguments about dayside aurora that constantly forced me to both reconsider and critically examine our work. Life at the GI would never have been nearly as much fun without the presence of Dr. Nettie La Belle-Hamer and Dr. Geoff McHarg.

Reproduced with permission of the copyright owner. Further reproduction prohibited without permission.

Dr. Roger Smith has supported me through many years of thesis work, when many advisors would have given up. His patience and belief that I would finish some day are remarkable, and in the end justified. I have been truly fortunate to work for a scientist who was willing to give me the space I needed to develop, the support I needed to keep going, and the help I needed to finish.

Finally, the constant support over the years I received from my parents deserves a word of thanks. They supported my decision to give up chemistry and pursue a degree in physics and were always there with a word of advice or encouragement if needed. Last, but certainly not the least, I thank Pam Croom who has stood by me for many years while I have worked on this thesis, certainly more than she ever imagined it would take when she first got involved with me and...IT! Even after proof reading drafts until she could no longer stand to look at them she is still here. Not only did she not give up, she married me instead...thanks Pam!

Reproduced with permission of the copyright owner. Further reproduction prohibited without permission.

*"...I feel a cold northern breeze play upon my cheeks, which braces my nerves, and fills me with delight. Do you understand this feeling? This breeze, which has travelled from the regions towards which I am advancing, gives me a foretaste of those icy climes. Inspirited by this wind of promise, my day dreams become more fervent and vivid. I try in vain to be pursuaded that the pole is the seat of frost and desolation; it ever presents itself to my imagination as the region of beauty and delight."*

*"Its productions and features may be without example, as the phenomena of the heavenly bodies undoubtedly are in those undiscovered solitudes. What may not be expected in a country of eternal light? I may there discover the wondrous power which attracts the needle; and may regulate a thousand celestial observations, that require only this voyage to render their seeming eccentricites consistent for ever"*

excerpts from *Frankenstein* by Mary W. Shelley

Reproduced with permission of the copyright owner. Further reproduction prohibited without permission.

# Chapter 1.
# Introduction and Overview of Thesis

## 1.1 Dayside Aurorae and the High Latitude Region

This thesis considers aspects of the use of ground based observations of dayside auroral emissions to monitor the transport of solar wind mass and momentum across the magnetopause and into the magnetosphere. Studies of solar wind interactions with the terrestrial magnetosphere are difficult because the process occurs a great distance from the Earth. Satellites provide detailed measurements of charged particle populations, magnetic field orientation, and field magnitude as they pass through the magnetospheric boundary. Little information can be obtained from a single satellite on either the temporal or spatial variations in the plasma and magnetic field conditions remote from the satellite. Complementary to satellite studies are ground based observations of auroral displays and plasma motions in the high latitude daytime ionosphere. If the morphological and spectral features of dayside auroral displays and variations in ionospheric plasma motions can be related to specific physical processes occurring at the magnetopause then the ground-based observations may provide the missing spatial and temporal information currently unavailable in the satellite studies.

*Hartz and Brice* [1967] used riometer observations to show that two regions of charged particle precipitation occur in the dayside region: the "soft zone" nearest the magnetic pole where electron energies are typically a few hundred eV and the "hard zone" equatorward of the soft zone where electron energies are on the order of a few keV to 10's of keV. A variety of terms are found in the literature for the auroral emissions within these regions. Examples include " aurora", "midday aurora","dayside auroral oval", "630.0 nm dominated aurora","dayside transients", "cusp aurora", "cleft aurora", "mantle aurora", and "daytime discrete aurora". The context in which the term "dayside aurora" is used depends on the author [c.f., *Murphree et al.*, 1990]. Some authors have applied "dayside aurora" exclusively to the soft particle zone [*Eather et al.*, 1979; *Sandholt et al.*, 1983] while others use the term in a general sense to include all auroral emissions in the midday region including the hard and soft precipitation zones [c.f.,*Eather and Mende*, 1971; *Sivjee and Hultqvist*, 1975; *Murphree et al.*, 1980].

"Dayside aurora" and "midday aurora" are used in this thesis as generic terms for any auroral emission found in the high-latitude daytime sector whether they are associated with the soft or hard zone precipitation. Similarly, "midday aurora" is used as a generic term for auroral emissions within a few hours of local noon. "Midday auroral oval" and "dayside auroral oval" are reserved specifically for auroral emissions within the day time soft particle zone. Emissions within the hard particle precipitation zone equatorward of the dayside auroral oval are referred to as "mantle aurora", the term originally applied by *Sandford* [1964, 1968]. A potential for confusion exists in terminology for two regions of dayside aurora since *Rosenbauer et al.* [1975] chose to label the magnetospheric boundary layer poleward of the cusp the "plasma mantle" tempting authors to use

Reproduced with permission of the copyright owner. Further reproduction prohibited without permission.

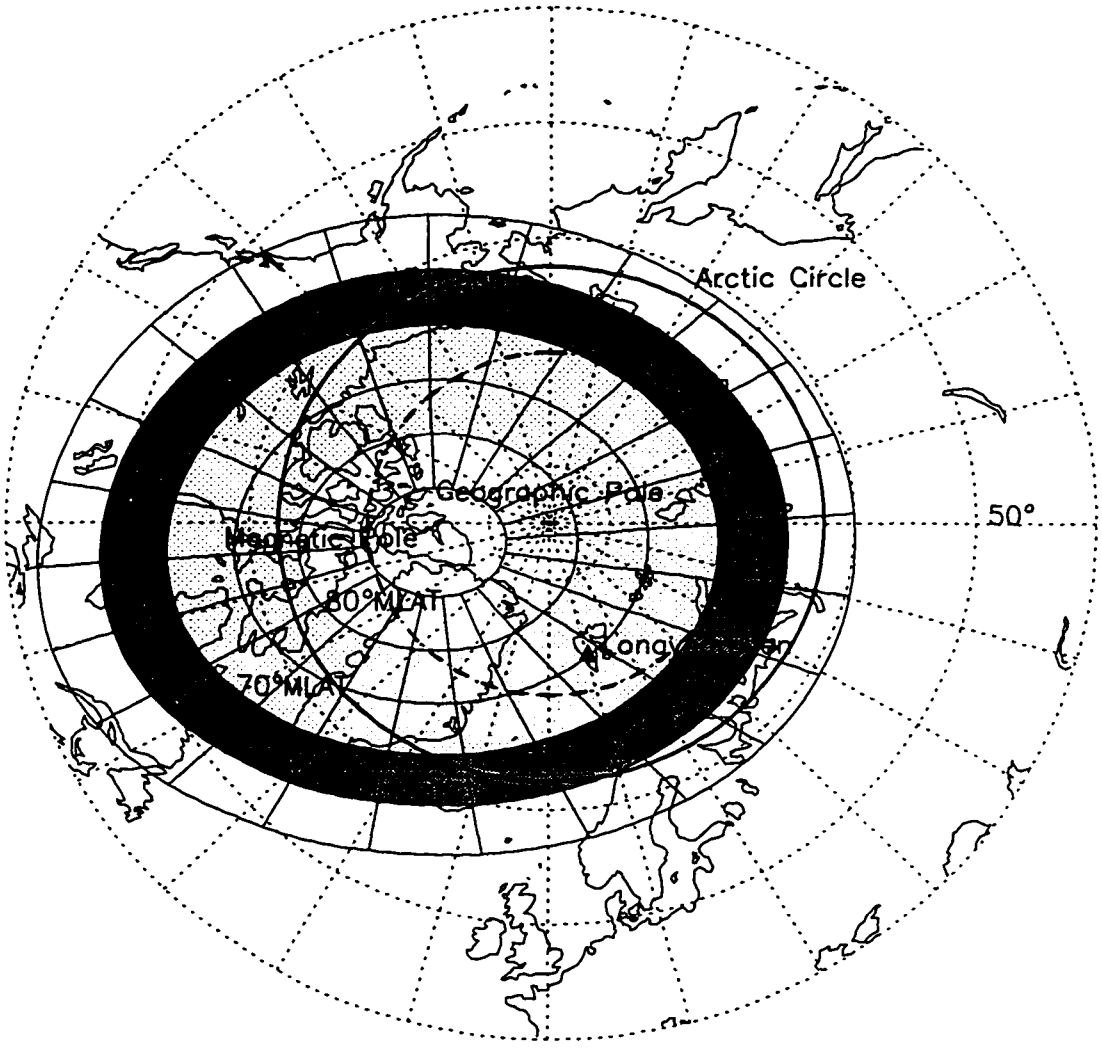


Figure 1.1 Northern Polar Region Map. The geographic and PACE magnetic coordinate systems are given by the dot and solid grids, respectively. Dayside "soft zone" aurorae and the maximum latitude at which the poleward border of the "hard zone" electron fluxes are measured most commonly occur between magnetic latitudes of 70° and 80° (lightly shaded region) with the peak probability near 75° magnetic latitude. This is poleward of the region where night time aurorae is observed nearly 100% of the time (darkly shaded region). The sun will remain below 7 degrees solar depression angle on the winter solstice above the dashed line at 75° N permitting daytime optical observations for a matter of weeks.

Reproduced with permission of the copyright owner. Further reproduction prohibited without permission.

the term mantle aurora for emissions poleward of the cusp [*Newell et al*, 1991a]. When referring to auroral forms on field lines that thread the plasma mantle use of the term "aurora within the plasma mantle" rather than "mantle aurora" will serve to distinguish the two regions.

Dayside aurora is restricted to magnetic latitudes between 70° and 80° . Optical observations of aurora require a ground site with a dark atmosphere above it to eliminate scattered light that will mask the auroral signal. This condition is easily satisfied for the night time aurorae since the entire auroral zone is located in darkness throughout the northern hemisphere winter. Daytime aurorae are more difficult to observe since they form in the auroral region nearest the sun. In order to obtain the dark skies required for daytime auroral observations the possible observatory sites are further restricted from the entire range given in Figure 1.1 to only those between 70° and 80° magnetic latitude which are at high geographic latitudes. Possible observations sites in the northern hemisphere include a band across the east coast of Greenland, the north Atlantic, Barents Sea, Arctic Ocean north of Siberia, and the Beaufort Sea north of Alaska and western Canada. Sites on solid ground where permanent field stations can be constructed are limited to East Greenland, the Svalbard Archipelago, Franz Josef Land, the northern edge of Novaya Zemlya, and Severnaya Zemlya as well as a limited region of the western Canadian high Arctic. A large sector of the Antarctic continent lies within the 70° to 80° magnetic latitude range at high geographic latitudes yielding a large region on which observatories may be built. The relative inaccessibility of the polar ice cap limits dayside auroral observations to South Pole Station, McMurdo Station, or unmanned observatories distributed over the ice cap.

Observations for this thesis were obtained at Nordlysstasjonen (The Northern Lights Station) research station on the island of Spitsbergen in the Svalbard Archipelago at 78.2° N and 15.7° E geographic coordinates. The approximate geomagnetic latitude of the station is 74.9° MLAT in the PACE geomagnetic system [*Baker et al.*, 1989] and magnetic noon occurs at approximately 0830 UT. The observing conditions at the site, facilities, and instrumentation have been described by *Deehr et al.* [1980] and *Deehr and Smith* [1991]. Details of instrumentation used for this work are given in the appendices.

## 1.2 Thesis Overview

Solar-terrestrial interactions and the formation and distribution of auroral displays are reviewed in the first two chapters. Chapter 2 begins with a discussion of the solar wind and its interactions with the terrestrial field. The topology of the solar magnetic field and the Earth's field are discussed. The concepts of open and closed magnetic field lines and the separatrix boundary between them are introduced. Three proposed models for solar wind energy and momentum transport into the magnetosphere are described with special emphasis on the magnetic reconnection model and the characteristics of flux transfer events. Finally, the characteristics of plasma populations within the magnetosphere are reviewed, providing a basis for interpreting the spatial and temporal variations in precipitating particles within the dayside magnetosphere and the resulting variations in dayside aurorae.

Reproduced with permission of the copyright owner. Further reproduction prohibited without permission.

The morphological, spectroscopic characteristics, and dynamic behavior of dayside aurorae are reviewed in Chapter 3. Emissions from atomic oxygen, ionized nitrogen, and neutral hydrogen are routinely monitored in auroral studies. Problems associated with the particular emissions with respect to dayside aurorae are discussed. Evidence shows dayside aurora is the result of physical processes occurring at the dayside magnetopause providing justification for the use of ground based dayside auroral observations as a monitor for solar wind/magnetosphere interactions. Evidence suggesting that transient arcs within the dayside auroral oval are the ionospheric signature of magnetopause flux transfer events is reviewed.

Considered in Chapter 4 is the origin of the diffuse [OI] 630.0 nm emissions observed in the midday auroral oval. An auroral model is developed to study the morphology of [OI] 630.0 nm auroral emissions. A hypothesis is tested that ground based photometer records of 630.0 nm emissions can be reproduced by photons emitted by $O(^1D)$ populations formed by a series of poleward drifting latitudinally thin auroral arcs.

The presence of a diffuse 630.0 nm background emission in which transient arcs are imbedded has been interpreted as prima facie evidence for continuous particle transport from the magnetosheath across the magnetopause boundary and into the polar cusp. The model demonstrates that the observations can be reproduced by discrete auroral events alone and is the result of remnant populations of metastable $O(^1D)$ . A variety of auroral morphologies observed in photometer records from the midday period can be duplicated in special cases using a time dependent azimuthal drift of the transient arcs.

An analysis of a set of dayside auroral records is presented in Chapter 5 including a description of previously unreported features in dayside auroral displays and a proposed mechanism to explain the observations. Temporal variations at the poleward boundary of the mantle correlate with the formation of the 630.0 nm transient aurorae suggesting the events are related. The character of the auroral variations is consistent with the behavior of particle populations reported from satellite observations of flux transfer events near the dayside magnetopause. An interpretation of the events in terms of impulsive magnetic reconnection yields a new observation that relates poleward moving transient auroral arcs in the dayside auroral oval to flux transfer events.

The instrumentation used to obtain the auroral records in the study are meridian scanning photometers and all sky cameras which have been widely used in studies of airglow and aurorae for many years. Data analysis and results from the first five chapters do not depend in detail on any special features or modifications of the existing instrumentation therefore the descriptions of the principles, design, and operation of the scanning photometer and camera systems used to obtain the auroral records are left to Appendix A and B, respectively.

Reproduced with permission of the copyright owner. Further reproduction prohibited without permission.

# Chapter 2
# Solar Wind and Magnetosphere

## 2.1 Introduction

The topics reviewed in this chapter provide a basis for an understanding of the interaction between the solar wind and the terrestrial magnetic field. The characteristics of the solar wind, geometry of the solar magnetic field, and the interaction of the solar wind with the Earth's magnetic field are considered first. Second, mechanisms that have been proposed to explain how solar wind energy is transported across the outer boundary of the magnetosphere are reviewed. Special emphasis is placed on the magnetic reconnection model since it is largely favored today as the best explanation for the variety of interplanetary magnetic field dependent phenomena observed in the magnetosphere and high latitude ionosphere. Finally, the structure of the geomagnetic field and the major plasma populations found within the magnetosphere are described. The emphasis is placed on the relationship of magnetospheric plasma populations to the precipitating particles observed at low altitudes above the dayside ionosphere.

## 2.2 Solar Wind and the Earth's Magnetic Field: Bow Shock, Magnetosheath, and Magnetopause

The solar wind is a stream of charged particles expanding outward from the solar corona into interplanetary space. It is a secondary energy source for the terrestrial upper atmosphere and the primary source of energy driving plasma dynamics in the magnetosphere. Charged particles, unlike photons, cannot penetrate directly into the atmosphere since the terrestrial magnetic field will deflect the majority of charged particles and shield the neutral atmosphere from direct bombardment by the solar wind. Solar wind energy transport into the magnetosphere, ionosphere, and neutral upper atmosphere is a process complicated by the shielding effect of the magnetic field. Two mechanisms couple solar wind energy to the upper atmosphere. First, solar wind plasma flow across the magnetospheric surface generates electric fields that penetrate to ionospheric altitudes thus driving plasma convection throughout the magnetosphere and ionosphere and heating the neutral atmosphere. Second, energetic particles from populations held in the Earth's magnetic field or penetrating directly from the magnetosheath produce aurora and heat the ionospheric plasma. In the winter hemisphere where solar photon input is negligible particle precipitation may become the dominant energy source to the upper atmosphere apart from advection.

The velocity moments (number density, momentum, and energy) for the solar wind plasma have been established by a large number of satellite measurements. The plasma is quasi-neutral with an equal number of ions (usually protons) and electrons. Plasma number densities are approximately 2-10 $cm^{-3}$ with mean values of 5 $cm^{-3}$ in the vicinity of Earth orbit. The most common minor species is $He^{++}$ [*Neugebauer and Snyder*, 1966] accounting for approximately 4-5% of the total ion number density and 16-20% to the total solar wind momentum flux. Other common minor species include $O^{6+}$, $O^{7+}$,$Si^{7+}$ to $Si^{9+}$, and $Fe^{7+}$ to $Fe^{13+}$, [*Bame et al.*, 1968].

Reproduced with permission of the copyright owner. Further reproduction prohibited without permission.

$He^{++}$ and other minor ion species carry only a fraction of the total solar wind momentum which is due primarily to protons because of their greater concentration. $He^{+}$ and $O^{+}$ ions are also observed within the solar wind but they are of terrestrial magnetospheric origin (Section 2.6) since a negligible quantity is discharged from the sun. Consistent with values predicted by the *Parker* [1958] theoretical model, satellite measurements show bulk solar wind velocities to vary from a minimum 200 km $s^{-1}$ to a maximum 750 km $s^{-1}$. The average value is approximately 400 km $s^{-1}$. Low solar wind velocities are associated with quiet solar conditions. Large velocities are observed during coronal disturbances such as shocks and high speed streams. The average 400 km $s^{-1}$ solar wind velocity results in energies on the order of 1 keV for protons and 0.5 eV for electrons. Bulk motion of the plasma dominates the thermal contribution to solar wind energy. The ratio of energy variations due to thermal velocities to bulk flow energy is approximately $\delta E/E \sim 0.1$ The particle energy associated with the solar wind flow is insufficient to explain the particle energies observed in the aurora since electron energies of 100-300 eV are typical for dayside aurorae and 1-10 keV for night time aurora.

The orientation and strength of the solar magnetic field is an important factor governing the solar wind-magnetosphere coupling process. Solar magnetic field strengths in the vicinity of the Earth are weak compared to the magnitude of the terrestrial field. Magnitudes of the solar magnetic field vary from approximately 2 to 10 nT with an average value of 5 nT [ Ness et al., 1966] compared to the 50-100 nT terrestrial magnetic field at the dayside magnetopause and the approximately 60,000 nT magnetic field on the planet's surface in the polar regions. During quiet solar wind conditions the average orientation of the solar magnetic field is a spiral as predicted by *Parker* [1958]. Typically the magnetic field vector is aligned with the ecliptic plane and rotated approximately 45° with respect to the Sun-Earth line in near Earth space. *Wilcox and Ness* [1965] identified a large-scale sector structure in the interplanetary magnetic field in the plane of the Earth's orbit. Interplanetary magnetic fields with components $B_x > 0$ and $B_y < 0$ are classified as "towards" in reference to the direction the magnetic field vector points relative to the sun and those with components $B_x < 0$ and $B_y > 0$ are classified as "away." The sector structure is primarily due to oscillations in the heliospheric current sheet separating regions of opposite polarity in the magnetic fields originating in the northern and southern solar hemispheres [*Schulz*, 1973; *Smith*, 1979]. Magnetic field data from the Pioneer 10 and 11 spacecraft obtained between 1 and 8.5 AU demonstrate the Parker spiral model is a good approximation to the IMF orientation over a wide range of distances [*Thomas and Smith*, 1980]. The solar $B_z$ component may be either positive ("$B_z$ northward") or negative ("$B_z$ southward") due to the oscillation of the current sheet but generally the horizontal components dominate and $B_z$ component which fluctuates between 1 and 2 nT about the mean zero value.

Solar wind interactions with the magnetosphere depend critically on the solar wind plasma velocity moments, magnetic field magnitude, and magnetic field orientation. The plasma and field parameters encountered in interplanetary space are the initial conditions that establish the rate at which the solar wind-magnetosphere interaction occurs as well as the total energy available to the magnetosphere. Interaction with the magnetosphere alters a number of these parameters upstream of the magnetopause where the interaction occurs, which is the subject of the next section.

Reproduced with permission of the copyright owner. Further reproduction prohibited without permission.

## 2.3 Solar Wind and the Magnetosphere

The magnetosphere is an obstacle to the solar wind. Momentum associated with the bulk flow must be lost for the solar wind to flow around the magnetosphere. Since the solar wind is supersonic plasma flows into the obstacle faster than the velocity that Alfvén waves can travel outward. New plasma arrives before waves can transport momentum upstream to slow the plasma flow allowing plasma to pile up in front of the magnetosphere. A shock front forms approximately $2-3\,R_E$ ($1\ R_E = 6371\,km$, the mean Earth radius) upstream of the magnetosphere where the plasma velocity abruptly increases and density decreases. The shock front is termed the " shock" and is the site where the plasma flow is thermalized converting energy associated with the bulk plasma flow to thermal energy within the plasma.

Shocked and thermalized solar wind plasma within the bow shock forms the region known as the "magnetosheath." The inner boundary of the magnetosheath is the outer boundary of the terrestrial magnetic field termed the "magnetopause." Satellite measurements of ion composition within the magnetosheath showed the plasma to be nearly identical to the solar wind [*Peterson et al.*, 1979], the primary difference is the increased number density and thermal velocity of the decelerated solar wind particles after encountering the bow shock. Observations of the magnetopause thickness vary from 100 to 1000 km with the minimum values appearing near the subsolar magnetosphere [*Cahill and Amazeen*,1963: *Kaufmann and Konradi*, 1973; *Berchem and Russell*, 1982]. The magnetopause boundary is always in motion radially from the Earth with velocities varying from 10 km $s^{-1}$ to 80 km $s^{-1}$ [*Kaufmann and Konradi*, 1973; *Berchem and Russell*, 1982] due to an oscillation with a period of approximately 10 minutes and amplitude of approximately 1 R *E*.

The magnetopause boundary is the surface over which the pressure exerted by the shocked solar wind flow is balanced by the magnetic pressure of the terrestrial field. The shape of the magnetopause surface can be computed from the pressure balance, but the equations must be solved self-consistently [*Wu et al.*, 1981] since the terrestrial field which balances the solar wind pressure is due not only to the Earth's internal magnetic field but also to the Chapman-Ferraro currents flowing on the surface of the magnetosphere generated by solar wind plasma flow over the terrestrial field. The origin of the Chapman-Ferraro current is the charge dependent $q\vec{v} \times \vec{B}$ Lorentz force acting on solar wind ions and electrons as they encounter the terrestrial field. Ions are deflected toward dusk and electrons toward dawn as they are ejected from the terrestrial field back into the magnetosheath. The relative motion of these particles while penetrating the surface of the terrestrial field generates the Chapman-Ferraro current flowing from dawn to dusk.

The number density $\rho$ and flow velocity $v$ (and dynamic pressure $\rho v^2$) of the plasma within the magnetosheath as well as the orientation of the interplanetary magnetic field immediately outside the magnetopause are important parameters required for studies of solar wind-magnetosphere interactions, though values obtained by satellites in interplanetary space upstream of the bow shock are often substituted due to their more general availability. Conditions within the compressed and thermalized solar wind plasma of the magnetosheath are not the same as the plasma upstream of the bow shock. Plasma densities near the subsolar point in the magnetosheath are predicted

Reproduced with permission of the copyright owner. Further reproduction prohibited without permission.

by magnetohydrodynamic (MHD) models [*Spreiter and Alksne*, 1969] to be enhanced by a factors of approximately 4 over the ambient solar wind values. The interplanetary magnetic field, frozen into the solar wind flow, is dragged into the magnetosheath and may be similarly compressed to magnitudes of nearly seven times the value outside the bow shock or may be reduced to zero depending on the orientation of the interplanetary magnetic field [c.f., *Spreiter et al.*, 1966; *Spreiter and Alksne*, 1969]. Further, the compressed magnetic field regions have lower plasma density due to loss of particles streaming outward along the field lines [*Zwan and Wolf*, 1976; *Crooker*, 1977] leading to an increase of the magnetosheath to interplanetary magnetic field ratios by factors up to 8. *Reiff et al.* [1981] noted that while application of the amplification factors may yield enhancements of the magnetic field of 5-10 times within the magnetosheath, if the sheath field exceeded the terrestrial field magnitude the results are erroneous because the total plasma pressure in the solar wind (field and plasma) must balance the pressure due to the terrestrial field at the magnetopause. Theoretical calculations and observations show the bulk velocity of magnetosheath plasma varies from 0 km $s^{-1}$ to near solar wind values depending on the distance from the subsolar point the plasma crosses the bow shock. Number densities increase up to four times the solar wind values with the largest increases occurring near the subsolar point [*Spreiter and Alksne*, 1969].

Many studies of the magnetopause are based on direct observations of magnetosheath fields and plasma conditions using data from the HEOS, ISEE, and AMPTE satellite missions but values obtained by satellites upstream of the bow shock in the solar wind are often substituted if magnetosheath values are not available. *Russell et al.* [1980] and *Crooker et al.* [1982] showed that magnetic field and plasma parameters from the ISEE 3 satellite in orbit about the sunward libration point approximately 200 Re in front of the Earth must be used with caution. Propagating IMF structure and large variations in the normals to planes separating interplanetary magnetic fields of differing polarity or regions with varying number densities lead to large variations in time lags between solar wind magnetic field or plasma parameter time series obtained at the libration point and in the vicinity of the Earth. For this reason magnetic field orientation information is best obtained as near the bow shock as possible and the satellites most often used for IMF parameters are in the Interplanetary Monitoring Platform (IMP) series in near circular orbits at radial distances of approximately 40 Re from the Earth.

*Fairfield* [1967] tested the validity of using solar wind observations to estimate the conditions within the magnetosheath by comparing satellite observations of the IMF upstream from the bow shock and within the magnetosheath. Discontinuities observed at the two satellites are nearly always correlated on a one-to-one basis demonstrating that the interplanetary field is convected into the sheath with the solar wind flow. Further, the comparison showed that even as the magnitude of the field increases in the sheath and is distorted to force the interplanetary field lines to align tangentially to the magnetopause, the relative polarity of the $B_z$ component and the sense of the interplanetary towards and away polarity remain constant. Similarly, plasma density and pressure variations appear to be magnified within the magnetosheath allowing interplanetary values to be used to estimate the existence of variations within the magnetosheath plasma environment although the magnitude of the variations is subject to the error in determining the correct amplification factors. *Freeman and Southwood* [1988] found that variations in the transverse component of the

Reproduced with permission of the copyright owner. Further reproduction prohibited without permission.

IMF with time scales greater than approximately 100 seconds pass unchanged through the bow shock and magnetosheath. In addition, the magnetic field in the sheath was shown to convect at approximately the plasma flow velocity allowing the magnetosheath flow model developed by *Spreiter and Stahara* [1980] to be used to obtain time lags between the IMF and magnetosheath fields.

## 2.4 Magnetic Field Topology: Open and Closed Field Lines and the Separatrix

Currents generated in terrestrial plasma populations resulting from the solar wind interaction with magnetosphere are sources of additional magnetic fields external to Earth's internal field. Addition of the external fields to the terrestrial field generated in the Earth's core and crust distorts the dipole magnetic field geometry by compressing the dayside and the stretching the nightside field into a long tail. The distorted geometry of the magnetosphere is the result of the self-consistent fields produced by the interaction of the terrestrial magnetic field with the solar wind plasma and the generation of the currents within magnetospheric plasma populations. A diagram of the Earth's magnetic field geometry in the noon midnight plane is given in Figure 2.1. Two regions of reduced magnetic field intensity are found in the high latitude dayside regions. Termed the "polar cusps", they are the result of the solar wind-magnetosphere interaction sweeping flux tailward from the dayside magnetosphere. Since the cusps are formed by the solar wind-magnetosphere interaction, their size and location are also strongly dependent on the details of the interaction, a subject that will be considered in more detail below.

Three topologically distinct types of magnetic field lines are found in the Earth-solar wind open magnetosphere system. Each type shown schematically in Figure 2.2 can be distinguished by considering the behavior of a low energy test charge found in each region. Lines labelled (1) are the closed terrestrial field lines. A test particle initially located within the region of closed field lines may encounter the Earth or remain trapped in the terrestrial field but will never move into the region dominated by the solar magnetic field. Field lines labelled (2) originate in the Sun and are carried into interplanetary space by the solar wind. These field lines are not connected with the terrestrial field line and a test charge located within the region will never move into the region of closed terrestrial field lines. The final class are the open geomagnetic field lines labelled (3) and (4) which are topologically connected to the solar magnetic field. A test particle initially in the solar wind may enter the magnetosphere along open field lines. Similarly test particles initially located in the terrestrial magnetic field may flow out into the solar wind on open field lines. The open lines are labelled differently in the northern and southern hemisphere since their topology depends on the sign of the interplanetary magnetic field $B_y$ component (see Section 2.6.4). The three classes are often colloquially described as having no ends on the earth (solar wind), two ends on the earth (closed), or one end on the earth and one in interplanetary space (open). This description is not strictly correct, of course, since magnetic field lines do not have ends without requiring the existence of a magnetic monopole (c.f., the discussion by *Jackson*, 1975).

A variety of magnetic field models have been developed which describe the magnetosphere as being either open or closed [*Axford and Hines*, 1961; *Dungey*, 1961,1963; *Dessler*, 1964; *Williams*

Reproduced with permission of the copyright owner. Further reproduction prohibited without permission.

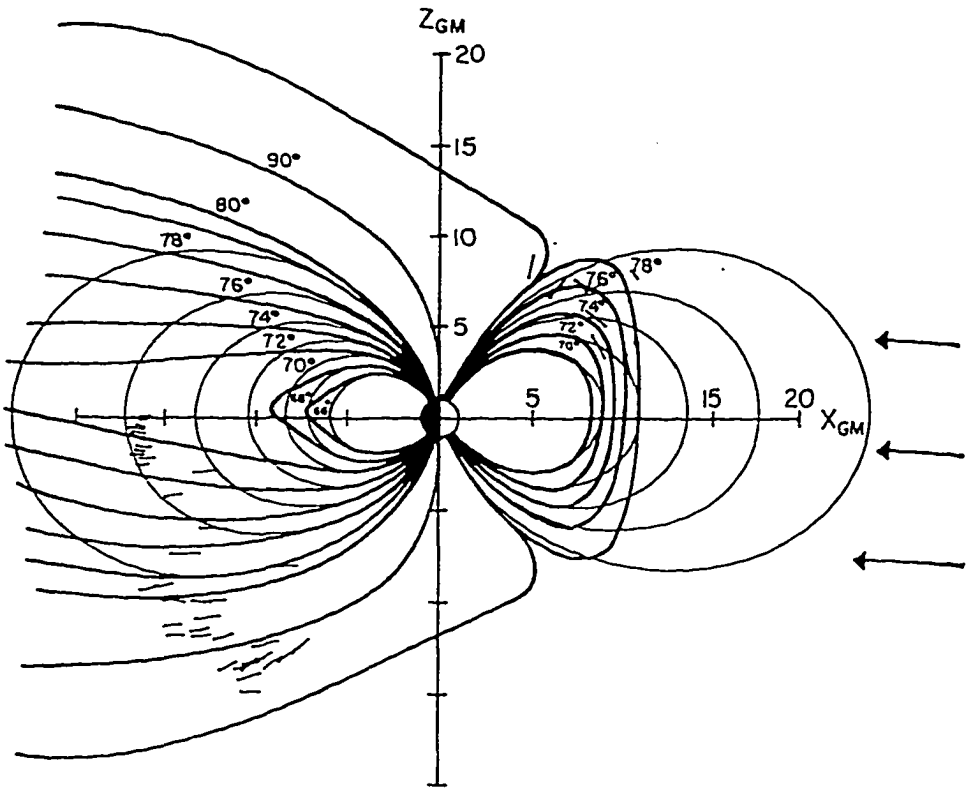


Figure 2.1 Magnetic Field of the Earth. The distorted magnetic field lines (heavy) due to the solar wind interaction with the Earth's dipole magnetic field (light). The projection is in the noon-midnight meridian plane. The light arrows indicate magnetic field vectors measured by satellites. The latitude at which the field line intersects the Earth's surface is labelled for the distorted field. This field model indicates that field lines on the dayside poleward of 78° are swept tailward. The cusps are the indented regions in the field between the last closed dayside field line and the first field line that is swept into the tail. The compression of the dayside field is also evident forming regions of minimum $\vec{B}$ off the equatorial plane. On the night side of the planet the field lines are stretched rather than compressed as they are on the dayside and by latitudes above 70° they extend deep into the magnetotail. [from *Fairfield*, 1968].

Reproduced with permission of the copyright owner. Further reproduction prohibited without permission.

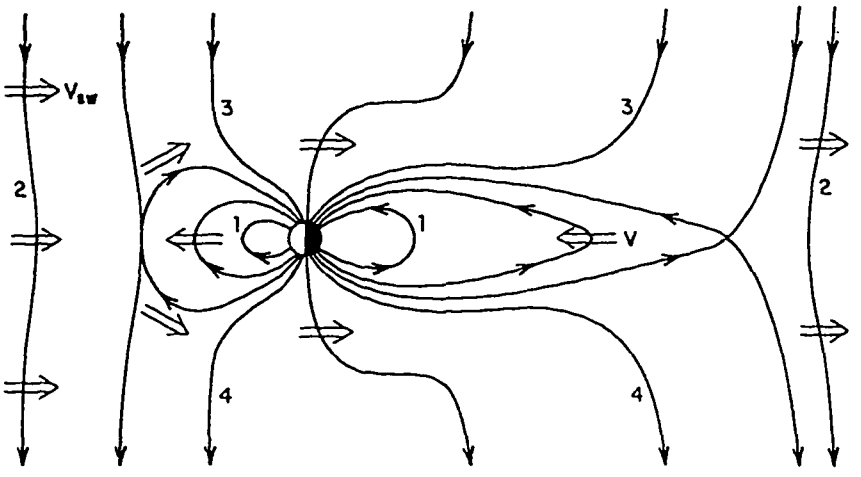


Figure 2.2 Field Line Topology of an Open Magnetosphere. Field lines labelled (1) are closed terrestrial field lines that do not connect with the interplanetary field lines (2). Lines (3) and (4) are open terrestrial field lines that connect with the solar field lines in interplanetary space [from *Lyons and Williams*, 1984].

*and Mead*, 1965; *Roederer*, 1969; *Beard and Choe*, 1974; *Choe and Beard*, 1974; *Olson and Pfitzer*, 1974; *Tsyganenko*, 1987, 1989; *Tsyganenko and Usmanov*, 1982]. Closed magnetospheres contain only magnetic field lines of terrestrial origin aud the solar wind plasma and interplanetary magnetic fields are entirely excluded. Energy transfer from the solar wind into such a magnetosphere may be accomplished by either an impulsive penetration process (Section 2.7.2) or a viscous process acting on the boundary (Section 2.7.3) but neither process is thought to contribute significantly to the total magnetosphere energy budget. An open model contains a set of terrestrial field lines connected to the solar wind allowing the direct penetration of solar wind plasma and electric field into the magnetosphere (and conversely the magnetospheric plasma into the solar wind). Strong evidence for the open model is found in the behavior of magnetic fields and plasma at the dayside magnetopause consistent with the reconnection models for the solar wind interaction (Section 2.8.1) and the asymmetric access of high energy solar wind particles to the polar caps (Section 2.6.4). The current consensus is that the magnetosphere is open and that magnetic field line merging (Section 2.8.1) between the solar and terrestrial fields is the dominant mechanism for the transport solar wind mass and energy across the magnetopause.

A boundary between topologically distinct types of magnetic field lines, a line in two dimensions or a surface in three dimensions, is termed a "separatrix." Two such lines are found in the

Reproduced with permission of the copyright owner. Further reproduction prohibited without permission.

two dimensional picture of Figure 2.2. The first is the last closed magnetic field line on the dayside in contact with the solar magnetic field near the subsolar point and the second is the last closed field line on the nightside. The dayside separatrix in an open magnetosphere divides magnetic field lines that connect through the dayside magnetosphere to the conjugate hemisphere from field lines that connect to the solar magnetic field. A dayside separatrix near the noon-midnight meridian plane may still be defined for a closed magnetosphere between field lines that close through the dayside magnetosphere to the conjugate hemisphere from field lines that close through the distant tail region to the conjugate hemisphere although strictly speaking the topology of all field lines within a closed magnetosphere is the same.

The question of how solar wind energy and mass is transferred across the separatrix into the magnetosphere is one of the central problems of space physics and one of the prime motivations for the study of dayside aurora. Many details of the energy transfer process are still controversial. The time dependence of the merging rate is poorly understood even though dayside reconnection is thought to be the primary mechanism for solar wind particle transport across the magnetopause. Attempts to identification the magnetospheric source regions for the precipitating particles observed at low altitudes producing dayside auroral displays are still fraught with problems in mapping particles from the ionosphere to the magnetosphere. Finally, the identification of ionospheric signatures of boundary layer processes is currently in its infancy since unique correlation between magnetopause events and ionospheric response has yet to be generally established.

## 2.5 Charged Particle Motion in the Magnetosphere

Drift motions of ions and electrons in the Earth's magnetic field are primarily due to the presence of electric fields and magnetic field inhomogeneities [c.f., *Northrup*, 1963; *Roederer*, 1970; *Krall and Trivelpiece*, 1973; *Lyons and Williams*, 1984; *Walt*, 1994]. The electric field drift

$$\vec{V}_{d,E} = \frac{\vec{E} \times \vec{B}}{B^2} \tag{2.1}$$

is independent of charge, mass, and energy of the particle yielding the same drift for both ions and electrons. The curvature drift

$$\vec{V}_{d,C} = \frac{m v_{\parallel}^2}{qB^2}(\hat{b} \times \nabla \vec{B}) \tag{2.2a}$$

and gradient B drift

$$\vec{V}_{d,\nabla B} = \frac{1}{2}\frac{m \vec{V}_{\perp}^2}{qB^2}(\hat{b} \times \nabla \vec{B}) \tag{2.2b}$$

where $\hat{b}$ is a unit vector in the direction of the terrestrial field, $m$ and $q$ the mass and charge of the particle, and $v_{\parallel}$ and $v_{\perp}$ are the components of the particle velocity parallel and perpendicular

Reproduced with permission of the copyright owner. Further reproduction prohibited without permission.

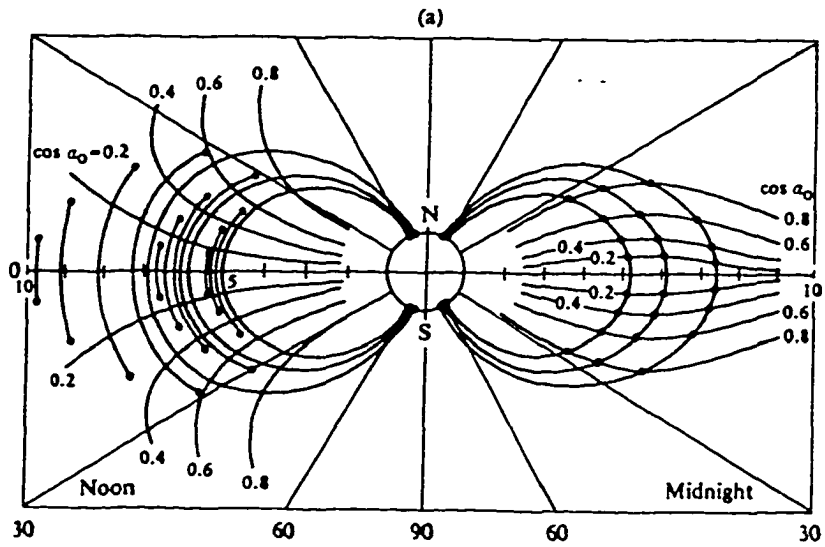


Figure 2.3 Drift Shell Splitting for Particles Originating in the Midnight Meridian. The mirror points are indicated as dots and are labelled with the cosine of the equatorial pitch angle. Particles with small equatorial pitch angles mirroring near the equatorial plane must move radially outwards to conserve the adiabatic invariant I. If the drift shells pass near the magnetopause pitch angles near 90° are lost. Injection of charge particles near 8-10 $R_E$ on the nightside is a source of quasi-trapped electrons near the magnetopause.

to the magnetic field. The drifts in equations (2.2a) and (2.2b) are in the same direction and may be combined to yield

$$\vec{V}_{d,\nabla B-C} = \frac{T}{qB^3}(1+cos^2\alpha)(\vec{B}\times\nabla\vec{B}) \tag{2.3}$$

which describes the combined drift due to curvature and gradients of the magnetic field.

Low energy plasma in the high latitude ionosphere drifts primarily in response to the magnetosphere and corotation electric fields and is not strongly affected by the curvature and gradient B drifts. High energy particle populations of the ring current and radiation belts are strongly driven by the gradient B and curvature drifts. Since these drifts are charge dependent, electrons drift eastward while ions drift westward producing a current. The relative drift between ions and electrons within the inner magnetosphere where particles can drift completely around the Earth gives rise to the ring current. The curvature and gradient drifts are approximately the same magnitude in the inner regions of the magnetosphere but the curvature drift dominates in the magnetotail due to the strong curvature in the field near the neutral sheet [*Burke et al.*, 1985].

Reproduced with permission of the copyright owner. Further reproduction prohibited without permission.

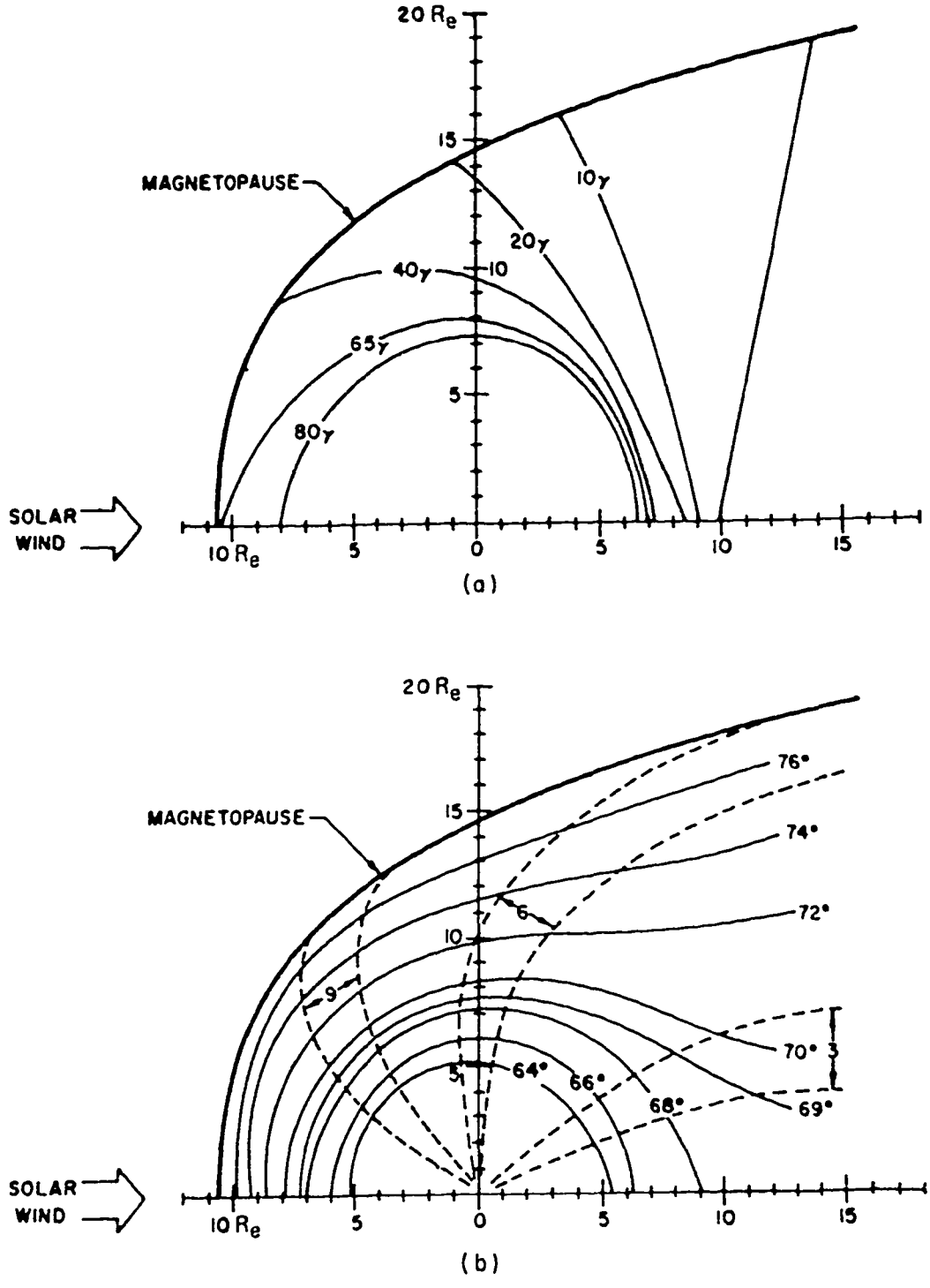


Figure 2.4 Lines of Constant $|\vec{B}|$ and Mapping the High Latitude Ionosphere to the Equatorial Plane. (a) Particles with 90° pitch angles (mirroring on the equatorial plane) will drift on lines of constant B shown here in the equatorial plane. (b) Lines of constant magnetic latitude and longitude mapped to the equatorial plane [from *Fairfield*, 1968].

Reproduced with permission of the copyright owner. Further reproduction prohibited without permission.

The dynamics of charged particles within the Earth's magnetic field of interest here can be described in terms of the first two adiabatic invariants (general discussions on the derivation and use of adiabatic invariants can be found in *Northrup*, 1963, *Stone*, 1963, *Roederer*, 1969, and *Lyons and Williams*, 1984). The first is due to the particle oscillating between two mirror points in a field with a nonzero gradient in the direction of the field and is given by the ratio of the kinetic energy of the particle perpendicular to the field to the magnetic of the magnetic field

$$J_1 = E_\perp(s)/B(s) = constant \tag{2.4a}$$

or, in terms of the particle pitch angle (the angle between the particle velocity and magnetic field vectors),

$$\frac{sin^2\alpha(s)}{B(s)} = \frac{sin^2\alpha_i}{B_i} = constant \tag{2.4b}$$

where $\alpha(s), B(s)$ are the particle pitch angle and magnetic field intensity at some distance $s$ along the field line and $\alpha_i, B_i$ are the pitch angle and field intensity at an arbitrary initial point. Pitch angles are often referred to the equatorial plane where the magnetic field intensity $B_0$ is a minimum for a dipole field. The equatorial pitch angle $\alpha_0$ will be a minimum for all particles travelling on a given field line. A particle moving away from the equatorial plane into the increasing magnetic field intensity must increase its pitch angle for the first adiabatic invariant to remain constant. When the pitch angle becomes 90° the particle is at the "mirror point" and is reflected. Particles with mirror points at altitudes where the atmospheric density is sufficiently low that collisions are improbable are said to be "trapped". The probability of loss through collisions with the atmosphere for particles mirroring below approximately 100-150 km is very high. An altitude of 100 km is typically accepted as the critical altitude below which high energy radiation belt particles are efficiently loss to the atmosphere. Particles with equatorial pitch angles less than

$$\alpha_0 = arcsin(B_0/B_{100})^{1/2} \tag{2.4c}$$

mirror below 100 km and are said to be in the "loss cone" and "precipitate" into the atmosphere.

Loss cones are small for particles on field lines in the outer radiation belts. For example, consider a closed field line that intersects the Earth near 75° magnetic latitude and passes near the magnetopause. The magnitude of the magnetic field varies from only 60-100 nT at the equatorial plane near the magnetopause to nearly 60,000 nT near the Earth's surface. The equatorial pitch angle defining the loss cone for particles mirroring at 100 km along this field line are on the order of 2° . Precipitation of particles from trapped populations may result if the parallel velocity is increased reducing the altitude of the mirror point. Some examples of processes which result in changes to the pitch angle are wave-particle interactions, formation of parallel electric fields, and collisions with the atmosphere.

Reproduced with permission of the copyright owner. Further reproduction prohibited without permission.

The bounce period between mirror points can not be solved analytically for a dipole field but may be estimated using the approximation [*West*, 1994]

$$\tau_b = 0.117\left(\frac{r_0}{R_E}\right)\frac{1}{\beta}[1 - 0.4635(sin\alpha_{eq})^{3/4}] \ seconds \tag{2.5a}$$

applicable for both electrons and ions. Alternatively, a simplified form is given by *Lyons and Williams* [1984]

$$\tau_b = \frac{4r_0}{v}s(\alpha_0) \quad seconds \tag{2.5b}$$

where the parameter $s(\alpha_0)$ is approximated by either [*Hamlin et al.*, 1961]

$$s(\alpha_0) \sim 1.30 - 0.56sin\alpha_0 \tag{2.5c}$$

or [*Wentworth*, 1960]

$$s(\alpha_0) \sim 1.38 - 0.32(sin\alpha_0 + \sqrt{sin\alpha_0}) \tag{2.5d}$$

The latter approximation for $s(\alpha_0)$ is the most accurate of the two.

The second adiabatic invariant requires the summed momentum along the field line remain constant

$$J_2 = \oint mv_{\|} = \oint p_{\|} = constant \tag{2.6a}$$

or in terms of the magnetic field through the use of Equation 2.4

$$I = \int_{B_{m,1}}^{B_{m,2}} \left[1 - \frac{B(s)}{B_m}\right]^{1/2} ds = constant \tag{2.6b}$$

where $B_m$ is the magnetic field intensity at the mirror points [c.f., *Roederer*, 1970; *Lyons and Williams*, 1984]. The oscillation between the mirror points and the azimuthal drift due to the combined curvature and gradient drifts define a fixed surface on which the particle motion is confined due to the conservation of the adiabatic invariant I. The L-shell [*McIlwain*, 1961] defines the locus of trajectories available to a population of particles with a given equatorial pitch angle. All particles passing through the equatorial plane at the same radial distance from the Earth lie on the same drift shell in an azimuthally symmetric magnetic field.

The two applications of the adiabatic invariants of greatest interest here are the identification of trapped and quasi-trapped particle populations and sources of particles near the magnetopause. The compressed magnetic field on the dayside is stronger near the equatorial plane than the field at an equivalent radius on the nightside where the field is stretched and weakened. Particles with pitch angles near 90° drifting towards the dayside due to the combined effects of the curvature and gradient B drifts must move radially outward to conserve $I$ resulting in drift shell splitting, the removal of the degeneracy of drift shells for particles with different equatorial pitch angles. Figure 2.17 shows the result of a calculation by *Roederer* [1967] using a model magnetic field showing the effects of drift shell splitting for particles with a variety of pitch angles originating on common field lines in the midnight meridian. Particles drifting nearest the Earth where the nondipolar components of the magnetic field are relatively weak are not affected as strongly as

Reproduced with permission of the copyright owner. Further reproduction prohibited without permission.

particles in the distorted field of the outer magnetosphere. Note that particles with large equatorial pitch angles (near 90° ) originating at 7-8 Re on the night side approach the magnetopause at 10 Re on the dayside. These particles may encounter the magnetopause and are lost from the magnetosphere. Electrons with pitch angles near 90° are lost preferentially due to drift shell splitting producing "butterfly" electron pitch angle distributions in the afternoon magnetosphere from magnetopause shadowing [*West et al.*, 1972, 1973]. Butterfly pitch angle distributions are indicative of trapped particle populations with the usual field aligned decrease in intensity due to the atmospheric loss cone but with an additional decrease at 90° due to the loss of particles through the magnetopause. Natural particle populations exhibiting butterfly distributions are typically encountered in the dayside magnetosphere near the magnetopause, prenoon for ions and postnoon for electrons, indicating the outer radiation belts are full of particles to the magnetopause.

Particles initially injected in the night time sector which drift through the daytime sector and return without encountering the magnetopause or the atmosphere are stably trapped. The drift period of trapped particles can be estimated for a dipole magnetic field from the approximate relationship (accurate to approximately 0.5%) [*Walt*, 1994]

$$\tau_d = C_d\left(\frac{R_E}{r_0}\right)\frac{1}{\gamma\beta^2}[1 - 0.333(sin\alpha_{eq})^{.62}] \quad seconds \tag{2.7a}$$

where $r_0$ is the radial distance of the equatorial crossing of the field line, $\beta$ is the ratio of the particle velocity $v$ to the speed of light $c$, and $\gamma = [1 - \beta^2]^{-1/2}$. The constant $C_d$ contains the particle dependent parameters

$$C_d \quad = 1.557 \times 10^4 (electrons) \tag{2.7b}$$

$$= 8.481(protons) \tag{2.7c}$$

The approximate form is often used since the drift period, like the bounce period, cannot be obtained analytically in a dipole field.

The approximations for the bounce and drift periods as well as results using a dipole field model should only be used to obtain a qualitative estimates of particle motions in the magnetosphere since particle drifts in realistic fields may be more complicated. For example, *Reeves et al.* [1991] numerically computed particle drifts in the *Tsyganenko and Usmanov* [1982] semi-empirical model magnetic field to show that particles with 30° pitch angles will drift faster than 85° pitch angle particles near noon due to the solar wind compression of the magnetic field, behavior that is not predicted by the equations for motion in a symmetric dipole field.

Particles originating in nightside injections which encounter the dayside magnetopause are termed quasi-trapped or pseudo-trapped since they cannot drift completely around the Earth. Fluxes of quasi-trapped particles are quite variable since only recent injections provide fresh sources and all particles within the quasi-trapped zone are lost through the magnetopause before returning to the point of origin [*Frank*, 1965; *Craven*, 1966].

Reproduced with permission of the copyright owner. Further reproduction prohibited without permission.

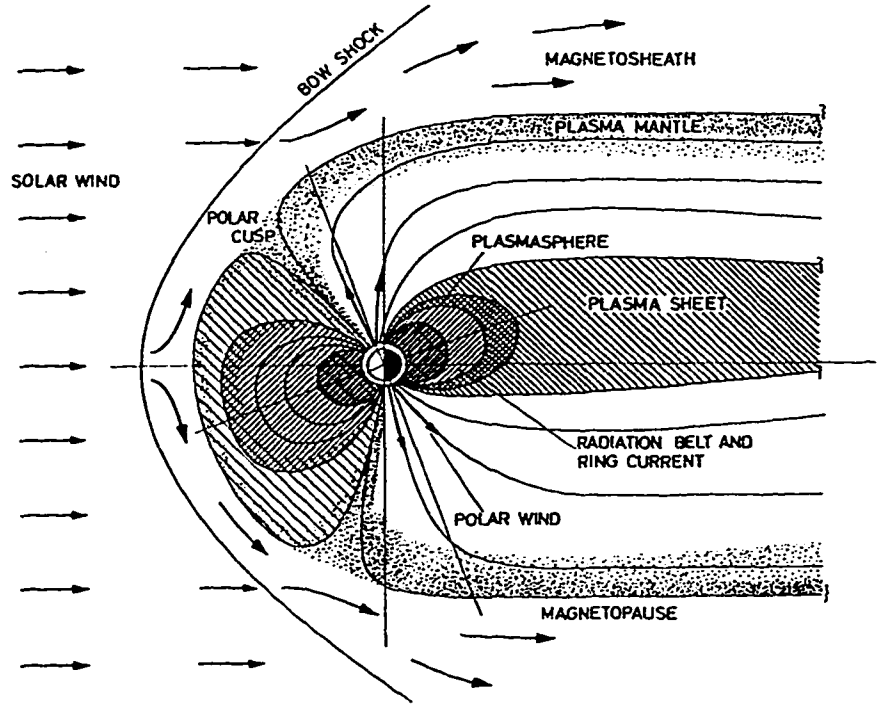


Figure 2.5 Schematic of the Magnetosphere. The principle plasma and current regimes in the magnetosphere are indicated (from *Rosenbauer et al.* [1975]).

## 2.6 Magnetospheric Structure and Plasma Populations

The principle particle populations in the magnetosphere and adjoining regions of space are shown in Figure 2.5. Characteristics of the plasma and magnetic fields within these regions have been determined over the last thirty years by direct measurements from Earth orbiting satellites (c.f., the reviews given by *Ness*, 1965; *Frank*, 1971; *Cowley*, 1980; and *Feldstein and Galperin*, 1985; *Schultz*, 1991). The magnetosphere is the source of the charged particles that create auroral displays. Any study of auroral processes therefore requires an understanding of the magnetic structure, particle populations, and plasma motions in the magnetosphere.

### 2.6.1 Boundary Layers

Immediately inside the magnetopause are the "boundary layers", regions of the terrestrial magnetic field where the dominant plasma populations are characteristic of the solar wind and magnetosheath [*Vasyliunas*, 1979]. Satellite observations show the plasma flows within the boundary layers are generally antisunward at variable velocities and number densities suggesting a temporally varying plasma source [*Hones et al.*, 1972; *Akasofu et al.*, 1973; *Eastman et al.*, 1976]. Boundary layers are found over the entire surface of the magnetosphere with thicknesses varying from a fraction of an Earth radius at the subsolar point to nearly 10 Re in the flanks of the

Reproduced with permission of the copyright owner. Further reproduction prohibited without permission.

magnetosphere. A number of specialized terms are applied to the dayside boundary layer regions based on their locations in the magnetosphere. The polar cusps are localized regions of minimum magnetic field intensity in the dayside magnetosphere [*Fairfield and Ness*, 1972] where magnetosheath plasma can penetrate directly to ionospheric altitudes [*Frank*, 1971; *Frank and Ackerson*, 1971; *Heikkila and Winningham*, 1971]. An extended region associated with the cusp referred to as the "polar cleft" separates magnetic field lines closing through the dayside magnetosphere in the conjugate hemisphere with field lines that are swept into the geomagnetic tail. At ionospheric altitudes the term cleft is often associated with the footprint of the boundary layers located equatorward of the cusp and magnetic cleft [c.f., *Lundin*, 1988] where particle fluxes similar to the cusp are encountered but are accompanied by isolated accelerated electron events. Equatorward of the cleft the boundary layer is termed the "low latitude boundary" layer [*Eastman et al.*, 1976]. The "entry layer" [*Paschmann et al.*, 1976] is found near the equatorward edge of the cusp where magnetosheath plasma flow is turbulent. A region of stagnant plasma found near the outer reaches of the polar cusp is called the "exterior cusp" [*Hansen et al.*, 1976; *Sckopke et al.*, 1979]. Boundary layers poleward of the cusp and cleft on the surface of the tail lobes is the "plasma mantle" [*Rosenbauer et al.*, 1975; *Sckopke and Paschmann*, 1978]. The polar cusps and mantle are considered in more detail in the next section since their extensions into the ionosphere are the regions to where dayside aurorae form.

Plasma transport across the magnetopause is required to obtain the magnetosheath ion composition found within the boundary layers [*Peterson et al.*, 1982; *Lundin et al.*, 1982]. Magnetosheath plasma may have direct access to the magnetosphere through the polar cusp and cleft if the magnetic field lines threading the boundary layers are connected to the solar wind. However, if the boundary layer field lines are closed then the magnetosheath plasma does not have direct access to the boundary layer and some form of viscous or impulsive process is required for the plasma transport across the magnetopause to occur. The question of whether the boundary layer field lines are open or closed is still a subject of debate. As noted in Section 2.8.1, *Eastman and Hones* [1979] and *Eastman and Hones* [1982] used high time resolution measurements of the boundary layer plasma to show that electron pitch angle distributions are strongly peaked at 90 ° , characteristic of trapped populations on closed field lines. *Roeder and Lyons* [1992] found similar energetic particle pitch angle distributions in S3-3 satellite data during traverses of the boundary layer and concluded the low latitude boundary layer was partially on open and partially on closed field lines. *Daly and Fritz* [1982] explained that electrons may retain their anisotropic distributions even on newly opened field lines since the electrons may be reflected from the converging magnetic fields near the reconnection site and, therefore, electron distributions within the boundary layers may exhibit characteristics of trapped populations even though they are on newly opened field lines. The ions, due to their greater mass and gyroradius, should not be reflected and would be expected to exhibit a loss cone distribution as observed by *Scholer et al.* [1982a].

A number of recent studies indicate that at least in the region near magnetic noon the magnetic the particle characteristics of the low latitude boundary are explained by time-of-flight effects on magnetosheath plasma injected on recently merged field lines [*Gosling et al.*, 1990b; *Onsager et al.*, 1993; *Lockwood et al.*, 1993; *Lyons et al.*, 1994]. The low energy magnetosheath plasma takes

Reproduced with permission of the copyright owner. Further reproduction prohibited without permission.

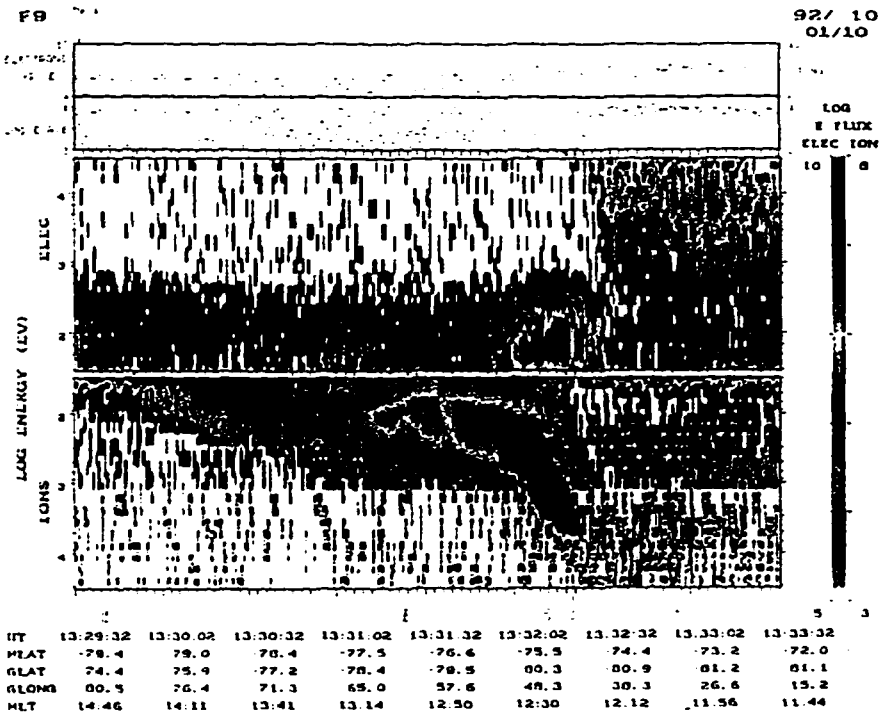


Figure 2.6 Dayside Ion and Electron Energy Spectrum. DMSP satellite measurement of ion and electron energy from 30 eV to 30 keV (note the energy scale on the ions is inverted). The decrease in average ion energy with latitude is characteristic of dayside passes through the cusp.

approximately 2 minutes to travel from the subsolar magnetopause to the ionosphere, in this time it convects poleward some 50-100 km for typical solar wind speeds. High energy electrons and ions can leak from the bulk magnetosheath flow explaining the low fluxes of high energy particles within the low latitude boundary layer. The bulk of the low energy plasma is identified as "cusp". This description of the low latitude boundary layer suggests that the cusp and the low latitude boundary layer are essentially the same region and the width of the low latitude boundary layer during IMF $B_z$ negative conditions is determined by the distance poleward the magnetosheath ions will convect before arriving in the ionosphere.

### 2.6.2 Polar Cusp and Mantle

The polar cusps were predicted theoretically by *Chapman and Ferraro* [1931, 1933]. Confirmation of their existence was obtained by *in situ* satellite measurements of the Earth's magnetic field showing a permanent localized region of weak magnetic field at high latitudes near local noon. *Heikkila and Winningham* [1971] and *Frank* [1971] showed that the high density and low energy plasma found on cusp field lines in the outer magnetosphere and at low altitudes was characteristic of the magnetosheath and not the low density and high energy plasma typically found throughout the magnetosphere (Section 2.4.5), demonstrating that magnetosheath plasma penetrates the

Reproduced with permission of the copyright owner. Further reproduction prohibited without permission.

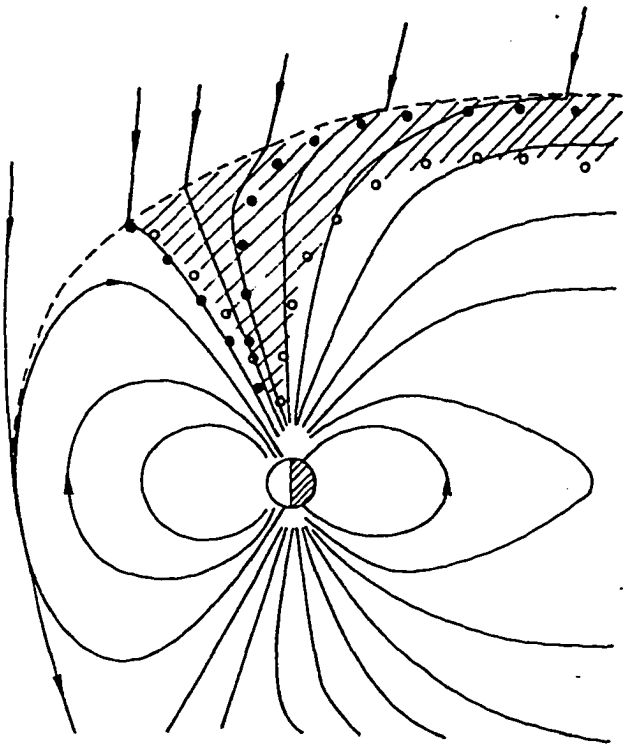

Figure 2.7 Origin of the Ion Energy Dispersion in the Cusp and Mantle. Ions with large (dark) velocities parallel to the field line rapidly penetrate the cusp to low altitudes, mirror, aud then travel upwards and tailwards. Ions with small (light) velocities parallel to the magnetic field convect further polewards before they mirror aud travelling further tailward. High energy ions are observed closer to the open/closed field line boundary at low altitude and the average energy decreases poleward [from *Rosenbauer et al.*, 1975].

magnetosphere to ionospheric altitudes in the cusp region. Further evidence for direct access of magnetosheath plasma into the magnetosphere has been demonstrated by the excellent correlations between plasma densities obtained by the IMP satellite in the solar wind and simultaneous observations of cusp plasma densities by the Viking satellite at altitudes of approximately 2 Re [*Aparicio et al.*, 1991].

Estimates of the size of the polar cusp have been obtained by a number of satellites. ISIS 1 and IMP 5 intersected regions of plasma with characteristics similar to the magnetosheath typically over a latitude range of approximately 2 degrees near the noon meridian [*Heikkila and Winningham*, 1971; *Frank*, 1971]. *Burch* [1973] estimated the cusp width to vary from 4° to 7° using the 0.7 keV to 23.9 keV electron data from the OGO-4 satellite, the small and large values associated with IMF $B_z$ southward and northward, respectively. Studies from satellites in the DMSP series have yielded estimates for widths of the polar cusp on the order of 0.7 ° to 3.5 ° invariant latitude [*Meng*, 1981; *Newell and Meng*, 1987, 1988]. *Carbury and Meng* [1986] noted that the cusp width is correlated with $B_z$, narrowing for periods of strong $B_z$ negative. A later study by *Carbury and*

Reproduced with permission of the copyright owner. Further reproduction prohibited without permission.

*Meng* [1988] obtained values varying from 1° to 8° and which showed that the latitudinal width of the cusp decreases with geomagnetic activity, consistent with the *Burch* [1973] study. *Newell and Meng* [1987] however noted that DMSP observations show the cusp is narrowest during periods when the IMF $B_z$ component is negative and widest when $B_z$ is positive. Statistical analysis of the DMSP particle data give an average value of approximately 1 ° invariant latitude [*Newell et al.*, 1991b]. Analysis of Viking dayside particle data yields values of approximately 2 ° for the latitude width of the cusp [*Kremser and Lundin*, 1990; *Aparicio et al.* 1991]. Finally, *Escoubet et al.* [1995] reported a cusp width of 0.5° invariant latitude from a DE 2 satellite traverse of the cusp during a period of high auroral activity.

Estimates of the longitudinal extent of the cusp have also been obtained from satellite observations of precipitating electrons and protons. *Newell et al.* [1989] obtained statistical values for the longitudinal width of the cusp to be 2.1 (2.8) hours for $B_z > 0 (B_z < 0)$ using particle data from the DMSP satellite consistent with the value of approximately 2 hours obtained by *Aparicio et al.* [1991] using Viking data.

Discrepancies between the different estimates result from a number of factors including varying sensitivities of the particle detectors flown on different satellites, the varying altitudes at which the cusp is sampled, varying geomagnetic conditions, and variations in criteria used to determine the poleward and equatorward boundaries of the cusp. The satellite measurements indicate the average cusp is approximately 1 ° -3 ° in latitude. This latitude range is approximately 100-300 km at auroral altitudes. This value will be an important parameter in comparison to the reported widths of the midday aurorae given in Chapter 3 and the choice of latitudinal width of the electron precipitation in the auroral model described in Chapter 4.

The plasma mantle is the high latitude extension of the boundary layers and extends over the entire surface of the magnetosphere tailward of the cusp [*Rosenbauer et al.*, 1975]. The thickness of the mantle and the density of the plasma is greatest during periods when the interplanetary magnetic field $B_z$ component is negative [*Sckopke et al.*, 1976]. Plasma composition within the mantle is similar to the magnetosheath and cusp suggesting a common solar wind source. The mechanism by which the dayside boundary layers is populated by magnetosheath plasma was described by *Rosenbauer et al.* [1975]. Ions and electrons enter the polar cusp from the magnetosheath and travel along the magnetic field lines into the magnetosphere where they either mirror or collide with the atmosphere. Mirrored particles move outward and tailward under the influence of the convection electric field populating the mantle region. Particles that encounter the atmosphere before mirroring from the precipitated flux responsible for the dayside aurora. A characteristic feature of ion energy spectra obtained by low altitude satellites in the cusp and mantle is a decrease in average ion energy with increasing latitude. Figure 2.6 shows an example of this feature in energy spectra obtained by a DMSP satellite. This feature is due to the velocity filter effect of the convective electric field [*Rosenbauser et al.*, 1975; *Reiff et al.*, 1977] shown schematically in Figure 2.7. Both high and low energy ions are driven antisunward by the convective electric field as they move along the magnetic field lines. High speed ions either reach the atmosphere or mirror sooner than the low speed ions. The average ion energy is therefore greatest at the equatorward edge

Reproduced with permission of the copyright owner. Further reproduction prohibited without permission.

of the cusp where only the high speed ions may be found and decreases with increasing latitude where lower speed ions finally reach the ionosphere.

Plasma in the magnetosheath and in the cusp is quasi-neutral [*Burch*, 1985] and the ions due to their greater mass will govern the motion of the plasma. If it were not for this requirement, electrons would precipitate over the entire polar cap since their thermal velocity is far greater than their convection velocity. Ions however can only enter the magnetosphere if the vector sum of the bulk convection and thermal velocities are approximately field aligned. This condition is trivially satisfied for ions moving poleward towards the cusps since the convection velocity adds to the fraction of the ion velocity distribution with velocities aligned along the magnetic field. Once the plasma is sufficiently far poleward that the magnetic field lines are nearly radial, however, it becomes more difficult for the ions to enter, and a cut off is found.

DE-1 plasma observations at altitudes of approximately 3 $R_E$ reported by *Burch et al.* [1982] show an energy-pitch angle dispersion for ions injected within the cusp in addition to the energy-latitude dispersion. The energy-pitch angle effect is not present in the low altitude observations *Reiff et al.* [1977]. Ions are initially observed nearly field aligned as the injection begins but soon significant fluxes are observed at larger pitch angles, including nearly antiparallel to the inflow direction. This is dramatic evidence of particle injection into the cusp, mirroring at low altitudes, and moving back upwards into the mantle as they convect antisunward. The evolution of the "V"-shaped ion energy-pitch angle signature was interpreted in terms of a spatially restricted region of plasma injection. The "V"-shaped energy-pitch angle signature is observed in both proton and alpha particle spectra, consistent with a solar wind source for the light ions. A particularly interesting feature of these observations is the time duration of the field aligned component which provides an estimate of the spatial extent of the particle injection *Menietti and Burch* [1988]. The size of the injection region perpendicular to the magnetic field was estimated to be 1000 $km < D <$ 6000 $km$ at a radial distance of approximately 10 $R_e$ similar to the *Burch et al.* [1982] estimate of of 8 $R_e$

The equatorward edge of the cusp, where midday transients form, maps to the subsolar region rather than the lobes or tail. Auroral arcs in the prenoon sector and postnoon sector have been mapped to the flank regions of the magnetosphere to the low latitude boundary layer or boundary plasma sheet [*Burke et al.*, 1993; *Maynard et al.*, 1994].

### 2.6.3 The Polar Cap

In his review of the polar cap, *Sergeev* [1990] notes that the term "polar cap" has two meanings. The first is a rigorous definition using magnetic field models. The polar cap is the region of open magnetic flux and the polar cap boundary is the separatrix between open and closed field lines. The polar cap boundary in the midday sector is the separatrix dividing the magnetic field lines equatorward of the cusp with those lines that sweep tailward in the plasma mantle. The night sector polar cap boundary divides the open high latitude lobe field lines from the field lines closing through the plasma sheet. The second definition is based on observations, yielding different boundaries based on the technique used to observe the magnetosphere and ionosphere.

Reproduced with permission of the copyright owner. Further reproduction prohibited without permission.

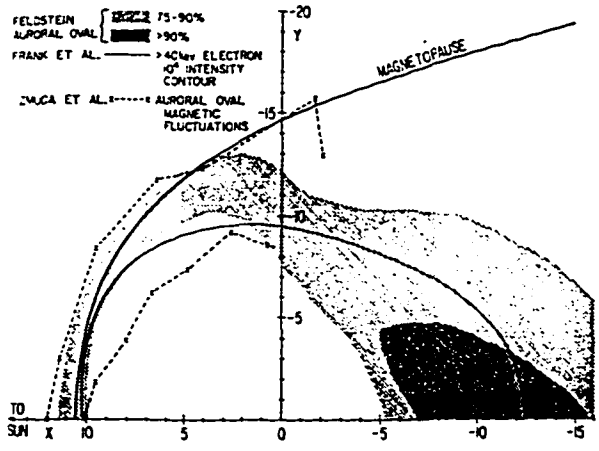


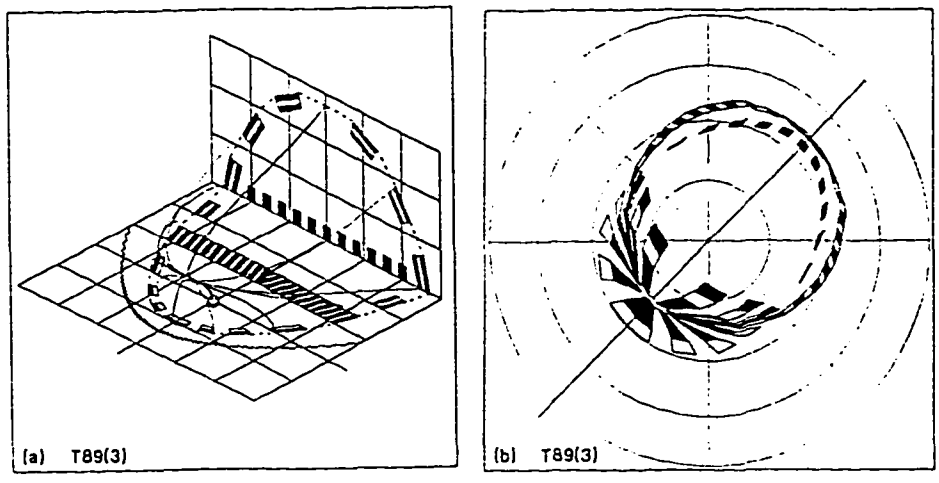


Figure 2.8 Mapping Between Dayside Magnetosphere and Ionosphere. (a) Mapping the northern hemisphere auroral oval along magnetic field lines to the equatorial plane. Note that the dayside portion of the auroral oval lies outside of the magnetopause in this model suggesting the formation of the arcs on open field lines [from *Fairfield*, 1968]. (b) A recent mapping of the dayside boundary layers to the ionosphere using the *Tsyganenko* [1989] magnetic field model. This figure highlights how a large surface area of the dayside magnetosphere near the magnetopause maps to a relatively small region near local noon in the ionosphere [from *Stasiewicz*, 1991].

Reproduced with permission of the copyright owner. Further reproduction prohibited without permission.

The poleward edge of intense auroral precipitation obtained by satellites generally agrees with the ground based observations of the poleward edge of auroral luminosity. This is true of course since the auroral emissions are the result of the energetic particles penetrating the atmosphere. Adopting the poleward edge of auroral precipitation as the polar cap boundary assumes that all of the processes resulting in auroral emissions occur on closed field lines.

Comparison of the auroral zone particle and optical boundaries with other techniques result in less agreement. The polar cap boundary obtained by ground based radars and magnetometers and *in situ* using driftmeters on satellites is defined as the region of strong plasma shear flows associated with the plasma convection reversal boundary. This definition yields a boundary which is often different than the high latitude particle precipitation boundary and the poleward edge of the associated auroral emissions [c.f., *Heelis et al*, 1980;*Torbert et al.*, 1981; *Sandholt et al.*, 1983; *Coley et al.*, 1987; *Newell et al.*, 1991b; *Burke et al.*, 1993; *Blanchard et al.*, 1995].

The topological boundary preferred by *Sergeev* [1990] is adopted in this work defining the polar cap boundary as "...the sharp boundary separating the open magnetic flux tubes connected to the IMF (polar cap) from the closed flux tubes of the plasma sheet (auroral zone)." The questions is therefore how well experimental observations are capable of detecting the boundary. This definition is particularly suited to dayside studies where high energy particles trapped in the Earth's magnetic field may be used to identify the poleward boundary of the open field lines.

*Winningham and Heikkila* [1974] reported that the polar cap is frequently filled with a weak, uniform low energy (100 eV - 500 eV) electron precipitation that they named the "polar rain". Observations of the polar rain at low altitudes [*Fennell et al.*, 1975; *Mizera and Fennell*, 1978; *Fairfield and Scudder*, 1985; *Riehl and Hardy*, 1986] and at distances of 3-7 $R_E$ from the Earth [*Yeager and Frank*, 1976] showed the intensity of polar rain is not symmetric in the two hemispheres, the intensity depending on the polarity of the IMF. Northern (southern) hemisphere fluxes are more intense when the solar magnetic field is pointed away from (towards) the sun. The spectra of these particles is similar to those found in the magnetosheath [*Yeager and Frank*, 1976] and the polar cusp [*Winningham and Heikkila*, 1974]. *Meng et al.* [1977a] noted dawn-dusk gradients in the polar rain intensity that depend on the sign of the IMF $B_y$ component. The evidence from these studies suggests that the polar rain electrons are solar wind electrons with direct access to the polar cap along open field lines. Two models have been developed to explain the distribution of polar rain. Solar electrons enter the polar cap along field lines that open to the solar wind through the distant tail in the "direct entry model" [*Fairfield and Scudder*, 1985]. *Foster and Burrows* [1976] proposed a second model in which the cusp electrons which mirror and convect tailward encounter a potential barrier reflecting a fraction of the plasma mantle population back into the ionosphere where they precipitate as polar rain electrons. *Gussenhoven* [1989] reviewed the experimental observations obtained by satellites and concluded that the data collected did not fully support either model although the evidence did show that regardless of the mechanism, low energy polar rain electrons enter the polar cap on open field lines.

Compelling evidence for the open nature of the magnetic field lines in the polar cap can be found in the direct access of high energy solar wind particles to the polar cap region. [c.f., *Van Allen et al.*, 1971; *Scholer and Morfill*, 1972; *Morfill and Scholer*, 1973]. Velocity distributions of

Reproduced with permission of the copyright owner. Further reproduction prohibited without permission.

solar wind protons and electrons at high energies are anisotropic, particularly during solar particle events when enhanced fluxes of high energy particles are ejected into interplanetary space from the solar corona. The solar particles moving away from the sun are found in greater numbers than the inward flowing galactic cosmic rays and particle fluxes from the outer planets precipitating particle fluxes. If the solar sector structure is "towards" the sun the open magnetosphere model predicts the northern hemisphere polar cap will be connected directly to the solar magnetic field while the southern hemisphere field lines are guarded by the Earth, predicting stronger fluxes of solar particles in the northern than southern hemisphere. The southern hemisphere will have the stronger fluxes if the solar structure is the "away" orientation. Further, the open magnetosphere model predicts the particles will have rapid access to the entire polar cap. The arrival of the high energy particles is nearly instantaneous over the entire polar cap, consistent with the field lines being open to the solar wind. The prediction of the closed magnetic field model for a gradual spread of the particles from the edge of the polar cap inward as the particles diffuse across field lines is not observed.

### 2.6.4 Geomagnetic Tail and Plasma Sheet

The terrestrial field lines on the nightside are extremely distorted due to the solar wind interaction forming the geomagnetic tail. Magnetic field lines in the tail are antiparallel with the field vectors pointing towards the Earth in the northern half of the tail and away from the Earth in the southern half of the tail. A current sheet (often called the neutral sheet) separates the antiparallel field lines. A weak magnetic field on the order of 2 nT permeates the neutral sheet and on the average points northward [*Fairfield*, 1979]. The gross departure from a dipole geometry is due to the self-consistent interaction of currents and fields in the region.

The magnetic tail is the largest structure in the magnetosphere. *Dessler* [1964] predicted on theoretical grounds the tail should extend approximately $10^6 Re$ in the antisolar direction while *Dungey* [1965] estimated $10^3 Re$ based on the latitude of the last closed field line and the convection speed of plasma in the polar cap. *Fairfield* [1968] confirmed that magnetic field structures consistent with the tail can be found near 1000 $R_E$. Observations of a stable magnetic tail structure [*Slavin et al.*, 1983] and plasma regimes similar those found in near Earth measurements [*Bame et al.*, 1983] were reported from the ISEE 3 deep tail mission at distances of 220 $R_E$ tailward of the Earth. More recently the GEOTAIL satellite has made a number of encounters with the geomagnetic tail up to distances of $210 Re$ [*Nishida*, 1994] allowing detailed examination of both magnetic structures [*Yamamoto et al.*, 1994b] and dense plasma regimes [*Yamamoto et al.*, 1994a] of the distant geotail. Depressed ion flux intensities interpreted as traversals of the geotail have been reported at distances of 500 $R_E$ tailward of the Earth by Pioneer 8 [*Intriligator et al.*, 1969] and even as far as 1000 $R_E$ [*Wolfe et al.*, 1967] and 3100 $R_E$ [*Intriligator et al.*, 1979] by Pioneer 7, consistent with the *Dungey* [1965] prediction of tail lengths on the order of $10^3 R_E$.

The plasma sheet, along with the ring current and radiation belt particles (Section 2.6.6), are a continuous population of particles trapped within the closed field lines of the magnetosphere [c.f., the review by *Schulz*, 1991]. The region of the plasma sheet confined to closed field lines

Reproduced with permission of the copyright owner. Further reproduction prohibited without permission.

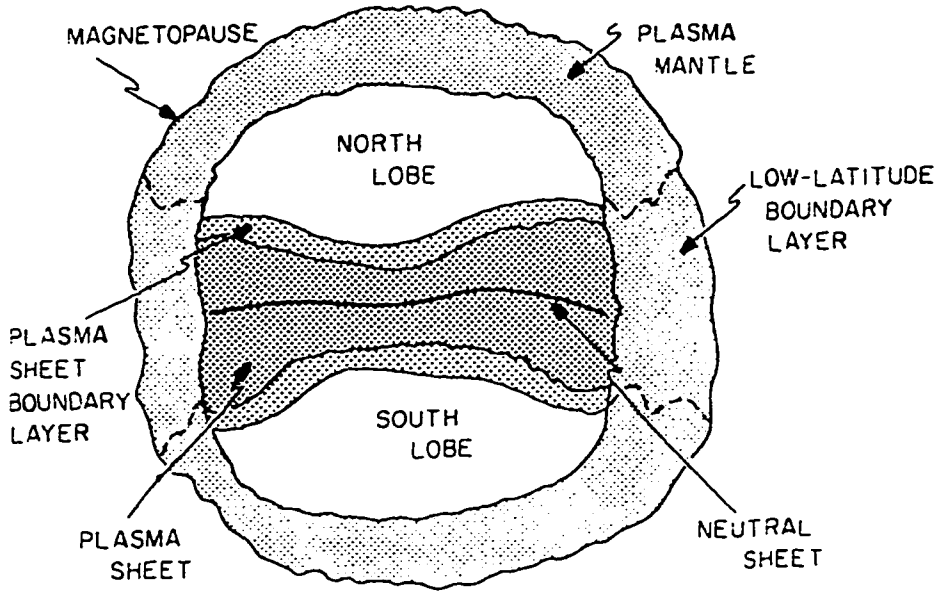


Figure 2.9 Cross Section of the Magnetotail Showing Main Plasma Regions. The distributions of the primary plasma regimes in the tail at a distance of 40 $R_E$ antisunward of the Earth are indicated in this schematic. The (central) plasma sheet surrounds the neutral (current) sheet in the center of the tail and is bounded above and below by the plasma sheet boundary layer. The plasma mantle and low-latitude boundary layer lie immediately inside the magnetopause and are populated with plasma characteristic of the magnetosheath. The lobe regions have much lower plasma densities than the plasma sheet, mantle and low latitude boundary layers. [from *Frank*, 1985].

around the current sheet in the geomagnetic tail is termed the "central plasma sheet" while the outer regions are referred to as the "boundary plasma sheet". The term central plasma sheet and boundary plasma sheet are something of a misnomer since they are not boundaries in the sense of the magnetospheric boundary layers discussed in Section 2.6.1 and 2.6.2. The field lines originating in the polar cap which extend into the high latitude lobes (Section 2.6.4) lie between the boundary plasma sheet and the plasma mantle. Field lines in the boundary plasma sheet extend from the vicinity of the auroral oval to extreme distances down the magnetic tail. The central plasma sheet is not the central structure of the magnetic tail, but lies above and below the current sheet.

Central plasma sheet densities are greatest near the current sheet where electrons and ions are on the order of 0.5 $cm^{-3}$ and electron energies are typically on the order of 0.5-1 keV and ions 5-10 keV. The particle energies are approximately the same within the current sheet and central plasma sheet but the number density is about five times greater in the current sheet. The density decreases in the plasma sheet boundary layer to only 0.1 $cm^{-3}$, tenuous but still more dense that

Reproduced with permission of the copyright owner. Further reproduction prohibited without permission.

the 0.01 $cm^{-3}$ densities which characterize the high latitude lobes. Particle energies are less in the plasma sheet boundary layers, typical values for electrons are 0.5 keV and ions 1 keV.

Central plasma sheet particles are generally thought by many authors to be responsible for the diffuse 557.7 nm aurora equatorward of the discrete auroral arcs in the auroral oval including the diffuse 557.7 nm aurora observed in the hard precipitation zone in the morning sector and the boundary plasma sheet particles the discrete auroral arcs of the auroral oval. Mapping high latitude particle precipitation to magnetospheric source regions is still a controversial topic however and no clear consensus has developed on how the night time aurora maps to particle populations in the tail. *Feldstein and Galperin* [1985] reviewed many of the proposed relationships between large-scale plasma structures and various types of auroral luminosity and they will not be repeated here.

An interesting proposition is that dayside processes may influence the nighttime aurora by altering the ion composition of the plasmasheet. *Baker et al.* [1982] proposed a substorm trigger mechanism that requires a large fraction of heavy ions in the plasma sheet to increase the growth rate of the ion-tearing instability leading to substorm onset. *Cladis and Francis* [1992] suggested the source of the ions was in the dayside cleft ionosphere where outflows of $O^+$ ions have been observed [*Lockwood et al.*, 1985; *Waite et al.*, 1985]. Numerical simulations show the dayside outflows are an efficient method of populating the both the high latitude lobes and the magnetotail with the required $O^+$ ions [*Horwitz and Lockwood*, 1985; *Swift*, 1990]. *Lennartsson and Shelley* [1986] reported observations of $O^+$ fractions as high as 50% of the plasma sheet ion density yet little $O^+$ is found in either the magnetosheath or the solar wind requiring a terrestrial source for the plasma sheet ions.

### 2.6.5 Ring Current and Radiation Belt

The plasma sheet, along with the ring current and radiation belt particles, are a continuous population of particles trapped within the closed field lines of the magnetosphere [*c.f.*, *Schulz*, 1991]. The plasma sheet (Section 2.6.5) is confined to closed field lines around the current sheet in the geomagnetic tail while the ring currents and radiation belts lie further within the magnetosphere.

Particles observed near the magnetopause within the quasi-trapped zone in the prenoon sector must have been injected within $\tau_d/2$. Strong pitch angle scattering due to wave-particle interactions is the dominant loss mechanism of the trapped electrons [*Kennel and Petschek*, 1966] leading to pulsating aurora in the morning sector which is observed from the ground equatorward of the soft zone midday aurora [*Davidson* 1986a,b]. VLF waves propagating along the magnetic field in the whistler mode are often considered to be the major source of wave energy controlling the populations of radiation belt electrons [*Kennel and Petschek*, 1966; *Davidson*, 1986a,b; *Davidson et al.* 1988]. Recently *Hardy et al.* [1990] described energy dispersed electron precipitation events in the morningside auroral zone and noted that equatorial electron cyclotron resonance is not consistent with the observations. An alternative mechanism in terms of off-equatorial wave-particle interactions with intense, asymmetric packets of VLF waves was proposed that explained the time delays of the electron precipitation bursts demonstrating that resonances may occur at a range of

Reproduced with permission of the copyright owner. Further reproduction prohibited without permission.

altitudes along a field line. Regardless of the type of resonance, fluxes of radiation belt electrons are limited by wave-particle interactions as originally described by *Kennel and Petschek* [1966]. They balanced the loss of electrons due to wave-particle interactions against sources to show that waves are produced spontaneously above a critical number flux threshold which then act to reduce the electron number flux. Figure 2.19 is reproduced from *Kennel and Petshek* [1966] and shows the computed theoretical limit of $> 40keV$ electron fluxes due to losses by whistler wave interactions against observations of outer zone electron fluxes to show the maximum fluxes agree with the computed theoretical limit. Number fluxes in the morning sector for L values of 8 and 10 do frequently exhibit values greater than the theoretical limit suggesting wave energy should be particularly strong in that region accompanying regions of pulsating aurora.

High energy trapped particles in the Earth's field were one of the first major features of the magnetosphere to be mapped in detail [*Vernov et al.*, 1960; *Frank et al.*, 1964a,b; *Frank*, 1965; *Lyons*, 1979, and references therein]. The radiation belt consists of electrons and ions with energies from approximately 1 keV to $> 100MeV$ distributed throughout the magnetosphere from approximately L=1.1 to 10. There is an inner zone with peak electron intensity near L=1.2-2 and an outer zone with peak fluxes near L=4-6. The region of depressed electron fluxes between the two zones is the electron slot. The proposal that whistler wave interactions limit the trapped fluxes [*Lyons et al.*, 1972] has been confirmed by coordinated measurements of electron fluxes, electromagnetic wave frequency distributions, and plasma density profiles within the slot region [*Imhof et al.*, 1982]. The outer boundary of the radiation belts is the magnetopause although particle fluxes often rapidly decrease beyond the last closed drift shell and only variable fluxes are observed in the quasi-trapped zone between the last closed drift shell and the magnetopause. The poleward boundary of the stably trapped fluxes (the last closed drift shell) is identified with the poleward boundary of the hard precipitation zone identified by *Hartz and Brice* [1967] (see Figure 1).

Electron intensities in the outer radiation belt are variable, increasing during periods of magnetic activity and decaying with time constants on the order of days for $L > 4$ and weeks for $L < 4$ [*Frank et al.*, 1964; *Craven*, 1966; *McDiarmid and Burrows*, 1966; *Williams et al.*, 1968]. Dependence on magnetic activity is greatest at large distances from the Earth [*Williams and Smith*, 1965], electrons at $L = 2$ show little correlation with magnetic activity, those at $2.5 \leq L \leq 3$ show increases only during periods of strong magnetic activity, and at $L \sim 6$ the electron fluxes are strongly correlated with magnetic activity. The behavior of electron populations for $L > 6$ is sensitive to the detailed variations in geomagnetic activity. Electron number fluxes are greatest at energies near 40 keV and decrease with higher energies but significant fluxes are observed at energies into the MeV range [*Frank et al.*, 1964]. The source of the particles are plasma injections in the midnight sector which subsequently drift in response to the curvature-gradient B forces [*DeForest and McIlwain*, 1971; *Smith and Hoffman*, 1974; *Ejiri*, 1978; *Moore et al.*, 1981].

As noted above, the ring current results from the differential motion of high energy ions and electrons due to charge dependent curvature and gradient B drifts. The greatest contribution to the energy density of the ring current is due to ions of approximately 10 keV to 100 keV [*Smith and Hoffman*, 1973; *Williams*, 1981] which originate in the plasma sheet but are energized and injected

Reproduced with permission of the copyright owner. Further reproduction prohibited without permission.

into the near Earth magnetosphere during magnetic storms dramatically increasing the number of particles in the ring currents. Ions increase by factors of 5 to 10 during storms at distances of 4-5 $R_E$. Ion composition of the ring currents is dominated by $H^+$ and $O^+$ during quiet times with trace quantities of $N^+$, $He^+$, $He^{++}$, and $O^{++}$ [*Shelley et al.*, 1972; *Young et al.*, 1977; *Johnson*, 1979; 1983; *Chappell et al.*, 1982]. Although the proton energy density typically dominates during quiet periods and for small magnetic storms, during intense disturbances $O^+$ may become the dominant species [*Gloeckler et al.*, 1985; *Hamilton et al.*, 1988]. The induced current is antiparallel to the main terrestrial field and since the greatest density of particles in the ring current is near the magnetic equator, the perturbation field is stronger at low latitudes than at high latitudes. The *Dst* index, an average of equatorial horizontal magnetic field intensities, is designed to monitor the variations in the strength of the ring current [*Mayaud*, 1980].

### 2.6.6 Plasmasphere

The plasmasphere is the inner most region of the magnetosphere where magnetic field lines are nearly dipolar. The high density plasma ($10^2 - 10^3 cm^{-3}$) is composed of low energy ions (less than 1 eV) and electrons corotating with the Earth. Corotation is the result of an electric field generated by the motion of the Earth's magnetic field through the charged particles of the plasmasphere driving the plasma to $ExB$ drift at exactly the same rate as the rotation speed of the planet [*Mozer*, 1973]. Gradient B and curvature drifts are unimportant for the low energy plasmasphere particles which is driven by the corotation field at the electric field drift velocity.

Corotation allows plasma on dipolar flux tubes to approach equilibrium with the ionosphere since the high density plasma formed on the dayside from photoionization of the neutral upper atmosphere can flow out along the nearly dipolar field lines. The time constants for loss of ionization in the corotating plasma is longer than the rotation rate of the Earth and the plasma spends insufficient time on the nightside of the Earth for the plasma concentration to decay before it is replenished on the dayside by solar UV photoiouization.

The plasmapause, the outer edge of the plasmasphere, is the boundary between regions of the magnetosphere where the cold plasma motion is dominated by the corotation electric field and the convection electron field from the magnetosphere [*Nishida*, 1966; *Brice*, 1967]. Corotation electric fields are determined by the angular rotation rate of the Earth, the strength of the terrestrial field, and the size of the planet and is constant to first order. Electric fields generated by the solar wind interaction with the magnetosphere are, however, highly variable and exhibit a strong dependence on geomagnetic activity and the location of the plasmapause has been shown to correlate with Kp [c.f., the review by *Chappell*, 1972].

The plasma in the outer edge of the plasmasphere may be heated by collisons with energetic particles on the inner edge of the plasma sheet leading to excitation of the stable aurora red (SAR) arc phenomenon [c.f., *Cornwall et al.*, 1971; *Rees and Roble*, 1975; *Kozyra et al.*, 1990]. These events form equatorward of the auroral oval at latitudes of approximately 40° . The great altitude of SAR arcs, often in excess of 300-400 km, and the association with low energy electron fluxes

Reproduced with permission of the copyright owner. Further reproduction prohibited without permission.

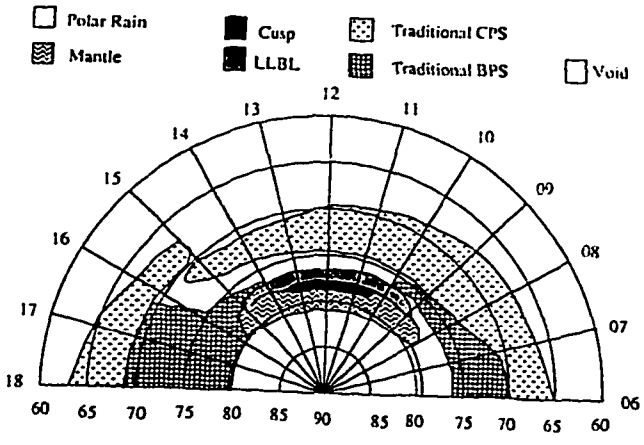


Figure 2.10 Distribution of Particle Precipitation Types in the High Latitude Ionosphere. Utilizing the categories adopted in Table 2.1, *Newell et al.* plotted the distribution of particle populations in the daytime sector based on a study of the probability of encountering a particular category of precipitating particles as a function of latitude and local time . [from *Newell et al.*, 1991].

suggests that aspects of their formation may be similar to cusp aurorae and the matter will be discussed further in Section 3.7.1.

## 2.7 Identification of Particle Precipitation by Low Altitude Satellites

Low altitude satellites have been instrumental in identifying the particles responsible for auroral emissions since they obtain energy, energy flux, and pitch angle distributions of particles immediately before they enter the atmosphere and after any acceleration that may occur between the outer magnetosphere and the top of the atmosphere. A survey of the characteristics adopted to identify categories of particle precipitation related to the regions of the magnetosphere discussed in Section 2.4 is important because these are the types of particles which will result in the luminous auroral signatures observed from the ground that will be discussed in the following chapter.

*Newell and Meng* [1988] adopt the criteria listed in Table 2.1 and used it to classify precipitating particle populations observed by the DMSP satellites. The probability of observing each category of precipitating particles as a function of latitude and magnetic local time was obtained by *Newell et al.* 1991] and is reproduced here in Figure 2.10. The plot should only be considered

Reproduced with permission of the copyright owner. Further reproduction prohibited without permission.

as a probability distribution of observing a population of precipitating particles consistent with the definitions given in Table 2.1 but should not treated as implying a mapping to source regions in the magnetosphere in the same sense of the mapping displayed in Figures 2.12 and 2.13(b). The two "mappings" represent two different methods of comparing particles observed at ionospheric altitudes with possible source regions in the magnetosphere. In the latter case the magnetic field lines in a magnetic field model were traced between the ionosphere and magnetosphere to establish a topological relationship between the two regions but plasma characteristics in the magnetosphere and the ionosphere were not used. The plot given in Figure 2.14, while labelled with terms consistent with magnetospheric particle types, has not been mapped along field lines. The characteristics of the particle energy spectra have been compared.

The figure shows the relationship of the low energy electron precipitation regions associated with the soft precipitation zone (cusp, mantle, low latitude boundary layer) and the hard electron precipitation zone (central plasma sheet). A particularly interesting feature is the gap between the plasma sheet and the boundary plasma sheet and low latitude boundary layers in the midday period. Certainly much of this gap results from the numerous satellite overpasses during which the pseudo-trapped electron fluxes were very low. Auroral observations often show a similar gap which will be described in more detail in Chapter 3 and 5.

Ground based observations of auroral emissions cannot provide the detailed information listed in Table 2.1 since the ion information is missing and the electron energy information is convolved with atmospheric structure. However, the soft electron regions are easily discriminated from the hard electron regions. In addition, ground based observations provide temporal and spatial variations of the particle precipitation, an additional set of diagnostic information that is unavailable to the satellite particle detectors which may be used to categorize particle precipitation regions. This will be discussed in further detail in Chapter 3.

Reproduced with permission of the copyright owner. Further reproduction prohibited without permission.

**Table 2.1**
**Characteristics and Classification of Dayside Particle Types**

| Region | Ion and Electron Characteristics | References |
|---|---|---|
| Cusp (CU) | $\epsilon_i > 1 \times 10^{10}$eV/cm$^2$ s sr<br>$\epsilon_e > 6 \times 10^{10}$ eV/cm$^2$ s sr<br>$300 < E_i < 3000$ eV and $E_e < 220$ eV | *Heikkila and Winningham*, 1971<br>*Newell and Meng*, 1988 |
| Mantle (MA) | Soft ions poleward of cusp | *Newell et al.*, 1991 |
| Low Latitude Boundary Layer (LLBL) | $3000 < E_i < 6000$ eV or $220 < E_e < 600$ eV<br>$n_{i,llbl} < 5n_{i,cusp}$<br>$\epsilon_i \sim 1 \times 10^7$eV/cm$^2$ s sr eV | *Newell and Meng*, 1988<br>*Newell et al.*, 1991 |
| Plasma Sheet Boundary Layer (BPS) | Like CPS but includes more low energy electrons<br>Poleward of CPS<br>Spatial structured due to discrete auroral arcs | *Winningham et al.*, 1975<br>*Newell et al.*, 1991 |
| Central Plasma Sheet (CPS) | $\epsilon_{e,2keV}$ or $\epsilon_{e,5keV} > 1 \times 10^7$eV/cm$^2$ s sr eV<br>$E_i > 10$ of keV and $E_i >$ 1keV<br>Little spatial structure in electrons<br>Maxwellian plus power law electron energy spectrum | *Winningham et al.*, 1975<br>*Newell and Meng*, 1988 |
| Polar Rain (PR) | Maxwellian electrons in polar cap<br>$T_e \sim 60 - 110eV$ or higher<br>Little or no structure | *Winningham and Heikkila*, 1974 |
| Photoelectrons (PH) | $E_e <$ 68eV<br>Low latitude, require sunlight on local or conjugate hemisphere, no structure | *Peterson et al.*, 1977<br>*Newell et al.*, 1991 |

Reproduced with permission of the copyright owner. Further reproduction prohibited without permission.

## 2.8 Transfer of Solar Wind Energy into the Magnetosphere

Solar wind mass and momentum must be transported across the magnetopause in order for the solar wind to drive convective plasma flows within the magnetosphere and for solar wind plasma to populate regions of the magnetosphere inside of the magnetopause (Section 2.6.1 and 2.6.2). The mechanisms proposed to explain how this transport is possible are grouped into one of three categories:

(1) magnetic reconnection of the interplanetary magnetic field with the terrestrial field leading to plasma flow across the magnetopause [*Dungey*, 1961],

(2) impulsive plasma penetration of solar wind irregularities into the magnetosphere [*Lemaire*, 1977; *Lemaire and Roth*, 1978; *Heikkila*, 1982; *Lundin and Evans*, 1985], and

(3) viscous interactions between the magnetosheath and the adjacent magnetospheric boundary layer plasma [*Axford and Hines*, 1961; *Eviatar and Wolf*, 1968; *Coleman*, 1971].

The success of each model is evaluated by considering the significance of each process to the total energy budget of the magnetosphere as well as the ability to explain features of the high latitude magnetosphere-ionosphere system including the distribution of plasma within the magnetosphere boundary layers, cold plasma convection patterns, and the formation and distribution of dayside aurorae. The reconnection process will be considered first since the preponderance of evidence obtained to date indicates that magnetic reconnection between the interplanetary and terrestrial fields is the most significant process responsible for the transfer of solar wind energy into the dayside magnetosphere and ionosphere. The process is important because it provides an efficient mechanism by which solar wind mass and momentum may be transferred directly from the shocked solar wind plasma found in the magnetosheath to the magnetosphere along magnetic field lines. Impulsive penetration of plasma irregularities and viscous interactions may also contribute to the formation of polarization electric fields and currents in the outer magnetosphere providing the energy necessary for magnetospheric plasma convection and to drive magnetospheric particles into the ionosphere but both processes require particle transport across field lines. Recent work suggests their total contribution to the magnetospheric energy budget is approximately 5% to 20% for IMF $B_z < 0$ conditions only becoming important when $B_z > 0$ [*Reiff et al.*, 1981; *Wygant et al.*, 1983; *Reiff and Luhmann*, 1986].

### 2.8.1 Reconnection

A closed magnetosphere immersed in the solar wind plasma and magnetic field of the sun contains only two types of magnetic field lines, the interplanetary field exterior to the magnetosphere and the magnetosphere itself which is formed entirely on closed terrestrial field lines. The two regions are separated by the magnetopause current layer where the normal component of the magnetic field is zero, i.e., the magnetopause is a tangential magnetic field discontinuity since magnetic field lines do not cross the boundary. In an open magnetosphere the situation is more complex, the open field lines crossing the magnetopause boundary and into the solar wind require a process that allows the terrestrial and solar fields to merge. *Dungey* [1961] proposed that interplanetary

Reproduced with permission of the copyright owner. Further reproduction prohibited without permission.

field lines merging with terrestrial field lines when the IMF $B_z$ component is negative allows the direct flow of solar wind plasma into the magnetosphere.

The fundamental consequence of a magnetic reconnection process in contrast to viscous processes is a change in a magnetic field topology [*Haerendel and Paschmann*, 1982]. *Vasyliunas* [1975] proposed a specialized definition for reconnection as a "...process whereby plasma flows across a surface containing topologically different magnetic fields." Vacuum annihilation of magnetic field lines between two magnetic sources is eliminated as a reconnection process by this definition since the presence of a plasma is required which alters the character of the fields at the boundary between the two regions by producing a current layer. *Sonnerup* [1984] alternatively defines reconnection as occurring when an electric field is present along the x-line in a sheared magnetic field geometry. These definitions are not independent since in reality each one simply highlights a specific aspect of the merging process.

Reconnection occurs at the boundary between two plasmas imbedded in antiparallel magnetic fields. Before the onset of merging the two fields are separated by a current sheet dividing the two regions of differing magnetic field orientation. The two fields must approach one another at some localized point for reconnection to be initiated. This is generally accomplished by the motion of the plasma in which the magnetic fields are frozen and the inflow of the magnetic field in the plasma is often described in terms of ideal MHD theory since the field is frozen into the plasma and a plasma inflow will bring the two regions into contact. Merging cannot occur under the conditions assumed by ideal MHD since the frozen-in-field condition does not allow the solar wind plasma exterior to the magnetosphere to penetrate the terrestrial field and the terrestrial field cannot diffuse into the solar wind. Merging requires a non-ideal MHD process: a diffusion of the magnetic fields in the inflow region (called the diffusion region) allowing the two fields to reconnect.

A schematic of the dayside merging site is given in Figure 2.11 showing the earthward separatrix (S2) that divides the closed and open field lines. A boundary layer is found on open field lines immediately inside the magnetopause. The plasma in the magnetosheath flows into the merging region where the separatrix S1 and S2 meet with a velocity $v_1$ and flows poleward away from the merging site with a velocity $v_2$. The newly merged field lines have a sharp bend near the merging site, an undesirable geometry for a magnetic field since the small radius of curvature represents a high magnetic "tension" and the field line will immediately begin to unbend by moving away from the merging site to decrease the curvature of the field line. As magnetic energy is converted into kinetic energy, plasma associated with the field line is accelerated away from the merging site yielding outflow velocities $v_2$ greater than the inflow velocity $v_1$. A fundamental prediction of the reconnection model therefore is the existence of accelerated plasma flows in the boundary layer immediately inside of the magnetopause.

Flux tube motion during the unbending phase depends on the orientation of the IMF. In the two dimensional case depicted in Figure 2.11 the only direction the field and plasma can move is poleward. The process is shown in Figure 2.12 for a three dimensional case where the IMF $B_z$ component is negative. The flux tube will move initially east or west in the northern hemisphere if the IMF $B_y$ component is negative or positive, respectively, driving the IMF $B_y$ dependent convective plasma flows observed in the ionosphere [c.f., *Heelis*, 1984]. If the IMF is

Reproduced with permission of the copyright owner. Further reproduction prohibited without permission.

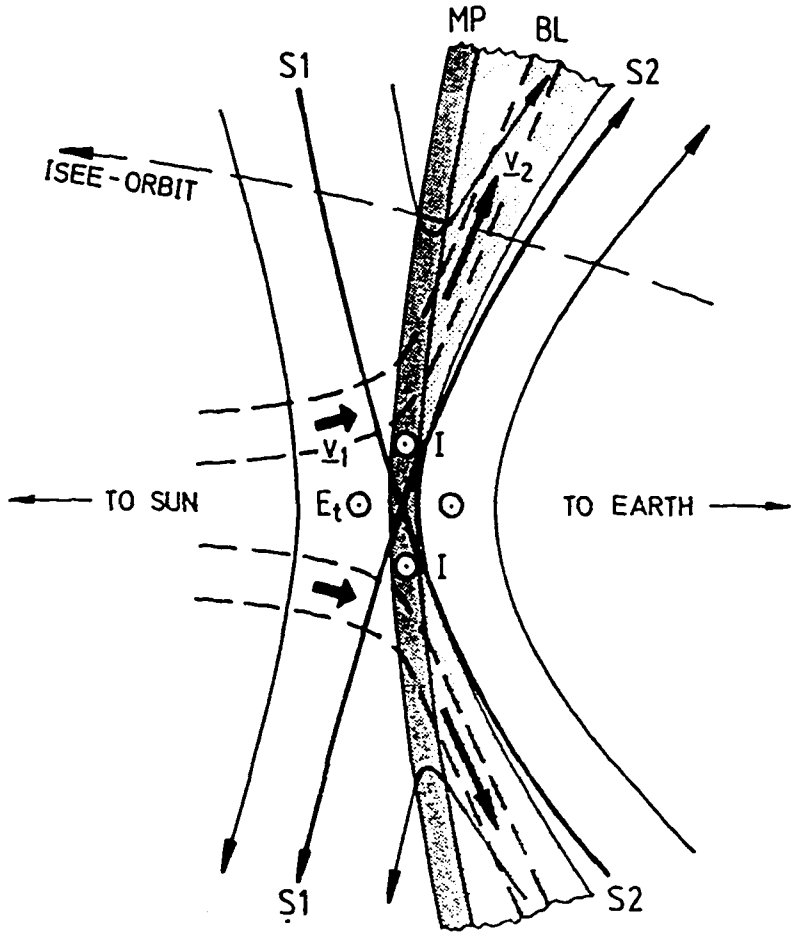


Figure 2.11 Detail of the Dayside Merging Site. The separatrix S1 divides the IMF from the region of reconnected (open) field lines and separatrix S2 divides reconnected and closed terrestrial field lines. Field line merging occurs at the diffusion region where the S1 and S2 meet allowing magnetosheath plasma flowing inward at velocity $v_1$ to cross the magnetopause (MP) and flow into the boundary layer (BL) at velocity $v_2$. Ions and electrons accelerated away from the merging site yield flows with $v_2 > v_1$ inside the boundary layer. Note that the magnetopause and either separatrix are in contact only at the merging site, the separatrix S2 which is the last closed terrestrial field line lies inside the magnetopause at all other locations [from *Paschmann*, 1991].

Reproduced with permission of the copyright owner. Further reproduction prohibited without permission.

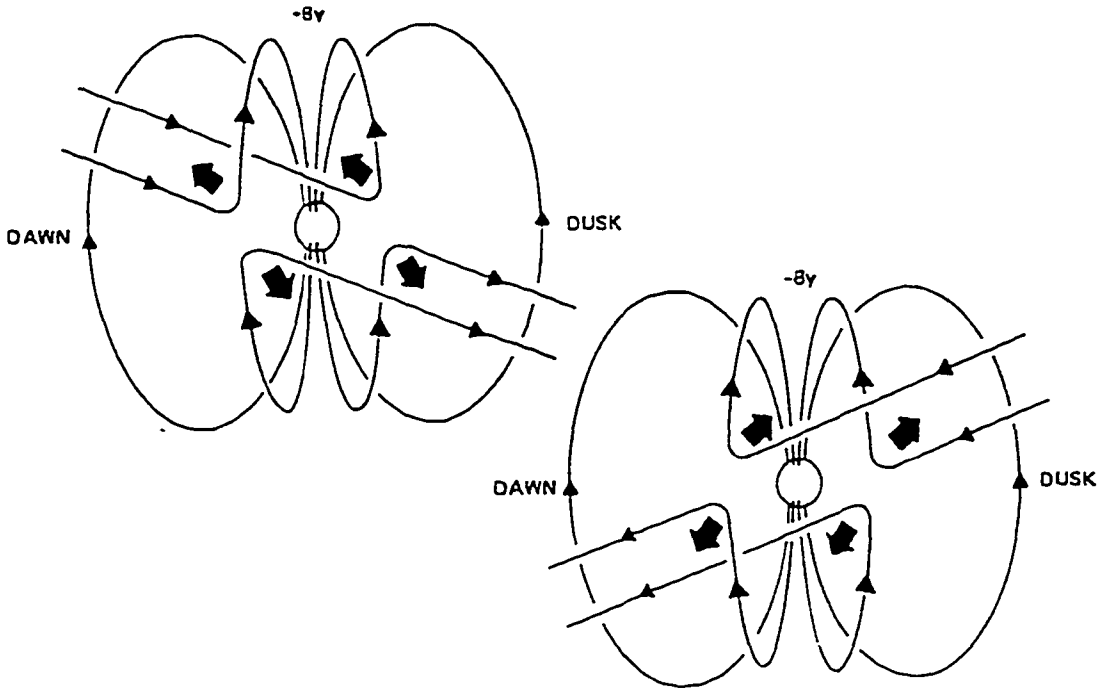


Figure 2.12 IMF $B_y$ Effect on Dayside Merging. Tension on the newly merged field lines produce asymmetric plasma flows in the high latitude ionosphere [from *Gosling et al.*, 1990a].

aligned exactly antiparallel to the terrestrial field the accelerated plasma flows are poleward but under more typical conditions where the IMF is aligned in the Parker spiral orientation the IMF is dominated by the $B_y$ component plasma flows toward dawn or dusk are to be expected in the high latitude dayside region. Magnetic reconnection explains very simply not only how solar wind plasma may enter the magnetosphere but also the subsequent motion of the plasma once it has crossed the magnetopause.

Currently it is widely accepted that reconnection is the principle mechanism controlling the input of solar wind energy into the Earth's magnetosphere [c.f., the review by *Southwood*, 1989]. A wide variety of phenomena observed iu the dayside magnetosphere and ionosphere can be understood within the framework of the reconnection model including

(1) IMF dependence of magnetospheric plasma convection [c.f., the review by *Cowley*, 1986],

(2) IMF dependent asymmetries in the high latitude ion convection pattern in the ionosphere [*Heelis*, 1984; *Burch et al.*, 1985; *Heppner and Maynard*, 1987],

(3) the IMF dependent asymmetric horizontal current flows in the noon region responsible for the Svalgaard-Mansurov effect [*Svalgaard*, 1972, 1973; *Mansurov*, 1969; *Friis-Christensen et al.*, 1975, 1985],

Reproduced with permission of the copyright owner. Further reproduction prohibited without permission.

(4) the equatorward motion of the dayside cusp when the interplanetary magnetic field $B_z$ component is negative [*Burch*, 1973] and a correlated increasing geomagnetic activity during these periods [*Akasofu*, 1972a,b],

(5) the interplanetary magnetic field $B_y$ dependent shift towards prenoon and postnoon magnetic local times for the region of maximum low energy electron precipitation [*Meng et al.*, 1977; *Candidi et al.*, 1983; *Newell et al.*, 1989],

(6) the IMF dependent asymmetric distribution of ion precipitation in the plasma mantle region poleward of the cleft [*Meng et al.*, 1977; *Xu et al.*, 1995],

(7) reports of IMF dependent initial east or west motion followed by poleward motion for dayside transient arcs [*Sandholt et al.*, 1986],

(8) IMF dependent ion energy dispersion in cusp and mantle [*Reiff et al.*, 1980],

(9) accelerated plasma flows in the dayside magnetosphere observed by satellites near the magnetopause [*Paschmann et al.*, 1979; *Sonnerup et al.*, 1981], and

(10) non-zero components of the magnetic field perpendicular to the magnetopause current layer implying that field lines must cross through the magnetopause [*Paschmann et al,*, 1979; *Russell and Elphic*, 1979].

Terrestrial and interplanetary field lines are assumed to continuously merge at the dayside in the original reconnection model of the magnetosphere developed by Dungey [*Dungey*, 1961; *Levy et al.*, 1964] as long as the magnetosheath field is favorably oriented. The presence of plasma flows inside the magnetopause accelerated relative to the magnetosheath flow is a fundamental prediction of the merging model and should be observed whenever a satellite crosses the magnetopause when the IMF $B_z$ component is negative if the process is indeed quasi-steady. Early attempts to identify such flows met with little success [*Hones et al.*, 1972; *Eastman et al.*, 1976; *Haerendel et al.*, 1978; *Paschmann et al.*, 1978; *Eastman and Hones*, 1979] suggesting that reconnection does not occur as a quasi-stationary process. *Heikkila* [1975], for example, concluded that the lack of an increase in plasma kinetic energy within the boundary layer was evidence the magnetopause is an equipotential (i.e., the tangential electric field at the X-line is not present and reconnection does not occur at the magnetopause). When the expected accelerated flows were finally reported [*Paschmann et al.*, 1979; *Sonnerup et al.*, 1981; *Southwood et al.*, 1986] they were not found on all boundary crossings, even during periods when the magnetic field in the magnetosheath was oriented favorably for reconnection. Evidence for quasi-stationary reconnection in the form of repeated observations of accelerated flows during multiple boundary crossings was finally reported by *Gosling et al.* [1982] for an unusual interval when the magnetopause moved outwards to approximately 20 Re during a period of extremely low solar wind dynamic pressure. *Gosling et al.* [1986] later reported accelerated plasma flows consistent with quasi-steady reconnection in the near tail flank of the magnetosphere for average solar wind conditions. These results show that quasi-steady reconnection may occur at least under some conditions and locations on the magnetopause although the missing accelerated flows are problematic to the steady state concept of the merging process.

The independent discovery by *Haerendel et al.* [1978] and *Russell and Elphic* [1978, 1979] of impulsive magnetic field variations near the magnetopause provided the first evidence for temporal

Reproduced with permission of the copyright owner. Further reproduction prohibited without permission.

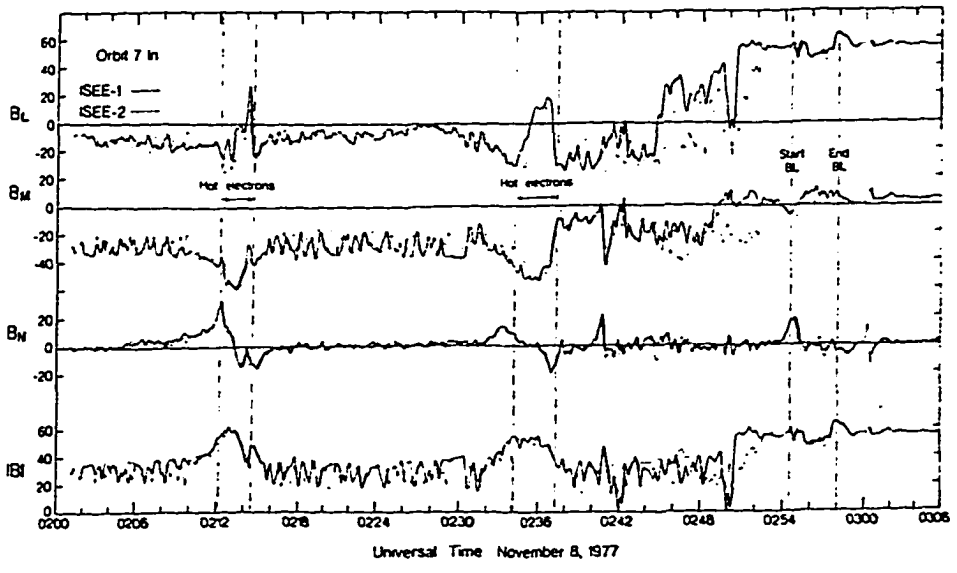


Figure 2.13 Flux Transfer Events. The magnetosheath magnetic field measurements obtained during an inbound orbit of the ISEE 1 and 2 satellites show the characteristic bipolar FTE $B_n$ signature at 0212 UT and 0236 UT. Particle measurements indicate the presence of "hot electrons" with energies greater than 2 keV within the FTE's. The magnetopause is crossed between 0244 UT and 0252 UT [from *Russell and Elphic*, 1979].

variations in magnetopause merging rates suggesting a resolution to the problem of the missing flows within the structure of the reconnection model. *Haerendel et al.* [1978] proposed that large fluctuations in the magnetic field for short periods (on the order of 10's of seconds) in HEOS-2 satellite data obtained within the magnetosphere immediately before crossing the magnetopause in the vicinity of the polar cusps are the signature of impulsive merging. Similar events identified in the subsolar magnetosheath by *Russell and Elphic* [1978, 1979] in ISEE 1 and 2 magnetic field data were similarly interpreted as impulsive merging events and given the name "flux transfer events" (FTE).

*Russell and Elphic* [1978, 1979] plotted magnetic field data in the boundary normal coordinate system where $\hat{n}$ is a unit vector normal to the magnetopause boundary, $\hat{l}$ is perpendicular to $\hat{n}$ in the direction along the projection of the $Z_{GSM}$ coordinate, and $\hat{m}$ the third component of the right-handed coordinate system ($\hat{m} = \hat{n} \times \hat{l}$). In this system FTE's within the magnetosphere and magnetosheath are identified both identified by a characteristic bipolar variation in the $B_n$ magnetic field component indicating the magnetopause is a rotational discontinuity, exactly what is expected for magnetic merging. Two examples of magnetosheath FTE's originally published by

Reproduced with permission of the copyright owner. Further reproduction prohibited without permission.

*Russell and Elphic* [1978] are identified in Figure 2.5 near 0212 UT and 0236 UT. The presence of hot ($> 2keV$) electrons as noted in the Figure 2.5 is an important characteristic of FTE's and is consistent with the merging model of FTE formation. This and other details of the time dependent behavior of particle populations in FTE's is considered in further detail in Chapter 5.

Important information on the characteristics of FTE's have been obtained from a number of statistical studies [*Rijnbeek et al.*, 1984; *Berchem and Russell*, 1984; *Southwood et al.*, 1986; *Kuo et al.*, 1995]. FTE's occur over the entire region of the dayside magnetopause available to the satellites although relatively fewer events are detected at low latitudes. *Russell et al.* [1985] suggested FTE's form at low latitudes and the probability of observing them is greater at high latitudes as they move away from the merging line. The events are common features when the IMF $B_z$ component is negative but are rarely observed if $B_z$ is positive. On a number of occasions, satellite passes through the magnetopause failed to detect any FTE's even when the magnetosheath magnetic field was negative suggesting the IMF $B_z < 0$ conditions are a necessary but not sufficient condition for the formation of FTE's. Dimensions of the events are estimated to be approximately 1 Re both normal to the magnetopause and along the magnetopause although smaller events are also observed [*Russell and Elphic*, 1978, 1979;, *Saunders et al.* 1984; *Walthour et al.*, 1993]

*Rijnbeek et al.* [1984] used ISEE data to determined that on average 5 magnetosheath FTE's are observed at intervals of approximately 8 minutes and 4 magnetospheric FTE's are observed at intervals of 7 minutes during a boundary crossing indicating the magnetosheath and magnetosphere events are related to the same phenomenon. *Lockwood and Wild* [1993] reexamined the ISEE magnetic field data and showed the distribution of intervals between FTE's is skewed with a mode (most probable) value of 3 minutes, a mean value of 8 minutes, and upper and lower decile values of 1.5 minutes and 18.5 minutes, respectively.

Magnetic field merging was originally thought to occur continuously when the IMF orientation was favorable for reconnection. However, satellite observations during magnetopause encounters generally failed to find any evidence for large scale quasi-steady merging. The lack of evidence for merging was problematic. If the process was to contribute significantly to the transport of solar wind mass and momentum across the magnetopause then evidence for reconnection is expected on at least some, if not all, magnetopause crossings. Identification of the flux transfer event in magnetic field data was an important discovery since it was the first clear evidence that merging between solar and terrestrial field lines did in fact occur at the magnetopause although in an impulsive rather than steady manner.

A variety of unsteady reconnection models have been proposed to explain the intermittent nature of magnetic reconnection and the formation of FTE's. The original model proposed by *Russell and Elphic* [1978] to explain the FTE required merging to occur intermittently at a single X-line. *Scholer* [1988] and *Southwood et al.* [1988] similarly developed FTE models based on time-dependent reconnection along a single X-line. Multiple X-line processes have also been considered [c.f., the reviews by *Lee*, 1986, 1995]. *Lee and Fu* [1985, 1986] proposed that merging occurred along a set of multiple X-lines leading to the formation of magnetic flux ropes. Evaluation of the multiple X-line model has been accomplished primarily by computer simulation and the transient

Reproduced with permission of the copyright owner. Further reproduction prohibited without permission.

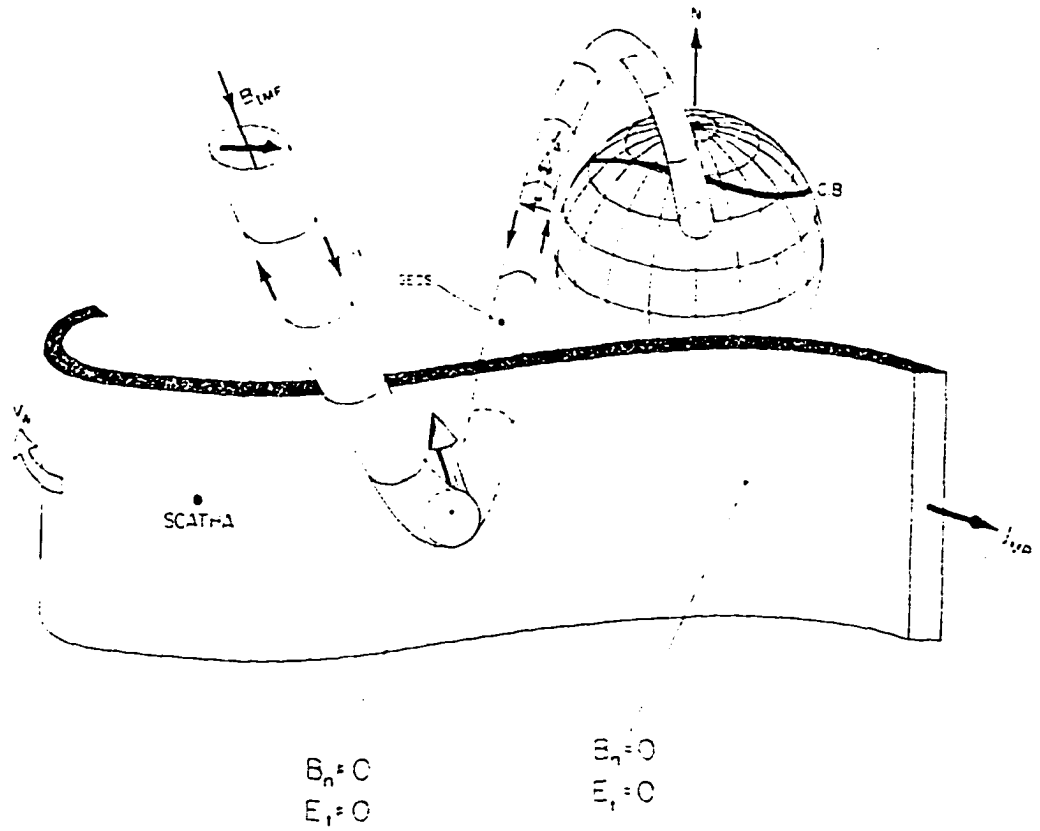


Figure 2.14 Cartoon of Flux Transfer Event. One widely accepted model of the flux transfer event is an isolated bundle of magnetic flux threading the magnetopause producing the nonzero $B_N$ and $E_t$ field components observed by satellites during passes through the magnetopause [from *Goertz et al.*, 1985].

nature of the merging process appears in both local and global simulations [*Fu and Lee*, 1985; *Shi et al.*, 1988, 1991; *Ip and Jin*, 1991; *Ding et al.*, 1992; *Lee*, 1995 and references therein].

Magnetic flux transported by the solar wind into the magnetopause will accumulate unless it can either move around the magnetosphere or reconnect with terrestrial field lines. Reconnection in two-dimensional computer models is the only mechanism provided to remove the accumulated flux. The two-dimensional models are artificial in the sense that no alternative to reconnection for loss of accumulated flux is provided in the codes and the results must not be interpreted as confirmation that solar wind flux must reconnect with terrestrial field lines. Flux may be deflected and slide over the surface of the magnetopause without reconnection in a realistic three-dimensional geometry, a process which is favored over reconnection since only a fraction of the solar wind flux incident on the magnetosphere ever becomes connected to the terrestrial field [*Reiff and Luhmann*, 1985] The important results obtained from two-dimensional computer codes is the demonstration that reconnection rates for multiple X-line processes are inherently variable in time. Variations in the plasma inflow velocity or particle density are not required to obtain temporal variations in the plasma outflow rates. The formation of a flux tube decreases the merging rate since the increase in cross section of the new flux tube shields the active merging site from the magnetosheath field.

Reproduced with permission of the copyright owner. Further reproduction prohibited without permission.

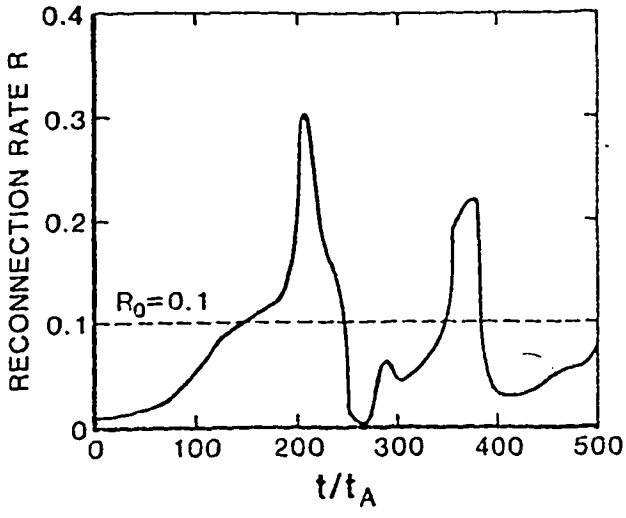


Figure 2.15 Simulated Magnetopause Reconnection Rates. The imposed reconnection rate $R_0$ is the ratio of the inflow speed to the Alfven velocity and is a constant for the simulation. The rate at which magnetic flux is found to reconnect is temporally varying [from *Fu and Lee*, 1985].

As the merging rate comes to a stop the flux tube accelerates polewards away from the merging site allowing the process to start again.

An example of time varying reconnection rates for multiple X-line merging is given in Figure 2.15 showing the merging rate obtained by *Fu and Lee* [1985] from a two-dimensional computer simulation of magnetopause field line merging. The simulation assumed the reconnection was driven, i.e. the magnetosheath plasma was driven into the magnetopause at an externally imposed fixed rate by the magnetosheath plasma flow. Temporal variations in the merging rate, and hence the plasma outflow rate, arise naturally from the physical process. This simulation demonstrates that even for a constant plasma inflow rate supplying the merging region with magnetic flux at a fixed rate, the outflow from the merging site will vary with time, predicting variable plasma fluxes injected into the dayside magnetosphere. It also shows that while the merging rate may periodically decrease to very small values, or even cease entirely, in general the merging process may best be described as short intervals of enhanced merging rates superimposed on a lower rate of continuous merging. The implications of these results on ionospheric phenomenon will be discussed in Chapter 3.

The possibility of multiple active merging sites coexisting simultaneously have also been proposed to explain the intermittent and patchy formation of flux transfer events [*Kan*, 1988] and a

Reproduced with permission of the copyright owner. Further reproduction prohibited without permission.

number of applications of the models have appeared in the literature. *Nishida* [1989] discussed the possibility of forming the boundary layer through random reconnection at a large number of sites across the magnetopause. *Fasel et al.* [1994] invoked the patchy multiple X-line reconnection model developed by *Lee et al.* [1993] as an explanation of temporal variations in the luminosity of dayside transient arcs. More recently, *Weiss et al.* [1995] invoked multiple merging sites to explain observations of aurora and plasma drifts in the high latitude daytime region. Multiple regions of enhanced flows may also be due to localization of strong electric fields along a single merging line as described by *Moses et al.* [1988].

Reconnection may occur anywhere on the magnetopause surface provided the conditions necessary for merging are present. *Cowley* [1976] showed that merging may occur as long as the component of the magnetic field perpendicular to the X-line changes sign across the X-line, but the change in the parallel component is arbitrary. *Crooker* [1979] proposed the antiparallel hypothesis in which the magnetosheath field must be antiparallel to the terrestrial field. In either case the requirement that a component of the IMF must be antiparallel to the geomagnetic field explains the origin of the strong correlation between a variety of phenomena in the magnetosphere and ionosphere and the orientation of the IMF.

*Reiff and Burch* [1985] showed that merging is possible for nearly all orientations of the IMF using the anti-parallel merging hypothesis proposed by *Crooker* [1979] which requires the magnetosheath magnetic field vector to be aligned antiparallel to the terrestrial field for reconnection to occur. Relaxation of the stringent antiparallel merging model to a requirement that only a component of the IMF need be parallel [*Gonzalez and Mozer*, 1974: *Cowley*, 1976] leads to possibilities for reconnection regardless of the IMF orientation, especially if the reconnection process is driven by the solar wind flow. Indeed, *Kuo et al.* [1995] have shown that the rate of FTE formation correlates highly with the IMF $B_z$ component and solar wind pressure, suggesting that merging occurs under favorable conditions due to antiparallel merging but may be moderated by the pressure. The lack of a high correlation with the IMF $B_y$ component suggests that a pure antiparallel alignment of the magnetosheath and terrestrial fields is not required for the merging process.

In general these sites are all thought to map to the ionosphere in the region of the dayside oval, i.e., in the reconnection model the merging of the IMF with the geomagnetic field lines provides the energy and particle flux required to excite the dayside auroral emissions in either the form of currents associated with Alfven waves generated by the release of magnetic tension at the reconnection site or the solar wind particles entering on the recently reconnected field lines.

The conditions required for magnetic merging are not the same over the surface of the entire dayside magnetopause. Subsolar reconnection may occur for even modest magnetic field shears, and may even occur if the magnetosheath field is slightly northward [*Gosling et al.*, 1990a]. *Gosling et al.* [1986] pointed out that reconnection along the near-tail flanks requires large magnetic shears ($> 135$ degrees) between the magnetosheath and geomagnetic field. The sign of $B_z$ is not important in this case as long as the field lies mainly in the x-y plane, but the $B_y$ component becomes critical to obtain the necessary shear. Hence, a strong $B_y$ effect is expected for flank merging. *Gosling et al.* [1991] noted that the reason the differences exist for merging near the subsolar point and in the near earth flanks is that reconnection is more strongly controlled by the magnetosheath flow in the

Reproduced with permission of the copyright owner. Further reproduction prohibited without permission.

subsolar region where the plasma impacts at near normal incidence on the magnetopause than in the flanks where it moves tangentially past the boundary. Merging is also expected tailward of the cusp and has been reported by *Gosling et al.* [1991] from mid latitudes and *Kessel et al.* [1996] at high latitudes.

It is not sufficient to merely reconnect two magnetic field lines to produce an ionospheric response. The bulk speed of the plasma within the magnetosheath at the reconnection site may carry the reconnected plasma tailward faster than effects from the site can propagate into the ionosphere. A necessary condition for information to travel from the reconnection site to the ionosphere in the form of cold plasma waves or current pulses is for local Alfvén velocity, $V_A$ to be greater than the convection velocity $V_c$ of the magnetosheath flow velocity [*Reiff et al.*, 1977]. Failure to satisfy this condition results in the loss of the information Earthward of the reconnection site as the reconnected field lines and associated plasma is swept tailward with the magnetosheath flow [*Gosling et al.*, 1986, 1991]. Merging in the region of the flanks is more restrictive as a possible source of plasma to low altitudes since $V_c$ and $V_A$ directed in the opposite direction, limiting the access of particles from the merging site to the ionosphere.

The requirement that $V_A$ exceed $V_c$ condition is trivially satisfied for subsolar merging where both the magnetosheath flow and the accelerated flows associated with the release of the Maxwell tension in reconnected field lines carries the plasma antisunward from the reconnection site towards the cusp region. Even so, ion thermal temperatures in the magnetosheath are sufficiently low that typically only those ions with velocities nearly parallel to the local magnetic field can cross the magnetopause, the bulk of the ion population is simply swept tailward [*Reiff et al.*, 1977]. For this reason, ion densities observed within the cusp are often well correlated with magnetosheath densities [*Aparacio et al.*, 1991].

While the existence of flux transfer events is not questioned (in the sense that isolated events with the requisite bipolar $B_n$ variation are observed in magnetic field data during satellite passes through the magnetopause) exactly what they are and their significance to the magnetosphere is still a controversial subject. *Lui and Sibeck* [1991] have argued the magnetic field signature is also explained in terms of surface waves propagating along the magnetopause boundary in response to impulsive variations in the solar wind dynamic pressure and they have also been interpreted as the signature of the impulsive penetration of solar wind into the magnetosphere (Section 2.5.2).

The significance of the merging process to the magnetospheric energy budget has been analyzed by *Reiff et al.* [1981] and *Wygant et al.* [1983] from satellite observations of the cross polar cap potential drop as a measure of the rate of plasma flow through the magnetospheric convection system. Polar cap potentials vary from minimum values of 10 kV to maximums of over 150 kV. The minimum values are obtained during periods of prolonged IMF $B_z$ northward periods when merging is expected to be completely inactive. Even at these times weak circulation of plasma is observed in the ionosphere due to viscous processes. However, if $B_z$ becomes negative the potential rapidly increases, the value depending on the magnitude of the IMF $B_z$ component. Magnetic reconnection provides approximately 80% to 90% of the coupling between the solar wind and the magnetosphere [*Hill and Dessler*, 1991].

Reproduced with permission of the copyright owner. Further reproduction prohibited without permission.

Much of the current controversy surrounding flux transfer events involves their significance to magnetospheric energetics. A variety of estimates of the contribution to the cross polar cap potential drop are available for FTE's and candidate ionospheric FTE signatures. For example, *Russell* [1995] estimate an average of 3 kV contribution per FTE to the cross polar cap potential based on FTE's with a diameter of 1 $R_E$, field strength of 50 nT, and a reccurence rate of one event per 8 minutes. Estimates from ground based radars and optical data obtained by *Lockwood et al*, [1990] suggest the ionospheric transients are associated with an average of 30 kV assuming periods of enhanced merging occurred for 2 minutes. *Lockwood and Smith* [1992] obtained estimates of the dayside reconnection rate using low-altitude satellite observations of cusp region particle precipitation. Assuming the size of the merging gap was 1500 km, they obtain an average of 58 kV for a period during which approximately 87% of the potential contribution occurs during three bursts of merging. This result is consistent with *Lockwood et al.* [1992] if the assumption of 2 minutes for the period of active merging in the latter estimate is in *Lockwood et al.* [1992] is reduced to 1 minute.

**Table 2.2**
**Estimated Upper Limit of FTE Contributions to Polar Cap Potential[1]**

| Reference | Ionospheric Dimensions (km) Azimuthal | Longitudinal | Average $\Delta V_{rec}$ (kV) |
|---|---|---|---|
| *Russell and Elphic*, [1984] | | | 20 |
| *Rijnbeek et al.*, [1984] | | | 6 |
| *Goertz et al.*, [1985] | | | 5 |
| *Egeland and Sandholt*, [1992] | 300-500 | 50 | 2 |
| *Denig et al.*, [1993] | | 50-100 | <1 |
| *Lockwood et al.*, [1993c] | 2750 | 300 | 33 |
| *Pinnock et al.*, [1993] | 900 | 100 | 7.1 |

[1]From Newell and Sibeck [1993b].

*Newell and Sibeck* [1993b] surveyed reports of candidate FTE signatures and summarized the upper limit to the contribution that each event could make to the polar cap potential drop. These results are reproduced in Table 5.2 where it is shown that the average contribution is less than the 100-150 kV potential that is common during active periods. Flux transfer events at best can only produce a fraction of the total convective electric field suggesting that a continuous merging process must also be present at the dayside magnetopause.

The search for ionospheric signatures of flux transfer events has received wide interest. Theoretical models for current systems associated with FTE's were proposed by *Saunders et al.* [1984], *Lee* [1986], and *Southwood* [1985, 1987]. The ionospheric responses due to these systems have been modelled by *McHenry and Clauer* [1987], *Basinska et al.* [1989], *Zhu and Kan* [1989], and *Wei and Lee* [1990]. The predicted size of the disturbance is generally based on the dimensions of the current structure and is expected to extend over a few hundred kilometers in the ionosphere.

Reproduced with permission of the copyright owner. Further reproduction prohibited without permission.

The upward field aligned current where the associated auroral luminosity should be confined is restricted to a fraction of the total event [*Lockwood et al.*, 1993a]. Estimates of the dimensions of the ionospheric disturbances may be quite different based on radar or optical studies (see Section 3.4.8).

Candidate events reported in the literature as ionospheric signatures of FTE's include radar observations of enhanced ion flows [*Goertz et al.*, 1985; *Todd et al*, 1986], magnetometer records of impulsive variations in the magnetic field [*Lanzerotti et al.*, 1986], optical observations of transient poleward drifting auroral arcs [*Sandholt et al.*, 1986] alone or with complimentary radar data [*Lockwood et al.*, 1989a,b; *Sandholt et al.*, 1990] and precipitating particle and drift meter data on low altitude satellites [*Basinska et al.*, 1989; *Lockwood and Smith*, 1989].

The interpretation of many of these events in terms of ionospheric signatures of flux transfer events is not without controversy and a number of the events have been reexamined in recent years. An alternative explanation of the *Todd et al.* [1986] events proposed by *Sibeck et al.* [1989] is the ionospheric response to solar wind pressure pulses. Similar events are now known to appear during both $B_z > 0$ and $B_z < 0$ conditions, inconsistent with the strong $B_z$ negative dependence for FTE's [*Saunders*, 1989]. Similarly, events typical of those reported by *Lanzerotti et al.* [1986] from a single magnetometer have been identified in the chain of magnetometers on the coasts of Greenland. The network of instruments show that the motion of the events are inconsistent with that predicted for FTE's [*Friis-Christensen et al.*, 1988]. *Lanzerotti et al.* [1987, 1988] later arrived at the same conclusion. The consensus now is that large magnetometer responses on closed field lines are due to currents generated in the ionosphere when the magnetosphere responds to solar wind pressure pulses. *Lui and Sibeck* [1991] have similarly argued that the optical events reported by *Sandholt et al.* [1986] can be explained by solar wind pressure pulses.

### 2.8.2 Impulsive Penetration

*Lemaire* [1977], *Lemaire and Roth* [1978], and *Lemaire et al.* [1979] developed a model in which magnetosheath plasma elements with momentum in excess of the ambient solar wind flow, termed "plasmoids", impulsively penetrate the magnetopause. The model is offered as an alternative mechanism to reconnection or viscous processes to explain the excitation of high latitude plasma convection, the formation of boundary layers with characteristics of magnetosheath plasma, flux transfer events, and dayside aurorae. Solar wind plasma density irregularities with scale sizes smaller than the magnetosphere are proposed as the source of the excess momentum flux. An alternate theory for impulsive penetration was proposed by *Heikkila* [1982] based on the similar premise as Lemaire and Roth's that small plasma regions with excess momentum were responsible for the mass and momentum transfer at the magnetopause. Differences in the details of the two models have been described by *Roth* [1992]. Impulsive penetration models have been invoked by *Lundin and Evans* [1985] and *Meng and Lundin* [1986] to explain the discrete auroral arcs in the prenoon and postnoon sectors of the auroral oval which radiate from the midday region. A schematic of the process published by *Lemaire and Roth* [1978] is reproduced in Figure 2.17.

Reproduced with permission of the copyright owner. Further reproduction prohibited without permission.

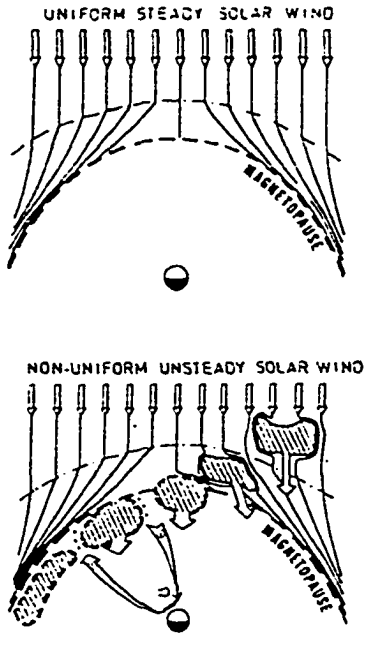


Figure 2.16 Schematic of the Impulsive Penetration Process. A steady solar wind flow [from *Lemaire and Roth*, 1978].

Impulsive penetration as a source of the dayside boundary layer plasma and an energy source driving high latitude convection has been severely criticized in recent years. Theoretical work by *Schindler* [1979] using ideal MHD showed that the *Lemaire* [1977] version of the impulsive penetration process can result in plasma transport across the magnetopause only under the very restrictive conditions where the magnetosheath field is either parallel or antiparallel to the geomagnetic field. The process has also been analyzed numerically by 2-D computer simulations [*Ma et al.* 1991; *Dai and Woodward*, 1994; *Savoini et al.*, 1994] confirming the *Schindler* [1979] results. The computer codes demonstrate that trapping of plasmoids is possible after entering the magnetosphere if reconnection occurs in the field lines draping around the penetrating plasma. The reconnection process occurs even if the fields are not exactly parallel or antiparallel if the initial kinetic energy density of the plasmoid exceeds the magnetic energy density of the transverse component of the magnetic field by a factor of 50. Since the magnetosheath flow velocity rarely exceeds a few hundred kilometers per second the 2-D model predicts that impulsive penetration is unlikely unless the fields are within 5° of being parallel or antiparallel. *Ma et al.* [1991] also noted that the threshold for penetration may not be as restrictive in the three dimensional case which was not considered in their simulation as long as the field-aligned dimension of the plasma irregularity is small in comparison to the dimensions of the magnetosphere, in which case the plasmoid may align itself with the geomagnetic field by stretching the interplanetary field lines.

Reproduced with permission of the copyright owner. Further reproduction prohibited without permission.

*Cowley* [1984] objected to the *Heikkila* [1982] version of the penetration problem and formation of the boundary layer on the grounds that the magnetospheric model used in developing the model was unrealistic. *Owen and Cowley* [1991] further argued that while the mechanism may result in plasma on open field lines it cannot produce a boundary layer plasma on adjacent closed field lines and cannot provide the energy necessary to obtain the large potential drops observed in the high latitude ionosphere.

Predictions for the IMF dependence of the impulsive penetration of solar wind filaments into the magnetosphere were described by *Lemaire et al.* [1979]. The regions of enhanced solar wind plasma density (nm) or bulk speed (v) are expected to be rejected by the magnetosphere if the IMF $B_Z$ component is strongly positive due to an induced magnetic moment within the plasmoid aligned in the same direction as the terrestrial dipole creating a magnetic field with the same direction as the magnetosphere [c.f., Figure 1. of *Roth*, 1995]. Penetration is possible for IMF $B_z < 0$ because the induced magnetic moment is aligned antiparallel to the terrestrial dipole and the induced magnetic field is antiparallel to the field in the dayside magnetosphere. This prediction agrees with the formation of the flux transfer event during $B_z$ negative or weakly positive periods [*Berchem and Russell*, 1984]. The penetration of the solar wind filaments into the lobe regions of the magnetotail is also expected to be controlled by the orientation of the IMF. The field must be oriented towards (away) from the Sun for the filaments to be captured in the southern (northern) hemisphere according to *Lemaire et al.* [1979]. *Lemaire* [1987] further suggests that the optical observations of poleward drifting auroral forms by *Sandholt et al.* [1986] and the detection of poleward drifting ionospheric plasma irregularities by radar reported by *Goertz et al.* [1985] are entirely consistent with the impulsive penetration model since the IP model predicts the poleward motion of the transient events.

### 2.8.3 Viscous Interaction

The term "viscous interaction" is a general one and applies to a variety of mechanisms that result in drag on the geomagnetic field by magnetosheath plasma flowing along the magnetopause [*Paschmann*, 1991] and diffusive penetration of magnetosheath plasma across the magnetopause as a result of wave-particle interactions from lower-hybrid turbulence [*Labelle and Treumann*, 1988; *Gary and Sgro*, 1990; *Treumann et al.*, 1992] or kinetic Alfvén waves [*Lee et al.*, 1994] and plasma wave instabilities that form along the boundaries of the magnetosphere. Streaming instabilities can arise in a plasma with different ion and electron velocities or if two or more components of the plasma have different velocity distributions. In the context of the magnetosphere this, instability may form when high speed magnetosheath plasma flows through low speed magnetospheric plasma allowing momentum transfer across the magnetopause [*Eviatar and Wolf*, 1968]. An early proposal by *Parker* [1967] suggested that viscous drag may even be responsible for field line erosion from the surface of the dayside magnetosphere and lead to the increase in the magnetic flux of the tail. This model predicts that dayside flux erosion and the subsequent increase in lobe flux should be correlated with the solar wind velocity and density and uncorellated with the orientation of the solar magnetic field, inconsistent with observations. However, it may be a useful model of the

Reproduced with permission of the copyright owner. Further reproduction prohibited without permission.

baseline viscous effect of the magnetosheath flow over the magnetopause and the effects noted during $B_z > 0$ periods.

Wave structures propagating along the magnetopause boundary can also lead to current generation through excitation of the Kelvin-Helmholtz instability. The presence of electrons with pitch angle distributions strongly peaked near 90° in the boundary layer led *Eastman and Hones* [1979] to believe the field lines were closed requiring an alternative to reconnection to explain the transport of plasma into the boundary layer. A strong velocity shear is present within the magnetospheric the boundary layer, providing conditions appropriate for the growth of the Kelvin-Helmholtz instability. This same region has been identified by a number of authors as a possible site for a growth of unstable waves in the plasma. Observational evidence for these waves was obtained by the ISEE satellites [*Hones et al.*, 1981]. *Ogilvie and Fitzenreiter* [1989] showed that the velocity shear across the magnetopause is generally stable but marginal or unstable conditions may be found in the density transitions in and at the inner edge of the boundary layer. Numerical simulations of the plasma behavior at the magnetopause and within the afternoon boundary layer [*Wei et al.*, 1990; *Lee and Wei*, 1993; *Wei and Lee*, 1993; *Thomas and Winske*, 1993] have demonstrated growth of instabilities at both boundaries. The instabilities lead to formation of vortices in the plasma flow and an associated current flow along the magnetic field line where the direction of current flow is into the ionosphere in the morning and out of the ionosphere in the afternoon. The simulation produced by *Wei and Lee* [1993] attempted to explain the formation of the "spots" in dayside aurora reported by *Lui et al.* [1987] from the 1300-1600 MLT sector in images obtained by the Viking satellite. *Lui et al.* [1989] later reported that the "spots" (as they have come to be called) were found in the afternoon oval independent of substorm and IMF conditions, suggesting that they are unrelated to merging. The growth of the instability is limited to the postnoon and prenoon sectors and is unlikely to explain auroral arcs in the midday sector.

The total contribution of viscous interactions to the large scale energetics of the magnetosphere is small. As noted in Section 2.8.1 the results obtained by *Reiff et al.* [1981] demonstrate that viscous processes account for less than 10% of the energy extracted from the solar wind. Experimental evidence for ionospheric effects of viscous processes has also been found in a number of other studies. Comparison of particle precipitation boundaries to ion convection reversal boundaries shows the presence of closed convection cells equatorward of the $> 35keV$ electron boundary, consistent with a viscous process [*Heelis et al.*, 1980, 1986; *Coley et al.* [1987].

It is unlikely that the viscous process can explain poleward moving transient auroral arcs in the midday sector nor the formation of the FTE's since both phenomenon are commonly found during $B_z$ negative conditions but rare for $B_z$ positive while the viscous process is independent of the orientation of the IMF. Convection cells have been observed at high latitudes during periods of $B_z$ northward [*Heelis et al.*, 1986], but the flow is often sunward and evidence exists that reconnection between IMF and open lobe field lines is responsible for the convection of the plasma.

Reproduced with permission of the copyright owner. Further reproduction prohibited without permission.

# Chapter 3
# Spectral Characteristics and Morphology of Dayside Aurorae

## 3.1 Introduction

There are two primary scientific motivations for the extensive studies carried out in recent years of atmospheric emissions in the Earth's high-latitude regions. First, the aurorae, airglows, and twilight emissions pose intrinsically interesting aeronomical problems, many unique to high latitudes. Observations of atmospheric emissions from the ground can be used to obtain a wide variety of information including winds and plasma drifts, temperatures, concentrations of neutral and excited species, and details of chemical reactions and other important physical processes that influence the state of the atmosphere. Second, the close association of the auroral oval with the high latitude limit of trapped particles [*Akasofu*, 1968] suggests that monitoring high latitude aurorae may provide a method of studying physical processes in the magnetosphere using low altitude satellite and ground based observations. A further motivation for many studies carried out during the Cold War era was the practical need to characterize natural transient optical phenomenon in the high latitude regions and to understand their relationship to the variety of radio interference problems that often limit communications in the polar regions during magnetically disturbed periods. A need today still exists to characterize charged particle distributions and dynamics within the magnetosphere since interactions of spacecraft with the space environment are often detrimental to electronic equipment onboard the spacecraft. General discussions relevant to the problem of the origin and behavior of dayside aurorae include publications by *Sandford* [1964, 1968], *Eather et al.* [1979], *Shepherd* [1979], *Feldstein and Galperin* [1985], *Meng and Lundin* [1986], *Sandholt et al.* [1986], *Sandholt and Egeland* [1988], *Leontyev et al.* [1992], *Sandholt* [1988, 1993], and *Smith* [1994].

This chapter is a review of the characteristics of dayside auroral forms reported in the literature and the evidence for associating high latitude midday aurorae with the dayside magnetospheric boundary layers. The spectral characteristics of dayside aurorae will be considered first. The standard wavelengths at which the meridian scanning photometer (MSP) in Longyearbyen has been operated are the traditional [OI] 630.0 nm, [OI] 557.7 nm, ($N_2^+$)1NG 427.8 nm, ($H_\beta$) 486.1 nm emissions widely used for monitoring aurorae and airglows throughout the world. A number of important limitations are discussed that must be considered when using these emissions for studies of dayside aurorae. Finally, the morphology and dynamics of dayside aurorae is reviewed with special emphasis on the use of dayside auroral emissions to monitor plasma entry from the magnetosheath into the magnetosphere.

## 3.2 Spectral Characteristics of Dayside Aurorae

Two regions of electron precipitation occur in the dayside auroral zone producing markedly different types of auroral displays. A "soft zone" is found at the highest latitudes produced by electrons with characteristic energies in the hundreds of electron volts. This region is the dayside

Reproduced with permission of the copyright owner. Further reproduction prohibited without permission.

continuation of the auroral oval and is associated with the penetration of electron populations from the dayside boundary layers. The "hard zone" lies immediately equatorward of the soft zone and is the result of the loss of high energy electrons from trapped particle populations drifting on closed field lines from the nightside into the daytime region. Aurora in this region was termed the "mantle aurora" by *Sandford* [1964, 1968]. Spectra obtained from the soft zone in the midday auroral oval differ from spectra of night time aurorae in a number of important aspects. The low energy electrons responsible for producing the predominantly red auroral forms common in the soft zone dayside aurorae have a limited range in the atmosphere, depositing most of their energy at high altitudes where the neutral atmosphere is dominated by atomic rather than molecular species [*Deehr et al.*, 1980; *Gault et al.*, 1981; *Sivjee and Deehr*, 1980; *Sivjee*, 1983a,b]. A relatively simple spectrum results where atomic emissions dominate over molecular emissions. Nightside aurora, in contrast, is rich in molecular emission bands. A survey of column emission rates reported in the literature for selected atomic and molecular emissions in the near UV to near IR characteristic of dayside aurora are presented in Table 3.1. A spectrum of dayside aurora has also been obtained in the ultraviolet region at wavelengths of 50.0-150.0 nm by *Gentieu et al.* [1989] but this radiation is absorbed by the atmosphere and is unavailable to ground based observers. For comparison of dayside aurora with a typical night time aurora, Table 3.2 lists relative intensities of atomic and molecular emissions given by *Vallence Jones* [1974] with values from table 3.1. To facilitate the comparison, the *Vallence Jones* [1974] values appropriate for an aurora with peak emission near 110-120 km are scaled to I(557.7 nm)=10 kR, a typical value for night time auroral displays. For the interested reader, references to dayside auroral spectra available in the literature are given in Appendix F.

The spectral content of the hard zone emissions have not received the same attention as the soft zone emissions but are expected to display essentially the same spectral content as pulsating aurorae observed in the night time and morning hours since they are produced by the same mechanism (see Section 3.3). The spectrum is dominated by the 557.7 nm and 427.8 nm emission lines in the MSP records with little or no 630.0 nm emission, indicative of significant electron energy losses deep in the atmosphere where $O(^1D)$ is completely quenched. Electron energies in the $> 5 - 10$ keV range are required for this to occur, and are consistent with rocket and satellite observations of the precipitating electron energy spectrum in the region [*Carlson and Torbert*, 1980; *Lorenzten et al.*, 1996 ] *Meng*, 1981; *Meng and Akasofu*, 1983].

Reproduced with permission of the copyright owner. Further reproduction prohibited without permission.

**Table 3.1**
**Survey of Measurements of Dayside Emission Rates at Visible Wavelengths**

| Emitter | Wavelength[1] (nm) | Brightness (kR) | Reference |
|---|---|---|---|
| OI | 630.0 | 0.90-1.2 | *Sivjee et al.*, 1982 |
| | | 2.0 | *Deehr et al.*, 1980 |
| | | 1.5-3.0 | *Sivjee*, 1983a |
| | | 0.20-2.9 | *Sandholt et al.*, 1980 |
| | | 0.35-0.99 | *Gault et al.*, 1981 |
| | | 1.0-2.0 | *Duncan and McEwen*, 1979 |
| | | 1.0-4.0 | *Peterson and Shepherd*, 1974 |
| | | 4.0-8.0 | *Sandholt et al.*, 1992 |
| | | 0.5-3.0 | *Vorobjev et al.*, 1983 |
| | 636.4 | 0.12-0.34 | *Gault et al.*, 1981 |
| | 557.7 | 0.255-0.99 | *Gault et al.*, 1981 |
| | | 1.0 | *Deehr et al.*, 1980 |
| | | 0.5-1.0 | *Duncan and McEwen*, 1979 |
| | | 0.4-2.7 | *Cogger et al.*, 1977 |
| | | 10. | *Sandholt et al.*, 1989 |
| | | 0.5-3.0 | *Vorobjev et al.*, 1983 |
| | 844.6 | 0.2-0.89 | *Gault et al.*, 1981 |
| | | 0.2-3.0 | *Sivjee et al.*, 1984 |
| | | 0.44 | *Deehr et al.*, 1980 |
| | 777.4 | 0.035-0.12 | *Gault et al.*, 1981 |
| | | 0.035-1.0 | *Sivjee et al.*, 1984 |
| | | 0.10 | *Deehr et al.*, 1980 |
| | 799.5 | 0.14 | *Gault et al.*, 1981 |
| | | 0.100-1.3 | *Sivjee et al.*, 1984 |
| | | 0.10 | *Deehr et al.*, 1980 |
| OII | 731.9-733.0 | 0.065-0.115 | *Gault et al.*, 1981 |
| | | 0.25-0.50 | *Sivjee et al.*, 1982 |
| | | 0.1 | *Sivjee and Deehr*, 1980 |
| | | 0.4 | *Deehr et al.*, 1980 |
| | 372.7-372.9[1] | - | *Sivjee and Deehr*, 1980 |
| | | 0.04 | *Deehr et al.*, 1980 |
| | | 0.045 | *Sivjee*, 1991 |
| NI | 346.6 | 0.050 | *Deehr et al.*, 1980 |
| | 520.0 | 0.010 | *Gault et al.*, 1981 |
| | | 0.015-0.075 | *Shepherd et al.*, 1976 |
| | | 0.040 | *Deehr et al.*, 1980 |
| | 694.5-695.1 | 0.015 | *Sivjee*, 1983b |
| | 597.9-598.2 | 0.015 | *Sivjee*, 1983b |

[1]Rarely detected at night due to proximity to strong $N_2 2P$ bands [*Sivjee*, 1983b, 1991].

Reproduced with permission of the copyright owner. Further reproduction prohibited without permission.

**Table 3.1**
**(continued)**

| Emitter | Wavelength[2] (nm) | Brightness (kR) | Reference |
|---|---|---|---|
| HI Balmer $\alpha$ | 656.3 | 0.015-0.030 | *Gault et al.*, 1981 |
| | | 0.080-1.0 | *Sigernes et al.*, 1995 |
| | | 0.010 | *Deehr et al.*, 1980 |
| | | 0.040 | *Derbloom*, 1975 |
| | | 0.030-0.090 | *Henriksen et al.*, 1985. |
| Balmer $\beta$ | 486.1 | 0.020-0.040 | *Gault et al.*, 1981 |
| | | 0.010 | *Eather and Mende*, 1971 |
| | | <0.020 | *Henriksen et al.*, 1978 |
| | | 0.004 | *Deehr et al.*, 1980 |
| | | 0.016-0.200[3] | *Sigernes et al.*, 1995 |
| HeI | 388.9 | 0.003-0.070 | *Sivjee*, 1983a |
| | | 0.004 | *Deehr et al.*, 1980 |
| | | 0.002-0.013 | *Sivjee et al.*, 1980 |
| | | 0.010-0.070 | *Henriksen et al.*, 1985 |
| | 587.6 | 0.003 | *Deehr et al.*, 1980 |
| | | 0.004[4] | *Sivjee et al.*, 1980 |
| $N_2$VK | | <0.002 | *Sivjee*, 1983 |
| $N_2$1P (2.0) | 775.4 | 0.265-0.440 | *Gault et al.*, 1981 |
| (4,2) | 750.5 | 0.33-0.44 | *Gault et al.*, 1981 |
| $N_2$2P (0,1) | 357.7 | <0.002 | *Sivjee*, 1983 |
| (1,2) | 353.7 | <0.002 | *Sivjee*, 1983 |
| $N_2^+$1NG (0-0) | 391.4 | 0.3-2.7 | *Cogger et al.*, 1977 |
| (0-1) | 427.8 | 0.10-0.50 | *Gault et al.*, 1981 |
| | | 0.2 (0.05[5]) | *Deehr et al.*, 1980 |
| | | 0.751 (0.15[5]) | *Link et al.*, 1983 |
| | | 0.2-1.0 | *Sandholt et al.*, 1986 |
| | | 0.5-1.0[5] | *Lanchester and Rees*, 1987 |
| M (2-0) | 782.6 | <0.52 | *Gault et al.*, 1981 |
| (3,0) | 685.3 | <0.24 | *Gault et al.*, 1981 |
| (3,1) | 805.4 | <0.24 | *Gault et al.*, 1981 |
| $O_2$ atm (1,1) | 770.8 | 0.44-0.62 | *Gault et al.*, 1981 |
| (2,2) | 780.2 | <0.20 | *Gault et al.*, 1981 |
| (3,3) | 790.1 | <0.36 | *Gault et al.*, 1981 |

[2]Wavelength is the band head for the diatomic molecules.
[3]Based on the reported $H_\alpha$ intensity and $H_\alpha/H_\beta$ ratio.
[4]Based on laboratory measurements of HeI excitation by charge exchange of HeII in air.
[5]Intensity with resonance scattering contribution removed.

Reproduced with permission of the copyright owner. Further reproduction prohibited without permission.

Table 3.2
**Comparison of Relative Intensities for Day and Night Aurora**

| Emitter | | Wavelength (nm) | Night[1] (kR) | Day[2] (kR) |
|---|---|---|---|---|
| OI | | 557.7 | 10. | 1.3 |
| | | 630.0 | 0.14-6.8 | 1.9 |
| | | 636.4 | 0.6-3.2[3] | 0.23,0.61[3] |
| | | 297.2 | 0.6 | |
| | | 777.4 | 0.96 | 0.085 |
| | | 844.6 | 1.15 | 0.510 |
| OII | | 731.9-733.0 | 0.040-10. | 0.216 |
| | | 372.7-372.9 | | 0.042 |
| NI | | 868.0 | 1.05 | |
| | | 1039.5-1040.4 | 0.60 | |
| | | 346.6 | | 0.050 |
| | | 520.0 | | 0.027 |
| | | 694.5-695.1 | | 0.015 |
| | | 597.9-598.2 | | 0.015 |
| HI | Balmer $\alpha$ | 656.3 | | 0.114 |
| | Balmer $\beta$ | 486.1 | | 0.21 |
| HeI | | 388.9 | | 0.20 |
| | | 587.6 | | 0.004 |
| $N_2^+$1N | total | | 15. | 0.40-3.7 |
| | (0,0) | 391.4 | 9.80 | 0.3-2.7 |
| | (0,1) | 427.8 | 3.00 | 0.1-1.0 |
| | (0,2) | 470.9 | 0.60 | |
| | (1,0) | 358.2 | 0.68 | |
| $N_2^+$M | total | | 63.0 | 1.0 |
| | (0,0) | 1108.7 | 12.3 | |
| | (0,1) | 1461.0 | 3.7 | |
| | (1,0) | 918.1 | 15.8 | |
| | (1,1) | 1147.2 | 1.00 | |
| | (1,2) | 1521.0 | 3.20 | |
| | (1,3) | 2239.6 | 0.58 | |
| | (2,0) | 782.6 | | 0.52 |
| | (3,0) | 687.4 | 1.40 | 0.24 |
| | (3,1) | 808.2 | 3.90 | 0.24 |
| | (3,2) | 977.4 | 0.96 | |
| | (4,1) | 706.4 | 1.10 | |
| | (4,2) | 832.8 | 1.10 | |
| | (5,2) | 726.3 | 0.52 | |

[1] From *Vallance Jones* [1974] scaled to $I(557.7nm) = 10$ kR.
[2] Single values unless otherwise noted are averages from Table 3.1 (extreme values excluded).
[3] Estimated from $I(636.4\,nm) = (A_{636.4\,nm}/A_{630.0\,nm})I(630.0\,nm)$.

Reproduced with permission of the copyright owner. Further reproduction prohibited without permission.

**Table 3.2**
**(continued)**

| Emitter | | Wavelength (nm) | Night (kR) | Day (kR) |
|---|---|---|---|---|
| $N_2$1P | total | | 88. | 0.60-0.88 |
| | (0,0) | 1050.8 | 9.6 | |
| | (0,1) | 1237.3 | 5.5 | |
| | (0,2) | 1497.7 | 1.7 | |
| | (1,0) | 891.2 | 12.4 | |
| | (1,2) | 1192.5 | 2.6 | |
| | (1,3) | 1426.9 | 2.1 | |
| | (1,4) | 1768.7 | 0.81 | |
| | (2,0) | 775.3 | 5.4 | 0.265-0.44 |
| | (2,1) | 872.3 | 7.4 | |
| | (2,2) | 993.4 | 1.5 | |
| | (2,4) | 1363.5 | 1.3 | |
| | (2,5) | 1664.3 | 8.8 | |
| | (3,0) | 687.5 | 8.8 | |
| | (3,1) | 762.7 | 6.4 | |
| | (3,2) | 854.2 | 1.8 | |
| | (3,3) | 968.0 | 2.34 | |
| | (3,6) | 1571.7 | 0.52 | |
| | (4,1) | 678.9 | 1.80 | |
| | (4,2) | 750.5 | 4.90 | 0.33-0.44 |
| | (4,4) | 943.6 | 1.70 | |
| | (5,2) | 670.5 | 1.80 | |
| | (5,3) | 738.7 | 2.40 | |
| | (5,5) | 920.4 | 0.66 | |
| | (5,6) | 1044.8 | 0.53 | |
| | (6,3) | 662.4 | 1.40 | |
| | (6,4) | 727.4 | 0.84 | |
| | (7,4) | 654.5 | 0.89 | |
| $N_2$2P | total | | 11. | |
| | (0,0) | 337.0 | 3.10 | |
| | (0,1) | 357.6 | 2.00 | |
| | (0,2) | 380.4 | 0.82 | |
| | (1,0) | 315.8 | 1.50 | |
| | (1,2) | 353.6 | 0.68 | |
| | (1,3) | 375.4 | 0.60 | |

Reproduced with permission of the copyright owner. Further reproduction prohibited without permission.

**Table 3.2**
**(continued)**

| Emitter | | Wavelength (nm) | Night (kR) | Day (kR) |
|---|---|---|---|---|
| $O_2$ Atm | total | | 130.2 | 1.00-1.18 |
| | (0,0) | 761.9 | 117.6 | |
| | (0,1) | 864.5 | 5.8 | |
| | (1,1) | 770.8 | 1.4 | 0.44-0.62 |
| | (2,2) | 780.2 | 0.68 | 0.20 |
| | (3,3) | 790.1 | 1.1 | 0.36 |
| $O_2$ IR | total | | 251.7 | |
| | (0,0) | 1268.7 | 250.0 | |
| | (0,1) | 1580.8 | 1.7 | |
| $O_2^+$1N | total | | 2.60 | |
| | (1,0) | 560.9 | 0.59 | |

### 3.2.1 [OI] 630.0 nm and [OI] 557.7 nm Emissions

The red "nebular" [OI] 630.0 nm and "auroral green" [OI] 557.7 nm emission lines originate from the excited atomic oxygen O($^1D$) and O($^1S$) states. O($^1D$) and O($^1S$) are the first and second excited states of atomic oxygen lying 1.96 eV and 4.17 eV, respectively, above the O($^3P$) ground state. Excitation within the atmosphere is accomplished by charged particle impact on O($^3P$) and a variety of chemical reactions and energy transfer mechanisms due to the low energy of the excited states above the ground state. The two emission lines are typically the brightest features in the visible spectrum giving the aurora its characteristic green color at low altitudes and red color at high altitudes. Traditionally the 630.0 nm and 557.7 nm emissions are monitored in auroral and airglow studies because the emissions are relatively bright and easy to measure and the ratios of the column intensities (the volume emission rate summed along the magnetic field) are qualitatively related to the energy and energy flux of precipitating electrons (Section 3.1.5). Detailed descriptions of the status of work regarding the sources and sinks of O($^1D$) and O($^1S$) and the production of 630.0 nm and 557.7 nm emission lines have been reviewed by *Bates* [1978], *Torr and Torr* [1982], *Solomon* [1991], and *Link et al.* [1992]. A brief discussion of the production of O($^1D$) and O($^1S$) and the resulting altitude dependent 630.0 nm and 557.7 nm volume emission rates will be presented here since the red and green lines will be the primary auroral emissions studied in Chapters 4 and 5.

Emission of a 630.0 nm photon results from a 1.96 eV magnetic dipole transition from $O(^1D_2)$ to $O(^3P_2)$. The radiative lifetime $\tau_{O(^1D)}$ of the O($^1D$) state most widely adopted for aeronomical calculations is 110 seconds although evidence exists for larger values [c.f. *Link et al.*, 1981; *Torr and Torr*, 1982; *Solomon et al.*, 1988]. The most probable radiative decays of O($^1D$) are the magnetic dipole $O(^3P_2)$- $O(^1D_2)$ and $O(^3P_1)$ - $O(^1D_2)$ transitions producing 630.0 nm and 636.4 nm

Reproduced with permission of the copyright owner. Further reproduction prohibited without permission.

**Table 3.3**
**$O(^1D)$ Einstein Coefficients and $\tau_{O(^1D)}$**

| $A_{6300} \times 10^{-3}$ $s^{-1}$ | $A_{6364} \times 10^{-3}$ $s^{-1}$ | $A_{O(^1D)} \times 10^{-3}$ $s^{-1}$ | $\tau_{O(^1D)}$ s | Reference |
|---|---|---|---|---|
| 7.5 | 2.5 | 10.0 | 100 | *Condon*, 1934 |
| 7.8 | 2.6 | 10.4 | 96 | *Pasternack*, 1940 |
| 6.9 | 2.2 | 9.1 | 110 | *Garstang*, 1951 |
| 7.023 | 2.278 | 9.301 | 107 | *Froese Fischer and Saha*, 1983 |
| 5.608 | 1.815 | 8.849 | 113 | *Baluja and Zeippen*, 1988 |
| — | — | 5.3 | 187 | *Omholt*, 1960 |
| — | — | 8.3 | 120 | *Stoffregen and Derblom*, 1960 |
| 5.69 | 1.85 | 7.54 | 133 | *Yamanouchi and Horie*, 1952 |
| 5.1 | 1.64 | 6.74 | 148 | *Garstang*, 1968 |
| 5.15 | 1.66 | 6.81 | 147 | *Kernahan and Pang*, 1975 |

photons. Reported values for the Einstein coefficients (the radiative transition probability) for these transitions are summarized in Table 3.3 where they are grouped according to the magnitude of the estimated radiative lifetime of the $O(^1D)$ state. The $A_{6392}$ Einstein coefficient for the final $O(^3P_0)$ - $O(^1D_2)$ transition is approximately $2.2 \times 10^{-6} s^{-1}$ [c.f. *Krassovsky et al.*, 1962] and does not contribute appreciably to radiative loss of $O(^1D)$ . The radiative or characteristic lifetime $\tau_i$ for an excited state $i$ is given by the reciprocal of the sum of the radiative decay probabilities for each possible transition to $j$ lower states

$$\tau_i = \frac{1}{\sum_j A_{ij}} \tag{3.1}$$

and the radiative lifetime of an excited state $N_i$ is understood to be the characteristic decay time governing the exponential decay

$$[N_i]_t = [N_i]_0 e^{-t/\tau} \tag{3.2}$$

where $[N_i]_0$ is the initial concentration of the excited state. The lifetime $\tau$ is characteristic of the excited state and is independent of time. Further, $\tau$ does not depend on the method of preparing the unstable state nor does it depend on the time history of the unstable state (c.f., the definition of the lifetime and discussion of the probabilistic nature of the decay of excited states by *Cohen-Tannoudji et al.*, 1977).

The 557.7 nm photon is emitted in the 2.21 eV electric quadrupole transition between $O(^1S_0)$ and $O(^1D_2)$. There is less disagreement on the radiative lifetime of this state than $O(^1D)$ . Reported Einstein coefficients are 1.32 $s^{-1}$ [*Garstang*, 1956], 1.41 $s^{-1}$ [*Garstang*, 1968], 1.11 $s^{-1}$ [*Kernahan and Pang*, 1975], 1.057 $s^{-1}$ [*Froese Fisher and Saha*, 1983], and 1.291 $s^{-1}$ [*Baluja and Zeippen*, 1988] leading to a radiative lifetime of 0.7 to 0.95 seconds. The most recent value gives the 0.77 second $O(^1S)$ radiative lifetime commonly adopted for aeronomic calculations.

The altitude dependence of the 557.7 nm and 630.0 nm volume emission rates are a result of altitude variations in both the production and loss rates for the excited states. Electron impact on

Reproduced with permission of the copyright owner. Further reproduction prohibited without permission.

atomic oxygen is the dominant source of excitation for both $O(^1D)$ and $O(^1S)$ over a wide range of altitudes and energies and coupled with the energy dependent excitation cross sections provide a first order explanation for the altitude variations in the emission intensity.

Considering production first, the volume excitation rate by electron impact is given by

$$\eta_i(z) = n_{O(^3P)}(z) \int_{E_{th,i}}^{E_{maximum}} \sigma_i(E) I(E,z) dE \tag{3.3}$$

where $n_{O(^3P)}(z)$ is the atmospheric density of atomic oxygen in the ground state at altitude $z$, $\sigma_i(E)$ the cross section for excitation by electron impact into state $i = O(^1D), O(^1S)$, and $I(E,z)$ the intensity of primary and secondary electrons with energy $E$ at altitude $z$. The limits of the integration are between the threshold energy required to produce the excited state and a maximum energy for which the product of the cross section and electron intensity term, $\sigma_i(E)I(E,z)$, is nonzero.

The distance an electron can penetrate the atmosphere before being thermalized governs the altitude range over which $I(E,z)$ is significant. Electrons lose energy during collisions with neutral constituents and are gradually slowed down as they penetrate to lower altitudes. The energy loss mechanism involves inelastic scattering of the primary electron leading to excitation, dissociation, or ionization of the collision partner. A significant contribution to $I(E,z)$ are the secondary electrons produced by ionizations of neutral atoms. The peak in the secondary electron energy spectrum between 2 eV and 10 eV [*Rees and Jones*, 1973; *Banks et al.*, 1974; *Sharp and Hays*, 1974; *Feldman and Doering*, 1975] is coincident with the maxima in the $O(^1D)$ and $O(^1S)$ excitation cross sections [*Vaughan and Doering*, 1986; *Shyn and Sharp*, 1986a,b; *Doering*, 1992]. Precipitating primary auroral electrons are less efficient at exciting atomic oxygen because their energies are generally on the order of $10^2$eV to $10^3$eV. While the number of secondary electrons produced for each collision is nearly independent of the primary electron energy, the mean free path between collisions is strongly energy dependent. Low energy electrons collide frequently, producing secondaries at high altitudes where they deposit most of their energy. High energy electrons suffer fewer collisions at high altitudes than low energy electrons, penetrating to lower altitudes before they begin to produce significant quantities of secondary electrons. The result is that low energy electrons deposit energy entirely at high altitudes while high energy electrons deposit energy over a range of altitudes but the maximum is at low altitudes.

Excitation cross sections for $O(^1D)$ and $O(^1S)$ by electron impact are strongly energy dependent [*Shyn and Sharp*, 1986a,b]. The $O(^1D)$ cross section peaks near 6 eV but drops by a factor of 10 by approximately 2 eV and 100 eV. The $O(^1S)$ cross section is similar in form to the $O(^1D)$ cross section but is reduced by a factor of 10 and the peak is near 10 eV favoring $O(^1D)$ production over $O(^1S)$ for a wide range of electron energies. Emissions from high altitude due to low energy electron impact are therefore dominated by the red 630.0 nm emission. High energy electrons will similarly produce both $O(^1D)$ and $O(^1S)$ at high altitudes but at reduced rates due to the smaller secondary electron production rate. The maximum production of excited oxygen states by high energy electrons occurs low in the atmosphere although $O(^1D)$ is still produced more often than $O(^1S)$ due to the differences in the excitation cross section. If the source and loss of the excited

Reproduced with permission of the copyright owner. Further reproduction prohibited without permission.

oxygen states was due solely to electron impact and radiative decay then 630.0 nm emissions should dominate 557.7 nm emissions over the entire altitude range and the only difference between auroral arcs formed by precipitating populations of low and high energy electrons would be the altitude distribution of the 630.0 nm emission. The dominance of the green 557.7 nm emission at lower altitudes is due to the differences in the radiative lifetimes of $O(^1D)$ and $O(^1S)$ and an additional collisional energy loss mechanism which is more efficient than radiative decay.

If every excited state formed by electron impact were to radiate the altitude profile of the photon emission rate will be the same as the altitude profile of the production rate of the excited state. This is only true for prompt emissions for which the transitions are allowed by electric dipole selection rules and the lifetimes are on the order of microseconds. The probability of a radiative decay of either the $O(^1D)$ by a magnetic dipole transition or $O(^1S)$ by an electric quadrupole transition are greatly reduced compared to the electric dipole transition leading to the long lifetime of the states. Radiative decay is not the only energy loss mechanism. Collisions with a neutral atom, molecule, or electron provides an alternative energy loss mechanism for the excited state which does not involve the emission of a photon. The collision process, known as "quenching", dominates at low altitudes where the atmospheric density is large and the probability for de-excitation through a collision is greater than the probability of photon emission.

The effect of quenching on the lifetime of an excited state population $N_i(z)$ at altitude $z$ can be illustrated by considering the continuity equation governing the time dependent concentration of the excited state

$$\frac{\partial[N_i(z)]}{\partial t} = P_i(z) - L_i(z)[N_i(z)] \tag{3.4a}$$

where transport and diffusion has been neglected and $P_i(z)$ and $L_i(z)[N_i(z)]$ are the production and loss rates of state $i$, respectively, at altitude $z$. $L_i(z)$ is the altitude dependent loss coefficient for the excited state. Alternatively, Equation 3.4a is often written

$$\frac{\partial[N_i(z)]}{\partial t} = P_i(z) - L_i'(z) \tag{3.4b}$$

where $L_i'(z) = L_i(z)[N_i(z)]$ is the loss rate. The advantage of the first form is that concentrations of the excited state at equilibrium where the production and loss rates are balanced are given simply by

$$[N_i(z)] = \frac{P_i(z)}{L_i(z)} \tag{3.4c}$$

Equation 3.4 governs the time dependence of the excited state and will be solved in Chapter 4 to derive concentrations of the $O(^1D)$ as a function of altitude and time. For now simply assume that some quantity of the excited state has built up after a period of excitation and the production has stopped, that is, $P_i(z) = 0$ with $[N_i(z)] > 0$. Only the loss term contributes to the time

Reproduced with permission of the copyright owner. Further reproduction prohibited without permission.

dependence of the excited state in these conditions. The loss due to radiation and quenching is given generally by

$$L_i(z) = \sum_j A_{ij} + \sum_k \alpha_{ik}(z)[M_k(z)] \tag{3.5}$$

where $A_{ij}$ is the Einstein coefficient for a radiation transition between the excited state $i$ and state $j$ and $\alpha_{ik}(z)$ the rate coefficient for quenching reactions of the type

$$N_i + M_k \rightarrow N_j + M_k^*$$

indicating that energy transferred from the excited state $i$ to one of the ground states $j$ through a collision with an atmospheric species $M_k$. Rearranging equation (3.5) using Equation 3.1 an effective lifetime $\tau_{eff}(z)$ is obtained

$$\tau_{eff}(z) = \tau\left[1 + \frac{\sum_k \alpha_{ik}(z)[M_k(z)]}{\sum_j A_{ij}}\right]^{-1} \tag{3.6}$$

which is always less than or equal to the radiative (unquenched) lifetime $\tau$. The surviving excited species after a time $t$ at altitude $z$ in the presence of quenching is given by

$$[N_i(z,t)] = [N_i(z,0)]e^{-t/\tau_{eff}(z)} \tag{3.7}$$

Collision rates are very low at high altitudes and quenching is negligible. A useful parameter indicating the altitude at which quenching becomes significant is the quenching height, the altitude at which the emission rate is reduced to one half its unquenched value [*Vallance Jones*, 1974]. The quenching altitude varies from 250 km to 350 km for $O(^1D)$ due to variations in thermospheric temperature and density. In contrast, the quenching altitude for $O(^1S)$ for which the radiative lifetime is approximately 0.7 second is approximately 95 km. $O(^1D)$ is efficiently quenched at low altitudes and the dominant emission is the green 557.7 nm emission from the $O(^1S)$ state. At high altitudes neither state is quenched but the cross section favors the production of $O(^1D)$ and auroral emissions are dominated by the 630.0 nm emission.

Quenching reduces the lifetime of the $O(^1D)$ population and hence the emission rate of 630.0 nm photons by removing the excited state before emission can occur. A ground based camera or photometer sampling 630.0 nm photons emitted from populations of $O(^1D)$ over a range of altitudes at some magnetic zenith angle $\chi$ near the magnetic zenith will obtain an integrated intensity

$$I(630.0\ nm) = \frac{A_{6300}}{cos\chi}\int_0^\infty [N_{O(^1D)}(z,t)]dz \tag{3.8}$$

or

$$I(630.0\ nm) = \frac{A_{6300}}{cos\chi}\int_0^\infty [N_{O(^1D)}(z,0)]e^{-t/\tau_{eff}(z)}dz \tag{3.9}$$

This integral is best solved numerically since the excited state concentration $[N_i z,0]$ at time $t = 0$ depends on the altitude dependent excitation mechanism and $\tau_{eff}(z)$ depends on the altitude dependent composition aud temperature of the neutral atmosphere. Integration along a path through the atmosphere samples emissions from a range of altitudes with a range of effective

Reproduced with permission of the copyright owner. Further reproduction prohibited without permission.

lifetimes. The time dependence in the column sums I(630.0 nm) observed on the ground are due to the product of the unquenched concentration of the excited state after time $t$ with a factor due to the quenching also at time $t$ within the integrand

$$[N_i(z,0)]\exp\left(-\frac{t}{\tau}\left(1+\frac{\sum_k \alpha_{ik}(z)[M_k(z)]}{\sum_j A_{ij}}\right)\right) \tag{3.10}$$

Since the dominant contribution to the column emission rate is due to photons arriving from near the peak emission altitude, the lifetime observed from the ground will be an apparent lifetime [*Henriksen et al.*, 1978; *Ono and Hirasawa*, 1992]. Only in cases where the energy deposition by low energy electrons is above altitudes where quenching is significant will the observed lifetime be close to the radiative lifetime of the excited state.

The explanation just presented for the high altitude of the 630.0 nm emission and the low altitude 557.7 nm emission is based on impact excitation of atomic oxygen by secondary electrons as the only source of atomic oxygen. This model is a useful first order approximation, but the process is more complicated due to the variety of chemical sources of $O(^1D)$ and $O(^1S)$ in addition to electron impact. Production and loss mechanisms for $O(^1D)$ are summarized in Table 3.4. The chemical rate coefficients and branching ratios are those used in the GLOW model (see Chapter 4). The most important auroral source of $O(^1D)$ is electron impact excitation of atomic oxygen (3.11a) and dissociative recombination of the diatomic oxygen ion (3.12) [*Torr and Torr*, 1982; *Meier et al.*, 1989]. The energetic electrons required for reaction (3.11) are generally secondary electrons although low energy primary electrons may also contribute. Electrons from the ambient thermal plasma population are responsible for dissociative recombination. A high temperature electron gas is an additional source of energetic electrons which may drive reaction (3.12) if the thermal plasma electron temperature exceeds approximately 3000 K. In this case the fast electrons in the high energy tail of the electron velocity distribution have energies above the threshold required to excite $O(^1D)$ allowing 630.0 nm photons to be observed that are unrelated to direct impact by precipitating particles. Efficient heating of the electron gas by soft electron precipitation is often invoked to explain the strong $O(^1D)$ production rate observed within the midday period [*Wickwar and Kofmann*, 1984; *Lockwood et al.*, 1993a]. Other significant contributions to $O(^1D)$ production are impact dissociation of diatomic oxygen (Equation 3.8) and cascading from $O(^1S)$ (Equation 3.7).

The interchange reaction (3.14) has also been suggested as a source of the $O(^1D)$ state within aurora although its importance is controversial. *Rusch et al.* [1978] originally proposed the reaction to explain discrepancies between calculated 630.0 nm emission rates with those observed by *Sharp et al.* [1979] in an aurora. Modelling efforts by *Rees and Roble* [1986] appeared to confirm that the traditional sources in reactions (3.11a)-(3.13) were not sufficient to account for the observed emission rates and that reaction (3.14) is the major source for $O(^1D)$ within an auroral arc. The significance of the reaction for production of auroral $O(^1D)$ was questioned by *Link* [1983] and later *Solomon et al.* [1988] who concluded that the traditional sources adequately explained their observations of 630.0 nm emissions in auroral arcs from the Atmosphere Explorer satellite. More recently, *Meier et al.* [1989] reexamined the rocket data published by *Sharp et al.* [1979] and

Reproduced with permission of the copyright owner. Further reproduction prohibited without permission.

showed that the bulk of the observed 630.0 nm emissions can be explained by the traditional sources with no compelling need to include reaction (3.14) if the atomic oxygen model used in the calculation is reevaluated. *Link and Swaminathan* [1992] recently reviewed the important points of the controversy and concluded the interchange mechanism is not required to explain auroral observations.

The mechanism by which the $O(^1S)$ state is excited is similarly controversial [c.f, the reviews by *Torr and Torr*, 1982; *Henriksen and Egeland*, 1988; *Solomon*, 1991]. The primary reactions are summarized in Table 3.5. Although impact excitation produces $O(^1S)$ in aurora at high altitudes, the energy transfer reaction (3.29) appears to dominate at altitudes below approximately 130 km [*Meyer et al.*, 1969; *Deans and Shepherd*, 1978; *Sharp and Torr*, 1979; *Gattinger et al.*, 1985] where the molecular nitrogen concentration is greater than atomic oxygen and the greater atmospheric density permits frequent collisions.

A number of nonauroral processes may also result in the emission of 630.0 nm and 557.7 nm photons. These reactions are summarized in Table 3.6. Photodissociation and photoionization of $O_2$ by ultraviolet photons will also produce $O(^1D)$ and $O(^1S)$ directly as well as the $O_2^+$ and $O^+$ precursors required for reactions 3.13 and 3.19. Photoelectrons produced in the photoionization of diatomic oxygen at low altitudes may also become a source of electrons with sufficient energy to produce $O(^1S)$ at greater altitudes. Strong absorption by atmospheric oxygen limits the penetration of the ultraviolet light and dayside observations during the midwinter period are generally obtained when the UV screening height in the zenith of the station is near 400 km. Under these conditions the excited photolysis products of diatomic oxygen should not be observed. The station is located sufficiently close to the terminator that even on the winter solstice the emissions from the photolysis products are observed at high altitudes far to the south of the station. Emissions at 630.0 nm are particularly prominent in the photometer plots from this source although they are easily distinguished from auroral sources based on morphology. Twilight and airglow 630.0 nm emissions are recognized by their lack of structure, maximum intensity near the southern horizon, and maximum development between magnetic and local solar noon.

Reproduced with permission of the copyright owner. Further reproduction prohibited without permission.

**Table 3.4**
**$O(^1D)$ Production and Loss Mechanisms**

| | | |
|---|---|---|
| | Sources[1] | |
| $O(^3P) + e^* \rightarrow O(^1D) + e^*$ | | (3.11a) |
| $O(^3P) + e_{th} \rightarrow O(^1D) + e$ | $k_{O,e} = 2.6 \times 10^{-11} T_e^{0.5} exp(-22740/T_e)\ cm^3 s^{-1}$ | (3.12) |
| $O_2^+ + e \rightarrow O(^1D) + O$ | $k_{O_2^+,e} = 1.9 \times 10^{-7} (300/T_e)^{0.7}\ cm^3 s^{-1}$ $\beta = 1.20$ | (3.13) |
| $N(^2D) + O_2 \rightarrow NO + O(^1D)$ | $k_{N,O_2} = 6.0 \times 10^{-12}\ cm^3 s^{-1}$ $\beta = .10$ | (3.14) |
| $N(^2D) + O(^3P) \rightarrow N(^S) + O(^1D)$ | $k_{N,O} = 1.0 \times 10^{-12}\ cm^3 s^{-1}$ $\beta = .10$ | (3.15) |
| $O(^1S) \rightarrow O(^1D) + h\nu(557.7nm)$ | $A_{5577} = 1.06 s^{-1}\ cm^3 s^{-1}$ | (3.16) |
| $O_2 + e^* \rightarrow O(^1D) + O + e^*$ | | (3.17) |
| $N^+ + O_2 \rightarrow O(^1D) + NO^+$ | $k_{N^+,O_2} = 6 \times 10^{-10}\ cm^3 s^{-1}$ $\beta = .30$ | (3.18) |
| $O^+(^2D) + O(^3P) \rightarrow O(^4S) + O(^1D)$ | $k_{O^+,O} = 1.0e-11\ cm^3 s^{-1}$ $\beta = .50$ | (3.19) |
| | Loss[2] | |
| $O(^1D) \rightarrow O(^3P_2) + h\nu(\lambda = 630.0nm)$ | $A_{6300} = 0.00585 s^{-1}$ | (3.20) |
| $O(^1D) \rightarrow O(^3P_1) + h\nu(\lambda = 636.4nm)$ | $A_{6364} = 0.00185 s^{-1}$ | (3.21) |
| $O(^1D) + N_2 \rightarrow O(^3P) + N_2^*$ | $k_{O,N_2} = 2.0 \times 10^{-11} exp(107.8/T_n)\ cm^3 s^{-1}$ | (3.22) |
| $O(^1D) + O_2 \rightarrow O(^3P) + O_2^*$ | $k_{O,O_2} = 2.9 \times 10^{-11} exp(67.5/T_n)\ cm^3 s^{-1}$ | (3.23) |
| $O(^1D) + O(^3P) \rightarrow O(^3P) + O(^3P)$ | $k_{O,O} = 3.0 \times 10^{-12}\ cm^3 s^{-1}$ | (3.24) |
| $O(^1D) + e \rightarrow O(^3P) + e*$ | $k_{O,e} = 8.1 \times 10^{-10} (T_e/300)^{0.5}\ cm^3 s^{-1}$ | (3.25) |

[1]Reactions included in GLOW model (courtesy of *S. Solomon*, 1994) for $O(^1D)$ production.
[2]Reactions included in present work for time dependent $O(^1D)$ loss.

Reproduced with permission of the copyright owner. Further reproduction prohibited without permission.

**Table 3.5**
**$O(^1S)$ Production and Loss Mechanisms**

| | | |
|---|---|---|
| | Sources[1] | |
| $O(^3P) + e^* \rightarrow O(^1S) + e^*$ | | (3.11b) |
| $O_2^+ + e \rightarrow O(^1S) + O$ | $k_{O_2^+,e} = 1.95 \times 10^{-7}(300/T_e)^{0.7}\ cm^3s^{-1}$ | (3.26) |
| | $\beta = 0.12 + 0.02log_{10}([n_e]/[O](300/T_e)^{0.7})$ | |
| | $\beta = 0.03\ if\ \beta < 0.03$ | |
| $O_2^+ + N \rightarrow O(^1S) + NO^+$ | $k_{O_2^+,N} = 1.2 \times 10^{-10}\ cm^3s^{-1}$ | (3.27) |
| | $\beta = .21$ | |
| $N(^2D) + NO \rightarrow N_2 + O(^1S)$ | $k_{N,NO} = 7.0 \times 10^{-11}\ cm^3s^{-1}$ | (3.28) |
| | $\beta = .20$ | |
| $N_2(A^3\Sigma_u^+) + O(^3P) \rightarrow O(^1S) + N_2$ | $k_{N_2,O} = 3.1 \times 10^{-11}\ cm^3s^{-1}$ | (3.29) |
| | $\beta = .19$ | |
| | Loss[1] | |
| $O(^1S) \rightarrow O(^1D) + h\nu(\lambda = 557.7nm)$ | $A_{5577} = 1.25s^{-1}$ | (3.30) |
| $O(^1S) \rightarrow O(^3P) + h\nu(\lambda = 297.2nm)$ | $A_{2972} = 0.071s^{-1}$ | (3.31) |
| $O(^1S) + O_2 \rightarrow O(^3P) + O_2^*$ | $k_{O,O_2} = 4.0 \times 10^{-12}exp(-865/T_n)\ cm^3s^{-1}$ | (3.32) |
| $O(^1S) + O(^3P) \rightarrow O(^3P) + O(^3P)$ | $k_{O,O} = 2.0 \times 10^{-14}\ cm^3s^{-1}$ | (3.33) |

[1]Reactions used in GLOW model (courtesy of *S. Solomon*, 1994) to obtain equilibrium values of 557.7 um photon volume emission rate.

**Table 3.6**
**Nonauroral Sources of $O(^1D)$, $O(^1S)$, and $O_2^+$**

| | |
|---|---|
| $O_2 + h\nu(\lambda < 174.9\ nm) \rightarrow O(^3P) + O(^1D)$ | (3.34) |
| $O_2 + h\nu(\lambda <\ nm) \rightarrow O(^3P) + O(^1S)$ | (3.35) |
| $O_2 + h\nu(\lambda < 102.6\ nm) \rightarrow O_2^+ + e_{ph}$ | (3.36) |
| $O_2 + h\nu(\lambda < 66.2\ nm) \rightarrow O_2^+ + O + e_{ph}$ | (3.37) |
| $O_2 + e_{ph} \rightarrow O(^1D) + O + e$ | (3.38a) |
| $\rightarrow O(^1S) + O$ | (3.38b) |
| $O + e_{ph} \rightarrow O(^1D) + O + e$ | (3.39a) |
| $\rightarrow O(^1S) + O$ | (3.39b) |

Reproduced with permission of the copyright owner. Further reproduction prohibited without permission.

### 3.2.2 Hydrogen and Helium Emissions

The presence of hydrogen emissions in dayside aurora is expected due to the large number flux of protons in the penetrating magnetosheath plasma. A proton incident on the atmosphere must charge exchange with atmospheric species to obtain the electron necessary to form neutral hydrogen before photons can be emitted. The neutral atom, no longer constrained to move along the magnetic field, drifts across the field until a collision removes the electron. The proton is repeatedly transformed into hydrogen and back into a proton through a series of collisions leading to a random walk of the proton guiding center from the point of origin [c.f., *Davidson*, 1965; *Johnstone*, 1972]. Hydrogen emissions in the dayside aurorae are rather weak even with the large fluxes of magnetosheath protons found in the cusp. The average energy of a magnetosheath proton is approximately 1 keV which is rapidly lost in a few collisions high in the atmosphere, limiting the number of charge exchange reactions that may take place and hence the number of photons that can be emitted.

The choice of which hydrogen emission to use to monitor for proton precipitation depends on the instrument and the type of aurora. $H_\alpha$ yields are greater than $H_\beta$ but the $H_\alpha$ line is located in a region of $N_2$1PG band emissions which often obscures the hydrogen line in night time aurorae. Erroneous intensities will be obtained if an MSP using interference filters is used to isolate the spectral line in night time aurorae due to contamination from the molecular emission band. The $H_\beta$ emission, although weaker by a factor of 6 to 8 than the $H_\alpha$ emission when produced by approximately 1 keV protons [*Van Zyl et al.*, 1984; *Sigernes et al.*, 1995], is generally chosen for the MSP to monitor proton precipitation in night time aurorae.

The $H_\beta$ 486.1 nm emission is not totally free of contaminating lines. *Eather* [1967] cautioned that photometric observations of the $H_\beta$ 486.1 nm emission requires careful consideration of the background in the vicinity of the Doppler shifted emission line. Numerous bands from molecular nitrogen are found in the 470.0-490.0 nm region, the most troubling of which is the $N_2$VK (2,15) band [*Lofthus and Krupenie*, 1977; *Degen*, 1982]. The baud head is located at 483.6 nm and rotational structure spreads over nearly 10 nm to higher wavelengths. The signal from a photometer must be corrected for the $N_2$VK (2,15) band before $H_\beta$ 486.1 nm observations are meaningful if energetic electrons are present [*Stringer*, 1971; *Romick et al.*, 1974].

*Henriksen et al.* [1985] argue that either the $H_\alpha$ 656.3 nm or $H_\beta$ 486.1 nm emission could in principle be used for dayside studies of proton precipitation in the dayside auroral oval due to the general lack of molecular band contamination but note that if Fraunhofer absorption in scattered solar radiation (which is stronger on the blue end of the spectrum) is present then even the use of $H_\beta$ may be limited. *Eather* [1967] similarly cautions against the use of either $H_\alpha$ or $H_\beta$ observations if scattered twilight or moonlight is present. In either case a spectrometer is more useful than a scanning filter photometer since the complete spectrum is available allowing the Fraunhofer line shape and contributions from weak OH bands to be removed before the hydrogen line shape is analyzed [*Sigernes et al.*, 1995].

Energy deposition due to proton precipitation contributes to populations of excited atomic and molecular species. *Eather* [1968] reported ratios of several common auroral emissions to the

Reproduced with permission of the copyright owner. Further reproduction prohibited without permission.

intensity of $H_\beta$ in auroral displays excited by protons. These values are summarized in Table 3.7. Adopting the range of 10-40 R $H_\beta$ intensities listed in Table 3.1 as typical for dayside aurora, the contributions from proton excitation to atomic and molecular emissions within dayside aurora are also estimated. Contributions to 557.7 nm and 630.0 nm intensities due to protons are on the order of the airglow intensities at these wavelengths (Section 3.2.4).

Photometer records of hydrogen emissions will not be analyzed in detail in this thesis since they are not suitable for identification of particle precipitation boundaries. Spatial information in precipitating proton populations above the atmosphere is quickly removed by the charge exchange process. Numerical simulations of proton injection from point and sheet sources above Svalbard show that sharp boundaries originally present in a proton source will expand over distances of hundreds of kilometers removing the spatial information [*Davidson*, 1965; *Eather*, 1967b; *D. Lorentzen*, unpublished manuscript, 1995]. *Iggesias and Vondrak* [1974] have shown that observations of proton angular distributions within the atmosphere can be used to determine the original arc thickness and proton current intensity but this information must be obtained by satellite and is not available to ground based observers. Lack of information on the spatial distribution of the proton precipitation from the ground is unfortunate since many of the criteria adopted by the satellite community to categorize populations of precipitating particles require the knowledge of proton characteristics (Section 2.7). Further, resolution on the order of 10 km or less is required to identify some of the narrow precipitation regions and the boundaries between them on the dayside. Hydrogen emissions from latitude dispersed proton beams do not carry sufficient information to resolve features this narrow.

Helium emissions are weak but are interesting due to the possibility of their use as an alternative to hydrogen emissions for detecting solar wind plasma penetration into the cusp. Helium within the solar wind is predominantly doubly ionized (Section 2.2) while terrestrial helium within

Table 3.7
**Intensity Ratios Due to Proton Excitation**[1]

| Emission | Ratio[2] | Dayside Intensity[3] (R) | Reference |
|---|---|---|---|
| I(391.4 nm) | 10.0-17.5 | 100-700 | *Eather*, 1968 |
| | 10-100 | 100-4000 | *Omholt*, 1959 |
| I(470.9 nm) | 0.9-1.3 | 9-52 | *Eather*, 1968 |
| I(557.7 nm) | 9.0-12.5 | 90 -500 | *Eather*, 1968 |
| | 4-12 | | *Eather*, 1967a,b |
| I(630.0 nm) | 2.5-3.3 | 25 - 132 | *Eather*, 1968 |
| $N_2$ 1P (6,3) | 1.6 | 16-64 | *Vaisberg*, 1962 |
| $N_2^+$(1,0)M | 5.4-7.3 | 54 - 290 | *Vaisberg*, 1962 |

[1]These results are also summarized in Table 4.21 of *Vallance Jones* [1974].
[2]Relative to $H_{beta}$ I(486.1 nm).
[3]Predicted from ratios assuming I(486.1 nm)=10-40 R.

Reproduced with permission of the copyright owner. Further reproduction prohibited without permission.

the magnetosphere is singly ionized and the different charge states may be used as a tracer of the source region for the auroral particles. Precipitating $He^{++}$ has been detected in aurora by instruments on suborbital rocket flights and satellites [*Reasoner et al.*, 1968; *Axford et al.*, 1972; *Whalen and McDiarmid*, 1968, 1972; *Reasoner et al.*, 1968; 1973; *Sharp et al.* 1974; *Bühler et al.*, 1976; *Moore and Evans*, 1979]. While charge exchange of terrestrial $He^{+}$ may also produce a quantity of $He^{++}$ ions, the relative abundance of $^3He$ to $^4He$ in $He^{++}$ populations sampled within the magnetosphere identifies the source unambiguously as the solar wind [*Bühler et al.*, 1976; *Lind et al.*, 1979]. *Bühler et al.* []1976] first reported the detection of $^3He$ in aurora. The isotopic ratio $^4He/^3He \sim 2950 \pm 250$ was nearly the solar wind value of 2350 rather than the atmospheric value which is 250 times larger than ratios in the solar wind confirming the solar wind source of the precipitating helium. $He^{++}$ precipitating within the dayside cusp and cleft has been identified by *Shelley et al.* [1976] from low altitude satellite measurements and *Carlson and Torbert* [1980] using rocket borne instrumentation providing further evidence for solar wind plasma penetration into the dayside ionosphere. Further evidence that $He^{++}$ precipitates with $H^{+}$ from the solar wind was obtained by *Burch et al.* [1982] who showed that both light ions in the polar cusp exhibit a characteristic "V"shaped energy dependent pitch angle dispersion as well as a latitude dependent energy dispersion consistent with ions injected into the magnetosphere from the magnetosheath (Section 2.6.4).

Initial ground based attempts to detect optical emissions from precipitating helium in night time aurora were unsuccessful [*Eather*, 1967, 1968; *Reasoner et al.*, 1968] although *Stoffregen* [1969] later reported observation of the [HeI] 587.6 nm line as evidence for the presence of helium in a very bright night time aurora. *Reasoner* [1973] however concluded that the report was doubtful since the observations were limited to emission profiles from the horizon. Comparison of Doppler shifted zenith profiles to Doppler broadened horizon profiles are required to unambiguously determine if the emissions are the result of precipitating particles instead of geocoronal or extraterrestrial sources [*Eather*, 1966]. Later attempts by *Sears* [1975] to observe the 587.6 nm line from neutral helium in night time aurora similarly failed to obtain evidence for auroral helium emissions.

Interest in detecting helium from ground based optical observations has been revived in recent years in the context of identifying magnetosheath plasma within the dayside ionosphere. Observation of helium optical emissions within the dayside aurora are difficult due to the low emission rates [*Henriksen et al.*, 1978; 1985]. The solar wind alpha particles must gain at least one electron before they can be detected by optical emissions. *Reasoner et al.* [1968] calculated that a beam of 200 keV alpha particles which is 100% $He^{++}$ above altitudes of approximately 400 km will result in approximately 36% $He$ and 60% $He^{+}$ at 150 km. Optical transitions in either the neutral or singly ionized helium are available in the visible spectrum for ground based monitoring but studies to date have focused on the neutral atom. *Sivjee et al.* [1980] identified the HeI 388.9 nm and HeI 587.6 nm emission lines in spectra of dayside aurora with Doppler shifts less than 0.3 nm implying average energies for the precipitating $He^{+}$ of less than 8 keV. The $He^{+}$ ions, if solar wind in origin, must have been formed by previous charge exchange of $He^{++}$ with atmospheric species. Excited $He^{+}$ ions from the conjugate hemisphere was discounted as a source since photoionization will produce ions at energies of tens of electron volts while the excitation cross section required

Reproduced with permission of the copyright owner. Further reproduction prohibited without permission.

to produce the excited helium are quite small below 1 keV. *Henriksen et al.* [1985] showed the HeI 388.9 nm feature is found throughout the midday period with intensities correlated with the solar depression angle. Periodic enhancements in the intensity are superimposed on a smoothly varying component suggesting two sources of the emission. The periodic intensity enhancements are likely due to solar wind $He^+$ precipitation while resonance scattering of sunlight from terrestrial $He^+$ produces the smoothly varying component. None of the dayside studies compared zenith with horizon (or other off zenith) profiles to test if the profiles passed the Doppler shifted zenith/Doppler broadened horizon test required to identify the source as particle precipitation. The small Doppler shifts reported by *Sivjee et al.* [1980] were on the order of the wavelength resolution of the instrument and differences between zenith and horizon profiles would have been difficult or impossible to detect. Measurements of electron and ion distributions in the dayside region by *Kremser and Lundin* [1990] have shown that $He^{++}$ of magnetosheath origin is localized in the cusp but is not detected in the plasma mantle or the low latitude boundary layer. It would appear than further work on detecting helium emissions from ground based observations is warranted due to the possibility of obtaining a unique optical signature of the cusp.

### 3.2.3 Molecular Band Emissions

The $N_2VK$ band, a common feature of the night time aurorae, is usually weak [*Deehr et al.*, 1980] or absent [*Sivjee et al.*, 1981; *Sivjee*, 1983b] in dayside aurorae. Photons of the $N_2$VK bands are emitted if the $N_2(A^3\Sigma_u^+)$ state required for the energy transfer reaction producing $O(^1S)$ at low altitudes (Equation 3.20) decays radiatively to $N_2(X^1\Sigma_g^+)$. Relatively low concentrations of $N_2(A^3\Sigma_u^+)$ will be produced at high altitudes due to the lack of a significant $N_2$ source and few electrons with sufficient energy to penetrate to low altitudes are thought to precipitate within the cusp. Reports of 557.7 nm emissions observed during dayside "breakup" events have been interpreted as evidence for acceleration of electrons to energies greater than 1 keV [*Sandholt et al.*, 1989, 1990] posing an interesting problem: why are the $N_2VK$ bands not observed during these events? A partial resolution of this problem may be found by considering that the radiative lifetime of $N_2(A^3\Sigma_u^+)$ is approximately 2 seconds [*Shemansky*, 1969]. If formed at low altitudes by accelerated electrons accompanying the dayside breakup events, $N_2(A^3\Sigma_u^+)$ may be efficiently quenched through reaction 3.20 producing $O(^1S)$ and 557.7 nm photons but only limited quantities of $N_2VK$ photons, consistent with the note by *Sivjee* [1983b] that $N_2VK$ emissions are observed in mixtures of long-rayed and cusp aurorae. Reports of weak $N_2 2P$ emissions from dayside aurora [*Sivjee*, 1976; *Vlaskov and Henriksen*, 1985] are consistent with this picture since the average lifetime against radiative decay of the $N_2 2P$ bands are on the order of 50 ns [*Nicholls*, 1969], much less than the $N_2VK$ transition reducing the effect of quenching. It should also be noted that observation of 557.7 nm photons does not necessarily require an accompanying emission of the $N_2VK$ band. $O(^1S)$ can be produced by low energy electrons at altitudes greater than the typical peak 557.7 nm emission altitude near 110 km for energetic electrons although at reduced rates. If $O(^1S)$ is formed directly by electron impact at high altitudes where atomic oxygen dominates over molecular nitrogen, little $N_2(A^3\Sigma_u^+)$ is expected to be formed and weak 557.7 nm emissions

Reproduced with permission of the copyright owner. Further reproduction prohibited without permission.

may be observed without an accompanying $N_2VK$ signal. Finally, it may well be that the lack of reports of $N_2VK$ emission bands associated with energetic electron events in dayside aurora is simply the result of the lack of any concerted effort to detect the emissions.

Acceleration events may result in strong molecular band emissions even within a few hours of magnetic noon. A record in my field notes from November 1991 describes an arc at approximately 0600 UT (0930 MLT) observed from Longyearbyen with a pink lower border, a phenomenon attributed to strong emissions of the $O_2^+1N$ and $N_2 1P$ systems [*Shemansky and Vallance Jones*, 1968] which requires electron penetration to altitudes below 95 kilometers [*Gattinger et al.*, 1985].

The $(N_2^+)1NG$ (0-1) 427.8 nm and $(N_2^+)1NG$ (0-0) 391.4 nm emission bands are strong compared to other molecular emissions throughout the midday region. The excited $B^2\Sigma$ parent state decays by an electric dipole transition with characteristic lifetimes on the order of $10^{-6}$ seconds allowing the state to relax radiatively even at altitudes where the $O(^1S)$ state is quenched. *Vallance Jones* [1974] lists a quenching altitude of approximately 48 km for $(N_2^+)1NG$ compared to 95 km for $O(^1S)$ . Since energy deposition by very energetic auroral electrons rarely occurs below 60-85 km, the altitudes over which pink lower auroral borders are observed [*Störmer*, 1955; *Shemansky and Vallance Jones*, 1968; *Vallance Jones*, 1974], the ionized nitrogen bands in aurora are essentially unquenched. Resonance scattering of sunlight may account for appreciable fractions (or even dominate) the signal observed at 391.4 nm and 427.8 nm when the upper atmosphere is sunlit, a common condition for northern hemisphere dayside observations where the proximity of ground stations to the terminator results in shadow heights below 300-400 km. The Swings effect [*Swings*, 1949] has been found in spectroscopic measurements of the $N_2^+(1NG)$ band at Svalbard providing direct evidence for resonance scattering of solar photons [*Deehr et al.*, 1980; *Sivjee and Deehr*, 1980; *Sivjee*, 1983a; *Degen*, 1987]. Estimates of the resonance scattering contribution to the 427.8 nm band include 25% [*Degen*, 1987], 75% *Deehr et al.* [1980], 83% by *Link et al.* [1983], and the range of 10% to 50% by *Lanchester and Rees*, [1987]. In cases there the resonance scattering contribution can be removed from sunlit aurorae the 427.8 nm signal can be used to obtain an estimate of the total energy deposition rate [c.f., *Lanchester and Rees*, 1987]. Estimates of the brightness of the 427.8 nm emission for unit energy influx from precipitating electrons vary from 200 R/erg cm-2 sec-1 to 300 R/erg cm-2 sec-1 [*McEwen and Venkatarangan*, 1978; *Christensen et al*, 1987; *Steele and McEwen*, 1990].

A beneficial aspect of the presence of resonance scattering from aurorally produced $N_2^+$ is the additional strength of the 427.8 nm signal. The presence of precipitating electrons may be indicated even in situations where the electron number or energy flux would otherwise result in weak or undetectable 427.8 nm signals. Consider that the electron energy flux within the midday aurora is typically on the order of $0.1 - 1.0$ erg/cm$^2$ s predicting a 427.8 nm emission of 20-200 R (see Section 3.2.5). Based on the reports that resonance scattering contributes 25% to 83% of the total observed 427.8 nm signals within dayside aurora, predicted intensities including resonance scattering may range from a modest 24 R to and extreme of 800 R.

### 3.2.4 Airglow

Reproduced with permission of the copyright owner. Further reproduction prohibited without permission.

Airglow emissions from the OH molecule and free sodium are also present in dayside auroral spectra obtained from the ground but are not listed in Table 3.1 since they are ubiquitous to the mesosphere and do not result from auroral excitation. These emissions originate at altitudes of approximately 80 km to 110 km in the case of sodium and 85 km to 95 km for the hydroxyl molecule [c.f., *Kirchhoff*, 1986, *Abreu and Yee*, 1989; *Viereck*, 1991]. The OH emission intensity in the dayside region, which may reach values of 400-1000 R in the near infrared [*Gault et al.*, 1981], and the Na 589.0-9.6 nm emission intensity, approximately 35 R [*Gault et al.*, 1981] are often significant fractions of (or even equal to) the weaker atomic emissions originating from auroral excitation. Detailed analysis is often required to remove the OH contributions before meaningful consideration of weak features in auroral spectra is possible.

The $H_\alpha$ 656.3 nm, [OII] 732.0 nm, [OI] 630.0 nm and [OI] 557.7 nm lines all are located in spectral regions with OH emission lines [c.f., *Chamberlain*, 1961; *Krassovsky et al.*, 1962]. Components of the OH (9,3) band at 628.7 nm, 629.8 nm and 630.7 nm may contaminate measurements of a weak 630.0 nm emission when a wide bandpass filter is used to isolate the emission line [*Broadfoot and Kendall*, 1968]. Airglow studies by *Hernandez* [1974b] and *Burnside et al.*, [1977] show that the OH contribution to intensity measurements at 630.0 nm is less than 10% if the instrumental bandwidth is less than 0.5 nm and the 630.0 nm intensity is greater than 20 R. This condition is easily satisfied by the MSP using a 0.4 nm bandpass 630.0 nm filter when observing dayside aurora where I(630.0 nm) is typically on the order of $10^3$ R and airglow backgrounds are rarely less and 100-200 R. The 557.7 nm region contains lines from the OH (7,1) band at 556.2 nm and 559.0 nm [*Krassovsky et al.*, 1962; *Broadfoot and Kendall*, 1968] but the line OH lines are sufficiently removed from the green auroral line to contribute to the transmitted signal in the 558.0 nm/0.4 nm filter in use at Longyearbyen as long as the angles selected for the background position on the MSP is not over 5° -6° from the peak position. Even in a case where the background position is selected near the 556.2 nm line the reduction in filter transmission should reduce the effect of a weak airglow line in comparison to a strong 557.7 nm emission line. In the author's experience the minimum intensity of the 630.0 nm at 557.7 nm lines at Longyearbyen rarely are less than 100 R to 200 R (and then only at night) eliminating any concern for significant OH contribution to the auroral oxygen lines. The strong OH emissions reported by *Gault et al.* [1981] are a possible source of background for the white light television cameras although the effect is limited by the reduced sensitivity of the camera in the near infrared. None of the emission lines monitored by the MSP are located in the near infrared avoiding the complication of the strong OH emissions. One exception is the [OII] 732.0 nm emission which is occasionally monitored for which the OH (8,3) band may contribute as much as 400 R [*Gault et al.*,1981].

[OI] 630.0 nm and [OI] 557.7 nm emissions are also found in airglow layers produced by chemical reactions listed in Table 3.2.6 and discussed in Section 3.2.1. [OI] 557.7 nm emissions peak in two layers, the lower occurring at approximately 97 km with a half width of 8 km [*Yee and Abreu*, 1987] and an upper layer in the F-region. Typical 557.7 nm and 630.0 nm column emission rates are on the order of $10^2$ R in the nightglow while twilight intensities of the 630.0 nm emission may reach values of 500 – 1000 R [*Chamberlain*, 1961; *Broadfoot and Kendall*, 1968].

Reproduced with permission of the copyright owner. Further reproduction prohibited without permission.

### 3.2.5 Excitation Efficiencies and Emission Ratios

Ratios of spectral emissions are powerful tools for auroral studies since they allow the determination of characteristics of the primary particle flux from ground based observations [*Rees and Luckey*, 1974]. Spectral ratios have been widely used to classify types of auroral emissions and to relate the auroral features to particle precipitation regions as observed by polar orbiting satellites.

Column intensities of auroral 427.8 nm, 630.0 nm, and 557.7 nm emissions produced by electron impact have been determined from auroral models. Output from these models are used to determine emission rates as a function of the average energy and energy flux of the precipitating electrons. *Rees and Roble* [1986] obtained the equations

$$\frac{4\pi I(427.8nm)\,kR}{ergcm^{-2}s^{-1}} = .213E_0^{0.0735} \qquad 0.1 < E_0 < 2.0\,keV \tag{3.40}$$

$$\frac{4\pi I(630.0nm)\,kR}{ergcm^{-2}s^{-1}} = 0.42E_0^{-0.9} \qquad 0.1 < E_0 < 2.0\,keV \tag{3.41}$$

which have been widely used to estimate 427.8 nm and 630.0 nm emission rates or determine energy and energy flux from measurements of emission intensities. The equation

$$\frac{4\pi I(557.7nm)\,kR}{ergcm^{-2}s^{-1}} = 1.4E_0^{-0.2} \qquad 0.5 < E_0 < 2.0\,keV \tag{3.42}$$

for the 557.7 nm emission was obtained by *Rees et al.* [1988]. The characteristic energy $E_0$ and energy flux $\epsilon$ are defined in terms of the energy spectra of the incident electrons. An example is a Maxwellian of the form

$$N(E)dE = N_0 E e^{-E/E_0} dE \tag{3.43a}$$

with a total electron number flux

$$F = N_0 E^2 electrons\,cm^{-2}s^{-1} \tag{3.43b}$$

and total energy flux

$$\epsilon = 2EF erg\,cm^{-2}s^{-1}. \tag{3.43c}$$

The equations relate the total light output along a field line due to the energy deposited in the neutral atmosphere by a precipitating electron population with a given characteristic energy and energy flux. The column intensities are obtained from integration of the volume emission rates along the magnetic field. Equations (3.40)-(3.42) are not valid for integrated emission rates at elevation angles other than the local magnetic zenith. The use of a Maxwellian energy distribution is not crucial, experience from auroral modelling has shown that the results are relatively insensitive to the exact form of the primary electron spectrum. Gaussian, anisotropic, and other non-Maxwellian spectra yield different altitude profiles of the optical emissions, but the emission integrated along the field line yields similar results [*Christensen et al.*, 1987; *Lummerzheim et al.*, 1990].

Reproduced with permission of the copyright owner. Further reproduction prohibited without permission.

Determination of the characteristic energy from equations (3.40)-(3.41) requires the elimination of the energy flux to yield the equations

$$\frac{I(630.0\ nm)}{I(427.8\ nm)} = 1.97E_0^{-0.9735} \qquad 0.1 < E_0 < 2.0\,keV \tag{3.44}$$

$$\frac{I(630.0\ nm)}{I(557.7\ nm)} = 0.33E_0^{-0.7} \qquad 0.5 < E_0 < 2.0\,keV \tag{3.45}$$

Application of equations (3.40) - (3.45) to auroral emissions with the intent to obtain quantitative estimates of incident energy fluxes aud characteristic energies requires careful consideration of a number of important assumptions that are made in development of the auroral models. Equations (3.40) and (3.41) are obtained from fitting curves to column intensities obtained from an auroral model as a function of characteristic energy and energy flux *Rees and Roble* [1986]. These equations are strictly only applicable to auroral displays which form under the same conditions assumed for the model aurora. *Rees and Luckey* [1974] and *Rees and Roble* [1986] note that equations (3.40), (3.41), and (3.44) are not generally applicable if aurorae is either illuminated by sunlight or if large populations of suprathermal electrons are present as neither effect was included in the auroral model used to obtain the equations. Resonance scattering, as already noted in Section 3.1.3, may account for appreciable fractions of the observed 427.8 nm signal in dayside aurora observed at Svalbard due to the proximity of the midday oval to the terminator requiring special analysis of the photometer records to remove the effect [c.f., *Deehr et al.*, 1980; *Link et al.*, 1983; *Lanchester and Rees*, 1987]. Low energy electron precipitation resulting in strong heating such that a fraction of the ambient electron gas will have sufficiently large energies (> 1.96 eV) to become an excitation source of the $O(^1D)$ state. Calculations by *Mantas and Walker* [1976] suggest that this mechanism may account for much of the enhanced 630.0 nm emissions when the dominant particle source is soft electrons. Equation (3.41) cannot be used in quantitative work when electron heating is present without including the contribution to the total energy flux due from the hot electrons [*Rees and Roble*, 1986].

The use of equations (3.42) and (3.45) requiring I(557.7 nm) is problematic due to the strong dependence of the 557.7 nm photon yields on the composition of the neutral atmosphere. Large variations in 557.7 nm column intensities may be obtained for a given input particle energy distribution. Uncertainties in the chemistry of $O(^1S)$ production leads to uncertainties in the output from auroral models. Unlike equations (3.40) and (3.41) which were obtained from models, *Rees et al.* [1988] obtained equation (3.42) empirically by comparing photometer observations of magnetic zenith 557.7 nm intensity against values of characteristic energy and energy flux derived from equations (3.40) and (3.41). The large variability in the I(557.7 nm) values in the data set resulted in poor statistical fits limiting the use of equation (3.42) and (3.45) for quantitative work [*D. Lummerzheim*, personal communication, 1995].

A further complication arises if there is significant transport of excited species. The models used to derive the column intensities in Equations (3.38-3.43) neglected transport assuming that all sources of excited species through electron impact or chemical reactions and all losses through radiation or quenching must occur on the same field line. Diffusion in latitude and neutral winds

Reproduced with permission of the copyright owner. Further reproduction prohibited without permission.

act as either additional sources or losses of excited atoms which are not included in the models. The excited $O(^1D)$ , due to its long lifetime, is especially prone to intensity variations due to transport.

Finally, auroral models used to obtain relationships between input electron energy input and optical emission output are either (1) equilibrium models or (2) time dependent but run for sufficiently long periods that all of the excited species have obtained equilibrium. Application of the ratios assumes, therefore, that the aurorae in question is in equilibrium. Electron sources which move rapidly or have rapid temporal variations rarely allow the concentration of metastable species to reach equilibrium and the emission ratios will be time dependent [*Rees and Jones*, 1973], limiting the quantitative application of the ratios in equations (3.44) and (3.45) in these cases [*Vallance Jones et al.*, 1987]. An alternative technique proposed by *Christensen et al.* [1987] is to use early time values from auroral models thereby neglecting the contributions from slow reactions.

An alternative technique to auroral modelling is to use empirical values for excitation efficiencies (the brightness of an emission per unit energy flux) based on observations of incident electron fluxes with simultaneous observations of auroral emission rates. *Steele and McEwen* [1990] obtained the values

$$I(557.7\ nm) = 1.23\ kR/ergcm^{-2}s^{-1} \quad E_e = 1.8keV \tag{3.46a}$$

$$= 1.73\ kR/ergcm^{-2}s^{-1} \quad E_e = 3.1keV \tag{3.46b}$$

from measurements of incident electron fluxes from satellites and simultaneous ground based optical observations of auroral emissions. Equation (3.46a) compares favorably with the *Rees et al.* [1988] model results summarized by equation (3.42) and (3.46b) differs by a factor of 1.5. Using simultaneous records from the soft particle spectrometer and the 630.0 nm photometer on the ISIS 2 spacecraft, *Shepherd et al.* [1980] obtained the values

$$I(630.0\ nm) = 1120 \pm 263\ R/ergcm^{-2}s^{-1} \quad 5 - 60eV \tag{3.47a}$$

$$= 1520 \pm 84\ R/ergcm^{-2}s^{-1} \quad 60 - 300eV \tag{3.47b}$$

$$= 277 \pm 22\ R/ergcm^{-2}s^{-1} \quad 0.3 - 1keV \tag{3.47c}$$

$$= 14.3 \pm 1.2\ R/ergcm^{-2}s^{-1} \quad 1 - 10keV \tag{3.47d}$$

for the 630.0 nm excitation efficiencies. Comparison with the *Rees and Roble* [1986] results in equation (3.41) indicate the model results predict lower 630.0 nm yields than the empirical results by factors of 5-10 for electron energies less than 1 keV and greater yields than the empirical results by factors of 15-30 for energies greater than 1 keV.

### 3.2.6 Classification of Dayside Aurorae Based on Emission Ratios

Even with the caveats presented in the previous section, emission rates and intensity ratios do provide a convenient qualitative method to classify types of dayside auroral emissions. Hard zone electrons are sufficiently more energetic than soft zone electrons that strong differences exist

Reproduced with permission of the copyright owner. Further reproduction prohibited without permission.

in ratios of spectral features in the two regions. Ratios of spectral emissions may therefore be used as a diagnostic tool to determine precipitation regions from optical observations. Sharp latitudinal gradients in electron precipitation produce pronounced boundaries in auroral luminosity that may be used to identify the edges of the electron precipitation regions.

A number of schemes have been described using ratios and absolute intensities of auroral emissions to classify particle precipitation zones in the dayside ionosphere. Auroral forms in the dayside auroral oval are characterized by enhancements in the ratio of I(630.0 nm) to I(427.8 nm) by nearly an order of magnitude over typical nightside aurorae [*Eather and Mende*, 1971] due to the intense fluxes of low energy electrons ($E \sim 100-200eV$) and protons ($E \sim 1keV$) which precipitate in the high-latitude midday region *Heikilla and Winningham* [1971]. The I(630.0 nm)/I(427.8 nm) ratio can be used to identify distinct regions of electron precipitation [c.f., *Eather and Mende*, 1971, *Romick and Brown*, 1971]: (i) a region equatorward of the auroral oval where electrons of energy $> 1-3$ keV produced emissions with the ratio I(630.0 nm)/I(427.8 nm) $< 1.$; (ii) the region of the cusp or cleft where precipitation of low energy magnetosheath electrons produce aurora dominated by 630.0 nm emissions with very large I(630.0 nm)/I(427.8 nm) ratios. *Sandholt* [1988] suggested that dayside aurora may be further subdivided into four categories utilizing the I(630.0 nm) to I(557.7 nm) spectral ratio and the location of the emissions within the dayside auroral oval. The scheme is reproduced in Table 3.8 to demonstrate the variety of emission ratios found in the midday period.

Table 3.8
Classification of midday aurorae [from *Sandholt*, 1988]

| Category | Spectral Ratio $\frac{I(630.0nm)}{I(557.7nm)}$ | Latitudinal Location | Electron Energy | Plasma Source |
|---|---|---|---|---|
| 1 | $< 1$ | Poleward of cusp | ~1 keV | plasma mantle? |
| 2 | $> 2$[1] | Cusp | <200 eV[1] | magnetosheath |
| 3 | $> 1$ | Equatorward of Cusp | 0.2-1 keV | LLBL |
| 4 | $< 1$ | Equatorward of Cleft | 1-10 keV | plasmasheath |

[1]Transient increases in the 557.7 nm emission may temporarily yield ratios $< 2$.

The choice of which emissions to monitor with the MSP is determined primarily by the scientific question that is to be addressed although practical considerations also constrain the possible choices. The interest here is not only to obtain records of auroral distribution and intensity for which monitoring any bright emission would suffice, but to use the auroral emissions to estimate properties of the precipitating particles from which the magnetospheric source regions can be inferred. The ideal situation would be to monitor a set of emissions providing sufficient information to unambiguously identify the polar cusp, boundary layers, radiation belts, and polar cap. Unfortunately, not only has an unambiguous optical identification of the longitudinal boundaries of the cusp never been found [*Eather et al.*, 1979] mapping particle precipitation patterns from the ionosphere to the magnetosphere is still a controversial topic due to mixing of particle types due

Reproduced with permission of the copyright owner. Further reproduction prohibited without permission.

to time-of-flight effects which effect low energy particles [c.f. *Sergeev*, 1990; *Lockwood and Smith*, 1993; *Newell and Meng*, 1993; *Smith*, 1994].

*Sivjee and Hultqvist* [1975] compared ESRO satellite particle measurements with simultaneous airborne photometric observations of midday aurora to show that photometric measurements of 630.0 nm and 557.7 nm emissions in the magnetic noon sector are sufficient to map the particle precipitation regions occurring in the vicinity of the cusp due to the energy sensitivity of the emissions as indicated by equations (3.41), (3.42), and (3.45). In contrast, *Eather et al.* [1979] have adopted the criteria that an enhanced I(630.0 nm)/I(557.7 nm) ratio indicative of soft electron precipitation concomitant with an $H_\beta$ 486.1 nm signal indicating the presence of proton precipitation is required for an identification of the cusp. *Sivjee and Hultqvist* [1975] argue that the proton emissions are useful extra information as long as signals from the high energy protons drifting in the outer radiation belts through the dusk into the noon sector can be clearly separated from the low energy magnetosheath protons.

Ground based photometer and camera systems can, at best, only provide the same information on the origin of precipitating particles as satellites or rockets equipped with charged particle detectors. The advantage of using the ground based optical instruments is the continuous monitoring capability in both space and time in contrast to the snapshots in time obtained along satellite or rocket trajectories during overflights of an area of interest. However, ground based observations at the current time cannot even provide the same detailed information as satellites since the spatial information in precipitating protons due to the charge exchange process is lost once the proton beam enters the atmosphere and the pitch angle information that may obtained from charged particle detectors cannot be determined from the auroral emissions. Emissions that yield information related to precipitating electron average energy and total energy flux are therefore emphasized for the MSP. The traditional choice for auroral studies has been to monitor at least the green [OI] 557.7 nm and red [OI] 630.0 nm emissions, the $(N_2^+)$1NG 427.8 nm band, and a hydrogen emission, generally $H_\beta$ 486.1 nm. These emissions have been measured at the field site from 1979 to the present. The atomic oxygen lines are sensitive to the energy of the primary electron stream due to the wide difference in their lifetimes and are therefore useful to provide a qualitative estimate of characteristic energies and energy fluxes of the precipitating particles. The ionized molecular nitrogen emission is prompt and depends only on the incident energy flux. It is traditionally favored over the 557.7 nm emission since the lack of complicated chemical sources allows the physics of its excitation to be readily quantified. As noted in Section 3.1.3 the presence of resonance scattering complicates its use in dayside studies so the 557.7 nm emission will be used here in its place. The hydrogen emission is used to monitor for proton precipitation.

### 3.3 Morphology of Dayside Aurora

The spectral content of auroral emissions is but one set of diagnostics of use to studies of aurorae. The distribution, morphology, and behavior of auroral emissions are an important source of information that may be used to determine possible magnetospheric sources of precipitating particles which excite the auroral emissions. In addition, the behavior of temporal and spatial

Reproduced with permission of the copyright owner. Further reproduction prohibited without permission.

characteristics of auroral emissions may be used to infer characteristics of the physical processes which result in particle precipitation.

### 3.3.1 Large-scale Distribution of Aurorae and the Geomagnetic Field

Scientists of the $18^{th}$ and $19^{th}$ centuries accepted the concept of the aurorae occurring in a circular ring surrounding the polar region. Early polar expeditions found that the maximum frequency of appearance occurred over a wide range of longitudes at some distance from the north pole suggesting the ring distribution. (c.f., the historical accounts of auroral science by *Chapman* [1967, 1969] and *Brekke* [1984]). It was not until the 1957-1958 International Geophysical Year with the establishment of numerous field stations throughout the polar regions that instantaneous records of auroral activity were routinely obtained at widely different local times. Examination of these records firmly established two important features of the global auroral distribution. First, aurora is found instantaneously at all local times in a region surrounding the magnetic poles termed the "auroral oval." Second, the size of the region varies with magnetic activity establishing that the distribution of auroral activity is controlled by the geomagnetic field [*Khorosheva*, 1961; *Feldstein*, 1964a,b, 1967; *Feldstein and Starkov*, 1967]. The link between auroral activity and the Earth's magnetic field geometry was further illuminated when *Feldstein and Starkov* [1970] found that daily variations in auroral latitude in relation to a fixed ground station results from diurnal variations of the magnetic dipole axis with respect to the ecliptic plane.

Images of auroral emissions obtained from satellites have demonstrated that the auroral ovals in the northern and southern hemispheres are not completely symmetric. The instantaneous distribution of aurora in the southern hemisphere can be approximated by a circle offset from the magnetic pole by 3° -5° from the sun [*Holzworth and Meng*, 1975; *Meng et al.*, 1977] while the aurora in the northern hemisphere, similarly offset, is distorted into an ellipse. The hemispheric asymmetry in the shape of the auroral oval is due to the geometry of the magnetic field. Magnetic field geometry is largely dipolar in the southern hemisphere at auroral altitudes than the northern hemisphere where the nondipolar contributions from the outer magnetosphere are more significant. The result of this hemispheric difference in the structure of the magnetic field can be seen in the lines of constant magnetic latitude. They are nearly circular in the southern hemisphere while they are ellipses in the northern hemisphere [c.f., Appendix 10 of *Akasofu and Chapman*, 1972]. Variations in the latitude of the auroral oval observed at a ground site are due to the combined effects of diurnal variations due to the constant antisolar offset of the auroral oval from the geomagnetic pole [*Eather et al.*, 1979; *Eather*, 1984; *Akasofu*, 1978] as well as variations produced by expansion and contraction of the auroral oval due to changes in geomagnetic field geometry due to erosion of flux from the dayside magnetosphere and generation of field perturbations by substorm current [*Starkov and Feldstein*, 1967; *Akasofu*, 1972; *Sandholt et al.*, 1985].

*Starkov and Felstein* [1967] analyzed all sky camera images of aurora from Svalbard and showed that the latitude of the dayside emissions moved equatorward during periods of high magnetic activity. Images from South Pole Station analyzed by *Akasofu* [1972] exhibited the same behavior and were interpreted as observational evidence supporting the *Dungey* [1961] reconnection

Reproduced with permission of the copyright owner. Further reproduction prohibited without permission.

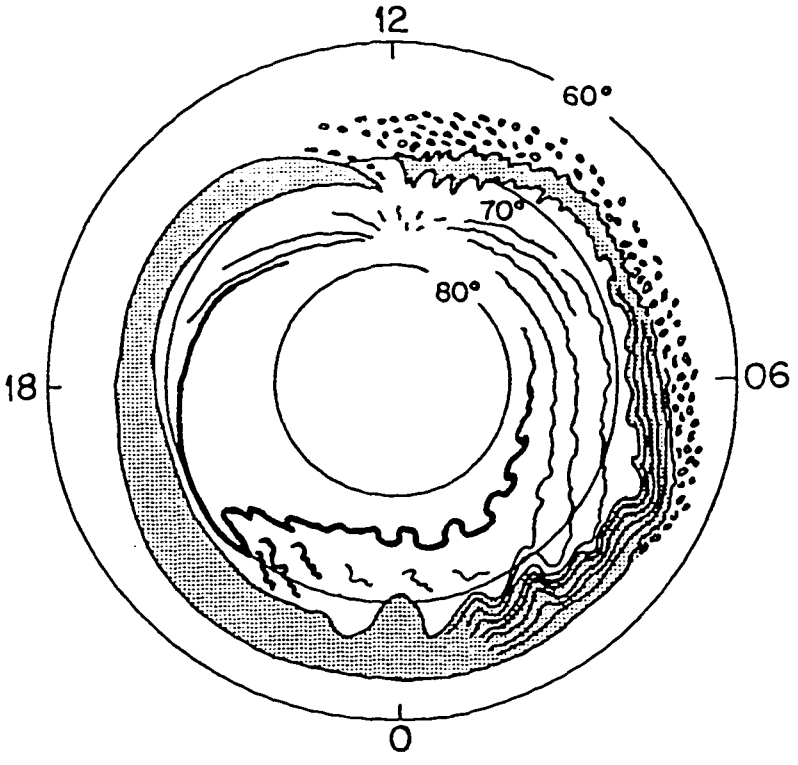


Figure 3.1 Global distribution of auroral forms. The schematic is from *Akasofu* [1976] and is the synthesis of many DMSP images. Discrete arcs are found on the poleward edge of the auroral oval while a broad region of diffuse aurora (shaded) is found at lower latitudes at all local times.

model. This view was supported when *Aubrey et al.* [1970] reported satellite observations of an inward motion of the magnetopause following the turning of the IMF $B_z$ component from northward to southward. Cusp motion has been shown to correlate with the IMF $B_z$ component, further supporting the interpretation that motion of the dayside auroral oval is due to erosion of magnetic flux from the dayside magnetosphere [*Pike et al.*, 1974; *Horwitz and Akasofu*, 1977; *Burch*, 1979]. Current systems associated with substorm activity has also been suggested as a possible mechanism to reduce the latitude of the dayside auroral oval [*Eather et al.*, 1979]. There has been some disagreement over the mechanism responsible for the equatorial shift of the cusp. One set of studies favor dayside merging as the cause of equatorward cusp shifts due to close correlations with the IMF $B_z$ component [*Burch*, 1973; *Meng*, 1983; *Sandholt et al.*, 1983, 1985, 1986]. Alternatively, a number of investigations have concluded that cusp latitude is more closely correlated with the AE index rather than the IMF suggesting the motion is due to current systems forming due to substorm activity [*Eather et al.*, 1979; *Eather*, 1984, 1985; *Mende et al.*, 1979]. A resolution of the controversy was given by *Carbury and Meng*, 1986] by showing that cusp latitude correlates well with both the AE index and the IMF $B_z$ component but that careful elimination of one or other effect is required to determine the primary effect which is due to the IMF $B_z$ component.

Reproduced with permission of the copyright owner. Further reproduction prohibited without permission.

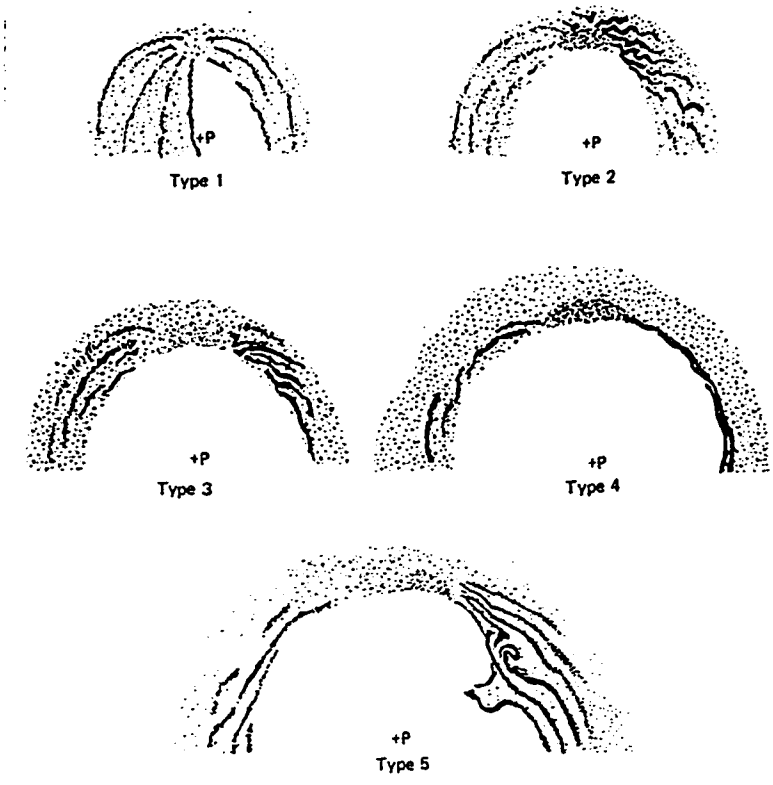


Figure 3.2 Global distribution of auroral forms for increasing levels of geomagnetic activity. The schematic is derived from examination of DMSP images [from *Meng and Lundin*, 1976].

### 3.3.2 Distribution of Dayside Auroral Emissions

Dayside auroral emissions are always present even if there is little significant nightside auroral activity [*Lassen*, 1967, 1970]. This observation is consistent with the model that dayside aurora is the result of a continuously active process which couples solar wind energy into the dayside magnetosphere. In contrast, nightside aurora which maps to the outer boundary of the plasma sheet [*Lassen*, 1974] results from intermittent processes producing active displays during the substorm cycle from energy stored in the magnetotail [c.f., *Akasofu*, 1968; 1977; *McPherron et al.*, 1973; *Baker et al.*, 1996]. Although the numerous models proposed for the substorm process leading to the auroral displays in the night time sector may conflict on some very important points, they do at least agree that the process is the result of the growth of some form of instability in the geotail region leading to catastrophic loss of energy from the distorted tail configuration. This process may occur when the IMF $B_z$ component is oriented either northward or southward if there is sufficient energy stored in the tail. In fact, it has been established that substorms form after the IMF $B_z$ has been negative for some period allowing excess magnetic flux and particles to accumulate in the magnetotail [*Rostoker et al.*, 1983] The trigger for the substorm onsets may be a reduction in the southward component of the IMF or a complete northward turning [*Caan et al.*, 1975; *Samson and Yeung*, 1986; *Lyons*, 1996] or compression of the magnetosphere by solar wind shock waves

Reproduced with permission of the copyright owner. Further reproduction prohibited without permission.

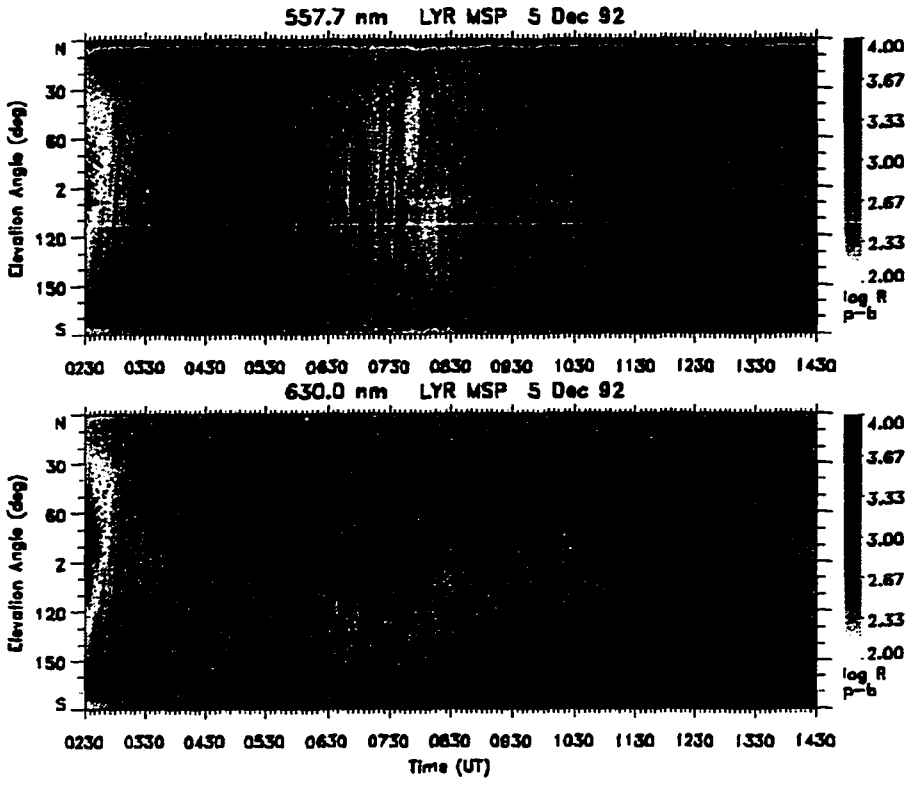


Figure 3.3 Photometer records of dayside aurora. The 557.7 nm and 630.0 nm emissions are plotted.

[*Kokubun et al.*, 1977]. In contrast, the dayside aurora appears to be driven by a direct coupling between the solar wind and the magnetosphere. An immediate equatorward shift of the dayside auroral oval occurs when the IMF $B_z$ component turns southward [*Feldstein and Starkov*, 1967] due to flux erosion at the dayside magnetopause and the latitude of the dayside aurora has been shown to correlated closely with the orientation of the IMF [*Eather*, 1985; *Carbury and Meng*, 1986].

Satellite images of aurora in the dawn and dusk sectors show that the dayside arc systems are not necessarily continuous with the nightside systems suggesting the current systems responsible for the two regions of the auroral oval arise from different sources in the magnetosphere [*Akasofu and Kan*, 1980]. The gap between the dayside and nightside arc systems is most clear in the afternoon sector. In cases where it is possible to clearly distinguish the two systems, the dayside arcs lie equatorward of the nightside arc system. *Akasofu and Kan* [1980] suggest that the dayside arc systems are associated with field-aligned currents fed by the low-latitude boundary layer dynamo while the nightside arc systems are associated with field-aligned currents fed by the magnetotail dynamo.

ISIS [*Cogger et al.*, 1977] and DMSP satellite images show that a gap in discrete dayside arcs occurs in the noon sector [*Dandekar and Pike*, 1978; *Dandekar*, 1979]. The term "midday gap" was applied to the lack of discrete forms only. Auroral forms dominated by 630.0 nm emission observed during airborne photometric observations of the midday aurora [*Buchau et al.*, 1970; *Heikilla et al.*,

Reproduced with permission of the copyright owner. Further reproduction prohibited without permission.

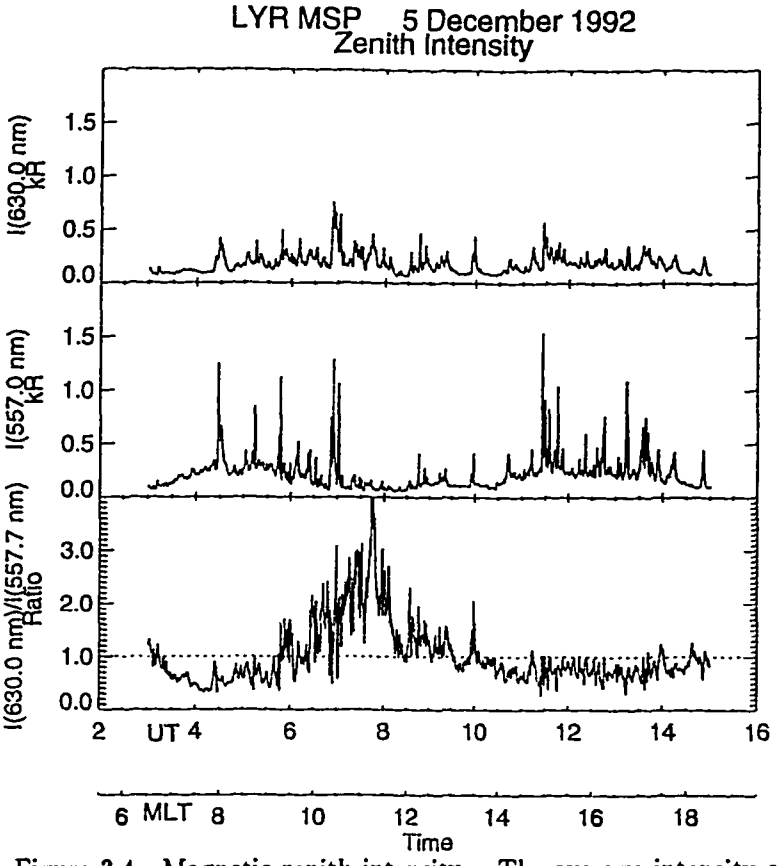


Figure 3.4 Magnetic zenith intensity. The average intensity of 11 degrees centered on the magnetic zenith (-8° ) is plotted as a function of time for the individual emissions in (a) and (b) and the ratio in (c).

1972; *Whalen and Pike*, 1972] suggested that the auroral oval was continuous through the daytime sector. *Shepherd and Thirkettle* [1973] confirmed these results using observations from the ISIS-2 satellite and *Shepherd et al.* [1976b] found the region of 630.0 nm emission to be a continuous and permanent feature of the midday sector where the 391.4 nm emission is usually a local minimum. *Cogger et al.* [1977] examined ISIS-2 images to show that the 391.4 nm while a local minimum does persist throughout the midday region as well. *Shepherd* [1979] suggests the 391.4 nm photons may result from resonance scattering of sunlight from $N_2^+$ but may also arise from high energy particle precipitation. If the 391.4 nm emission is found in the same region as the enhanced 630.0 nm emission, the former explanation is more likely since the dominant 630.0 nm emission is consistent with low energy precipitation.

*Meng* [1981] showed that DMSP electron spectra within the midday gap is consistent with magnetosheath plasma and proposed that the ionospheric projection of the cusp is coincident with the midday gap. *Elphinstone et al.* [1992] compared the particle spectra obtained by the DMSP satellite and identified as "cusp" by the *Newell et al.* [1991b] neural network technique with Viking UV auroral images and concluded the regions labelled "cusp" should not be associated on a one-to-one basis with the optical midday gap. The midday gap, where the dayside arcs tend to converge, was most typically found near local noon in the Viking images while the DMSP particle data often indicated the presence of magnetosheath like plasma at prenoon and postnoon locations.

Reproduced with permission of the copyright owner. Further reproduction prohibited without permission.

Consistent with *Meng* [1981, 1994], *Elphinstone et al.* [1992] identifies the ionospheric projection of the cusp with the midday gap.

Equatorward of the discrete auroral arcs of the dayside auroral oval is a broad region of diffuse auroral emissions excited by energetic electrons ($E \sim 1 - 20keV$) drifting from the midnight sector [*Lui et al.*, 1973] through dawn and into the daytime sector [*Meng and Akasofu*, 1983]. This region, shaded in Figure 3.2 and dotted in Figure 3.2, was originally termed the "mantle aurora" by *Sandford* [1964,1968] who showed that the auroral emissions are a uniform glow in the 427.8 nm and 391.4 nm emissions but lacking in 630.0 nm emissions. The term "mantle arcs" is now unfortunately also used occasionally in reference to auroral arcs in the region of open field lines poleward of the discrete aurora which connects with the "plasma mantle" [*Rosenbauer et al.*, 1975] but as noted by *Newell et al.* [1991a] should not be confused with the diffuse aurora which results from high energy electrons lost into the atmosphere from the outer radiation belts.

Pulsations observed in the diffuse aurora are thought to result from wave-particle interactions leading to pitch angle scatter into the atmospheric loss cone. *Kennel and Petschek* [1966] showed theoretically that trapped and quasi-trapped electron populations beyond a critical flux level are unstable to the spontaneous growth of whistler mode waves in the VLF region of the electromagnetic spectrum. Resonance interactions of the whistlers with the trapped electrons lead to pitch angle scattering and loss of the electrons to the atmosphere. Consistent with this mechanism *Taylor and Gurnett* [1968] have reported that the probability of observing VLF waves with intensities greater than the threshold required to efficiently reduce radiation belt electron fluxes peaks in the 8-13 MLT sector at latitudes of approximately 55° -75° magnetic latitude.

*Nemzek et al.* [1995] showed the close relationship between pulsating aurorae and the injection of electrons in the magnetotail by comparing all sky camera records of aurora with geosynchronous satellite observations of electron injections on conjugate field lines. This study establishes that electron injections during substorms studied at geosynchronous orbit and in the outer radiation belts [*Parks and Winckler*, 1968, 1969; *Pfitzer and Winckler*, 1969; *Hoffman and Burch*, 1973; *Akasofu*, 1977; *Reeves et al.*, 1990; *Borovsky et al.*, 1993] produce the unstable particle populations responsible for the pulsating aurorae observed in the dawn and morning sector. *Imhof et al.* [1994] have reported bursts of 1.7 keV to 288 keV electron precipitation coincident with enhanced electromagnetic wave activity in the 311 Hz to 3.11 Hz range, consistent with the equatorial wave-particle cyclotron resonance interaction mechanism for radiation belt particle loss. The observation frequency increased with increasing L shell, peaking between L=7.5 and the outer limit of the observations at L=8.5. As noted in Chapter 2, the decay time of outer radiation belt electrons is on the order of days such that large particle injections should result in pulsating aurorae for extended periods. Even if strong pulsating aurorae is associated only with the initial period of magnetic storms when the injected fluxes are greatest, the large size of the injected regions–from 30° -60° [*Pfitzer and Winckler*, 1969] to 90° [*Reeves et al.*, 1990] predicts the peak fluxes associated with the injection of 40 keV electrons for which $\tau_d \sim 2.7$ hours to be observed for .08-.25 $\tau_d$, or 16-40 minutes. The duration of enhanced electron fluxes is almost certainly longer on closed drift shells due to circulation of the particles leading to drift echos [*Brewer et al.*, 1969; *Reeves et al.*, 1990]

Reproduced with permission of the copyright owner. Further reproduction prohibited without permission.

The diffuse auroral emissions in the mantle aurora terminate near local noon or in the early afternoon with few or no emissions observed in the afternoon and evening sectors [*Sandford*, 1964, 1968; *Meng and Akasofu*, 1983]. The lack of mantle aurora emissions is due to the distribution of electrons in the outer radiation belts. Electrons drifting into the morning sector at radial distances that map to the ionosphere equatorward of the dayside auroral oval may be lost through the magnetopause. If the electron drift path passes near the magnetopause drift shell splitting (Section 2.5) may remove the fraction of the electrons with pitch angles near 90° while the entire population may be lost if the drift shell intersects the magnetopause (magnetopause shadowing). In either case the electron population is reduced in the postnoon sector resulting in a reduction or complete absence of mantle auroral emissions [*Meng and Akasofu*, 1983].

*Kvifte and Petersen* [1969] and *Brekke and Pettersen* [1971] studied the diffuse 557.7 nm aurora from Svalbard and showed that the luminosity varied in a manner similar to pulsating aurora commonly observed at lower latitudes in the postmidnight and dawn sectors. The pulsations were quasi-periodic with nearly constant periods and amplitudes for several minutes. A peak in the occurrence of the aurora was found in the period from 0500-0700 UT (0830 MLT - 1030 MLT) with activity limited to the prenoon period. Similar observations were later reported by *Craven and Burns* [1990] for the postnoon sector from observations at Antarctica and were attributed to the wave-particle interaction between trapped (or pseudo-trapped) electrons and whistler mode VLF waves [*Davidson*, 1986a,b]. *Synder et al.* [1972] reported simultaneous observations of patchy aurora with a riometer absorption event confirming the identification of the diffuse auroral patches with the hard precipitation zone described by *Hartz and Brice* [1967].

The region of soft particle precipitation on the poleward edge of the oval and the hard precipitation on the equatorward edge are often not contiguous, however, but can be separated by a well defined decrease in luminosity in both the 630.0 um and 557.7 nm emissions [*Chernouss et al.*, 1986; *Yagodkina et al.*, 1989] This gap is not to be confused with the "midday gap" reported by *Dandekar and Pike* [1978], the "luminosity trough" or "intensity dip" [*Yagodkina et al.*, 1989, 1990] is a decrease in the latitude profile of the midday 557.7 nm auroral emissions while the latter is a longitude modulation in the distribution of bright, discrete, 557.7 nm dominated arcs. *Yagodkina et al.* [1989, 1990] notes that the intensity of 557.7 nm emissions is less than that in both the diffuse auroral region and the dayside auroral oval, but is above the airglow background with typical magnitudes of approximately 1 kR.

Much of the recent effort devoted to studies of the diffuse 557.7 nm aurora and the luminosity gap has been to compare the distribution of the auroral types with magnetic pulsations [*Yagodkina et al.*, 1989, 1990, 1992]. *Yagodkina et al.*, 1990] divide the pulsating 557.7 nm aurora into two distinct types: (1) quasi-periodic irregular increases in intensity and the formation of short lived diffuse bands of width 50-150 km and (2) quasi-periodic poleward expansions of the hard electron precipitation. They suggest that, consistent with the scheme of *Feldstein and Galperin* [1985], the diffuse luminosity on the equatorward edge of the dayside auroral oval maps to the outer edge of the radiation belts. Micropulsations may modulate the high-frequency wave interactions resulting in precipitation pulses at periods significantly longer than the cyclotron bounce periods [*Coroniti and Kennel*, 1970a,b]. Micropulsations cannot result in precipitation directly

Reproduced with permission of the copyright owner. Further reproduction prohibited without permission.

since the electron number density at energies required for a resonance is too small to trigger an instability. In addition, the precipitating particles which produce the auroral pulsations appear to be largely 10-100 keV electrons, requiring waves in the VLF and ULF frequency range to satisfy the electron cyclotron-electromagnetic wave resonance condition. The gain and loss of electron energy through interaction with the electric field component of the electromagnetic wave required for pitch angle scattering in the electromagnetic wave-electron cyclotron interaction is not possible with micropulsations. Electrons will move adiabatically through the relatively slow micropulsation magnetic field variations and will not be scattered in pitch angle (electron bounce periods are typically the order of seconds while the micropulsation wave periods are on order of minutes). Correlations between pulsating aurora and micropulsations has been explained by the variation in the local magnetic field intensity and cold plasma number density due to the micropulsation which alters the resonance condition for the VLF mechanism and result in electron scattering into the loss cone [*Coroniti and kennel*, 1970a,b].

### 3.4 Characteristics of Transient Midday Arcs

The transient auroral forms which form at the equatorward edge of the dayside auroral oval and drift poleward are especially interesting. They are thought by many to be the best candidates for the ionospheric signature of the FTE and have been heavily studied as a result. A brief note on terminology is in order before describing the characteristics of transient midday aurorae. Transient discrete arcs in the daytime sector have been variously termed the "midday auroral breakup" by *Sandholt et al.* [1989b], "poleward running epherial forms" by *Atkinson et al.* [1989], and "poleward moving auroral forms" (PMAF) by *Fasel et al.* [1995]. Neither *Eather* [1984] nor *Rairden and Mende* [1989] chose to adopt a specific term, but rather chose to generally refer to "discrete auroral structures" as "poleward moving features" when a significant poleward drift velocity component was observed. All of these terms describe the same phenomenon and are often used interchangeably.

Reports of an initial east (west) motion of the transients for IMF $B_y < 0$ ($B_y > 0$) before turning northward have led to their selection as the most likely candidates of an ionospheric signature of the flux transfer event [c.f., the discussions by *Lockwood et al.*, 1989b; *Lockwood et al.*, 1990; *Saunders*, 1990]. The phenomenon which has been reported in the literature that has been interpreted as evidence for relating the transient arcs to flux transfer events is summarized as follows:

(1) Transient optical events in the dayside aurorae and FTE's at the magnetopause occur primarily during periods when IMF $B_z$ is southward [*Berchem and Russell*, 1984; *Rijnbeek et al.*, 1984; *Southwood et al.*, 1986].

(2) *Rijnbeek et al.* [1984] obtained a mean repetition period of 7 minutes for FTE's which compares favorably to the mean of $8.3 \pm 0.6$ min [*Lockwood et al.*, 1989b] Sandholt et al. [1986].

Reproduced with permission of the copyright owner. Further reproduction prohibited without permission.

(3) The 5-15 minute duration of the transient events [*Sandholt et al.* 1986] are consistent with predictions of the time required to form an open flux tube [*Lockwood and Cowley*, 1988; *Lockwood et al.*, 1990c].

(3) East-west motion of the transient optical features controlled by the IMF $B_y$ component [*Sandholt et al.*, 1986; *Sandholt et al.*, 1989; *Sandholt*, 1988].

(4) Transients are accompanied by impulsive variations in the magnetic field the polarity which depends on the IMF $B_y$ component *Oguti et al.* [1988].

(5) $B_y$ related dependent asymmetry of the occurrence rates of transient aurora. *Karlson et al.* [1996] report results from a statistical study of dayside aurora to show that transients are more common in the prenoon (postnoon) sector for IMF $B_y > 0$ ($B_y < 0$), consistent with predicted ionospheric signatures of FTE's [*Cowley et al.*, 1991].

A number of characteristic features of the transient arcs including their dimensions, drift velocities, and repetition periods are used in developing the auroral model described in Chapter 4 that will be applied to the morphology of 630.0 nm emissions in the midday auroral oval. The remainder of Section 3.3 will consider a number of the characteristics of transient dayside auroral arcs in more detail to provide a basis for the features selected in the auroral model.

### 3.4.1 Poleward and IMF $B_y$ Dependent East-West Motion

Transient auroral arcs are observed to form in the dayside auroral oval and drift poleward primarily when the IMF $B_z$ component is negative [*Vorobjev et al.*, 1975; *Horwitz and Akasofu*, 1977, *Eather*, 1985]. Examples of zonal and meridional velocities of transient arcs which are typically on the order of 0.5-3 kms$^{-1}$ are listed in Table 3.9.

An IMF $B_y$ dependent initial eastward or westward motion of transient arcs was originally reported by *Sandholt et al.* [1986] from studies of television images filtered for the 630.0 nm emission recorded on Svalbard. Other studies have observed zonal motion in the auroral luminosity with cameras filtered for the 557.7 nm emission and white light television cameras as well. The latter are typically more sensitive towards the blue end of the spectrum and emphasize the 557.7 nm component. East-west motions are therefore not solely due to the 630.0 nm component but appear to be a characteristic of the electron precipitation source. Studies reporting IMF dependent zonal motion, a number of which are summarized in Table 3.10, are consistent with the prediction of an initial east-west motion of newly reconnected field lines by the magnetic merging model [*Jørgensen et al.*, 1972; *Cowley et al*, 1981, 1991]. The geometry of the newly reconnected flux tubes is an unstable magnetic field configuration due to the sharp bend at the reconnection site. A magnetic tension is associated with sharp bend which will drive the flux tube azimuthally even as the magnetosheath flow drags the reconnected field line poleward. The resulting motion of the plasma injected across the magnetopause on the open field lines is azimuthal and poleward (see Figure 2.4 in Section 2.5.1) driving asymmetric IMF $B_y$ dependent flows in the high latitude ionosphere.

Reproduced with permission of the copyright owner. Further reproduction prohibited without permission.

**Table 3.9**

**Velocities of Selected Transient Auroral Events**

| Date[1] | MLT [1] | $V_{north}$ (km/s) | $V_{east}$ (km/s) | Reference |
|---|---|---|---|---|
| 30 Nov 1979 | 1130 | .75 | | *Sandholt et al.*, 1985 |
| | | 0.5-1.0 | | *Sandholt et al.*, 1986 |
| | | 1 | -5 | *Sandholt et al.*, 1988a |
| 24 May 1984 | 1225 | 0.6 | | *Rairden and Mende*, 1989 |
| 24 Nov 1987 | 1145 | 1.3 | | *Sandholt et al.*, 1989b |
| 12 Jan 1988 | 1250 | 0.63 | -3 | *Sandholt et al.*, 1990 |
| | | | | *Lockwood et al.*, 1993a |
| 9 Jan 1989 | 1230 | 0.6 | 1.1-2.5 | *Lockwood et al.*, 1993a |
| 2 Dec 1989 | 1100 | 0.18 | -1.3 | *Denig et al.*, 1993 |
| | 1100 | .36-.54 | -2 | |
| 20 Dec 1990 | 1230 | | 1.3-1.8 | *Minow et al.*. 1994 |
| 2 Dec 1991 | 1245 | ~0 | -1.5 | *Sandholt et al.*, 1992a |

[1]Date and MLT are listed for individual events but are left blank for results from survey papers.

**Table 3.10**

**IMF $B_y$ Dependent East-West Motion of Transient Arcs.**

| Date | Time | Direction | IMF $B_y$ (nT) | Wavelength[1] (nm) | Reference |
|---|---|---|---|---|---|
| 30 Nov 79 | 0757-0820 | W | ~0,+20, -5 | 630 | *Sandholt et al.*, 1986 |
| | | | | | *Sandholt et al.*, 1985 |
| 29 Dec 81 | 0530-1000 | W | -10,+10,-10 | 630 | *Sandholt et al.*, 1986 |
| 1 Dec 86 | 0900-0930 M | W | ~0,+40,-15[2] | 558 | *Elphic et al.*, 1990 |
| 12 Jan 88 | 1200-1230 M | W | $B_y > 0$ [4] | white[3] | *Lockwood et al.*, 1989b |
| | | | | white[3] | *Sandholt et al.*, 1990 |
| 12 Jan 91 | 0520-0615 | W | -2, +8, -6 | 630 | *Sandholt et al.*, 1993 |
| 30 Dec 81 | 0815-0825 | E | -3, -8, -7 | 630 | *Sandholt et al.*, 1986 |
| 10 Dec 82 | 0820-0905 | E | +10,-20,-20 | 630 | *Sandholt et al.*, 1986 |
| 10 Dec 83 | 0810-0835 | E | +7,-10,+13 | 630 | *Sandholt et al.*, 1986 |
| 10 Jan 93 | 10-14 MLT | E | +4, -8, -5 | 630 | *Sandholt et al.*, 1994 |
| 20 Dec 90 | ~ 12 M | E | +6, -4, -4 | white[3] | *Minow et al.*, 1994 |
| 17 Dec 92 | 1000-1200 | E | +8,-10,±2 | 630 | *Farrugia et al.*, 1995 |

[1]Wavelength sensitivity of filtered camera systems are rounded to nearest nanometer.

[2]Components are along the $\hat{n}, \hat{l}, \hat{m}$ directions of the boundary normal system.

[3]Television camera sensitivity is greater at 557.7 nm than 630.0 nm.

[4]Field orientation changed from 0900-0930 UT: $B_x$ from -7 to -12 nT, $B_y$ from 11 to 16 nT, and $B_z$ from -8 to -3 nT.

Reproduced with permission of the copyright owner. Further reproduction prohibited without permission.

It should be noted that in the publication by *Sandholt et al.* [1986] where the azimuthal motion of transient auroral events was first reported eight events did not exhibit detectable longitudinal motion. The IMF $B_z$ component was positive for some of the intervals and negative for others, but in general the magnitude of the $B_y$ component is less than 2 to 3 nT suggesting that strong zonal motion only occurs if the $B_y$ component of the interplanetary magnetic field is large. Recently, *Sandholt et al* [1992] noted that "...although the statistics are still poor the presently available data indicate that the direction of east-west motion around magnetic noon is determined by IMF $B_y$..." and further indicated that no events with velocities inconsistent with the merging model have been discovered.

Motion of the arcs in the midday, soft electron, region are nearly always poleward. Statistics studies of dayside arc motion indicate that the minimum of equatorward motion occurs near local noon coincident with the maximum in the number of arcs with a poleward velocity component [*Eather*, 1984]. This distribution was also noted by *Lassen and Danielson* [1978] and *Lassen* [1979] who associated the quiet time patterns and motions of auroral arcs with average convection patterns.

### 3.4.2 Correlation of Transient Arcs with Ion Flow Velocity Enhancements

Comparisons of the motion of transient arcs obtained by all-sky cameras on Svalbard to F-region plasma convection measured by the EISCAT radar in the midday period has established that the optical transients are closely related to enhancements in the plasma flow velocity, indeed, a number of the reports show the arcs move at the same velocity as the plasma drift within the error of the measurements [*Lockwood et al.* 1989a,b, 1990a,b; *Sandholt et al.* 1990, *Lockwood et al.*, 1993a]. These observations have been interpreted to mean that the same process responsible for the formation of the flow burst also provides the precipitating particles necessary to excite the transient arc [*Smith and Lockwood*, 1990; *Lockwood*, 1991; *Smith et al.*, 1992]. There is some ambiguity since only line of sight observations are possible using the EISCAT radar over Svalbard. Two dimensional field perpendicular flows may be derived using a single radar with a beamswinging technique where the single radar obtains observations at two separate azimuths [*Willis et al.* 1986; *Lockwood et al.*, 1988; *Lockwood*, 1991]. Alternatively, two radars operating simultaneously from the EISCAT site at two azimuths can provide the same information without requiring the beamswinging. Either method requires that the flow is uniform between the two azimuths and that any variations in flow occur linearly during the observation period. Errors in recovering the two dimensional flow field from the radar measurements may occur if rapid variations in the ionospheric flow occur during the observations or if if shears exist in the region of observation [*Lockwood et al.*, 1988; *Etemadi et al.*, 1989, *Lockwood*, 1991; *Freeman et al.* 1991; *Yeoman et al.*, 1992]. Even if the 2-D auroral arc velocity proves to differ from the cold plasma flow, a close relationship must still hold between the meridional components as measured by the line of sight velocities along the radar beams, showing the optical transients are related to the ion flow bursts. Further, *Lockwood et al.* [1989b] note that spurious mixing effects due to the erroneous generation of westward flow due to temporal variations in the northward flow and vice verse depends on the phase of the flow variations with respect to

Reproduced with permission of the copyright owner. Further reproduction prohibited without permission.

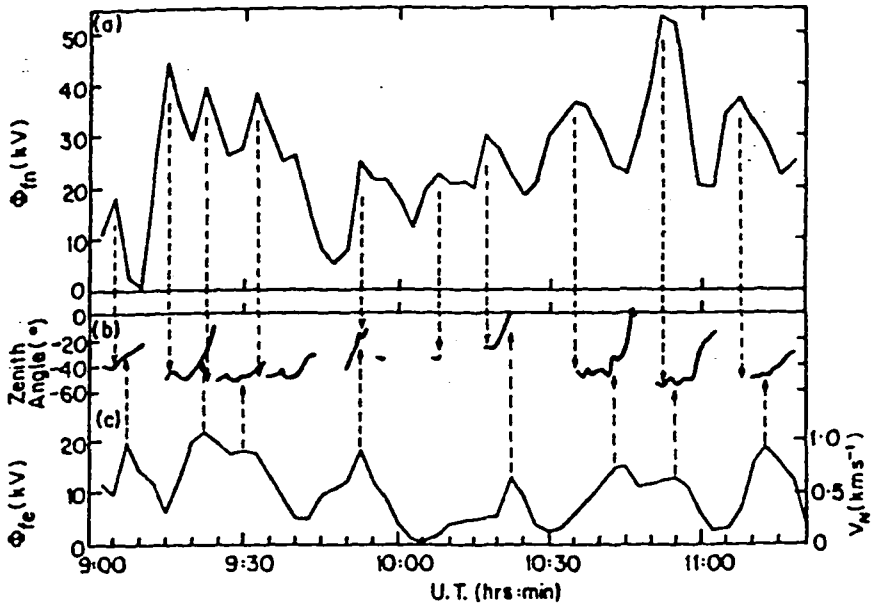


Figure 3.5 Radar Observations of Ion Drift and Transient Aurora. The radar observations are the potential integrated across N-S dimension of the radar scan. Zenith angles of peak 630.0 nm emissions for intensities greater than 3 kR. [from *Lockwood et al.*, 1989b].

the cycle in the sequence of azimuth scans. Spurious effects are expected to result in a variety of recovered flow velocities rather than the uniform flows reported from the EISCAT events.

It is important to note that there is no reason to assume *a priori* that auroral arcs must always move at the same velocity and direction as the $\vec{E} \times \vec{B}$ convecting plasma. There is often a relative velocity between auroral arcs in the night sector or within the polar cap and the cold plasma in which they are imbedded. For example, *Kelley et al.* [1971] compared electric fields measured from balloons to simultaneous all-sky camera images of aurora to show the magnitude of the meridional component of the auroral arc drift velocity was the same as the plasma drift approximately 75% of the time and smaller than the plasma drift approximately 25% of the time. *Haerendel* [1972] report on a series of barium releases used to trace cold plasma motion in the auroral ionosphere which show auroral arcs associated with poleward expansions of the auroral oval and westward travelling surges are independent of the plasma motion. The plasma continued to drift southeast as a series of irregular auroral forms moved poleward in the case of the poleward expansion of a substorm. The auroral arcs associated with the westward travelling surge were inferred to be parallel to the plasma flow in one area of the surge and perpendicular in others. *Haerendel* [1972] suggests that these observations, along with those of *Kelley et al.* [1971] and *Wescott et al.* [1970] are consistent with a reconnection process at the neutral sheet within the tail. Measurements of

Reproduced with permission of the copyright owner. Further reproduction prohibited without permission.

electric fields in the vicinity and within auroral arcs have often shown that fields inside arcs are less intense by a factor of ten than outside the arc [*Westcott et al.*, 1969; *Potter*, 1970; *Whalen et al.*, 1974]. *Westcott et al.* [1969] attributes the decrease to the increased conductivity within the auroral form which reduces the electric field.

*Mende et al.* [1988] compared radar observations of plasma drifts with all-sky camera images of sun-aligned polar cap arcs to determine the relative motion of ionospheric plasma with respect to high latitude auroral arcs. The components of the motion of the auroral luminosity and the plasma drift perpendicular to the polar cap arcs was found to generally agree in direction. The parallel components were far more variable with both sunward and antisunward plasma drifts found outside the arcs and predominantly antisunward drifts within the arcs, suggesting the presence of highly structured electric fields. *Doolittle et al.* [1990] presented results from a similar study of auroral arcs and polar cap patches in the 2030 MLT sector. Images from an all sky camera filtered at 630.0 nm were compared to Soudrestrom radar measurements of the ion drift velocity to determine the relationship between the two motions. The auroral arc was found to move slowly opposite the direction of the ion drift. A small component of the ion drift velocity was also observed parallel to the arc showing the arc was not an equipotential. The drift velocities of faint 630.0 nm airglow patches associated with regions of enhanced plasma density were also observed during this study and shown to agree in both direction and magnitude with the ambient plasma flow. The auroral arc which is formed by precipitation of electrons from populations exterior to the F region plasma could not have been driven by the magnetospheric electric fields while the airglow patches associated with regions of enhanced plasma imbedded within the ionosphere were simply drifting with the ambient plasma flow as originally reported by *Buchau et al.* [1983] and *Weber et al.* [1984]. *Frey et al.* [1996] and *Haerendel et al.* [1993, 1996] have recently reported relative velocities between auroral arcs and the plasma as large as 100-200 m/sec when comparing all-sky camera images to 3-D plasma drift velocities obtained by the tristatic EISCAT radar system.

It would appear that reports of auroral arc motion at the same velocity as the plasma drift should be considered a special case in the midday period. Further work in this area is needed, especially in the area of high resolution measurements of electric fields within the dayside cusp region.

### 3.4.3 Transient Arc Formation Rates and Lifetimes

Case studies of transient arc behavior originally showed the arcs form once every 3 to 15 minutes [*Vorobjev et al.*, 1975; *Horwitz and Akasofu*, 1977; *Sandholt et al.*, 1986]. Recent statistics of a large number of arcs that drift poleward [*Fasel et al.*, 1993; *Fasel.*, 1995] indicate the average time between formation of the transient arcs is 6 minutes and the mode (most probable) time between transients is approximately 3 minutes. Most recently, statistical studies of intervals between FTE's observed at the magnetopause [*Lockwood and Wild*, 1993] have shown that the most probable and mean intervals are 3 and 8 minutes, respectively. Results from studies of intervals between the formation times of dayside arcs in the subclass of poleward moving auroral forms (the "PMAF" arcs studied by *Fasel et al.* 1993] are similar with a most probable and mean interval of 3 and 6

Reproduced with permission of the copyright owner. Further reproduction prohibited without permission.

minutes, respectively. *Fasel* [1994] tested the null hypothesis that there is no difference between the distributions of intervals between FTE's and poleward moving transient auroral arcs using a Mann-Whitney test and found no statistically significant reason to reject the hypothesis.

### 3.4.4 Temporal Variations in Luminosity

The time history of luminosity within transient arcs is variable. Examples presented by [*Vorobjev et al.* [1988] include cases where the luminosity not only simply decayed with time following the initial formation of the arc, but also examples where the arc rebrightened. In the latter cases *Vorobjev et al.* [1988] find that the rebrightening in the meridian plane is due to transient enhancements of small regions of rayed arcs that move into the photometer field of view.

Temporal variations in the discrete arc luminosity, however, are not solely restricted to localized regions. *Fasel et al.* [1992] considered examples of the rebrightings in which entire the entire section of the arcs within view of an all sky camera are observed to increase in luminosity. The interpretation of the rebrightening in terms of current surges associated with multiple reconnection events have been discussed by *Fasel et al.* [1992] and *Fasel et al.* [1993].

An alternate interpretation proposed by *Lockwood* [1994] attributes the 557.7 nm emissions (and any low lifetime 630.0 nm emissions) observed within the arc to $> 1$ keV electrons accelerated by an unspecified plasma instability in the upward field aligned current associated with the arc. The rebrightenings in this model are the result of variations in the plasma instability rather than multiple reconnections of the convecting field lines. A prediction that the rebrightenings are only observed in the 557.7 nm emissions (and low lifetime 630.0 nm emissions) and not the long lifetime 630.0 nm emissions excited by the magnetosheath electrons has yet to be tested.

More recently *Kan et al.* [1996] proposed a model for the recurrent increases in luminosity of the dayside arcs. They propose that bright auroral arcs must occur on closed field lines and that dayside forms will simply fade once the field line is opened to the solar wind. The rebrightening is suggested to result from Alfven waves reflecting between the ionosphere and the equatorial plane in the magnetosphere. The interval between rebrightenings is determined by the travel time of the Alfven pulse, approximately 2-4 minutes is estimated by the authors. The model predicts that the rebrigtenings can only occur on closed field lines, and the transient arcs should rapidly fade once the field line is opened. Also, the intensity of each rebrightening decreases due to the diminished intensity of the Alfven wave.

### 3.4.5 Ion Flow Enhancements, Transient Aurora, and Energy Dispersed Ions

The "cusp plume" of energy dispersed ions (Section 2.6.2) is one of the definitive signatures used to identify the cusp and mantle in records of precipitating particles obtained by low and mid-altitude satellite data. Demonstration that the poleward moving transient optical features and the ion flow bursts in the high-latitude region form on the same field lines as energy dispersed ions is an important piece of evidence linking the transient ionospheric phenomenon with the cusp precipitation. Relatively few such coincidences have been published and they are generally limited to DMSP satellite overpasses of the prenoon oval with simultaneous ground based observations by

Reproduced with permission of the copyright owner. Further reproduction prohibited without permission.

photometers and all sky cameras in Svalbard [*Sandholt and Newell*, 1992; *Sandholt*, 1993; *Sandholt et al.*, 1993; *Minow et al.*, 1994].

Analysis of electron and ion precipitation records obtained onboard rockets in the prenoon auroral oval by *Carlson and Torbert* [1980] and *Clemmons et al.* [1995] have yielded results with important implications for correlations between ions and electrons within dayside aurora. In both cases energy dispersed ions consistent with time-of-flight effects from spatially localized sources were observed. The high time and space resolution available on the rockets demonstrated the electron precipitation is highly structured and generally uncorrelated with the impulsive ion injections. Signatures of electron acceleration and ion deceleration were noted in both studies consistent with the formation of potential structures at near Earth ($\sim 1 - 2R_E$) distances.

*Lockwood et al.* [1993b] presented a study of transient flow bursts identified by regions of ionospheric plasma with enhanced plasma density moving with increased drift velocities. Ion energy spectra obtained during an overpass of the region by a DMSP satellite demonstrated the presence of the characteristic cusp plume and confirmed the transient ionospheric events were forming in the cusp region. Auroral records were not available due to the season the observations were obtained but the flow bursts were similar to those often observed during the winter when it has been shown that transient optical events accompany the flow bursts [*Lockwood et al.*, 1989a,b, 1990b; *Rodger et al.*, 1995].

The intense number fluxes of charged particles characteristic of the cusp precipitation [*Heikkila and Winningham*, 1971; *Winningham*, 1972; *Newell and Meng*, 1988] suggests that hydrogen emissions associated with cusp precipitation should be observed from ground based observatories and may provide an important diagnostic of the relationship of transient aurora to the cusp plume. Few ground based studies of the temporal and spatial distributions of hydrogen emissions within the dayside oval have been reported in the literature. Studies by *Eather et al.* [1979] at South Pole Station show $H_\beta$ emissions accompanying the soft electron precipitation in the midday sector. Proton precipitation is generally poleward of the soft electron precipitation in the morning region, concomitant with the soft aurora in the midday aud afternoon sectors, and equatorward of the soft electrons in the afternoon region.

More recently *Sigernes et al.* [1995] report case studies of midday auroral events in which the relative timing of the transient arc and hydrogen emissions are examined. Hydrogen $H_\alpha$ emissions monitored by spectrometer sampling in the local zenith and a scanning photometer obtaining $H\beta$ intensities in the magnetic meridian plane. In one case study, 17 December 1992, the auroral forms are not drifting poleward but rather are fixed in latitude. The authors note that hydrogen emissions are apparently coincident with the 557.7 nm and 630.0 nm emissions in the auroral electron events in this case. A second case, 12 January 1992, in which poleward drifting auroral forms are noted led to authors to report that hydrogen emissious lag the 557.7 nm emissions from the corresponding auroral transient. There is some question to the validity of these results since the same records from the 17 December 1992 case was presented by *Deehr* [1994] but a time lag between the hydrogen and electron signals was reported, contradictory to the *Sigernes et al.* [1995] result. The results are not entirely clear however since the photometer records appear to show hydrogen emissions which are in fact coincident in both space and time with the 557.7 nm

Reproduced with permission of the copyright owner. Further reproduction prohibited without permission.

records within the time resolution of the instrument. It is possible that contamination from the $N_2VK$ (5,12) band (Section 3.1.2) is the cause of the correlations between the MSP $H_\beta$ and the 557.7 nm emissions. This hypothesis cannot be tested since the spectra from a second spectrometer in the vicinity of the $H_\beta$ emission line required to show the presence of the nitrogen band is not available due to an instrument failure.

If the emissions interpreted as $H_\beta$ in the photometer records do in fact result solely from precipitating magnetosheath protons, then the ground base observations are inconsistent with the *Carlson and Torbert* [1980] and *Clemmons et al.* [1995] rocket measurements of proton and electron precipitation in the cusp and cleft which show no significant correlations between structured electron events producing auroral arcs and energy dispersed ion injections. Further work in this area is needed.

### 3.4.6 Structured Electron Fluxes and Electron Acceleration within the Cusp

Before considering the dimensions of the transient forms in the following section, a few notes about the possibility of electron acceleration within the precipitating magnetosheath plasma is in order. Two characteristics of transient arcs observed from the ground support the view that acceleration of the magnetosheath plasma must occur within the cusp. First, descriptions of transient arcs often note the presence of internal ray structure within the transient arcs which are described as discrete auroral forms [*Sandholt et al.*, 1986, 1989b, 1990b; *Sandholt*, 1988a,b, 1990]. Second, the transient arcs may exhibit 557.7 nm intensities of 1-10 kR and ratios $I(557.7\ nm)/I(630.0\ nm) > 1$ requiring the presence of keV electrons. The average energy of the magnetosheath plasma in the cusp is only on the order of a few hundred electron volts. Presence of strong green line emissions in transient arcs which are spatially restricted in latitude suggests that acceleration of the magnetosheath plasma must occur within the cusp [*Sandholt et al.*, 1989b; *Lockwood et al.*, 1989b; *Sandholt et al.*, 1990b]. The best evidence however is obtained from *in situ* observations of precipitating electron and ion energies from both satellites and rockets.

Evidence for electron acceleration in electron energy spectra obtained by the HILAT satellite during a traverse of the northern hemisphere cusp was reported by [*Sandholt*, 1988b]. A series of three precipitation structures marked by factor of ten increases in the electron energy flux over the background precipitation were observed within the polar cusp. Electron energy spectra with distinct shoulders are reported to occur in the regions of the flux enhancements suggesting acceleration of the magnetosheath electrons. The energy fluxes within the structured events peak at values of 5 erg/cm$^2$ s over the background fluxes of 0.05 erg/cm$^2$ s. Average electron energies within the structured events was approximately 100 eV although peak values in excess of 850 eV are apparent in Figure 3 of *Sandholt* [1988]. Using the empirical values given by *Shepherd et al.* [1980] summarized in equation (3.47), the 630.0 nm intensities due to background precipitation of 100 eV electrons and energy flux of 0.05 erg/cm$^2$ s are predicted to be approximately 76 R. The 5 erg/cm$^2$ s electron fluxes with both 850 eV and 100 eV electrons predict yields of 630.0 nm emissions on the order of 7.6 kR, in agreement with the coincident optical observations obtained from a ground site under the satellite flight track.

Reproduced with permission of the copyright owner. Further reproduction prohibited without permission.

Accelerated electron events were present in the study of dayside particle injection by *Carlson and Torbert* [1980] and *Torbert and Carlson* [1980]. High time resolution records of ion and electron precipitation obtained by a sounding rocket launched through the prenoon auroral zone showed the presence of the characteristic energy dispersed ions associated with cusp injection. DC electric fields parallel to the magnetic field lines are indicated by the presence of periodic features in which field aligned bursts of accelerated electrons are observed coincident with protons decelerated by an equal amount. The accelerated electrons were noted to be field aligned within 3° in some of the events. The acceleration region was estimated to be located within several thousand kilometers of the Earth's surface based on time-of-flight delays between the protons and the electrons (assuming a common time of acceleration). More recently, a similar set of rocket observations was published by *Clemmons et al.* [1995] in which electron acceleration events are also found in the particle energy spectra although in contrast to the results obtained by *Carlson and Torbert* they conclude that dayside merging is not a viable source of the injected ions based on field line mapping with the Tsyganenko magnetic field model.

A study of AE-C and AE-D spacecraft encounters with the cusp by *Zanetti et al.* [1981] revealed that a common feature of the cusp was events in which electrons stream down field lines. The pitch angle of the streaming electrons were less than 15° and the energy spectra peaked at a few hundred electron volts. *Zanetti et al.* [1981] noted that the observations of dayside auroral emissions reported by *Shepherd* [1979] included small-scale enhancements of the 630.0 nm emissions accompanied by the 557.7 nm and 427.8 nm emissions. They considered the low energy electrons responsible for producing the ambient 630.0 nm cusp emission were not a possible source of the enhanced emissions, suggesting rather that the field aligned fluxes associated with upward currents were responsible. The events were common in the AE data sets, approximately half of the cusp traverses exhibited the features.

*Escoubet et al.* [1995] report DE 2 observations of narrow enhancements of electron precipitation within the cusp that are well above the background values which are considered typical. Estimated of the 557.7 nm emission intensity showed the values to be highly peaked with widths typical of an inverted V of 40 km but others were below 25 km. *Escoubet et al.* [1995] note that the size of the electron structures with values less than 50 km are consistent with the *Sandholt et al.* [1989, 1990] reports of midday arc widths and suggests that the accelerated electrons are responsible for the 557.7 nm emissions observed within midday transients.

Electron acceleration at the merging site is an alternative source of the keV electrons within the transient arcs [*Osso and Arendt*, 1991]. However, electrons with the keV energies required to produce the increases in luminosity and 557.7 nm/630.0 nm > 1 ratios within the transient arcs can only $\vec{E} \times \vec{B}$ drift on the order of a few kilometers poleward of the field line on which they were originally injected before encountering the atmosphere. If the merging site remains fixed near subsolar region their effect must be observed near the poleward edge of the mantle aurora, not well poleward of the mantle aurora in the dayside auroral oval. Electrons accompanying the 1 keV ions of the magnetosheath plasma required for quasi-neutrality are governed by the ion motion and will drift approximately 50-100 kilometers poleward of the merging site before encountering the atmosphere. The keV electrons observed within the transient auroral forms must be formed

Reproduced with permission of the copyright owner. Further reproduction prohibited without permission.

near the atmosphere to be observed coincident with the transient arcs, most likely within 1-2 $R_E$ in a low altitude acceleration process, after travelling most of the distance from the magnetopause at the ion velocity. This description of the dayside auroral arc as the result of an acceleration processes in the near Earth ionosphere rather than bulk electron precipitation at the merging site explains a number of observations of dayside auroral arcs:

(1) structured electron fluxes,

(2) narrowness of the transients

(3) enhanced 5577/6300 ratios and the discrete nature of the majority of the 630.0 emissions,

(4) internal ray structure within the transient arcs

(5) fluctuations of the 557.7 emission intensity due to current instabilities.

### 3.4.7 Dimensions of Transient Events

Estimates of the significance of transient increases in the dayside electric field to the energy budget of the polar magnetosphere have are often based on the dimensions of transient auroral arcs [*Lockwood et al.*, 1993a *Sandholt et al.*, 1993], the dimensions of enhanced ion flow events [*Lockwood et al.*, 1989a], and the integrated potential drop across transient events obtained from satellite measurements of ion drift velocity through the transient [*Denig et al.*, 1993]. The importance of the event dimensions arises because the significance if individual transient events to the magnetospheric energy budget is often estimated based on their contribution to the cross polar cap potential drop. Faradays Law

$$\frac{d\Phi}{dt} = -\Delta V_{rec} \qquad 3.48$$

relating the change of magnetic flux

$$\Phi = \int \vec{B} \cdot d\vec{S} \qquad 3.49$$

to the resulting potential $\vec{B}$ contribution to the polar cap potential drop is the basis of the estimate (Section 5.6). Magnetic flux transported into the polar cap in large transient events can provide a large contribution to the polar cap potential, especially if the events occur over short intervals. Small events conversely add little flux to the polar cap and are not significant contributers to the total polar cap potential drop. Therefore, the size of the events and the rate at which they occur determine their importance to the energy budget iu the high altitude ionosphere.

The altitude of the peak emission within transient arcs is required to convert all sky camera images of auroral arcs to estimates of the dimension of the arc. Usually, accepted values for the altitude of the peak emission is adopted for the estimate. For example, 120 km for 557.7 nm and 240 km for 630.0 nm are often accepted if the electron source is relatively low energy (~100 eV). However, *Lockwood et al.* [1993a] noted that altitudes of the 630.0 nm emission may vary from the accepted 240 km altitude to values as high as 300-400 km. If the latter estimates are valid the images of transients obtained by filtered cameras at 630.0 nm may cover very large areas, significantly increasing the estimated contribution of the transient to the cross cap potential.

Reproduced with permission of the copyright owner. Further reproduction prohibited without permission.

Early attempts to measure auroral altitudes from Svalbard date to the late 1800's and early 1900's but are limited to night time arcs [*Carlheim-Gyllenskiöld*, 1887; *Wegener*, 1914]. Triangulations have similarly been used by Sandholt et al. [1982] to obtain altitudes of night time auroral arcs during the poleward expansion phase of a substorm. Table 3.11 lists estimates of dayside auroral altitudes obtained within the 0600-1800 MLT sector. The majority of measurements are restricted to the prenoon and postnoon sectors with relatively few values from the hour surrounding magnetic noon, especially the studies using ground based cameras and photometers. Triangulations generally require stable bright arcs with significant ray structure to yield accurate values and weak or structureless emission feature are generally avoided [*Deehr et al.*, 1980; *Sigernes et al.*, 1995]. Most investigations obtained altitudes of either the peak emission or the lower border, although the upper border was also measured by *Jack and Hallinan* [1994]. The *Jack and Hallinan* and *Starkov* [1968] studies are interesting as they appear to be one of the few systematic observations of dayside arc altitudes over a range of magnetic local times. Both studies show a decrease in altitude of the peak emission as a function of magnetic local time difference from noon, consistent with satellite observations that soft particle fluxes dominated near noon while more structured, energetic fluxes are present in the prenoon and postnoon sector producing aurora with lower altitude peak emissions.

Most of the peak 630.0 nm emission altitudes are in the 200-300 km range with the exception of the 400-500 km example reported by *Lockwood et al.* [1993a]. Direct measurements do exist for auroral arcs at altitudes exceeding 300 km but they are primarily limited to the stable auroral red (SAR) arc phenomenon reported from midlatitudes. *Roach and Roach* [1963] reviewed the properties of the SAR arcs noting that the mean altitude of the peak emissions are approximately 400 km and the 630.0 nm to 557.7 nm ratio may be 50:1 to 80:1. More recently *Okano and Kim* [1978] reported photometric observations of a mid-latitude stable auroral red (SAR) arc from two stations showing the bulk of the emission originated from altitudes between 370-460 km with an average of 401 km. The intensity of the weak emission varying from 20-60 Rayleighs, increasing in intensity when the emission peak moved lower in the atmosphere.

Reproduced with permission of the copyright owner. Further reproduction prohibited without permission.

**Table 3.11**
**Altitude Estimates of Dayside Aurora in the 0300-1800 MLT Sector**

| Reference | Time (MLT) | Wavelength (nm) | Altitude (km) | Technique [1],Site, and Notes |
|---|---|---|---|---|
| *Lloyd et al.*, 1967 | 1141,1518 | 5577 | 100-100[2] | RP, Churchill |
| | | 4278 | 100[2] | |
| *Starkov*, 1968 | 0830-0845 | white | 140-155[3] | AA, Svalbard |
| | 1645 | white | 160-180[3] | Unfiltered film camera |
| *Lassen*, 1969 | 0430-0930 | white | | AA, Greenland |
| *Shepherd et al.*, 1976a | 1245 | 6300 | 200-300[5] | RG, N.W.T. |
| *Deehr et al.*, 1980 | 1030 | 4278 | 220[2] | MM, Svalbard |
| | | 5577 | 140[2] | |
| | | 6300 | 220[2] | |
| *Sandholt et al.*, 1983 | 1330-1530 | 6300 | 200-250[2] | ER, Svalbard |
| | 1630 | 6300 | 200[2] | |
| | 1730 | 6300 | 200[2] | |
| *Lanchester and Rees*, 1987 | 1030-1100 | 4278 | 150 [2] | MM, Svalbard altitude profiles |
| | | 5577 | 150[2] | |
| *Lockwood et al.*, 1993a | 1250 | 6300 | 250[2] | M, Svalbard |
| | 1230 | 6300 | 400-500[2] | |
| *Jack and Hallinan*, 1994 | 0600-1000 | white | 120-150[3] | P, space shuttle unfiltered TV |
| | | white | 200-250[4] | |
| | 1500-1800 | white | 100-125[3] | |
| | | white | 190-210[4] | |
| *Sigernes et al.*, 1995 | 1000 | 5577 | 125-160[2] | MM, Svalbard altitude profiles |
| | | 6300 | 200-220[2] | |
| *Wu et al.*, 1996 | 1100 | 6300 | 325[2] | SFPI |
| | 1042 | 6300 | 325[2] | |

[1] The most common techniques are triangulation from two stations using (MM) scanning photometers or (AA) all sky camera images. Alternatives include observations using a (RP) rocket borne photometer or a (RG) a rocket borne photometer and ground based scanning photometer, (M) a single ground based photometer, triangulation using (P) parallactic images (television) from spacecraft, estimates using the *Rees and Luckey* [1974] altitude dependent emission ratios (ER), and limb scans from a satellite borne Fabry-Perot interferometer (SFPI).

[2] Peak emission.

[3] Lower border.

[4] Upper border.

[5] Altitude range.

Reproduced with permission of the copyright owner. Further reproduction prohibited without permission.

Two possible mechanisms may result in 630.0 nm emissions at great altitudes (~300-500 km). *Lockwood et al.* [1993a] suggested that dayside arcs may be excited by a mechanism similar to the low latitude SAR arc (see Section 2) where strong electron heating at high altitudes selectively excites the $O(^1D)$ state. Dayside observations of electron temperatures in the range of 3000 K to 4000 K have been reported [*Wickwar and Kofman*, 1984; *Lockwood et al.*, 1993a,b] providing evidence that thermal excitation may be a significant contribution to the cusp $O(^1D)$ populations. However, the analogy to SAR arcs should not be carried too far since ratios of 630.0 nm to 557.7 nm may often exceed 50:1 in SAR arcs where the 557.7 nm emission is rarely if ever observed [*Rees and Roble*, 1975]. Virtually all publications describing the 630.0 nm and 557.7 nm intensities in transient dayside arcs indicate the 557.7 nm emission is present in the transient auroral events (Table 3.14). The second possibility is that the high altitude emissions are the result of remnant populations of $O(^1D)$ left behind a poleward moving transient arc (this process is modelled in Chapter 4). Low altitude populations of $O(^1D)$ will be removed due to quenching. The population above 350 km to 400 km will remain nearly unquenched and the only significant source of loss is radiative decay of the excited state. Estimates of emission altitudes in the 300-500 km range may be obtained by waiting a suitable period after the excitation source has terminated and the low altitude component has decayed due to quenching.

Reports of transient arcs in the literature generally refer to regions of emission which are elongated in longitude and very narrow in latitude with internal ray structure. Longitudinal dimensions are summarized in Table 3.12. In most cases the transient arcs are much larger in their longitudinal dimension than in latitude. It is difficult to determine east-west extents of the dayside arcs because they are typically on the order of or greater than the field of view of a single all sky camera. At best a single ground station can obtain an estimate of the minimum size of the arcs if it is stationary. Lengths of arcs with an azimuthal velocity can be estimated by measuring the time required for the arc to pass through the camera field of view if the velocity of the arc is known. The latter method is not without ambiguities since it is often difficult to determine if apparent motion of an arc is due to the motion of the arc itself or to ray motion within the arc.

Reproduced with permission of the copyright owner. Further reproduction prohibited without permission.

**Table 3.12**
**Latitudinal and Longitudinal Dimensions of Transient Dayside Events**

| Reference | Time (MLT) | Width (km) | Length (km) |
|---|---|---|---|
| | Optical Observations of Auroral Arcs | | |
| *Sandholt et al.*, 1986 | 1215 | | 400-500 |
| "small scale" events | | 100-200 | <500 |
| "large scale" events | | | >1000 |
| *Sandholt*, 1988 | 1130 | 45 | |
| | | 300-500 | |
| *Sandholt et al.*, 1988 | 0900 | 15 | |
| *Rairden and Mende*, 1989 | 1225 | 70 | >500 |
| *Sandholt et al.*, 1990b | 1250 | 50 | 500 |
| *Sandholt et al.*, 1990a | 1400 | | 300 |
| *Sandholt et al.*, 1992a | 1230 | 200 | 300 |
| *Sandholt et al.*, 1993 | 1030 | 200 | 500-1000 |
| *Lockwood et al.*, 1993a | 1251 | 300 | |
| | 1232 | 320-640 | |
| *Denig et al.*, 1993 | 1100 | 14 | 240 |
| | 1100 | 20 | 200 |
| *Lockwood et al.*, 1989b | 1250 | 10 | |
| | Radar Observations of Ion Drift Velocity | | |
| *Foster and Doupnik*, 1984 | 1100-1200 | 100 | |
| *Lockwood et al.*, 1989a | 1430 | >700[1] | 300 |
| | | 300-700[1] | 200 |
| *Pinnock et al.*, 1983 | | 100 | 900 |

[1] Magnetometer data provides estimate of disturbance outside of radar range.

A sample of estimates of latitudinal widths for dayside auroral arcs reported in the literature is given in Table 3.12. Values vary from 14 km to greater than 300 km with a number of values in the 100 km to 200 km range. Satellite particle measurements between 800 km and 14000 km altitude (Section 2.6.2) indicate average north-south dimensions for the cusp of 100 km to 200 km with extreme values up 400 km or greater. Comparison of the dayside arc widths in Table 3.12 to the statistical width of the cusp suggests the latitude range over which the particles responsible for the dayside arcs are distributed may range from large fractions to nearly the full statistical width of the cusp. Many of estimates are inconsistent with the original description of the midday arcs.

Some discrepancy also occurs due to the difference in the width of the optical arc and the width of the transient event. *Lockwood et al.* report widths of transient flow events on the order of 300-600 km but note that the optical event is collocated with the upward field aligned current and is only a fraction of the total event. It should be remembered however that the resolution available for optical observations is much better than radar. Scanning photometers are typically operated

Reproduced with permission of the copyright owner. Further reproduction prohibited without permission.

with approximately one degree field of views yielding approximately 2 km to 4 km resolution when sampling features in the zenith at altitudes of 120 km to 240 km, respectively. Range gates on the radars are typically a factor of ten larger. The EISCAT range gates, for example, used in experiments over Svalbard are on the order of 50 km [*Lockwood et al.*, 1989b]. In the case of the radar observations however the enhanced flows are observed over a wide range of gates indicating the flow events are in fact much larger than the optical events.

The largest of the transient events reported by *Lockwood et al.* [1989a] are over 300 km in the east-west and greater than 700 km north-south based on the region over which the radar and ground based magnetometers observe a disturbance. The optical event, a 5 kR 630.0 nm arc with nearly equal 557.7 nm intensities, is limited to the poleward edge of the event. The 630.0 nm emissions in the photometer records cover over 60° of elevation angle south of the station to near zenith, suggesting a latitude range of over 350 km. However, the 557.7 nm emissions are more narrowly peaked in the region of the strong arc, suggesting a more narrow region of strong electron precipitation, most likely less than 50 km (based on mapping 1 degree of elevation angle to approximately 2 km at E-region altitudes for the 557.7 nm emission). A projection of a 557.7 nm all-sky camera image of an event in this same series reported by *Lockwood et al.* [1989b] would suggest that the latitude width of a single arc is on the order of 10 km.

It is interesting to contrast the reported widths for dayside arcs to measurements of the widths of nightside forms where reports of thin arcs are the rule. *Maggs and Davis* [1986] used an image orthicon television camera system with a 12 by 16 ° field of view to obtain images of auroral structures located in the magnetic zenith. Measurements of thickness for 581 structures with an assumed altitude of 100 km for the lower border yielded widths from 70 m to 1440 m with a median value of 230 m. The lower values were determined by the 70 m minimum resolution of the television system leading *Maggs and Davis* to conclude that arcs thinner than 70 m must exist. *Borovsky et al.* [1991] repeated the measurements with an intensified television camera system connected to a 10-inch $f/6.3$ Schmidt-Cassegrain telescope to obtain a field of view of 0.31° x 0.41° . The narrower field of view in *Borovsky's* system limited the resolution to 2.1 m at an altitude of 105 km a significant improvement over the system operated by *Maggs and Davis.* Thicknesses were found to be typically 100 m while the thinnest values obtained were 40 m. *Borovsky* confirmed the prediction by *Maggs and Davis* that auroral structures may be thinner than 70 m, but could not determine if they approach the theoretical limit of 9.5 m due to limitations imposed by the minimum resolution of their camera system.

Narrow widths are not solely the product of television technology, estimates of the thickness of auroral structures using film records give similar results to the television observations. *Kim and Volkman* [1963, 1965] used all sky cameras to obtain widths from 3.5 to 18.2 km for a set of homogenous auroral arcs in the geographic zenith, a geometry that will yield excessively large estimates. *Störmer* [1955] reported 7.42 km for the width of an arc observed over Oslo with a lower border at 200 km while *Akasofu* [1961] used color photographs to estimate widths for two separate night time arcs to to be no larger than 336 m for the first and 144 km for the second arc.

Reproduced with permission of the copyright owner. Further reproduction prohibited without permission.

Field line curvature is a fundamental limit to the minimum thickness that can be obtained from a ground based observation *Maggs* [1967]. Other experimental problems may also be encountered including light scattering by aerosol layers producing artificially thick regions of emissions associated with an arc [c.f., *Romick and Belon*, 1967a,b; *Mende and Eather*, 1971].

Why are so many of the dayside widths reported in the literature and summarized in Table 3.9 so large compared to the night time arcs? One answer is the two sets of observations relate to different phenomena. Spatial scales of auroral emissions have been outlined by *Borovsky* [1993] as varying from fine-scale auroral arcs on the order of 100 meters, dynamic arc systems approximately 1 km in width composed of several fine scale arcs, the approximately 100 km distance between auroral arcs, and the hundreds of kilometer thickness of the auroral zone. The estimates of night time arcs have been limited to the fine scale structures. *Maggs and Davis* and Borovsky et al. make the critical distinction between a greater region of diffuse luminosity surrounding the narrow arcs and limited their observations to the bright, thin imbedded structures as a measure of the width of the primary electron beam. The source of the diffuse emissions was attributed to diffusion of metastable neutrals.

A similar point applies to dayside aurora, especially since the dominate 630.0 nm emission originates from metastable $O(^1D)$ . Significant redistribution of the neutral excited species is expected before many of the metastable states may radiate. Consider a case where infinitely thin arcs are moving poleward at 500-1000 m/s through a neutral atmosphere that is moving poleward at a neutral wind velocity of 120-240 m/s in the same direction. The arc will move poleward a distance of 60-250 km assuming it is excited by particle precipitation for a period of 2-4 minutes. The weakly coupled neutral atmosphere including the $O(^1D)$ formed by the auroral arc will only drift 14-28 km during the same period, resulting in a distribution of $O(^1D)$ over a distance of of $\sim$ 90-460 km behind the arc. Radiative decay of $O(^1D)$ from these remnant populations will produce 630.0 nm photons over a range latitudes equatorward of the transient arc. Measurements of the total width of the 630.0 nm emissions from the poleward to equatorward border does not measure the width of the electron source but rather the distribution of metastable $O(^1D)$ and results in an overestimate of the width of the electron precipitation. Errors in measuring latitudinal widths of 630.0 nm emissions are likely to contribute to many of the extreme widths of transient arcs listed in Table 3.12. The only valid method of measuring auroral arc widths with photometer or all sky camera data is to use the records where the arc passes through the magnetic zenith and then to only use emissions which originate from short lifetime states.

### 3.4.8 Persistent 630.0 nm Emissions

Auroral emissions in the midday sector are thought to be composed of two general forms [c.f. *Shepherd*, 1979; *Sandholt*, 1988; *Sandholt et al.* 1989a,b, 1990]:

(i) Discrete arcs that form intermittently and drift poleward. The arcs are dominated by [OI] 630.0 nm emission excited by electrons with energies on the order of 100 eV originating from magnetosheath plasma that penetrates the cusp, but may also contain

Reproduced with permission of the copyright owner. Further reproduction prohibited without permission.

significant ray structure in [OI] 557.7 nm emissions suggesting there is also a source of accelerated keV electrons.

(ii) A "persistent" or "pre-existing cusp arc" [*Sandholt*, 1988] auroral emission dominated by the [OI] 630.0 nm emissions.

The presence of 630.0 nm emissions throughout the midday period is the basis for the [*Newell and Sibeck* [1993] argument that "...the cusp optical observations cannot be explained in the limit of discrete events only." Examples of reported persistent backgrounds are listed in Table 3.13. It is interesting to note that there does not appear to be any obvious correlation between the difference in peak and background intensity and the interval between auroral transients. Such a correlation may be expected if the background is simply due to the decaying population of $O(^1D)$ excited within the transient arc. The source of and time dependence of 630.0 nm emissions is considered in more detail in Chapter 4.

**Table 3.13**
**Transient Events and Persistent Background Aurora**

| Date[1] | Time [1] (MLT) | I(630.0 nm) transient (kR) | Mean background (kR) | Interval (Minutes) | Reference |
|---|---|---|---|---|---|
| 10 Dec 1983 | 1100 | 5 | 3 | 2.5 | *Sandholt and Newell*, 1992 |
| 24 Nov 1987 | 1145 | 4 | 1 | 9 | *Sandholt et al.*, 1989b |
| 2 Dec 1991 | 1230-1255 | 8 | 4 | 9 | *Sandholt et al.*, 1992a<br>*Sandholt et al.*, 1993 |
| 12 Jan 1991 | 0930 | 5 | 2 | ~10 | *Sandholt et al.*, 1993 |
| 9 Jan 1989 | 1400 | 5-10 | 3-5 | 10 | *Sandholt et al.*, 1990a |

[1]Date and time are indicated only for individual events.

Transient auroral events observed within the midday region typically are characterized by emission rate ratios $I(630.0nm)/I(557.7nm) > 1$. While most commonly dominated by emissions of 630.0 nm photons, the transients are always accompanied by 557.7 nm emissions. The intensity of the 557.7 nm emission is variable, extremes vary from reports of 10 kR to 15 kR [*Sandholt et al.*, 1989, 1990] to barely above the airglow level of a few hundred Rayleighs. This is borne out by considering the auroral events published by ground based observers in recent years. Table 3.10 catalogs many of these events and represents the bulk of observations of dayside aurora reported in the literature on which theoretical models of dayside aurorae are currently based. Photometer records of both the 557.7 nm and 630.0 nm emission rates are available in the references for all of the events included in the table. All of the transients show a corresponding enhancement of the 557.7 nm emission rate accompanying the 630.0 nm emissions within the transients. Therefore, some recent suggestions that midday transients are always observed in 630.0 nm light but only sometimes in 557.7 nm light [*Lockwood*, 1995] are surprising since the published record of dayside transients show the 557.7 nm emission to be an integral part of the events. The events in Table 3.14 include the original series of transients published by *Sandholt et al.* [1986] which were interpreted

Reproduced with permission of the copyright owner. Further reproduction prohibited without permission.

in terms of the ionospheric signatures of plasma transfer at the magnetopause, the auroral events shown to occur simultaneously with radar observations of enhanced plasma flow [Lockwood et al, Sandholt et al], as well as the observations of FTE's at the magnetopause with optical and radar transients in the dayside ionosphere [*Elphic et al.*, 1990]. In all of the photometer plots in the publications listed in Table 3.14 an obvious 557.7 nm component accompanies the 630.0 nm transients.

Why is this important? Because it has also been suggested that strong heating of the electron gas by low energy particle precipitation in the cusp creates an appreciable population of suprathermal electrons, providing the primary source of $O(^1D)$ within dayside aurorae. This is the mechanism thought to be responsible for the midlatitude SAR arcs and predicts very large I(630.0nm)/I(557.7nm) ratios or often no detectable 557.7 nm emission. In the case of the cusp a directed flow of electrons with a Maxwellian energy distribution with a peak at 100-300 eV are observed entering the atmosphere (for example, *Newell and Meng* [1995] have published examples of electron energy spectra obtained within the cusp). This electron distribution must excite not only $O(^1D)$ but $O(^1S)$ as well on the same field line and the 557.7 nm signals will be weaker than the 630.0 nm signals, but not absent.

Reproduced with permission of the copyright owner. Further reproduction prohibited without permission.

**Table 3.14**
**Photometer Records of 630.0 nm Aurora with 557.7 nm and 427.8 nm Component**

| Event Date | Approx. MLT | Reference |
|---|---|---|
| 26 Dec 78 | 0855, 1100, 1445 | Deehr et al., 1980 |
| 21 Jan 82 | 0935-1100 | Vorobyev and Turyanskiy, 1983 |
| | 1138-1142 | |
| 10 Dec 83 | 1142-1206 | Sandholt et al., 1986a; Sandholt et al., 1990 |
| | 1131-1142 | Sandholt et al., 1988a,b, Sandholt and Egeland, 1988 Sandholt, 1993 |
| 13 Dec 83 | 0925 | Sandholt et al., 1989 |
| 4 Jan 84 | 1130-1315 | Sandholt et al., 1986b |
| 16 Dec 87 | 1300-1320 | Jacobsen et al., 1991 |
| 27 Dec 84 | 1330-1700 | Sandholt et al., 1986a |
| 31 Dec 84 | 1130-1530 | Fasel et al., 1992,1994a |
| 16 Jan 85 | 1230-1330 | Fasel et al., 1994b |
| 17 Jan 85 | 1353-1407 | Sandholt et al., 1986a |
| 23 Jan 85 | 0945 | Sandholt, 1988b, Sandholt et al., 1989 |
| 1 Dec 86 | 1230-1300 | Elphic et al., 1990 |
| 31 Dec 86 | 0930 | Sandholt et al., 1989 |
| | 1000,1035-1115 | Sandholt, 1990 |
| 24 Nov 87 | 1140-1200 | Sandholt, 1988b |
| 7 Jan 88 | 1410-1520 | Sandholt, 1990 |
| 12 Jan 88 | 1235-1300 | Sandholt, 1990; Sandholt et al., 1990 Lockwood et al., 1989b, 1993a |
| | 1410-1440 | Lockwood et al., 1989a |
| 16 Dec 88 | 1120-1135 | Jacobsen et al., 1991 |
| 9 Jan 89 | 1334-1400 | Denig et al., 1993; Sandholt, 1993 |
| | 1220-1245 | Lockwood et al., 1990b, 1993a |
| | 1535-1610 | Sandholt and Lockwood, 1990 |
| 12 Jan 89 | 0330-1130 | Jacobsen et al., 1991, 1995; Burke et al., 1993 |
| | 1100-1400 | Fasel, 1995 |
| 2 Dec 89 | 1100 | Denig et al., 1993; Sandholt 1993 |
| | 1125-1147 | Moen et al., 1993 |
| | 1245(HEI) | Denig et al., 1993; Sandholt, 1993 |
| 20 Dec 90 | 1200 | Minow et al., 1994 |
| 12 Jan 91 | 0845-1145 | Sandholt et al., 1993 |
| 13 Jan 91 | 1000-1100 | Fasel, 1995 |
| 2 Dec 91 | 1230-1255 | Sandholt et al., 1992; Sandholt et al., 1993 |
| 27 Dec 91 | 1130-1230 | Fasel et al., 1994a |
| 7 Jan 92 | 1330-1445 | Lockwood et al., 1993c |
| 10 Jan 92 | 1100-1200 | Fasel et al., 1994b |
| 12 Jan 92 | 1000-1100 | Fasel, 1995 |
| 17 Dec 92 | 1330-1630 | Farrugia et al., 1995 |
| 23 Dec 92 | 0930-1030 | Fasel et al., 1994b; Fasel, 1995 |
| | 1230-1330 | |
| 10 Jan 93 | 1230-1530 | Sandholt et al., 1994 |

Reproduced with permission of the copyright owner. Further reproduction prohibited without permission.

### 3.5 Evidence for a Causal Relationship between FTE's and Optical Transients

A large body of evidence has been collected to date suggesting that the transient discrete aurorae in the midday sector have many characteristics consistent with the predicted ionospheric response to FTE's. There is however remarkably little direct evidence for a causal relationship between an individual impulsive increase in the rate of plasma transport across the dayside magnetopause and the formation of a transient auroral event in the midday aurorae. *Crooker and Burke* [1991] summarized the status of research on the physics of the cusp and cleft regions by noting that while the ultimate goal is to determine the nature of the magnetopause and boundary layer processes from ground based or low altitude satellite observations, it is more typical that researchers simply accept one of the standard models for the solar wind-magnetosphere interaction which has been widely accepted by the community and then attempt to describe how their observations fit into the model. The field line merging model (Section 2.5.1) has been most widely adopted to explain the formation and motion of dayside aurora.

It is not too difficult to propose a merging scenario to explain a particular auroral arc in the daytime ionosphere since for a given orientation of the IMF there is nearly always a terrestrial field line with an antiparallel component to the solar wind somewhere on the magnetopause [*Reiff and Burch*, 1985; *Crooker*, 1979]. Relaxing the conditions for merging from a strict antiparallel criteria to requiring that only a component of the fields in the magnetosheath be antiparallel to the terrestrial field allows reconnection over a much wider area of the magnetopause [*Gonzalez and Mozer*, 1974; *Cowley*, 1976]. Attributing auroral arcs to merging often becomes an exercise of picking the merging site for a given IMF orientation and comparing the high latitude plasma flows which must be excited by the particular merging process to observations if coincident satellite observations are available.

The difficulty in obtaining simultaneous observations at the magnetopause and in the ionosphere on the same field line is due to the great expense and difficulty of placing satellites in the locations required to obtain data complementary to a ground station. For this reason, most studies to date have had to resort to comparison of statistical records of magnetopause events with those in the ionosphere or choosing ionospheric events which appear to match the predicted signatures of events near the magnetopause. Parameters from the magnetopause and in the ionosphere include event formation rates, distributions of intervals between events, directions of event propogation. In virtually none of the magnetopause studies of FTE's are ground based data available to confirm a response and ionospheric observations which are shown to be consistent with the merging models are rarely compared to complementary satellite observations near the magnetopause to confirm that FTE's are indeed forming as expected. It has certainly been shown that transient auroral events form during periods when merging is active. An unambiguous causal relationship between FTE's forming at the magnetopause and transient arcs forming in the ionosphere remains to be demonstrated.

The only example of apparent correlations between satellite observations of FTE's and ground based measurements of transient optical and ion flow phenomenon obtained to date was published by *Elphic et al.* [1990]. A fortuitous conjunction between the ISEE 1 and 2 satellites near the

Reproduced with permission of the copyright owner. Further reproduction prohibited without permission.

magnetopause with magnetic field lines mapped to the vicinity of Svalbard allowed a direct comparison of transient magnetopause and ionospheric events. For each FTE identified in the satellite magnetometer data before the satellite entered the magnetosphere, an auroral arc and increase in ion drift velocity was observed to follow after an interval of time consistent with the time required for plasma to flow from the magnetopause to the ionosphere. These results are consistent with the model that transient auroral arcs are the optical signatures of FTE's and are the only measurements which show that FTE's are present at the magnetopause while transient arcs are forming in the ionosphere.

Lacking satellite observations from the magnetopause, *Sandholt et al.* [1994] and *Farrugia et al.* [1995] have compared time series of solar wind densities obtained by the IMP 8 spacecraft to the formation of transient optical events in the midday and postnoon aurorae. The apparent correlation between the times that number density maxima were observed in the solar wind with the brightening of auroral events in the dayside ionosphere led the authors to conclude that a causal relationship existed between the two sets of events. Magnetic merging driven by pressure pulses was suggested for a mechanism to explain the apparent correlations between the events. A similar set of auroral transients was published earlier by *Sandholt et al.* [1993] were not considered to be due to driven reconnection due to a lack of any correlation between pressure variations and the formation of optical events.

Reproduced with permission of the copyright owner. Further reproduction prohibited without permission.

# Chapter 4
# A Study of 630.0 nm Emission Morphology in the Midday Auroral Oval

## 4.1 Introduction

The "pulsating cusp" model developed by *Smith and Lockwood* [1990] proposes that low energy magnetosheath plasma in the polar cusp is injected into the magnetosphere in a series of flux transfer events produced by periodic enhancements in the dayside reconnection rate. *Smith et al.* [1992] expanded the model to suggest that cusp formation varies from the extreme of steady state during periods of continuous reconnection to an entirely discrete nature in the limit of discontinuous merging events. In its general form the pulsating cusp model covers the entire range of possible variations in merging rates at the dayside magnetopause. The most common dayside auroral forms observed during IMF $B_z < 0$ intervals are individual poleward drifting auroral arcs, suggesting that the merging process is most typically impulsive in nature.

Descriptions in the literature of discrete auroral arcs forming on the equatorward edge, propagating through, and fading on the poleward edge of a region of stable or persistent 630.0 nm emissions [c.f., *Sandholt*, 1988; *Sandholt et al.*, 1989a,b] suggest an inconsistency in interpreting dayside auroral forms entirely in terms of pulsed reconnection and FTE's. *Newell* [1990] notes "...the fact that ground observations show a fairly stable near-noon cusp arc to be the normal pattern seems to rule out the possibility that the cusp is actually a series of FTE's". *Newell and Sibeck* [1993] considered the existence of the "pre-existing cusp arc" as evidence that reports of transient arcs drifting poleward through a 630.0 nm background cannot be explained in the extreme limit of discrete events. These authors interpret persistent 630.0 nm emissions in the noon sector as the signature of continuous merging of magnetosheath and terrestrial field lines allowing free access of magnetosheath plasma to the magnetosphere along newly opened field lines. Further, *Newell and Sibeck* [1993] noted that reports of transient arcs forming on the equatorward edge and drifting through a persistent cusp emission is contradictory to the predicted auroral signature of the pulsed reconnection model since "...individual field lines do not propagate through other open field lines..." as the auroral observations might suggest. This criticism of the pulsed cusp model is based on an interpretation of 630.0 nm emissions as a tracer of low energy magnetosheath plasma precipitation. Finally, *Newell and Sibeck* [1993] criticized the pulsed-cusp model on the grounds that since "...there should be no relative motion between the new merging and the open lines just poleward (i.e., the pre-existing cusp arc), unless either the IMF or the magnetosheath flow has changed in the interval between the two merging epochs..." and proposed that midday transient arc morphology must arise due to variations in the magnetosheath $B_y$ or $B_z$ values rather than discontinuous pulses of enhanced merging.

The origin and interpretation of the persistent 630.0 nm emission in the midday auroral oval relative to transient auroral arcs, then, has important implications to physical models of the solar wind-magnetosphere coupling process. This chapter presents a study of the morphology of the 630.0 nm emissions in the midday aurora. An example of 630.0 nm and 557.7 nm emissions

Reproduced with permission of the copyright owner. Further reproduction prohibited without permission.

obtained by a scanning photometer in the midday aurora is presented in Section 4.2. Features of the auroral display including transient auroral arcs and two types of background 630.0 nm emissions are described. Section 4.3 is an overview of earlier work describing stable or persistent 630.0 nm arcs and efforts to identify the precipitating particle sources in the magnetosphere. An analysis of ion and electron energy spectrograms obtained during low altitude satellite overflights of the midday auroral oval are presented in Section 4.4 to consider the distribution of 630.0 nm emissions in the cusp. Simulated spectrograms obtained from theoretical auroral models of magnetosheath plasma entry into the cusp are considered as well as data records from the Defense Meteorological Satellite Program (DMSP). The theoretical models indicate the cusp electron fluxes are smooth predicting featureless 630.0 nm emissions within the cusp. The relationship of structured electron fluxes observed in real data to ground based observations of transient auroral arcs and persistent background emissions are considered next. Estimates of the relative contributions of the structured and diffuse background electron fluxes to the total energy deposition in the cusp are derived to determine the relative importance of the discrete events to energy input into the polar cusp. Section 4.5 describes an auroral model developed to simulate photometer records of 630.0 nm emissions. Low altitude satellite records are only "snapshots" in time and cannot yield information on the temporal and spatial variations in $O(^1D)$ populations excited by moving transient arcs. It is known from ground based observations that a prominent feature of dayside aurora are transient auroral arcs drifting poleward through a diffuse background 630.0 nm emission. The auroral model provides insight into the morphology of the transient arcs as observed by scanning photometers and will be used to estimate the transient arc contribution to the 630.0 nm emissions in the dayside auroral oval. A further purpose of the work is to test whether the continuous 630.0 nm emissions observed in midday auroral displays necessarily eliminate the discrete merging limit of the pulsating cusp model as suggested by *Newell and Sibeck* [1993]. Results from the auroral model are presented to test if discrete transient auroral events within the dayside oval can explain:

(1) formation of a persistent background 630.0 nm emission in which dayside transient arcs are imbedded,

(2) formation of transients on the equatorward edge, and subsequent poleward motion through, a persistent 630.0 nm emission, and,

(3) the presence of a persistent auroral arc on the equatorward edge of the cusp.

Comparison with auroral observations will demonstrate that excitation of auroral emissions within discrete arcs can reproduce the primary distribution of 630.0 nm emissions within the midday aurorae.

### 4.2 Observations: 10 January 1992

Photometer records of 557.7 nm and 630.0 nm emissions from 0700 UT to 0800 UT (1030 MLT-1130 MLT) on 10 January 1992 at Longyearbyen, Svalbard, are given in Figure 4.1. The format of the plot is Universal time on the horizontal axis, elevation angle measured from the northern horizon on the vertical axis, and the emission intensity is coded in increasing levels of gray. Each

Reproduced with permission of the copyright owner. Further reproduction prohibited without permission.

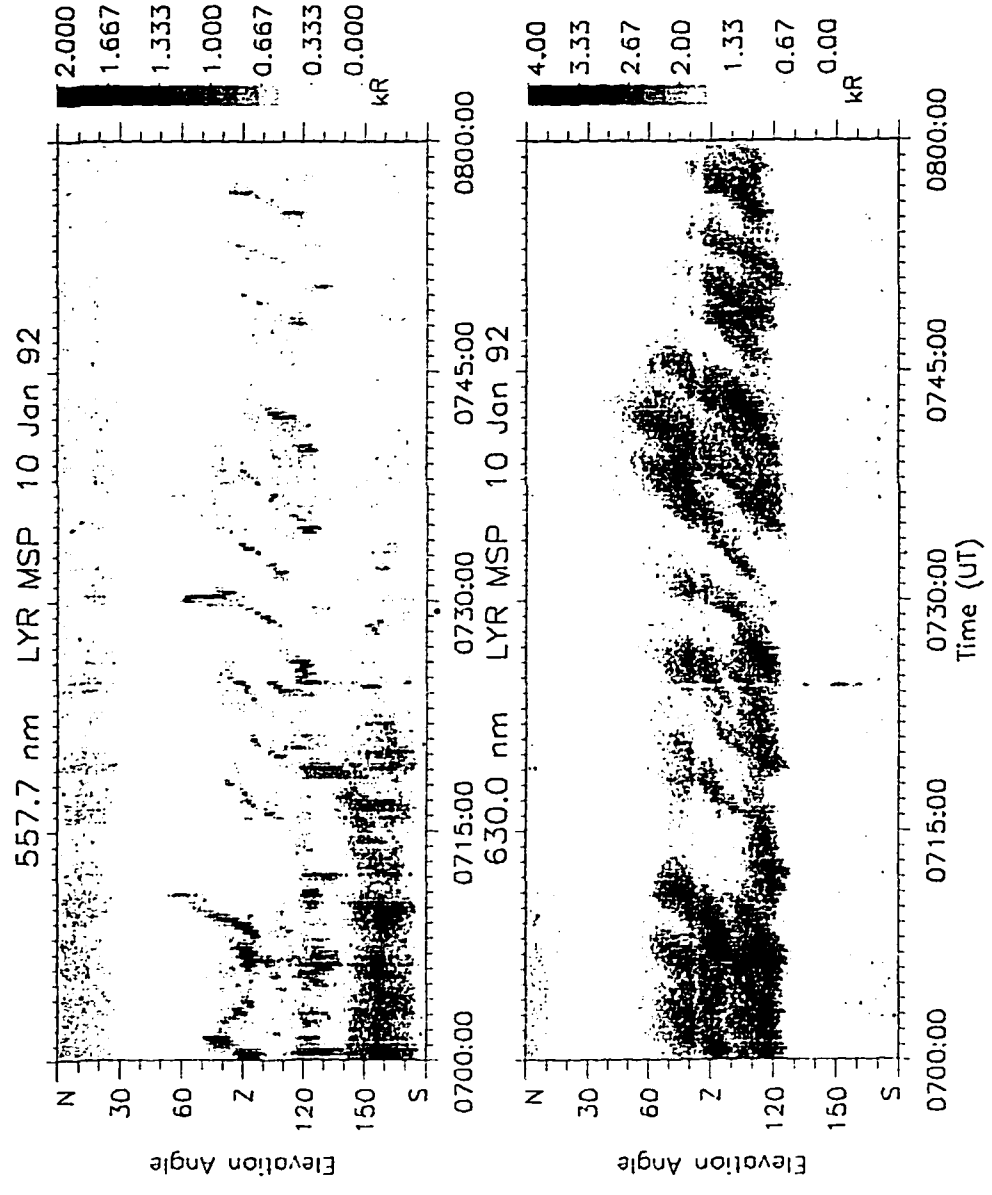


**Figure 4.1 MSP records from Longyearbyen on 10 January 1992. 557.7 nm and 630.0 nm emissions are plotted with the emission intensity coded in increasing levels of grey.**

Reproduced with permission of the copyright owner. Further reproduction prohibited without permission.

image is composed of a series of individual photometer scans which are apparent in the images as thin vertical stripes.

The 630.0 nm and 557.7 emissions sampled by the photometer between elevation angles of approximately 40° to 130° is the dayside auroral oval. Red line emissions are brighter than the green line emissions by a factor of nearly 10 throughout the study period. Transient arcs of the type considered as likely candidates for the auroral response to dayside FTE's (Section 3.4) are forming on the equatorward edge of the dayside oval where the photometer initially samples the emissions at elevation angles between 120° -130° . The arcs subsequently drift poleward to the poleward edge of the auroral oval where the photometer records their fading at elevation angles between 50° to 70° . At least 15 individual transients may be discerned from the photometer plot for the hour period for an average interval of 4 minutes between each transient. The total distance the arcs move is estimated at 115-200 km based on the 557.7 nm component (assuming an altitude of 120 km for the peak emission). This distance is consistent with the width of the cusp or cusp and a fraction of the plasma mantle (Section 2.6.2).

The events which cross through the magnetic zenith between approximately 0730 UT and 0800 UT are particularly amenable to study since each event appears to be an individual arc, is clearly separated in time from adjacent events, and exhibits sharp onset and termination times. Table 4.1 lists a number of characteristics of the individual events. The series of arcs between 0700 UT and 0730 UT are more complicated. Multiple arc structures (e.f., the series from 0700-0710 UT) make estimation of the event velocities and durations difficult and precise measurements of the onset times are precluded by the presence of a persistent emission at the equatorward edge of the dayside oval. Zenith crossing times are given in Table 4.1 to identify each event. The duration is the time from the initial onset of the transient to the time its intensity fades to the background values. The average duration is 7.6 minutes. Distances the arc moved poleward are computed from the duration of each even and the meridional velocity. The average distance, based on the average duration of 7.6 minutes and average velocity of 370 m/s is approximately 170 km, consistent with the 115-200 km estimate obtain from converting the elevation angles to latitudes by assuming and emission altitude.

A time series of 630.0 nm and 557.7 nm intensities in a 5 degree range centered on the magnetic zenith are plotted in Figure 4.2(a). As each transient drifts through the the zenith the intensity of the auroral emissions increases to values in the range of 2-3 kR. Coincident pulses of 557.7 nm emissions are also observed ranging from 0.4-0.6 kR although early in the interval between 0700-0710 UT there are three pulses of 557.7 nm which exceed 1 kR. Between the pulses, when the transient arc has drifted away from the zenith, the 557.7 nm emission decreases to a background of approximately .2-.3 kR. The 630.0 nm emission requires longer to return to the background of 1.6 kR due to the 110 second lifetime of the metastable $O(^1D)$ state.

Velocity of the arc in the magnetic meridian plane is determined from the slope of the peak emission for each transient in Figure 4.1. Velocities of individual transients are listed in Table 4.1 and the average velocity for all of the events is approximately 370 m/s. A zonal component of arc velocity cannot be determined directly from the photometer records but is suggested from the morphology of the auroral emissions. A variation in the slope of the transient can be due to an

Reproduced with permission of the copyright owner. Further reproduction prohibited without permission.

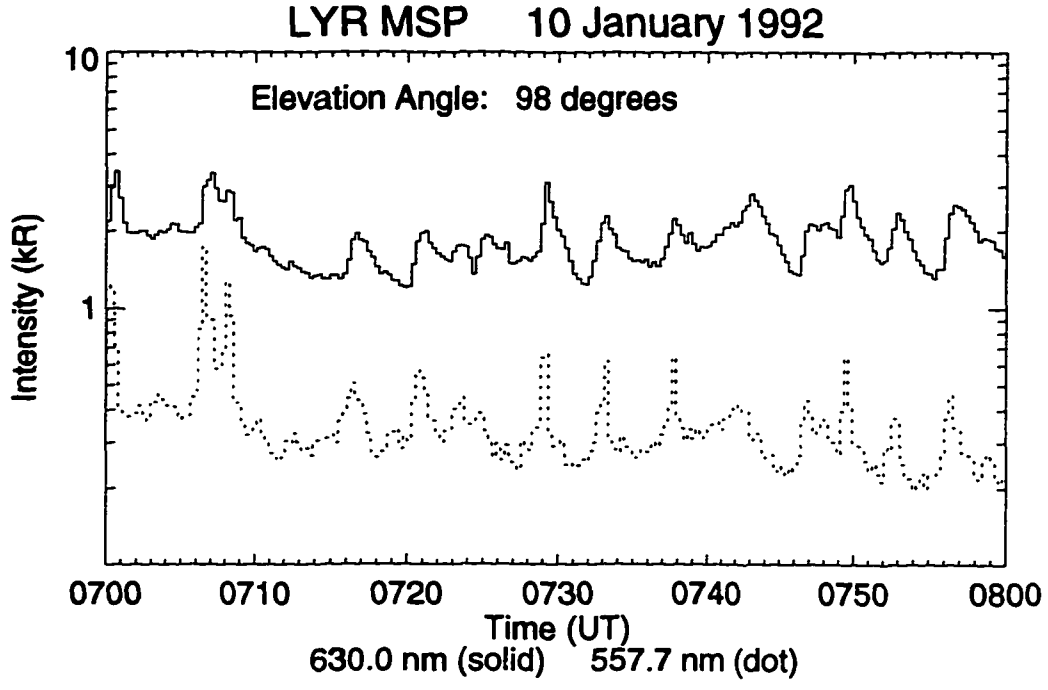


Figure 4.2 Column Intensity of I(630.0 nm) and I(557.7 nm) in Magnetic Zenith. A series of pulses in the 557.7 nm column emission are observed when the transient arcs drift through magnetic zenith. 630.0 nm emissions associated with the arcs are observed to reach a maximum a nearly the same time but decay over a longer period of time due to the longer radiative lifetime of $O(^1D)$ compared to $O(^1S)$ .

initial east-west motion of the arc before drifting poleward (c.f., Figure 2 of *Lockwood et al.* [1989a] and Figure 1b of *Sandholt et al.*, 1989b]. The only arc which appears to drift directly poleward with no detectable azimuthal motion in the 0730-0800 UT interval is the event with crosses the zenith at 0733 UT. The slope of all of the other transient arcs increase within a few minutes of their formation, consistent with the initial east-west motion predicted for newly reconnected field lines [*Cowley et al.*, 1991] and observed for transient dayside arcs (see Section 3.4.1).

The brightness of each transient varies during its lifetime. Many of the events in the 0730-0800 UT period have been previously identified by [*Fasel et al.*, 1994a,b] as exhibiting the periodic intensity fluctuations termed "rebrightenings" by *Fasel et al.* [1992] with intervals of approximately 2 minutes between each intensification [*Fasel et al.*, 1994a]. Mechanisms proposed to explain the origin of the rebrightenings include patchy multiple reconnections at the dayside magnetopause [*Fasel et al.*, 1993; 1994b], an unspecified instability in the upward field aligned current associated with the transient arc [*Lockwood*, 1994], and bouncing of Alfvén waves launched by dayside reconnection [*Kan et al.*, [1996].

Two forms of "persistent" emissions are present in the 0700-0800 UT interval. The first is a diffuse background 630.0 nm emission distributed throughout the dayside oval. Transient arcs are

Reproduced with permission of the copyright owner. Further reproduction prohibited without permission.

**Table 4.1**
**Characteristics of Transient Arcs on 10 January 1992**

| Event Onset (UT) | Zenith[1] Crossing (UT) | Duration (min) | Meridional Velocity (m/s) | Distance (km) |
|---|---|---|---|---|
| 0729:00 | 0733:13 | 11 | 234 | 155 |
| 0733:00 | 0738:00 | 10 | 234 | 140 |
| 0736:30 | 0742:30 | 10.5 | 341 | 215 |
| 0742:00 | 0747:15 | 8 | 395 | 190 |
| 0747:00 | 0749:45 | 4 | 395 | 95 |
| 0750:00 | 0752:30 | 4 | 500 | 120 |
| 0754:00 | 0756:30 | 5.5 | 470 | 155 |

[1]Magnetic zenith, the 98° elevation angle at Longyearbyen.

imbedded in this emission, forming on its equatorward edge and drifting poleward through it. The persistent background lies between elevation angles of approximately 40° and 130° . An estimate of 500 km for the latitudinal width of the persistent background is obtained by adopting an emission altitude of 250 km for the 630.0 nm emission. The latitude over which the transient arcs are observed is less than the persistent background by approximately 50-150 km suggesting that either $O(^1D)$ is transported poleward from the auroral oval or that a flux of low energy electrons is present beyond the highest latitude the transients may penetrate. This subject is considered further in Section 4.4 where the relative contribution of structured and unstructured electron fluxes throughout the polar cusp and plasma mantle to the production of 630.0 nm emissions is determined from DMSP satellite records of precipitating electrons. Transport is considered in Section 4.7.1 by including neutral winds of varying magnitudes in a series of computer simulations to determine the contribution of $O(^1D)$ excited within transient arcs to the diffuse 630.0 nm background.

A number of transients appear to form at greater elevation angles than the diffuse background. Examples in Figure 4.1 include arcs forming at 0712, 0719, 0736, 0750, and 0753 UT. Arcs of these type have been interpreted as forming equatorward of, and subsequently drifting poleward through, the persistent background emission [*Sandholt*, 1988; *Sandholt et al.*, 1986,1989a,b]. Examination of the photometer records in intervals between transients suggests that 557.7 nm emissions are reduced or lacking throughout the diffuse 630.0 nm background emission. For example, the intensity of the 557.7 nm emission in the magnetic zenith (98° ) at 0745 UT is only slightly greater than 100 R while the 630.0 nm emission is approximately 1500 R, a I(630.0 nm)/I(557.7 nm) ratio of 15.

A second type of persistent emission is that sampled by the photometer between elevation angles of 110° and 130° from ~0700-0730 UT where a "ridge" of 630.0 nm emissions are present on the equatorward edge of the auroral oval. The continuous presence of 557.7 nm emissions within this region provides evidence that electron precipitation in this region. This feature is likely the

Reproduced with permission of the copyright owner. Further reproduction prohibited without permission.

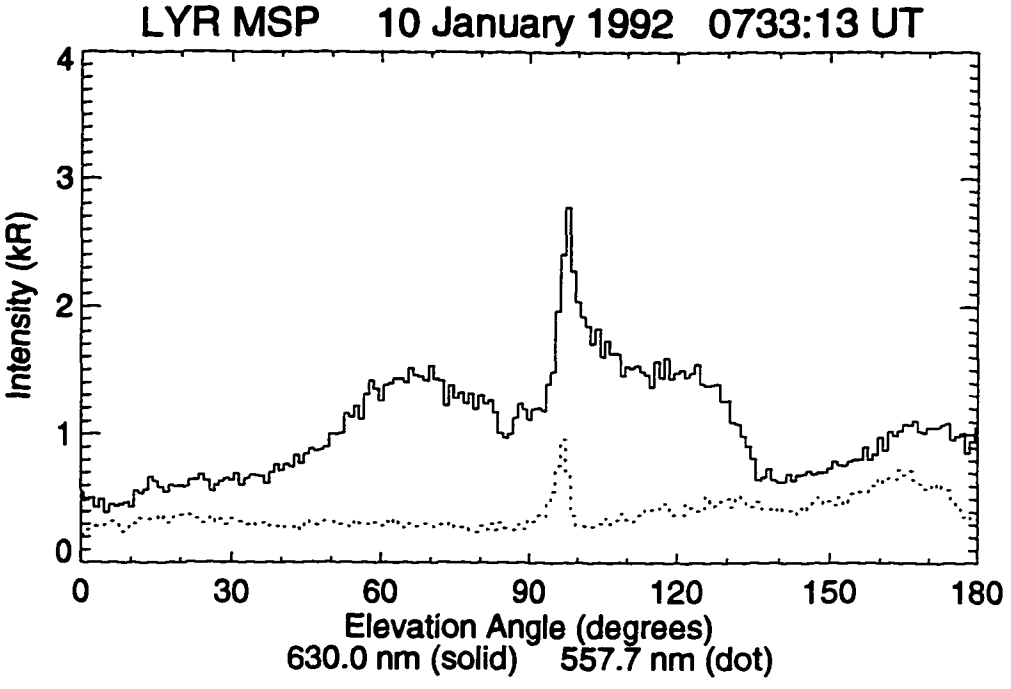


Figure 4.3 Single I(630.0 nm) and I(557.7 nm) Scans. The scan, obtained at 0733:13 UT, shows a transient arc in the magnetic zenith (98° ). The narrowly peaked 557.7 nm emission is indicative of a narrow region of electron precipitation while the 630.0 nm emission is distributed over a wider range of elevation angles equatorward of the green line emission.

"persistent cleft arc" or "stable 630.0 nm arc" that has been noted by a number of authors [c.f., *Sandholt et al.*, 1990b, 1992a, 1994; *Denig et al.*, 1993].

A single scan obtained at 0733:13 UT is plotted in Figure 4.3 showing a narrow emission feature due to a transient arc passing through the zenith. The latitudinal width of the arc is estimated to be approximately 12 km based on the distribution of 557.7 nm emission over a 6° -7° range of elevation angles and an assumed altitude of 110 km. The estimated width is relatively insensitive to the assumed altitude for the emission since the arc is observed near the local zenith.

The 557.7 nm component is on the poleward edge of a broader region of 630.0 nm emission. A mechanism proposed by *Lockwoood et al.* [1993a] and *Lockwood* [1994] to explain asymmetries in the distribution of 630.0 nm and 557 nm emissions within auroral transients is an IMF $B_y$ dependent position of the upward and downward field aligned currents within dayside transients. In the northern hemisphere, the upward field aligned current is predicted to lie on the poleward (equatorward) side of the transient for an IMF $B_y > 0$ ($B_y < 0$). The bulk of the 630.0 nm emission is equatorward of the 557.7 nm emission in the transient passing through zenith in Figure 4.3 predicting an IMF $B_y$ component that is positive. IMF data is unavailable to test this prediction since the IMP 8 satellite was located at $X_{gsm}$ =-17 $R_E$ and $Y_{gsm}$ =-19.5 $R_E$ at this time. Although

Reproduced with permission of the copyright owner. Further reproduction prohibited without permission.

magnetopause crossings have been detected inside of 20 $R_E$ at a distance of 20 $R_E$ behind the Earth they are improbable events [c.f., Figure 2 of *Roelof and Sibeck*, 1993] and the magnetic field data from the IMP satellite for the period is consistent with a satellite location inside the dawn flanks of the magnetosphere. I propose that an aeronomical explanation can explain the observation equally as well even if production of the excited states are confined to the same field lines. $O(^1D)$ excited in the neutral atmosphere by the auroral arc is not constrained to move with the arc. Populations formed equatorward of the arc as it passes through zenith will continue to radiate producing an asymmetric distribution of 557.7 nm and 630.0 nm emission. This proposal is tested with the auroral model in Sections 4.6 and 4.7.

Two other features in Figure 4.3 are of interest. The first is the broad region of 1.5 kR 630.0 nm and weak 557.7 nm emission at elevation angles between 110° and 130° . Consulting Figure 4.1 is it apparent that this is the onset of a new transient forming equatorward of the zenith arc. Poleward of the zenith arc between elevation angles of 40° and 90° is a broad region of unstructured 630.0 nm emission with peak intensity on the order of 1.5 kR. Green line emissions throughout the region are reduced or absent, at most only 30-50 R of 557.7 nm are detectable above the airglow background. The relative position of the broad unstructured 630.0 nm dominated emission poleward of a narrow arc is reminiscent of the "cusp" identified in photometer scans by *Sivjee et al.* [1982] and *Sivjee* [1983] poleward of a long rayed aurora. Consulting the photometer records in Figure 4.1 it is apparent that another interpretation of the unstructured 630.0 nm in the northern sky is a decaying population of $O(^1D)$ from a previous transient. In this view all three 630.0 nm features in the scan, the narrow arc in the zenith and the broad structures in the northern and southern skies, are transient arcs at different stages in their lifetime. This proposal for the origin of the "cusp" emissions poleward of discrete arcs is tested in Sections 4.6 and 4.7 with the auroral model.

### 4.3 Previous Work on Persistent 630.0 nm Dayside Emissions

The origin of persistent emissions in dayside aurora has been considered in a number of studies although the observations have generally been confined to either the prenoon or postnoon sector. A brief review of the most pertinent studies are presented here to provide a background on the status of the work and to emphasize that the studies are generally removed from the local time sector where particle precipitation is likely to be the result of merging at the dayside magnetopause.

*Sandholt et al.* [1989a] and *Burke et al.* [1993] describe coordinated ground and satellite observations of dayside aurorae in the $\sim$ 9 MLT sector. Photometers and all sky cameras record of auroral emissions were compared with energy spectra of precipitating protons and electrons as well as magnetic field deflections obtained during DMSP overflights of the ground site to determine the relationship between particle precipitation and field aligned currents in the aurora. The case studies showed that persistent red structures and discrete transient arcs lie in a region of filamentary field aligned currents. Both studies concluded that the particle source for the persistent 630.0 nm emission were electrons originating in the low latitude boundary layer or plasma sheet and not the dayside magnetopause.

Reproduced with permission of the copyright owner. Further reproduction prohibited without permission.

*Sandholt et al.* [1993] presented a particularly interesting case study of dayside aurora containing persistent 630.0 nm emissions observed on 12 Jan 1991 in the ~ 0930 MLT sector. Photometer observations from two sites in the Svalbard Archipelago were used to compare observations of a single aurora from different aspect angles. Photometers at the Ny Ålesund field site sampled a series of transient arcs and persistent emission in the dayside auroral oval located far to the south of Ny Ålesund. A second photometer at Hopen was located under the auroral oval and sampled the same auroral emissions near the local zenith. Drift meter records of the cold plasma drift velocity obtained from an overpass of a DMSP satellite east of the ground site confirm the location of the persistent emissions near the convection reversal boundary. The origin of the particle fluxes responsible for the persistent 630.0 nm component are identified by the authors as the low latitude boundary layer or boundary plasma sheet and not magnetosheath plasma entering through the polar cusp.

A unique aspect of the *Sandholt et al.* [1993] study is the comparison of the persistent 630.0 nm emission from two sites. The instrument at Ny Ålesund, far to the north of the auroral emissions, sampled the auroral emissions near the southern horizon. A nearly constant 630.0 nm emission in the auroral oval is reported from the northern site. The photometer at Hopen is nearly underneath the auroral oval providing a much better observation of the auroral emissions. The same auroral forms that appear to include a very stable 630.0 nm arc when observed from Ny Ålesund appears to be a series of individual arcs in the Hopen data with strong temporal variations even on the equatorward edge of the "background cleft emission." Comparison of the two data sets is a good example of the problems inherent in interpreting photometer data for auroral structures that are far from a ground site. Reports of stable 630.0 nm emissions in these cases should be considered suspect and only examples where the auroral oval is sampled within 45° -50° degrees of local zenith should used in studies of persistent emissions.

This may be the case for the *Denig et al.* [1993] study where a similar set of photometer and satellite data in the 11 MLT sector were examined. Photometer data indicated the presence of persistent 630.0 nm emissions to the south of the Ny Ålesund site. Transient arc fragments were reported to form either poleward of, or within, the persistent 630.0 nm emissions and were thought to be due to motion of arcs into the field of view of the camera from a merging site located closer to local noon. Comparison of the optical records with energy spectra of the precipitating particles from a DMSP satellite overpass showed that the region of the persistent 630.0 nm emissions was composed of three distinct zones of precipitation related to the morning boundary layers that were not resolved in the optical data. *Lockwood and Cowley* [1994] pointed out that the background 630.0 nm emissions are not stable in this case, rather, temporal and spatial variations exist in the photometer data that are consistent with westward travelling transient arc events described by *Lockwood et al.* [1990].

A pertinent observation, although not optical in nature, is that of *Wickwar and Kofman* [1984] who measured elevated electron temperatures sufficient to produce $O(^1D)$ in the auroral oval associated with the afternoon convection reversal boundary. Calculation of $O(^1D)$ concentrations predicted that 1-2 kR of 630.0 nm emissions could be produced by the heated electron gas suggesting a source for a postnoon persistent red arc. Direct observation of a red arc to confirm the

Reproduced with permission of the copyright owner. Further reproduction prohibited without permission.

prediction was not possible however since the study was performed in daylight conditions. The results are consistent with a suggestion by *Reiff et al.* [1978] that strong and persistent 630.0 nm emissions are expected in the prenoon and postnoon sectors associated with shears in the ion drift velocity at convection reversal boundaries. In contrast to the conclusions reached in the *Sandholt et al.* [1989a, 1993], *Burke et al.* [1993], and *Denig et al.* [1993] studies where particle precipitation from the boundary layer/plasma sheet interface was identified as the energy source for excitation of atomic oxygen to the $O(^1D)$ state, the *Reiff et al.* [1978] mechanism invokes ion drag on the neutral atmosphere at the ion velocity shear to produce the excited states.

*Evans* [1985] reported satellite observations of a persistent energetic electron flux in the 1400 MLT sector with average energy fluxes of 0.50 ergs/cm$^2$ s sr and energies of 0.3-3 keV. The highly structured precipitated electron fluxes showed evidence of acceleration in the form of peaks at keV energies. Most of the precipitation occurred in one or several narrow regions with widths on the order of 10 km. Peak energy fluxes within the narrow structures often exceeded 3 ergs/cm$^2$s and in some exceptional cases exceeding 30 ergs/cm$^2$ s. Auroral emissions in the 14-16 MLT sector, often referred to as the "afternoon hot spot", when observed from the ground [*Sandholt et al.*, 1990a; *Moen et al.*, 1994] or satellite [*Murphree et al*, 1981; *Meng and Lundin*, 1986; *Lui et al.*, 1989; *Vo and Murphree*, 1995] are seen to be multiple, longitudinally extended arcs often dominated by 557.7 nm emissions in accord with *Evans* [1985] report of keV electrons within the structured electron fluxes.

The results from the previous studies of persistent emissions in the daytime region may be summarized by noting that the majority of the reports are not generally applicable to the region near local noon. They have focussed on either the prenoon sector [*Burke et al.* 1993, *Sandholt et al.*, 1989a] or postnoon sector [*Wickwar and Kofman*, 1984; *Evans*, 1985] where the large field aligned currents map along magnetic field lines to the flank regions of the magnetospheric boundary layers and near Earth tail (see Figure 2.8) and strong shears in the convection velocity provide ample energy to excite a persistent 630.0 nm emission [*Reiff et al.*, 1978]. These mechanisms are not directly related to the dayside merging process which maps along field lines into the midday sector.

These papers appear to suggest that a region of stable and persistent 630.0 nm emissions may be found in the 9 MLT sector but temporal variations in the red emissions are found near 11 MLT, i.e., nearer local noon. The results of these cases suggest that the stationary persistent 630.0 nm emissions observed in the prenoon sector is excited by charged particles originating in the prenoon boundary layers either poleward of or in the region of the convection shear, consistent with the proposal that the nonuniform flow pattern is responsible for the excitation of the dayside auroral arcs [*Reiff et al.*, 1978]. Within the region where the merging line is most likely to be found, however, the temporal behavior of the 630.0 nm emissions is of greatest interest since it is there that the auroral emissions are thought to be the best monitor of the dayside merging process. The hypothesis that series of discrete poleward drifting auroral events may be capable of producing the 630.0 nm emissions observed within the midday oval was not considered in any of these studies.

Reproduced with permission of the copyright owner. Further reproduction prohibited without permission.

## 4.4 Estimates of I(630.0 nm) from DMSP Cusp Overflights

Overflights of the midday aurora by low altitude satellites offer one possible solution to determine the origin of the midday "persistent" 630.0 nm background emission. Satellite records of the average energy and energy flux of precipitating electrons may be converted to column emission rates using equations (3.40)-(3.42) or alternatively the empirical excitation efficiencies listed in equation (3.47). This method is applied here to a number of DMSP spectrograms obtained during cusp overflights to estimate relative contributions of structured and diffuse electron fluxes to the total energy deposition in the cusp ionosphere.

### 4.4.1 Minimum I(630.0 nm) Predicted by [*Newell and Meng*, 1988] Definition of Cusp

The criteria *Newell and Meng* [1988] adopted for identifying the polar cusp in DMSP records of precipitating particles (Table 2.1) can be used to establish minimum intensities for auroral emissions within the cusp. A population of energetic particles is classified as "cusp" if:

(i) average electron energy is $E_e < 220$ eV and average ion energy is
in the range $300 < E_i < 3000$ eV, and
(ii) electron energy fluxes $J_e > 6 \times 10^{10}$ eV/cm$^2$ s sr and
ion energy fluxes $J_i > 1 \times 10^{10}$ eV/cm$^2$ s sr.

An increase in the energy flux will increase the photon yields. Decreasing the average electron energy to values less than the threshold of 220 eV will similarly increase the photon yields since the O($^1D$) and O($^1S$) excitation cross sections increase with decreasing energy to a maximum value near 10 eV. Any population of charged particles meeting the *Newell and Meng* [1988] criteria will produce 630.0 nm and 557.7 nm emissions exceeding a minimum value which can be estimated using equations (3.40)-(3.42).

Consider the effect of the energy deposition by the electrons first. Electron thermal velocities far exceed the bulk ion flow velocity in the cusp [*Reiff et al.*, 1977] so that electron pitch angle distributions are isotropic over the downward hemisphere throughout the cusp [c.f., the observations reported by *Reiff et al*, 1977; *Burch et al.*, 1982; *Burch*, 1985; *Menietti et al.*, 1988; *Yamauchi and Lundin*, 1994]. Assuming the DMSP detectors are sampling the field aligned fraction of an isotropic pitch angle distribution, the downgoing hemispherical electron flux is $J_e > 6\pi \times 10^{10}$ eV/cm$^2$ s to meet the criteria identifying the precipitating particles as cusp. Equation (3.41) and (3.42) predicts I(630.0 nm) $\geq$495 R and I(557.7 nm) $\geq$550 R due to the electron component of the magnetosheath plasma within the cusp using the limiting electron energy of 220 eV. Note that the ratio I(630.0 nm)/I(557.7 nm)$\sim$0.9 is smaller than values normally adopted for optical identification of the cusp. For example, *Sandholt et al.* [1988] suggests the ratio should be greater than 2 with only transient increases of the 557.7 nm component yielding temporary ratios less than 2. Values of I(630.0 nm)$\sim$1 kR and I(557.7 nm)$\sim$0.65 kR result from using an electron energy of 100 eV, an electron energy typical of the cusp. The ratio in this case the I(630.0 nm)/I(557.7 nm)$\sim$1.5.

Pitch angle distribution of precipitating ions in the cusp depend on altitude and the the travel time from the reconnection site and are not in general isotropic when sampled at mid-altitudes

Reproduced with permission of the copyright owner. Further reproduction prohibited without permission.

[*Frank*, 1971; *Burch et al.*, 1982; *Burch*, 1985; *Menietti et al.*, 1988]. *Reiff et al.* [1977] have shown that ions are isotropic over the downward hemisphere when measured at low altitudes. The same argument applied to electrons may therefore be used for ions at low altitude and the DMSP ion angular fluxes are converted to downgoing omnidirectional fluxes by assuming the detectors sample a fraction of an isotropic distribution. The limiting ion energy flux to identify a region as cusp is $J_i > \pi \times 10^{10}$ eV/cm$^2$ s Precipitating ion energies and energy fluxes cannot be converted to I(630.0 nm) and I(557.7) as readily as the electron case since proton excitation efficiencies analogous to equations (3.40)-(3.42) are not generally available in the literature. Instead, an estimate of the proton contribution to the auroral red and green lines within the cusp can be obtained by adopting the I(486.1 nm)$\sim$10-40 R range from Table 3.1 for $H_\beta$ within the cusp. Values of I(630.0 nm)$\sim$25-132 R and I(557.7 nm)$\sim$90-480 R due to protons are obtained using the I(630.0 nm)/$H_\beta$ and I(557.7 nm)/$H_\beta$ ratios in Table 3.7.

Addition of the electron and proton contributions yield predicted background intensities of I(630.0 nm)$\sim$ 0.5-0.6 kR for 220 eV electrons and 1.0-1.1 kR for 100 eV electrons, consistent with reports of strong red line emission backgrounds throughout the midday cusp. The proton contributions are likely to be reduced from the estimated provided here due to expansion of the particle flux over a wide range of latitudes once the precipitating particles encounter the atmosphere. Electrons will therefore provide the dominant contribution to 630.0 nm emissions in the polar cusp.

### 4.4.2 Distribution of 630.0 nm Emissions in Cusp from Theoretical DMSP Records

Conversion of the average ion and electron energy and energy flux along a satellite track to I(630.0 nm) during a traverse of the cusp provides an estimate of the latitudinal dependence of cusp 630.0 nm emissions. A list of column emission rates are given in Table 4.2 to convert the average energy and energy fluxes on the standard Applied Physics Laboratory DMSP particle format [*c.f.*, *Wing et al.*, 1996] to intensities of the 630.0 nm, 557.7 nm, and 427.8 nm emissions. In all cases the electron pitch angles are assumed to be isotropic over the downgoing hemisphere. Each of the column intensities are computed using an energy flux value of $1.0 \times 10^{10}$ eV/cm$^2$ s sr. Column intensities may be determined for other values of the energy flux by simply multiplying by the appropriate value.

Reproduced with permission of the copyright owner. Further reproduction prohibited without permission.

**Table 4.2**
**I(630.0 nm) and I(557.7 nm) from Cusp Electrons**

| Average Energy (eV) | Energy Flux $10^{10}$(eV/cm$^2$ s sr) | I(630.0 nm) (R) | I(557.7 nm) (R) | I(427.8) (R) |
|---|---|---|---|---|
| 100 | 1 | 170 | 110 | 9 |
| 200 | 1 | 90 | 96 | 10 |
| 300 | 1 | 62 | 90 | 10 |
| 400 | 1 | 48 | 85 | 10 |
| 500 | 1 | 39 | 81 | 10 |
| 600 | 1 | 33 | 78 | 10 |
| 700 | 1 | 29 | 76 | 10 |
| 800 | 1 | 26 | 73 | 10 |
| 900 | 1 | 23 | 72 | 11 |
| 1000 | 1 | 21 | 70 | 11 |

The numerical models of magnetosheath proton and electron entry into the magnetosphere developed by *Onsager et al.* [1993] and *Wing et al.* [1996] successfully reproduce DMSP spectrograms for ions in the cusp, mantle, and polar cap. The original *Onsager et al.* [1993] model predicts electrons with average energies of 100 eV throughout the cusp with an energy flux decreasing from a maximum of approximately $5 \times 10^{11}$ eV/cm$^2$s sr at the equatorial edge of the cusp to a minimum of $1 \times 10^{11}$ eV/cm$^2$ s sr at the poleward edge of the intense cusp ion precipitation (c.f., Plate 1 of *Wing et al.* [1996]). The 630.0 nm emission produced by the electrons would vary smoothly from 8.5 kR at the equatorial edge of the cusp to 1.7 kR at the poleward edge. Distribution of electron precipitation in the *Onsager et al.* [1993] model does not correspond well with real data, however, lacking a sharp decrease in electron flux at the poleward edge of the cusp. In fact, the model predicts precipitating electron energy fluxes poleward of the cusp in excess of $1 \times 10^{10}$ eV/cm$^2$ s sr up to the highest latitudes sampled by the satellite. A uniform glow of 630.0 nm emissions in excess of 170 R is predicted by the model.

*Reiff et al.* [1977] pointed out that electron thermal speeds are much greater than the magnetosheath flow speed allowing electrons to enter the magnetosphere along any open field line throughout the polar cap. Ion thermal speeds in contrast are much smaller than magnetosheath flow speeds, limiting ion entry into the magnetosphere to regions where the magnetosheath flow is subsonic. Observations of electron precipitation at high latitudes shows that large fluxes of electron precipitation is limited to regions of ion precipitation suggesting the presence of an ambipolar electric field requiring the electrons to precipitate with the ions. This was confirmed when *Burch* [1985] showed that magnetosheath plasma within the midaltitude cusp is quasi-neutral. *Wing et al.* [1996] introduced an electric potential from the magnetopause to the Earth to the *Onsager et al.* [1993] model to ensure precipitating magnetosheath plasma remains quasi-neutral. Simulated DMSP spectrograms produced by the improved model successfully reproduce the main features of both ion and electron precipitation in the cusp, mantle, and polar rain. The distribution of electrons throughout the cusp is still smooth in the *Wing et al.* [1996] model, decreasing from

Reproduced with permission of the copyright owner. Further reproduction prohibited without permission.

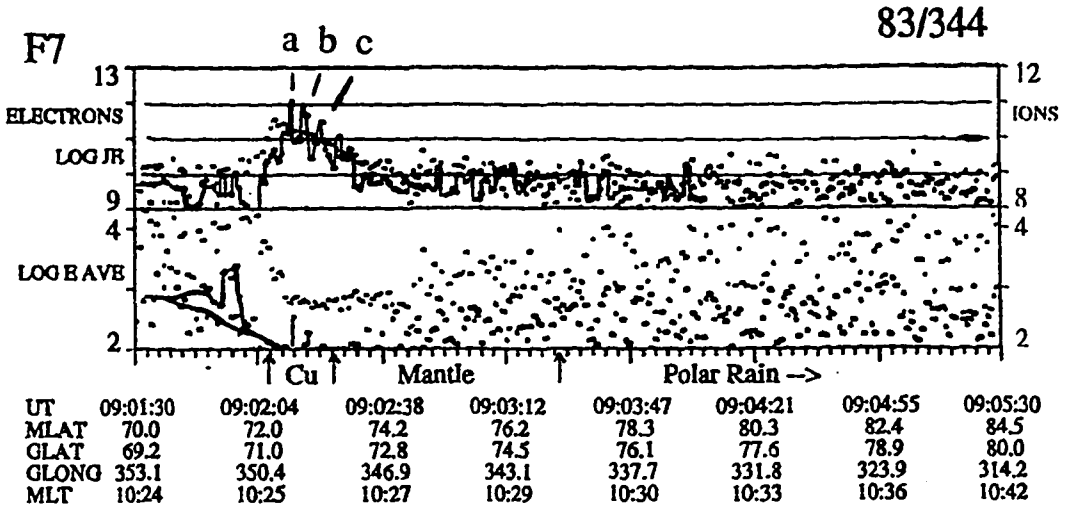


Figure 4.4 Energy Flux and Average Energy for Electrons and Ions, 10 December 1983. Electron and ion energy flux (eV/cm$^2$s sr) is given in the top plot and average electron and ion energies (eV) in the lower plot. Electron values are emphasized by the solid line. Events labelled a,b, and c are discussed in the text. Identification of the precipitating particles is based on the technique described by *Newell et al.* [1991c]. [adapted from *Wing et al.*, 1996].

$5\times10^{11}$ eV/cm$^2$s sr to $1\times10^{11}$ eV/cm$^2$s sr in the cusp but rapidly decreasing below $7\times10^{9}$ eV/cm$^2$s sr at latitudes where dayside magnetosheath plasma can no longer penetrate. Predicted column intensities of the 630.0 nm emission are the same as the *Onsager et al.* [1993] model throughout the cusp with 630.0 nm intensities between approximately 2 and 8 kR but an abrupt decrease in electron energy fluxes on the poleward edge of the cusp reduces the auroral emission to values below 17 R within 30-50 km poleward of the cusp.

### 4.4.3 Case Study of 630.0 nm Emissions in Cusp from DMSP Records

DMSP satellite overpasses of the cusp often show the structured electron fluxes in contrast to the relatively featureless precipitation predicted by the models. An example of structured electron fluxes superimposed on a diffuse background flux is given in Figure 4.4 where the average energies and energy fluxes from a DMSP F7 spectrogram obtained on 10 December 1983 are plotted. The figure is an adaptation from the original spectrogram published as Plate 2 of *Wing et al.* [1996]. Three enhanced electron energy flux structures are identified within the cusp (labelled a,b, and c) and a fourth is present at the equatorward edge of the plasma mantle superimposed on a

Reproduced with permission of the copyright owner. Further reproduction prohibited without permission.

broad featureless background. Identification of the precipitating particle types is based on the neural network method described by *Newell et al.* [1991c]. Electron energy fluxes are greater than $1 \times 10^{10}$ eV/cm$^2$s sr between magnetic latitudes of 72° and 74.2° , a distance of approximately 220 km, predicting I(630.0 nm) values >170 R. This includes the cusp and low latitude edge of the plasma mantle. Energy fluxes in a more restricted range (~160km) sampled by the satellite between 09:02:07 UT and 09:02:27 UT lie above $6 \times 10^{10}$ eV/cm$^2$s sr where I(630.0 nm)> 1 kR.

The structured electron events within the cusp are observed at 09:02:13 UT, 09:02:16 UT, and 09:02:20 UT. Electron energy fluxes for all three of the events exceed $10^{11}$ eV/cm$^2$s sr predicting I(630.0 nm)> 1.7 kR. The width of each enhancement is approximately 20 km based on the ~3 second period required for the satellite to cross each structure at a velocity of 7 km/s. Estimates of the average energy and energy fluxes within the structures (labelled in the time column) encountered by the satellite in the cusp are given in Table 4.3 in the second and third columns. Estimates of the background energy fluxes are given in the fourth column. The average energy of the background precipitation is 100 eV, typical of magnetosheath plasma. Electron acceleration is suggested in two of the structures by the 500 eV and 700 eV average energy within the events, values exceeding typical magnetosheath electron energies.

The fractional contribution of the structured events above the background to the total energy deposition within each event

$$F_{energy} = \frac{J_{E,p} - J_{E,b}}{J_{E,p}} \tag{4.1}$$

is listed in the final column. Note that over 90% of the energy deposition within each structured electron event is due to the electron flux above the background. The contribution of the structured electron events to the total energy deposition within the cusp is obtained by comparing the energy flux within the structured events above the background flux, $27.0 \times 10^{11}$ eV/cm$^2$s sr, to the total energy flux measured during the satellite traverse of the cusp, $28.6 \times 10^{11}$ eV/cm$^2$s sr. The fraction is approximately 94% demonstrating that the structured electron events are the dominant source of electron energy input into the cusp.

**Table 4.3**
**Characteristics of Cusp Electron Fluxes, 10 December 1983**

| | Peak Flux | | Background Flux | | $F_{energy}$ |
|---|---|---|---|---|---|
| Time (event) (UT) | $J_E \times 10^{11}$ (eV/cm$^2$s sr) | $< E >$ (eV) | $J_E \times 10^{11}$ (eV/cm$^2$s sr) | $< E >$ (eV) | |
| 09:02:07 | | | 0.6 | 100 | |
| 09:02:10 | | | 0.9 | 100 | |
| 09:02:13 (a) | 10 | 700 | 1.0 | 100 | 0.90 |
| 09:02:16 (b) | 10 | 500 | 0.9 | 100 | 0.91 |
| 09:02:20 (c) | 7 | 100 | 0.5 | 100 | 0.93 |
| 09:02:23 | | | 0.1 | 100 | |

Reproduced with permission of the copyright owner. Further reproduction prohibited without permission.

The estimated peak and background 630.0 nm intensity for each of the three structures are given in Table 4.4 using the results from Table 4.2. An emission fraction

$$F = \frac{I_{peak} - I_{background}}{I_{peak}} \tag{4.2}$$

is computed for the red and green lines and listed in the final two columns. Note that while the energy deposition in the cusp due to the structured events dominates the contribution by the background fluxes, the fraction of the 630.0 nm emission due to the electron flux enhancement varies from 41% to nearly 90% of the light production. The discrepancy occurs because the light production depends not only the electron energy flux but the electron energy as well. Even though the energy flux contained in the first event is greater than the third, the third event produces more 630.0 nm photons because of its lower average energy. Yields of 557.7 nm emissions in all three of the events are in excess of 7 kR. The green line due to the background electron fluxes are dominated by the 630.0 nm emission. The auroral display suggested by these results is a diffuse aurora dominated by a > 1 kR 630.0 nm emission over a latitudinal width of 160 km. Three to four intense green dominated arcs with widths < 21 km are imbedded in the background emission. This auroral morphology is substantially what is observed in the 10 January 1992 example presented in Section 4.2. The differences in absolute intensities and ratios of the 557.7 nm and 630.0 nm between the 10 January 1992 example and the DMSP case study presented here are not significant considering that auroral emissions may vary by factors of 4 to 5 due to differences in atmospheric composition [*Meier et al.*, 1989]. Variations in the ratios of the 557.7 nm and 630.0 nm emissions arise due to variations in average electron energies between the two events.

**Table 4.4**
**Predicted Cusp I(630.0 nm) and I(557.7 nm) Intensities, 10 December 1983**

| Time (UT) | Peak Emission 630.0 (kR) | Peak Emission 557.7 (kR) | Background Emission 630.0 (kR) | Background Emission 557.7 (kr) | 630.0 Fraction | 557.7 Fraction |
|---|---|---|---|---|---|---|
| 09:02:07 | | | 1.0 | 0.66 | | |
| 09:02:10 | | | 1.5 | 0.99 | | |
| 09:02:13 | 2.9 | 7.6 | 1.7 | 1.10 | 0.41 | .86 |
| 09:02:16 | 3.9 | 8.1 | 1.5 | 0.99 | 0.61 | .88 |
| 09:02:20 | 11.9 | 7.7 | 0.85 | 0.55 | 0.93 | .93 |
| 09:02:23 | | | 0.17 | 0.11 | | |

Electron features with enhanced energy fluxes and increased average energies have been previously described by *Escoubet et al.* [1995] in DE 2 satellite data from the cusp/cleft region. The electron energy spectrum within the electron structures exhibit a peak near 500 eV but is otherwise similar to electron energy spectra within the magnetosheath and in the background cusp plasma (i.e., outside of the structured events). FTE's were eliminated as the source of the energetic electrons by noting that the spectrum of electrons energized on the edge of an FTE peak near 100 eV *Farrugia et al.* [1988]. The acceleration of the magnetosheath plasma must occur somewhere

Reproduced with permission of the copyright owner. Further reproduction prohibited without permission.

between the magnetopause and the ionosphere. The width of the events varied from 14 km to 50 km and energy fluxes varied from 1-3 ergs/cm$^2$s sr. Assuming an isotropic distribution, the omnidirectional energy flux is approximately 3-9 ergs/cm$^2$ s within these events. Equations (3.41) and (3.42) predict and aurora with 2-7 kR of 630.0 nm and 5-14 kR of 557.7 nm emissions consistent with observations of strong transient 557.7 nmn emissions in midday auroral arcs [*Sandholt et al.*, 1989b]. The electron structures are imbedded in a background electron flux of approximately 0.1 ergs/cm$^2$s sr and energy of 100 eV predicting 1 kR 630.0 nm and 0.7 kR 557.7 nm emissions.

*Escoubet et al.* [1995] noted the strong similarity of the structured events in the DE data to the fluxes responsible for transient arcs in the dayside aurora. The events are a common feature of the cusp being observed on 80% of the DE cusp crossings with an average of 2 events per crossing. This value is consistent with the photometer data in Figure 4.1 where at least one, usually two, and sometimes three transient arcs are present at any time within the 0700-0800 UT interval. The average number of electron structures in the DE cusp data may also be compared with the statistical results *Fasel* [1995] obtained for transient auroral arcs in the midday aurora. The distribution of transient event lifetimes peaks at 3-4 minutes with a mean of 5 minutes and the distribution of intervals between successive transient auroral events peaked at 3-4 minutes with a mean of 6 minutes. The accumulated probability of a new arc forming within the approximately 5 minute mean lifetime of an existing arc is 53%. This estimate is based on summing the probability given in Figure 5 of *Fasel et al.* [1995] over five minutes. If the ~7 minute average lifetime of the 10 January 1992 events in Figure 4.1 is used rather than the mean value from *Fasel* [1995] then the probability of a second arc forming while a previous arc is still active is 67%. These results are consistent with the DE average of 2 events per crossing.

The events identified by *Escoubet et al.* [1995] were found at magnetic latitudes between 65° and 85° and distributed throughout local times between 0930 MLT to 1430 MLT (times outside of this interval were excluded from the study). The structured electron events associated with electron acceleration in the DMSP records described above are within the cusp as well. Identifying the narrow electron structures as acceleration events may appear inconsistent with the *Kremser and Lundin* [1990] definition of the cusp proper which is based on the lack of acceleration events and the recent results obtained by *Newell et al.* [1996] which show that electron acceleration events are rare or absent in the midday auroral oval.

*Kremser and Lundin* [1990] distinguished two particle populations in the cusp region from measurements obtained by the Viking satellite: a "cusp proper" subregion connected to the entry layer imbedded within a larger "cusp" region connected to the exterior cusp. Plasma with magnetosheath characteristics is present in both regions but electron acceleration is not observed within the cusp proper. It is possible that the events described by *Escoubet et al.* only occur within the cusp but not the localized cusp proper. An alternative explanation is that the altitude of the Viking observations between 12,000-13,000 km ($\sim 2\ R_E$) during cusp encounters was above the acceleration region. If the *Escoubet et al.* [1995] study is taken as evidence of electron acceleration throughout the cusp then the lack of acceleration through a fraction of the cusp places the acceleration region at 1-2 $R_E$.

Reproduced with permission of the copyright owner. Further reproduction prohibited without permission.

The apparent contradiction with the *Newell et al.* [1996] study is resolved by noting that the neural network used to identify acceleration events was trained to recognize inverted V events [*Lin and Hoffman*, 1979, 1982] as a method of detecting electron acceleration. Inverted V events also appear in the data sets examined by *Escoubet et al.* [1995] but are distinct from the electron structures identified as accelerated electrons. Therefore the structured electron events described by *Escoubet et al.* would not be identified by *Newell et al.* as acceleration events.

A plausible explanation for the unstructured background electron fluxes within the cusp which produce a diffuse 630.0 nm background emission is suggested by the origin of the structureless electron energy fluxes in the *Onsager et al.* [1993] and *Wing et al.* [1996] theoretical models for magnetosheath plasma entry into the magnetosphere. The *Wing et al.* [1993] model is the most successful of the two in predicting the distribution of electrons in the cusp, plasma mantle, and polar cap yet the only mechanism provided to alter the distribution of electron fluxes within the cusp is the introduction of an electric field to maintain charge quasi-neutrality. The electrons, constrained by the ambipolar electric field that is generated when the electrons start to outrun the ions, are bound to travel with the ions. The ions, due to their much greater mass, determine the distribution of magnetosheath plasma in polar cap region. Electron distributions in latitude and time are governed entirely by the ion behavior.

Ions will be observed over a wide range of times at low altitudes even if they cross the magnetopause at the same time due to large differences in flight times between the high and low energy ions. Reconnection models predict that ion velocity distributions immediately inside the magnetopause will exhibit a characteristic "D" distribution in velocity [*Cowley*, 1982] which have been observed by a number of spacecraft near the magnetopause [*Gosling et al.*, 1990b; *Fuselier et al.*, 1991; *Smith and Rodgers*, 1991]. The distributions peak between 250 km/s and 500 km/s with a low velocity cut off at 130-200 km/s [*Smith and Rodgers*, 1991; *Smith*, 1994] corresponding to the de Hoffman-Teller velocity [*Cowley*, 1982; *Smith*, 1994]. Ions are observed with velocities up to 1000 km/s [*Smith and Rodgers*, 1991]. Assuming a distance of 15 $R_E$ from the magnetopause to the ionosphere, the high energy ions may arrive as soon as 1.5 minutes after crossing the magnetopause. The bulk of the ions will take 3-6 minutes and the slowest ions near the cut off velocity 8-12 minutes. Considering that the mean interval between injections is on the order of 8 minutes with the most probable value near 3 minutes [*Lockwood and Wild*, 1993], many of the low energy ions from previous injections will not have arrived in the ionosphere before they are overtaken by high energy ions from a more recent injection [*Lockwood and Smith*, 1992; *Lockwood et al.*, 1984]. Ions must therefore be continuously present in the cusp during periods when magnetic field line merging is actively eroding flux from the dayside magnetopause [*Lockwood and Smith*, 1994]. Accompanying the continuous ion flux is a continuous electron flux to maintain charge quasi-neutrality.

Time of flight effects alone cannot explain the distribution of plasma in cusp and mantle. Electric fields within the magnetosphere are responsible for redistributing plasma by driving charged particles across magnetic field lines [*Lockwood and Smith*, 1993]. The effect of flight time variations due to particles of differing energies in the presence of an electric field produces the decrease in average ion energy with latitude characteristic of the polar cusp and plasma mantle when IMF $B_z$ is southward [*Rosenbauer et al.*, 1975; *Reiff et al*, 1977; see also the discussion in Section 2.6.2].

Reproduced with permission of the copyright owner. Further reproduction prohibited without permission.

Ions can enter the magnetosphere over a wide range of locations as reconnected field lines convect antisunward–even in the case where the reconnection is discontinuous–producing a continuous precipitation of ions into the atmosphere over a wide range of latitudes [*Cowley et al.*, 1991 *Onsager et al*, 1993; *Lockwood and Smith*, 1993]. The electrons accompanying the ions are similarly distributed in latitude as well.

The source of the persistent, structureless background electron fluxes described in this section which appear to be responsible for diffuse 630.0 nm emissions on the order of 0.1-1 kR is the magnetosheath component of the precipitating magnetosheath plasma bound to precipitate with the ions due to the requirement of charge quasi-neutrality. The structured electron energy fluxes which are commonly observed during satellite traverses of the cusp do not appear in the models, requiring an additional mechanism to the ambipolar electric field to explain the observed distribution of electrons.

## 4.5 Auroral Model Study

The analysis of DMSP records presented in Section 4.4 demonstrates that 80% to 90% of the energy deposition within the cusp by charged particles is due to enhancements in the electron energy flux in restricted latitude ranges on the order of tens of kilometers in width. The average electron energy within the structured electron events is often greater than the surrounding plasma suggesting that an acceleration process is active even within the cusp. Values of I(630.0 nm) and (557.7 nm) computed from the average energy and energy flux as well as the restricted latitude range for the events are consistent with ground based observations that the prominent feature of midday auroral displays are thin auroral arcs. However, the satellite records cannot be used to consider time dependent effects due to the motion of the structured electron fluxes or the decay of metastable states produced by the precipitating particles.

An auroral model is described in this section that will be used to investigate the temporal variations in 630.0 nm emissions arising from $O(^1D)$ populations produced in discrete arcs and to determine what fraction of the diffuse 630.0 nm background can be attributed to the discrete auroral structures. There are a number of advantages in considering an auroral model over computing I(630.0 nm) directly from the DMSP satellite overpasses of the cusp. First, an auroral model allows careful examination of the morphology of 630.0 nm emissions in MSP plots. The scanning photometer is widely used as a record of auroral emissions in the meridian plane so it is useful to understand the latitude-altitude ambiguities introduced by the photometer line of sight integration. Second, the time dependence in $O(^1D)$ concentrations and 630.0 nm photon yields inherent to the moving excitation source within the midday aurora may be considered using an auroral model. Finally, the auroral model allows the contribution of $O(^1D)$ from transient auroral arcs to the background 630.0 nm emission to be evaluated.

### 4.5.1 Numerical Basis and Philosophy for a Simple Auroral Model

Development of a complete self consistent model of the thermospheric response to energy input from particle precipitation is a formidable task. A general solution requires the simultaneous

Reproduced with permission of the copyright owner. Further reproduction prohibited without permission.

solution of a set of coupled equations governing the not only the transport and energy loss of the incident particles but also consideration of the mass, momentum, and energy conservation of the charged and neutral species within the ionosphere [c.f., *Rees*, 1989]. Mass conservation is described by the continuity equation

$$\frac{\partial n_j}{\partial t} + \nabla \cdot (n_j \mathbf{v}_j) = P_j - L_j \tag{4.3}$$

where $n_j$ and $\mathbf{v}_j$ are the density and velocities and $P_j$ and $L_j$ the production and loss rates of the $j^{th}$ species. Production of excited states may include not only electron impact by primary and secondary electrons but a host of chemical reactions as well. Loss due to radiative transitions yields the photon emission rates required to predict auroral emissions and quenching reactions must also be included at altitudes where collision rates are a significant fraction of the radiation transition probabilities. Momentum of the $j^{th}$ species is described by

$$\rho_j \frac{D_j \mathbf{v}_j}{Dt} + \nabla \cdot \vec{\mathbf{P}}_j = \sum_j n_j \mathbf{F}_j \tag{4.4a}$$

where $\vec{\mathbf{P}}_j$ and $\mathbf{F}_j$ are the pressure tensor and the external forces acting on the plasma and the convective derivative is given by

$$\frac{D_j}{Dt} = \frac{\partial}{\partial t} + \mathbf{v}_j \cdot \nabla \tag{4.4b}$$

The temperature of each component is described by the energy equation

$$n_j k \frac{D_j T_j}{Dt} = Q_j - L_j^T - n_j k T_j \nabla \cdot \mathbf{v}_j - \nabla \cdot \mathbf{q}_j + \sum_j n_j \mathbf{F}_j \cdot \mathbf{v}_j \tag{4.5}$$

where $Q_j$ is the heat loss rate, $L_j^T$ is compressional heating or cooling, and $\mathbf{q_j}$ is the heat flow rate for species $j$. These coupled equations for the mass, energy and momentum must be solved for all $j$ species at all altitudes, latitudes, and times.

The volume excitation rate by electron impact into the state $l$ of a species $j$ required for the production term in (4.3) is given by

$$\eta_j(z)^l = n_j(z) \int_{E_{threshold,j}}^{E_{maximum,j}} \sigma_j^l(E) I(E,z) dE \tag{4.6}$$

requiring values of the energy dependent cross sections $\sigma_j^l(E)$ for each reaction over the entire energy range where the product $\sigma_j^l(E)I(E,z)$ yields a significant contribution to the integral. The electron intensity due to upward and downward moving electrons $I(E,z,\mu)$ as a function of energy $E$, altitude $z$, and pitch angle $\alpha$ ($\mu = cos\alpha$) is determined from the electron transport equation

$$\mu \frac{dI(E,Z,\mu)}{dz} = -n(z)\sigma(E,\mu)I(z,E,\mu)$$
$$+n(z) \int_E^\infty \int_{-1}^{+1} \sigma(E' \rightarrow E, \mu' \rightarrow \mu) I(E',z,\mu') dE' d\mu'$$
$$+n_e(z) \frac{\partial [L(E) I(E,z,\mu)]}{\partial E} \tag{4.7}$$

Equations (4.3)-(4.7) are presented here to formally introduce the necessary components of a complete auroral model. A self-consistent solution to these equations for the dayside auroral

Reproduced with permission of the copyright owner. Further reproduction prohibited without permission.

problem is formidable. First, a model for the temporal and spatial variations of the plasma transport process at the magnetopause is required to determine the energy spectrum of the electron and proton fluxes injected into the cusp. Next, the transport of the plasma along the magnetic field into the mid and low altitude cusp (including any process required to structure or accelerate electrons) must be modelled to determine the incident energy spectrum for the charged particle fluxes before they encounter the atmosphere. Only then can the number densities, velocities, and temperatures of all neutral and charged species within the ionosphere be obtained from equations (4.1)-(4.3). Variations in the electron spectrum as a function of altitude are obtained from equations (4.4) and (4.5) but also require input from equation (4.3) since secondary electrons produced by primary electron impact on atmospheric constituents is a major source of electrons with energies capable of exciting auroral emissions.

**Table 4.1**
**Comparison of Models for O($^1D$) Distribution in Dayside Aurora**

| Reference | Continuity Equation | Dimension | Neutral Wind, Source |
|---|---|---|---|
| *Link et al.* [1983] | $\frac{\partial n_j}{\partial t} = 0$ $= -\nabla \cdot (n_j \mathbf{v}_j) + P_j - L_j n_j$ | 2-D | $v_n =$ $v_0 \frac{T_n(z) - T_n(120km)}{T_n(500km) - T_n(120km)}$ $v_{source} = 0$ |
| *Davis et al.* [unpub. manuscript] | $\frac{\partial n_j}{\partial t} + \nabla \cdot (n_j \mathbf{v}_j) =$ $= P_j - L_j n_j$ | 2-D | $v_n = v_d$ $v_{source} = v_d$ |
| Present work | $\frac{\partial n_j}{\partial t} + \nabla \cdot (n_j \mathbf{v}_j) =$ $= P_j - L_j n_j$ | 2-D | $0 < v_n = constant < v_d$ $v_{source} = v_d$ |

Self consistent computer models of magnetosheath plasma transport into the cusp including the dayside reconnection process, transport of plasma in the cusp, response of the ionosphere, and the formation of dayside aurora have yet to be developed. A variety of models applicable to individual components of the process have been reported in the literature [*Alad'yev*, 1989; *Onsager et al.*, 1993; *Winglee et al.*, 1993; *Waterman et al.*, 1994a,b; *Wing et al.*, 1996]. Models developed to obtain estimates of auroral emissions within the midday cusp by *Link et al.* [1983] and *Davis et al.* [unpublished manuscript] are particularly pertinent to the work described here. The transport terms used in the continuity equations (Section 4.5.2) are summarized in Table 4.3. *Link et al.* [1983] include an altitude dependent neutral wind but fix the latitude of the auroral precipitation. Comparison of results from the model with observations obtained in the postnoon auroral oval demonstrated that transport by neutral winds significantly effect the distribution of metastable species. The *Davis et al.* model was designed to model auroral transients which may accompany steps in ion energy dispersion in the cusp.

The primary interest here is to estimate the 630.0 nm volume emission rates created by the passage of transient arcs through the daytime ionosphere as realistically as possible without resorting to the drudgery of treating the intricate details of the electron interactions and subsequent

Reproduced with permission of the copyright owner. Further reproduction prohibited without permission.

chemistry. A reasonable estimate of the O($^1D$) concentration as a function of time can be obtained by including much of the physics contained in equations (4.3)-(4.7) in an *ad hoc* manner. A test of the hypothesis that discrete auroral arcs can reproduce the spatial and temporal variations in 630.0 nm photon volume emission rates observed in the midday sector is possible through the use of the auroral model. Although the analysis of DMSP records in Section 4.4 established that a background 630.0 nm emission is expected throughout the cusp due to the presence of an unstructured electron component in the precipitating electron flux, this component is not included in the model. The purpose of the auroral model is to determine the relative contribution of the transient arcs to the 630.0 nm emissions observed in the midday oval.

### 4.5.2 Continuity Equation and O($^1D$) Production and Loss

The model is based on solving the continuity equation (4.3) for O($^1D$) as a function of altitude, latitude, and time in the form given by *Rees and Jones* [1973]

$$\frac{\partial[O(^1D)]}{\partial t} = D\frac{\partial^2[O(^1D)]}{\partial x^2} - v_n\frac{\partial[O(^1D)]}{\partial x} + P(x,z,t) - L(x,z,t)O(^1D) \qquad (4.8a)$$

where $v_n$ is the velocity of the neutral wind, $D$ the molecular diffusion coefficient. If emission regions on the order of tens of kilometers or greater are treated then diffusion has little effect on the emission rates within the center of the emitting region and can be neglected [*Rees*, 1961]. Using these simplifications, equation (4.8a) is

$$\frac{\partial[O(^1D)]}{\partial t} = -v_{n,x}\frac{\partial[O(^1D)]}{\partial x} + P(x,z,t) - L(x,z,t)O(^1D) \qquad (4.8b)$$

This is the form of the continuity equation used in the auroral model. Solution of this equation requires that the sources P(x,z,t), loss rates L(x,z,t), and neutral wind wind $v_n$ be known for all altitudes, latitudes, and times.

Equation (4.8b) is approximated by the upwind difference scheme

$$\frac{n_j^{t+1} - n_j^t}{\Delta t} = -v\frac{n_j^t - n_{j-1}^t}{\Delta x} \qquad (4.9)$$

and the chemistry is explicitly incorporated in a subsequent step as

$$n_j^{t+1} = \frac{n_j^{t+1} + P_j^{t+1}\Delta t}{1 + L_j^{t+1}\Delta t} \qquad (4.10)$$

providing a stable solution for values of $v\Delta t/\Delta x \leq 1$.

Calculations are performed on a two-dimensional 800x800 cell grid where each cell is 1 km in altitude and 0.01 degree in latitude giving a simulation region approximately 890 km in length at the ground and 1000 km at 800 km altitude. The location of the ground station is an input to the simulation but is always placed at 0 km altitude. Simulated MSP response in the 630.0 nm and 557.7 nm channels at each elevation angle are obtained by numerically integrating the 630.0 nm and 557.7 nm volume emission rates along lines of sight from the ground station to the edge of the

Reproduced with permission of the copyright owner. Further reproduction prohibited without permission.

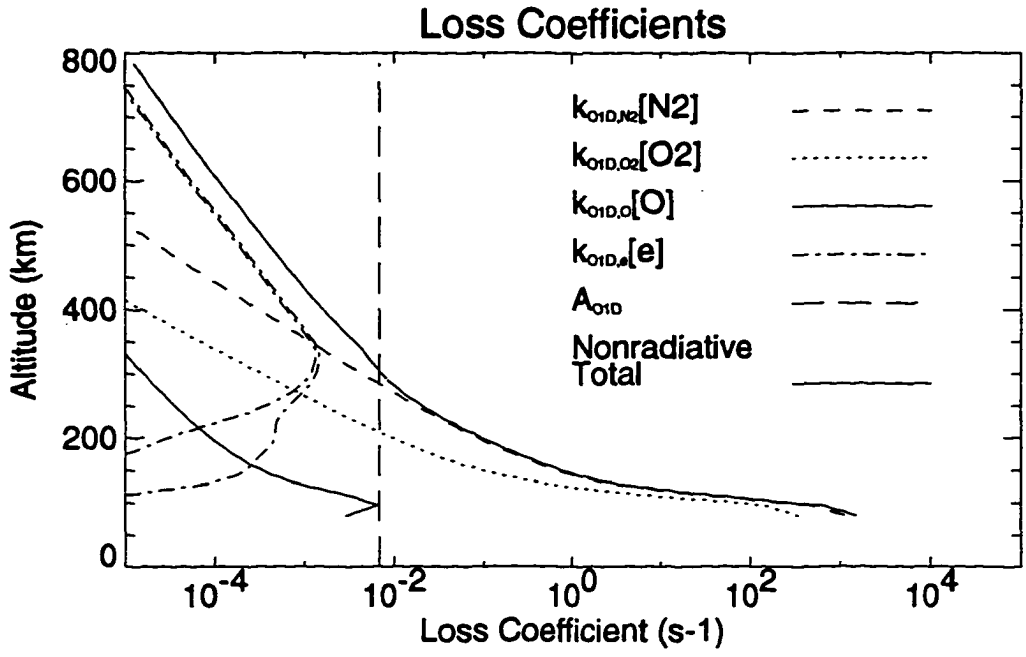


Figure 4.5 Loss Coefficients. Quenching by $N_2$ dominates the nonradiative loss at altitudes below 300 km and radiative decay is the dominant loss mechanism above 300 km.

simulation domain. Each scan is converted to Rayleighs ($1.0 \times 10^6$ photons/cm$^2$ s) for comparison with data obtained from the Longyearbyen field site.

Sources and losses of $O(^1D)$ included in the model are summarized in Table 3.3. The dominant production mechanisms of $O(^1D)$ are electron impact excitation of atomic oxygen

$$O(^3P) + e^* \rightarrow O(^1D) + e^* \tag{4.11}$$

and dissociative recombination of the diatomic oxygen ion

$$O_2^+ + e \rightarrow O(^1D) + O \tag{4.12}$$

The excitation cross section for production of $O(^1D)$ by electron impact on atomic oxygen is a maximum near 10-100 eV but decreases rapidly for electron energies approaching 1000 eV. Characteristic energies of primary electrons in the cusp and cleft region are typically on the order of 100-200 eV so reaction (4.11) may proceed through either the low energy primary or secondary electrons. Energetic electrons in the high energy tail of the ambient thermal plasma may have sufficient energy to excite oxygen to the $O(^1D)$ state if the electron temperature exceeds approximately 3000 K [c.f., *Rees and Roble*, 1986]. This latter source is thought to be important to $O(^1D)$ production within the cusp due to the efficient heating of the electron gas by soft electron precipitation [*Roble and Rees*, 1977; *Wickwar and Kofmann*, 1984; *Lockwood et al.*, 1993a].

Reproduced with permission of the copyright owner. Further reproduction prohibited without permission.

The primary interest here is the $O(^1D)$ distribution that results from moving regions of particle precipitation through a neutral atmosphere with the subsequent redistribution of the excited metastable oxygen atoms due to neutral winds. A simplified model for the $O(^1D)$ chemistry and transport has been chosen to explore this system rather than attempting a full self consistent treatment of the E and F region chemistry.

Production rates of $O(^1D)$ within auroral arcs are obtained from the GLOW airglow and aurora model developed by S. Solomon. The model, described in detail by *Solomon et al.* [1988], includes the traditional sources of the $O(^1D)$ state from primary, secondary, and thermal electron impact, dissociative recombination of $O_2^+$ , and cascade from the $O(^1S)$ state listed in Table 3.3. Two loss mechanisms of $O(^1D)$ are considered in the model, quenching due to collisions with the neutral atmosphere and radiative decay of the excited state with the emission of photons. Radiative decay

$$O(^1D) \rightarrow O(^3P) + h\nu(\lambda = 630.0nm) \tag{4.13}$$

which yields the model 630.0 nm volume emission rates is dominant at high altitudes but must compete with the quenching reactions

$$O(^1D) + N_2 \rightarrow N_2^* + O(^3P) \tag{4.14}$$

$$O(^1D) + O_2 \rightarrow O_2^* + O(^3P) \tag{4.15}$$

$$O(^1D) + O \rightarrow O^* + O(^3P) \tag{4.16}$$

$$O(^1D) + e \rightarrow e* + O(^3P) \tag{4.17}$$

at low altitudes where collisions are more probable than radiative decay. Although included in the model, electron quenching is of minor importance to the loss of $O(^1D)$ and quenching proceeds primarily through collisions with the neutral atmosphere [*Hunten and McElroy*, 1966].

Quenching reactions are of the general form

$$O(^1D) + M \rightarrow M^* + O(^3P) \tag{4.18}$$

where $M$ is the species which carries the energy away from the excited state. The form of the reaction rate is

$$\alpha = k[M][O(^1D)] = k'[O(^1D)] \tag{4.19}$$

where $k$ is a parameter which may depend on the temperature of the reacting species. The loss coefficient $k' = k[M]$ due to quenching may be compared for reactions (4.14)-(4.17) and with the Einstein coefficient $A_{O(^1D)}$ to determine the relative importance of each loss mechanism. Loss coefficients are plotted in Figure 4.5

GLOW model equilibrium values are used for 557.7 nm volume emission rates. Use of equilibrium values is acceptable because the 0.7 second lifetime of the $O(^1S)$ state is less than the time step used in the simulations and much less than the 16 second rate at which synthetic MSP scans are computed. The purpose of including the 557.7 nm emission in the output of the model is to

Reproduced with permission of the copyright owner. Further reproduction prohibited without permission.

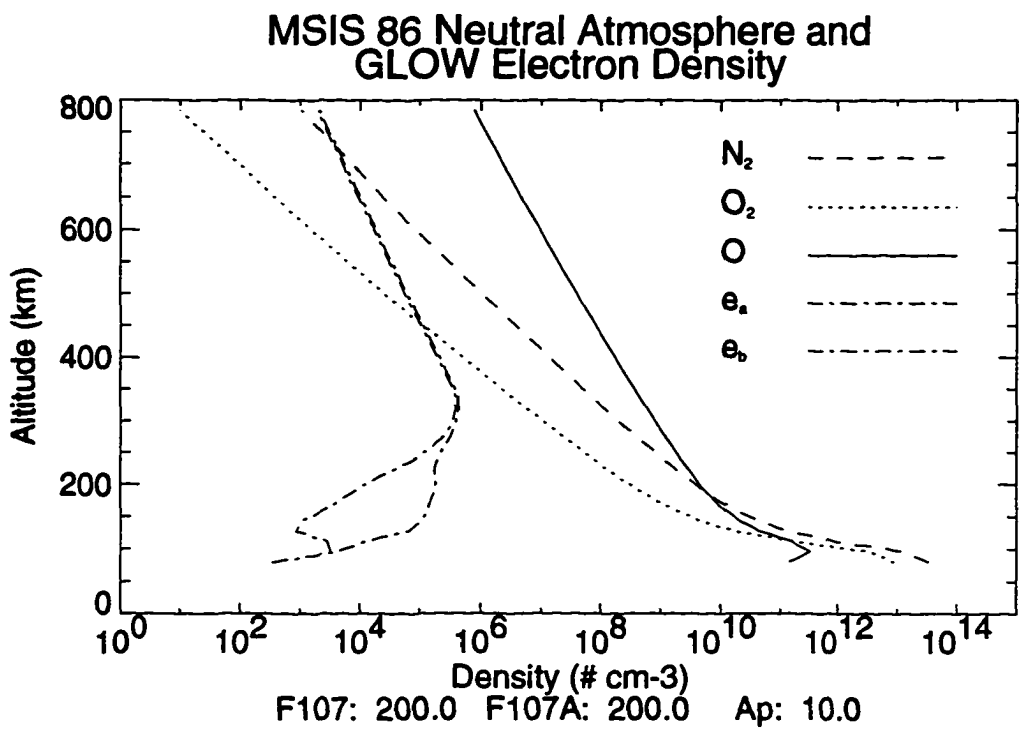


Figure 4.6 MSIS-86 Neutral Atmosphere and GLOW Electron Density. Input parameters for MSIS used in all of the simulations are 200 for the 3 month average F10.7 cm radio flux, 200 for the previous day F10.7 value, and an AP index of 10. Atomic oxygen is the dominant neutral species above 200 km and $N_2$ dominates below 200 km.

indicate the presence of precipitating electrons in the simulations since the equilibrium assumption will result in no emission if the electron precipitation is terminated.

Altitude dependent concentrations of $O_2$, $O$, and $N_2$ are obtained from the MSIS-86 neutral atmosphere model [*Hedin*, 1987]. Parameters appropriate for winter solstice conditions at magnetic noon (~0830 UT) for Longyearbyen are used as inputs for the model. Solar driven photochemistry is neglected as the solar depression angle at this time is -13.8° .

Electrodynamics is included in the sense that auroral arcs and the ionized atmosphere is assumed to move poleward at the same $\vec{E} \times \vec{B}$ drift velocity with values chosen that are consistent with measurements obtained in the midday aurora. This choice was made based on reports from simultaneous observations of dayside ionospheric plasma and auroral arcs using radar and cameras, respectively, which indicate that the dayside arcs move with speed and direction consistent with the ambient cold plasma flow (Section 3.4.2). The enhanced temperatures and density of the electron and ion gas associated with the particle precipitation also appears to drift at the same rate as the transient arc [*Lockwood et al.*, 1993a]. GLOW model equilibrium concentrations of ions and electron densities are adopted within the moving frame of the auroral arc. Variations in the $O(^1D)$ populations left behind as the arc sweeps poleward through the simulation domain are explicitly calculated by solving equation (4.8b). A radial magnetic field is adopted with a constant

Reproduced with permission of the copyright owner. Further reproduction prohibited without permission.

magnitude of 60,000 nT over the domain of the simulation. Magnetic zenith will therefore coincide with local zenith (90° ) in the simulation. All plasma motions are horizontal and vertical transport is neglected.

The model is generally applicable for any process that results in temporal and spatial variations in the particle flux within the cusp region giving rise to 630.0 nm dominated auroral arcs. Observations have consistently shown that transient dayside arcs are rayed with narrow latitude extent but extended in longitude, suggesting particle precipitation is confined to a restricted range of latitudes. A particle input source consistent with these observations is adopted for the model to test if a persistent background can be derived from the remnant populations of oxygen atoms in the $O(^1D)$ state excited during the passage of the particle source through the neutral atmosphere. The model is quite general in the sense that any mechanism capable of producing particle streams that are narrow in latitude, extended in longitude, and move poleward at convection velocities will give the same results.

Temporal variations for the particle fluxes are simulated in the following manner: an event is modelled by assuming that at time $t_i$ magnetosheath particles begin to arrive at ionospheric altitudes. The particle source is allowed to persist for a time $\tau_R$ and is terminated at time $t_f$. A constant zonal convection electric field is assumed to exist throughout the simulation period resulting in a constant meridional drift of the plasma poleward. The drift rates are determined from the data sets to which the simulations are to be compared. The period between events is given by $\delta t$. The time $\tau_R$ is referred to as the "merging" time in the simulations because it may be considered the time that merging is opening magnetic flux to the solar wind at the dayside magnetopause. Widths of the arcs are determined by the product of the merging time and the convection velocity of the arc.

The electron energy spectrum used for input in the GLOW model is a Maxwellian with a low energy tail [*Meier et al.*, 1989] with an energy flux of 1 erg/cm$^2$ s and a characteristic energy of 500 eV, greater than typical cusp energy spectra [*Winningham*, 1972; *Valladares et al.*, 1989]. The choice of the 500 eV energy is based on the values observed in the narrow electron features which give the arc structures in dayside aurora. *Newell and Meng* [1988] require electron energy fluxes $> 6 \times 10^{10}$ eV/cm$^2$ s sr (0.03 erg/cm$^2$ s for isotropic fluxes) to classify an electron spectrum as "cusp" (see Table 2.1). Electron fluxes within the structured events described in Section 4.4 however are significantly greater, often exceeding $10^{11} - 10^{12}$ eV/cm$^2$ s sr (0.5-5 erg/cm$^2$ s). I am interested in simulating the structured electron fluxes so an energy flux of approximately $2 \times 10^{11}$ eV/cm$^2$s sr (1 erg/cm$^2$ s) was used in all of the simulations. An added advantage is that the intensity of the auroral emissions in all of the simulations are based on unit energy flux (in erg/cm$^2$ s) and may be scaled appropriately to compare with experimental results with differing energy fluxes.

### 4.5.3 Electron and Neutral Temperatures

Similar to the computations reported by [*Rees and Luckey*, 1974], the ion chemistry and electron and ion temperature computations have not been coupled in the model. The model will

Reproduced with permission of the copyright owner. Further reproduction prohibited without permission.

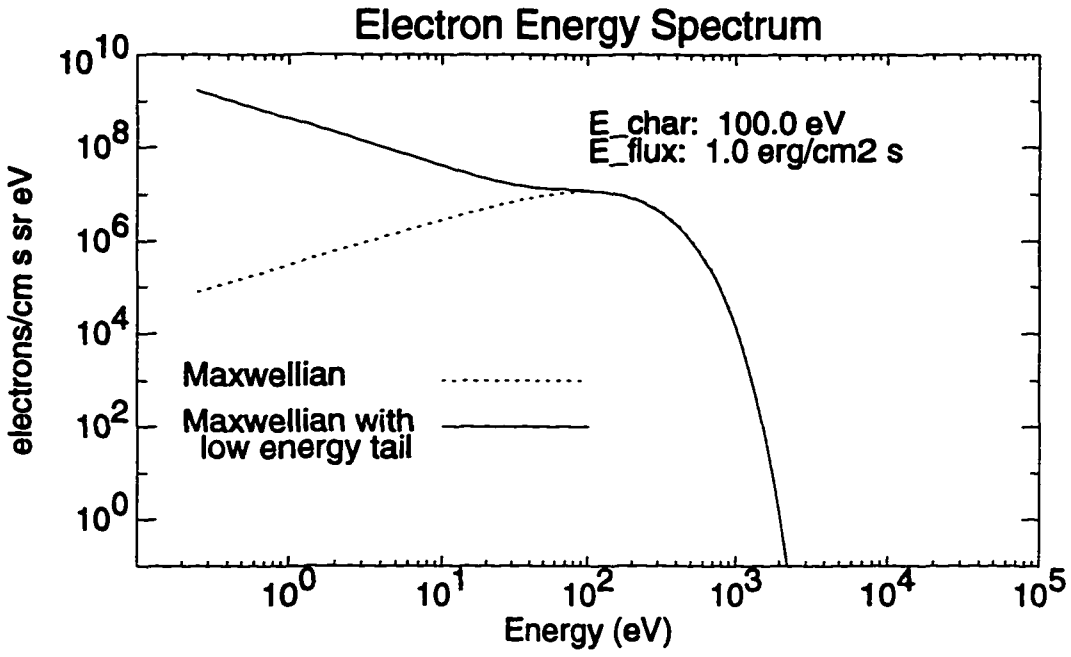


Figure 4.7 Electron Energy Spectrum. A Maxwellian with a low energy tail [*Meier et al.*, 1989] is used for all of the simulations. The characteristic energy is 500 eV and the energy flux 1 erg/cm$^2$ s.

simply assume that the electron and ion temperatures are in equilibrium both within auroral arcs and in the background ionosphere. Electron temperature profiles are obtained from the International Reference Ionosphere (IRI 90) Model are used for background electron temperatures. The temperatures are arbitrarily doubled within the transient arcs where electron precipitation heats the ambient electron gas to obtain temperature profiles appropriate for cusp conditions. Further, no heat flow will be considered and the ionosphere is assumed to be incompressible. Equation (4.5) is trivially solved under these conditions by simply adopting ion, electron, and neutral temperatures consistent with observations reported within auroral arcs and in the ambient ionospheric background.

Neglecting the ion and electron temperature computations is based on theoretical auroral calculations which show that heating of the electron gas during electron precipitation occurs on time scales of a few to tens of seconds with cooling occurring at nearly the same rate [c.f., *Min*, 1993; D. Lummerzheim, personal communication, 1995]. Electron temperatures adopted for the simulations are based on reports that values on the order of, or exceeding, 3000 K are present in dayside [*Curtis et al.* 1982; *Kofman and Wickwar*, 1984; *Lockwood et al.*, 1993b; *Watermann et al.*, 1994a,b].

Reproduced with permission of the copyright owner. Further reproduction prohibited without permission.

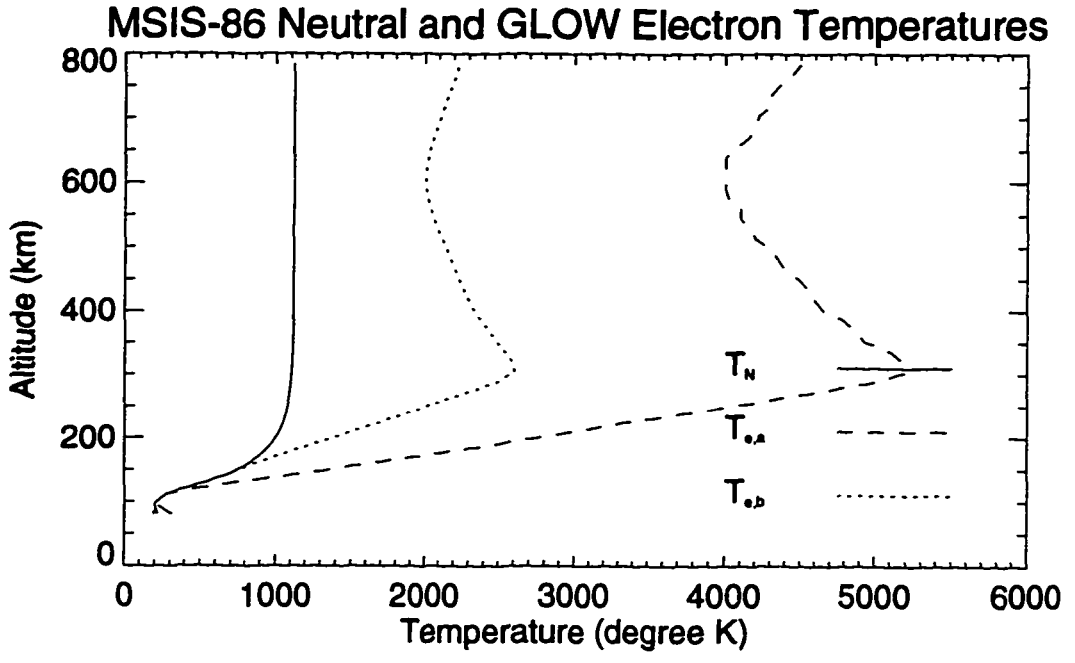


Figure 4.8 Electron and Neutral Gas Temperatures. Electron temperatures from the IRI 90 model are used for the background ionosphere temperature $T_{e,b}$. Electron temperatures within auroral arcs $T_{e,a}$ are doubled to obtain values consistent with observations of high electron temperatures within the cusp. All of the neutral species have the same temperature $T_N$ which is obtained from MSIS-86 model.

### 4.5.4 Momentum Equation and Neutral Winds

It has long been recognized that the morphology of the 630.0 nm emission is subject to transport effects. Even if the $O(^1D)$ atoms are formed in a thin sheet in a restricted range of altitudes, the observed 630.0 nm emission rate will occur over a broadened range of latitudes [*Rees*, 1961] and altitudes [*Rees et al.*, 1967] due to molecular diffusion. Even if the diffusion rates are slow, the distortion of emissions from neutral metastable species formed within auroral arcs are known to be a significant factor in the shape of auroral forms due to motions of the neutral atmosphere [*Hays and Atreya*, 1971]. *Link et al.* [1983] examined 630.0 nm emissions in the prenoon sector sampled by rocket borne photometers and concluded that neutral winds are a significant factor in controlling the distribution of the dayside 630.0 nm emissions. Other studies showing the strong effects of neutral winds on the distribution of metastable species in the high latitude regions include *Rees and Roble* [1980], *Gérard and Roble* [1982], and *Duboin et al.* [1984]. These studies all demonstrate that a successful model for time dependent 630.0 nm emissions in the midday region must explicitly include transport due to neutral winds requiring that equation (4.4) for the neutral gas be included in the model.

Reproduced with permission of the copyright owner. Further reproduction prohibited without permission.

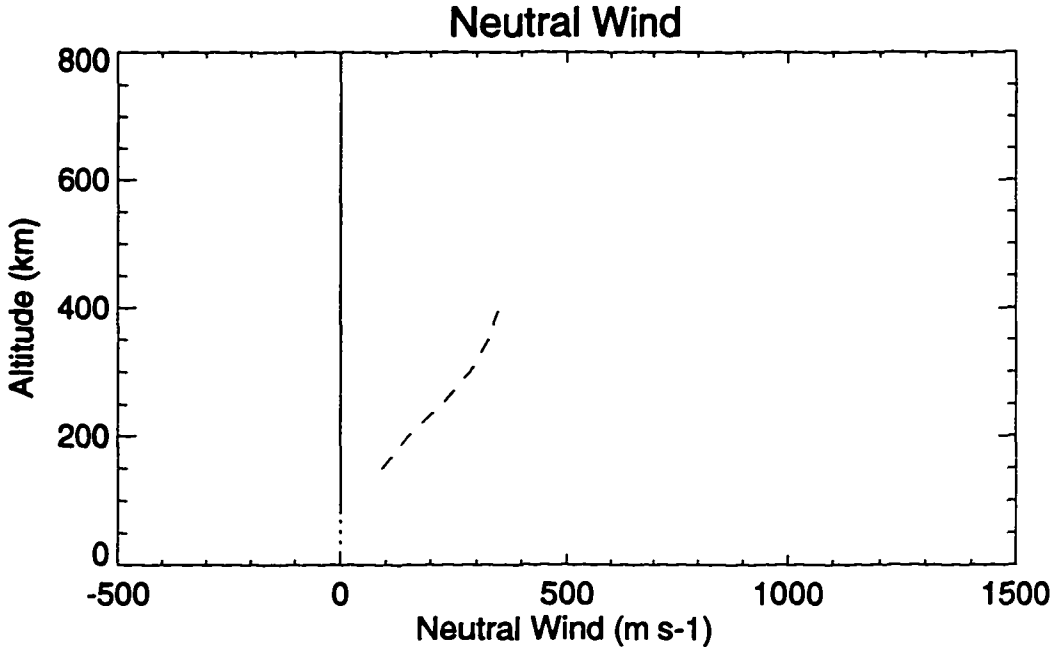


Figure 4.9 Neutral Wind Model. The wind was assumed to be constant over the full altitude range of the model. In the example given here the wind speed of 120 m/s northward is indicated by the solid line. Experimental wind profiles obtained by *G/' e rard and Roble* [1982] (dotted line) and *Pereira et al.* [1980] (dashed line) are given for comparison.

Inclusion of the momentum equations leads to significant complication of the model. Solution of the momentum equation may be conveniently avoided by adopting two simplifying conditions. First, the neutral gas moves at a velocity consistent with values measured in the dayside auroral oval which is constant on the time scales of transient arc formation. Second, the ions and electrons move at the electric field drift speed which is determined by an externally imposed electric field. The $\vec{E} \times \vec{B}$ velocity need not be a constant but its magnitude and direction is imposed by processes external to the auroral ionosphere. The effect of ion-neutral coupling is included in the model in the sense that realistic ion and neutral flow speeds are used in the simulations.

Transport of ions and electrons in the ionosphere, assumed to be due entirely to the electric field drift, was discussed in Section 4.5.3. The electric fields governing the motion of the auroral arc and cold plasma are assumed to be imposed by processes occurring in the magnetosphere, i.e., they are externally imposed, and no equation of motion is required for the ions and electrons.

Assumption of a constant neutral gas velocity in the presence of periodic enhancements of the ion drift velocity (Section 3.4.2) requires some justification. Equation 4.4 for the neutral gas can

Reproduced with permission of the copyright owner. Further reproduction prohibited without permission.

be written as

$$\frac{\partial \mathbf{v}_n}{\partial t} = \frac{n_i}{n_n}\nu_{in}(\mathbf{v}_i - \mathbf{v}_n) \qquad 4.18$$

where $\nu_{in}$ is the ion-neutral collision frequency. Terms describing pressure and temperature gradients have been neglected since I am only interested in the acceleration of the neutral gas in the cusp, not the ambient flow. A time constant $\tau_{ni}$ for the e-folding time required for the neutrals to reach the ion velocity following a change in velocity is found from equation (a) to be [*Killeen et al.*, 1984]

$$\tau_{ni} = \frac{n_n}{n_i \nu_{in}} \qquad 4.19$$

assuming the neutral wind is accelerated exponentially towards the ion drift speed.

Values for $\tau_{ni}$ have been estimated by *Baron and Wand* [1983] to vary from 38 minutes in the lower thermosphere to over 6 hours in the upper thermosphere. *Killeen et al.* [1984] computed values of $\tau_{ni}$ along the track of the Dynamics Explorer 2 satellite for three passes through the high latitude ionosphere at altitudes varying from 347 km to 390 km. Values of the ion-neutral time coupling constant were found to vary from a minimum of approximately 25 minutes to maximums of nearly 200 minutes with typical values of 50-100 minutes. These time scales are much longer than the 3-5 minute repetition period expected for the transient enhancements of the ion drift velocities so that on time scales of transient arc formation and drift the neutral wind velocity may be assumed to be constant. Explicit inclusion of equation (4) in the model is therefore not required while a constant neutral gas velocity $V_n$ is retained in equation (1).

Ground based observations of thermospheric wind patterns are used to establish typical velocities for the model. Descriptions of dayside neutral winds determined from Fabry-Perot measurements of Doppler shifted 630.0 nm photons are given by *Smith and Sweeney*, [1980], *Deehr et al.*, [1980], *Smith et al.*, [1985], *McCormac and Smith*, [1984], and *Smith et al.*, [1986] from Svalbard and *Hernandez et al.* [1991] from South Pole Station. *McCormac and Smith*, [1984] showed a pronounced dependence neutral wind speed and direction on the IMF $B_y$ component due to the coupling between the ionized and neutral gases in the F region ionosphere. Poleward neutral wind velocities on the order of 50-200 m/s are commonly encountered near 12 MLT. The magnitude and direction of the zonal flows depend on the sign of the IMF By component, and values of 0-50 m/s are found for IMF $B_y < 0$ while 50-150 m/s are observed when IMF $B_y > 0$.

Fabry-Perot measurements can only provide a mean value of the wind since the signal is derived from a line of sight integration. The wind values therefore represent the mean wind near the peak of the 630.0 nm emission profile. Direct measurements of altitude profiles of the neutral wind suggest the velocity is a minimum near the lower edge of the thermosphere and asymptotically approaches a maximum above 400-600 km [*McCormac et al.*, 1987; *Gérard and Roble*, 1982]. Velocity shears in the meridional wind are often present at altitudes between 120-140 km [*Pereira et al.*, 1980] but $O(^1D)$ is strongly quenched at these altitudes and transport effects are negligible. The model was originally run with profiles similar to those described by *Gérard and Roble* [1982] but the results were the same as the constant velocity profiles so the more complicated form was dropped.

Reproduced with permission of the copyright owner. Further reproduction prohibited without permission.

### 4.5.5 Comparing Photometer Records to Model

The distance to a feature in the ionosphere scattering radio waves is measured by a radar from the time required for a pulse to travel from the transmitter to the feature and return to a receiver. Dividing the radar beam into distance increments, or range gates, allows a unique altitude, latitude, and longitude to be determined for each increment from the travel time of the transmitted wave and the orientation of the transmitter. Measurements from charged particle detectors onboard satellites are identified with a unique altitude, latitude, and longitude from the knowledge of the satellite trajectory. Finally, the grid on which auroral models are solved establishes an altitude and location for each pixel within the simulation. In contrast, the response of a scanning photometer at a particular elevation angle and azimuth is an integrated intensity through an emitting region. A unique latitude, longitude, and altitude cannot be determined from the response of a single photometer. Comparing photometer records with radar, satellite particle detectors, and models is complicated by the fact that photometer measurements cannot in general be associated with a unique location in space.

Assumptions based on the altitude distributions of emissions in aurora and airglows may be used to associated altitudes and geographic position with a photometer response but the results are not unique. For example, a photometer aimed at an angle of 45° above the horizon produces an output indicating the presence of an emitting gas. The volume of excited gas may be relatively localized at an altitude of 100 km and a distance of 100 km from the station (assuming a flat Earth). It may just as well be 500 km in altitude and 500 km from the station, there is no information in the photometer response that will distinguish between the two locations. Another possibility is the emitting gas may be distributed uniformly along the sight line between altitudes of 100 km and 500 km.

The basis of one common technique for converting photometer scans to intensities as a function of latitude is to assume an altitude for the emission and compute a latitude (see Appendix A). Latitudes determined for emission features will be a good approximation to the true latitudes as long as the emission arises from a restricted range of altitudes, the emission feature covers a restricted range of latitudes, and the correct emission altitude is chosen. The final requirement may be a great source of error if the altitude distribution of a spectral emission is variable [*c.f., Lockwood et al.*, 1993a]. The technique has been widely used as a quick method of comparing photometer records with data obtained by radar [*Lockwood et al.*, 1990, 1993 *Rodger et al.*, 1995], and satellite [*Sandholt et al., Denig et al., Minow et al., 1994*] records or to compare the intensities of emissions with different peak emission altitudes [*Sivjee et al.*, 1982].

Alternative methods of analyzing photometer records have been devised that more correctly deal with the altitude-latitude ambiguities. A technique developed by *Eather et al.* [1976], for example, uses the assumption that the volume emission ratio I(630.0 nm)/I(427.8 nm) is nearly independent of the primary electron energy and only the altitude of the emission determines the ratio. This is true for energetic electron precipitation since it is generally the secondary electrons that are responsible for the majority of excitation and emission ratios depend only weakly on the primary energy over a wide range of altitudes [*Rees and Luckey*, 1974]. To obtain meaningful

Reproduced with permission of the copyright owner. Further reproduction prohibited without permission.

spectral ratios, the *Eather et al.* technique requires simple auroral situations where only single arcs or well separated multiple arcs with narrow horizontal extents are present such that the photometer sight lines will not intersect two auroral arcs. Applications of the technique include the conversion of photometer records to latitude maps of auroral column intensity and estimates of space-time variations in auroral energy [*Eather et al.*, 1976], ionospheric conductivity [*Mende et al.*, 1984] and field aligned currents responsible for conductivity enhancements [*McHarg*, 1993].

Both techniques for converting photometer records to altitude and latitude were rejected for this study for a number of reasons. First, poleward moving auroral forms characteristic of active dayside aurora must create significant concentrations of $O(^1D)$ as they sweep poleward through the neutral gas producing 630.0 nm emissions within the arc and over an extended region equatorward of the arc as well. This distribution of emissions is in violation of the assumption of thin emitting regions. Second, the formation of series of closely spaced transient arcs often results in photometer sight lines passing through the low altitude regimes of one arc and the high altitude regimes of neighboring arcs, violating the assumption of single arcs within the photometer sight lines. Third, the existence of diffuse 630.0 nm emission due to a background electron flux in addition to the electron flux within the arc will produce an extended emitting region that violates the requirement of thin emitting regions.

The *Eather et al.* [1976] technique was rejected for two further reasons. First, the soft electron fluxes characteristic of the cusp may violate the assumption that the emission ratio is independent of the primary electron energy since electron-electron collisions become important at these energies. The *Rees and Luckey, 1974* model on which the technique is based is no longer applicable in these conditions. Finally, for the *Rees and Luckey* technique to work the aurora must be in equilibrium, or nearly in equilibrium, since those are the conditions for which *Rees and Luckey* computed the ratios of 630.0 nm and 427.8 nm column intensities. The purpose of the work described in this chapter is to consider time dependent concentrations of a metastable species and the resulting emissions when it radiates. Adopting a model which requires equilibrium would violate the spirit of the analysis.

Fortunately, there is a simple solution to the problem of comparing photometer records with an auroral model: the auroral model may be sampled in the same manner of an MSP. Model volume emission rates obtained over the grid summed along sight lines from a ground station yield an integrated intensity. Synthetic photometer records are produced by computing the integrated intensity for a variety of elevation angles. The resulting synthetic records are directly comparable to data. This is the format that will be used here.

### 4.5.6 Testing and Validation of Model Output

Before presenting results from the model a few words are in order about the tests that were used to determine if the model was (i) numerically stable, if (ii) the results were physically meaningful, and (iii) how sensitive the model was to changes in parameter. A variety of tests were run as the model was in the development phase as well as after the final version was completed. These will only be briefly summarized here.

Reproduced with permission of the copyright owner. Further reproduction prohibited without permission.

Problems with numerical stability arose in transport term in the $O(^1D)$ continuity equation. Stability required that $v_n \Delta t / \Delta x \leq 1$. If the model was run at the full resolution of 1 km in altitude, 1 km in latitude, and 1 second time steps, the largest neutral wind velocity that could be simulated was 1 km/s. A neutral wind of 1 km/s exceeds values expected for the high latitude ionosphere (Section 4.5.4). Tests with neutral winds exceeding the 1 km/s were run to verify that the instability would produce obvious artifacts that could not be mistaken for distributions of aurorally produced $O(^1D)$ . The model was also run for a variety of grid sizes and time steps to determine if the results were dependent on the resolution of the model. The results were essentially the same for a wide range of grid sizes. It was often more efficient to test new results by running the model on a 50x50 grid rather than the full 800x800 but significant changes in the results never appeared once the model was run at the full resolution.

Column sums for the 630.0 nm emission were compared with the results from models and data to determine if the absolute 630.0 nm intensity was physically meaningful. Peak values of I(630.0 nm) within model transient arcs were typically on the order of 1 kR to 10 kR, consistent with observations in dayside aurora. Column emission rates are consistent with the results obtained by [*Meier et al.* [1989] for characteristic electron energies of 100 eV but are larger by a factor of 2.5 to 3 at 1 keV.

In one test the model was run to equilibrium to verify that using the $O(^1D)$ production rates from the GLOW model and computing the time dependent loss rates would yield the same equilibrium concentrations of $O(^1D)$ and 630.0 nm emission rate as the equilibrium values obtained directly from the GLOW model. The results showed the equilibrium values to be the same.

Finally, the model was run for a variety of inputs to the MSIS-86 model to determine how sensitive the 630.0 nm emission rates were to variations in changes in the neutral atmosphere. Changing the Ap value from 5 to 150 resulted variations in the 630.0 nm column emission rate by a factor of 2 over a range of energies from 100 eV to 1 keV. The emission rates were greater for the smaller Ap value. These results are consistent with those obtained by *Meier et al.* [1989] in testing the sensitivity of a model of red line processes to changes in the model atmosphere.

## 4.6 Results I: Effects of Spatial and Temporal Variations in $O(^1D)$ Populations on 630.0 nm MSP Records

Output from a photometer at an arbitrary elevation angle is the integrated photon emission rates along the photometer sight line. Sight lines colinear with the magnetic field provide estimates of the column intensity while sight lines at an angle with respect to the magnetic field contain information from a range of altitudes and latitudes. The information content in photometer records obtained for arcs drifting through the magnetic zenith depend on the relative distance of the arc from the station. If the auroral emissions are located near the zenith then the resulting records can be interpreted as a column intensity while emissions located far from the station result in altitude profiles. Interpretation of a series of photometer scans obtained during an auroral display can often be confused, however, since the resulting emission profiles are a combination of spatial distributions of excited species in both altitude and latitude as well as temporal variations. The

Reproduced with permission of the copyright owner. Further reproduction prohibited without permission.

proper interpretation can only be made once the various effects that contribute to the resulting records are understood.

It is instructive to consider the differences between photometer records that would result if the lifetime of the $O(^1D)$ state was similar to the $O(^1S)$ state. Comparison of results obtained by the artificial modification of the $O(^1D)$ lifetime permits spatial effects due to altitude-latitude ambiguities to be clearly separated from temporal effects due to the lifetime of the metastable states.

### 4.6.1 Stationary Arcs and $O(^1D)$ Lifetime

The first example is an auroral arc at 72° latitude equatorward of the station at 75° . The position of the arc remains fixed throughout the simulation. Electron precipitation is constant for a period of 600 seconds and then terminated. Variations in the 630.0 nm emission intensity are due entirely to the time and altitude dependent production and loss of $O(^1D)$ . Locating the arc 3° (approximately 300 km) south of the station and restricting the electron input to a narrow range of latitudes (1 km) assures that the simulated photometer response is due entirely to the altitude distribution of the excited state.

Results are given for $O(^1D)$ lifetimes of $\tau_{O(^1D)}$ = 110sec and $\tau_{O(^1D)}$ = 147sec in Figure 4.10(a) and (b), respectively, to test the sensitivity of the model results to the value chosen for the Einstein coefficients (see discussion in Section 3. The results are similar using either the 110 second and 147 second $O(^1D)$ radiative lifetimes in the simulation. A gradual build up of $O(^1D)$ and therefore an increasing 630.0 nm emission rate is noted within the first few minutes of the simulation. The system rapidly attains equilibrium at low altitudes (large elevation angles) where the 630.0 nm emission rate is nearly constant throughout the excitation period. The approach to equilibrium is more gradual at high altitudes (small elevation angles) where the 630.0 nm emission rate continues to increase even after the low altitude emission rate is constant. The peak of the 557.7 nm emission rate, a constant throughout the excitation period, exhibits a maximum near the lower border although populations of $O(^1S)$ exist at greater altitudes resulting in a distribution of 557.7 nm emissions over a range of elevation angles. The peak in the 630.0 nm emission rate lies at a smaller elevation angle, and therefore greater altitude, because quenching efficiently removes $O(^1D)$ in the low altitude portion of the arc.

Once the electron precipitation is terminated, 557.7 nm emissions are no longer observed due to the rapid decay of the 0.7 second lifetime $O(^1S)$ state but the 630.0 nm emission persists. The origin of the 630.0 nm emission are remnant populations of $O(^1D)$ formed by the electron precipitation. Low altitude (large elevation angle) $O(^1D)$ populations decay more rapidly because of strong quenching at lower altitudes where collisions are frequent. The shift of the emission towards smaller elevation angles from 150° is characteristic of low altitude quenching. This feature will be observed in many of the simulations to follow.

The 630.0 nm emissions are present for a longer period after the termination of electron precipitation if $\tau_{O(^1D)}$ = 147 sec although the lifetime is significantly long for both the 110 and 147 second examples for 630.0 nm emissions to persist for at least five minutes. The differences

Reproduced with permission of the copyright owner. Further reproduction prohibited without permission.

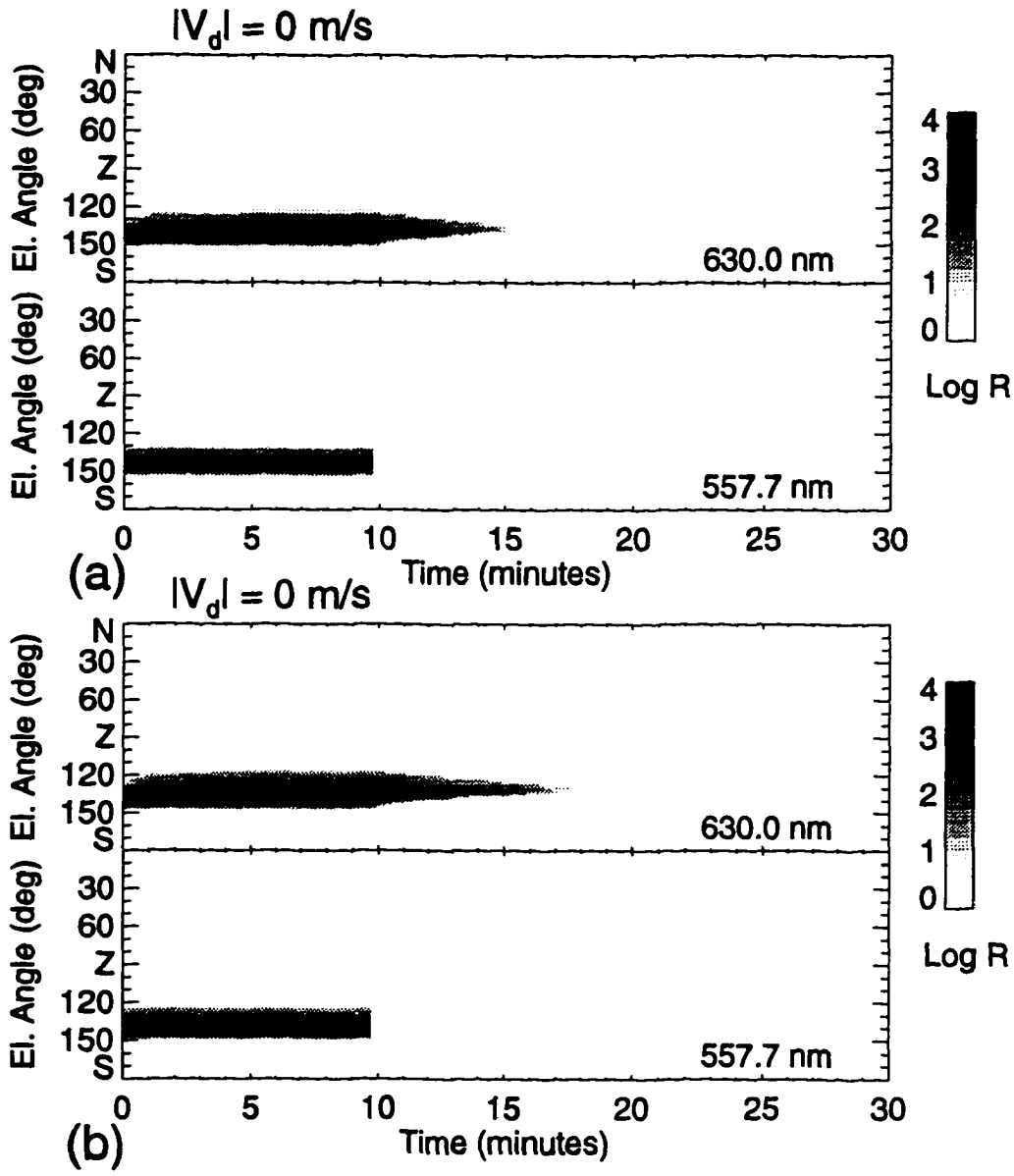


Figure 4.10 MSP Records of an Arc at a Fixed Latitude. The excitation producing the arc is terminated after 600 seconds. The arc is 3° south of the station so the distribution of emissions over a range of scan angles is primarily due to an altitude distribution of the source. (a) $\tau_{O(^1D)}$ = 110sec (b) $\tau_{O(^1D)}$ = 147sec. The neutral wind velocity is zero for both cases.

Reproduced with permission of the copyright owner. Further reproduction prohibited without permission.

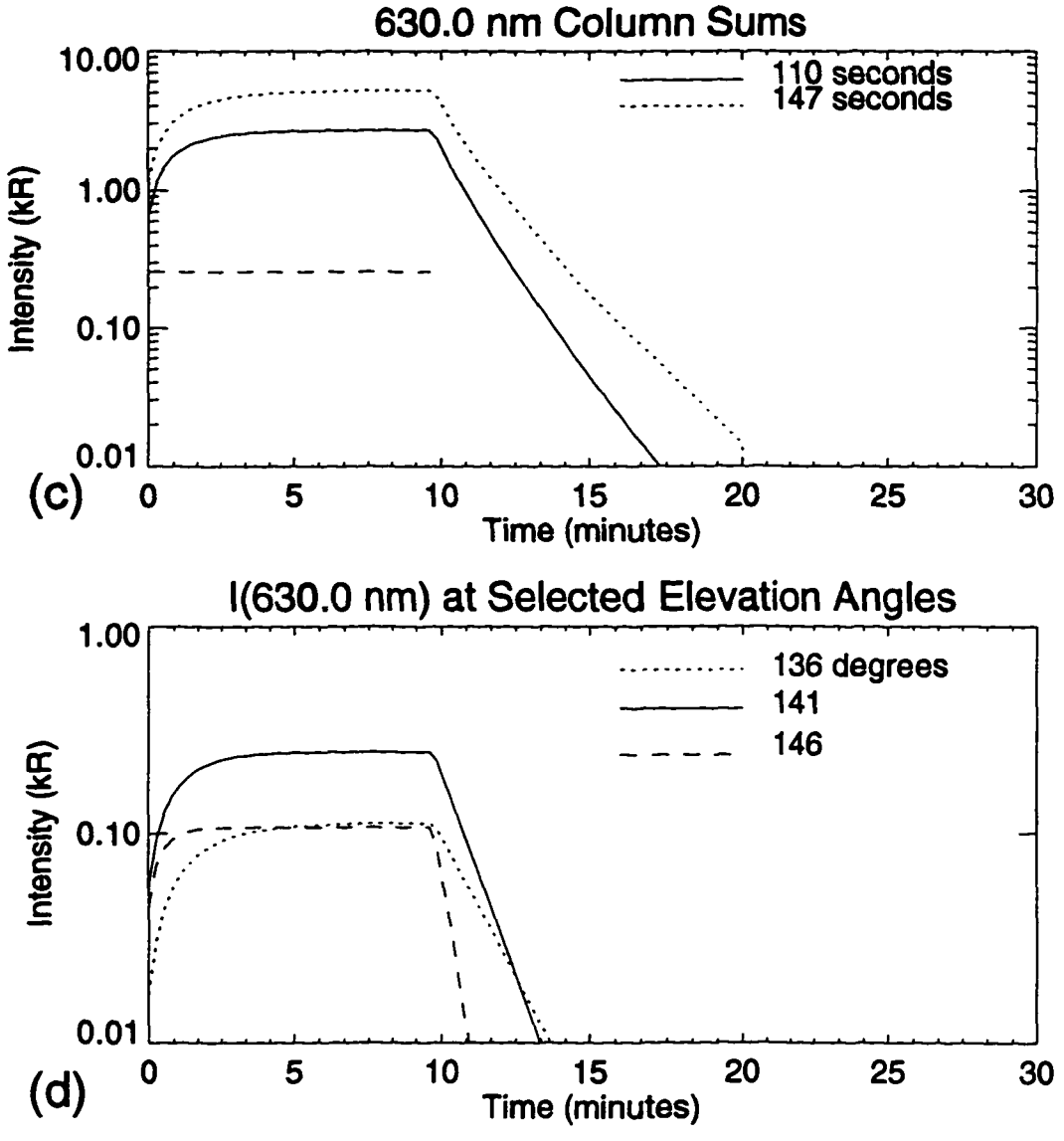


Figure 4.10 (continued) (c) Column intensities obtained by summing the photometer response from 90° to 180° are plotted for both the 110 and 147 second lifetime arcs. The presence of electron precipitation is indicated by the 557.7 nm emission (dashed line). (d) Intensity at selected elevation angles for the 110 second lifetime example in Figure 4.10(a). Emissions at the 141° elevation angle originate near 250 km, the peak emission altitude. Elevation angles greater than this sample emissions at lower altitudes and smaller elevation angles sample emissions from greater altitudes than the peak emission. In this case the 146° and 136° scans sample 200 km and 300 km.

Reproduced with permission of the copyright owner. Further reproduction prohibited without permission.

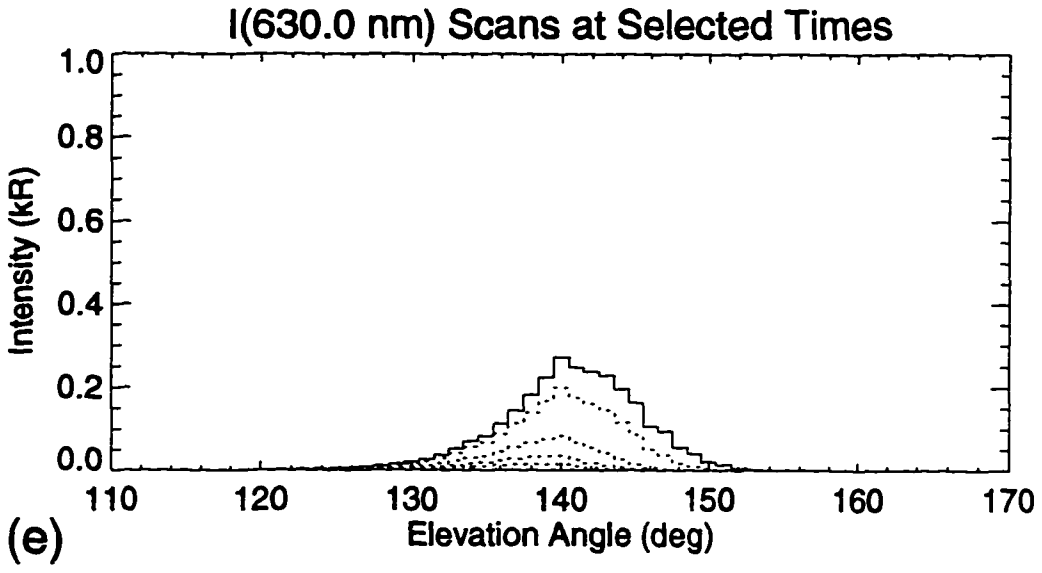


Figure 4.10 (continued) (e) Single scans are plotted once every 64 seconds starting at 10 minutes into the simulation (immediately after termination of the electron precipitation) to exhibit the time dependent 630.0 nm signal due to the altitude dependent decay of $O(^1D)$ .

between the two lifetimes is better appreciated by comparing the column sums plotted in Figure 4.10(c). The excitation period is indicated by the presence of the constant 557.7 nm emission. Concentrations of $O(^1D)$ are greater in the arc with the 147 second lifetime during the excitation period. By the end of the excitation period both arcs are near equilibrium and the 630.0 nm emission in the 147 second lifetime arc is approximately double the 110 second lifetime arc. A simple explanation for the difference is provided by considering the continuity equation (4.3) for $O(^1D)$ in the absence of transport at equilibrium is

$$\frac{\partial[O(^1D)]}{\partial t} = P_j - L_j[O(^1D)] = 0 \tag{4.20}$$

yielding an equilibrium concentration of $O(^1D)$

$$[O(^1D)] = P_j/L_j \tag{4.21}$$

The equilibrium concentration of the excited state is greater if the loss rate is reduced by increasing the lifetime of the state.

Altitude dependent time variations of $O(^1D)$ and 630.0 nm emissions are better considered by plotting individual elevation angles as a function of time rather than column sums. Figure 4.10(d)

Reproduced with permission of the copyright owner. Further reproduction prohibited without permission.

shows intensities at three elevation angles. Each elevation angle can be associated with a unique altitude because the location of the arc is known from the input to the model. Scans obtained at elevation angles of 136° , 141° , and 146° intersect the arc at altitudes of approximately 300 km, 250 km and 200 km, respectively. The 141° scan was chosen because it is the peak emission within the arc. 630.0 nm emissions at 250 km are 90% of the equilibrium value within three minutes and approach equilibrium within 5 minutes.

Populations of $O(^1D)$ below the peak emission altitude attain equilibrium more rapidly but the total concentration is reduced. For example, the 146° elevation scan in Figure 410(d) samples emissions originating at altitudes of 200 km. Emission rates of 630.0 nm at this altitude are reduced from those 50 km higher by a factor of 3, but equilibrium is attained within 2 minutes. Populations of $O(^1D)$ at greater altitudes, shown here by the 136° elevation angle scan sampling populations at 300 km, are not in equilibrium as the emission rate of 630.0 nm is still increasing up to the time the electron precipitation is terminated. The intensity is reduced by a factor of three from concentrations at the peak emission altitude due to the reduced oxygen concentrations at the greater altitude.

The bulk of the emission in the arc originates from altitudes near the peak emission altitude of 250 km where precipitation must be present for at least 5 minutes to yield equilibrium concentrations of $O(^1D)$ and constant 630.0 nm emission rates. It is important to consider that transient auroral arc formation rates and lifetimes are on the order of 5 minutes and they move at velocities of 0.5-1 km/s. Energy input into the neutral atmosphere of the cusp by electron precipitation in the transient arcs is anything but constant. Therefore, dayside auroral emissions can rarely be assumed to be in equilibrium; an important point if attempting to utilize the *Rees and Luckey* [1974] method to infer energy characteristics of the primary particle stream.

Figure 4.10(e) is a series of 630.0 nm intensities between elevation angles of 110° and 170° . Scans are plotted once every 64 seconds starting at 10 minutes into the simulation, immediately after termination of the electron precipitation. Note that the elevation angle at which the peak 630.0 nm emission is sampled decreases as the $O(^1D)$ population decays due to the increase in altitude of the peak emission. Variations of elevation angle at which the photometer detect 630.0 nm emission due to the altitude dependent decay of $O(^1D)$ may be misinterpreted as shifts in latitude of the auroral arc.

The intensity at the peak altitude is reduced by approximately 1/e between each successive scan in Figure 4.10(e), suggesting the lifetime of $O(^1D)$ at the peak emission altitude is approximately 64 seconds, smaller than the 110 second lifetime used as input in the simulation. This value is the effective lifetime in the presence of quenching described in Section 3.2.1. Decay curves of 630.0 nm emissions obtained from aurora arcs will exhibit effective lifetimes rather than the radiative lifetime as long as a significant fraction of the $O(^1D)$ production is at altitudes where quenching limits the emission of 630.0 nm photons. The approximate theoretical value of 64 seconds obtained here for the effective lifetime is consistent with the experimental values obtained by [*Ono and Hirasawa*, 1992].

Quenching results in a characteristic compound decay curve due to altitude variations in the effective lifetime. This feature is shown in Figure 4.11 where a one minute period of excitation

Reproduced with permission of the copyright owner. Further reproduction prohibited without permission.

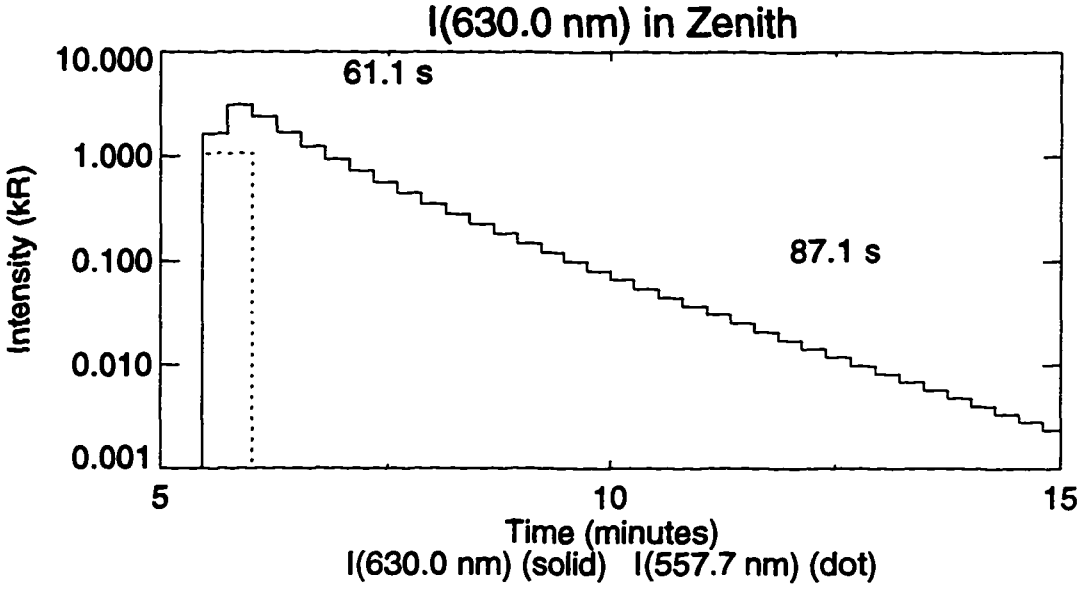


Figure 4.11 Compound Decay Curves in Column Sums. The column intensity of 630.0 nm resulting from a one minute period of electron precipitation in the magnetic zenith is plotted as a function of time. The slope of the decay curve varies in time and predicts a 63 second decay constant early in the decay and 90.7 seconds late in the decay. The compound decay curve is characteristic of a quenched emission.

produces ~4 kR of 630.0 nm which subsequently decays. The lifetime computed from the first 2 minute of the decay is 64.4 seconds but increases to 90.7 seconds when computed from intensities after 7 minute of the decay. The compound decay curve is the result of the rapid loss of the quenched population at at or below the peak emission altitude (yielding effective lifetimes of 64 seconds) and the more gradual decay of the high altitude portion of the arc (yielding values nearer the unquenched 110 second lifetime). Compound decay curves are expected for photometer scans which include emissions from a variety of altitudes. For example, the decay curves in Figure 4.10(c) exhibit the decreasing slope characteristic of a compound decay curve because they are obtained by summing the 630.0 nm emission rate over a range of altitudes. Decay curves in the single elevation angle scans in Figure 4.10(d) are straight lines because the emission originates in a narrow altitude range.

In practice it is difficult to observe the compound decay due to background emissions. The emission rate in Figure 4.11 approaches the 0.5-1 kR level while the effective lifetime is still approximately 65 seconds. Once the emission rate decreases below the statistical variation in the background it will no longer be detectable. For example, consider an instrument with a sensitivity on the order of 1 R/count. The statistical fluctuations in a 0.5-1 kR background is approximately

Reproduced with permission of the copyright owner. Further reproduction prohibited without permission.

20-30 R. The effective lifetime will approach the radiative lifetime only as the intensity approaches the background in this case. Attempts to detect compound decay curves in photometer data are also complicated by the variation in the background particle precipitation rate.

### 4.6.2 Poleward Moving Aurora

Auroral arcs within the midday aurora are characterized by a poleward motion (Section 3.4.1). which frequently moves the auroral arcs through the magnetic zenith. It was noted in the introduction to this section that the information content in photometer records varies as an arc moves closer to a station and passes overhead. Altitude distributions of the auroral emissions are probed if the arc is located some distance from the station but no information is obtained on the width of the arc. The thickness of auroral arcs may be conveniently measured when the arc is located in the magnetic zenith although the brightness represents a sum along the entire emitting column of gas and no altitude information is available. Production of $O(^1D)$ has been limited to discrete altitude ranges for the plots in Figure 4.12 to demonstrate the change in information content. The ranges are 5 km in width and centered on altitudes of 92.5, 102.5, 122.5, 202.5, 252.5, 302.5, 352.5, 402.5, 452.5, 502.5, and 552.5 km. Production rates of $O(^1D)$ are the same within each altitude range. The arc initially forms at a latitude of 72° and moves poleward with a velocity of 1 km/s. Electron precipitation is terminated when the arc reaches a latitude of 76.5° . The station is located at 75° , approximately 330 km north of where the arc initially forms (1° in latitude is approximately 110 km at ionospheric altitudes). Arcs forming at 72° and moving at 1 km/s cross the magnetic zenith 5.5 minutes after forming.

The neutral atmosphere is motionless and the lifetime of $O(^1D)$ is once again set to 1 second in Figure 4.12(a). The width of the arc is 30 km, determined by the "merging time" of 30 seconds and the poleward drift velocity of 1 km/s. None of the observed variation in the auroral emissions as the arc drifts from equatorward to poleward of the ground site can be attributed to changes in the energy flux and characteristic energy of the precipitating electrons. These parameters are held constant during the lifetime of the arcs. The observed variation is entirely due to the different sampling geometry as the arc moves over the station. The 557.7 nm emissions trace the locus of the particle energy deposition within the atmosphere. The appearance of slanting lines is indicative of the poleward motion of the arcs. The oblique "bow tie" form in the 557.7 nm signal results from the variation of the MSP sampling geometry as the arc moves from equatorward to poleward of the ground station. Emissions originating in arcs poleward or equatorward of the latitude of the ground site appear over a wide range of elevation angles as the photometer response at a given elevation angle is the integrated photon volume emission rate through a small range of altitudes. The response of the photometer over the range of elevation angles is primarily due to the altitude distribution of the photon emission rate assuming the arc is thin. Emissions observed at elevation angles nearest the horizon arrive from the lowest altitudes in the auroral arc while the high altitude regions of the arc are found in the regions nearest the zenith. The "pinch" of the bow tie occurs when the arc lies along the same magnetic field line that passes through the ground station. The photometer response for these conditions at a given elevation angle is the

Reproduced with permission of the copyright owner. Further reproduction prohibited without permission.

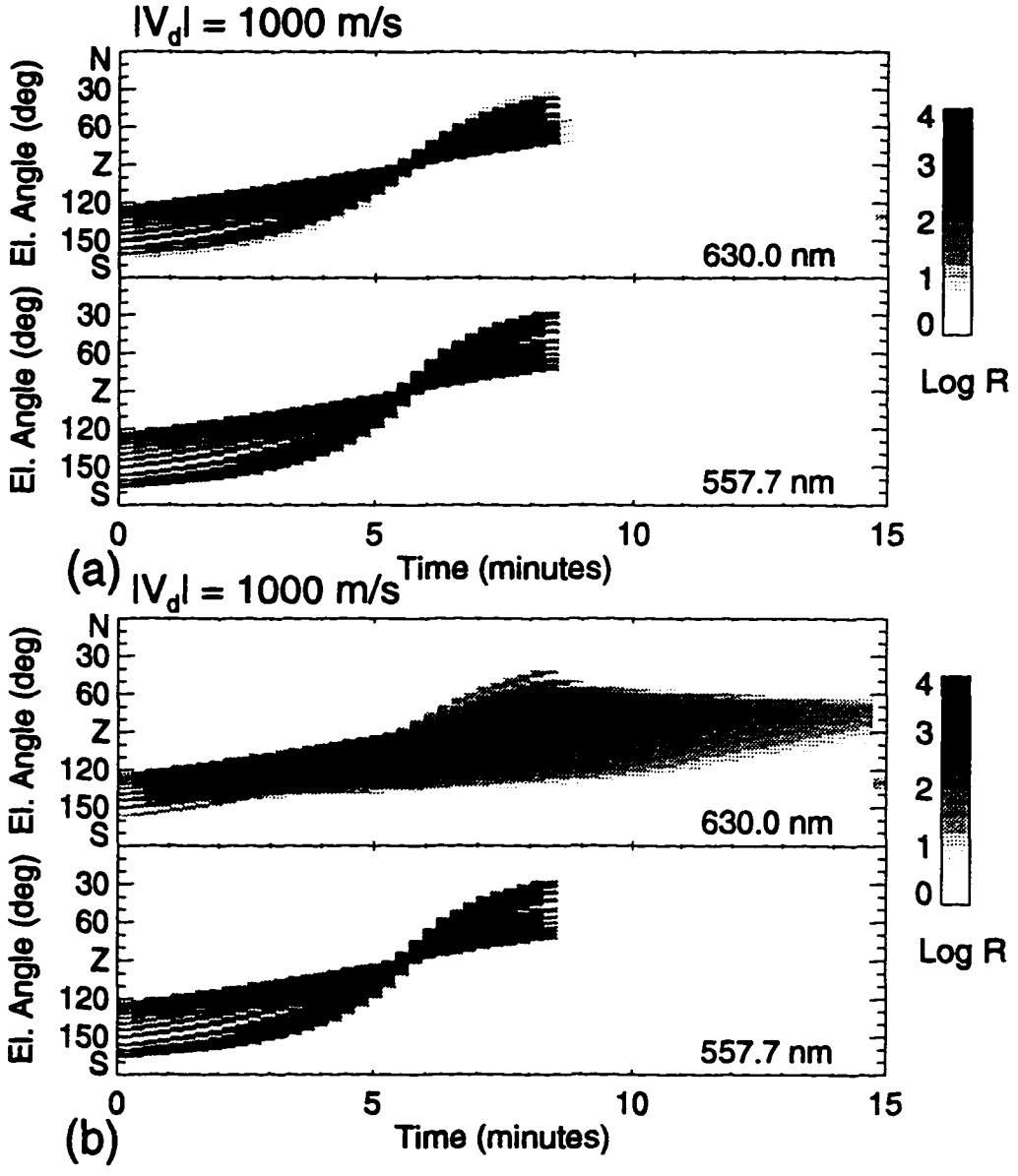


Figure 4.12 Single Poleward Moving Arc with Producton of $O(^1D)$ in Discrete Altitude Ranges. (a) $\tau = 1sec$ for $O(^1D)$ (b) $\tau = 110sec$ for $O(^1D)$ . The neutral wind is zero for both cases. Production of $O(^1D)$ is arbitrarily limited to discrete altitude increments to demonstrate how the information in an MSP scan varies from altitude distributions when the arc is distant from the station to a column sum when the arc is overhead.

Reproduced with permission of the copyright owner. Further reproduction prohibited without permission.

integrated volume emission rate of the entire arc yielding the column emission rate. The response of the photometer over a range of elevation angles near the zenith is due to a latitude distribution of the photon emission rate (i.e., the width of the arc). Note that the auroral emissions are diffuse (i.e., structureless) over a range of elevation angles as the arc approaches the station even though the production of $O(^1D)$ occurs within discrete altitude ranges.

Results for the realistic case of a 110 second $O(^1D)$ radiative lifetime is given in Figure 4.12(b). Production of $O(^1D)$ is discretized in this example using the same altitude ranges as Figure 4.12(a). The discrete emission ranges can be discerned only when the arc initially forms. Populations of $O(^1D)$ created by the arc decay with time constants longer than the motion of an individual emission altitude through given elevation angle producing a persistent 630.0 nm emission. A "pennant" of decaying 630.0 nm intensity is observed between 5-15 minutes in the simulation between elevation angles of 60° and 130° following the arc. The pennant is due to the remnant $O(^1D)$ populations produced by the arc since it is equatorward of the arc at all times. Since the neutral atmosphere is not moving in this example (and diffusion is neglected) the remnant populations remain at the excitation location producing the pennant. Finally, I emphasized that the diffuse 630.0 nm pennant feature present in Figure 4.12(b) is the result of a discrete arc in which the production of $O(^1D)$ has been arbitrarily limited to fixed altitude ranges. A diffuse background 630.0 nm emission is observed even in this artificial example.

Figure 4.13 presents results from a simulation using the same inputs as the previous example except the $O(^1D)$ production in discrete altitude ranges has been replaced by realistic GLOW model altitude profiles for production of $O(^1D)$ . Once again the lifetime of the $O(^1D)$ state has been set to 1 second for the results in Figure 4.13(a) and 110 seconds in 4.13(b). The results are similar to those in Figure 4.12 for the case of $O(^1D)$ production in discrete altitude ranges except the 630.0 nm signal is considerably more diffuse and a strong "ridge" of 630.0 nm emission is observed within the bowtie feature. The ridge is observed at elevation angles where the photometer samples emissions originating from near the peak emission altitude and the diffuse nature of the plot reflects the use of a smooth altitude profile for $O(^1D)$ production. The "pennant" morphology of the 630.0 nm emissions is particularly strong in the realistic case due to the strong ridge of 630.0 nm within the transient arc.

A feature characteristic of altitude dependent quenching in Figure 4.13(b) is the variation in the highest elevation angle at which the 630.0 nm emission is observed. The elevation angle changes from 160° to 145° within the first 2 minutes of the simulation but remains relatively constant as long as the arc is south of the magnetic zenith. Once the arc moves north of the station the equatorward border begins to decay more rapidly. Rapid quenching of $O(^1D)$ formed at altitudes near 250 km or less is the cause of the rapid variation of 630.0 nm emission at the large elevation angles for the first two minutes after the arc initially forms (Section 4.6.1). Once the low altitude $O(^1D)$ populations strongly effected by quenching have been removed a more gradual decrease in 630.0 nm emission rate is observed due to the slower radiative loss of the remnant $O(^1D)$ populations at high altitudes. Emissions within the pennant at a fixed elevation angle are due to primarily to $O(^1D)$ produced within the arc at low altitudes near the station but remnant populations of $O(^1D)$ over a range of altitudes at greater distances from the station also contribute. Decay of the 630.0 nm emission

Reproduced with permission of the copyright owner. Further reproduction prohibited without permission.

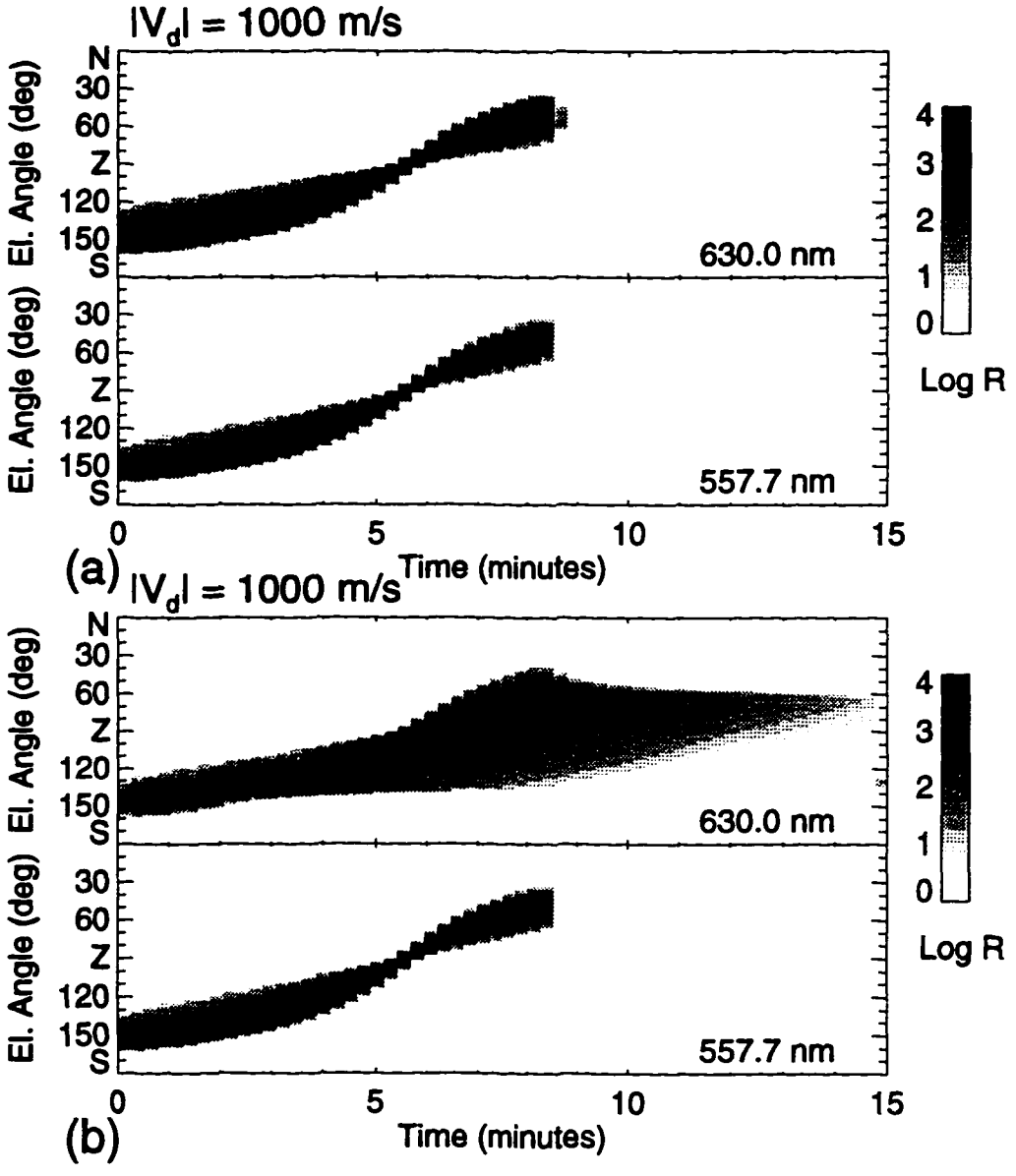


Figure 4.13 Single Poleward Moving Arc. Production rates of $O(^1D)$ from GLOW model are used to obtain realistic altitude profiles of the emission rate. The lifetime of $O(^1D)$ is arbitrarily set to $\tau = 1sec$ in (a) to isolate spatial effects in sampling the auroral arc. When the $O(^1D)$ lifetime is set to $\tau = 110sec$ in (b) the pronounced effects of the long lifetime become apparent.

Reproduced with permission of the copyright owner. Further reproduction prohibited without permission.

rate is therefore reduced as long as the photometer samples emissions from O($^1D$) produced within the arc as well as the remnant populations, explaining the slow decrease in elevation angle for the lower border between 2.5-6 minutes into the simulation. Once the arc has moved into the northern sky all of the 630.0 nm emissions observed in the southern sky are due to remnant O($^1D$) and the angle at which the lower border is sample once again begins to shift to smaller elevation angles.

A series of single scans from Figure 4.13(b) at selected times are given in Figure 4.14. The transient is initially observed south of the station at 02:08 minutes into the simulation. The arc exhibits the classic altitude variation in the 630.0 nm and 557.7 nm emission lines. The strong 630.0 nm emission at high altitude is sampled at smaller elevation angles and the low altitude 557.7 nm emission is detected at larger elevation angles. Note that at elevation angles between 125° and 150° both emissions are present since mechanisms that produce O($^1S$) also produce O($^1D$) and quenching can only remove a fraction of the O($^1D$) population. The transient lies in the magnetic zenith at 05:36 minutes. The 557.7 nm emission is narrowly peaked but the 630.0 nm emission trails to greater elevation angles because of the remnant O($^1D$) produced while the arc was south of the station. Once the arc has moved into the northern sky as in the scans obtained at 08:00 minutes the relative position of the 557.7 nm emission with respect to the magnetic zenith has changed. The 557.7 nm emission appears to be equatorward of the 630.0 nm emission while the arc is south of the station but changes to poleward of the 630.0 nm emission when north of the station. This interpretation is based on erroneously treating the elevation angle scans as intensity as a function of latitude. The effect is geometric since it is known from the input of the simulation that both the 630.0 nm and 557.7 nm emissions are produced on the same field line within the discrete arc. Photometer records should be interpreted as the 557.7 nm emission occurring nearest the horizon for arcs poleward and equatorward of the station. There is no 557.7 nm emission in the scans obtained at 08:48, 10:56, and 13:04 minutes because the electron precipitation has terminated. The 630.0 nm emissions are due to the decaying remnant population of O($^1D$) produced by the arc as it drifted over the station. Note that even though electron precipitation is not present in the 08:00 and 08:48 minute scans that 630.0 nm photons are observed in the magnetic zenith.

Figure 4.14 also highlights a problem encountered when utilizing the 630.0 nm emissions to determine the latitudinal width and duration of energy deposition by electrons within transient arcs. The input to the model produces a precipitation region of 30 km in north-south extent, yet the 630.0 nm emissions may be found over a wide range of elevation angles. As the arc moves through the zenith, the 557.7 nm emission is sampled over an elevation angle range of approximately 16° yielding a width on the order of 30 km if the emission is peaked at 110 km (see Appendix A for converting elevation angles to distance). A similar calculation based on the full angular range over which the 630.0 nm emission is observed, approximately 30-50° , and assuming an emission altitude of 250 km yields an estimated arc width of 130-180 km. The erroneous value results from including 630.0 nm emission originating in remnant O($^1D$) populations. Many of the extreme values reported for widths of dayside transient events (Section 3.4.7) may result from erroneous estimates based on the 630.0 nm emission.

Finally, the pennant feature produced by the simulation in Figure 4.13(b) compares favorably with observations of 630.0 nm emissions in dayside aurora published as Figure 1b of *Sandholt et al.*

Reproduced with permission of the copyright owner. Further reproduction prohibited without permission.

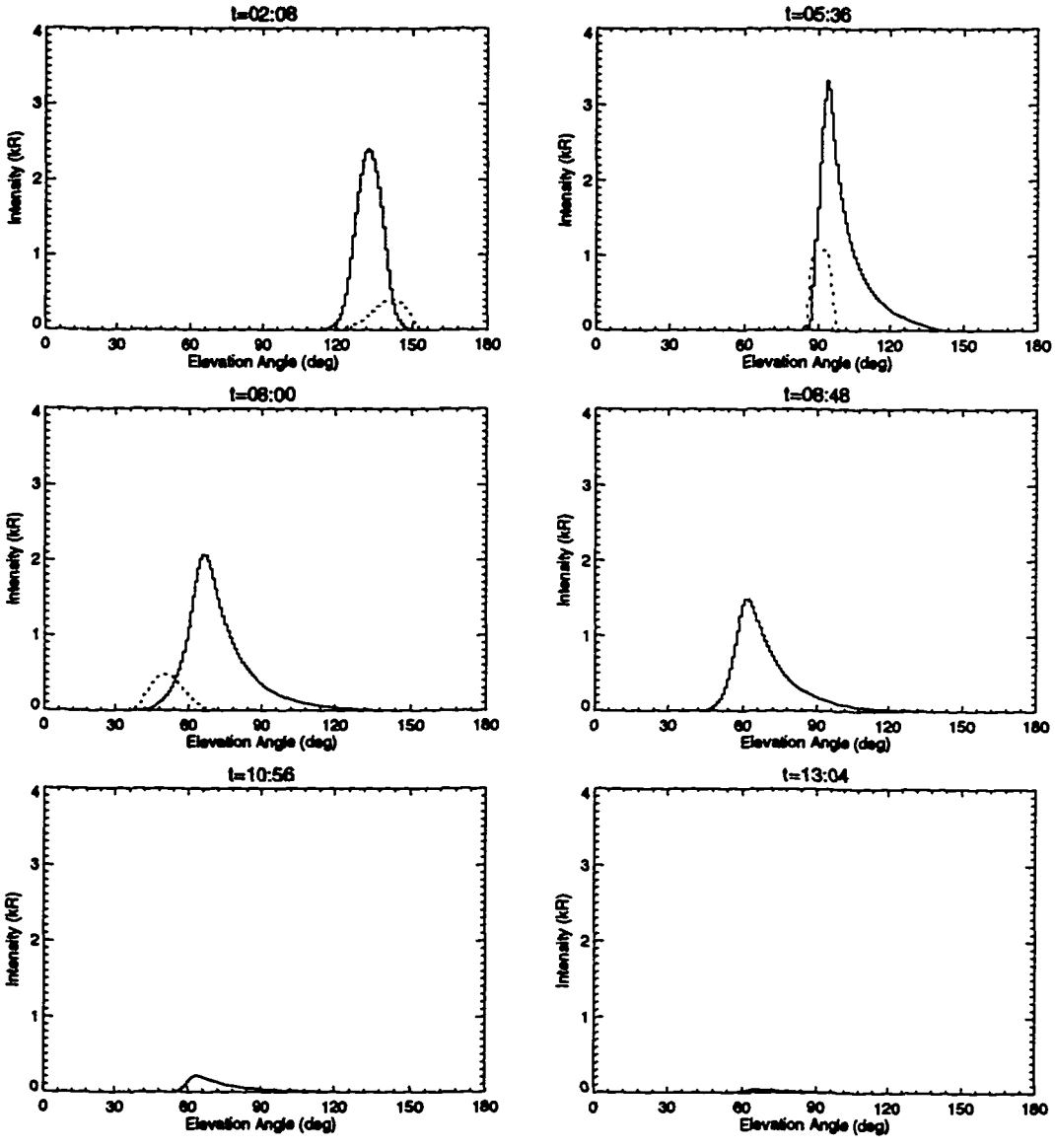


Figure 4.14 Elevation Scans From Figure 4.13(b). A series of scans at selected times are given. The 630.0 nm emission is the solid line and 557.7 nm emission the dotted line. See text for details.

Reproduced with permission of the copyright owner. Further reproduction prohibited without permission.

[1989b], Figure 2 of *Fasel et al.* [1994a], and Figure 2 of *Fasel* [1995]. A number of the transient arcs in Figure 4.1 also exhibit the pennant feature, particularly the events crossing the zenith between 0730 UT and 0800 UT. The full development of the pennant is rarely realized in data since series of arcs overlap, the subject of the next section.

## 4.7 Model Results II: Application to Dayside Aurora

The cases considered to this point have been used to understand the distribution of 630.0 nm emissions arising from a single auroral arc. Daytime aurora, however, is characterized by series of arcs. Statistical studies show the transients which persist for an average of 5 minutes form on the average of once every 6 minutes with a peak in the probability distribution of once event every 3 minutes *Fasel* [1995]. The 7.6 minutes event lifetimes in the case study presented in Section 4.2 are somewhat longer than the average value. The series of events simulated in this section form with 5 minute intervals between events. Each arc initially forms at 73.5° latitude and drifts poleward 333 km to 76.5° latitude where the electron precipitation is terminated. The 0.5 km/s drift speed used in all of the simulations results in arc lifetimes of approximately 11 minutes.

### 4.7.1 Series of Transients with Neutral Wind

Simulations of series of transient arcs are shown in Figure 4.15. The "reconnection time", $d\tau$, is 10 seconds and the interval between events is 5 minutes. Each arc appears to move poleward immediately after forming because the reconnection time is less than the sample time of 16 seconds. Poleward arc velocities are a constant 500 m/s for the lifetime of the arc yielding arc widths of 5 km. Neutral wind velocities of 0 m/s, 120 m/s and 240 m/s, and 500 m/s have been used in the different cases. Values of 120 m/s and 240 m/s are representative of neutral wind speeds observed in the dayside auroral oval (Section 4.5.5). Simulated photometer records in Figure 4.15(a) where the neutral atmosphere is not moving is included for comparison with the nonzero wind results. The final case where the neutral wind is the same as the arc drift speed, 500 m/s, has been included to demonstrate the 630.0 nm morphology that results from neglecting transport in 1-D models by assuming the neutral gas moves with the electron precipitation source [*Davis et al.*, unpublished manuscript].

Poleward and equatorward borders of the 630.0 nm emissions exhibit a serrated edge in all of the photometer plots, a characteristic of the discrete nature of the auroral arcs. The serration is due to the rapid decay of the low altitude $O(^1D)$ populations that suffer the greatest quenching, as discussed in Section 4.6.2. It can only be observed on the equatorial edge of the dayside auroral oval if the arcs move poleward once they form. Serrations are reduced or absent in the simulations presented in Section 4.7.3 where arcs remain at a constant latitude for a period after forming. Serrations on the equatorward edge of the dayside auroral oval in Figure 4.15(a),(b), and (c) are more obvious in the examples with greater wind speeds. This effect is due to the transport of $O(^1D)$ populations formed at the equatorial edge of the auroral oval poleward by the neutral wind. In contrast, serrations on the poleward edge of the auroral oval become less obvious as the wind speed increases due to the $O(^1D)$ transported into the region from lower latitudes.

Reproduced with permission of the copyright owner. Further reproduction prohibited without permission.

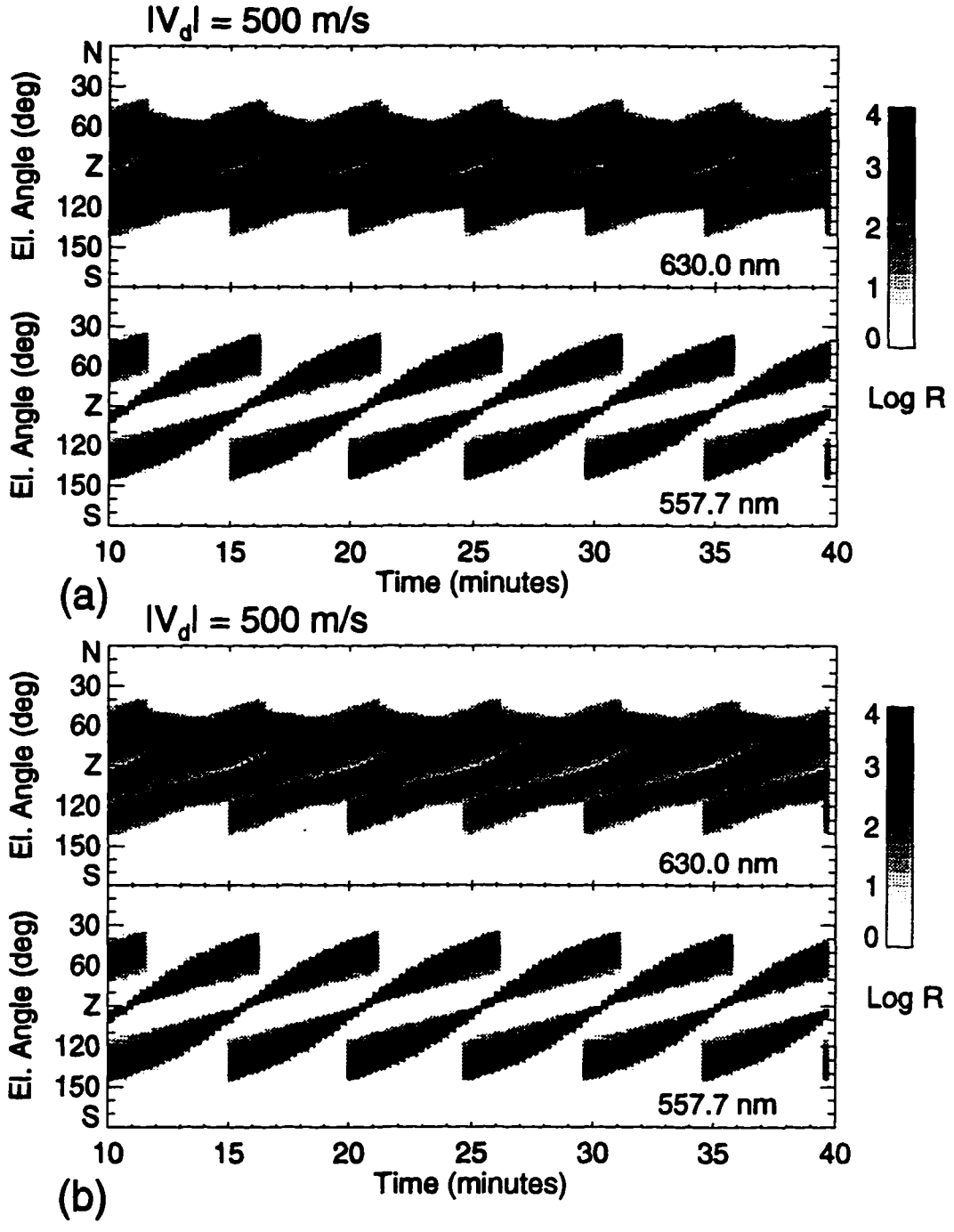


Figure 4.15 Series of Poleward Moving Arcs Including Neutral Wind. The arcs are drifting poleward at 500 m/s, $\tau = 110sec$ for $O(^1D)$ , and neutral wind speeds are (a) Vn = 0 (b) Vn =125. Transients are forming every five minutes.

Reproduced with permission of the copyright owner. Further reproduction prohibited without permission.

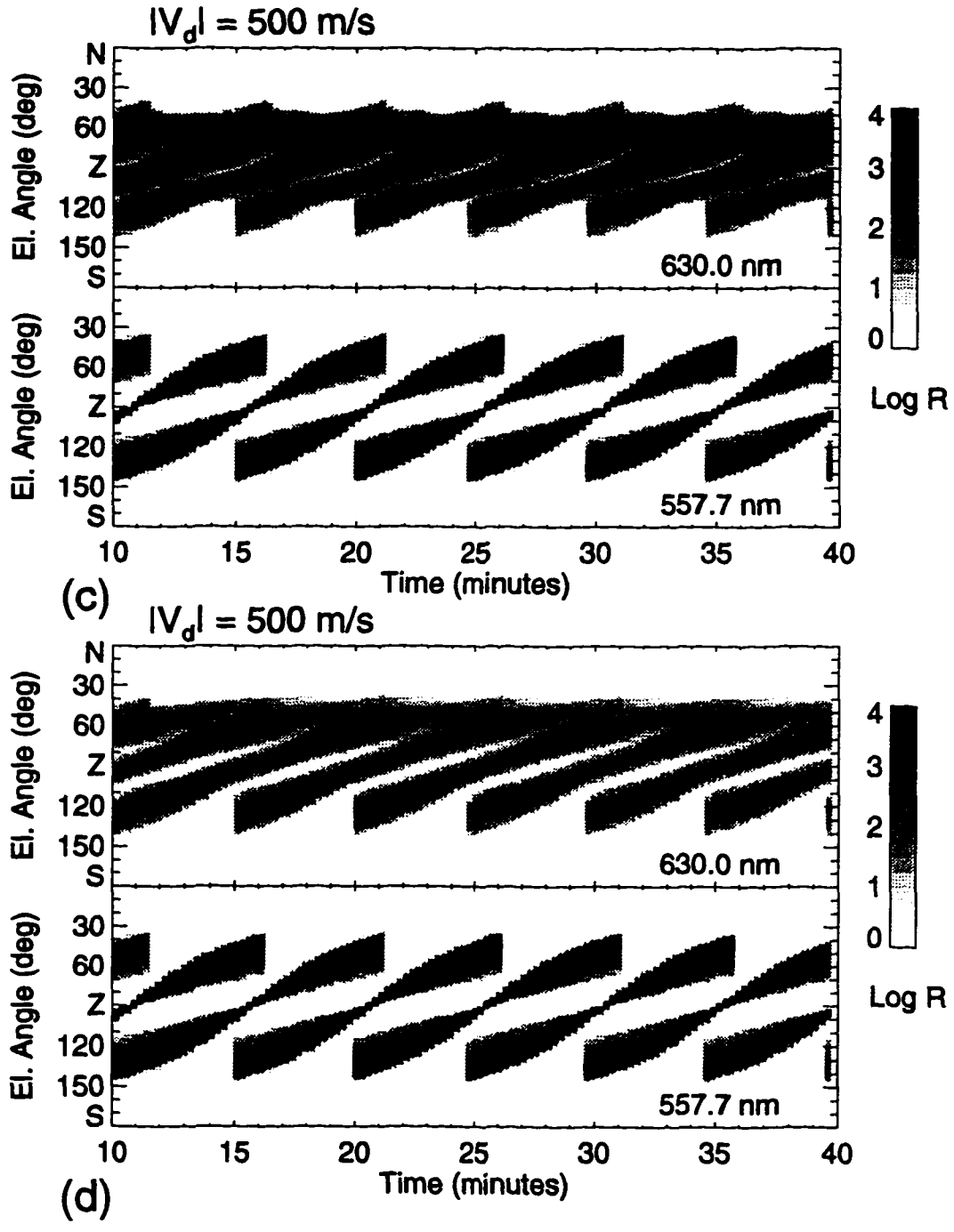


Figure 4.15 (continued). (c) Vn = 250 (d) Vn =500.

Reproduced with permission of the copyright owner. Further reproduction prohibited without permission.

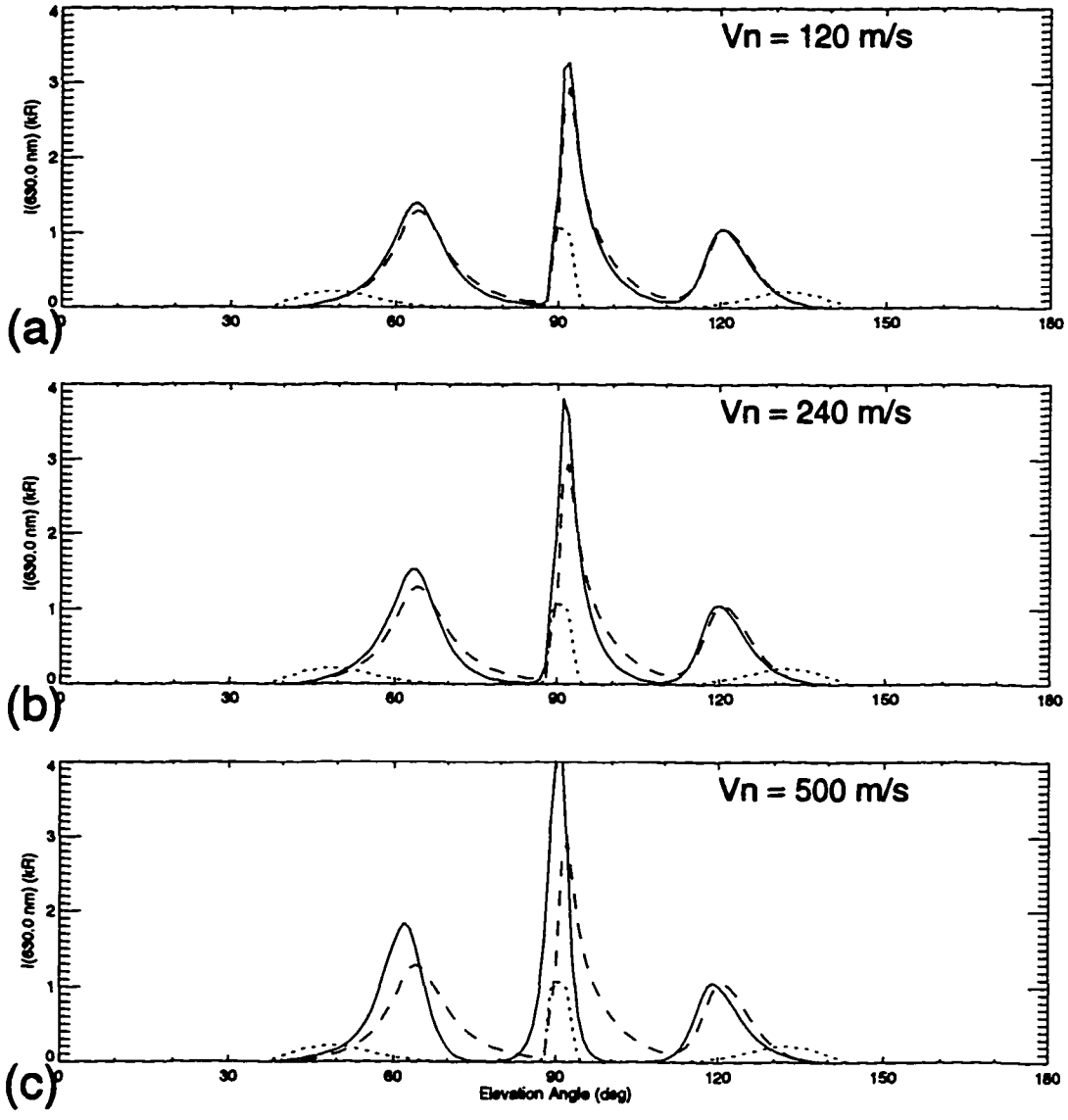


Figure 4.16 Comparison of Elevation Scans for Different Neutral Wind Velocities. Peaks in the 557.7 nm emission (dotted line) mark the regions of active electron precipitation. The solid line is the 630.0 nm emission in the presence of the varying neutral winds and the dash line the $V_n = 0$ 630.0 nm emission for comparison.

Reproduced with permission of the copyright owner. Further reproduction prohibited without permission.

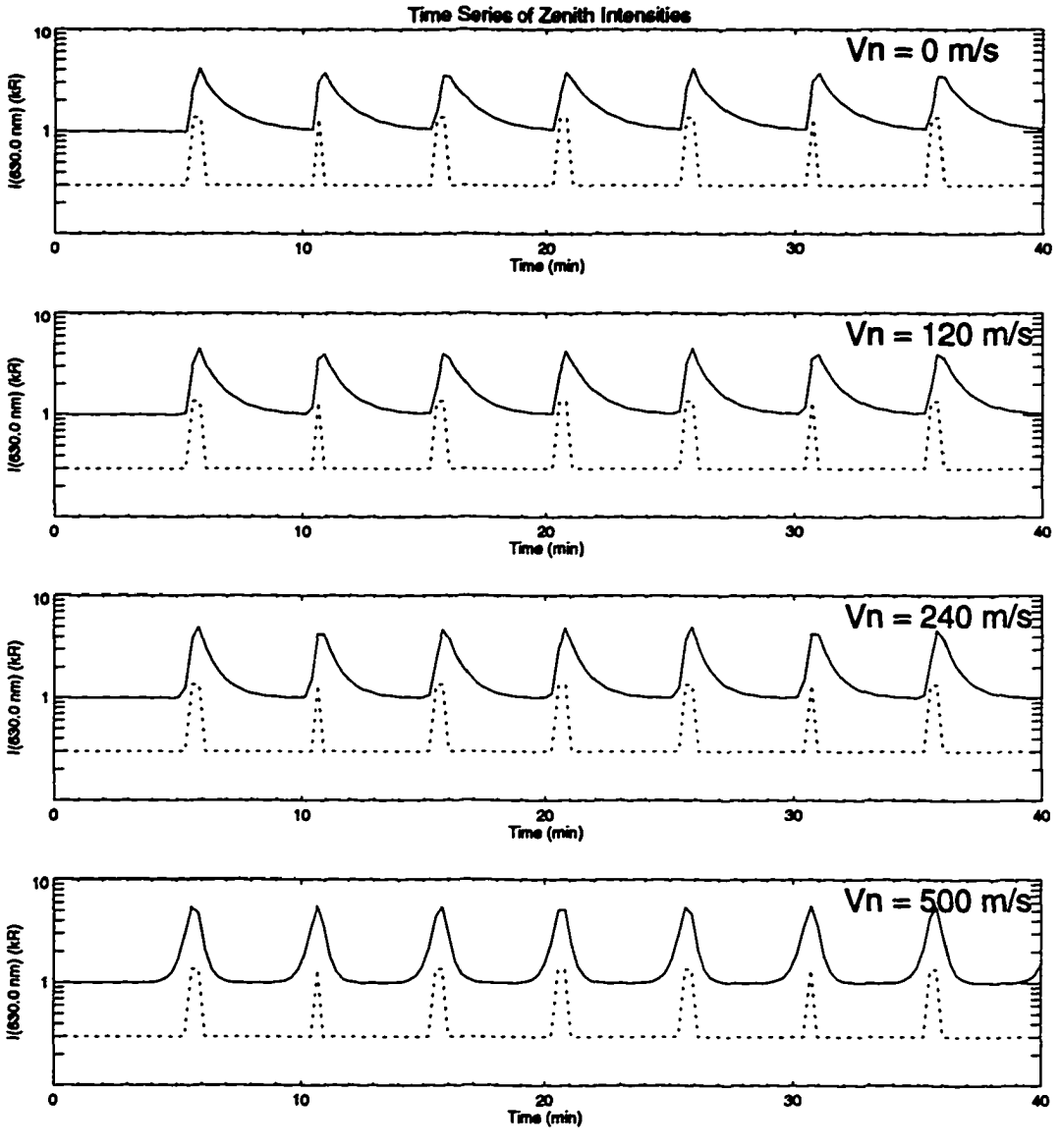


Figure 4.17 Zenith Scans for Neutral Wind Series. As the wind speed approaches the arc drift speed the characteristic decay curve is altered. Arbitrary background intensities of 1 kR 630.0 nm and 300 R 557.7 nm have been added.

Reproduced with permission of the copyright owner. Further reproduction prohibited without permission.

The effect of neutral wind transport is more easily observed in single elevation angle scans. Figure 4.16 shows a single set of scans obtained at 20.5 minutes in the simulation. Three prominent regions of auroral emissions are present in the record. The first is south of the station where the photometer detects emissions at elevation angles between 110° and 145° . The relative position of the 557.7 nm emission peak at larger elevation angles than the 630.0 nm emission peak suggests the structure is an auroral arc. This assumption is confirmed by consulting Figure 4.15 where a new transient is forming at the equatorward edge of the auroral oval. The emission in the zenith is a transient arc formed approximately five minutes earlier that has drifted into the vicinity of the ground station. Poleward of the station is another transient arc nearing the end of its life.

Three sets of curves are plotted in Figure 4.16, a solid line representing the 630.0 nm emission observed for the neutral wind conditions listed on the plot. The dashed line is the 630.0 nm emission in the absence of a neutral wind for comparison and the dotted line the 557.7 nm emission to indicate the location of electron precipitation. Neutral wind transport of the $O(^1D)$ produced with the transient arc is apparent in a number of features in the figure. One of the most obvious is the reduction of the 630.0 nm intensity at elevation angles of 100° to 110° and the increase in the zenith. The reduction is due to the wind acting as an additional loss of $O(^1D)$ due to transport of the excited state out of the photometer field of view. For the same reason, the zenith intensity increases since more $O(^1D)$ is transported into the field of view of the photometer although the wind is effectively an additional source of $O(^1D)$ in this case. The wind effect is very obvious in Figure 4.16(b) and (c) for the arc in the northern sky. The wind has removed much of the $O(^1D)$ which produces the 630.0 nm sampled near zenith and deposited it poleward increasing the brightness of the arc near the 60° elevation angles.

Column intensities obtained in the magnetic zenith for the neutral wind cases are plotted in Figure 4.17. An arbitrary background of 1 *kr* 630.0 nm and 0.3 *kR* 557.7 nm was added to the column sums to facilitate comparison with the 10 January 1992 data set in Figure 4.2. Each plot for the different neutral wind cases exhibits a 630.0 nm emission rate that increases rapidly as a transient arc arrives in the magnetic zenith and subsequently decays. The form of the decay depends on the magnitude of the neutral wind. When the neutral atmosphere is not moving the decays are the same as the examples given in Section 4.6 including a compound decay curve indicative of a quenched low altitude population. Including a neutral wind alters the form time series in two significant ways. First, an increased loss rate of $O(^1D)$ and therefore the 630.0 nm emission rate follows each excitation pulse. The greater the wind speed the faster the decay due to transport of $O(^1D)$ produced within the arcs out of the magnetic zenith. Second, an increase in $O(^1D)$ and associated 630.0 nm emission is noted as the transient arc arrives in the zenith. This increase is due to $O(^1D)$ formed equatorward of the station which is blown into the magnetic zenith. Neutral winds therefore may act either as an addition production or loss term depending on the direction of transport. The signature of neutral wind in the zenith scans is the rounding of the decay curves. Comparing these results with Figure 4.2 suggests the neutral winds on 10 January 1992 were consistent with the 120-240 m/s neutral wind simulation.

A number of interesting points can be made by comparing the series of scans in Figure 4.16 with experimental results. Consider first the single scans from the 10 January 1992 example

Reproduced with permission of the copyright owner. Further reproduction prohibited without permission.

plotted in Figure 4.3. The plots are similar in a number of important points. Transient arcs moving through the zenith have asymmetric 557.7 nm and 630.0 nm distributions which arise from the different lifetimes of the $O(^1S)$ and $O(^1D)$ states. Both the simulated and experimental arcs have a 557.7 nm component on the poleward edge of the transient. The 630.0 nm emission on the equatorward edge of the simulated photometer records is due to the remnant $O(^1D)$ populations excited by the arc (Section 4.6.2). The 630.0 nm emission with a peak near 120° in Figure 4.3 is due to a new transient forming equatorward of the zenith arc. This is substantially the same as the simulated feature in Figure 4.16. One important difference lies in the > 1 kR 630.0 nm emission at elevation angles near 110° and 80° in the experimental data that is lacking in the simulated set. The origin of the enhanced red line emission at high altitude in the data set may be due to an extra flux of very low energy electrons creating 630.0 nm emissions by thermal excitation, a process not explicitly included in the simulation. An additional difference is that the 557.7 nm emission is reduced or absent in the most poleward arc in Figure 4.3.

Photometer records published by *Sivjee et al.* [1982] and *Sivjee* [1983] provide another interesting comparison with the simulated photometer records. The photometric observations obtained at Longyearbyen exhibited a broad region of > 1kR 630.0 nm emission poleward of a discrete zenith arc. *Sivjee et al.* and *Sivjee* interpreted the broad red dominated feature as the cusp. The similarity of the 1982 and 1983 observations to the scans plotted in Figure 4.3 was noted in Section 4.2 where it was noted that remnant $O(^1D)$ populations decaying in the north due to a previous transient arc provided an alternative explanation to the broad red feature. The simulation confirms that the *Sivjee et al.* and *Sivjee* results can be explained in terms of transient arcs drifting poleward in the polar cusp.

One final set of observations that is interesting to compare with the simulation results is Figures 4 and 7 of *Lockwood et al.* [1993a]. Two examples of photometer scans obtained near zenith at the Ny Ålesund field site were presented which demonstrate an asymmetric distribution of 557.7 nm and 630.0 nm emissions dependent upon the sign of the IMF $B_y$ component. *Lockwood et al.* [1993a] and *Lockwood* [1994] suggest the photometer data is evidence confirming the *Cowley et al.* [1991] prediction of asymmetries in auroral emissions within dayside transients arcs, the 557.7 nm component predicted to form on the poleward (equatorward) edge of the 630.0 nm auroral transient when $B_y > 0$ ( $B_y < 0$ ). The results from the simulation of transient arcs described here show that asymmetries in the red and green line component are expected to appear due to the differences in lifetimes of $O(^1S)$ and $O(^1D)$ states even if the electron precipitation within the transient is confined to the same field line. Therefore, the results reported by *Lockwood et al.* [1993a] must be considered tentative since a simple aeronomical explanation exists for at least one of the cases required to confirm the $B_y$ dependent asymmetry.

The cases for $V_n$ =0 m/s and 120 m/s both yield results that appear generally consistent with published MSP data, especially in the distribution of 630.0 nm emissions on the poleward border. Examples of photometer records consistent with the simulated morphology include Figure 1 of *Sandholt et al.* [1989b], Figure 7 of *Lockwood et al.* [1990b], Figures 1 and 14 of *Fasel* [1995], and Figures 2 and 11 of *Oieroset et al* [1996]. Reduction of the serration in the poleward edge of the

Reproduced with permission of the copyright owner. Further reproduction prohibited without permission.

630.0 nm emission for the 10 January 1992 case in Figure 4.1 of this study suggest large neutral wind velocities.

A resolution to the apparent paradox as to how the transient events can form on the equatorward side of, travel through, and decay on the poleward side of the "preexisting cusp arc" [*Sandholt*, 1988; *Sandholt et al.*, 1989] is suggested by the results from the simulated series of arcs. A persistent background 630.0 nm emission feature is produce by excitation of atomic oxygen as a transient arc drifts poleward through the cusp. Neutral atomic oxygen is not controlled by the electrodynamic forces that drive the ionized components of the atmosphere poleward at the same rate as the poleward moving electron precipitation region. Remnant populations of $O(^1D)$ originating within the arcs are simply left behind as the arc moves rapidly poleward. Neutral winds alter the form of the background emission by transporting $O(^1D)$ poleward but in general do not strongly alter the distribution of background 630.0 nm emissions because neutral wind velocities are generally less than transient arc velocities. There is no contradiction to the frozen in flux theorem as suggested by *Newell and Sibeck* [1993] because the electrodynamic forces driving the transient arcs do not effect the neutral atmosphere. The transient arcs alone can produce a diffuse 630.0 nm background but the addition of the diffuse electron fluxes which pervade the cusp due to the requirement of charge neutrality of the precipitating plasma assure a uniform background 630.0 nm emission will be present even if merging at the magnetopause is entirely discrete.

### 4.7.2 Series of Transients with Different Widths (Reconnection Rates)

The spatial and temporal variations of 630.0 nm emissions may also be the result of variations in the electron source. The proposition that the dominant excitation source of the 630.0 nm emissions is due to magnetosheath electrons and the width of a transient arc is determined by the period reconnection is active at the magnetopause [*Cowley et al.* 1991; *Lockwood*, 1994; *Davis et al.*, 1995]. is the basis for the series of simulations in this section which represents a departure from the simple assumption of narrow transient arcs that has been used in the proceeding simulations.

Figure 4.18 displays series of arcs forming at 73.5° magnetic latitude and drifting poleward over the station at 75° latitude. Electron precipitation within the arcs are terminated at 76.5° . A series of "merging" times have been used to alter the width of the arc. As long as merging is active high energy ions will arrive some distance poleward of the ionospheric projection of the separatrix (see Chapter 5). In the simulation the low latitude edge of the arc is determined by the latitude at which ions arrive from the merging site. Lower energy ions take longer to travel from the magnetopause to the ionosphere and will convect further poleward due to the influence of the dawn-dusk convection electric field present in the cusp. After the onset of merging ions begin to arrive in the ionosphere at a minimum latitude and spread poleward. Electrons similarly spread poleward due to the requirement of quasi-neutrality. After a time $d\tau_R$ the merging is terminated and the last open magnetic field line convects poleward. Ions continue to cross the magnetopause and precipitate in the cusp on the convecting open field lines but the low latitude edge of the

Reproduced with permission of the copyright owner. Further reproduction prohibited without permission.

arc moves poleward as the minimum latitude that ions can reach moves steadily poleward at the convection velocity.

Simulations for merging times $d\tau$ of 30, 60, 120, and 180 seconds are given in Figure 4.18. The interval between the formation of individual arcs is once again 5 minutes. The temporal width of the low latitude edge of the arc or, alternatively, the time required for the arc to move through the zenith, is determined by the time the magnetopause is open to magnetosheath plasma. This suggests that photometer records provide a simple method of obtaining information on the time behavior of the reconnection process at the magnetopause. A caveat is that the arc must convect poleward from the formation site. Any zonal motion will introduce additional temporal width that is unrelated to merging. The simulations for $d\tau$ values less than a minute appear consistent with photometer observations of dayside aurora while in the author's experience photometer records comparable to the 120 and 240 second merging times do not exist.

An increase in 630.0 nm brightness with increasing merging times is present in the simulated photometer plots. The maximum 630.0 nm emission rate from the magnetic zenith is plotted in Figure 4.19 as a function of arc width to highlight this increase. The origin of the increase is simply due to the duration of electron precipitation in the zenith which depends on the arc velocity and arc width. The description of transient arc formation used here to obtain varying widths predicts the increase in brightness. I have attempted to compare zenith brightness with arc widths in photometer records from Longyearbyen without much success for two reasons. First, all of the emission rates must be converted to an apparent brightness for unit energy flux and unit energy to compensate for variations in electron energy spectrum. A quantitative method to obtain average energy and energy flux with the 630.0 nm and 557.7 nm emissions is required for this technique to work. Second, the presence of accelerated electron features produce temporary rebrightenings [*Fasel et al.*, 1992] which are unrelated to duration of electron precipitation governed by the transient arc width and velocity. It is interesting to note however that the maximum and minimum brightness observed in a series of transients is often within about a kilorayleigh of the mean, i.e., there is often little fluctuation in the brightness of a series of transients. For example, the average zenith intensities on 10 January 1992 given in Figure 4.2 is approximately 2.5 kR with maximums near 3 kR and minimums near 2 kR. A relatively constant peak emission is certainly expected for a series of arcs drifting through the zenith at nearly the same velocity.

### 4.7.3 Series of Transients with Variations in Drift Azimuth

Transient arcs have been reported to first move east or west dependent on the orientation of the interplanetary magnetic field before moving poleward into the polar cap (Section 3.4.1). The east-west motion is not sampled by the MSP directly but appears as a period of time when the poleward motion is stopped. A series of simulations of the east-west effect are now displayed. A constant arc drift velocity is assumed from the time when the arc forms until it decays, but the azimuth of the velocity vector is varied during the lifetime of the arc. Each arc moves with an initial zonal velocity before turning and drifting poleward. The series presented in Figure 4.20 spend sequentially longer periods moving eastwards before turning poleward. Note that even

Reproduced with permission of the copyright owner. Further reproduction prohibited without permission.

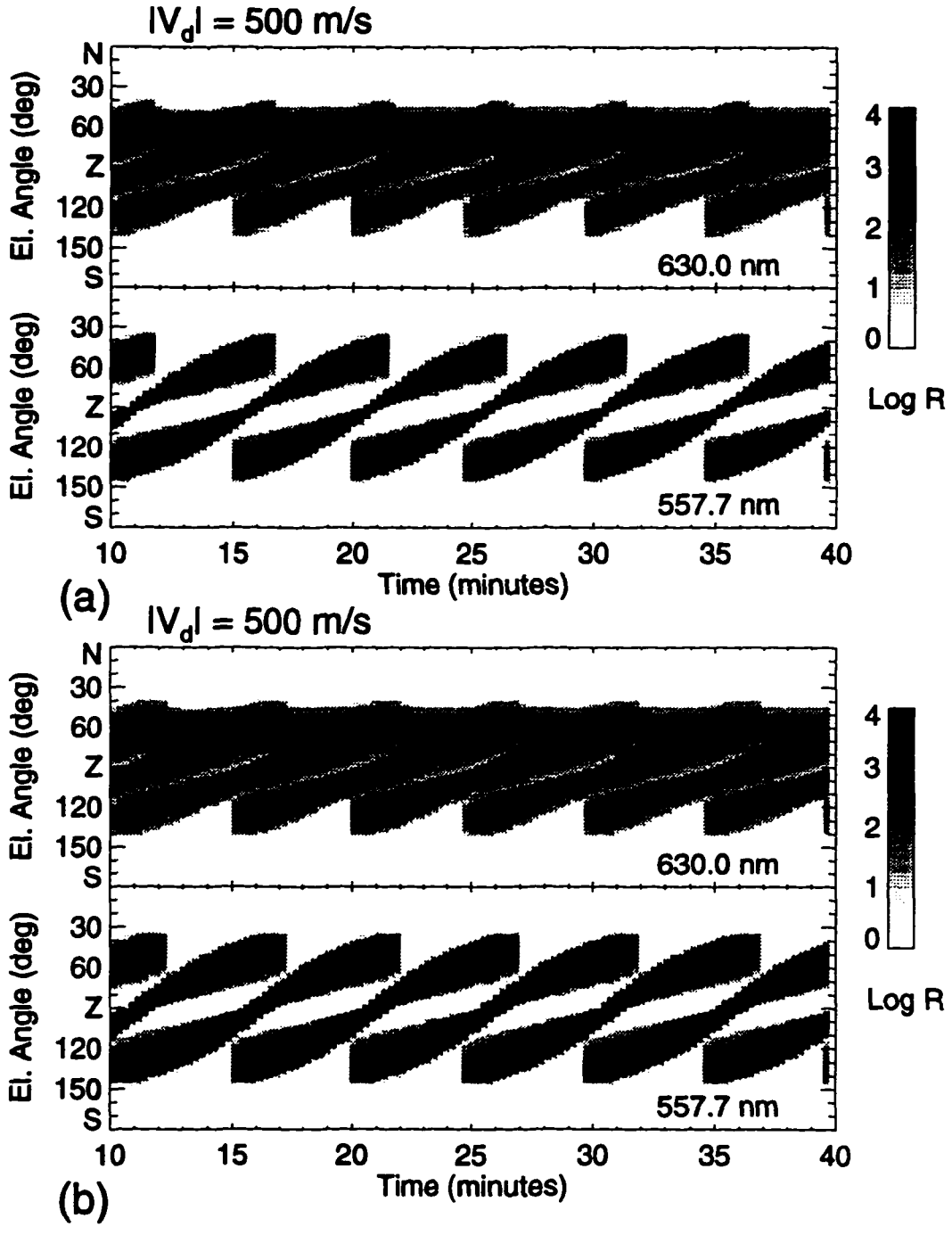


Figure 4.18 Simulated MSP observations for varying "merging times", $d\tau$. The arc drift velocity is poleward at 500 m/s and a neutral wind value of $V_n = 300m/s$ is used for all cases. The "merging times" are (a) $d\tau = 30s$, (b) $d\tau = 60s$.

Reproduced with permission of the copyright owner. Further reproduction prohibited without permission.

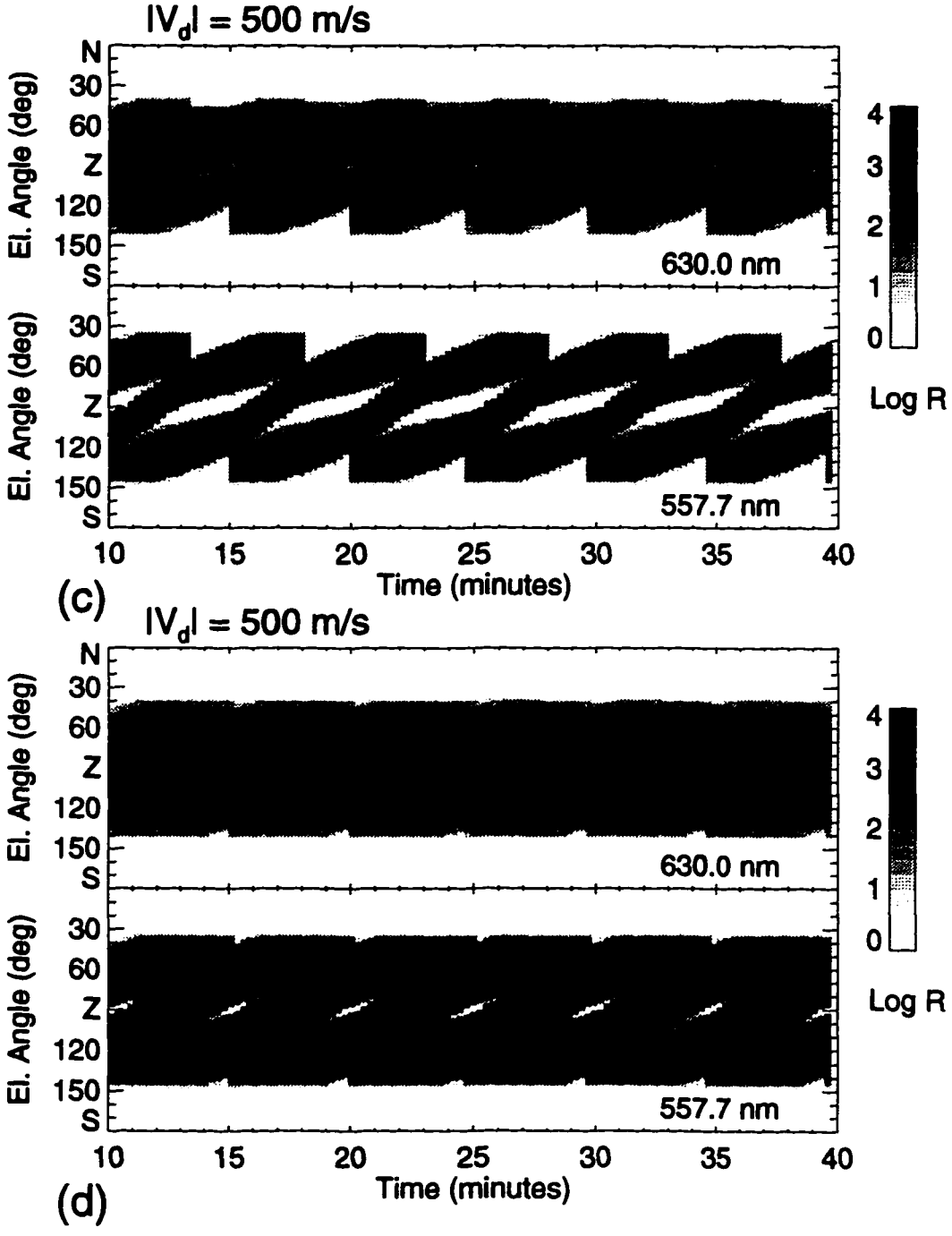


Figure 4.18 (continued) (c) $d\tau = 120s$, and (d) $d\tau = 180s$.

Reproduced with permission of the copyright owner. Further reproduction prohibited without permission.

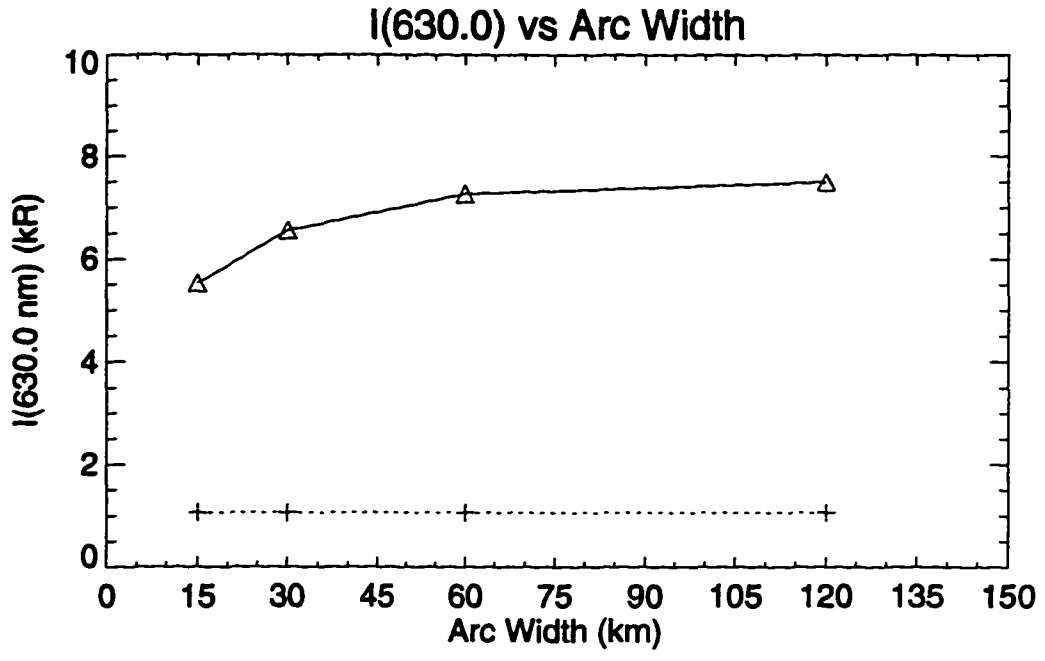


Figure 4.19 Maximum Zenith Intensity as a Function of Arc Width. The longer a transient arc spends in the zenith the closer the 630.0 nm emission can approach to equilibrium.

though the same 60 second merging period is used in each simulation the temporal width of the arc at the 140° elevation angle increases with the increase in the time the arc drifts zonally. The final example in Figure 4.20(d) is a series of discrete arcs which simply drift zonally. Although the perception from the photometer records is that of an arc excited by a fixed electron precipitation source it is produced by the same discrete events that have been used throughout this study. This mechanism is a possible source of the second type of persistent emission discussed in Section 4.2

## 4.8 Conclusions

DMSP satellite overpasses of the cusp exhibit structured electron features that may be identified as the fluxes responsible for the dayside auroral arcs. These features are superimposed on a structureless electron flux distributed throughout the cusp and low latitude edge of the plasma mantle. The persistent, structureless background electron fluxes, a viable source of diffuse 630.0 nm emissions on the order of 0.1-1 kR in the cusp, is the magnetosheath component of the precipitating magnetosheath plasma bound to precipitate with the ions due to the requirement of charge quasi-neutrality.

An auroral model was described that was used to examine the temporal variation in 630.0 nm emissions produced by transient arcs in the cusp. The model demonstrates that even very thin auroral arcs drifting poleward will produce a diffuse background of 630.0 nm emissions due to the

Reproduced with permission of the copyright owner. Further reproduction prohibited without permission.

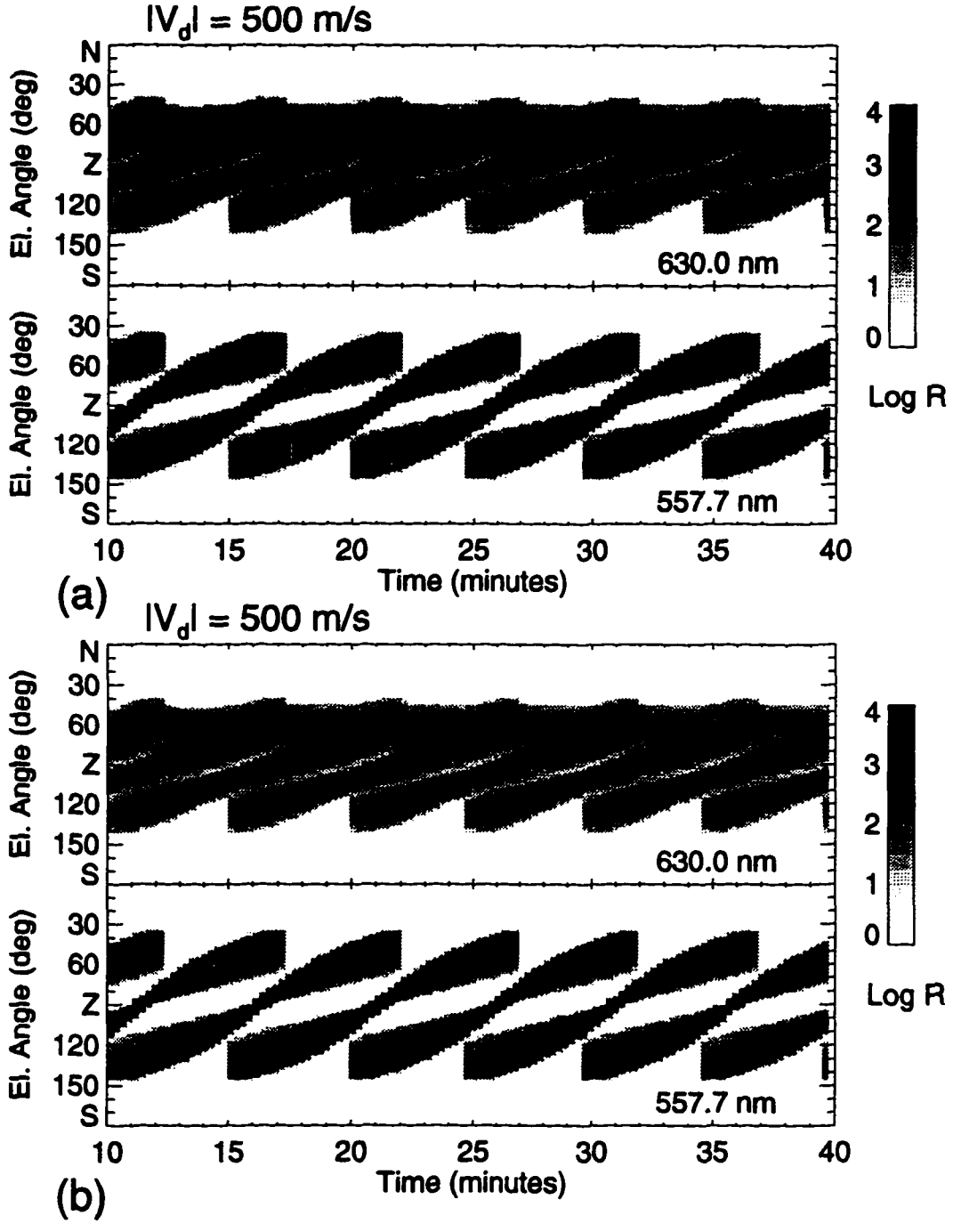


Figure 4.20 Simulated MSP observations for varying poleward arc drift velocity. The arc drift velocity is fixed at 500 m/s but the azimuth of the drift velocity is varied as a function of the lifetime of the arc. The coordinate system and time variation of the azimuth is given in Figure 4.15. The neutral wind is 300 m/s. (a) Transients drift directly poleward, no zonal velocity. (b) Arcs drift eastwards for 30 seconds before turning poleward.

Reproduced with permission of the copyright owner. Further reproduction prohibited without permission.

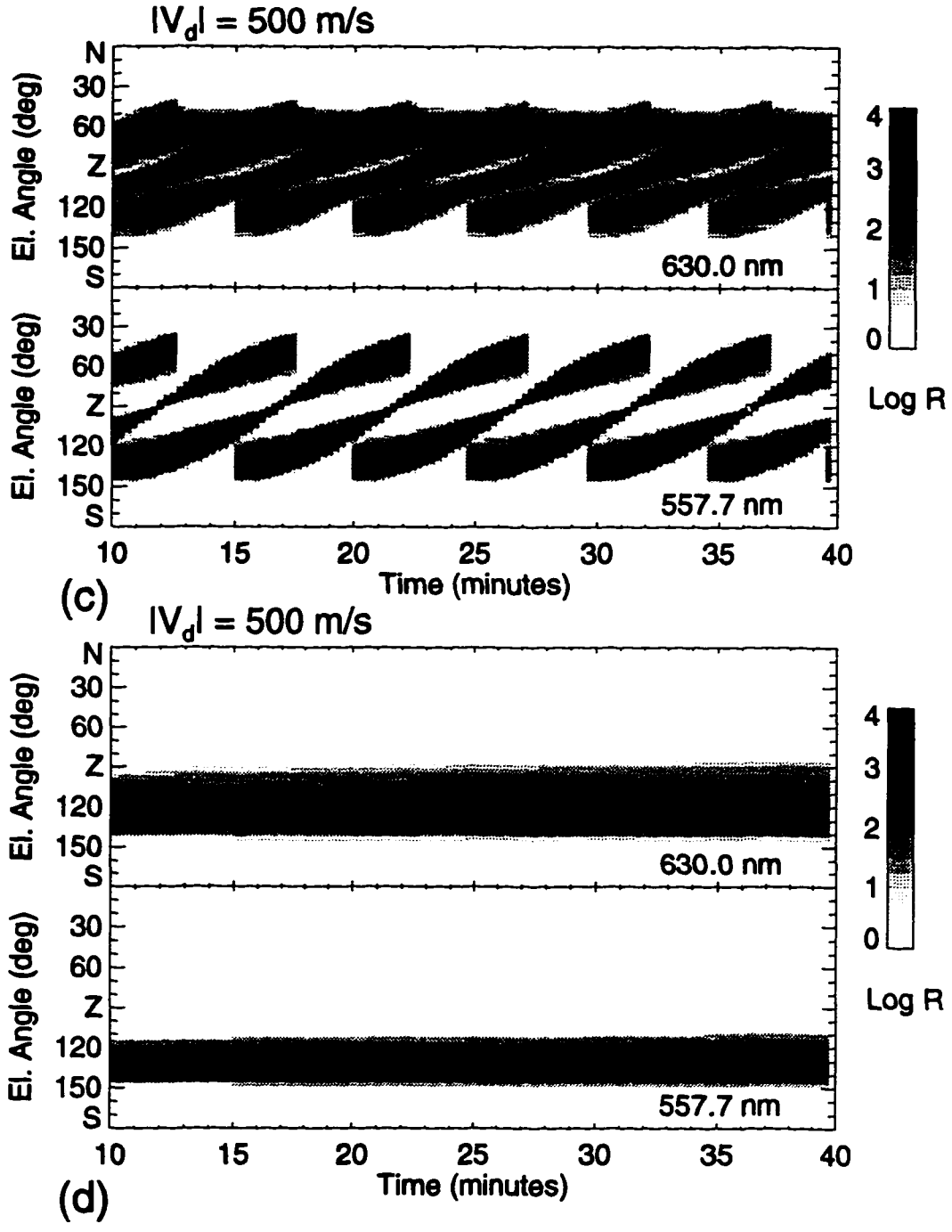


Figure 4.20 (continued) (c)Arcs drift eastwards for 60 seconds before turning poleward (d) Constant eastward drift.

Reproduced with permission of the copyright owner. Further reproduction prohibited without permission.

uncoupling of the excitation source from the neutral atmosphere. Neutral winds modify the diffuse background, but the wind speeds on average are expected to be slower than the electrodynamic drifts leaving $O(^1D)$ behind the excitation region. Transient arcs produce an additional background 630.0 nm emission in addition to that produced by the diffuse electron fluxes required to maintain charge quasi-neutrality in the cusp. Both sources of electrons may originate in discrete merging events at the dayside ionosphere and produce a diffuse 630.0 nm emission. Therefore, observations of diffuse 630.0 nm emissions in the dayside aurora cannot be used to discount discrete merging.

If the arcs are allowed to drift in a zonal direction before moving poleward significant $O(^1D)$ populations accumulate near the equatorward edge of the cusp and may even approach near equilibrium. Zonal drifts are expected if the IMF field is dominated by the $B_y$ component, the typical configuration for the IMF (Section 2.2), explaining why dayside aurorae is often described as moving through a persistent arc. Departures from the Parker spiral orientation are often the result of coronal mass ejections, corotating shocks, or solar flares leading to compression of the solar field ahead of the disturbed region. In these cases the total field increases and very large Bz values are observed but the By component is generally the strongest component, therefore the transient arcs should exhibit even stronger azimuthal drifts during disturbed periods leading to even stronger persistent red emissions.

The model highlights that 630.0 nm emissions within the dayside aurorae are rarely in equilibrium. The 110 second radiative lifetime of $O(^1D)$ is on the order of the most probable interval between formation of individual transients, approximately 180 second. Significant concentrations of $O(^1D)$ are always present due to previous arcs and the 630.0 nm emissions are rarely in equilibrium, limiting the use of the I(630.0 nm)/I(557.7 nm) ratios to quantitatively estimate the average energy flux of the precipitating particles.

The simulation of a wide variety of photometer observations of dayside 630.0 nm emissions including the formation of diffuse 630.0 nm backgrounds from the assumption that all of the electron precipitation arrives in discrete arcs points out that the presence of diffuse 630.0 nm emissions is not evidence for a continuous background of precipitating particles either throughout the cusp or localized at the equatorward boundary of the dayside auroral oval. However, I must emphasize that these results do not show the lack of diffuse electron fluxes. Satellite overpasses of the cusp routinely record unstructured electron fluxes in excess of $1^{10}$-$6 \times 10^{10}$ erg/cm$^2$s sr predicting diffuse 630.0 nm emissions on the order of 1 kR. Results from the simulation should be interpreted as describing the temporal variations in 630.0 nm emissions due to transient arcs. Diffuse emissions in the midday cusp are due to at least two electron precipitation sources: transient auroral arcs and the unstructured electrons required for charge quasi-neutrality. The structured fluxes represent 80% to 90% of the energy deposition within the cusp explaining why ground based observers describe dayside aurora as a series of bright arcs on a diffuse background aurora.

Reproduced with permission of the copyright owner. Further reproduction prohibited without permission.

# Chapter 5.
# A Case Study of Dayside Aurora near the Ionospheric Projection of the Separatrix

## 5.1 Introduction

Flux transfer events (FTE) are widely believed to be the magnetic field signature of impulsive increases in the dayside magnetic reconnection rate [*Russell and Elphic*, 1978]. The search for ionospheric signatures of these events has received considerable attention in recent years. One motivation for these studies is the interest in monitoring dayside plasma processes using ground based observations. Poleward drifting auroral arcs, typical of dayside auroral displays, have been associated with magnetic flux erosion at the dayside magnetopause since their discovery [*Vorobjev et al.*, 1975; *Horwitz and Akasofu*, 1977]. In recent years it has been proposed that the transient arcs are the best candidates for an optical signature of the FTE in the ionosphere [see Section 3.4]. The consensus in the space science community is that electrons with energies on the order of 100's of eV producing the dayside auroral oval originate in the magnetosheath plasma which penetrates to ionospheric altitudes through the polar cusp [*Heikkila and Winningham*, 1971; *Frank*, 1971; *Eather and Mende*, 1972; *Heikkila et al.*, 1972; *Shepherd and Thirkettle*, 1973; *Sivjee and Hultqvist*, 1975; *Shepherd et al.*, 1976a,b]. The question of whether individual poleward moving transient arcs can be attributed to impulsive increases in the rate at which the plasma enters the polar cusp remains unanswered.

Evidence that an individual transient arc is a causal result of an individual FTE formed during an interval of pulsed merging consists primarily of comparisons between average characteristics (repetition periods, drift rates, drift directions, strong correlation with southward IMF $B_z$ orientation) of the auroral phenomena with the predicted ionospheric response to pulses of dayside merging (Section 2.5.1). As noted in Section 3.5, few studies have ever been reported which critically compare the formation times and intervals between individual FTE's observed at the magnetopause with simultaneous and conjugate observations of auroral events in the ionosphere. Studies of this nature are generally lacking in the literature due to the great difficulty and expense in obtaining simultaneous conjugate observations within the ionosphere and at the dayside magnetopause. In the single example obtained to date where simultaneous observations were available, *Elphic et al.* [1990] reported ground based observations of transient auroral and enhanced ion flow events forming in the ionosphere following a series of FTE's detected by a satellite near the magnetopause. This is consistent with the model that transient ionospheric features are the response to an FTE, but the apparent correlation may in fact be spurious. The possibility exists that the processes forming FTE's and auroral transients are operative during $B_z < 0$ conditions when dayside merging allows plasma to cross the magnetopause. The FTE and ionospheric transients may simply be produced with the same average interval between events but without a one-to-one correspondence between the events at the magnetopause and in the ionosphere. Further evidence is therefore required to confirm that individual arcs are the result of impulsive merging events at the

Reproduced with permission of the copyright owner. Further reproduction prohibited without permission.

dayside magnetopause. Extensive studies along the same lines as *Elphic et al.* [1990] would provide the necessary statistical basis for establishing a causal relationship between dayside aurora and the impulsive merging events but as previously noted the simultaneous observations are difficult to obtain. Alternatively, identification of features in dayside auroral displays which are shown to be specific to a merging process would similarly provide evidence of a causal relationship between the auroral forms and the impulsive merging events. If a causal relationship can be established then the use of ground based optical observations of transient arcs can be considered a valid method of monitoring the energy transfer rate across the dayside magnetopause.

The purpose of this work is to report a set of previously undescribed features of dayside auroral displays and to propose a mechanism to explain the observations. A "latitudinal gap" approximately 50-100 km in width between the poleward border of the mantle aurora and the equatorward border of the dayside auroral oval is described. The [OI] 557.7 nm emission rate is continuously depressed within the gap relative to emission rates in the auroral structures bounding the gap. *Yagodkina et al.* [1989, 1990] used the term "intensity dip" for the region of $\sim$ 1 kR 557.7 nm pulsating aurora approximately 4° to 6° in latitudinal width on the poleward side of the mantle aurora and suggested the electrons producing the aurora within the intensity dip originate in the quasi-stable trapping region in the dawn and dayside magnetosphere. The equatorward boundary of the intensity dip was identified as the durable trapping boundary [*Vorobyev et al.*, 1984; *Yagodkina et al.*, 1989, 1990], consistent with the earlier results of *Buchau et al.* [1972].

The narrow region of reduced 557.7 nm intensity reported here is the boundary between the mantle aurora and the dayside auroral oval and should be located in the vicinity of the separatrix (the boundary between open and closed field lines) in the dayside magnetosphere. A series of "drop out" events are described where the 557.7 nm luminosity on the poleward edge of the intensity dip decreases to values found in the latitudinal gap. The drop outs are followed by formation of 630.0 nm dominated transient poleward moving arcs in the dayside auroral oval. Correlations between the drop outs and the subsequent formation of the transient 630.0 nm dominated arcs suggest the events form as a result of the same physical process. Finally, a narrow region of continuous emission on the poleward edge of the pulsating mantle aurora is described. It will be shown that the auroral observations can be successfully interpreted in terms of the electron and ion populations associated with the dayside boundary layers and FTE's providing new evidence consistent with the hypothesis that transient dayside auroral events are auroral signatures of FTE's.

### 5.2 Instrumentation and Constraints on Observational Geometry

Auroral observations described here were obtained on 30 November 1986 at the Nordlysstajonen field station near Longyearbyen, Svalbard, located at 78.2° N, 15.7° E geomagnetic coordinates. The interval selected for examination is from 0700 UT to 0800 UT (approximately 1030 MLT to 1130 MLT) where the probability of observing the cusp is the greatest [*Newell and Meng*, 1988]. Line-of-sight integrated emission rates at fixed wavelengths in the magnetic meridian plane is obtained by the meridian scanning photometer (MSP) at elevation angle intervals of one degree from

Reproduced with permission of the copyright owner. Further reproduction prohibited without permission.

the northern to southern horizon. A tilting filter mechanism is used to provide background correction for each wavelength. Time resolution is 16 seconds for a complete observation including the emission line observation and background correction. Unfiltered image orthicon television camera images are used to determine the spatial and temporal variations in auroral morphology. Details of these instruments are described in detail in Appendix A and B.

The location of the boundary between the mantle aurora and dayside oval relative to the ground station is important in considering the observations in this study since detection of reductions in auroral intensity over distances on the order of 10's of kilometers at the boundary is required to resolve the latitudinal gap. In cases where the boundary between the two auroral zones is located poleward of the station the slanted sight lines may pass through both the low altitude mantle aurora and the high altitude dayside oval as shown in Figure 5.1 masking the latitudinal gap between the two auroral regions. The gap in emission intensity between the two regions must either be overhead or equatorward of the ground station for details of auroral features on the boundary between the mantle aurora and dayside auroral oval to be successfully studied with optical instrumentation. This special geometry limits the number of days on which the boundary between the regions may be observed (see Section 5.5).

Two other examples have been found in the archive of photometer records from Longyearbyen similar to the example presented here as a case study: 3 December 1986 and 10 January 1982. The latter of the two was presented in Chapter 4. Further examples are not common in Longyearbyen data sets. The implications for the sparse nature of the phenomenon within the Longyearbyen MSP archive is discussed further in Section 5.5.

### 5.3 Case Study: 30 November 1986

MSP records of 557.7 nm and 630.0 nm emissions from 0700 UT to 0800 UT on 30 November 1986 are given in Figure 5.2. Auroral emissions are plotted as a function of Universal Time on the horizontal axis, elevation angle of the photometer scan above the northern horizon on the vertical axis, and the emission brightness is scaled in increasing levels of grey. The sloping lines decreasing in elevation angle with time are a series of transient auroral arcs in the dayside auroral oval. Transient arcs form south of the station where the photometer initially records the emissions near the 110-120° elevation angles. Poleward of the station the arcs fade below the approximately 150 R 557.7 nm and 200 R 630.0 nm airglow background near an elevation angle of 30° . The total range of elevations angles over which the transient arcs are detected is approximately 90° centered on the local zenith, mapping to a horizontal distance of 200-300 km for an assumed peak emission altitude of 90-120 km for the 557.7 nm emission (details of the calculation and a plot of latitude shift as a function of elevation angle are given in Appendix A). These arcs are typical of the type of auroral structures excited by magnetosheath particle precipitation in the cusp that have been associated with the process transferring magnetic flux from the dayside magnetosphere into the geotail [*Heikkila and Winningham*, 1971; *Frank*, 1971; *Heikkila et al.*, 1972; *Vorobjev et al.* [1975]; *Horowitz and Akasofu* 1977; *Sandholt et al.*, 1986]. Peak [OI] 630.0 nm emission rates are

Reproduced with permission of the copyright owner. Further reproduction prohibited without permission.

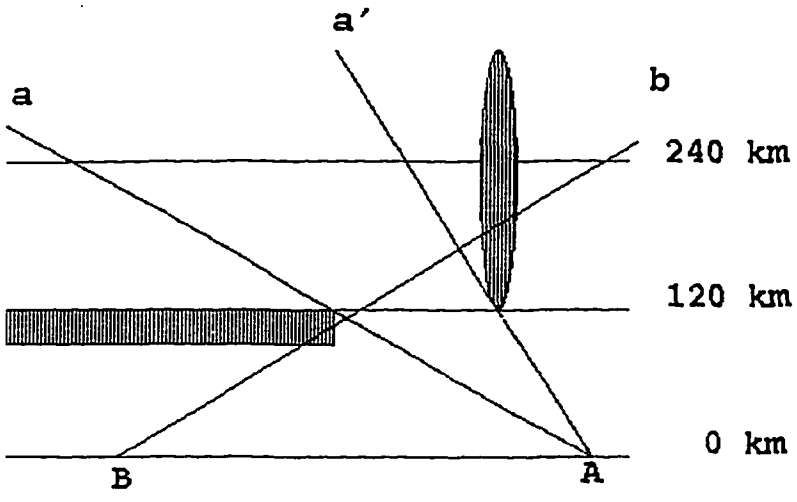


Figure 5.1 MSP Observation Geometry. Auroral emissions within the mantle aurora are indicated by the horizontal shaded region below 120 km altitude. An arc in the dayside oval distributed over a broad altitude range is indicated by the vertical shaded ellipse. The sight line (a) from a station (A) intersects the poleward edge of the mantle aurora and the upper altitude portion of the arc. The latitudinal gap will not be visible from ground station (A). Photometers at station (B) will detect a decrease in auroral emissions between the sight lines (b) and (b') due to the gap in auroral emissions.

on the order of 1-2 kR within the transient arcs with I(630.0 nm)/I(557.7 nm) $\geq$ 1 and a significant 557.7 nm component is present in each transient arc, often in excess of 1 kR.

The unmodulated 630.0 nm emission sampled by the photometer between 150° and the southern horizon is not due to electron precipitation. This feature occurs daily regardless of whether a pulsating aurora is present and is organized in local solar rather than geomagnetic time. The emissions are due to photochemical reactions 5° to 10° south of the observing site where the ionosphere is illuminated by solar UV photons [*Stamnes et al.*, 1985].

The component of arc velocity in the magnetic meridian plane is estimated from the change in elevation angle as a function of time. In this case the slope is positive due to the poleward drift of the arc and meridional drift velocities ranging from 420 m/s to 900 m/s with an average value

Reproduced with permission of the copyright owner. Further reproduction prohibited without permission.

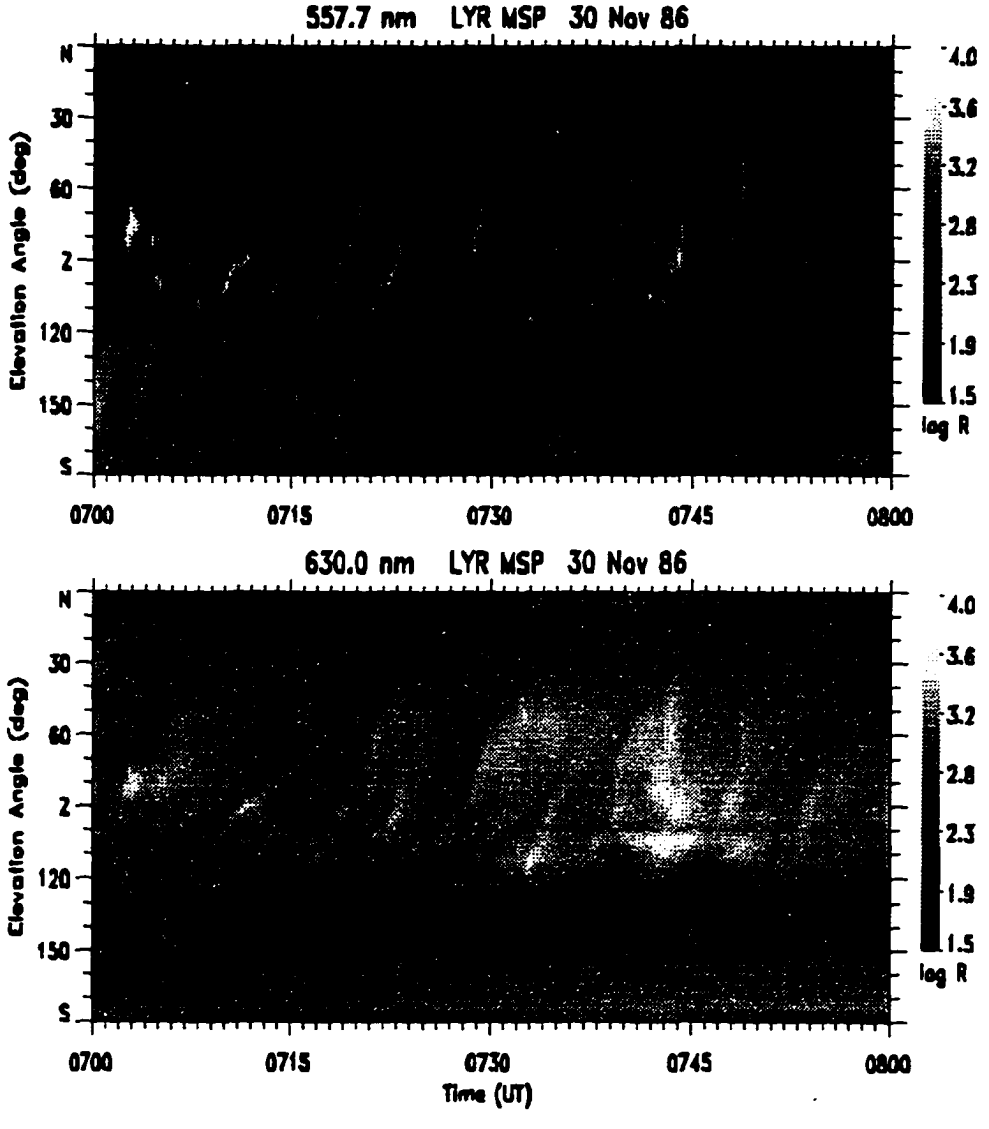


Figure 5.2 MSP records of 557.7 nm and 630.0 nm emissions on 30 November 1986.

Reproduced with permission of the copyright owner. Further reproduction prohibited without permission.

**Table 5.1**
**I( 630.0 nm) Accompanying 150 R, 250 R, and 1 kR 557.7 nm Aurora**

| Characteristic Energy (keV) | $\epsilon$ (erg/cm$^2$/s) | I(630.0 nm) (R) |
|---|---|---|
| | *Rees and Roble* [1986], *Rees et al.* [1988] | |
| 1 | 0.11,0.18,0.71 | 46 ,76 ,298 |
| 1.8 | 0.12,0.20,0.80 | 27 ,44 ,176 |
| 3.1 | 0.13,0.22,0.90 | 20 ,33 ,137 |
| 5 | 0.15,0.25,0.99 | 15 ,25 ,99 |
| 10 | 0.17,0.28,1.13 | 8 ,13 ,53 |
| 20 | 0.20,0.33,1.30 | 4 , 7 ,28 |
| | *Shepherd et al.* [1980], *Steele and McEwen* [1990] | |
| 1.8 | 0.12,0.20,0.81 | 1.7, 2.9,12 |
| 3.1 | 0.09,0.14,0.58 | 1.3, 2.0, 8.3 |

of approximately 500 m/s are determined from the 557.7 nm plot assuming an emission altitude of 120 km.

The transient arcs and associated emissions within the dayside auroral oval is centered on 75° magnetic latitude, consistent with IMF $B_z < 0$ conditions (c.f., *Sandholt et al.*, 1985 and references therein). If the IMF $B_z$ component is positive the auroral oval generally contracts poleward of the station and few of the transient arcs are observed. The hypothesis that $B_z < 0$ cannot be confirmed using IMP 8 records since the satellite is located in the flanks of the magnetosphere during the interval considered here.

Equatorward of the dayside auroral oval in Figure 5.2 is the mantle aurora [*Sandford*, 1964, 1968] sampled by the 557.7 nm photometer between elevation angles of approximately 135° and 180° . The intensity of the 557.7 nm emission is variable with an average value of approximately 150-250 R above the 150 R background in the weaker pulsations near 0730-0800 UT to values on the order of 1 kR in the periods of strongest emission from 0700-0720 UT. The variability arises from auroral pulsations in the mantle aurora. Sampling of the auroral intensity in a fixed meridian by the photometer results in the vertical 'stripes' between approximately 135° to 165° in the photometer records. The variations occur on a number of time scales. The strongest maxima in auroral emission persists for 1-2 minutes at intervals of 4-7 minutes. A series of rapid pulsations are also detectable. This is especially apparent between approximately 07:05 UT to 07:20 UT, where the emission maxima persist for less than a minute and repeat on the order of every 1-2 minutes. The pulsating aurora forms as well as the narrow region lacking 557.7 nm emissions equatorward of the dayside auroral oval form the 'intensity dip' reported by *Yagodkina et al.* [1989,1990]. The 557.7 nm photometer samples the intensity dip between elevation angles of 120° and 165° at 0700 UT. Assuming an emission altitude of 110 km for the mantle aurora this range of elevation angles maps to a distance of 300 km or approximately 3° in latitude. The equatorward border of the intensity dip is marked by an increase in 557.7 nm signal and lack of pulsations. The 3° width of the dip described here is narrower than the 4° - 6° reported by *Yagodkina et al.* [1989,1990].

Reproduced with permission of the copyright owner. Further reproduction prohibited without permission.

A 630.0 nm emission corresponding to the auroral pulsations in the 557.7 nm line is not observed within the mantle aurora due to the large energy of the precipitating electrons. This is confirmed by estimating the 630.0 nm emission expected to accompany the observed I(557.7 nm). One widely used method utilizes the results from the auroral model described by *Rees and Roble* [1986] and Rees et at. [1988]. An alternative is to use the empirical excitation efficiencies derived from coincident satellite and ground based observations by *Steele and McEwen* [1990] and satellite observations by *Shepherd et al.* [1980]. These methods are described in more detail in Section 3.2.5. Results for 150 R, 250 R, and 1000 R 557.7 nm emissions within the pulsating mantle aurora are given in Table 5.1 indicating 630.0 nm brightnesses associated with the weaker 557.7 nm emissions as well as an extremely bright value. The values obtained from the empirical results are smaller than the model values by factors of 15-30. Comparison of the energy flux $\epsilon$ derived using the two methods indicates the model and empirical results are similar. The difference occurs in the red line results, the model producing 630.0 nm intensities on the order of 10 times greater than the empirical results for a given energy flux. The discrepancy may result from the different methods used to obtain the excitation coefficients in the *Steele and McEwen* [1990] and *Shepherd et al.* [1980] methods. Both methods predict 630.0 nm intensities less than the airglow background in the data records.

In order for 630.0 nm emissions to remain undetected the brightness must be less than the statistical variation in the airglow background. The photochemical and airglow sources south of the field station result in 630.0 nm emissions on the order of 200-500 R at the same elevation angles where the 557.7 nm emissions are strongest from 0700-0730 UT. Any additional 630.0 nm signal produced within the pulsating aurora which is less than either the count rate error in the background emission or the sensitivity of the instrument will not be detected by the photometer. The maximum 630.0 nm signal that may be expected from the pulsating aurora is therefore 14-22 R in the region of greatest 557.7 nm intensity in the mantle aurora. The results presented in Table 5.1 demonstrate that this is possible for incident electron populations with characteristic electron energies of 5 keV or greater satisfy this requirement. Electrons with characteristic energies of 5-10 keV or greater deposit their energy at altitudes where quenching of $O(^1D)$ dominates over radiative decay. These results are consistent with previous studies in which the charged particles producing the mantle aurora have been identified as electrons lost from the outer radiation belts [*Frank and Ackerson*, 1972; *Lui et al.*, 1973; *Winningham et al.*, 1975; *Meng and Akasofu*, 1983].

A number of apparent variations in the emission rates due to instrumental artifacts and environmental effects are found in the records plotted in Figure 5.2. Both the 557.7 nm and 630.0 nm channels exhibit sharp decreases in intensity between the 175° and 180° elevation angles at the southern horizon and the 0° and 5° elevation angles at the northern horizon due to snow and ice on the edge of the MSP window deposited during storms. Evidence of atmospheric light scattering is present in the records (particularly in the northern skies) in the form of a uniform airglow background departing from the van Rhijn intensity distribution typical for uniform airglow layers [c.f., *Chamberlain*, 1961]. Light scattering from defects in the MSP slit material may also contribute to scattering. Examples where scattering is particularly evident include the intervals from 0715-0717 UT and 0738-0744 UT on the 557.7 nm plot. Scattering effects are most prominent

Reproduced with permission of the copyright owner. Further reproduction prohibited without permission.

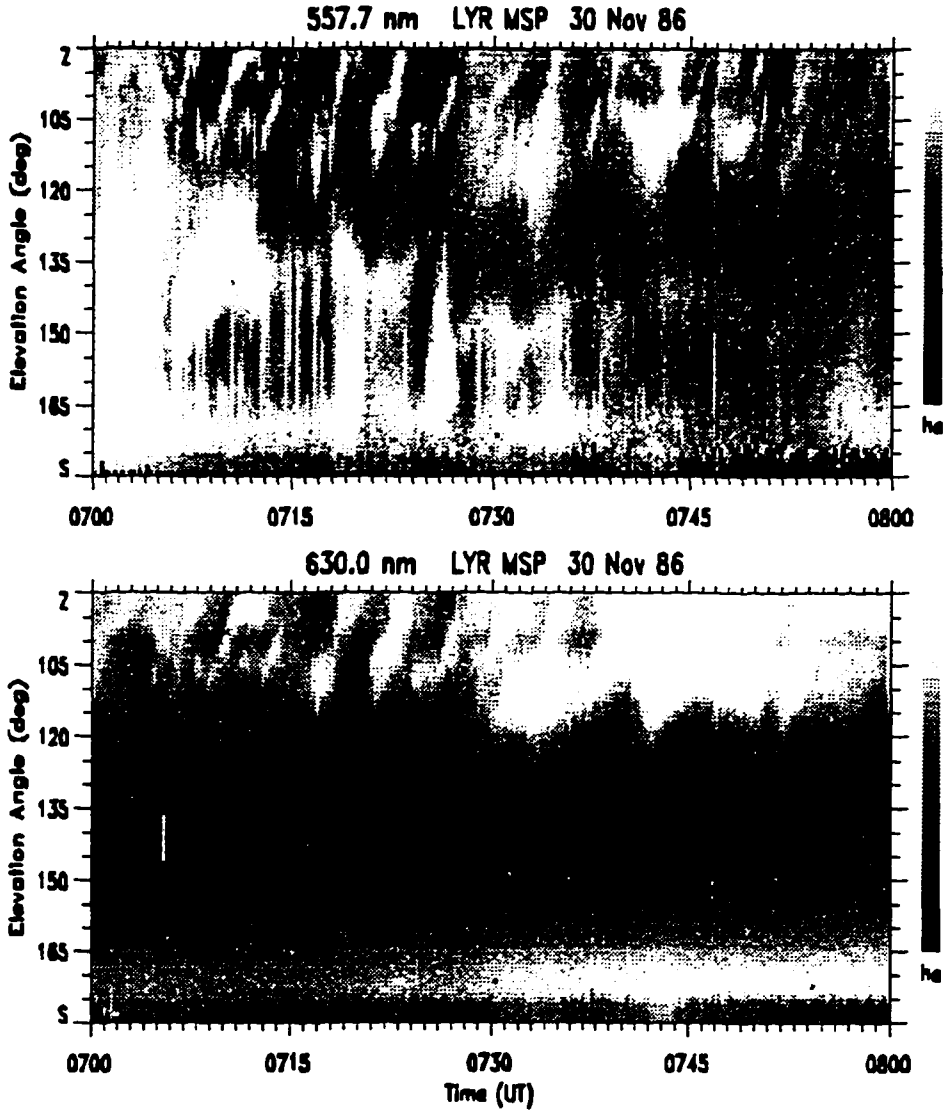


Figure 5.3 Histogram Equalized 557.7 nm and 630.0 nm Record. Histogram equalization has been applied to records from elevations between 90° and 180° to increase the contrast in the image and highlight the features in the vicinity of the latitudinal gap.

Reproduced with permission of the copyright owner. Further reproduction prohibited without permission.

for the 557.7 nm line since the scattered intensity is proportional to $\lambda^{-4}$. The presence of scattering effects suggests the presence of haze or thin clouds during the observation period. Complications of light scattering on the observations will be discussed in further detail below.

### 5.3.1 Latitudinal Gap in Auroral Emissions

Poleward of the mantle aurora and equatorward of the dayside auroral oval is a region where the auroral emissions are reduced to nearly background airglow values resulting in a meridional "latitudinal gap" in the dayside emissions. This region of continuously reduced auroral emissions within dayside aurora has not been reported in the literature to the author's knowledge. It is distinguished from the intensity dip by its lack of auroral pulsations and narrow range in latitude. The photometer samples the latitudinal gap over approximately 30° centered on the 125° elevation angle. Assuming an emission altitude of approximately 120 km, the width of the latitudinal gap is on the order of 60 km.

Auroral features in the vicinity of the latitudinal gap are enhanced in Figure 5.3 where a subset of the 557.7 nm photometer record from Figure 5.2 has been replotted using histogram equalization to increase the contrast in the image. This is a standard technique of image analysis (c.f., *Ekstrom*, 1984; *Jain*, 1989; *Jähne*, 1991) in which each pixel is assigned value based on the number of times its original value appears in the image. The intensity values in the histogram equalized image are no longer proportional to the integrated number of photons obtained by the photometer (although the increasing gray level assigned to increasing intensity values is preserved).

The auroral oval is slowly expanding equatorward from 0700 UT to 0730 UT. During this period the poleward border of the mantle aurora similarly moves equatorward and the width of the latitudinal gap increases in angular size. Elevation angles at which the 557.7 nm photometer samples the poleward border of the mantle aurora and the equatorward border of the dayside auroral oval are given in Table 5.2. Estimated values of the gap width and magnetic latitude of the gap center are computed using a constant peak emission altitude of 100 km for the 557.7 nm emissions. These results show the gap generally expanding in width toward local noon.

Single photometer scans from the 557.7 nm and 630.0 nm channels are plotted in Figure 5.4 to show the decrease in magnitude of the 557.7 nm signal through the latitudinal gap, the region between the 110° and 140° elevation angles marked by the vertical dotted lines. The mantle aurora is located equatorward of the latitudinal gap at elevation angles of 140° to 180° . Emissions from a discrete arc are detected by the photometer poleward of the latitudinal gap between elevation angles of approximately 90° and 110° . Note that the latitudinal gap is not devoid of 557.7 nm emissions. The 557.7 nm intensity, while greater than the airglow background (approximately 150 R), is reduced relative to the pulsating patches and dayside auroral oval equatorward and poleward of the latitudinal gap.

An all sky camera image from 07:19 UT is plotted in Figure 5.5 labelled with the features identified in Figure 5.4 to show the two dimensional distribution of auroral emissions. The image is an average of 128 television frames or 4 seconds of time. Averaging the video signal is done on the Quantex 50 video processor and the 151 video board was used to digitize the image (see Appendix

Reproduced with permission of the copyright owner. Further reproduction prohibited without permission.

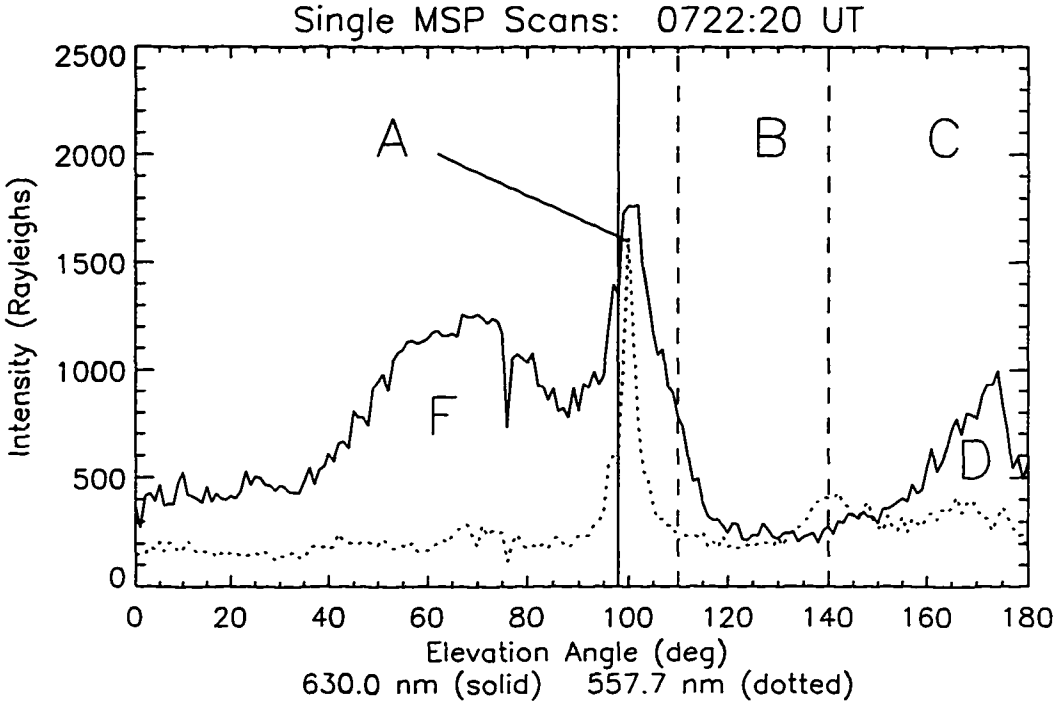


**Figure 5.4 Single MSP 557.7 nm and 630.0 nm Scan. The latitudinal gap (B) in the 557.7 nm emission is located between approximately 110 ° and 140 deg elevation angles (marked by the dashed vertical lines). The elevation angle scans have been chosen to highlight the intensity variations through a (A) transient arc (B) latitudinal gap, and (C) the diffuse 557.7 nm pulsating aurora. The region of 630.0 nm emission marked by (F) is the result of a previous transient arc.**

B). The images were grabbed between approximately 3-4 seconds after the time turned to the new minute but generally no later than 10 seconds after the new minute producing a smearing the seconds digits in the time code.

The poleward edge of the mantle aurora is well marked in this case by the strong gradient in luminosity between the mantle aurora and the latitudinal gap. This is not always the case since the unfiltered television camera is particularly prone to noise due to scattered sunlight near the southern horizon. If the mantle aurora and latitudinal gap is too close to the southern horizon, scattered sunlight often masks the auroral emissions completely hiding structure associated with the diffuse aurora.

Reproduced with permission of the copyright owner. Further reproduction prohibited without permission.

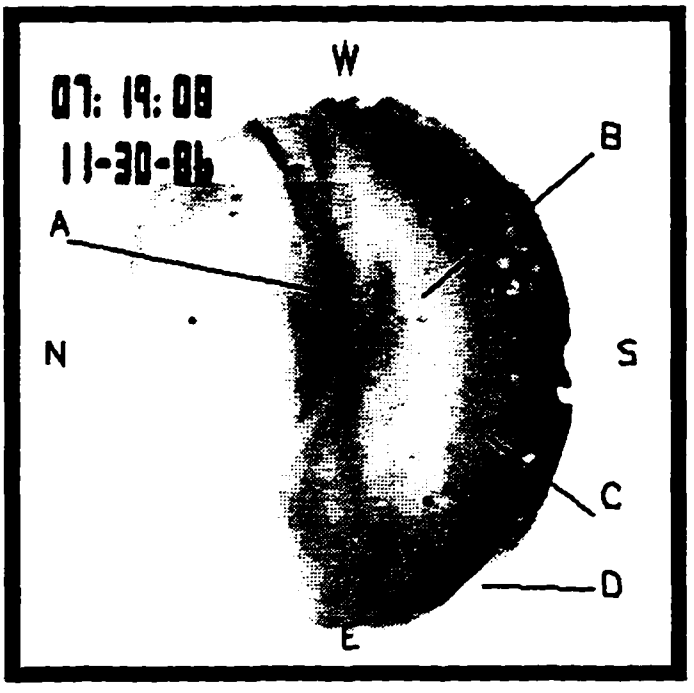


Figure 5.5 30 November 1986 07:19 UT Television Image. Geomagnetic directions are indicated by the N,S,E and W labels at the edge of the white light all sky television image. The image is plotted in negative with increasing brightness in the image is indicated by darker levels of gray. A transient arc (A) aligned east-west is located in the zenith. The latitudinal gap (B) is the region of reduced luminosity equatorward of the arc (A) and the diffuse 557.7 nm aurora (C). Twilight (D) is the very bright region near the southeastern horizon.

**Table 5.2**

**Estimates of Latitudinal Gap Width and Latitude as a Function of Time**

| Time (UT) | Elevation Angle (deg) $\theta_{pole}$ | $\theta_{eq}$ | ~ Width (km) | Magnetic Latitude (deg) |
|---|---|---|---|---|
| 0710 | 110 | 120 | 10 | 74.5 |
| 0720 | 114 | 133 | 50 | 74.4 |
| 0730 | 126 | 146 | 100 | 74.1 |
| 0740 | 120 | 140 | 100 | 74.2 |
| 0750 | 120 | 140 | 100 | 74.2 |

Reproduced with permission of the copyright owner. Further reproduction prohibited without permission.

**Table 5.3**
**Drop Outs in 557.7 nm Emissions at Poleward Border of Mantle Aurora**

| Event Time (UT) | Duration[1] (sec) | Elevation Angle (deg) $\theta_i$ | $\theta_f$ | ~ Altitude[2] (km) | ~ Distance[3] (km) |
|---|---|---|---|---|---|
| 0712:20 | ≤16 | 120 | 134 | 40 | 24 |
| 0718:30 | 135 | 125 | 138 | 36 | 23 |
| 0722:30 | 60 | 134 | 137 | 10 | 5 |
| 0726:30 | 120 | 134 | 146 | 36 | 21 |
| 0731:00 | ≤16 | 144 | 150 | 20 | 11 |
| 0734:00 | 120 | 138 | 142 | 12 | 7 |
| 0744:00 | 160 | 136 | 140 | 14 | 7 |

[1]The time required for poleward border of mantle aurora to change from initial to final elevation angle.
[2]Assuming the initial altitude is 100 km.
[3]Assuming a constant emission altitude of 100 km.

### 5.3.2 Variations in Auroral Luminosity on the Poleward Border of the Mantle Aurora

A series of "drop out" events occur at the poleward border of the mantle aurora. The drop outs are characterized by an increase in the elevation angle at which the photometer samples the poleward border of the mantle aurora. The auroral emission at a fixed elevation angle decrease in intensity from the initial mantle aurora values to nearly the airglow background. The total variation in elevation angle varies from 4° to 14° . Table 5.3 lists the elevation angle at which the photometer samples the poleward border of the mantle aurora at the onset of selected drop out events and the final elevation angle at which the 557.7 nm emissions are detected. The duration of the event listed in the first column is the interval between the scans in which the poleward border of the mantle aurora is detected at the initial and final elevation angles. A change in either altitude or latitude of auroral forms will result in variations in the elevation angle at which auroral emissions are detected by the photometer. Although it is impossible to determine which variation is the cause of the change in elevation angle using a monochromatic photometer, the combined information from the 557.7 nm and 630.0 nm channels provides sufficient evidence to indicate the variation is due to an equatorial shift of the poleward border of the mantle aurora.

Consider first the possibility that the variation in elevation angle is due to altitude variations in the mantle aurora. A decrease in the electron energy will result in a decrease in the 557.7 nm emission rate at a fixed elevation angle, consistent with the observations. However, a concomitant increase in 630.0 nm emission is expected since the energy deposition of a lower energy electron population will be at greater altitudes where reduced quenching allows greater numbers of $O(^1D)$ to radiate. No such 630.0 nm emission is detectable in the photometer records. In addition, an increase in the emission altitude requires a decrease in the elevation angle at which the emission is measured. Therefore, a decrease in electron energy is eliminated as the source of the equatorial shift in elevation angle in the drop out events. A shift of the peak emission to lower altitudes will result

Reproduced with permission of the copyright owner. Further reproduction prohibited without permission.

in the increase in the elevation angle at which the emission is sampled by the photometer. The fourth column in Table 5.3 gives the altitude changes required to explain the observed variations in elevation angle assuming the latitude of the poleward border of the mantle aurora remains constant. Large drop outs require auroral emissions to form at altitudes of 60 to 70 km, below the approximately 95 km quenching altitude of $O(^1S)$ [*Vallance Jones*, 1974], so few 557.7 nm photons are expected. Red lower borders of bright auroral arcs are known to originate at altitudes between 60 and 85 km [*Störmer*, 1955; *Shemansky and Vallance Jones*, 1968; *Vallance Jones*, 1974] where electrons with energies greater than 100 keV may penetrate. If the drop outs are due to energetic electron events then a coincident increase $O_2^+$1N, $N_2$1PG, and $N_2^+$1N emissions should accompany the decrease in 557.7 nm emission. The first emissions were not monitored by the MSP in the experiments described here and no increases in $N_2^+$1N 427.8 nm are noted within the drop outs. A large increase in electron energy is therefore ruled out as a possible cause of the drop out events.

A moving electron source may also yield apparent temporal variations in auroral luminosity at a fixed point due to the so-called "searchlight" effect even if the energy and number flux of the precipitating electrons is constant. If this is the origin of the drop outs then the mantle aurora should exhibit structures propagating along its poleward border. A series of images are presented in Figure 5.6 to show the temporal variations of the dayside auroral oval and the mantle aurora. The all sky camera records demonstrate the drop outs are not due to a searchlight effect. Difficult to note in the reproductions, the original tape clearly showed the change elevation angle of the poleward border of the mantle aurora was not due to structures propagating through the camera field of view.

The most likely explanation for the reduced auroral luminosity within the drop out events is a decrease in the electron number flux within the atmospheric loss cone on field lines threading the drop out events. Estimates of the latitudinal dimensions over which the loss is observed is tabulated in the final column in Table 5.3. The average distances are 14 km with a minimum of 5 km and maximum of 24 km for the events listed in Table 5.3. It is also possible that the entire electron population on the field lines threading a drop out event are lost regardless of pitch angle although the auroral records can only provide evidence for the behavior of electrons within the atmospheric loss cone. The loss cone is 1.74° at 100 km using a dipole magnetic field magnitude at 100 km and 75° magnetic latitude and 60 nT for the equatorial field at a distance of 10 Re. Thus, the auroral observations represent only a fraction of the particle population that may exist on the field line.

Intervals between the drop outs vary from 3 to 6 minutes with an average of approximately 4.5 minutes. Each decrease is followed in approximately 2-3 minutes by the formation of a poleward drifting transient within the dayside auroral oval. It is this apparent correlation between the drop outs and the formation of a transient arc in the dayside auroral oval that is particularly interesting. It appears that the transient event morphology includes the decreased intensity at the poleward border of the diffuse 557.7 nm aurora followed by the subsequent formation and poleward drift of the transient arc. A test of the hypothesis that the events are related is given in Figure 5.7a where the times of seven drop out events are plotted against the onset times of the corresponding transient auroral events. The drop out events occur at 0712:20, 0718:30, 0722:30, 0726:30, 0731:00,

Reproduced with permission of the copyright owner. Further reproduction prohibited without permission.

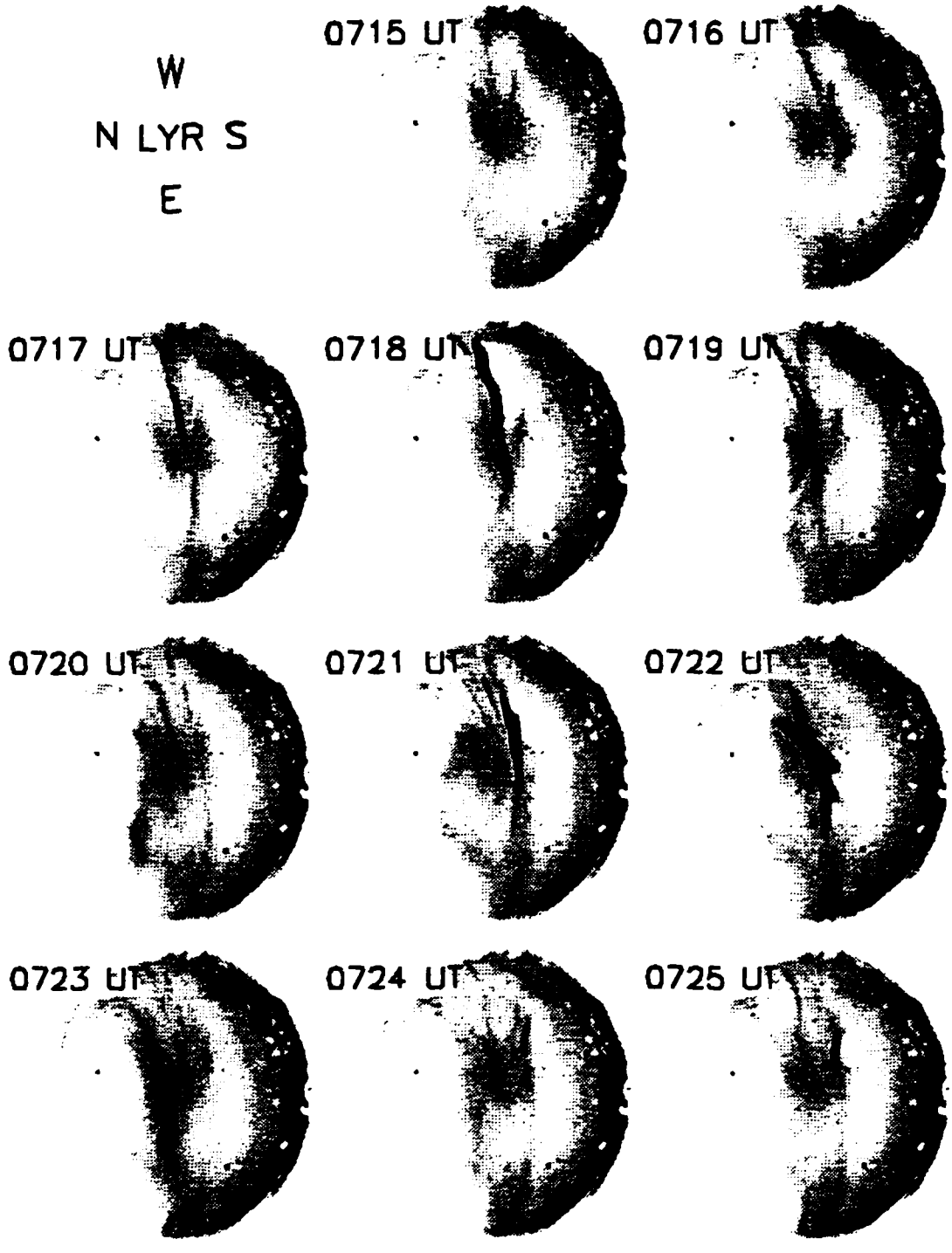


Figure 5.6 Selected 30 November 1986 Television Images. A series of images are plotted to exhibit the temporal variations in the auroral emissions over the entire sky. The series demonstrates that the drop outs are not due to spatial variations in the mantle aurora propagating through the camera field of view.

Reproduced with permission of the copyright owner. Further reproduction prohibited without permission.

0734:00, and 0744:00 UT while the corresponding transient arcs form at 0715:30, 0721:00, 0724:00, 0728:00, 0732:30, 0736:20, and 0746:00 UT. The error bars for the times are on the order of 1 minute reflecting the difficulty in obtain precise onset times for either the drop outs or transient arcs. A linear fit to the event times in Figure 5.5a yields a line with a slope of $0.96 \pm .02$ and an intercept of $3.1 \pm 0.4$ minutes. The coefficient of linear regression is 0.999, indicating a good fit. These results are necessary but not sufficient to demonstrate a causal relationship between the two series of events. It can easily be shown that similar results are obtained for any two unrelated time series with random intervals between successive events provided the average interval between events is the same for both time series. In the example plotted in Figure 5a the scatter plot indicates only that the drop out events occur at the same rate as the formation rate of the transient arcs (yielding the slope of $\sim 1$). The intercept indicates an approximately three minute interval between the drop outs and formation of the transient arcs.

A more sensitive test of a relationship between the two series of events is given in Figure 5.7b where a scatter plot is constructed of intervals between events rather than the event times. In this case a causal relationship requires the intervals between the drop outs to be the same as the intervals between the transient arcs yielding a best fit line with a slope of one passing through the origin. The best fit line resulting from the intervals between events indeed produces a line with a slope of $1.03 \pm 0.08$ and an intercept of $-0.3 \pm 0.5$. These results are consistent with the hypothesis that the drop outs on the poleward border of the mantle aurora are related to the formation of the transient arcs in the dayside auroral oval within the error of the measurements.

### 5.3.3 Continuous Emissions on the Poleward Border of the Mantle Aurora

The poleward border of the mantle aurora is continuously marked by 557.7 nm emissions over nearly the entire 0700 UT to 0800 UT period. These emissions are present even if the aurora further equatorward is in a minimum of the auroral pulsations. Examples in Figure 5.3 include the 557.7 nm emissions observed within an approximately 10° band centered on the 135° elevation angle at 0715 UT, 140° at 0722 UT, 152° at 0732 UT, and 142° at 0742 UT. The scan at 0722 UT is also plotted in Figure 5.4 where the continuous emission is the approximately 250 R 557.7 nm emission located on the poleward border of the 100 R 557.7 nm mantle aurora.

Sampled at elevation angles from 140° early in the period to 150° later in the period, this region of continuous emission is approximately 15-20 km in latitudinal width. Due to the relatively low lifetime of the $O(^1S)$ state ($\sim 0.7sec$) compared to the interval between MSP samples ($\sim 16sec$) this this feature must be due to a continuous source of precipitating electrons on the poleward edge of the mantle aurora. In addition, the lack of a corresponding modulation in the 630.0 nm channel at similar elevation angles requires an electron source with energies of 5-10 keV or greater. The continuous 557.7 nm emission form the equatorward boundary of the drop out events. An estimate of the energy flux required to produce the 250 R 557.7 nm emission is 0.17 erg/cm$^2$s where the average 557.7 nm excitation coefficient of 1.44 kR/erg/cm$^2$ s obtained by *Steele and McEwen* [1990] has been used. A crude estimate of the average number flux required to produce the 557.7 nm emission observed at 0722 UT may be obtained by adopting a characteristic energy

Reproduced with permission of the copyright owner. Further reproduction prohibited without permission.

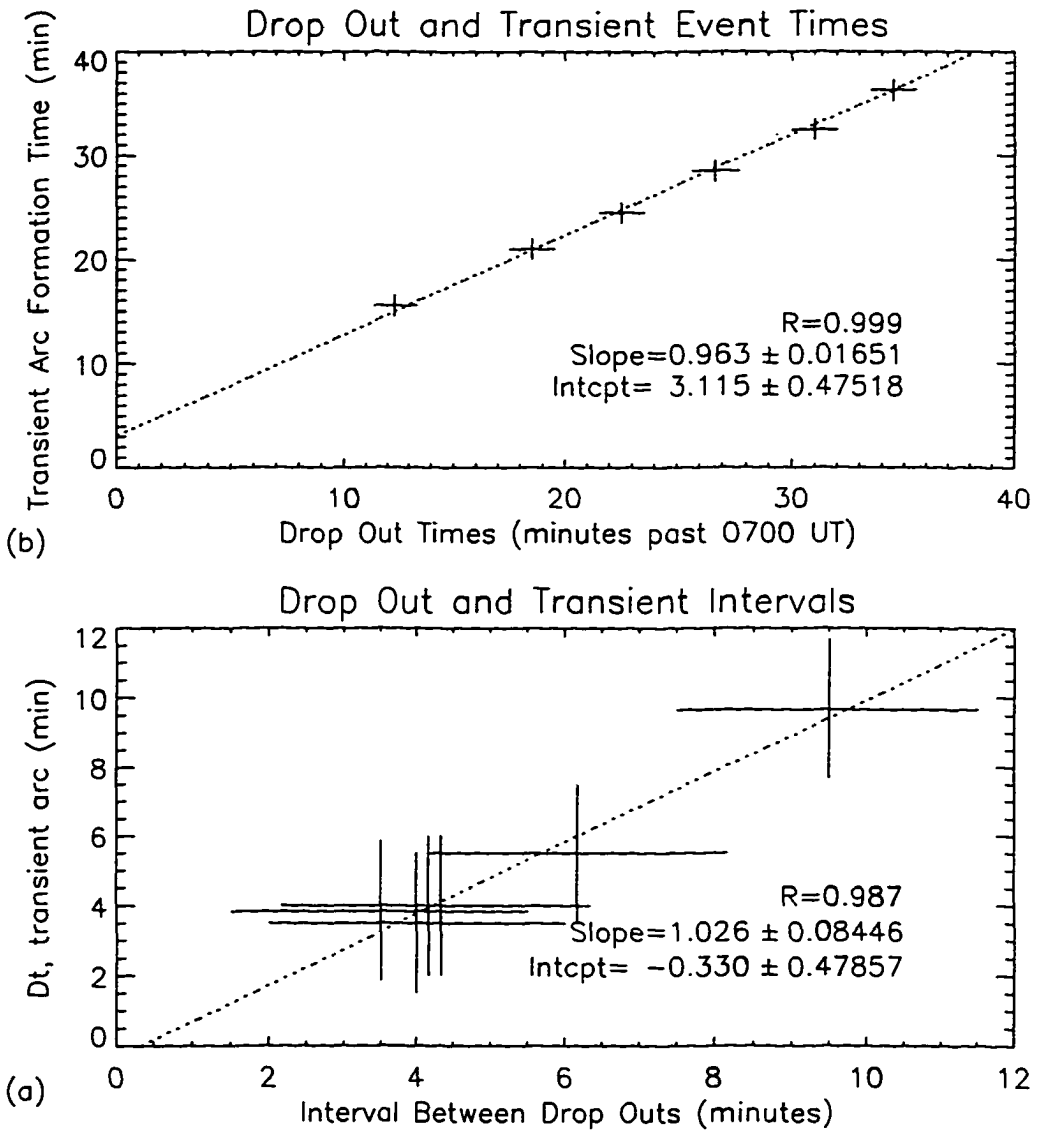


**Figure 5.7 Correlation Between Drop Outs and the Formation of Transient Arcs.** (a) Drop out event times versus formation times of transient arcs. Times on the horizontal axis are minute past 0700 UT. (b) Intervals between drop outs on the poleward border of the diffuse 557.7 nm aurora versus intervals between formation of transient arcs. Error bars in both plots are based on an estimated 1 minute uncertainty in obtaining drop out and transient arc formation times. Each plot shows linear correlation coefficients near one.

Reproduced with permission of the copyright owner. Further reproduction prohibited without permission.

for the precipitating electrons. Average energy values of 20, 10, 5 , and 1 keV yield precipitated number fluxes of $.53 \times 10^7 cm^{-2}s^{-1}$, $1.2 \times 10^7 cm^{-2}s^{-1}$, $2.1 \times 10^7 cm^{-2}s^{-1}$, and $12 \times 10^7 cm^{-2}s^{-1}$, respectively. The mechanism which produces the drop out events must be capable of modulating electron fluxes of these magnitudes over a latitudinal range of 10's of kilometers within the 16 second scan resolution of the MSP.

## 5.4 Discussion and Interpretation of Observations

There are a number of important points to be considered in proposing a mechanism to explain the drop out events on the poleward border of the mantle aurora and the poleward moving arcs within the dayside oval. First, the correlation between the drop out events and the subsequent formation of transient arcs suggest a common explanation for both phenomenon. Second, the drop out events form on the poleward border of an auroral emission that is associated with closed geomagnetic field lines. Third, the poleward moving arcs within the dayside oval are the result of magnetosheath plasma penetrating into the polar cusp in a region associated with geomagnetic field lines that are open to the solar wind.

Formation of the drop out events and the transient arcs across a boundary that is typically associated with the open/closed field line boundary suggests an interpretation of the events in terms of the magnetic reconnection model which will form the basis of the discussion to follow. Features of the auroral display described in the case study that are discussed here in further detail include

(1) The origin of the latitudinal gap and the location of the separatrix.

(2) The source of continuous 557.7 nm emissions on the poleward edge of the hard electron precipitation zone.

(3) Implications of the correlation between drop outs in 557.7 nm emissions on the poleward edge of the mantle aurora and the subsequent formation of 630.0 nm dominated arcs within the dayside auroral oval to models of solar wind magnetosphere coupling.

(4) The origin of the auroral emissions within the latitudinal gap.

(5) The origin of "trapped" electron pitch angle distributions within the low latitude boundary layer.

The final topic is included although it is not a feature in the auroral records. Electron pitch angle distributions near the outer edge of the low latitude boundary layer are often peaked near 90° , a characteristic of electron populations on closed field lines. These field lines are required to be open in the reconnection models. At other times the electron pitch angle distributions are nearly isotropic in the same regions. These observations have interesting applications to topic (3), the origin of auroral emissions within the latitudinal gap.

### 5.4.1 Origin of the Latitudinal Gap and Identification of the Separatrix

The 50-100 km gap between the 557.7 nm emissions of the mantle aurora and the dayside auroral oval may be explained as a result of differential flight times for precipitating particles from different dayside plasma populations in the presence of convective electric fields [*Rosenbauer*

Reproduced with permission of the copyright owner. Further reproduction prohibited without permission.

*et al.*, 1975; *Reiff et al.*, 1977; *Søraas et al.*, 1980]. In addition, convection of plasma in the magnetosphere is an important limitation on the use of low energy particles to map boundaries between magnetospheric plasma populations [*Lockwood and Smith*, 1993; *Newell and Meng*, 1993]. A charged particle in the presence of magnetic and electric fields has velocity components parallel

$$v_{\|} = v\cos\alpha \tag{5.1a}$$

and perpendicular

$$v_{\perp} = \left|\frac{\vec{E} \times \vec{B}}{B^2}\right| \tag{5.1b}$$

to the field lines where the pitch angle $\alpha$ is the angle of the velocity $v$ with respect to the magnetic field. E and B are the total electric fields at the location of the particle. The velocity of a particle with rest mass $m_0c^2$ and kinetic energy $T$ is given by

$$v = c\left[1 - \frac{1}{[1 + T/m_0c^2]^2}\right]^{1/2} \tag{5.2a}$$

where $m_0c^2$ is 938.2 MeV for a proton and 511 KeV for an electron. Equation 5.2a reduces to the nonrelativistic form

$$v = \left[\frac{2T}{m_0}\right]^{1/2} \tag{5.2b}$$

if the particle kinetic energy is much less than the rest mass. Equation 5.2a is retained for the computation of electron velocities in subsequent work since electron energies up to 100's of keV are considered. Ion energies in excess of 10 keV are not considered allowing the ion velocities to be computed from Equation 5.2b. Drifts across the magnetic field are independent of the particle characteristics and depend only on the orientation and magnitudes of the electromagnetic fields. An electromagnetic field acts as a velocity filter separating particles of different energies and mass and redistributing particles within the magnetosphere.

In applying the velocity filter to explain the latitudinal gap, consider first the low energy magnetosheath plasma injected across the magnetopause into the polar cusp when the $B_z$ component of the interplanetary magnetic field is negative (which physical mechanism results in the injection is not important here as long as a quantity of magnetosheath plasma is introduced into the magnetosphere). The plasma is quasi-neutral requiring the bulk of the electrons and ions to move at the same velocity [*Reiff et al.*, 1977; *Burch*, 1985]. This requirement is the result of an ambipolar electric field that develops between the ions and electrons decelerating the electrons while accelerating the ions [c.f., *Liu*, 1993]. Due to their much greater mass than the electrons, the ions govern the motion of the magnetosheath plasma while the electrons serve to ensure quasi-neutrality. The bulk plasma velocity along the field line is approximately the ion velocity.

At the same time the plasma moves inward, it is driven antisunward by the dawn to dusk convection electric field present in the dayside magnetosphere for $B_z < 0$ [c.f., *Heppner and Maynard*, 1987]. Traveling inward along the converging magnetic field, the high energy ions arrive first at either their mirror point where they are reflected or precipitate into the atmosphere. Since the poleward convection drift is independent of the particle characteristics, the low energy ions take longer

Reproduced with permission of the copyright owner. Further reproduction prohibited without permission.

**Table 5.4**
**Survey of Ion Energies at Low Latitude Edge of Cusp Plume**

| Year/ Day of Year | MLT | Ion Energy Low Cut Off | Mean | High Cut Off | Reference |
|---|---|---|---|---|---|
| 90/354 | 1200 | .250 | .5 | 1. | DMSP[1] |
| 11 Feb 77 | 1220 | — | .5-1. | — | *Roeder and Lyons* [1992][3] |
| 83/359 | 1200 | .2 | 1. | 20. | *Newell and Meng* [1987][2] |
| 83/344 | 1025 | .4 | 1. | 20. | *Wing et al.* [1996][2] |
| 29 July 76 | 1200 | — | 1-2 | — | *Roeder and Lyons* [1992][3] |
| 91/012 | 1200 | .4 | 1.1 | 8. | DMSP[1] |
| 92/011 | 1130 | 0.6 | 1.2 | 1.6 | DMSP[1] |
| 92/011 | 1200 | 0.3 | 1.6 | 4.0 | DMSP[1] |
| 83/358 | 1145 | 1.1 | 1.8 | 10. | *Newell and Meng* [1995][2] |
| 91/336 | 1220 | 3. | 4. | 8. | DMSP[1] |
| 84/026 | 1130 | 2. | 4. | 10. | *Newell et al.* [1991][2] |
| 6 Oct 89 | 1240 | 2. | 6. | 15. | *Pinnock et al.* [1993][2] |

[1] From DMSP ion energy spectra provided courtesy of P.T. Newell.
[2] DMSP satellite.
[3] S3-3 satellite.

to mirror or precipitate and move further poleward than the high energy ions. Therefore, measurements of ion energies by low altitude satellites within the polar cusp and mantle typically exhibit the characteristic "cusp plume" in which the average ion energy decreases with increasing latitude [*Rosenbauer et al.*, 1975; *Reiff et al.*, 1977].

The antisunward convective drift requires that magnetosheath plasma arrive in the ionosphere some distance poleward of the field line on which it was initially injected, the distance determined by the flight time of the ions and the poleward convection velocity. A crude estimate of this distance can be obtained if the time required for the ions to reach the ionosphere and the poleward convection velocity is known. Satellite measurements of the ion energy and convection electric fields are unavailable for this period so average values must be adopted for the estimate. A survey of ion energy spectra obtained by satellites in the vicinity of the dayside cusp is given in Table 5.4 indicating a range of average energies may be found for the ions sampled at the equatorward edge of a cusp plume, varying from maximums over 10 keV to minimums under 1 keV. I have adopted an ion energy of 1-2 keV based on the predominance of the low energy values. Based on a travel distance of 14-15 Re along a terrestrial field line from the merging site to the ionosphere [*Sibeck and Newell*, 1994], the time required for the ions to reach the ionosphere is on the order of 2-3 minutes. Typical dayside convection speeds are on the order of 500-1000 m/s within the midday region. Plasma convecting poleward at this rate will travel approximately 60-180 km across the magnetic field during the time required to travel from the subsolar point to the ionosphere. The ionospheric projection of the separatrix is therefore located an equal distance equatorward of the low latitude border of the dayside auroral oval along the direction of the plasma flow [*Lu et al.*, 1995; *Weiss et al.*, 1995]. It is not necessary that the separatrix represent a merging line in this

Reproduced with permission of the copyright owner. Further reproduction prohibited without permission.

description. Any process that allows plasma to cross the magnetopause and creates an electric field in the dayside magnetosphere to drive the antisunward convection will yield the same results.

The 14-15 $R_E$ distance to the merging site used to estimate the flight time of the ion requires some justification. I have used a simplified model for the magnetic field to obtain this result assuming the ions are injected across the subsolar magnetopause. The path of the ion along the magnetic field from the injection site to the ionosphere is approximated by a semicircle of radius 5Re so that the standoff distance of the magnetopause from the center of the Earth is 10 $R_E$. This model yields a distance from the subsolar merging point to the ionosphere at approximately 1 Re on the order of 14-15 Re without resorting to integration of the path length along a model field. The simplification of the magnetic field geometry is justified in the context of the current work since only the total length of the field line is required to obtain the flight time of the magnetosheath plasma. There is some debate whether merging occurs primarily at the subsolar magnetopause or at higher latitudes near the exterior cusp [*Newell and Sibeck*, 1994]. When the distance to the merging site is inferred from the dispersion in ion velocity a range of values from 7 $R_E$ [*Carlson and Torbert*, 1980] to 26 $R_E$ [*Reiff et al.*, 1977] have been obtained. *Newell and Sibeck* [1994] presented a survey of results from case studies available in the literature to show that the most likely distance to the merging site from the ionosphere is 10-15 $R_E$. Since distance along the field to the subsolar magnetopause is 20 $R_E$ while only 10 $R_E$ to the exterior cusp in a more realistic field their results would appear to confirm that particle injection occurs most often near the exterior cusp. *Smith and Lockwood* [1990] attempted to reconcile the distances obtained from ion velocity dispersion with the subsolar merging models by suggesting that the plasma injected during a merging event is constrained by a magnetic field within an FTE and can precipitate only when the FTE arrives at the exterior cusp. If 20 $R_E$ is adopted the estimated width of the latitudinal gap is 84-240 km.

The ionospheric projection of the separatrix cannot be obtained from ground based observations of the dayside auroral oval since the low energy magnetosheath plasma drifts poleward of this line. However, if sufficient fluxes of electrons are present near the magnetopause in the outer radiation belts then the poleward border of the mantle aurora may provide the auroral signature required for ground based monitoring of the separatrix. High energy electrons drifting on closed field lines in the outer radiation belt (Section 2.5) travel rapidly between mirror points with bounce periods on the order of seconds. These particles originate in substorm acceleration and injection mechanisms in the magnetotail and drift eastward into the dawn and midday sector where some are lost through the dayside magnetopause (pseudo-trapped) or return to the night sector (trapped). Particles injected with pitch angles inside the atmospheric loss cone mirror at altitudes where collisions with the atmosphere are probable and are rapidly lost within a few bounce periods. Only particles with pitch angles greater than the atmospheric loss cone can survive a half drift period around the Earth and arrive in the midday sector. However, auroral emissions require a particle loss from the drifting population to the atmosphere so a separate mechanism from that responsible for the original injection must be present to produce the mantle aurora.

The most widely studied and accepted mechanism to explain the loss of radiation belt electrons and production of the mantle aurora is the electron cyclotron-whistler wave interaction leading to pitch angle scattering of trapped electrons into the loss cone [*Cornwall*, 1964, 1965; *Kennel*

Reproduced with permission of the copyright owner. Further reproduction prohibited without permission.

*and Petschek*, 1966; *Lyons et al.*, 1972; *Lyons and Williams*, 1984]. Experimental observations supporting this mechanism include a variety of satellite and ground based observations showing that pulsating electron precipitation within the mantle aurora in the dawn and dayside magnetosphere is strongly correlated with VLF noise [*Oliven and Gurnett*, 1968; *Rosenberg et al.*, 1971; *Hargreaves and Bullough*, 1972; *Holzer et al.*, 1974; *Tsurutani and Smith*, 1977; *Maeda et al.*, 1978; *Trefall and Williams*, 1979 and references therein]. The electron cyclotron-whistler wave interaction occurs when an electron encounters a whistler wave of frequency $\omega$ moving in the opposite direction. In the electron frame of motion the wave frequency is Doppler shifted to the electron n $\Omega_e$ [*Kennel and Petschek*, 1966]

$$\omega - \vec{k} \cdot \vec{v} = \Omega_e \tag{5.3}$$

leading to either a gain or loss of particle energy perpendicular to the field line (and accompanying change in pitch angle) due to the particle interaction with the electromagnetic wave. Particles with kinetic energy $T_R$ associated with the parallel motion of the particle may be efficiently scattered into the loss cone near the equatorial plane where the resonance condition

$$T_R = \frac{B^2}{8\pi n_e} \frac{\Omega_e}{\omega} \left(1 - \frac{\omega}{\Omega_e}\right)^3 \tag{5.4}$$

is most easily satisfied. Resonant energies for particles interacting with waves in the VLF and ELF frequency range in the outer magnetosphere typically range from 1 to 100's of keV.

Estimated bounce periods for a range of electron energies typical of those expected in the mantle aurora are listed in the first column of Table 5.5. The results are obtained from Equation 2.5

**Table 5.5**
**Electron Bounce and Drift Periods for L=12[1]**

| Electron Energy (keV) | $\tau_b$ (sec) | $\tau_d$ (hr) | $V_{d,\nabla B-C}$ (km/sec) |
|---|---|---|---|
| 1 | 21 | 90 | 1.5 |
| 2.5 | 13 | 35 | 3.8 |
| 5 | 9.6 | 18 | 7.5 |
| 7.5 | 7.9 | 12 | 11 |
| 10 | 6.8 | 8.9 | 15 |
| 40 | 3.6 | 2.3 | 58 |
| 100 | 2.4 | 0.96 | 140 |

[1]L=12 is appropriate for a field line passing near the magnetopause which intersects the atmosphere at 100 km a few degrees south of Longyearbyen where the mantle aurora is observed.

using an equatorial pitch angle of 2° , the approximate loss cone for particles mirroring at 100 km altitude in a dipole field at a magnetic latitude of 75° . These values represent the maximum time required for particles to oscillate between mirror points on the field line since the bounce period is relatively insensitive to the particle pitch angle and within a factor of two is determined by the particle velocity. Particles with larger equatorial pitch angles travel more rapidly between their

Reproduced with permission of the copyright owner. Further reproduction prohibited without permission.

mirror points but will not contribute significantly to production of the 557.7 nm emission within the mantle aurora since they must mirror at altitudes where production rates of $O(^1S)$ is very low.

Examination of the bounce periods in Table 5.5 demonstrates that electrons with energies greater than 1-2 keV are less than one MSP sample period (16 sec) from either mirror point. Since the time required for an electron to travel from the equatorial plane to the ionosphere once its pitch angle has been scattered into the loss cone is a quarter bounce period, even 1 keV electrons are never longer than approximately 5 seconds from the ionosphere. Poleward convection at 500-1000 m/s during this period will only result in a drift of approximately 2.5-5 km. Resolution of the MSP is approximately 2 km at altitudes near 100 km so very little displacement is possible for even the lowest energy electrons which may precipitate due to wave-particle interactions. Within the spatial resolution of the MSP the 557.7 nm emissions in the mantle aurora may be used to infer the field line on which a wave-particle interaction has occurred. The poleward boundary of the mantle aurora therefore represents the outermost field line on which particles are lost from the radiation belts into the atmosphere. Any change in the loss process is communicated to the ionosphere and is visible in the auroral display on the time scale of a quarter bounce period, less than the temporal resolution of the MSP.

Values of the drift period and drift velocity in the equatorial plane due to the combined gradient B and curvature are also tabulated in Table 5.5 although the effect was neglected in the description that was just presented for origin of the latitudinal gap. Multiplication of the drift velocities by the 2 to 3 minutes required for low energy magnetosheath plasma to travel along the polar cusp field lines to the ionosphere yield eastward drifts on the order of $10^2$ to $10^3$ km) along the L shell which may explain the peak probability of observing cusp precipitation is approximately one hour in local time before local noon [*Newell and Meng*, 1988]. Only the electric field drift need to be considered to because it drives electrons and ions across L shells rather than along as in the case of the combined gradient B and curvature drifts.

The different distances over which convective drifts redistribute precipitating mantle and magnetosheath electrons provide a ready explanation for the formation of the latitude gap in the dayside 557.7 nm emissions described in the case study. In addition, identification of the ionospheric projection of the separatrix in the auroral emissions is also limited by the distribution of high energy electron fluxes in the outer magnetosphere. In summarizing the auroral observations with respect to the latitudinal gap and the possible location of the ionospheric projection of the separatrix, the following picture emerges:

Two populations of electrons precipitate within the dayside high latitude region producing auroral displays. The first is due to multiple keV electrons within the radiation belts drifting along lines of constant magnetic field intensity through the morning sector into the midday sector. Upon encountering the magnetopause the electrons are lost. Pitch angle scattering mechanisms which result in loss of these particles into the atmosphere produce the pulsating aurora. The poleward boundary represents the outward most field lines which contain sufficient particles to produce a luminous aurora. If there has not been a recent injection then large fluxes of trapped electrons are only expected to exist out to the stable trapping boundary. The stable trapping boundary is formed by the last closed drift shell and electrons within this boundary can drift

Reproduced with permission of the copyright owner. Further reproduction prohibited without permission.

completely around the Earth without encountering either the dayside or nightside magnetosphere. In this case the poleward boundary of the mantle aurora marks the stable trapping boundary. For significant fluxes of electrons to be present between the stable trapping boundary and the dayside magnetopause a recent particle injection event in the nightside region is required. Injection events typically produce electron fluxes greater than the stable trapping limit computed by [*Kennel and Petschek*, 1966] allowing the spontaneous growth of whistler mode electromagnetic waves which scatter electrons into the loss cone [*Borovsky et al.*, 1993; *Nemzek et al.*, 1995]. Drift paths of the electrons take them eastward towards the morning and midday sectors increasing the fluxes not only within the stable trapping region but between the last closed drift shell and the magnetopause boundary as well.

The high energy particles are capable of travelling rapidly along the field lines encountering the atmosphere within seconds of any location in the magnetosphere. Very little displacement is possible due to convection during this time and the particles arrive very near their initial field line. This is true if a strong convective electric field exists in the midday region since the horizontal drift is much smaller than the field aligned motion of the particle. Therefore, the ionospheric projection of the separatrix is located just equatorward of the most poleward field line which maps to the outermost edge of the pseudo-trapping region. This field line passes through the poleward edge of the mantle aurora if there are sufficient particles within the pseudo-trapping region and an active mechanism resulting in electron precipitation. The location of the separatrix as determined from the high energy auroral particles is little effected by convective electric fields and is certainly on the order of the resolution of the MSP. The optical records allow the decrease in emission intensity on the poleward border of the diffuse 557.7 nm aurora to be determined within a few degrees, yielding estimates of the latitude of the separatrix within 4 to 5 kilometers.

Magnetosheath plasma however must drift poleward distances on the order of 100 km due to its much slower field aligned velocity. Auroral emissions excited within the dayside auroral oval when this plasma encounters the atmosphere will be located poleward of the mantle aurora. The latitudinal gap is the region between the equatorward boundary of the dayside auroral oval and the poleward boundary of the mantle aurora where the energy flux of precipitating electrons is reduced. When electron fluxes are precipitated on field lines out to the magnetopause boundary, then the poleward border of the mantle aurora (the equatorward edge of the latitudinal gap) may be identified as the ionospheric projection of separatrix.

A quantitative test of this proposal can be made by using ground based photometer records and radar measurements of the cold plasma drift velocity and using the particle energy spectra obtained by the DMSP satellite. Since neither the radar or precipitating particle records are available for this case study the method will only be outlined here. The technique requires the velocity of the ion parallel to the magnetic field and the convective drift perpendicular to the field line to determine the width of the gap. The velocity of the magnetosheath plasma along the magnetic field is obtained from the energy of the ions immediately poleward of the keV electron precipitation. Coincident measurements of the poleward drift velocity is required to obtain the rate at which the ions move poleward allowing the distance from the separatrix to be estimated from the time required to travel from the magnetopause and the poleward convection velocity.

Reproduced with permission of the copyright owner. Further reproduction prohibited without permission.

Consider ions injected at the subsolar point a distance $d_b$ from the ionosphere along the magnetic field. The time required for an ion to move this distance is

$$t_{ion} = \frac{d_b}{v_{\|,i}} \tag{5.5a}$$

where the ion velocity parallel to the field line $v_{\|,i}$ is obtained from the ion energy and pitch angle. The electron and ion spectrometers on the DMSP satellites do not resolve pitch angle distributions but only field aligned particles are sampled at high latitudes since the acceptance angle of the detectors is only 3° to 4° [*P. Newell*, personal communication, 1995]. The satellite is spin stabilized so at high latitudes the instrument is pointed nearly straight up the field line. Both ions and electrons arriving at the detector must have travelled the majority of the distance along the magnetic field with very small pitch angles and are therefore well within the loss cone (since the loss cone is computed assuming a 90° pitch angle at 100 km altitude).

In general ions are also injected at other locations along the magnetopause boundary so the distance may be treated as $fd$ where $f$ is a factor $0 \leq f \leq 1$ where $f = 0$ at the ionosphere and $f = 1$ the subsolar magnetopause. Typical values of $f$ should lie in the range $0.5 \leq f \leq 1$ for injections over the surface of the magnetopause from the subsolar point to the magnetopause in the region of the cusp. Equation 5.5a is then

$$t'_{ion} = \frac{f d_b}{v_{\|,i}} \tag{5.5b}$$

Electric fields in the dayside magnetosphere drive the plasma poleward due to the $\vec{E} \times \vec{B}$ drift. The distance poleward the ions and electrons move is determined by the time required to arrive at ionospheric altitudes from the magnetopause given in equation (5.5b) yielding an estimate for the width of the gap

$$d_{poleward} = v_{convection} \frac{f d_b}{v_{\|,i}} \tag{5.6}$$

The ion velocity $v_{\|,i}$ is obtained from equations (5.1a) and (5.2b)

$$v_{\|,i} = v cos\alpha = \left[2\left(\frac{T}{m_0 c^2}\right)c^2\right]^{1/2} cos\alpha \tag{5.7}$$

Since the thermal velocity of the magnetosheath ions is less than the bulk velocity, only ions injected very nearly parallel to the field are most likely to penetrate to ionospheric altitudes [*Reiff et al.*, 1977] and $cos\alpha \sim 1$ and the average poleward distance that magnetospheric plasma drifts after injection is given by

$$d_{poleward} = f d_b \left[2\left(\frac{T_{ion}}{m_0 c^2}\right)c^2\right]^{-1/2} \tag{5.8}$$

Equation (5.8) may be used to obtain a quantitative estimate of the distance magnetosheath plasma drifts poleward after injection across the magnetopause. Satellite measurements of the ion energy spectra are required to obtain values of the average energy $T_{ion}$ of the ions precipitating on the equatorward edge of the cusp as well as the ion velocity dispersion to estimate the distance to the injection point $fd_b$. A standard field model may be employed but the radial distance to the

Reproduced with permission of the copyright owner. Further reproduction prohibited without permission.

magnetopause is required to establish the length of the field line. Measurements of the standoff distance are not generally available for many of the periods for which auroral records are available since it requires a satellite encounter of the magnetopause at the time of the auroral observations. An estimate of the standoff distance can be obtained from the *Roeloff and Sibeck* [1993] or *Petrinec and Russell* [1993] parameterizations of the dayside magnetopause if satellite records of solar wind pressure and the IMF $B_z$ component are known. Additionally, It has already been noted that there is some question as to the location of the injection site, observations favoring the exterior cusp rather than the subsolar region [*Sibeck and Newell*, 1994] so that the quantity $fd_b$ represents two rather than one unknown.

Locating the separatrix by the optical method is limited primarily by the distance the precipitating mantle aurora particles may convect during the time required to drift from the equatorial plane to the ionosphere. This fundamental ambiguity is on the order of a few kilometers. In comparison, previous estimates of separatrix locations have not been as precise. Consider the method reported by *Lu et al.* [1995] where the time-of-flight argument was used to determine the location of the separatrix from the lowest energy ions observed by the DMSP satellites during overflights of the cusp region. The satellite trajectory passed through the dayside auroral oval on a chord poleward of the expected region containing the merging line. The DMSP satellite provides records of average ion energy at low altitudes and the drift meter observations of horizontal drift speed of the ionospheric plasma. The minimum energy ions establish the field aligned flow velocity of the cold magnetosheath plasma arriving from the merging site [*Lockwood and Smith*, 1994] and the drift meter measurements of ion drift provide the direction and magnitude of the convection electric field. Using the time-of-flight argument, the location of the separatrix equatorward of the satellite trajectory is determined from these parameters. Due to the errors in the technique the true position of the separatrix is suggested to lie within 1° to 2° in latitude of the location estimated from the satellite data. Comparison with high latitude electric potential patterns obtained by the assimilative mapping of ionospheric electrodynamics (AMIE) technique [*Richmond and Kamide*, 1988] demonstrated the estimated location of the separatrix was near the outer edge of the dayside convection throat, consistent with the theoretical predictions of the location of the merging line.

The error is not significant for the grid size of the AMIE potential patterns but it is certainly a distance the ground based observations can easily resolve. In fact, 1-2° is on the order of 100-200 km in latitude, a serious discrepancy for ground based observations. The advantage of using the ground based optics is that a wide region can be imaged in the vicinity of the merging line. The *Lu et al.* [1995] estimate cannot determine if a sharp boundary occurs in the vicinity of the separatrix identified by their technique since satellite passes perpendicular to the auroral oval coincident in time with the oblique orbit were not available.

The increase in width of the gap toward local noon is also consistent with the time of flight model for the gap. Consider ions drifting a fixed distance from the merging line. They drift a set distance along a flow line (equipotential). Flow lines are near perpendicular near the separatrix while they have a large component parallel to adiaroic boundaries. Hence, as the station samples auroral emissions nearer local noon the ions drift further poleward. This is consistent with the meridional arc velocities observed in the data here. The arcs have smaller slopes from 0700-0730

Reproduced with permission of the copyright owner. Further reproduction prohibited without permission.

UT but increase to large values near 0730-0800 UT consistent with the MSP sampling the poleward component of arc motion that rotates from eastward in the morning (towards the cusp) to poleward in the vicinity of the cusp.

### 5.4.2 Latitudinal Gap in DMSP Satellite Data

The latitudinal gap can also be identified in satellite records of precipitating electrons. The gap appears as a region of reduced precipitating electron energy flux on the equatorward edge of the cusp and poleward of plasma sheet electrons. A good example is found in the DMSP F7 spectrogram presented as Plate 1 of *Newell et al.* [1991a]. Average electron energies and energy fluxes equatorward of the cusp are approximately 1-2 keV and $6 \times 10^{10}$ eV/cm$^2$ s sr. Using the excitation efficiency for production of 557.7 nm photons given by equation (3.42) with the assumption that the precipitated flux is isotropic over the downward hemisphere (see Appendix E), the predicted emission intensity I(557.7 nm) is approximately 400 R. The latitudinal gap is the region immediately poleward of the sharp drop in kilovolt electrons but equatorward of the region identified as the cusp by *Newell et al.*, [1991a] where the average energy drops to values near 400-600 eV and the energy flux is approximately $1 \times 10^{10}$ eV/cm$^2$ s sr. The cusp is characterized by energy fluxes of $10^{10}$ eV/cm$^2$ s sr to over $10^{11}$ eV/cm$^2$ s sr with average energies of only 100 eV. The predicted intensities I(557.7 nm) within the gap are on the order of 80 R and in the cusp 50-500 R. These values are consistent with the variations in 557.7 nm intensity across the latitudinal gap reported here.

*Newell et al.* [1991a] display a number of DMSP spectrograms obtained during traverses of the dayside auroral oval at a variety of local times. The latitudinal gap is visible in the 26 January 1984 example in which the satellite sampled the cusp near 1127 MLT at approximately 12:46 UT. On the next orbit the satellite intersected the postnoon cusp at 1335 MLT but no gap is apparent in the electron spectrogram since the outer radiation belts are void of electrons over the range of latitudes presented in the plot (Plate 5 of *Newell et al.*, [1991a]). The lack of a gap in the postnoon cusp may be explained by magnetopause shadowing (Section 2.5). Energetic electrons drift nearly along lines of constant magnetic field strength due to the combined effect of the gradient B and curvature drifts into the morning and day time sector. A fraction of the drifting quasi-trapped electron population may be lost to the atmosphere due to wave-particle interactions or some other process and are observed as precipitated fluxes by the satellite at 1127 MLT. All drift shells at radial distances greater than the shell in contact with the magnetopause at noon must intersect the magnetopause. Particles drifting in the quasi-stable trapping region between this last closed drift shell and the magnetopause will be lost through the magnetopause and the postnoon quasi-trapping region will be void of electrons. For this reason the latitudinal gap is predicted to be observed most frequently in the prenoon to noon sector where drift shells bring electrons into contact with the magnetopause. The gap should be difficult to detect or absent in the postnoon sector due to the loss of electrons in the outer radiation belts from magnetopause shadowing.

The presence of a convection electric field introduces an additional inward drift motion, altering the electron drift path and shifting the intersection with the magnetopause to later local times

Reproduced with permission of the copyright owner. Further reproduction prohibited without permission.

[*Lyons and Williams*, 1984]. A population of electrons on a common drift shell will be dispersed in energy due to the convection electric field. Low energy electrons drift further into the afternoon sector before encountering the magnetopause due to the added effect of the electric field drift to the gradient B-curvature drift. High energy electrons are less strongly effected so a gradient in electron energy is expected across the dayside magnetopause if the oroginal injection is localized. Significant populations of electrons in the postnoon quasi-trapping region require electrons to either drift eastwards into the noon and into the afternoon sector or westward through the dusk sector. The local times where the injected electrons encounter the magnetopause depend on the size of the injection region, the time since injection, and the magnitude of the convection electric field [*Ejiri*, 1978; *Smith et al.*, 1979; *Meng and Akasofu*,1983]. Therefore, observation of a latitudinal gap at a given magnetic local time past local noon depends on the convection electric field both to drive the low energy magnetosheath ions poleward from the last closed field line and to move the magnetopause intersection of the energetic electron drift path to later local times providing a particle source within the postnoon quasi-trapping region.

Examples of electron energy spectrograms from DMSP orbits which intersect the dayside auroral oval before 8-9 MLT do not show a latitudinal gap [c.f., Plate 2-4 of *Newell et al.*, 1991a and *Newell et al.*, 1992]. These results are consistent with mapping the merging line along magnetic field lines into the midday auroral oval near local noon. Convective flows must be perpendicular to the separatrix to observe a significant gap. At earlier local times convective flows are parallel to the auroral oval [*Heelis et al.*, 1980; *Heelis*, 1984; *Heppner and Maynard*, 1987]. Even though magnetosheath ions may be driven significant distances from the field line on which they were originally injected, strong azimuthal motion results in little difference between the latitude of the ionospheric projection of the separatrix and the location where the ions impact the ionosphere and no gap is observed.

One should remember that although large gaps between the equatorward edge of the dayside auroral oval and the poleward edge of the mantle aurora may exist in the postnoon sector caution is advised in identifying the poleward boundary of the mantle aurora as the projection of the last closed field line. Magnetopause shadowing can significantly reduce the electron fluxes in the postnoon quasi-trapping region resulting in a local time asymmetry of the high latitude boundary for energetic electrons [*McDiarmid and Burrows*, 1968; *Vampola*, 1971; *Rossberg et al.*, 1978]. The poleward border of the mantle aurora at best may represent the last closed drift shell rather than the ionospheric projection of the magnetopause.

Two excellent examples of latitudinal gaps are apparent in the DMSP spectrograms displayed in Appendix C. Figure C.1 shows a southern hemisphere pass of the DMSP F9 satellite on 10 January 1992 nearly perpendicular to the dayside oval in the 1230 MLT to 1300 MLT sector at 1332 UT. The satellite enters the gap at 13:56 UT and takes approximately 8-9 seconds to cross the gap before encountering the poleward border of the plasma sheet precipitation. The satellite orbital velocity is approximately 7 km/s, therefore the gap width is 42-63 km. In comparison, note that the average energy of the ions on the poleward edge of the gap is 10 keV. Ions of this energy have velocities of approximately 1400 km/s. For assumed distances of 10, 14, and 18 $R_E$ between the satellite and the x-line where the ions are injected across the magnetopause (c.f., *Lockwood et*

Reproduced with permission of the copyright owner. Further reproduction prohibited without permission.

*al.*, [1994]), the travel times are 45, 64, and 82 sec. A poleward convection velocity of 1 km/s will result in gap widths of 45, 64, and 82 km. More meaningful comparison between the predicted gap width and observations requires knowledge of the ion drift velocity in the ionosphere (to obtain the antisolar convection speed of the ions) and the distance to the injection site.

The width of the gap appears to be greater in the 2 December 1991 example given in Figure C.3. The DMSP F10 satellite enters the gap at approximately 08:37:00 UT and requires 15-18 seconds to cross the gap before encountering the keV electron precipitation of the plasma sheet. The estimated width of the gap is therefore 105-126 km, 2-2.5 times larger than the previous example. However, the satellite trajectory carries it at an angle of approximately 45° to lines of constant magnetic latitude. Assuming the auroral oval is parallel to lines of constant magnetic latitude, the width of the gap is 74-89 km.

An example of a DMSP satellite pass through the aurora oval where a latitudinal gap is not present is given in the spectrogram in Figure C.2. The equatorward boundary of the dayside auroral oval lies at approximately 71.8° to 72.0° magnetic latitude. There are no plasma sheet electrons present at magnetic latitudes $\geq 71°$ , the lowest latitude in the spectrogram. A region at least 800-1000 km wide without a mantle aurora is present in this case.

### 5.4.3 Origin of the Continuous 557.7 nm Emission on the Poleward Mantle Aurora Boundary

Noted in Section 5.4.1, the poleward boundary of the mantle aurora strictly marks the highest latitude at which the atmospheric loss cones are filled with sufficient electrons to excite detectable aurora. In general the mantle aurora boundary may only be used to indicate a low latitude limit for the ionospheric projection of the separatrix. For the poleward boundary of the mantle aurora to be indicative of the separatrix two conditions must be fulfilled: the outer radiation belts must be filled with electrons to the magnetopause and some physical process must result in scattering of these particles into the atmospheric loss cone at a sufficient rate to produce visible aurora. Even if satellite observations of particle fluxes are used to identify trapping boundaries there is an ambiguity as to the location of the open/closed field line boundary. The latitude of the trapping boundary simply indicates the outermost field line on which electron fluxes are greater than the detector thresholds. Electron fluxes in the outer radiation belts decay with time constants on the order of days so particle populations decrease over time [*Craven*, 1966; *Lyons and Williams*, 1975a,b; *Lyons*, 1984]. Closed field lines may exist at greater radial distances from the Earth where particle fluxes are too low to be detected, especially during periods when the geomagnetic field is relatively undisturbed [*Fritz*, 1968; *Vampola*, 1971; *McDiarmid et al.*, 1976; *Rossberg*, 1978; *Sergeev*, 1990]. Detecting the separatrix using auroral emissions is therefore a more difficult problem than using satellite observations since *in situ* measurements of electron fluxes do not require that an active process scatter electrons into the atmospheric loss cone, only that detectable fluxes of particles are present to the magnetopause.

The electron populations within the quasi-trapping region are filled with electrons from recent plasma injections during night side substorms within a half electron drift period (approximately a few hours for electrons of 10's of keV). It is expected that electrons will be present out to

Reproduced with permission of the copyright owner. Further reproduction prohibited without permission.

the magnetopause since electron drift paths intersect the magnetopause in the morning and noon sector (see Figure 2.4). Electrons which have drifted to the vicinity of the magnetopause without encountering the atmosphere must have equatorial pitch angles greater than the loss cone since they mirror above the atmosphere. Electrons within the loss cone are lost to the atmosphere resulting in electron pitch angle distributions within the outer radiation belts that are peaked at 90° with empty loss cones [c.f., *West et al.*, 1973]. A fraction of the trapped population must be scattered into the loss cone and precipitated into the atmosphere if the presence of a quasi-trapped electron population is to be detected from the ground by an auroral emission. The strong auroral pulsations detected by the photometer within the mantle aurora suggests a wave-particle interaction is a reasonable candidate for the loss mechanism of particles throughout most of the region sampled by the photometer. In order to have any confidence that the ground based observations of the poleward boundary of the mantle aurora represents the separatrix and not a low latitude limit, some feature of the auroral display unique to particle precipitation from near the magnetopause be identified.

Before discussing the auroral observations further, it is instructive to consider a set of satellite measurements of electromagnetic wave and charged particle properties obtained by the ISEE 1 and 2 during a series of magnetopause crossings originally reported by *Gurnett et al.* [1979]. On each of the magnetopause crossings the plasma wave instrument on ISEE 1 detected strong electric field oscillations (at frequencies of 10 to $10^5$ Hz) and magnetic field oscillations (at frequencies of 10 to $10^3$ Hz) which *Gurnett et al.* [1979] interpreted as resulting from a superposition of both electrostatic and electromagnetic waves excited on terrestrial field lines adjacent the magnetopause. The ISEE 2 satellite magnetopause crossings from which the charged particle observations were obtained are only 30 to 60 seconds from the ISEE 1 crossings allowing the two instruments to be compared. The particle detectors exhibit enhanced fluxes of 1-6 keV electrons and 5.4-6.6 keV protons coincident with the strong electric and magnetic field oscillations.

An analysis of these records by *Tsurutani et al.* [1981] showed that interactions between the observed waves and 1-10 keV electrons and protons at the magnetopause can result in pitch angle scattering near the strong diffusion limit continuously filling the atmospheric loss cone. *Tsurutani et al.* [1981] estimated the energy flux deposited in the atmosphere by the process was approximately 0.15 $erg/cm^2s$, on the order of values that have been obtained within the dayside auroral oval, and proposed that it was a significant contribution to the dayside aurora. It was described in Section 5.4.1, however, that electrons with energies in the keV range are not convected very far from the field line on which the pitch angle scattering process leading to precipitation originally occurred. Since the electromagnetic wave turbulence reported by *Gurnett et al.* [1979] is observed on closed field lines adjacent to the magnetopause, any precipitated electrons resulting pitch angle scattering by the waves must arrive at, or equatorward of, the separatrix. Therefore it is unlikely that the transient arcs within the dayside auroral oval can be explained by this process since they form poleward of the separatrix.

However, the contribution of the precipitated electrons is worth considering further since they may alternatively provide an explanation for the continuous emission of 557.7 nm photons at the poleward border of the mantle aurora. The narrow region near the magnetopause where the

Reproduced with permission of the copyright owner. Further reproduction prohibited without permission.

enhancements are observed in the satellite data map to a narrow range of latitudes equatorward of the separatrix. Precipitation of electrons within this region excite auroral emissions at the poleward border of the mantle aurora. Using the empirical estimates of the 557.7 nm excitation efficiency of 1.23 to 1.73 kR/erg/cm$^2$ s [*Steele and McEwen*, 1990], the *Tsurutani et al.* [1981] estimate of the energy flux deposited in the atmosphere (0.15 erg/cm$^2$ sec) yields a 557.7 nm emission of approximately 185 - 260 R. This value is consistent with the observations of the approximately 100-250 kR 557.7 nm emission on the poleward border of the mantle aurora reported here. Using the 630.0 nm excitation efficiency of 14.3 R/erg/cm$^2$ s obtained by *Shepherd et al.* [1980] for 1-15 keV electrons the predicted brightness of the red line emission in the same region is approximately 2 R, at the detection limit of the photometer. These results are consistent with the observations of a weak but continuous 557.7 nm emission unaccompanied by detectable 630.0 nm emission on the poleward edge of the diffuse aurora.

A size estimate of the turbulent region at the magnetopause and its projection into the ionosphere can be obtained from the estimated velocity of the magnetopause as it sweeps across the satellite and the duration of the wave and particle enhancements. The time period the enhanced

**Table 5.6**
**Estimates of Distance to Injection Site**

| Time (UT) | $\sim d_{gap}$ (km) | $V_{meridional}$ (m/s) | $fd_b(R_E)$ 0.5kev | 1kev | 5kev |
|---|---|---|---|---|---|
| 0710 | 10 | 210 | 2.3 | 3.3 | 7.3 |
| 0720 | 50 | 420 | 5.8 | 8.2 | 18 |
| 0730 | 100 | 700 | 7.0 | 9.9 | 22 |
| 0740 | 100 | 900 | 5.4 | 7.7 | 17 |
| 0750 | 100 | 700 | 7.0 | 9.8 | 22 |

particles and wave turbulence are observed is on the order of 1-2 minutes while the typical magnetopause velocity is approximately $10 - 80$ km s$^{-1}$ (see Section 2.3) yielding an estimated thickness of the interaction region of approximately $0.1 - 1.5R_E$. Mapping this region into the ionosphere using magnetic flux conservation results in distances of 10 km - 150 km. The lower limit is consistent with the observations here, the region of persistent particle precipitation is approximately 10° or 20 km (larger because the observations are at approximately 120-150° elevation angle).

It is not required to invoke a reconnection model to explain the continuous 557.7 nm emission. Indeed, the original work by *Tsurutani et al.* [1981] was an attempt to provide an alternative explanation for solar wind energy transfer to the magnetosphere in terms of wave-particle interactions at the magnetopause. Application of the *Tsurutani et al.* [1981] results to the case study described here suggest the poleward boundary of the continuous mantle aurora 557.7 nm emission is located at or near (within a few kilometers) of the ionospheric projection of the separatrix. If the separatrix can be shown to be an active merging line, then the ionospheric projection of the merging line is identified as well. This is a separate issue that is considered in the next section.

Reproduced with permission of the copyright owner. Further reproduction prohibited without permission.

Identification of the poleward boundary of the mantle aurora as the ionospheric projection of the separatrix does however allow the distance to the site where ions are injected across the magnetopause to be estimated from the auroral records. Rearranging equation (5.8) into the form

$$fd_b = \sqrt{2}c\frac{d_{gap}}{v_{convection}}\left[\frac{T_{ion}}{m_0c^2}\right] \tag{5.9}$$

where $d_{poleward}$ has been replaced by $d_{gap}$ since the width of latitudinal gap is now recognized as the distance the magnetosheath plasma drifts poleward of the separatrix. The $v_{convection} = \vec{E} \times \vec{B}$ drift velocity is also required. Direct measurements of this quantity from a radar would provide the best values but these are not available for the case study. Rather, the meridional drift velocity of the auroral arcs may be used to estimate the plasma drift assuming the transient dayside arcs move with the same velocity as the ambient plasma (see Section 3.5.6). Estimated distances to the injection site are given in Table 5.6 where a range of ion energies has been adopted which span the values listed in Table 5.4. The meridional velocity is obtained from the auroral arc passing through zenith nearest the time indicated in table. Values obtained for 0.5 keV ions are too small suggesting an (unphysical) injection site within the magnetosphere. The 1 and 5 keV ions yield distances consistent with the near cusp and subsolar injection sites, respectively. Coincident measurements of the ion energy are required to determine which distance is correct.

### 5.4.4 Correlations Between Drop Outs and Transient Poleward Moving Arcs

Identification of the ionospheric projection of the separatrix with the poleward boundary of the mantle aurora in the case study requires the drop out events and the transient arcs to form on either side of the open-closed field line boundary. The correlation between the two series of events suggests an interpretation of the events in terms of the magnetic reconnection model since it is the most likely process that will convert closed to open field lines. Before considering the auroral observations, variations in particle populations sampled within FTE's detected in the magnetosheath and magnetosphere by satellites during magnetopause crossings will be described first. Application of these ideas and the time-of-flight effects will then be extended to the auroral observations to provide an explanation of the correlated behavior of luminosity drop outs on the poleward border of the diffuse 557.7 nm aurora and the formation of the transient 630.0 nm arcs poleward of the latitudinal gap.

Reconnection of terrestrial and solar magnetic field lines provides a simple explanation for the origin of plasma populations within FTE's and the boundary layer which are characterized by an admixture of magnetosheath and magnetosphere plasma [*Daly et al.*, 1981; *Paschmann et al.*, 1982; *Scholer et al.*, 1982; *Thomsen et al.*, 1987]. Once a terrestrial and solar wind field line has merged the magnetosheath plasma is no longer excluded from the magnetosphere and low energy magnetosheath plasma may flow unrestricted along the open field line into the magnetosphere. At the same time high energy ring current particles (Section 2.6.6) originally drifting on closed field lines near the magnetospheric boundary and rapidly oscillating between mirror points in opposite hemispheres are no longer trapped. The formerly trapped populations of high energy particles flow along the open field lines into the magnetosheath. Episodic intervals of enhanced merging creating

Reproduced with permission of the copyright owner. Further reproduction prohibited without permission.

FTE's produce open field lines at accelerated rates and large increases of the former high energy ring current particles are observed in the magnetosheath. The loss of energetic particles from the magnetosphere to the magnetosheath explains the presence of the $> 2keV$ electrons coincident with the magnetosheath FTE $B_n$ signature in Figure 2.5 since keV electrons are not typical of the magnetosheath plasma energies.

An example of magnetic field and plasma data obtained during an outbound pass of the AMPTE-UKS satellite from the magnetosphere into the magnetosheath near local noon from a study by *Chaloner et al* [1986] is presented in Figure 5.8. Three events observed within the magnetosphere displaying the characteristic bipolar $B_n$ variation of an FTE are labelled. The first, event A at 1724 UT, is an example of a magnetospheric FTE. Electron fluxes at three energies 44 eV, 106 eV, and 205 eV characteristic of the magnetosheath plasma populations increase within the FTE consistent with the model that magnetosheath plasma flows into the magnetosphere along the reconnected field lines. The electron fluxes at 980 eV, characteristic of the magnetosphere, decrease during the event suggesting the loss of magnetospheric plasma into the magnetosheath along the same field lines. *Thomsen et al.* [1987] have examined the velocity distributions of ions and electrons within FTE's and confirmed that the energetic magnetosphere particles flow outward along the FTE field lines while the low energy magnetosheath plasma flows inward.

The FTE's labelled B and C are observed after the satellite has crossed the magnetopause boundary and is located in the magnetosheath. The transition from magnetosphere to magnetosheath is noted by the greater proton number density and fluxes of low energy electrons found after approximately 1740 UT and the decrease in thermal velocity (kT). The increase in the 980 eV electron fluxes expected in the magnetosheath are not found in this example since the count rate is too low but the loss of magnetosheath plasma into the magnetosphere is noted by a decrease in the low energy electron fluxes.

An ISEE 1 observation of a magnetosheath FTE published by *Scholer et al.* [1982b] is presented in Figure 5.9 in which high energy electron and proton fluxes are are available. A bipolar variation in the $B_n$ component of the magnetic field identifies the FTE near 0212 UT. Simultaneously, fluxes of protons between 30 and 36 keV and electrons between 75 and 115 keV are enhanced, consistent with the loss of high energy particle fluxes from the magnetosphere along the newly reconnected field lines. Two dimensional velocity distributions presented by *Scholer et al.* [1981, 1982b] obtained during FTE's show that the flow of the ions, with energies too great to be magnetosheath particles, is directed along the magnetic field and outward into the magnetosheath confirming their origin as ring current particles lost during the reconnection events. Field aligned ring current particles are expected to be preferentially lost predicting distributions on newly open field lines with a strong peak in the sunward direction. *Scholer et al.* [1982a] noted that while the ions behaved as predicted for the merging model within FTE's (i.e., the velocity distributions were strongly peaked in the outward direction along the magnetic field) electron distributions were generally peaked at 90° indicative of trapped particle populations. Similar results obtained by *Eastman and Hones* [1979, 1982], and *Roeder and Lyons* [1992] when examining particle data from the boundary layers obtained either near the magnetopause or at low altitudes led the authors to conclude that either a fraction or all of the boundary layer is on closed field lines. Mechanisms for

Reproduced with permission of the copyright owner. Further reproduction prohibited without permission.

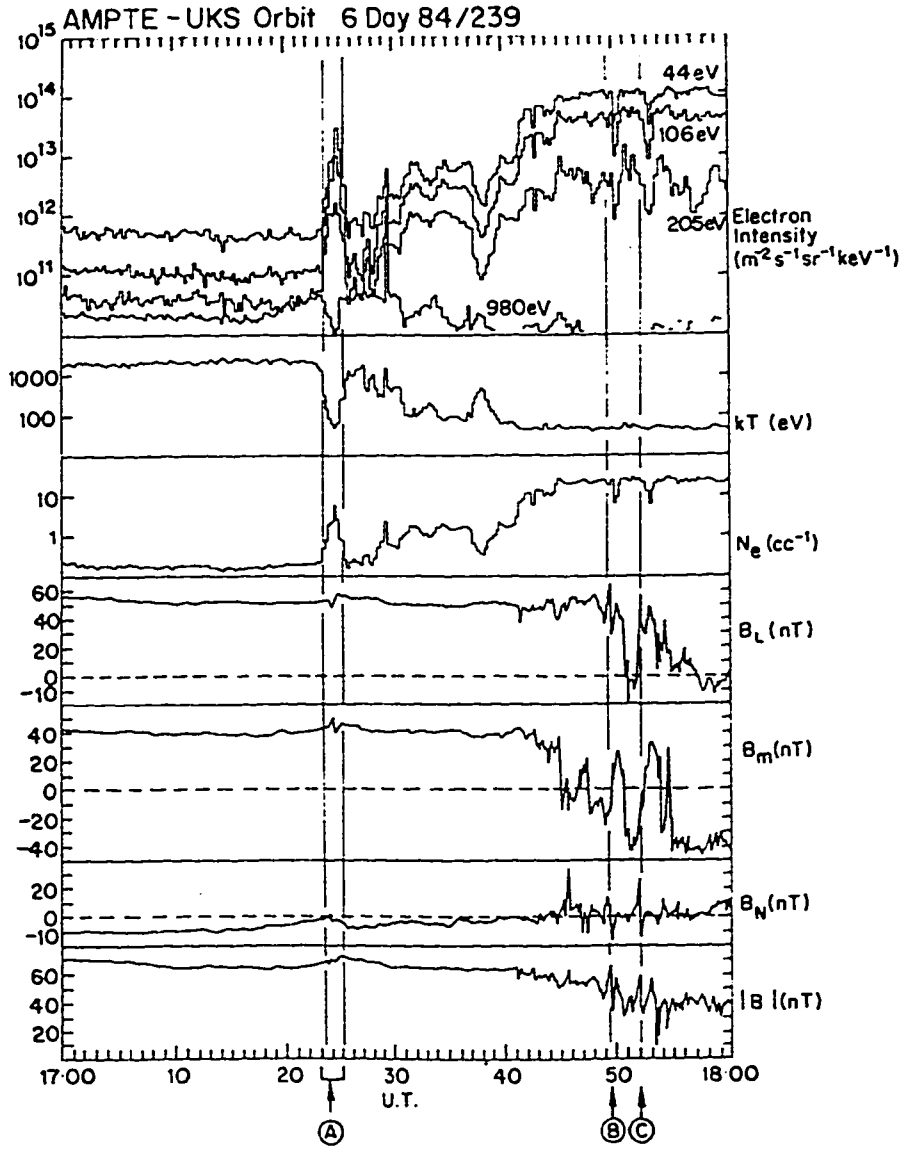


**Figure 5.8** Magnetic Field and Plasma Data for Magnetopause Crossing Exhibiting FTE Signatures. The magnetosphere FTE labelled A and magnetosheath FTE's labelled B and C are identified by the characteristic bipolar variation in the $B_n$ component of the magnetic field [from *Chaloner et al.*, 1986].

Reproduced with permission of the copyright owner. Further reproduction prohibited without permission.

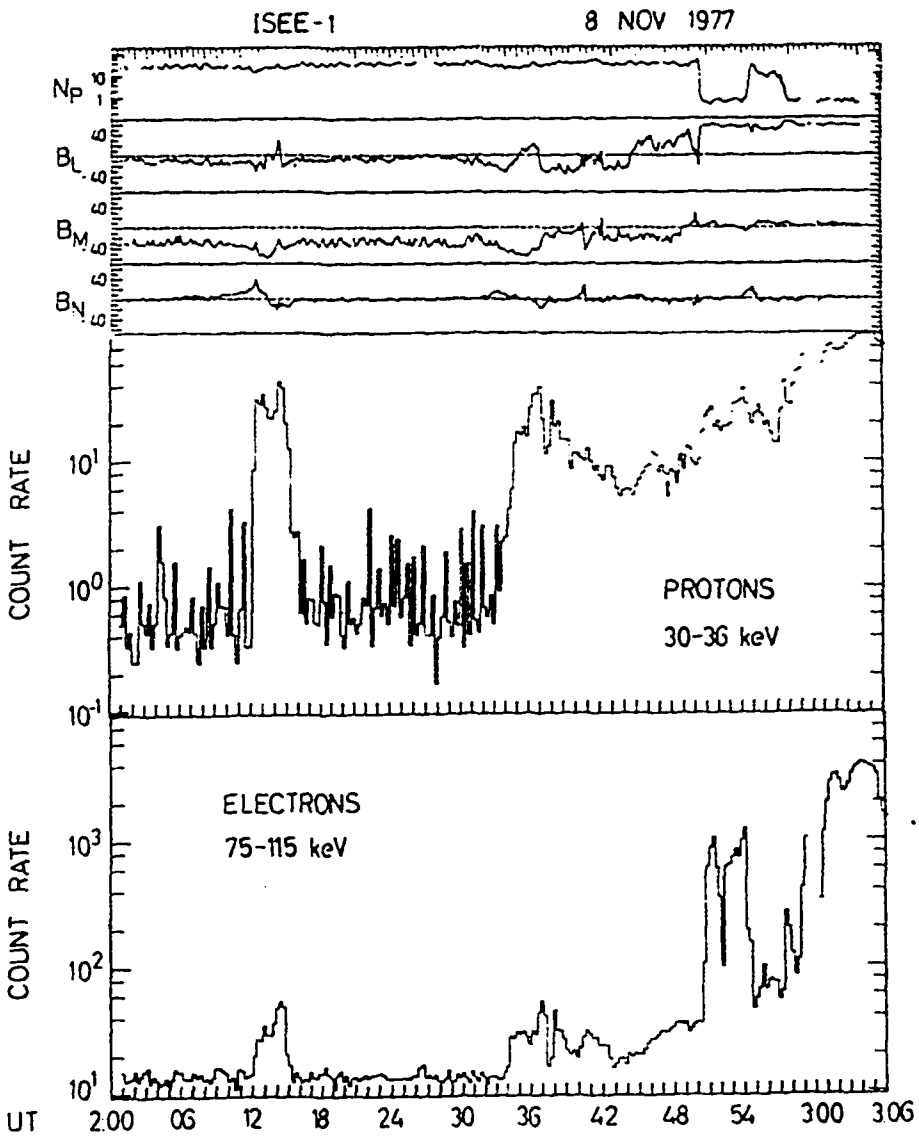


**Figure 5.9** Magnetic Field and Plasma Data for a Magnetosheath FTE. An example of a magnetosheath FTE exhibiting increases in the energetic electron and proton fluxes is observed at 0215 UT as the satellite is inbound from the magnetosheath into the magnetosphere [from *Scholer et al.*, 1982b].

Reproduced with permission of the copyright owner. Further reproduction prohibited without permission.

producing anisotropic electron pitch angle distributions on open field lines have been described by a number of authors and are considered in Section 5.4.6 in further detail.

Not all FTE's, defined by their characteristic magnetic field signature, exhibit the particle behavior just described. *Klumpar and Fuselier* [1990] reported a series of electron measurements associated with flux transfer events observed within the magnetosphere. A subset of the events do not exhibit the low energy particle enhancements and coincident loss of the high energy particles typical of magnetosphere FTE's. These observations show that clear FTE signatures in magnetic field data are not necessarily accompanied by the plasma signature. *Klumpar and Fuselier* [1990] suggested the lack of the low energy particle enhancements may be explained in terms of the standard FTE model if the region over which the magnetic field variations occurs is much larger than the region of open flux. A satellite must pass through the region of open field lines in the core of the FTE to record the particle variations. The satellite need only pass near the region of merged flux since the bundle of newly opened flux will disturb the neighboring closed flux producing the characteristic magnetic field variations.

A particularly instructive set of data is reproduced in Figure 5.10 from a study by *Gosling et al.* [1990] presenting two dimensional distributions of electron and proton velocities obtained by the ISEE satellite on an outbound pass through the dayside magnetopause. Velocity distributions are obtained within the magnetosphere (left hand plots), in the near Earth edge of the boundary layer (middle plots), and within the boundary layer (right hand plots). *Gosling et al.* [1990] interpreted the features in the ion and electron velocity distributions as time-of-flight effects on recently reconnected field lines. The electron and ion distributions are isotropic within the magnetosphere. This distribution is not typical for trapped particles which normally exhibit a loss cone distribution, but may result from strong diffusion of pitch angles into the loss cone through resonance with electromagnetic (whistler mode) waves [*Tsurutani et al.*, 1981; *Thorne and Tsurutani*, 1990].

High energy, field-aligned magnetosheath electrons are lost along the open field line yielding a pitch angle distribution that is peaked near 90° at large velocities in the boundary layer edge electron plot (bottom middle plot). At the same time the high density magnetosheath electrons begin to penetrate the boundary layer forming the anisotropic distribution peaked along the field. The down flowing magnetosheath plasma is directed along the field, but there is also a low energy electron component flowing up the field which is due to cold magnetospheric plasma.

The ion distribution has not changed significantly because they are slower and have convected further poleward and are not available to the satellite. In the final set of panels on the right hand side the satellite has moved further outward into the boundary layer where low energy ions are observed flowing down the field line into the magnetosphere. No mirror component is present due to the low ion velocity. Ions that mirror in the cusp do travel up the field line but the low velocity of of the ions allow them to convect so far tailward of the injection site that they are swept into the high latitude lobe forming the plasma mantle.

The particle observations at the magnetopause within FTE's are consistent with the auroral morphology reported in the case study plotted in Figures 5.2 and 5.3. Only the behavior of the inward flowing electrons or ions are considered to explain the auroral emissions since the majority of particles moving outward after mirroring in the increasing field strength near the Earth could

Reproduced with permission of the copyright owner. Further reproduction prohibited without permission.

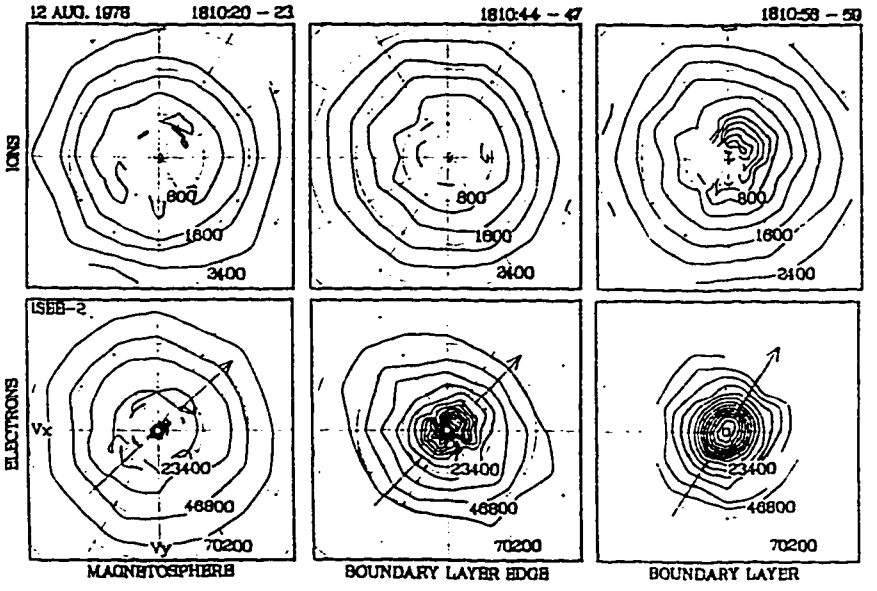


Figure 5.10 Boundary Layer Ion and Electron Velocity Distributions. The arrow on the electron plots indicate the direction of the magnetic field [from *Gosling et al.*, 1990].

Reproduced with permission of the copyright owner. Further reproduction prohibited without permission.

not have lost sufficient energy in collisions to produce a significant effect on the neutral atmosphere (i.e., produce auroral excitation). The ion motion along the field line governs the bulk flow of the injected magnetosheath plasma [*Reiff et al.*, 1977; *Burch et al.*, 1985] but is otherwise not an important consideration in interpretation of the sharp latitudinal variations in auroral luminosity in the region of the discrete transient auroral arcs due to beam spreading of the proton beam once they encounter the atmosphere.

Two questions arise from the proposal that formerly trapped energetic electron populations may rapidly evacuate a newly opened flux tube while magnetosheath ions and electrons entering the magnetosphere on the same flux tube must maintain quasi-neutrality and move at the ion velocity. The first question is to what extent the two populations interact altering the energy and pitch angle distributions of both the incoming and outgoing particle populations. Second, since the requirement that an ambipolar electric field form whenever an electron population attempts to flow from a slower ion population must be generally true [*Lui*, 1993] the outflowing electrons must affected as well as the incoming electrons.

The first question is answered by considering satellite measurements of thermal plasma distributions obtained at the magnetopause within FTE's. Measurements of this type reported by *Thomsen et al.* [1987] demonstrated that ion and electron populations within FTE's are well described by superimposed magnetosheath and magnetosphere velocity distributions. *Thomsen et al.* [1987] further noted that the lack of any significant variation in the component distributions within the FTE's from the individual velocity distributions in the magnetosphere and magnetosheath indicates the two populations do not interact strongly. The inflow of the magnetosheath plasma and the outflow of the magnetospheric plasma may therefore be treated as independent problems.

In considering the second of the two questions, first note that satellite measurements within the cusp confirm that penetrating magnetosheath plasma maintains quasi-neutrality [*Burch* 1985] which is the basis of computing the travel time from the merging site to the ionosphere based on the ion velocity. An ambipolar electric field must be present to insure the quasi-neutrality or the greater thermal velocity of the electrons would allow them to rapidly outrun the ions. However, the outflow velocity of the energetic electrons was computed above based simply on the electron energy neglecting any interaction with the energetic protons which are also trapped on the closed magnetic field lines. Since the formation of an ambipolar electric field due to charge separation must arise if there is differential motion of ions and electrons [*Lui*, 1993], it remains to be determined what the effect is on the outgoing electron populations.

Ion populations injected into the ring currents during substorms are dominated by particles with energies on the order of 10 keV to 100 keV [*Smith and Hoffman*, 1973]. Bounce periods for the 10-100 keV ions (assuming they are protons) at L=10 are approximately 136-43 seconds. The maximum time any ion is away from an equatorial merging site is given by the quarter bounce periods which are 34-11 seconds for the 10-100 keV protons. These values are greater than the 5-0.9 second bounce periods for 1-40 keV electrons listed in Table 5.5 but are still within a few 16 second MSP sample periods. Thus, the energetic electron populations will evacuate the newly opened flux tube on the order of 1-2 MSP scan periods, consistent with the observations reported

Reproduced with permission of the copyright owner. Further reproduction prohibited without permission.

here, even if the outgoing electron flux is constrained to move at a velocity determined by the ring current ions due to the formation of an ambipolar electric field

### 5.4.5 Source of Emissions within the Latitudinal Gap

In the process described in Section 5.4.1 to explain the latitudinal gap, particles do not precipitate within the gap itself. However, approximately 50 R of 557.7 nm emission above the airglow background was found in the case study suggesting that a low flux of energetic electrons may in fact be present within the gap.

Transport of $O(^1S)$ atoms from the mantle aurora cannot be the source of the 557.7 nm emissions within the latitudinal gap due to the short lifetime of the excited state. Typical neutral wind velocities in the vicinity of the dayside auroral oval are approximately 100-200 m/s [*Smith and Sweeney*, 1980; *McCormac and Smith*, 1984]. In one 0.7 second lifetime the excited species are transported only 0.07 km to 0.14 km. Even if the neutral wind is an extreme value of 200 m/s, the time required for the population to drift a distance of approximately 2 km (the minimum distance detectable by the MSP near 100 km) is on the order of 14 lifetimes of the $O(^1S)$ state. The transported population of $O(^1S)$ will be reduced to $6 \times 10^{-5}$% of the original population. Considering that typical 557.7 nm brightness in the mantle aurora described here is on the order of 150-250 R, brightness due to transported populations is predicted to be only fractions of a Rayleigh. Signals of this strength cannot be detected by the MSP and in any case are much less than the statistical variation in the approximately 100 R airglow background. Quenching has been neglected for this estimate and would act to further reduce the number of excited states. Therefore, poleward transport of $O(^1S)$ from the mantle aurora cannot be the source of 557.7 nm emissions within the latitudinal gap.

Scattering of light from the relatively brighter emissions within the mantle aurora and auroral arcs within the dayside auroral oval may also contribute to the 557.7 nm signal within the latitudinal gap. For example, consider the ground based observations reported by *Romick and Belon* [1967a,b] of an isolated auroral arc exhibiting an apparent wavelength dependent width and a diffuse "skirt" of emission within a restricted altitude range. The intensity of the "skirt" was reported to be 5% of the peak emission intensity within the core region of the arc. *Mende and Eather* [1971] showed the observations may be adequately explained by scattering since the features were not observed when similar observations were obtained above the bulk of the atmosphere during airplane flights. Adopting the 5% intensity reported for the "skirt" as typical for aerosol scattering on clear nights, the contribution from the 1550 R arc in the dayside auroral oval considered here is 77 R while the 400 R emission on the poleward edge of the mantle aurora contributes approximately 12 R. These values are consistent with the approximately 50 R 557.7 nm emission observed within the latitudinal gap suggesting all of the emission may result from light scattering. However, it is not clear that all of the 150 R "airglow background" is indeed the result of chemical reactions in the E-region ionosphere. A contribution due to scattering from the clouds or haze is most likely included in the background estimate suggesting that the 50 R 557.7 nm emission observed within the gap is greater than the intensity due to the local airglow and scattering contribution.

Reproduced with permission of the copyright owner. Further reproduction prohibited without permission.

Further work on this subject must await more detailed observations of similar auroral conditions as those presented in the case study although under clear conditions. Application of a spectral technique similar to that suggested by *Vallance Jones and Gattinger* [1990] would be useful in determining the presence of scattered light. The method requires monitoring two spectral lines, one at a short wavelength and one at a long wavelength, for which the ratio is constant. *Vallance Jones and Gattinger* [1990] advocate the $N_2$ First and Second Positive systems which they argue should be constant except for very low altitude aurora. Scattering preferentially removes the short wavelength component allowing identification of regions where the dominant source of light is scattering from adjacent emission features. The lack of strong band emissions within dayside aurorae (see Table 3.1) may limit the use of this technique unless another more suitable wavelength pair is identified.

Satellite measurements of precipitating particles during passes through the dayside auroral oval often show the presence of energetic electrons beyond the poleward edge of the 40 keV trapping boundary but equatorward of the dayside auroral oval [*Escoubet et al.*, 1995]. It is therefore expected that once any contribution due to scattering is eliminated as a source 557.7 nm emission within the latitudinal gap there will be an additional component that is still present due to precipitating particles. These particles may arise from any one of a number of sources.

One source of precipitating particles within the latitudinal gap are energetic electrons which leak out of the magnetosphere when their drift paths encounter the dayside magnetopause [*Sibeck et al.*, 1987b; *Sibeck and McEntire*, 1988]. Drifting onto newly open field lines, these particles may precipitate at latitudes poleward of the last closed field line. (c.f., *Escoubet et al.* [1995]). Satellite observations of energetic particles obtained within the magnetosheath show that electrons with energies >40 keV are typically found within approximately 1 Re of the magnetopause [*Meng and Anderson*, 1970] with the greatest fluxes located in the prenoon sector. A similar energetic ion layer peaks in the postnoon sector, consistent with the model that the particles are due to magnetospheric plasma gradient B-curvature drifting into the magnetopause [*Sibeck et al.*, 1987b]. Precipitation requires that the electron pitch angle lie within the atmospheric loss cone. Particle populations drifting into the magnetopause typically exhibit a strong loss cone distribution [*West et al.*, 1973]. An active pitch angle scattering mechanism must be present within the magnetopause current layer since the pitch angle distribution of the leaking particles are typically isotropic [*Daly et al.*, 1984; *Lyons et al.*, 1987]. The precipitated flux is due to the field aligned fraction of the isotropic population. Using magnetic flux conservation, the width of the layer maps to a region approximately 200 km in latitude in the ionosphere. This distance is on the order of the width of the latitudinal gap. Since the electron flux decreases with distance from the magnetopause [*Anderson et al.*, 1965], the observed auroral emission due to this source should decrease in intensity with increasing latitude from the poleward border of the mantle aurora.

A likely source of particles within the latitudinal gap is high energy electrons produced at an active dayside merging site. These particles can stream into the low latitude boundary layers ahead of the bulk flow of the cold magnetosheath plasma (c.f., *Gosling et al.* [1990b]). *Winglee et al.* [1993] simulated the entry of magnetosheath plasma injected at the dayside magnetopause using a particle code so the motions of individual electrons and protons could be examined. One

Reproduced with permission of the copyright owner. Further reproduction prohibited without permission.

result from the study was the demonstration that cold plasma arrived poleward of the injection site but a low flux of energetic (keV) electrons was able to precipitate through the region between the injection line and the arrival location of the cold plasma. Electrons populating the latitudinal gap from this mechanism are also subject to the velocity filter effect described in Section 5.4.1 predicting a gradual decrease in average energy poleward of the merging line. Auroral emissions associated with these particles may exhibit a decrease in the I(557.7 nm)/I(630.0 nm) ratio due to the softening of the electron energy spectrum with latitude. Such a variation is suggested in the photometer scan plotted in Figure 5.4. The 557.7 nm intensity decreases poleward of the boundary of the mantle aurora sampled at the 140° elevation angle while the 630.0 nm intensity gradually increases. It is difficult to make any quantitative statement about the ratios and particle energies however since the emissions are sampled so far from magnetic zenith. Further work on this subject must also await new records where the latitudinal gap is located near magnetic zenith.

Proton impact will also produce both $O(^1S)$ and $O(^1D)$. Lack of proton measurements during the period under consideration prevents any quantitative discussion of the proton contribution although some general comments are possible. Proton beams encountering the atmosphere will diffuse in latitude and longitude due to a charge exchange process with the neutral atmosphere [*Davidson*, 1965]. The protons may drift 100's of kilometers across the field resulting in a relatively unstructured hydrogen emission even if the original precipitating protons are relatively narrow in latitude (see Section 3.2.2). Protons injected into the cusp from the magnetosheath during merging processes as well as trapped magnetospheric protons pitch angle scattered into the loss cone by the wave-particle interaction at the magnetopause described by *Tsurutani et al.* [1981] can produce the excited atomic oxygen states. The I(557.7 nm) due to proton precipitation was estimated by [*Eather*, 1967] to be

$$I(557.7\ nm) \leq 3I(H\beta) \tag{5.10}$$

Average $H\beta$ intensities reported within the cusp region are 10-40 R (see Table 3.1). These emissions are spread over a wide range of latitudes and are generally unstructured so that the values reported for the cusp apply equally as well for latitudes immediately poleward or equatorward of the dayside auroral oval. The 557.7 nm intensity expected to accompanying these hydrogen emissions are 30-120 R. It would appear that much of the background 557.7 nm emission lacking in latitudinal structure observed near the cusp could be the result of proton precipitation.

The 557.7 nm intensity decreases within the gap relative to the emission intensity outside the gap while the 630.0 nm brightness increases towards the poleward edge of the gap, suggesting a change in electron energy over the latitudinal gap. The ratio $I(557.7\ nm)/I(630.0\ nm) > 1$ on the equatorward edge while $I(557.7\ nm)/I(630.0\ nm) < 1$ on the poleward edge of the latitudinal gap. The general lack of 630.0 nm emissions within the latitudinal gap indicates that while the electron energy flux must decrease within the gap, the average energy remains in excess of 1 keV near the poleward border of the mantle aurora and into the gap.

Reproduced with permission of the copyright owner. Further reproduction prohibited without permission.

### 5.4.6 Trapped Particle Fluxes at the Equatorward Edge of the Cusp

One issue that must be addressed with respect to the particle leakage out of the magnetosphere on open field lines is the observations of particle distributions peaked near 90° in the boundary layer observed by satellites both at low altitude [*Burrows et al.*, 1972; *McDiarmid et al.*, 1976] and near the magnetopause [*Palmer and Hones*, 1978; *Eastman and Hones*, 1979; *Williams et al.* 1985; *Mitchell et al.*, 1987]. These observations are the basis for the argument that the boundary layer, or at least the inner edge, must be formed on closed field lines and cannot result from a reconnection process.

These observations are problematic to the interpretation of the auroral events presented above since a model invoking rapid field line reconnection with loss of the trapped ring current electrons to explain the drop outs in the poleward border of the diffuse 557.7 nm aurora requires electrons to be rapidly lost to the magnetosheath on the order of an MSP scan period, approximately 15 seconds (on the order of 10 bounce periods for keV electrons). This would appear at first to be inconsistent with satellite observations of electron pitch angle distributions which suggest the boundary layer and the equatorward edge of the cusp is in fact on closed field lines. Reconciliation of the satellite observations with the model proposed here for the auroral observations requires that observations of particle pitch angle distributions peaked near 90° which can be shown to exist on open field lines within the boundary layer and cusp.

*Daly and Fritz* [1982] explained that electrons may retain their anisotropic distributions even on newly opened field lines since the electrons may be reflected from the converging magnetic fields near the reconnection site. Electron distributions within the boundary layers may therefore exhibit characteristics of trapped populations even though they are on newly opened field lines. The ions, due to their greater mass and gyroradius, are not reflected and exhibit a loss cone distribution as observed by *Scholer et al.* [1982].

An alternative method of obtaining 90° pitch angle distributions on newly opened field lines was suggested by Cowley and Lewis [1990] who invoked the local field maximum near the equator for field lines in the outermost magnetosphere [*Roederer*, 1966, 1969]. The compression of the dayside magnetosphere by the solar wind creates a local maximum in the field intensity near the equatorial plane and particles may be reflected from this region. The dynamics of particles in these regions were examined by *Vernov et al.* [1967] and *Antonova and Shabansky* [1968] using the Hones-Taylor magnetic field model [*Taylor and Hones*, 1965]. They showed that many particles with pitch angles near 90° drifting into the noon sector may move off the equatorial plane up or down into the minimum B pockets rather than drifting outward across the magnetopause and localized regions beyond 9 $R_E$ between 15° and 40° latitude may be filled with trapped particles. These early results were model dependent, however, since the branching was shown to be impossible if the Mead-Williams magnetic field model [*Williams and Mead*, 1965] was used for the calculations [*Roederer*, 1969]. Further analysis by *Shabansky* [1971] and *Buck* [1975] using alternative field models demonstrated the presence of a local field maxima near the equatorial plane in the outer magnetosphere. Experimental verification of the drift of field perpendicular particles away from the equatorial plane in the midday sector was presented by *West* [1979] in the form of pitch angle

Reproduced with permission of the copyright owner. Further reproduction prohibited without permission.

distributions of energetic electrons obtained near the magnetopause in the early afternoon. The distributions, originally obtained by [*West et al.*, 1973], exhibit not only the expected decrease in the 90° particles due to drift shell splitting but also a characteristic secondary loss of particles near 65° which they interpreted as resulting from the loss of particles when trajectories in the high latitude dayside field minimum pockets intersected the magnetopause. More recently, while evaluating the Tsyganenko magnetic field models by comparing model values against a wide variety of magnetic field intensity values obtained by satellite *Fairfield* [1991] noted that a field strength maximum does exist in the outer magnetosphere near noon near the equatorial plane.

Cowley and Lewis [1990] proposed that subsolar merging opens the terrestrial field in the region of the field maximum allowing the ring current particles to remain trapped for many bounce periods at higher latitudes within the minimum B pockets before they are lost from the magnetosphere into the magnetosheath. The auroral events described here require the ring current particles to be lost to the magnetosheath at least within an MSP scan period, approximately 15 seconds (on the order of 10 bounce periods for keV electrons). This would appear at first to be inconsistent with the results described above. The observations of trapped particle distributions in the boundary layer must be reconciled with the proposal that that rapid loss of trapped ring current electrons result in the drop out of the diffuse 557.7 nm aurora preceding the formation of the auroral transient if the FTE model for the auroral events is to be considered successful.

First, consider that a likely source of the charged particles observed immediately outside of the magnetopause is due to leakage of trapped particles drifting into the magnetopause [*Sibeck et al.*, 1987a,b, 1988; *Newell and Meng*, 1988]. Due to drift shell splitting, particles with large pitch angles drift outward at greater radial distances from the Earth on the dayside than those which are field aligned [*Roederer*, 1967] and particles leaking from the magnetosphere into the magnetosheath are dominated by the fraction of the trapped particles with velocities perpendicular to the field lines. The large pitch angle particles will mirror near the equatorial plane and cannot explain the observations by low altitude satellites. The particles detected by the low altitude satellites must have equatorial pitch angles within the atmospheric loss cone and may be the fraction of the population which are lost through the magnetopause with small pitch angles. In addition, during the passage through the current sheet the particles may be scattered in pitch angle while preserving the energy distribution [*Lyons et al.*, 1970]. Particle distributions due to leakage from the magnetosphere should be similar to those inside the magnetopause but more isotropic *Sibeck and McEntire* [1988]. The fraction of these populations observed by low altitude satellites will be peaked near 90° suggesting a trapped distribution since the magnetic mirror force increases the pitch angle as the particles move into the stronger field at lower altitudes [*Newell and Meng*, 1988]. The reduced flux of high energy particles outside the separatrix boundary will be observed at auroral heights as a reduced particle flux and 557.7 nm auroral luminosity within the latitudinal gap.

Butterfly pitch angle distributions observed in postnoon electron populations and prenoon ion populations in the outer magnetopause are due to magnetopause shadowing where the particles near 90° pitch angles are reduced due to losses into the magnetosheath [*West et al.*, 1973; *Sibeck et al.*, 1987a,b]. However, particles with pitch angles near 90° cannot be observed at low

Reproduced with permission of the copyright owner. Further reproduction prohibited without permission.

altitude since they mirror near the equatorial plane. One possibility is that interactions with the strong electromagnetic wave fields observed near the magnetopause *Gurnett et al.* lead to pitch angle scattering in the strong diffusion limit filling the loss cones. These waves should be equally as efficient on the closed field lines immediately inside the magnetopause, too, and in fact are observed there. Isotropic ring current particle distributions consistent with strong diffusion have been reported by *Gosling et al.*.

*Cowley and Lewis* [1990] discuss the possibility of magnetic trapping due to local magnetic field maximum in the outer dayside magnetosphere due to solar wind compression of the terrestrial field as an additional source of trapped particle populations near the magnetopause within the boundary layer. Magnetic merging opens the field lines to the solar wind allowing rapid escape of the trapped populations into the magnetosheath and interplanetary space on the order of one half a bounce period, typically seconds or less. Observations of particle pitch angle distributions peaked near 90° consistent with "trapped" populations near the magnetopause have been interpreted as evidence the boundary layer field lines must be closed [*Palmer and Hones*, 1978; *Eastman and Hones*, 1979; *Williams et al.*, 1985; *Mitchell et al.*, 1987].

These observations can be reconciled if the terrestrial field geometry is considered as a function of dipole tilt. *Cowley and Lewis* [1990] consider only the case where the terrestrial dipole is perpendicular to the ecliptic plane appropriate for near equinox conditions and show the *Tsyganeko* [1987] magnetic field model exhibits a maximum field intensity at the equatorial plane, consistent with predictions of off-equatorial field minimum due to solar wind compression of the dayside magnetic field [*Antonova and Shabansky*, 1968]. The local minima are not features of the *Tsyganenko* model alone but also appear in the Mead-Williams magnetic field model [*Mead*, 1964, *Williams and Mead*, 1965].

*Shabansky* [1971] noted however that the dipole tilt will shift the local field maximum in the outer magnetosphere from the equatorial plane into the summer hemisphere. The magnitude of the local field minimum in the winter hemisphere increases and a corresponding decrease is found for the local minimum in the summer hemisphere. At large dipole tilts, the minimum B region disappears completely in the summer hemisphere and the magnetic field intensity in the outer magnetosphere once again exhibits a single minimum. This is precisely the condition present during the boreal winter solstice conditions under which the Svalbard observations are obtained. In this case the ring current particles trapped in the magnetosphere should simply escape during reconnection events.

*Eastman and Frank* [1982] questioned the reconnection interpretation of the ISEE boundary layer traverse on 8 September 1978 reported in detail by *Paschmann et al.* [1979] and *Sonnerup et al.* [1976] on the grounds that the electron populations are peaked near 90° and appear trapped. These observations are obtained near the equinox when the dipole tilt is small and the high latitude minimum B pockets are expected to be well developed, consistent with the description by *Cowley and Lewis* [1990] although they do not explain the flank observations of *Palmer and Hones*, *Williams et al.*. Note that *Shabansky* [1971] shows three weak field intensity minima, one at the equatorial and two off equatorial, in the case of field lines crossing the geomagnetic equator

Reproduced with permission of the copyright owner. Further reproduction prohibited without permission.

90° from the subsolar region. These may in fact allow localized regions of trapped particles even for the case of flank observations.

### 5.5 Probability of Observing the Separatrix in Auroral Records

It should be noted that the two case studies presented here appear to be among the few examples in the Longyearbyen archive for which the conditions necessary to observe the ring current drop-outs are present and do not represent a large number of similiar examples. It is important therefore to examine if these limited cases are consistent with an expected probability of observing the events.

Approximately 11 winter field seasons (some are incomplete) were available in the Longyearbyen archive at the time of writing to search for auroral records matching the criteria:

(1) clear skies,

(2) pulsating aurora near the equatorward edge of the red arcs,

(3) red aurora forming near zenith or in southern sky.

A total of $660 \pm 154$ days is the maximum number of days for which observations are possible assuming that approximately 60 days of observation are possible during each two month field season. The error is based on variations in field seasons of approximately one week at the beginning and end of each season. The total number of days for which data is available to examine is given by

$$N_{obs} = P_{clear} P_{instrument}\, 660 \pm 154 days \qquad 5.11$$

where $P_{clear}$ is the probability of clear weather and $P_{instrument}$ is the probability of the instrument working correctly. Out of the 660 days theoretically available, 292 days were found to have sufficiently clear weather with data free from instrument errors to examine the photometer plots further for auroral features. This yields a probability of 31% to 58% clear days if the number of lost days due to instrument problems is neglected.

Strictly speaking, the fraction of acceptable days is given by the product of the joint probility of clear days and the time the instrument is running correctly. Neglecting the instrument failure days is a reasonable assumption for a quick estimate of the clear days since instrument failures occur as likely on cloudy days as clear days and often cloudy days are chosen to shut down the instrument for repairs. At least one channel is working on the MSP at nearly all times and the most reliable channels have always been reserved for the 557.7 nm and 630.0 nm filters. It is unlikely that an entire daytime period of bad red and green data was recorded since a problem of that magnitude would have resulted in instrument shutdown to correct the error. These periods simply have no data and are not counted in the total number of 262 days.

Reproduced with permission of the copyright owner. Further reproduction prohibited without permission.

The number of days events matching the criteria listed above are visible is given by

$$N_{obs} = P_{observation}\, 292 days \qquad 5.12$$

where the probability $P_{observation}$ of observing the separatrix is a joint probability of a number of independent probabilities

$$P_{observation} = P_{e^- injection} P_{\theta \geq 90} \qquad 5.13$$

where $P_{e^- injection}$ is the probability of observing the diffuse 557.7 nm aurora in the hard electron precipitation zone as a result of high$P_{observation} = P_{e^- injection} P_{\theta \geq 90}$g substorms in the night sector. The fraction $P_{\theta \geq 90}$ is a geometric factor representing the probability the transient auroral arcs form at elevation angles greater than or equal to 90 degrees (i.e., in the zenith of south of the station).

In order for the hard zone electron fluxes to produce observable auroral emissions up to the separatrix boundary a recent injection of particles is required in the night time sector. Trapped fluxes of energetic electrons are always drifting eastward into the day sector but as noted in Chapter 3 the electrons in the morning sector responsible for the diffuse 557.7 nm aurorae immediately equatorward of the soft zone aurorae include a fraction of pseudotrapped electrons which cannot complete a single azimuthal drift around the Earth before encountering the magnetopause. The best conditions to observe high fluxes of electrons near the outer edge of the magnetosphere occurs after a fresh injection of electrons and ions during a substorm. In order to observe the effects of these particles relative to the formation of transient auroral arcs in the dayside soft zone aurorae a ground station must be located in the 9-12 MLT sector. Dayside soft zone auroral displays earlier than 9 MLT are likely to be the result of processes within the magnetosphere deep in the tail and are less likely to result from dayside merging. In order to produce auroral emissions indicating the location of the last closed magnetic field line, electrons must pass very close to the magnetopause. The loss of the pseudotrapped component from the electron populations near the magnetopause at local noon limits the available flux to produce strong 557.7 nm auroral emissions in the postnoon sector. The night time injection event must have occured within one half azimuthal drift period earlier to provide the necessary flux of energetic electrons.

The size of the particle source is determined by the (1) duration [c.f., *Reeves et al.* 1992 describing multiple injections providing particles over approximately 30 minutes in the nightside ring current]. and (2) size of an individual injection region [c.f., *Reeves et al.* 1990] as well as (3) the lifetime of the injected particles since the outer radiation belt electrons rapidly decay with time [*see Craven et al*, 1966]. The size of the injection region is variable, initially only a few hours in local time but well developed injections are often typically 6 hours in local time and extreme cases may be even larger [*Reeves et al.*, 1990, 1992; *Friedel et al.*, 1994]

*Borovsky et al.* [1993] showed that the majority of injection events were greater than the stable trapping limit computed by *Kennel and Petschek* [1966] indicating that particle injections most commonly create pulsating aurorae. This is consistent with the results obtained by *Nemzek et al.* [1995] showing pulsating aurora when fluxes exceed the Kennel-Petschek limit. The latter study showed a greater proportion of events which failed to produce pulsations due to low fluxes than is present in the *Borovsky et al.* paper. The discrepency may be due to the fewer events in

Reproduced with permission of the copyright owner. Further reproduction prohibited without permission.

the Nemzek study or it may be that Borovsky's criteria of including only events observed within 1.5 hours of local midnight selected large injections. In either case, if the midnight values produce many injection events greater than the stable limit, pulsating aurorae will occur at least at those rates.

The probability distribution for intervals of time between charged particle injection events obtained from energetic particle detectors on geosynchronous satellites (see Figure 3 of *Borovsky et al.* 1993) provides an estimate of the probability of the injection events $P_{einjection}$. Integration of the normalized distribution over all intervals less than or equal to 3 hours yields a probability of approximately $P_{einjectionin3hourinterval} = 0.42$. This is the probability of a particle injection occuring within any three hour period during the day. There is no need to multiply by the factor 0.125 which is the fraction of the day the station is located in the 9-12 MLT sector if the probability desired in (5.11) is that of observing the events within the 9-12 MLT period.

The aurora must also be located in the zenith or equatorward of the station to clearly observe the luminosity gap between the diffuse aurora and the red dayside auroral oval. The best viewing geometry is limited to the region approximately 200 km south of the field stations at Svalbard which are located near 75° geomagnetic latitude. *Lockwood et al.* [1989b] estimated dayside transients form within this region approximately 30% of the time. The value $P_{\theta \geq 90} \sim .30$ is used for the observing geometry factor.

The joint probability is then

$$P_{observation} = (.42)(.30) \sim 0.12 \qquad 5.14$$

predicting the proper conditions should be found in (.12)(292 days) or 35 days.

This estimate assumes that all of the probabilities in Equation (5.13) are independent. The probabilities of clear weather, instrument function, and geomagnetic activity are all unrelated of course but $P_{substorm}$ and $P_{\theta \geq 90}$ are certainly related. Periods of substorm activity generally occur following an expansion of the polar cap leading to periods when the dayside oval is overhead or equatorward of the observatory. The estimate of 31 days is therefore a lower limit. If the joint probability $P_{substorm}P_{\theta \geq 90}$ are simply replaced by a single probability ranging from .3 to .056, the resulting number of days for which the luminosity gap should be apparent is then 1 to 20.7 days. The high value is certainly optimistic since it requires observable substorm effects during each period the ground station is located within the 9-12 MLT sector. A range of 3-7 days, however, seems reasonable based on the survey of the Longyearbyen archive and using these values it is expected that long term monitoring of dayside aurorae is required to obtain more of these cases.

## 5.6 Estimate of FTE Contribution to Polar Cap Potential Drop

The analysis presented in Section 5.4 demonstrates only that the drop out events and transient arcs within the dayside auroral oval are consistent with the predicted response of the dayside aurora to impulsive merging at the dayside magnetopause. The results are not adequate to prove that the events are in fact FTE's since simultaneous magnetic field observations from the magnetopause were not available. In this section I will accept the events as FTE signatures for the purpose

Reproduced with permission of the copyright owner. Further reproduction prohibited without permission.

of considering their possible contribution to the cross polar cap potential drop. This is a useful exercise since it will provide an estimate, should the events be validated as FTE signatures, of the importance of the events to magnetospheric energetics. The development is similar to that followed by *Newell and Sibeck* [1993b] who reviewed candidate FTE signatures described in the literature to show that the typical contribution to an active time polar cap potential drop of 100 kV is less than 10% for most candidate FTE events.

Estimates of the average potential contribution $\Delta V_{rec}$ of a candidate FTE event to the cross polar cap potential drop are based on application of Faraday's Law of Induction

$$\frac{d\Phi}{dt} = -\Delta V_{rec} \tag{5.15}$$

to the reconnected field. The magnetic flux $\Phi$ is defined as

$$\Phi = \int \vec{B} \cdot d\vec{S} \tag{5.16}$$

where $\vec{B}$ is the magnetic field within an area $d\vec{S}$. It is useful to apply these equations to the ionospheric end of the reconnected flux in magnetospheric problems for two reasons [*Newell and Sibeck*, 1993b]: first, the cross polar cap potential drop has been well studied by satellites indicating values of 100-150 kV are common for the IMF $B_z < 0$ conditions required for merging and, second, ionospheric plasma is incompressible so only the ionospheric area added to the polar cap per unit time need be considered.

The first method to estimate the average FTE contribution to the polar cap potential drop uses the dimensions and formation rate of the drop out events. Integration of equation (5.16) over an area $A$ of reconnected magnetic field with intensity $B$ within the ionosphere

$$\Phi = BA \tag{5.17}$$

so that application of Faraday's Law to obtain the reconnection potential is

$$\Delta V_{rec} = -\frac{d\Phi}{dt} \approx -\frac{BA}{\Delta t} \tag{5.18}$$

The area of the drop out events is required but only the meridional dimension is known from the auroral records from the latitude shift in auroral emission that forms a drop out event. Dayside auroral events are generally much larger in the zonal direction exceeding the all-sky camera field of view so the longitudinal dimension of the drop out events are not available. Lacking a direct measurement of this dimension from the optical events, satellite estimates of cross section areas for FTE's can be used. The size of the FTE's detected at the magnetopause are on the order of 1 $R_e^2$ [*Saunders et al*, 1984a,b; *Farrugia et al.*, 1987]. Invoking the conservation of magnetic flux between the magnetopause and the ionosphere

$$\Phi_{magnetopause} = \Phi_{ionosphere} \tag{5.19}$$

yields the area of the FTE within the ionosphere

$$A_{ionosphere} = A_{mp} \frac{B_{mp}}{B_{ionosphere}} \tag{5.20}$$

Adopting a dipole magnetic field value of 60,000 nT for the terrestrial field at ionospheric altitudes and 75° magnetic latitude and 60 nT for the field at 10 $R_e$ in the equatorial plane, an area of

Reproduced with permission of the copyright owner. Further reproduction prohibited without permission.

1 $R_e^2$ maps to $1.0 \times 10^{-3}$ $R_e^2$ or $4.1 \times 10^4$ $km^2$. The latitudinal widths of the drop out events listed in Table 5.3 range from 5 km to 24 km with an average of 14 km predicting longitudinal dimensions from 8200 km to 1700 km with an average of 2900 km. To put these results in another perspective, consider that at the azimuthal width of one hour in local time at 75° magnetic latitude is approximately 436 km. The events must span a range of 3.9 hours to almost 19 hours in local time with an average of 6.6 hours. The extreme value would appear to be almost certainly spurious since it suggests half of the auroral oval is an active merging line. The error is most likely the result of adopting a cross sectional area of the FTE at the magnetopause that is too large for the smaller events. In any case, the estimates are consistent with the observations in which all of the events are greater than the field of view of the all-sky camera at 100 km altitude (approximately 800 km).

**Table 5.7**
**Estimated Upper Limit of FTE Contributions to Polar Cap Potential[1]**

| Reference | Ionospheric Dimensions (km) Azimuthal | Longitudinal | Average $\Delta V_{rec}$ (kV) |
|---|---|---|---|
| *Russell and Elphic*, [1984] | | | 20 |
| *Rijnbeek et al.*, [1984] | | | 6 |
| *Goertz et al.*, [1985] | | | 5 |
| *Egeland and Sandholt*, [1992] | 300-500 | 50 | 2 |
| *Denig et al.*, [1993] | | 50-100 | <1 |
| *Lockwood et al.*, [1993c] | 2750 | 300 | 33 |
| *Pinnock et al.*, [1993] | 900 | 100 | 7.1 |
| This work | 2900 | 14 | 9 |
| | 1700 | 14 | 5.3 |
| | 1000 | 14 | 3.1 |
| | 800 | 14 | 2.5 |

[1]From Newell and Sibeck [1993b].

Once the area of the events has been established the average potential may be computed using the interval between events [*Goertz et al.*, 1985; *Lockwood et al.*, 1993a; *Newell and Sibeck*, 1993b]. In the 40 minute interval from 0710 UT to 0750 UT in Figure 5.3 there are approximately 9 drop out events. The average interval between events is therefore approximately 270 seconds. The average potential contribution of the events is therefore

$$\Delta V_{rec} = \frac{(60,000nT)(4.1 \times 10^{10} m^4)}{(270s)} \sim 9kV \tag{5.21}$$

This result is consistent with the upper limits obtained by *Newell and Sibeck* [1993b] for FTE contributions to the polar cap potential which are summarized in Table 5.2 and repeated here in Table 5.7 for continuity. Estimates of the potential contribution are also given for a number of smaller azimuthal dimensions less than the 2900 km estimated from mapping the average FTE

Reproduced with permission of the copyright owner. Further reproduction prohibited without permission.

into the ionosphere. In the case where the azimuthal dimension is 800 km, approximately the all sky camera field of view at 120 km, the potential contribution is only 2.5 kV. This value may be considered a lower limit to the FTE contribution established from ground based observations of transient arcs which are observed to stretch from horizon to horizon in the all sky camera images.

**Table 5.8**
**Reconnection Parameters Estimated From Drop Out Events**

| Onset Time (UT) | Duration[1] (sec) | ~ Distance[2] (km) | $V_{rec}$ (kV) | $E_{rec,i}$ (mV/m) | $E_{rec,mp}$ (mV/m) | $V_d$ (m/s) |
|---|---|---|---|---|---|---|
| 0712:20 | <16 | 24 | 150 | 90 | 2.9 | 1500 |
| 0718:30 | 135 | 23 | 18 | 10 | .32 | 166 |
| 0722:30 | 60 | 5 | 41 | 5 | .16 | 83 |
| 0726:30 | 120 | 21 | 21 | 11 | .35 | 175 |
| 0731:00 | <16 | 11 | 150 | 41 | 1.3 | 690 |
| 0734:00 | 120 | 7 | 21 | 4 | .13 | 58 |
| 0744:00 | 160 | 7 | 15 | 3 | .10 | 43 |

[1]The time required for poleward border of mantle aurora to change from initial to final elevation angle.

[2]Assuming a constant emission altitude of 100 km.

Much larger potentials may be obtained if the duration of the merging event is used in Equation 5.18 rather than the intervals between events. This is equivalent to computing the instantaneous rather than average potential assuming the merging rate varies in time. Examples of instantaneous potentials for the drop out events listed in Table 5.3 are given in Table 5.8 using the same FTE area projected to the ionosphere that was required to obtain the average potentials in Equation 5.18. The two largest values are 150 kV which would suggest that the events represent nearly all of the possible cross polar cap potential drop which may exist during active periods although most of the events are only on the order of 10's of a kilovolt. Since the estimates are based on mapping reported dimensions of FTE's from the magnetopause the results are of course dependent on how often FTE's are of the size adopted for the estimates in equation 5.21 and Table 5.7. The potentials from 15-41 kV are consistent with EISCAT radar observations of 10-50 kV electric potential enhancements associated with ion flow bursts forming simultaneously with transient auroral arcs [*Lockwood et al.*, 1989b].

Estimates of the reconnection electric field $E_{rec}$ may also be obtained from the drop out events by considering that

$$E_{rec} = -\frac{dV_{rec}}{dl} \tag{5.22}$$

where $dl$ is a differential unit of length along the ionospheric projection of the merging line. Integrating along the merging line of length $L$ gives

$$E_{rec}\Delta L = -\Delta V_{rec} \tag{5.23}$$

and substituting equation (5.18) results yields an estimate for the reconnection electric field inde-

Reproduced with permission of the copyright owner. Further reproduction prohibited without permission.

pendent of the length of the merging line

$$E_{rec} = B\frac{\Delta x}{\Delta t} \tag{5.24}$$

where $\Delta x$ is the latitudinal width of a drop out event. Values of the reconnection electric field in the ionosphere are listed in the fifth column of Table 5.8 and mapped to the magnetopause in the sixth column assuming the standard assumption that the ratio $E/\sqrt{B}$ remains constant. The final column are predicted plasma convection velocities using an ionospheric magnetic field magnetic of 60,000 nT and the electric fields listed in the fifth column.

An alternative estimate of the reconnection electric field may be obtained from the transient arcs within the dayside oval using a modification of the technique developed by *de la Beaujardiere et al.* [1991] to measure reconnection electric fields in the night time auroral oval. The method is again based on Faraday's Law of Induction. Inserting equation (5.16) into (5.15) and differentiating yields

$$\frac{d\phi}{dt} = \int_S \frac{\partial \vec{B}}{\partial t} \cdot d\vec{A} \tag{5.25}$$

Use of the Maxwell equation

$$\vec{\nabla} \times \vec{E} = \frac{\partial \vec{B}}{\partial t} \tag{5.26}$$

allows equation (5.25) to be rewritten as

$$\frac{d\phi}{dt} = \int_S (\vec{\nabla} \times \vec{E}) \cdot d\vec{A} \tag{5.27}$$

which is converted to

$$\frac{d\phi}{dt} = \oint \vec{E} \cdot d\vec{l} \tag{5.28}$$

where $d\vec{l}$ is a differential element along the integration path. Integrating around the polar cap boundary where the reconnection electric field $E_{rec}$ is applied only along the ionospheric projection of the merging line and the rest of the path is adiaroic, equation (5.28) is integrated to yield

$$\frac{d\phi}{dt} = E_{rec}\Delta L \tag{5.29}$$

Equation (5.15) can also be written

$$\frac{d\phi}{dt} = \frac{d(BA)}{dt} = B\frac{dA}{dt} \tag{5.30}$$

assuming that the only change to the polar cap is due to a small rectangular region of variable meridional dimension $dx$, fixed length $d\Delta L$, and area $dA = B\Delta L dx$. Equation (5.27) is then

$$\frac{d\phi}{dt} = B\Delta L\frac{dx}{dt} \tag{5.31}$$

However, the relative velocity of plasma with respect to the separatrix is

$$\frac{dx}{dt} = v_{relative} = v_{plasma} - v_{separatrix} \tag{5.32}$$

so

$$\frac{d\phi}{dt} = B\Delta L(v_{plasma} - v_{separatrix}) \tag{5.33}$$

and equating this result with equation (5.29) yields the relation

$$E_{rec} = B(v_{plasma} - v_{separatrix}) \tag{5.34}$$

obtained by *de la Beaujardiere et al.* [1991] for the reconnection electric field. The advantage of

Reproduced with permission of the copyright owner. Further reproduction prohibited without permission.

this method over the use of the drop out events to obtain the electric field is that it may be applied locally since the length of the merging line is not required.

Examples of the reconnection electric field calculated from equation (5.34) are listed in Table 5.9 for selected transient arcs. The meridional component of the arc velocity $V_m$ is computed from the

**Table 5.9**
**Reconnection Parameters Estimated From Transient Auroral Events**

| Onset Time (UT) | $V_m$ (m/s) | $V_{separatrix}$ (m/s) | $V_{rel}$ (m/s) | $E^1_{rec,i}$ (mV/m) | $E_{rec,mp}$ (mV/m) |
|---|---|---|---|---|---|
| 0715:30 | 420 | ~36 | 456 | 27 | .85 |
| 0721:00 | 560 | ~36 | 596 | 36 | 1.2 |
| 0724:00 | 700 | ~36 | 736 | 44 | 1.4 |
| 0728:00 | — | | | | |
| 0732:30 | 525 | ~0 | 525 | 32 | 1.0 |
| 0736:20 | 900 | ~0 | 900 | 54 | 1.7 |
| 0746:00 | 700 | ~0 | 700 | 42 | 1.3 |

[1] A value of 60,000 nT was assumed for the terrestrial field magnitude.

photometer plot in Figure 5.2 assuming an emission altitude of 100 km for the 557.7 nm component of the arc. Motion of the separatrix is obtained from the magnetic latitude of the equatorward edge of the latitudinal gap as a function of time listed in Table 5.2. The latitude decreases at an average rate of 0.2° in 10 minutes (36 m/s) from 0710 UT to 0730 UT and remains relatively constant thereafter. A value of 60,000 nT was used for the magnitude of the magnetic field in the polar ionosphere. Reconnection electric fields are on the order of 10's of mV/m within the ionosphere and approximately 1 mV/m when mapped to the magnetopause.

Estimates of the dayside reconnection rate in terms of the reconnection electric field available in the literature are listed in Table 5.10 for comparison with the results presented in Table 5.9 Values in parenthesis are the original results reported by the authors mapped along the field to obtain the electric field magnitudes within the ionosphere or at the magnetopause as required. *Lockwood et al.* [1995] and *Lockwood and Davis* [1996] used the ion energy dispersion characteristics in energy spectra obtained by the DMSP satellites during traverses of the low altitude cusp to estimate the magnitude of the reconnection electric field at the magnetopause. The values were variable ranging from minimums of 0 mV/m to maximums of 6 mV/m indicative of impulsive reconnection processes. The maximum values are best compared to the results in Table 5.8 since the electric field is expected to maximize during the lifetime of the transient arc [*Lockwood et al.*, 1989b]. Values of the reconnection electric field during impulsive increases in reconnection rate obtained by *Lockwood and Davis* [1996] are 1.3 mV/m, 6 mV/m, 3.7 mV/m, 0.5 mV/m, and 1.25 mV/m which are consistent with the results presented here. *Basinska et al.* [1989] showed electric fields of 50-100 mV/m within small scale vortical features they argued were due to FTE's, on the same order of magnitude of the values obtained from the drop out events and transient arcs given in

Reproduced with permission of the copyright owner. Further reproduction prohibited without permission.

Tables 5.8 and 5.9, respectively. *Shelley et al.* [1976] studied mass spectrometer measurements of $He^{++}$ and $H^{+}$ to obtain a values of 30-60 mV/m dawn-dusk electric field within the cusp. An electric field of 4 mV/m near the magnetopause was reported by *Maynard et al.* [1991], larger than any value obtained here yet within the same order of magnitude. Finally, electric fields of 10-100 mV/m within the ionosphere due to FTE's are predicted theoretically [*Lee*, 1986]. In summary, the ionospheric electric fields are approximately $10^1$ mV/m to $10^2$ mV/m while values applicable to the magnetopause are $10^{-1}$ mV/m to $10^1$ mV/m, consistent with the values obtained from the drop out events listed in Table 5.8 and those from the transient poleward moving auroral arcs listed in Table 5.9.

**Table 5.10**
**Reconnection Electric Fields from Literature[1]**

| Reference | $E^1_{rec,i}$ (mV/m) | $E_{rec,mp}$ (mV/m) |
|---|---|---|
| *Shelley et al.*, 1976 | 30-60 | (.96-1.9) |
| *Lee*, 1986 | 10-100 | (.32-3.2) |
| *Basinska et al.*, 1989 | 50-100 | (1.6-3.2) |
| *Maynard et al.*, 1991 | (125) | 4 |
| *Lockwood and Davis*, 1996 | 16-190 | 0.5-6[2] |

[1] Values in parenthesis have been mapped along the magnetic field using values of 60 nT and 60,000 nT for the magnetic field at the magnetopause and in the ionosphere, respectively.
[2]Values were variable, those listed here are the range of peak reconnection rates.

## 5.7 Conclusions

A set of dayside auroral observations have been presented describing a number of previously known features including:

(1) Transient poleward drifting auroral arcs dominated by red 630.0 nm emission produced by low energy electrons at high altitudes. These arcs are thought to result from magnetosheath plasma injected into the cusp by magnetic field reconnection at the dayside magnetopause.

(2) Equatorward of the transient arcs is a broad region of pulsating patches in the diffuse 557.7 nm aurora termed the "mantle" aurora. This aurora is produced by energetic electrons from populations trapped on closed field lines within the outer regions of the radiation belts. Pitch angle scattering due to a wave-particle interaction yields fluxes of particles within the atmospheric loss cone resulting in particle precipitation and the formation of the mantle aurora.

(3) A region of pulsating 557.7 nm emissions is observed in meridional photometer scans poleward of diffuse 557.7 nm aurora excited by electrons in the hard precipitation zone and equatorward of the dayside auroral oval. The width of the region reported by

Reproduced with permission of the copyright owner. Further reproduction prohibited without permission.

*Yagodkina et al.* [1989,1990] is on the order of 5° to 6° in latitude and was attributed to the quasi-trapping region.

A narrow region of continuously reduced 557.7 nm emissions between the poleward border of the mantle aurora and the equatorward boundary of the dayside auroral oval was described. This "latitudinal gap" is not the "intensity dip" reported by *Yagodkina et al.* [1989,1990]. since the dip is filled with pulsating aurora and is on the order of 500-600 km in width. Descriptions of previously undescribed phenomena occurring on the boundaries of the latitudinal gap include the identification of "drop out" events in the poleward border of the mantle aurora, correlations between the drop outs and the formation approximately 2 minutes later of a transient 630.0 nm dominated poleward drifting arc, and a region of nearly constant 557.7 nm emission on the poleward border of the mantle aurora.

The poleward moving 630.0 nm dominated arcs are typical of the auroral forms suggested to be the ionospheric signature of flux transfer events. This thesis provides an interpretation of the new observations as well as the origin of the latitudinal gap in terms of the reconnection model which successfully explains a number of features of the auroral display including the width of the intensity dip, the correlations between the events on the borders of the 557.7 nm and 630.0 nm emission formed by ring current electrons scattered into the atmosphere and magnetosheath electrons injected in the cusp, respectively.

Differences in flight times from the dayside magnetopause provide an explanation for the origin of the latitudinal gap in the 557.7 nm emission. Energetic electrons lost to the atmosphere from the ring current move rapidly along field lines and suffer little displacement due to electric field drifts. Electrons with energies in the keV range will arrive in the ionosphere within a few kilometers poleward of their initial field line (for $B_z < 0$) conditions, producing luminosity in regions of the ionosphere threaded by closed field lines. Electrons and ions from the magnetosheath are injected into the cusp as a quasi-neutral plasma. The velocity of the magnetosheath plasma is governed by the more massive ions and the electrons travel at the same velocity to maintain the quasi-neutrality. At typical ion energies of $\sim 1keV$ approximately 2-3 minutes is required for the magnetosheath plasma to arrive in the ionosphere. During this period electric field drifts carry the plasma approximately 80-100 km poleward, consistent with the width of the intensity dip. The origin of the latitudinal gap is therefore due to the differences in travel times for high energy electrons lost from the outer edge of the ring currents near the edge of the magnetosphere and cold plasma injected into the cusp on field lines which pass through the dayside magnetopause. It was noted that identification of the poleward border of the diffuse 557.7 nm aurora as the boundary between regions containing ring current electrons and regions devoid of ring current electrons is consistent with the identification of the boundary as the ionospheric projection of the the separatrix.

Drop outs in the poleward border of the mantle aurora and the equatorward boundary of the dayside auroral oval were shown to be correlated, the drop outs in the 557.7 nm signal preceding the formation of 630.0 nm dominated transient arcs by approximately 2 minutes, consistent with the time required for 1 $keV$ protons to travel from the subsolar magnetopause to the ionosphere. The correlation between the events suggests that the drop outs on the poleward border of the

Reproduced with permission of the copyright owner. Further reproduction prohibited without permission.

mantle aurora and the transient 630.0 nm arcs, previously identified as strong candidates for the auroral signature of flux transfer events, are formed by the same physical process.

Interpretation of the correlation between events forming on both sides of the latitudinal gap in terms of particle signatures of flux transfer events and the origin of the latitudinal gap due to differences in flight times provides a successful model for the events. In this description the drop outs are due to a rapid loss of formerly trapped high energy particles on recently merged field lines within flux transfer events so that insufficient electrons are available for scattering into the atmospheric loss cone to produce an auroral emission. The formation of the transient poleward moving auroral forms 80-100 km poleward of the poleward boundary of the mantle aurora and following the drop outs in time by approximately 2 minutes is consistent with the time required for cold magnetosheath plasma to travel from the subsolar magnetopause to the ionosphere. This interpretation of the correlations between the behavior of electrons on either side of the latitudinal intensity gap provides new evidence supporting the conclusion that poleward moving forms are manifestations of impulsive reconnection. Not only are the transient aurorae formed by impulsive reconnection but the particle populations in the outer regions of the magnetosphere are affected as well.

Attempts to invoke the plasma transfer event (PTE) model requiring the impulsive penetration of solar wind plasma across the magnetopause boundary to explain the events are not successful. The trajectory of the PTE after crossing the magnetopause boundary will take the enhanced plasma density region further into the the magnetosphere on closed field lines. The impulsive penetration model suggests that electric fields induced by charge separation within the penetrating plasma structure accelerate plasma into the ionosphere producing the dayside aurora. The trajectory of the penetrating plasma structure is deeper into the closed field line region of the magnetosphere predicting that auroral features associated with the PTE must form near the open/closed field line boundary and move equatorward, not poleward as observed [*Goertz et al.*, 1985; *Sandholt et al.*, 1986]. The observations presented here are consistent with the FTE model but do not support the PTE model.

The emission rate for 557.7 nm emissions within the intensity dip is reduced from values found in either the diffuse 557.7 nm aurora and the transient poleward moving arcs but is greater than the airglow background. Emission of 557.7 nm photons with no change in the 630.0 nm signal within the intensity dip requires a reduced flux of high energy particles within the gap. Three possible sources of these particles were considered in this thesis:

(a) formerly trapped ring current particles which leak from the magnetosphere when they drift through the magnetopause into the magnetosheath,

(b) high energy electrons from the boundary layer injected during field line merging which forming the low latitude boundary layer on open field lines between the separatrix and the location at which the cold magnetosheath plasma arrives in the ionosphere, and

(c) dispersed arrival locations of ring current particles from flux transfer events. Each of these mechanisms are equally plausible and may contribute to the emission rate within the intensity dip.

Reproduced with permission of the copyright owner. Further reproduction prohibited without permission.

The continuous emission on the poleward edge of the mantle aurora requires a continuous particle source in contrast to the impulsive nature of the electron precipitation producing the auroral pulsations further equatorward. I have proposed that satellite observations presented by [*Gurnett et al.*, 1979] of enhanced electromagnetic wave turbulence accompanied by an increase in the flux of 1-6 keV electrons in a narrow region near the magnetopause boundary are a plausible source of the continuous emissions. The emission is continuous since the enhanced wave activity produces a continuous supply of $> 1keV$ electrons, consistent with the evidence presented by *Gurnett etal.* [1979] that the electromagnetic wave and high energy electron enhancements were found on each encounter of the magnetopause. This interpretation further supports the identification of the poleward boundary of the diffuse 557.7 nm aurora as the separatrix.

An estimate of the number of days the intensity dip can be observed is presented. It is shown that although relatively few intervals have been found in the archive of Longyearbyen photometer records, the number is consistent with the theoretical number of times the events should be observed.

Interpretation of the events in terms of merging suggest that dayside auroral records from ground sites may be used to identify the separatrix between open and closed magnetic field lines and also to verify identification of the cusp in radar studies as well as provide a method of obtaining merging rates to compare with estimates obtained by radar. While the auroral observations have been successfully interpreted in terms of impulsive magnetic field reconnection, conclusive evidence for associating the transient aurora with FTE's must await further work since no direct evidence that FTE's are actually forming at the magnetopause during the period included in the study. Satellite observations demonstrating the present of FTE's at the dayside magnetopause coincident in time and on conjugate field lines as the mantle aurora drop outs and formation of the transient aurora would provide the required direct observation. Similarly, the few events that have been found to date suggest that further observations are required to confirm that under the proper circumstances drop outs in the poleward border of the mantle aurora will always be correlated with the subsequent formation of transient poleward moving auroral arcs.

Reproduced with permission of the copyright owner. Further reproduction prohibited without permission.

# Chapter 6.
## Summary of Thesis, Caveats, and Suggestions for Further Work

Charged particles producing midday auroral displays originate in the shocked solar wind plasma within the magnetosheath and the Earth's outer radiation belts suggesting that monitoring auroral displays can provide useful information on the interaction of the solar wind with the Earth's magnetosphere. *In situ* measurements of magnetic field and plasma characteristics obtained by satellites penetrating the magnetopause provide detailed information on conditions at the magnetospheric boundary, but only at the location of the satellite. Observations of variations in the magnetic field or plasma parameters are often ambiguous as to whether they represent spatial or temporal changes (or perhaps both). Ground based observations offer the advantage of a fixed observation site yielding both spatial and temporal information about auroral displays. If characteristics of the dayside auroral displays can be uniquely identified with specific processes at the magnetopause, the ground based auroral observations may be used as a convenient monitor of spatial and temporal variations in the solar wind-magnetosphere interaction. The use of dayside aurorae as a ground based monitor of magnetopause activity was the basis of the investigations described in this thesis.

A brief introduction to dayside aurora was presented in Chapter 1. Chapter 2 outlined the basic physics of the solar wind, magnetospheric structure, and mechanisms which are capable of transferring solar wind energy into the magnetosphere. The spectral characteristics and morphology of dayside auroral displays was described in Chapter 3 to provide a background to the observations described in this thesis.

The use of dayside aurora as a ground-based monitor of magnetopause was explored in two independent studies. The first, presented in Chapter 4 considered the origin and morphology of diffuse [OI] 630.0 nm emissions in the midday auroral oval. The continuous presence of red line emissions has been interpreted as evidence that the discrete limit of the pulsed cusp model developed by *Lockwood and Smith* [1992] can never be realized. The study described here considers satellite observations of precipitated electron fluxes within the cusp in relation to ground based observations of transient poleward moving auroral arcs and diffuse background 630.0 nm emissions. Results from Chapter 4 are described further in Section 6.1. A case study of dayside auroral emissions was presented in Chapter 5 relating temporal variations of the poleward boundary of the diffuse 557.7 nm mantle aurora with the formation of transient 630.0 nm auroral arcs in the dayside auroral oval. An interpretation of the events in the midday sector in terms of impulsive magnetic reconnection was proposed yielding a new observation relating dayside aurora to flux transfer events. Results from the case study are described in Section 6.2

### 6.1 Chapter 4: Diffuse 630.0 nm Emissions in Midday Aurora

The subject of diffuse 630.0 nm emissions in the midday auroral oval was introduced with the description of 557.7 nm and 630.0 nm photometer records obtained on 10 January 1992 at Longyearbyen, Svalbard, in Section 4.2. A series of transient poleward moving auroral arcs are

Reproduced with permission of the copyright owner. Further reproduction prohibited without permission.

present typical of the transient optical phenomenon associated with impulsive magnetic reconnection. Two types of persistent 630.0 nm emissions are noted: the first is a diffuse background in which the entire transient arc sequence is imbedded and the second a narrow arc-like feature on the equatorward edge of the dayside oval.

Precipitating electron energies and energy fluxes measured by low altitude satellites within the cusp are examined in Section 4.4 to determine the auroral morphology predicted from the incident particle populations on top of the atmosphere. Estimated intensities of the 557.7 nm and 630.0 nm emissions were obtained for three cases. First, it is pointed out in Section 4.4.1 that an electron population must have an energy flux sufficient to produce a 0.5-1 kR 630.0 nm emissions if it is to meet the criteria established by *Newell and Meng* [1988] to be classified as cusp. The satellite observations therefore predict that ground based observations of the cusp will always detect a strong red line emission. Second, latitudinal structure of electron fluxes predicted by models of magnetosheath plasma entry are examined in Section 4.4.2. Theoretical models (even the recent *Wing et al.* [1996] model which yields the most realistic distributions of electrons in the polar cusp, plasma mantle and polar cap to date) predict structureless electron fluxes throughout the cusp and, therefore, structureless 630.0 nm emissions. The presence of an ambipolar electric field required to ensure charge neutrality is identified as the origin of the diffuse electron fluxes. Motion of the precipitating electrons, due to their much smaller mass than ions, is governed by the ions within the magnetosheath plasma. Electron fluxes within the cusp are distributed ensure that the magnetosheath plasma remains quasi-neutral. The background electron fluxes are expected to remain diffuse even if merging occurs in the extreme limit of completely discrete events because the average interval between merging events is less than the time required for low energy ions to arrive in the ionosphere from the merging site. Discrete merging events result in ion injections overlapping in space and time at low altitudes producing a continuous flux of ions in the polar cusp. The electron flux required to ensure quasi-neutrality will similarly be continuously present at low altitudes. One component of the diffuse 630.0 nm background is the unstructured electron fluxes required to ensure quasi-neutrality.

The theoretical models are only an idealization of the actual processes present in the cusp since, as shown in Section 4.4.3, observations of electron fluxes within the cusp often show significant structure. Narrow electron features with widths of 10's of kilometers are often found in the cusp characterized by enhancements of the energy flux an order of magnitude above the unstructured background electron flux. The average energy within these events is often 500-700 eV, greater than the 100-200 eV typical of magnetosheath plasma within the cusp, suggesting the events are due to acceleration of the magnetosheath plasma. The relative importance of the structured electron events to energy deposition by particle impact in the cusp is estimated. It is found that 80% to 90% of the energy deposited within the cusp is due to the structured electron events, consistent with the ground based observation that dayside aurora is bright, discrete auroral arcs imbedded in a weak background emission.

The development of an auroral model is presented in Section 4.5 to study the morphology of 630.0 nm emissions produced by the transient arcs. While the satellite observations can provide useful information on distributions and energies of precipitating electrons they cannot be used

Reproduced with permission of the copyright owner. Further reproduction prohibited without permission.

to determine the time dependence of 630.0 nm emissions produced by moving auroral arcs. The auroral model is used to compute the [OI] 630.0 nm auroral emissions that would be observed from the ground if populations of excited neutral atomic oxygen are formed by the poleward drift of a series of latitudinally thin auroral arcs.

The formation rate of the dayside transients is such that the populations of excited atomic oxygen in the metastable $O(^1D)$ state will not have sufficient time to decay to background levels before reexcitation by a new flux of precipitating electrons arriving in a subsequent arc. Thus, the 630.0 nm emissions observed by ground based photometers will show an apparent persistent emission in the region of the transient arcs even in the case where the only source of electron precipitation is discrete arcs. The simple model of discrete auroral events with no extra particle source to produce a diffuse persistent emission is capable of reproducing the 630.0 nm emissions observed in dayside aurora.

The model demonstrates a diffuse 630.0 nm background emission will form due to production of $O(^1D)$ by the transient arcs sweeping poleward through the cusp. Sequences of transient arcs are imbedded in the diffuse background because they are a significant contribution to the background. A significant result from the model study is that diffuse 630.0 nm emissions which have been interpreted as prima facie evidence for continuous particle transport into the polar cusp may be explained by production of long lived metastable states within discrete auroral events.

In summary, two sources of diffuse background 630.0 nm emissions are described in Chapter 4. First, a relatively constant 0.5-1 kR 630.0 nm component produced by precipitating magnetosheath electrons required to maintain charge quasi-neutrality within the cusp. Second, the spatially and temporally varying 630.0 nm emissions produced by remnant populations of $O(^1D)$ excited by the passage of transient auroral arcs. Both sources will result in a diffuse 630.0 nm emission even if dayside merging allows access of the magnetosheath plasma to the cusp in discrete bursts. I must emphasize that the results from the auroral model do not prove that dayside merging only occurs in discrete bursts. The results from Chapter 4 only show that 630.0 nm emissions due to diffuse electron fluxes in the cusp and remnant populations of $O(^1D)$ excited by transient arcs cannot be used as evidence to discount the discrete limit of the pulsed cusp model.

Further work on the persistent 630.0 nm aurora would benefit from a more sophisticated auroral model. The simple model presented here was only capable of describing the first order effects due to production and quenching within narrow arcs. Interesting phenomenon such as enhanced 630.0 nm production at high altitudes due to electron heating is also expected (Section 4.7.1) which may be modeled if the electron temperatures are coupled into the model along with a self consistent ion chemistry.

Examination of the 630.0 nm morphology for case studies in which neutral wind values and ion drift measurements are available would also provide interesting results. Neutral wind and drift values adopted in Chapter 4 resulted in synthetic photometer records which compared favorably in a general sense with observations of midday aurora. More detailed and critical examination of neutral wind effects may be made if the actual neutral wind and ion convection velocity can be measured.

Reproduced with permission of the copyright owner. Further reproduction prohibited without permission.

### 6.2 Chapter 5: Drop Outs and Transient Arcs

Flux transfer events (FTE) are widely believed to be the magnetic field signature of an impulsive increase in the dayside magnetic reconnection rate. The search for ionospheric signatures of flux transfer events has received considerable attention in recent years motivated by the interest in monitoring dayside plasma processes using ground based observations. The candidate auroral events most widely accepted to date as the ionospheric signature of FTE's are poleward drifting auroral arcs typical of midday auroral displays.

Evidence that an individual transient arc is a causal result of an individual FTE consists primarily of comparisons between average characteristics (repetition periods, drift rates, drift directions, strong correlation with southward IMF $B_z$ orientation) of the auroral phenomenon with the predicted ionospheric response to pulses of dayside merging. If a causal relationship can be established then the use of ground based optical observations of transient arcs can be considered a valid method of monitoring the energy transfer rate across the dayside magnetopause.

A dayside auroral display was described in Chapter 5 featuring transient poleward moving auroral arcs poleward of a strong pulsating mantle aurora. The display also exhibited a number of previously undescribed features:

(1) A "latitudinal gap" in 557.7 nm emissions approximately 50-100 km in width between the poleward border of the mantle aurora and the equatorward border of the dayside auroral oval.

(2) A series of "drop out" events on the poleward edge of the mantle aurora in which the 557.7 nm luminosity decreases to values found in the latitudinal gap.

(3) The drop out events are followed by the formation of transient poleward moving arcs in the dayside auroral oval.

(4) A narrow region of continuous 557.7 nm emission on the poleward border of the pulsating mantle aurora.

An explanation of the latitudinal gap was proposed based on differences in ion travel times from the dayside magnetopause to the ionosphere in the presence of a dawn-dusk electric field. The high energy ions of the magnetosheath plasma (and electrons required for quasi-neutrality) require approximately 2-3 minutes to arrive in the ionosphere after crossing the magnetopause. During this period electric field drifts carry the plasma approximately 80-100 km poleward of the latitude at which they were initially injected. Trapped populations of energetic electrons in the outer ring current move rapidly along field lines and suffer little displacement due to electric field drifts. If scattered into the atmospheric loss cone, electrons with energies in the >5-10 keV range will convect only a few kilometers poleward before encountering the ionosphere. Auroral luminosity produced by these electrons marks regions of the ionosphere threaded by closed field lines. Electrons precipitating on field lines near the magnetopause will mark the ionospheric projection of the separatrix. The latitudinal gap is the region poleward of the separatrix but equatorward of the minimum latitude at which magnetosheath plasma has access to the ionosphere.

Correlations between the drop out events forming on the equatorward edge of the latitudinal gap and transient arcs on the poleward edge suggests that the phenomenon are due to a process

Reproduced with permission of the copyright owner. Further reproduction prohibited without permission.

converting closed magnetic field lines to open field lines. The impulsive nature of the process (i.e., discrete events) suggested an interpretation in terms flux transfer events. It was shown that the drop outs are consistent with a rapid loss of the trapped energetic electron populations which were the source of the pulsating aurora. The formerly trapped population is free to flow out of the magnetosphere on recently merged field lines. Reducing of the number of electrons available for scattering into the atmospheric loss cone results in a reduction in the auroral emission at the poleward border of the mantle aurora.

The formation of the transient poleward moving auroral forms 80-100 km poleward of the poleward boundary of the mantle aurora and following the drop outs in time by approximately 2 minutes is consistent with the time required for cold magnetosheath plasma to travel from the subsolar magnetopause to the ionosphere. This interpretation of the correlations between the behavior of electrons on either side of the latitudinal intensity gap provides new evidence supporting the conclusion that poleward moving forms are manifestations of impulsive reconnection. Not only are the transient aurorae formed by impulsive reconnection but the particle populations in the outer regions of the magnetosphere are affected as well.

It was noted in the introduction that one of the problems in accepting the *Elphic et al.* [1990] satellite/ground based study as confirmation of a causal relationship between FTE's and transient arcs on a one-to-one basis is that only the single series of events have ever been reported. A similar caveat exists in the auroral observations presented here. Although it was shown that the drop outs in the mantle aurora are correlated with the formation of transient arcs within the error of the measurements, only a single set of records was described. A limited set of similar records exist in the Longyearbyen data base providing some confidence the records are not a single unique event but represent a specific process. Continued accumulation of auroral records (or examination of records from Ny Ålesund or South Pole) must produce more such events under the proper geophysical conditions. If more of the drop out/transient arc correlations are not forthcoming, then the data set examined here is due to spurious correlations and another explanation for the events must be proposed. A large number of periods will allow the search for "signature" events such as long intervals (>7-15 minutes) between drop out events with similar intervals between individual transients. It may be possible to observe these events with the Polar satellite if the imager turns out to have the necessary sensitivity. This would be fortuitous as a very large number of auroral observations may be obtained without regard to weather conditions.

Ground based observations still have much to contribute due to their greater spatial and temporal resolution than is possible with a satellite imager. A series of all sky images or images centered on approximately 45° of the magnetic zenith obtained by a camera fitted with a bandpass filter would be the easiest method of obtaining further information. The choice of wavelength for the filter is governed by the desire to select an emission with a short radiative lifetime (less than the duty cycle of the imager) resulting predominantly from electron impact. Options include 557.7 nm or one of the high lying states producing either 777.4 nm or 844.6 nm. The green line is the brightest of the three allowing observations to be obtained at very low intensities. Even though there are possible chemical contributions to production of the excited state the lifetime is sufficiently small that the state is rapidly deactivated. The latter two lines of neutral atomic

Reproduced with permission of the copyright owner. Further reproduction prohibited without permission.

oxygen have an advantage since the airglow and astronomical background emission is reduced at these wavelengths relative to 557.7 nm [c.f., the work by *Shefov*, 1959 reproduced in Figure 9.6 of *Chamberlain*, 1961]. In addition, scattering is less efficient for longer wavelengths reducing possible scattering contributions within the latitudinal gap. Both are allowed transitions which avoids contributions due to transport of the excited species. This allows an improved estimate of the energy input into the atmosphere within the latitudinal gap due to solely to particle precipitation than was possible with the wavelengths in use in the analysis in Chapter 5.

Collaborative studies using optics, radars, and satellites is also desired to provide information on the velocity of the ambient ion flow in the vicinity of the drop out events and the transient arcs. Quantitative tests of the model proposed to explain the gap width may be conducted if values of the ion drift velocity and the energy of the precipitating ions are known.

Finally, a feature of the diffuse auroral oval that may be confused with drop outs are the "omega bands" and "auroral torch" structures which form on the poleward edge of the mantle aurora in the morning sector and drifting eastwards towards noon [*Akasofu*, 1974; *Lyons and Fennel*, 1986; *Tagirov*, 1993]. The possibility that the drop outs were omega bands was considered in the work discussed in Chapter 5 and subsequently eliminated because the morphology of the drop outs was inconsistent with the descriptions of the auroral torch or omega bands given by *Oguti et al.* [1981] and *Tagirov* [1993]. A more sophisticated study requiring a magnetometer array may be used to confirm this assumption by looking for the characteristic magnetic field variations which accompany the omega bands [*Andre and Baumjohann*, 1982; *Opgenoorth et al.*, 1983].

Reproduced with permission of the copyright owner. Further reproduction prohibited without permission.

# Appendix A The Meridian Scanning Photometer

## A.1 Introduction

The meridian scanning photometer (MSP) has been widely used as a standard method of obtaining records of airglow and auroral emissions. Descriptions of the instrument have been given by *Hunten* [1955, 1956], *Roach* [1957], *Eather and Reasoner* [1969], and *Romick* [1964, 1976]. The appendix will begin with a brief overview of the meridian scanning photometer followed by discussions of aspects of the photometer systems important to the use in the auroral observations presented in Chapters 4 and 5.

The MSP obtains records of the integrated photon emission rate along a line of sight at standard wavelengths in the magnetic meridian plane. The detector system consists of five individual photomultiplier tubes and associated counting electronics. Thermal noise is reduced within the photomultiplier tubes by cooling to approximately -30° C. Narrow band pass interference filters are used to isolate spectral regions of interest. Light from the magnetic meridian plane (approximately 45° west of geographic north) is collected by a mirror rotating continuously about an axis perpendicular to the meridian plane and parallel to the optical axis of the photometer systems. The rotation rate is 4 seconds per revolution with 2 seconds required to sample the sky from northern horizon to southern horizon. The angular resolution of each photometer is approximately 1° with 0.01 second required to sample each one degree in elevation angle. The photometer system was controlled by a Nova computer and the data logged on 9-track magnetic tape prior to the 1993/1994 field season when the computer was replaced by a personal computer and the data files logged on a hard disk with tape backup.

## A.2 Location of the Station and Observation Geometry

The scan plane of the MSP is aligned with the axis of the station, -45 degrees from the geographic north-south meridian (i.e., in the 135° - 315° azimuth plane). The station orientation was chosen empirically to fix the major and minor axis perpendicular and parallel, respectively, to the local L-shell. (*R.W. Smith*, personal communication, 1992). The choice, however, results in a scan plane that is not coaligned with any of the standard magnetic coordinate systems. The magnetic meridian according to the PACE system [*Baker et al.*, 1992] is approximately -35 degrees from geographic north. All of the optical systems in the station are adjusted to coalign with the axis of the building and are similarly misaligned with the magnetic axis.

The station is located at 78.2 deg N and 15.7 ° E geographic latitude and longitude with geomagnetic coordinates of 74.9° N and 114.7° E (in the PACE system). Although the local time that is equivalent to magnetic noon varies, it is generally near 0830-0900 UT (for example, 08:45 UT on 15 December 1990 is 1202 MLT).

Reproduced with permission of the copyright owner. Further reproduction prohibited without permission.

### A.2.1 Mapping Photometer Records to Geographic and Geomagnetic Latitudes

The geometry for an arbitrary observation by a photometer at S with latitude $lt$, longitude $ln$, and altitude $h_s$ along a line of sight at elevation angle $el$ and azimuth $az$ to a point P is given in Figure A.1(a). The distance between the station S and observation point P is $d$ and the altitude of the observation is $z$.

Two coordinate systems are useful to describe the observations. The first is a local cartesian reference frame for observations at the ground station at altitude $h_s$ defined by unit vectors $\hat{x}_s$ eastward from the station, $\vec{y}_s$ northward, and $\hat{z}_s = \hat{x}_s \times \hat{y}_s$ radially outward completing the right handed coordinate system. The origin of the system is the station. The azimuth angle $az$ is zero at geographic north and increases in a clockwise direction through east. The elevation angle $el$ is zero on the northern horizon and increases through 90° in the zenith and 180° on the southern horizon. A separate cartesian geocentric reference frame is defined with the origin at the center of the Earth and unit vectors $\hat{x}_{s,e}$ and $\vec{y}_{s,e}$ in the ecliptic plane with $\hat{x}_{s,e}$ in the direction of the sun and $\vec{y}_{s,e}$ perpendicular to $\hat{x}_{s,e}$ east, and $\hat{z}_{s,e}$ perpendicular to the ecliptic plane with $\hat{z}_{s,e} = \hat{x}_{s,e} \times \hat{y}_{s,e}$.

Coordinates of the station S in the cartesian geocentric reference frame are given by

$$x_{S,e} = (R_E + h_s)cos(lt)cos(ln) \qquad (A.1.a)$$

$$y_{S,e} = (R_E + h_s)cos(lt)cos(ln) \qquad (A.1.b)$$

$$z_{S,e} = (R_E + h_s)cos(lt)cos(ln) \qquad (A.1.c)$$

The latitude shift of the point P from S is obtained by solving the triangle SPO. The angle $\alpha$ is determined from the Law of Sines

$$sin(\alpha) = \frac{h_s + R_E}{z + R_E} sin(el + 90°) \qquad (A.2)$$

so that

$$\alpha = arcsin\left[\frac{h_s + R_E}{z + R_E} sin(el + 90°)\right] \qquad (A.3)$$

and using the sum of the triangles interior angles yields

$$\gamma = 90° - el - \alpha \qquad (A.4)$$

for the angle between the station and the observation point.

Reproduced with permission of the copyright owner. Further reproduction prohibited without permission.

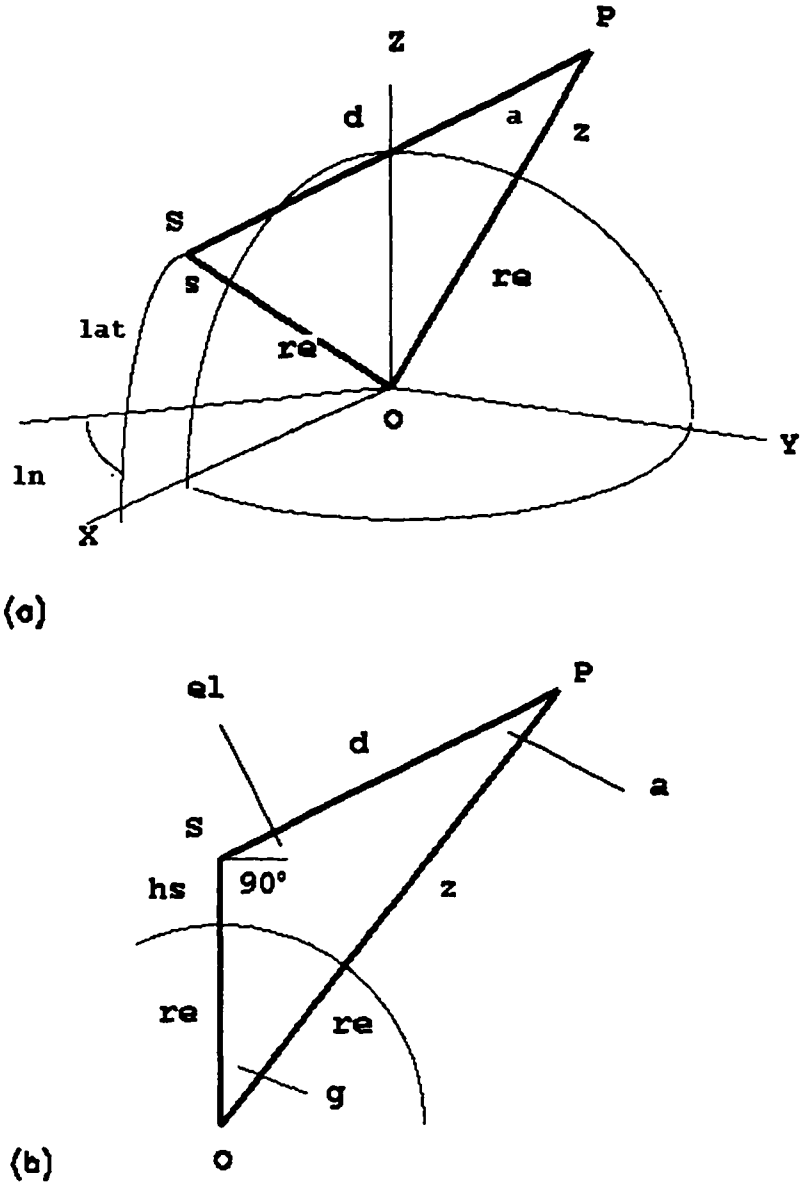


Figure A.1 Observation Geometry between Station and an Arbitrary Point. (a) Schematic of the observation geometry. The observation point P is located at an altitude z above the Earth's surface at a distance d from the station S. The difference in latitude and longitude from the station to the observation point is desired in terms of the elevation angle and azimuth of line of sight between S and P. (b) Solving the triangle SPO is required to obtain the shift in the latitude and longitude from the station to the observation point. Details of the computation are given in the text.

Reproduced with permission of the copyright owner. Further reproduction prohibited without permission.

The distance from the station to the observation point P is determined by applying the Law of Cosines

$$d = \sqrt{(h_s + R_E)^2 + (z + R_E)^2 - 2(h_s + R_E)(z + R_E)cos(\gamma)} \qquad (A.5)$$

The components of this distance in the local cartesian reference frame of the station is

$$d_{x,S} = dcos(el)sin(az) \qquad (A.6.a)$$

$$d_{y,S} = dcos(el)cos(az) \qquad (A.6.b)$$

$$d_{z,S} = dsin(el) \qquad (A.6.c)$$

To obtain the components of $d$ given in $A.6$ in the cartesian geocentric reference frame requires a rotation about the station $x$ axis by an angle

$$r_1 = -(90° - lt) \qquad (A.7.a)$$

aligning the station and geocentric $z$ axis followed by a subsequent rotation about the colinear station and geocentric $z$ axis through an angle

$$r_2 = -(270° - ln) \qquad (A.7.b)$$

aligning the station and geocentric $x$ and $y$ axis. Performing the rotation, the distance in the geocentric reference frame is given by

$$d_{x,e} = \quad d_{x,S}cos(r_2) + d_{y,S}sin(r_2)cos(r_1) + d_{z,S}sin(r_2)sin(r_1) \qquad (A.8.a)$$

$$d_{y,e} = -d_{x,S}sin(r_2) + d_{y,S}cos(r_2)cos(r_1) + d_{z,S}cos(r_2)sin(r_1) \qquad (A.8.b)$$

$$d_{z,e} = -d_{y,S}sin(r_1) + d_{z,S}cos(r_1) \qquad (A.8.c)$$

The station coordinates and the distance to the observation point are now in the cartesian geocentric reference frame. The cartesian location of the observation point is simply given by

$$x_{O,e} = x_{S,e} + d_{x,e} \qquad (A.9.a)$$

$$y_{O,e} = y_{S,e} + d_{y,e} \qquad (A.9.b)$$

$$z_{O,e} = z_{S,e} + d_{z,e} \qquad (A.9.c)$$

and the shift in the longitude $\delta(ln_P)$ and latitude $\delta(lt_P)$ of the observation point from the station latitude and longitude is given by the relations

$$\delta ln_P = arctan[y_{O,e}/x_{O,e}] \qquad (A.10.a)$$

$$\delta lt_P = arctan\left[\frac{z_{O,e}}{\sqrt{x_{O,e}^2 + x_{O,e}^2}}\right] \qquad (A.10.b)$$

These equation are generally valid for an arbitrary line of sight at any azimuth and elevation angle.

Reproduced with permission of the copyright owner. Further reproduction prohibited without permission.

If in the preceding development the geocentric reference frame is treated as the magnetic coordinate system then the equations can also be used to obtain shifts in magnetic latitude and longitude for an observation point a distance along a given line of sight at any geomagnetic azimuth and elevation angle. The MSP scan plane is fixed in the magnetic meridian plane so the observations are obtained at 0° magnetic azimuth and 0° -180° elevation angles. Equations (A.1)-(A.9) are used in the MSP software to convert auroral features at a given elevation angle and altitude to a distance from the station within the meridian plane. The elevation angle and azimuth of observation from the station at a known latitude, longitude, and altitude are known but the altitude and distance along the sight line is in general not known. Typically the altitude of the peak auroral emission is assumed to compute the latitude of the auroral feature. A set of curves are plotted in Figure A.2 converting zenith angle observations to distance from the station for a range of altitudes appropriate for the peak 557.7 nm and 630.0 nm emissions.

### A.3 Interference Filter Characteristics

Narrow bandpass interference filters are used to obtain the wavelength selection for the photometer system. The principle of the filter is based on the interference between reflected and refracted rays of light within multiple layers of dielectric materials with different refractive indices [c.f., *Macleod*, 1986].

The center wavelength of the passband (the wavelength of peak transmission) is a function of the incidence angle of the light on the filter

$$\lambda = \lambda_0 \left[ 1 - \left( \frac{N_{ext}}{N_{filt}} \right)^2 sin^2\theta \right]^{1/2} \qquad (A.11)$$

where $\lambda_0$ is the center wavelength at normal incidence, $N_{ext}$ the refractive index of the medium surrounding the filter (normally taken to be 1.0 for air), $N_{filt}$ the effective refractive index of the filter, and $\theta$ the incident angle of light on the filter. $N_{filt}$ is normally provided by the manufacturer but can also be determined experimentally by plotting $\lambda/\lambda_0$ as a function of $sin^2\theta$ if the value is required. The variation in the passband as a function of incident angle allows the interference filter to be used as a spectrometer.

The bandpass of the filter is also a function of angle [*Lissberger*, 1959; *Lissberger and Wilcock*, 1959; *Pollack*, 1966]. Approximations to the filter function have been derived [*Hernandez*, 1974a] that in principle would allow calculation of the transmission and half width as a function of tilt angle, but they are not generally applicable to filters of arbitrary construction. In general, the change in peak transmission and half width as the angle of incidence is varied is due not only to the change in the geometry due to the tilt angle but also on light scattering within the filter due to irregularities in the coatings and wavelength separation of polarized components of the transmitted light. While the variation in transmission due to polarization can be calculated for arbitrary angle, at large angles of incidence the decreased transmission is dominated by the scattering loss which is a unique property of an individual filter [*Eather and Reasoner*, 1969]. For this reason it is best

Reproduced with permission of the copyright owner. Further reproduction prohibited without permission.

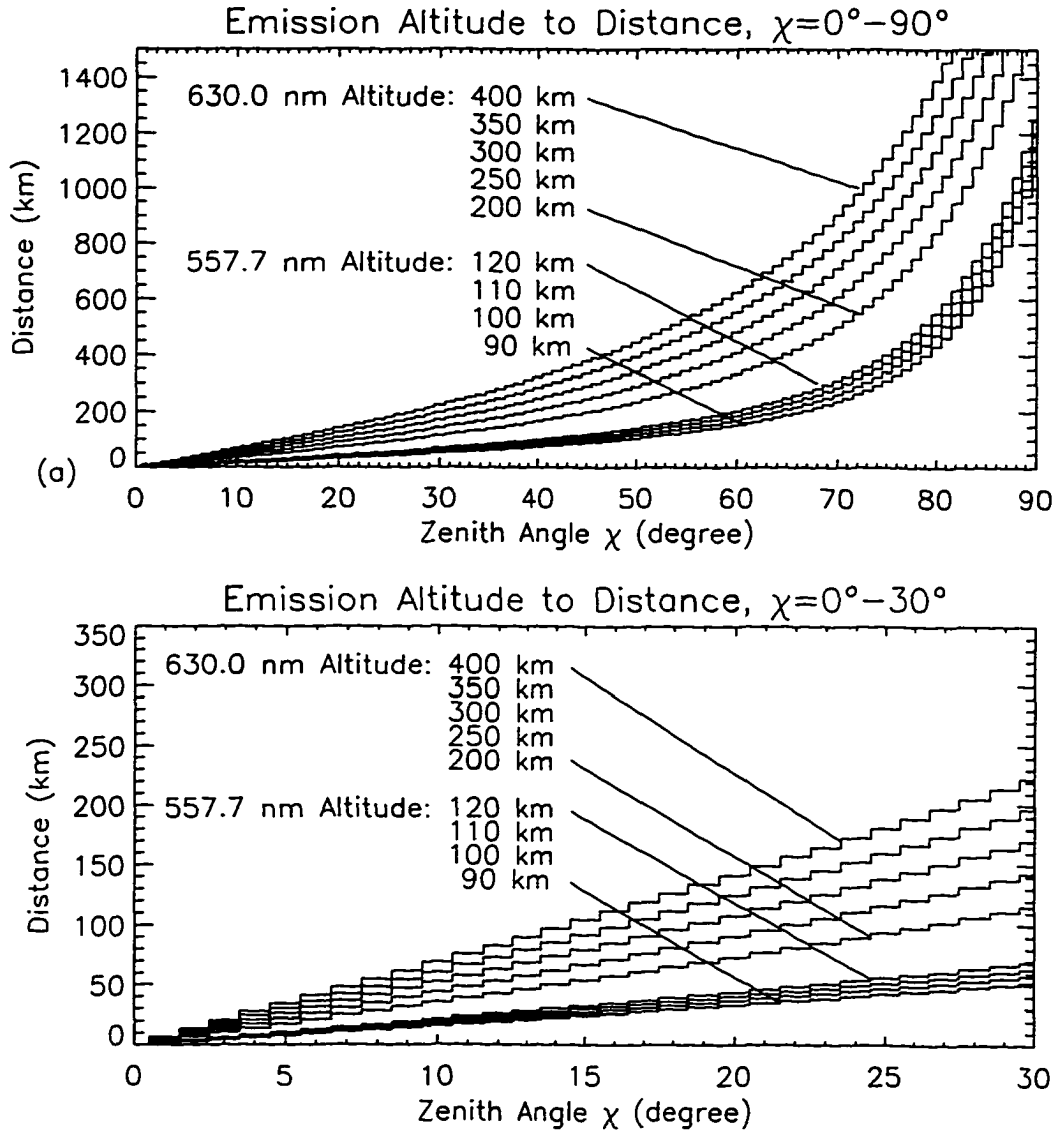


**Figure A.2 Conversions for Zenith Angle to Distance as a Function of Emission Altitude.**

Reproduced with permission of the copyright owner. Further reproduction prohibited without permission.

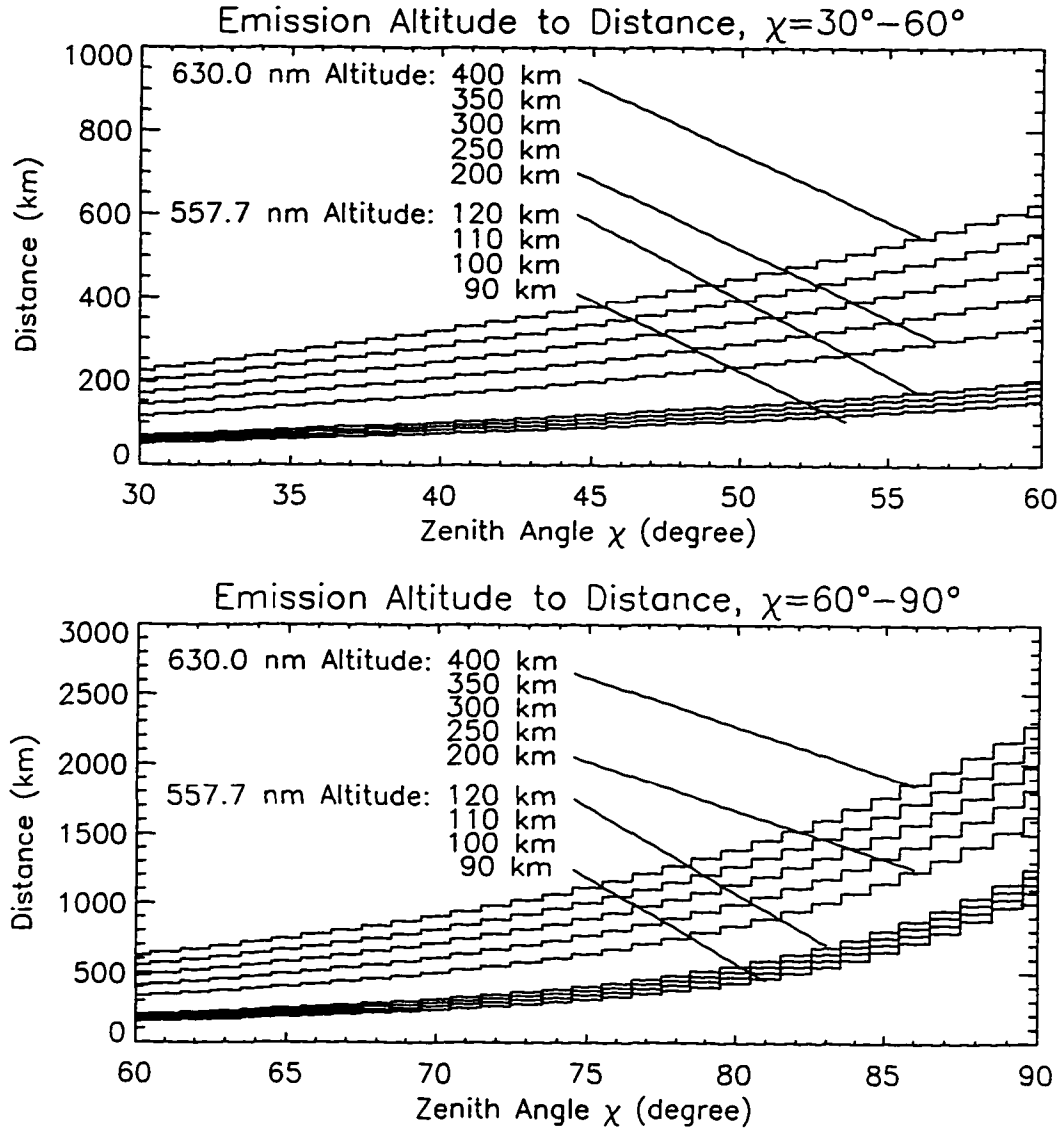


**Figure A.2 (continued).**

Reproduced with permission of the copyright owner. Further reproduction prohibited without permission.

**Table A-1**
**Interference Filter Characteristics**

| Filter[1] | $\lambda_{0,\alpha=0}$ | FWHM | $\%T_{\alpha_0}$ |
|---|---|---|---|
| 5580\4Å BARR #2 | 5584.9 | .43 | 53 |
| 6304\4Å BARR | 6303.8 | .43 | 54 |

[1]Label on filter.

to simply measure the transmission curves for the filters at each tilt angle for which the filters are to be used.

The transmission curves for the filters in use in Longyearbyen are well approximated by a Gaussian function for the range of tilt angles used in the MSP. Transmission curves for the filters used to isolate the 557.7 nm and 630.0 nm emission lines are plotted in Figure A.3 for a range of tilt angles as an example. The wavelength of peak transmission at normal incidence is 630.38 nm for the "6304\4A BARR" filter and 558.49 nm for the "5580\4A BARR" filter requiring the filters to be tilted to obtain the desired peak transmission. Measured values of transmission are plotted as a function of wavelength using a dotted line. Gaussian line fits are overplotted using a solid line. Variations between the fit and measured values are apparent only where the small dotted lines appear. It is fortunate that the curves are Gaussian as only three parameters are required to describe the filter at each tilt angle: the wavelength of the peak transmission, the full width of the peak at half of the maximum value (FWHM), and the value of the transmission at the peak. Measurement of these parameters for a set of standard tilts yield a set of values that can be interpolated to obtain the filter curves for arbitrary tilt angles.

(a) Transmission as a function of wavelength (top) for "5580\4A BARR" interference filter are plotted for tilt angles from 0° to 14° in two degree increments (increasing tilt from right to left). Peak transmission as a function of tilt angle (bottom). (b) Transmission as a function of wavelength (top) for "6304\4A BARR" interference filter and peak transmission as a function of tilt angle (bottom). —

Shifts of $\lambda_0$ also occur due to the expansion and contraction of the optical material as the temperature increases or decreases, respectively. Some examples of temperature coefficients for the change in wavelength at 400.0 nm and 800.0 nm for filters provided by the Andover Corporation are approximately 0.015 nm/° C and 0.020 nm/° C, respectively [*Andover Corporation Optical Filter Guide*]. Temperature coefficients were not measured for the filters in the MSP since the parameters are not required for use of the instrument. Temperature stability is maintained within a few degrees centigrade by the large thermal mass of the instrument and a thermostated heater in the instrument hut to avoid drifts in the peak wavelength of the filters. Compensation for large variations in temperature is accomplished by readjusting the angle to be used for the peak measurement during the instrument setup calibrations. Temperature drifts during routine operation will appear as a variation of the signal intensity. Significant variations in temperature are only expected during dramatic changes in the weather conditions outside the hut. Examples are the increase in the air

Reproduced with permission of the copyright owner. Further reproduction prohibited without permission.

temperature that often accompanies the onset of a storm or the rapid cooling that occurs when a strong wind blows a heavy cloud layer from the region. In the former case the MSP data is strongly contaminated by clouds and is not useful for auroral observations. The latter case is most commonly encountered following extended period of bad weather and is corrected by the operator when running the filter alignment calibrations.

### A.4 Background Correction.

Observations of very weak emissions of the night and twilight sky are complicated by the presence of a background continuum in addition to the line sources of interest. The background is the combination of stellar sources, unresolved atmospheric emissions, and scattered sunlight (in the case of twilight observations). *Broadfoot and Kendall* [1968] and *Sparrow et al.*,[1968] report values on the order of 5 R $nm^{-1}$ at 350.0 nm to 20 R $nm^{-1}$ at 750.0 nm for this background. *Chamberlain* [1961] reproduces a figure from work by *Shefov* [1959] indicating variations in the night sky continuum from 20 R $nm^{-1}$ to 40 R $nm^{-1}$ in the wavelength range from 520.0 nm to 650.0 nm. *Krassovsky et al.* [1962] suggests an average of 20 R $nm^{-1}$ over the entire visible range.

The wavelength dependence of the transmission peak on the angle of incidence is a useful technique to obtain a background correction for weak emission lines [*Eather and Reasoner* 1969] and is the one employed in the MSP. A signal intensity is obtained for the emission line of interest while the filter is rotated to an angle that yields a maximum in transmission. The continuum background contribution to the line is obtained by tilting the filter so that the passband shifts to a lower wavelength than the peak. The background light must be unmodulated and sufficiently slowly varying in the neighborhood of the emission peak for the intensity at the shifted wavelength to be a reasonable estimate of the background at the peak wavelength.

Tilting a filter, however, does not simply shift the wavelength but also changes the filter function. The change in filter function is assumed to be small for small angles, but may become a problem if large angles are used. An implicit assumption required to simply subtract the background intensity from the peak is that the integrated area under the transmission curve remains constant, even if the transmission curve varies slightly. Variations in the functional shape of the filter bandpass are tolerable at the background position if the assumption is valid that the light penetrating the filter is unstructured except for the emission peak of interest. Variations in the filter transmission curves are apparent in Figure A.3 where the peak transmission decreases with angle of incidence while the bandpass increases.

The general processing algorithm for using the peak and base values to compute the intensity at the wavelength $\lambda$ for a given elevation angle $\theta$ is

$$I(\lambda_p, \theta) = C_p(\theta)K_p^R(\lambda) - C_b(\theta)K_b^R(\lambda)\frac{A(\alpha_p)}{A(\alpha_b)} \qquad (A.12)$$

where $C_p$ and $C_b$ are the raw count rates while the filter are in the peak and background positions, respectively, $K_p^R(\lambda)$ and $K_b^R(\lambda)$ are the peak and background calibration constants converting

Reproduced with permission of the copyright owner. Further reproduction prohibited without permission.

count rates to a sensible photometric unit (generally Rayleighs). The areas under the transmission curves $A(\alpha_p)$ and $A(\alpha_b)$ are given by

$$A(\alpha_k) = \int_{\lambda_1}^{\lambda_2} W(\lambda, \alpha_k) d\lambda \tag{A.13}$$

for $k = p, b$ and the integration limits are over the wavelength range where $W(\lambda, \alpha_k)$, the filter response curve as a function of tilt angle $\alpha$, has nonzero values.

The constants $K_p^R(\lambda)$ and $K_b^R(\lambda)$ are taken to be equal so the equation reduces to

$$I(\lambda, \theta) = \left[(C_p(\theta) - C_b(\theta)\frac{A(\alpha_p)}{A(\alpha_b)}\right] K^R(\lambda) \tag{A.14}$$

if $A(\theta_p)/A(\theta_b) \sim 1$ then the equation for processing MSP data is given by the equation

$$I(\lambda, \theta) = [(C_p(\theta) - C_b(\theta)] K^R(\lambda) \tag{A.15}$$

Deviations from $A(\theta_p)/A(\theta_b) \sim 1$ are not generally important if the background is small compared to the peak intensity. However, for weak emissions (e.g., polar cap F-region patches and other weak airglow structures, faint diffuse aurora, or hydrogen emissions) or strong background intensities (e.g., observations in bright twilight) the background and signal may have approximately the same value and the assumption of equal areas may lead to poor corrections for the background. The ratio is a characteristic of each filter and is obtained in principle from the knowing the transmission curves as a function of tilt angle. An alternative method is to use the daily calibration values while the instrument is sampling the internal bulb in the instrument housing. Calibration bulb samples are available while the filter is in both the peak and base position. A required assumption is that the bulb is the same brightness at the peak and background wavelengths, valid for the limited wavelength range encountered during the filter shift operation. The ratio $A(\alpha_p)/A(\alpha_b) = 1$ when the area under the transmission curves are the same and $A(\alpha_p)/A(\alpha_b) > 1$ as the transmission decreases for large tilt angles.

## A.5 Field of View

The angular field of view is normally taken to be approximately 1 degree for the Longyearbyen instrument (*C.S. Deehr. personal communication*), approximately twice the angular size of the full moon. In the absence of a schematic for the optical system the value can be tested using the signal observed during the passage of a point source such as a star or planet through the magnetic meridian plane. The rate of change of zenith angle and azimuth of an astronomical object is given by *Smart* [1977] as

$$\frac{dz}{dH} = -sin(A)cos(\phi) \tag{A.16}$$

$$\frac{dA}{dH} = -[sin(\phi) - cot(z)cos(A)cos(\phi)] \tag{A.17}$$

where $\phi$ is the latitude of the observer, $z$ the zenith angle, and $H$ the hour angle (the angle between the geographic meridian plane and the location of the object) and the azimuth $A$ is

Reproduced with permission of the copyright owner. Further reproduction prohibited without permission.

measured positive eastward from north. The negative sign in equation (A.16) is positive in the notation given by *Smart* since his azimuth is measured positive westward from north.

Expressing the hour angle (the time from the passage of the meridian plane that contains the geographic north and south) in seconds and the azimuth and zenith angle in seconds of arc yields the forms

$$\frac{dz'}{dH'} = -15sin(A)cos(\phi) \qquad (A.18)$$

$$\frac{dA'}{dH'} = -15[sin(\phi) - cot(z)cos(A)cos(\phi)] \qquad (A.19)$$

where the prime quantities are in seconds and the unprimed in degrees.

The change in zenith angle with time is small at high latitudes and can be neglected so only the (A9) is required. Measurement of the time required for the object to transit the field of view of the instrument at a given zenith angle is used to determine the angular size of the field of view.

The error in the aperture is dominated by terms involving the zenith angle and time while those of the latitude and azimuth can be neglected. The error has the form

$$\delta(dA') = \left[\left(\frac{dA'}{dh'}\right)^2 \delta(dh')^2 + \left(\frac{15dH'cos(A)cos(\phi)}{cos^2(z)}\right)^2 \delta(z)^2\right]^{1/2} \qquad (A.20)$$

Table A-2 lists the zenith angle and time required for a series of planets and stars to cross the MSP scan plane on the 135° azimuth. The time and zenith angle measurements were obtained from plots of the background scans. Background subtraction cannot be used as the majority of radiation from stars is in a continuum emission, background subtraction will eliminate the signal from the star. Peak scans were not used to avoid competition between the signal from the star and airglow or auroral emissions. An example of a star transit is given in Figure A.4.

The standard deviation of the mean for the aperture widths given in Table A-2 is 0.09 degrees indicating the error is dominated by the propagation of measurement errors given by (A10) rather than statistical errors. Including the statistical error into the final error increases the value to approximately .24 degree. The field of view obtained from this measurement is therefore 1.52±.24 degrees, suggesting that within the error of the observations the field of view is greater than the nominal 1° value that is normally reported for the instrument.

Reproduced with permission of the copyright owner. Further reproduction prohibited without permission.

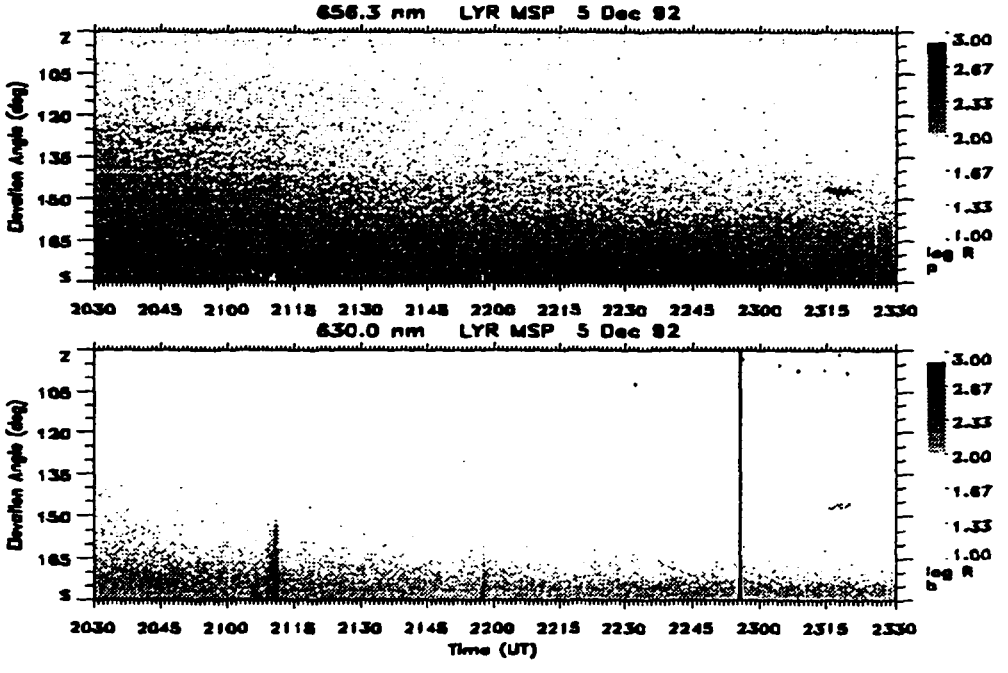


Figure A.4 MSP record of star transit. The star is observed in this case in the background scan of the 486.1 nm filter.

**Table A-2.**

**Transits of Astronomical Objects of the 135° Azimuth Scan Plane.**

| Object[2] | $dH'$ (sec) | $z$ (deg) | $dA'$ (deg) | $\delta(dA')$[1] (deg) |
|---|---|---|---|---|
| Arcturus | 300 | 62 | 1.32 | .21 |
| Arcturus | 345 | 62 | 1.52 | .21 |
| a[3] | 555 | 24 | 3.01 | .26 |
| b | 360 | 42 | 1.96 | .23 |
| c | 300 | 35 | 1.48 | .24 |
| d | 255 | 51 | 1.16 | .22 |
| e | 390 | 35 | 1.93 | .24 |
| f | 360 | 57 | 1.61 | .21 |
| g | 270 | 53 | 1.22 | .22 |
| h | 315 | 49 | 1.45 | .22 |
| | | | Mean 1.52 ± .22 | |

[1] Assuming Time error of three scans (48 seconds) and zenith angle error of 2 degrees.
[2] Objects not identified are simply labelled in order the measurements were obtained.
[3] Not included in the mean

Reproduced with permission of the copyright owner. Further reproduction prohibited without permission.

### A.6 Transmission Loss in Zenith Due to Window Joint.

The window material used for the slit is composed of two pieces requiring a joint. Light paths through the joint are sampled by the photometers near the zenith since the joint is at the midpoint of the slit. Aging of the glue holding the two pieces together and accumulation of sand and grit have conspired to darken the window material at the joint resulting in a decrease of signal transmission. It is particularly unfortunate that the channel normally assigned to the 557.7 nm filter suffers the transmission loss near the magnetic zenith. Ratios of the field aligned intensity at 630.0 nm and 557.7 nm using raw data are, therefore, questionable–especially for recent years.

A correction for the signal loss in the joint can be implemented in the MSP analysis software. The technique is based on the assumption that the loss of light in the joint is simply to do the increased optical thickness of the material in the joint region and does not depend on intensity of the signal. The factor $C^F(\theta,\lambda)_{joint}$ required to correct for the loss in the joint is determined from MSP observations of a uniform illumination source. The correction factor is implemented by multiplying

$$I_{corrected}(t,\lambda,\theta) = I_{uncorrected}(t,\lambda,\theta)C^F(\lambda,\theta)_{joint} \qquad (A.21)$$

Periods of cloudy weather provide a convenient source of uniform illumination to obtain the correction curves.

Two methods of calculating $C^F(\lambda,\theta)_{joint}$ are included in the analysis software. The first is to sum a set of cloudy weather scans and fit a straight line to the final curve. The ratio of the best fit line to the true curve is the correction factor. This method is very quick to implement but requires that the total light intensity remain constant for the period used for the calculation.

The second method is similar except that the best fit line and correction factor is calculated for each individual scan and the resulting set of correction factors averaged. The latter method, while requiring a greater computational effort than the first, is less sensitive to the shape of the cloudy night curves and can be used even if the total intensity is varying with time. It is the preferred method to use in correcting for the loss and yields better corrections than the first method.

Daytime records are likely to be contaminated by auroral signals, especially the 630.0 nm, 656.3 nm, and 732.0 nm emissions which may penetrate cloud layers. It is best to only use records from late afternoon or night where the probability of auroral contamination is minimal. The transmission loss depends on the aging of the joint and window material and the accumulated grit. The correction factor is therefore a function of time requiring a new set of of factors for each field season.

### A.7 Photomultiplier Detector and Counting System Characteristics

Photons transmitted through the interference filters fall on the photocathode surface of a photomultiplier tube resulting in the release of a photoelectron. An accelerating and focusing potential is applied between the photocathod and a dynode.

The photoelectron is accelerated through a potential drop to a secondary electrode where the impact of the energetic electron produces a number of electrons. The secondary electrons are again

Reproduced with permission of the copyright owner. Further reproduction prohibited without permission.

accelerated through a potential drop resulting in a larger number of ejected electrons. A series of potential drops results in the production of many electrons for each incident photon, typically in the range of $10^6$ for the tubes in use in the MSP. The size of the current pulse is proportional to the energy of the incident photon.

The phototubes are operated in pulse counting mode rather than current due to the low photon signal rates. The current pulses of the phototube are amplified in a preamplifier and shaped by a pulse shaper to obtain pulses of uniform width. A pulse amplitude discriminator (PAD) is used to reject pulses with amplitudes less than a critical threshold. The output of the PAD is fed into a computer for counting.

Noise in the counting system arises from a number of sources. One of the largest sources is thermionic emission of electrons from the electrodes within the phototube. This process occurs when an electron in the electrode has sufficient energy to escape the metal and is accelerated through the potential drop to the next electrode, producing a set of secondary electrons. The amplification is in general smaller for thermionic electrons that for those originating in photoemission at the photocathode since thermionic emission may originate in any of the electrodes within the tube. The current pulse is smaller for the thermionic electrons and are rejected in the PAD. In addition, the phototube is cooled to approximately -30° C by a Peltier cooler to reduce the chance of thermionic emission. The combination of cooling the tube and use of the PAD results in dark counts on the order of a few counts per second. Cosmic rays and radioactive decays within the tube material also lead to pulses. These sources are not rejected by the PAD since there is no upper threshold (i.e., the PAD is not a window) but are expected to give very low count rates.

The current output of a phototube may not be a linear function of the input rate of photons falling on the photocathode due to dead time effects in the phototube and the inability of the tube to supply sufficient current to maintain large pulse amplitudes at high count rates. Dead time refers to the loss of signal due to coincident arrival of photons. The counting system counts individual pulses above the minimum amplitude threshold as a single pulse. Two photons arriving within the response time of the phototube result in a single pulse of approximately double amplitude which will be counted as only a single pulse.

Space charge within the phototube also results in an inability of the tube to provide the necessary current to maintain the pulse height at high current rates for some of the output pulses. The pulse height discriminator will reject these pulses resulting in lost pulses.

A set of correction values must be used to adjust the output at large count rates for non-linearity. The linearity of the Longyearbyen instrument has never been checked to the authors knowledge as no linearity table have been found in the analysis programs in use at the Institute. Values from the Poker Flat instrument with similar phototubes can be compared to estimate the magnitude of the error if the count rates remain uncorrected. The correction values for Poker Flat are generally 1 for count rates below approximately 10000 counts but may reach 2 for count rates near the 50000 or 60000. Very large signals are therefore, undercounted, by the system. Count rates greater than 10000 are rare for dayside observations so the correction is not crucial for the work presented here. A set of multipliers as a function of count rates needs to be included in the MSP analysis software in the future, although it is not currently implemented.

Reproduced with permission of the copyright owner. Further reproduction prohibited without permission.

A shutter system was designed for the MSP system in at Poker Flat, Alaska, allowing routine measurement of the dark count level for the different photometer systems. The shutter system, however, was not installed in the Longyearbyen instrument and the data values stored in the dark count positions in the records are, therefore, not useful numbers. Typical dark counts for the Poker Flat instrument are generally less than 1 count and will be neglected in the analysis here. It would be useful in the future to run the instrument with the covers over the photometer barrels to obtain an estimate of the dark counts.

### A.8 Absolute Intensity Calibration.

Absolute intensity calibration for the system is obtained by sampling the light sources of known intensity during a field season. The calibration provides the constant, $K^R(\lambda)$ Rayleigh count$^{-1}$, which is required to convert the raw count rate output of the photometer, $I_u(t, \lambda, \theta)$, to Rayleighs ($4\pi \times 10^6$ photons cm$^{-2}$ sec$^{-1}$). The most general form of the constant is given by

$$K^R(\lambda) = \frac{\int B_i(\lambda) W(\lambda) d\lambda}{C_i} \qquad (A.22)$$

where $B_i(\lambda)$ is the brightness in $R\ nm^{-1}$ of the known light source, $W(\lambda)$ is the response of the bandpass of the filter in $nm$, and $C_i$ is the observed count rate while the MSP is sampling the light from the known source. The filter response as a function of wavelength are characteristic of each filter and have been described in section A-3.

Calibration is done on a daily basis by comparing the signal observed in each channel of the instrument while sampling the light from a tungsten bulb mounted inside of the MSP box and reflected through two barium oxide diffusing screens onto the main mirror.

Standard practice is to run the internal standard once in the morning before a midday "cusp" period near 0300-0400 UT, once in the afternoon after the midday period near 1400-1500 UT, and anytime a new tape is placed on the tape drive. In addition, internal calibrations are often obtained at other times chosen by the operator if there is a question about the status of the system or to simply obtain additional sets of calibration values. The internal lamp is operated at a fixed current of 1.6 Amps to obtain a constant light output for the daily calibrations.

If the variation in lamp brightness is small over the range of wavelengths where the filter transmission is significant, A12 can be rewritten as

$$K^R(\lambda) = \frac{B_i(\lambda) A(\alpha)}{C_i} \qquad (A.23)$$

where $B_i(\lambda)$ is now the brightness of the internal bulb and screen combination and $A(\alpha_p)$ is the integrated area of the transmission curve at the peak angle position given by A3.

The value of $B_i(\lambda)$ R nm$^{-1}$ used in this thesis for dates prior to February 1989 are obtained from Jerry Romick's original laboratory notes on the calibration of the Longyearbyen MSP system. A transfer photometer was used to compare the brightness of the internal calibration bulb and screens to a standard bulb and screen in the laboratory. This resulted in the brightness values for the internal bulb given in Table A-3. These values are simply adopted as correct for the pre 1989

Reproduced with permission of the copyright owner. Further reproduction prohibited without permission.

values since limited references can be found in the station logs to yearly checks on the internal lamp brightness by comparison with an external standard bulb. This is unfortunate as the internal bulb was never meant to be a standard bulb but rather was intended to be compared yearly with a transfer standard.

**Table A-3**
**Svalbard Internal Calibration Lamp Brightness at 1.6 A.**

| Wavelength[1] (nm) | Brightness | Wavelength[1] (nm) | Brightness (R/nm) |
|---|---|---|---|
| 427.8 | 510 | 614.2 | 7920 |
| (486.1) | (1530) | (630.0) | (8980) |
| (520.0) | (2660) | (656.3) | (10830) |
| 535.5 | 3320 | 670.8 | 11900 |
| (557.7) | (4440) | (732.0) | (17040) |

[1]Values for wavelengths in parenthesis are interpolated from the measure values.

The brightness of the internal bulb is determined by comparison with a standard bulb. The technique for the intercomparison is to reflect light from the station external standard tungsten-halogen bulb operated at 6.5 amps into the MSP slit. A reflecting barium oxide screen is used for the required 90 degree reflection to redirect the light from the bulb into the MSP slit and onto the mirror at approximately the zenith position of the mirror. The bulb is mounted 32.2 meters from the station approximately 2 meters from the ground on a tower. The MSP-bulb distance (31.2 meters) is the hypotenuse of the right triangle where the sides are the bulb-spectrometer periscope distance (30 meters) and the spectrometer-MSP slit distance (8.5 meters). The distance from the center of the reflecting screen on top of the MSP slit to the phototubes is approximately 1 meter. The total distance is approximately 32.2 meters.

The brightness of the standard bulb was determined by Romick by comparison with a reference standard at the Geophysical Institute and are given in the first column of Table A-4. These values are the brightness observed by a photometer system located 8.387 meters from a lambertian reflecting screen. This brightness must be corrected for the distance in Svalbard and the two 45 degree reflections (one incident and one exiting) the barium oxide screen. The brightness of the external lamp at the MSP, $B_{e,32.2m}R/nm$, is obtained from the values given by Romick at 8.387 m, $B_{e,32.2m}$, by the equation

$$B_{e,32.2m} = \left(\frac{8.387 meters}{32.2 meters}\right)^2 cos^2(45°) B_{e,8.387m} \qquad A.24$$

The values corrected for 32.2 meters and the reflection off the barium oxide screen are given in the third column of Table A-2. This assumes that the reflectivity of both the barium oxide screen and the mirror is 1.0.

Reproduced with permission of the copyright owner. Further reproduction prohibited without permission.

**Table A-4**
**Svalbard Standard External Calibration Lamp Brightness[1].**

| Wavelength ($\AA$) | $B_{e,8.387m} \times 10^3$ ($R\AA^{-1}$) | $B_{e,32.2m}$ ($R\AA^{-1}$) |
|---|---|---|
| 4278 | 1.8 | 61 |
| 4861 | 4.0 | 135 |
| 5200 | 5.8 | 197 |
| 5577 | 8.0 | 271 |
| 6300 | 13. | 441 |
| 6563 | 15. | 509 |
| 7320 | 20. | 678 |

[1]Brightness at 8.387 m obtained from Jerry Romick's notebooks.

Count rates from the photometer system were then compared with the count rates obtained while looking at the internal calibration bulb. The function of the photometer system was simply that of a transfer photometer between the external screen brightness and the internal screen brightness. The spectral response and total transmission of the interference filters are not important in this case as they simply cancel. The internal lamp brightness, $B_i R\AA^{-1}$, is obtained from the external lamp brightness transferred to the photometer system, $B_{e,32.2m} R\AA^{-1}$, from the ratio

$$\frac{B_i}{counts_{int}} = \frac{B_{e,32.2m}}{counts_{ext}} \qquad A.25$$

The results for both the December 1991 and the December 1992 calibration are tabulated in Table A-5. The original lamp values obtained by Jerry Romick (from Table A-3 above) are reproduced in the final column in Table A-3 for comparison.

**Table A-5**
**December 1991 and 1992 Internal and External Lamp Comparisons.**

| Wavelength | $B_{e,32.2m}$ ($R\AA^{-1}$) | $\frac{counts_{int}}{counts_{ext}}$ | $B_{i,1991}$ ($R\AA^{-1}$) | $\frac{counts_{int}}{counts_{ext}}$ | $B_{i,1992}$ ($R\AA^{-1}$) | $B_{i,1984}$ ($R\AA^{-1}$) |
|---|---|---|---|---|---|---|
| 4278 | 61. | 149.7/525 | 17.4 | 51.6/450 | 7.00 | 51 |
| 4861 | 135. | 1.75/40 | 5.91 | 44.2/750 | 7.96 | 153 |
| 5200 | 197. | | | | | |
| 5577 | 271. | 630.5/1200 | 142.3 | 631.5/103 | 142. | 444 |
| 6300 | 441. | 122/1500 | 35.9 | 129/2250 | 25.28 | 898 |
| 6563 | 509. | | | | | |
| 7320 | 678. | 220.9/5500 | 27.23 | 196.6/440 | 30.29 | 1704 |

13 December 1991 calibration approximately 0100-0200 UT
21 December 1992 at 0430-0530 UT

Reproduced with permission of the copyright owner. Further reproduction prohibited without permission.

A new bulb was chosen for the 1993/1994 field season to be used as the transfer standard for both the Longyearbyen and Poker Flat field sites. Unfortunately, the field crews did not use the new bulb so there was no standardization of calibration during the current field season. The only test of the old external standard as of the date this thesis is completed is the December 1992 comparison. These values have been adopted for the calibration of the internal standard between December 1989 to the current season. Prior to December 1989 the original values obtained by Gerry Romick are assumed to be correct. Calibration constants used for the results in this thesis are 3.65 kR/count for the 630.0 nm channel and 2.19 kR/count for the 557.7 nm channel.

Reproduced with permission of the copyright owner. Further reproduction prohibited without permission.

# Appendix B The Television Camera

## B.1 Introduction

The principle recording device of auroral morphology used in auroral studies for many years was the all sky film camera. Photographic film however is limited as a detecting medium if long series of high time resolution images are desired. Long exposures are required to obtain the photon fluxes necessary to create a latent image on a piece of photoactive material and a chemical development step is necessary to remove unreacted material and produce the final images. High speed films reduce exposure times if high time resolution is required but the technical problems of moving large quantities of film through a camera system, the labor and the necessity to store and work with the unprocessed film in darkness, and the specialized equipment required to handle large quantities of film have placed a practical limit on film rates to approximately 1 per minute for extended recording periods.

The conversion of light to an electric signal in photoelectronic devices offers a significant advancement over film due to the greater quantum efficiency of the photoelectric effect than the photoelectronic effect. The best emulsions in use for astrophotography have quantum efficiencies on the order of 4 per cent compared to the approximately 20 percent efficiency for the photocathode in an image orthicon television camera and 60 percent for the solid state charge-coupled device sensor [*Eccles et al.*, 1983]. Television systems are designed to amplify the incident light and yield images at rates of 30 images per second. These images are available for viewing on monitors as they are received from the system and the analog signal is recorded on magnetic tape for later processing. Records of auroral morphology used in this thesis were obtained by the image orthicon camera that had been the standard at the Nordlystassjonen field site until its failure in the fall of 1994.

## B.2 The Image Orthicon Television Camera

The first television system used for extensive auroral observations was the image orthicon (IO) television system [*Davis and Hicks*, 1964; *Davis*, 1966]. IO tubes are sensitive over a range of light levels from daylight to very low intensity and have been used in a wide variety of field and studio uses. The gain of an IO television system over direct photography is on the order of 100 [*Vallance Jones*, 1974] allowing records of weak light signals to be obtained at video rates. A brief description of the design and operation of the IO camera is given here following the descriptions found in *Rose et al.* [1946], *Redington* [1971], *Csorba* [1985], and *Benson* [1986].

A schematic of an IO tube is given in Figure B.1. The IO is a storage type device in which the photon image information is converted to a charge pattern on a target screen. The charge pattern is read by a scanning electron beam to convert the image information to an electrical signal that may be transmitted or recorded. The camera is composed of three main sections: the

Reproduced with permission of the copyright owner. Further reproduction prohibited without permission.

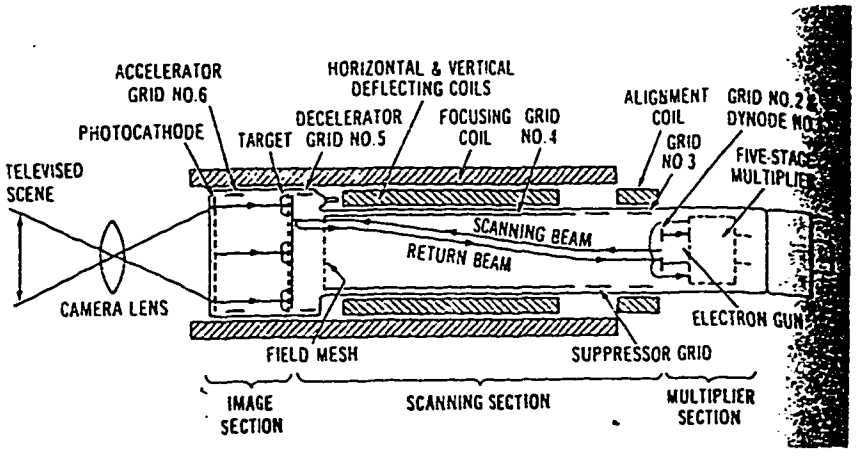


Figure B.1 Schematic of the Image Orthicon Television Camera Tube. The image, scanning, and multiplier sections are shown along with their major deflection coils and screens used to control electron motions within the tube (reproduced from Csorba, 1985). Details of the tube are discussed in the text.

image section, the scanning section, and the multiplier section. These sections are shown in the schematic in Figure B.1.

The image is initially converted from photons to an electron signal in the image section of the tube. Light from a luminous source is focused by the optical system onto the photocathode surface of the IO tube. Photoelectrons are released when the energy of the incident photon exceeds the work function of the photocathode material. The number of electrons emitted at any point on the photocathode is proportional to the intensity of the light that falls on the surface. The photoelectrons are accelerated through a potential drop on the order of 500 volts towards a target. An electric field serves to sweep the electrons away from the photocathode and accelerates them to the target screen where they arrive with sufficient energy to pass through the target mesh, colliding with the electrons on the target. Accelerated photoelectrons have enough energy to eject a number of secondary electrons from the target screen, resulting in a region of net positive charge. Secondary electrons produced at the target are collected at the target mesh on the image side of the target screen. The initial photon image is reproduced on the target in the positive charge regions where secondary electrons are removed on the image side of the target.

Glass, metal, and semiconductor materials have been used for target materials in production of IO tubes. The target material in the RCA-7967 IO tube in use in Longyearbyen is a thin

Reproduced with permission of the copyright owner. Further reproduction prohibited without permission.

film semiconductor. Specifications from the manufacturer (*Radio Corporation of America*) list the advantages of the semiconductor target as high sensitivity with minimal lateral charge leakage and superior performance in low light level conditions.

Positive charge patterns on the target are converted to an electrical signal in the scanning section of the tube. An electron gun in the scanning stage produces a beam of low energy electrons directed towards the target. The electrons drift along an axial magnetic field produced by the focusing coils while the position of the beam is controlled by a set of deflecting coils. In contrast to the accelerated photoelectrons, the scanning beam has insufficient energy to produce secondary electrons. The purpose of the scanning beam is to "read" the positive charge pattern on the target material. When the scanning beam encounters a region on the target which is positively charged a fraction of the electrons in the beam is lost in neutralizing the positive charge. The target cannot accept more electrons than those required to neutralize the positive charge without becoming negatively charged. Excess electrons in the beam are therefore repelled from the target forming a return beam. The video signal is derived from the modulation of the scanning beam by the charge pattern.

Scanning beam electron trajectories in the axial magnetic field are a helix. The decelerator grid and field mesh potentials form a deceleration lens to remove the radial and transverse velocity components after a few oscillation cycles of the electron beam assuring that the beam arrives perpendicular to the target. The return beam follows a path very close to the scanning beam and arrives in the vicinity of the electron gun with an excess energy sufficient to eject secondary electrons from a small disk near the electron gun. Amplification of the return beam is required since the modulation in the beam is small. The first step in the amplification is the creation of secondary electrons from the collision of the return beam with the disk. In turn, the secondary electrons are accelerated through potential drops across a series of electrodes creating successively greater numbers of secondary electrons. The video signal is typically amplified on the order of 500 times without reducing the signal-to-noise ratio established by the statistical fluctuations of the scanning beam.

IO cameras operated at the field station are mounted such that the vertical and horizontal axis of the images are aligned with the axis of the field station, approximately along the geomagnetic north-south and east-west directions. The camera is typically mounted vertically although options to mount them along the direction of the magnetic field are also provided by a steerable mount in the camera hut.

### B.3 Noise and Defects in IO Images

Noise in the IO image is predominantly the result of statistical fluctuations in both the photon source and the reading beam current. The variations in the source cannot be controlled but the reading beam current can be altered. The operator adjusts the beam current to the minimum value at which the scanning beam can completely discharge the positive charge on the target surface. Minimum fluctuations can be obtained in this manner. If the beam current is too low insufficient electrons are available to neutralize the positive charge accumulating on the target

Reproduced with permission of the copyright owner. Further reproduction prohibited without permission.

screen, the positive charge will begin to diffuse laterally over the target surface resulting in loss of beam current in adjacent regions not associated with the original image charge pattern. The return current in the reading beam is reduced or even completely fails to return. Reduction of the return beam current is found in regions where the initial image is bright so reduction or loss of the return beam is interpreted as bright light and "blooming" of the image results. This condition can be rectified by increasing the beam current at a penalty of increasing the noise in the image. Adjustments to either the gain or beam current are often required to keep the image within the dynamic range for the camera system. Neither are controlled automatically requiring the operator to monitor the image. Typically the operator attempts to use a minimum beam current to avoid blooming and the maximum gain which does not result in a noisy image.

A common problem that occurs in IO tubes is the formation of the "gas spot" artifact in the center of the image due to the increase in gas pressure of the evacuated tube over time. Collisions of the scanning and return beam electrons with gas atoms results in a reduction of the beam current and appears in the final signal as a bright spot near the center of the image. In recent years the gas spot in the Svalbard IO camera tube has become quite strong and may be confused with auroral emissions in the zenith. The gas spot is recognized as a structureless radially symmetric region in the center of the image. Comparison of images of from night time periods when aurora is absent allows the gas spot to be readily separated from auroral emissions.

### B.4 Spectral Response of the IO Camera

The spectral response of the camera is determined by the photocathode material. Figure B.4 shows a typical sensitivity curve for the S-20 material the manufacturers specifications indicate is used in the RCA-7967 IO tube (Radio Corporation of America). The spectral response of the tube used at the Longyearbyen station was not measured.

Peak S-20 response is near 420 nm with a rapid decrease in sensitivity towards the blue and a more gradual decrease into the red end of the visible spectrum. Wavelengths at which the sensitivity is half the peak value is approximately 330 nm and 600 nm and the quarter sensitivity wavelengths are approximately 310 nm and 685 nm. The camera response is greatest for light at a wavelength for which the product of the incident light spectrum and the photocathode sensitivity is a maximum. It is inappropriate in general to identify a single wavelength at which an unfiltered camera responds since the auroral spectrum is highly variable. Auroral emissions can easily vary over factors of 4 to 10 or more in short intervals of time. Since the relative sensitivity varies by a factor of four between 310 nm to 685 nm, nearly the entire visible spectrum may contribute to the camera response.

As an example of the varying response of the camera to different auroral conditions, consider two auroral displays with intensities given by the values listed in Table 3.2 for night and day aurora. The night aurora is due to energetic electrons which deposit energy at altitudes of 100-120 km exciting a number of molecular bands. Even though the 557.7 nm emission which gives the aurora its characteristic green color is 10 kR, response of the camera to the 14.1 kR $N_2^+1N$, 8.7 kR $N_2 1P$, and 14.7 kR $N_2 2P$ emissions will be much greater. In this case the camera response is

Reproduced with permission of the copyright owner. Further reproduction prohibited without permission.

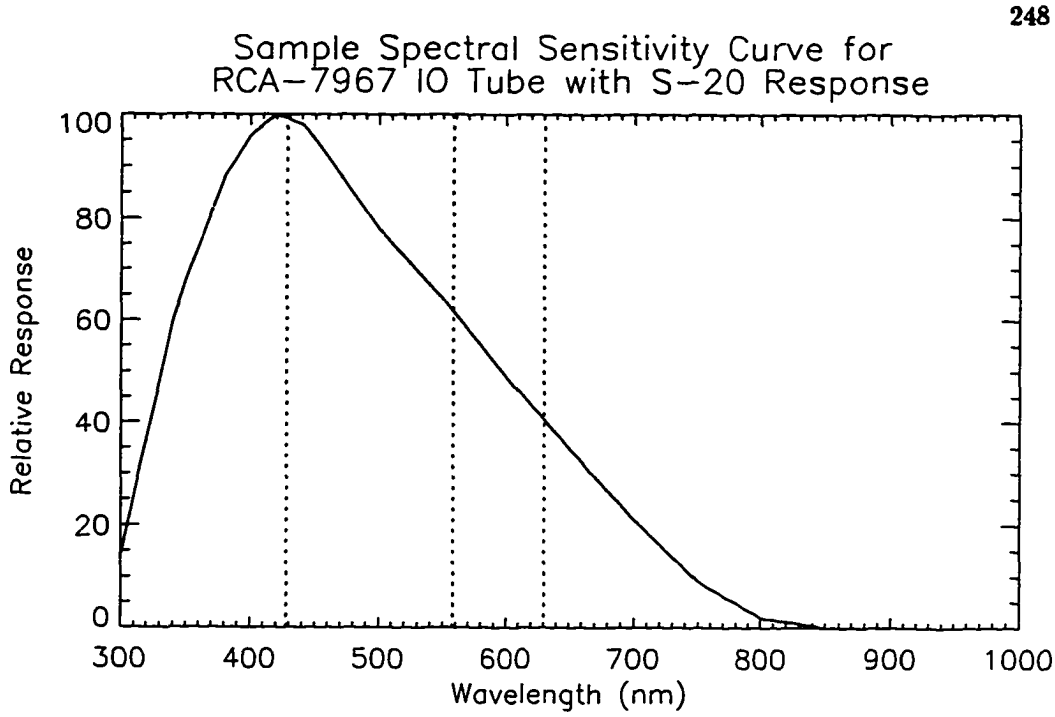


**Figure B.2 Relative Sensitivity of an Image Orthicon Tube. The relative response in terms of signal per photons at each wavelength are plotted for the Image Orthicon tube. Wavelengths of common auroral lines at 427.8 nm, 557.7 nm, and 630.0 nm are indicated by the vertical dotted lines.**

dominated by molecular emissions rather than atomic species. The low energy electrons in dayside aurora are thermalized at altitudes where the neutral atmosphere is dominated by atomic species and molecular emissions are reduced or absent. Average intensities of the 557.7 nm and 630.0 nm emission lines listed in the table are 1.3 kR and 1.9 kR, respectively, The cameras response at 557.7 nm and 630.0 nm is 0.6 and 0.4, respectively. The camera response to this aurora (given by product of the sensitivity and the emission intensity at the given wavelengths) is approximately equal for the red and green auroral lines. A decrease in electron energy resulting in an aurora with I(557.7 nm)/I(630.0 nm)<1 will shift the primary camera response to the 630.0 nm line while an increase in electron energy so that I(557.7 nm)/I(630.0 nm)>1 will similarly shift the camera response to the 557.7 nm line. Camera response to the 557.7 nm atomic emission and molecular bands are more apparent due to the strong spatial gradients that exist in those emissions. It is often difficult to determine from the camera output when the camera is responding primarily to 630.0 nm emissions since the diffuse nature of the emissions from $O(^1D)$ results in poor image contrast.

The images obtained by an unfiltered camera are an amplified version of all of the incident light weighted by the spectral response of the photocathode. There may be a few dominant spectral lines in an auroral image but the camera will also integrate photons at wavelengths intermediate

Reproduced with permission of the copyright owner. Further reproduction prohibited without permission.

to the auroral emissions contributing to an unwanted background noise. The problem is one of contrast, that of obtaining the form of a luminous object imbedded in a background of light. In the case of the dayside forms there is a background of continuum solar illumination that comes from scattered twilight, airglow, and extra terrestrial sources including unresolved stars and emission nebulae. This can be seen in many of the images as a bright region on the southern horizon for the case of the twilight. The auroral image may well be bright in the auroral lines, but the integrated intensity in all other lines across the visible spectrum will result in little variation of intensity inside the auroral form to that of the sky outside of the auroral form. Airglow is brighter near the horizon than the zenith due to the van Rihjn effect–that of integrating a uniformly emitting layer over longer path lengths near the horizon. Most of the extra-terrestrial sources are localized and are not readily misinterpreted as auroral signals. An exception is the Milky Way Galaxy (an example of which appears in Figure B.3). The many unresolved starts give the galaxy the appearance of a long arc and may be mistaken as an extended region of emission, especially at the high latitude of Svalbard where the Milky Way may be found within 10-15 degrees of the zenith.

Reduction of the unmodulated light requires limiting the wavelengths of the input photons. The easiest method is the use of a filter. A simple cutoff filter that transmits both the 557.7 nm and 630.0 nm lines but absorbs all of the blue end of the spectra is particularly useful in reducing the scattered twilight component since scattering is most efficient at the blue end of the spectrum. Use of narrow band interference filters is a particularly efficient method of limiting the wavelengths of the input light with the added advantage of obtaining images in light of known wavelength ranges. However, the optics of the camera system must be carefully designed to limit the angles of rays that are incident on the filter or the narrow passband of the filter simply opens due to the angle dependence of the filter transmission band discussed in Appendix A. All of the images used in this thesis are white light without use of any filters.

### B.5 Image Resolution.

Angular resolution in a television image is determined by the number of individual scan lines present in the original image. The NTSC standard is 280,000 information elements per frame with 440 picture elements in each scan line. A more practical limit on the image resolution here is the number of pixels obtained in digitizing the images since this defines the resolution of the image available for presentation and analysis. The 151 Image Processor is capable of grabbing and storing to computer disk digitized versions of NTSC video signals with 512 $\times$ 480 pixels in each image. This is the entire video image and fewer pixels are actually within the range of the all sky image. The IO images typically result in approximately 400 pixels across the all sky image, yielding 180 $^\circ$ /400 pixels, or .45$^\circ$ /pixel.

Temporal resolution is determined by the rate at which the beam current sweeps the target. Images are obtained at the NTSC rate of 60 interlaced half frames per second (even scans are obtained in the first 1/60 of a second and odd scans in the next 1/60 of a second) to obtain a full frame each 1/30 of a second. The interlacing feature is designed to "smear" motion so the television image appears smoothly varying to the human eye. The analog video signal is recorded

Reproduced with permission of the copyright owner. Further reproduction prohibited without permission.

on commercial VHS video tape at the same NTSC video rate. Original video signals are often noisy requiring further processing to increase contrast for analysis. Processing the video signal typically involves adding a series of full frames on either a Quantex DS-50 video processor or 151 Video Processor in the laboratory. The object in either case was to add together a series of frames to reduce the noise in the images. Averages of 32 frames to 128 frames were used to obtain approximately 0.5 to 4 second time resolution in the processed images.

The Quantex video processor [*Quantex Corporation*, 1981] utilizes a single 512 × 512 12 bit video memory buffer to store incoming digitized signals. Summing of images is implemented by adding successive incoming frames to the buffer. Summing is useful for photon limited images as a long integration can build up an image over a period longer than the 1/30 second required to obtain the original television image. The white light auroral images, however, have sufficiently large signals that summing can quickly overflow the buffers. The main problem to overcome in the auroral images was noise originating from the camera in the original image and tape noise related to recording and retrieving images from the video tape.

A more useful algorithm is to average the images. The "average" algorithm implemented by the Quantex [*Quantex DS-50 Digital Video Processor ...Manual*] is of the form

$$M = \frac{(I - M)}{N} + M = I/N + (N-1)M/N \qquad B.1$$

where M is the image in memory, I the incoming signal, and N is variable in powers of 2 from $2^0$ to $2^7$. This algorithm provides a continuous signal at 30 frames per second with no buffer overflow. In contrast, the common algorithm for averaging

$$M = (\sum_{k=1}^{N} I_k)/N \qquad B.2$$

first requires a sum process followed by the division and cannot yield processed images faster than 30/N images a second. In addition, since the sum step is required the buffer overflow limits the number of frames that can be used in the sum process.

The gain and black level of the incoming analog video signal is adjusted before the digitization step required for the internal buffering process used in the processor. The gain and offset of the resulting output signal was also adjustable for optimal contrast before being converted back to the processor output analog signal. Careful adjustment of the images on the processors gave great improvement to the images before digitizing. A digitized version of a poorly preprocessed signal was generally not useful for analysis on the computer. The final adjustment and enhancement of the digital images was accomplished through the application of a variety of computer algorithms (thresholding, median filtering, etc.) implemented in Interactive Data Language (IDL) on a DEC 5000 workstation.

The purpose of the IO camera was to provide records of auroral distribution. No attempt was made to obtain quantitative estimates of signal levels from the camera. In the future it may be of interest to consider quantitative estimates of the camera output. However, unless interference

Reproduced with permission of the copyright owner. Further reproduction prohibited without permission.

filters are used to limit the sensitivity to a restricted wavelength region it is of questionable merit to attempt any quantitative work.

### B.6 Contrast

The IO is a very sensitive instruments capable of forming images in very low light conditions. It is not unusual that the MSP is capable of recording faint emissions that are not visible on the camera systems. This is the result of poor contrast available in the white light images. Consider the equation

$$Contrast = \frac{I_s - I_b}{I_b} \qquad B.3$$

as a measure of the contrast in an image where $I_s$ and $I_b$ are the intensity of an object (the signal) and background, respectively. If the object is to be minimally visible over the background, then the difference $I_s - I_b$ must be at least as large as the error in the background, $I_b$. Assuming Poisson statistics, the error in the background is $\sqrt{I_b}$ resulting in a limiting contrast of 1. Values of the contrast less than one will result in the loss of the signal in the noise.

The response of a white light camera is given by the sum of the product of the incident light intensity $I(\lambda)$ and the relative response of the camera $W(\lambda)$, or

$$Signal = \int I(\lambda)W(\lambda)d\lambda \qquad B.4$$

where the integral is carried out over all wavelengths where the product is nonzero. Using the 20 R/nm continuum background reported by Krassovsky et al. (1962) for $I(\lambda)$ and the relative response of the IO camera, the integral given above yields a total of approximately 5 kR. Therefore, a monochromatic signal with intensity less than 70 R will not be detected by the camera while it may readily be detected by the MSP.

Reproduced with permission of the copyright owner. Further reproduction prohibited without permission.

# Appendix C Color Figures

## C.1 DMSP Electron and Ion Energy Spectrograms

Figure C.1 is an ion and electron spectrogram obtained during a southern hemisphere pass through the dayside auroral by the DMSP F9 satellite. A classic cusp/mantle ion energy dispersion feature is present between magnetic latitudes of -74.4° and -78° . Equatorward of the cusp plume is a region with electron energies $\geq$ 1 keV and average electron energy of nearly 10 keV. These electrons are part of the plasma sheet population in the dayside magnetosphere. Precipitation of these electrons produces the mantle aurora. The latitudinal gap (Chapter 5) is present between the poleward border of the plasma sheet electrons and the equatorward edge of the intense electron fluxes within the cusp.

Figure C.2 is a similar case from the northern hemisphere obtained by the DMSP F10 satellite. The high energy electron fluxes from the plasma sheet are not present at magnetic latitudes >71° in this case. A latitudinal gap would not be expected to appear in photometer records for these conditions.

The spectrogram in Figure C.3 obtained by the DMSP F10 satellite also shows a classic cusp plume between approximately 08:36 UT and 08:37 UT in the 1243 MLT to 1330 MLT sector. A second "mirror image" plume is present in the 1330 MLT to 1430 MLT sector. *Weiss et al.* [1995] propose that the "double cusp" feature is due to lobe reconnection. The oblique path of the satellite through the dayside oval allows the cusp precipitation to be sampled over longer time periods. Electron fluxes within the cusp are seen to be highly structured, not smooth as suggested in Figure D.1. The latitudinal gap is sampled between 08:37:00 UT and 08:37:15 UT.

Reproduced with permission of the copyright owner. Further reproduction prohibited without permission.

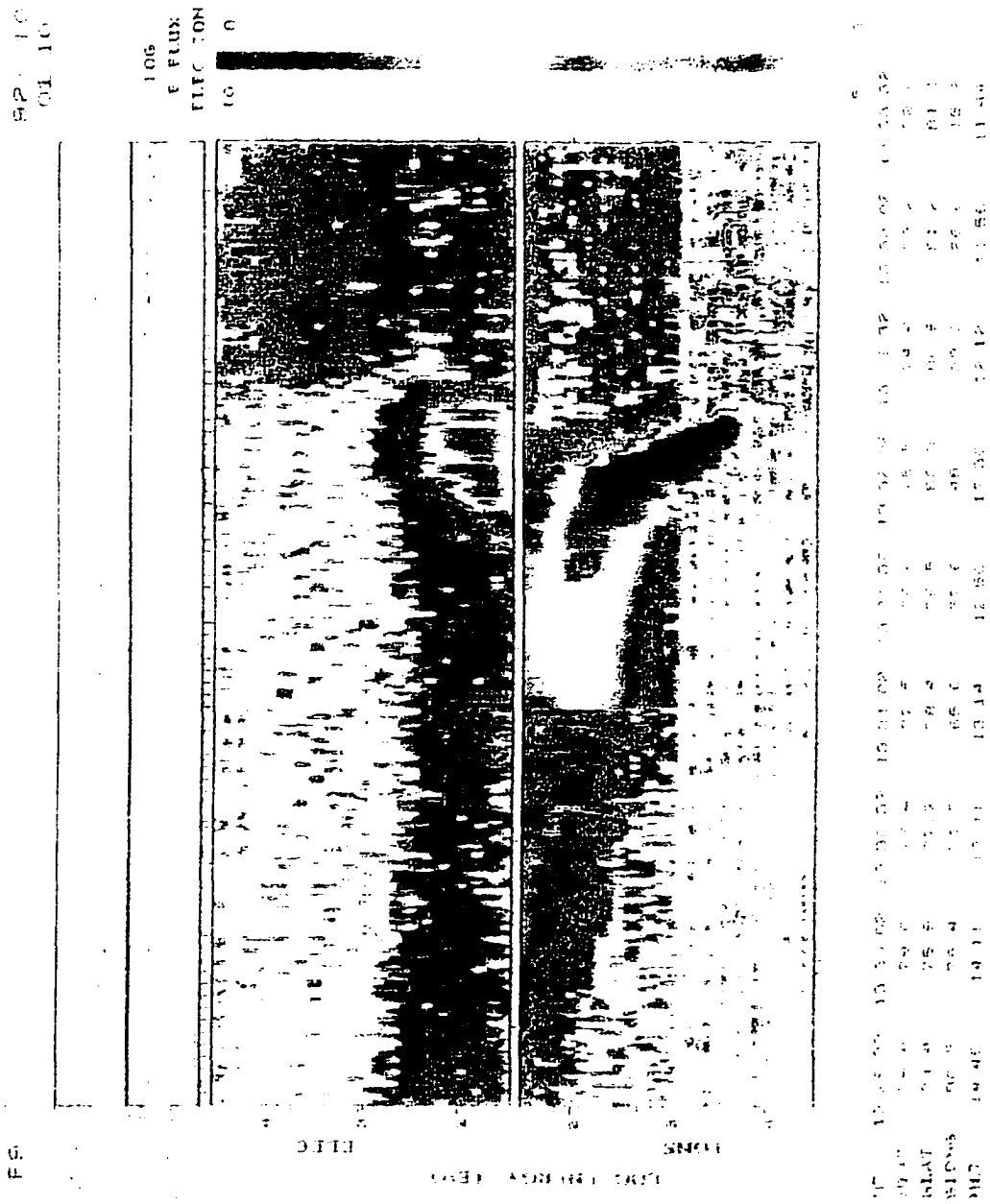

Figure C.1 DMSP F9 Electron and Ion Spectrogram, 10 January 1992. The satellite orbital track intersected the polar cusp in the southern hemisphere at approximately 13:32 UT. Ion and electron energy fluxes in the top plot are in units of eV/cm$^2$ s sr, the average energy is in eV, and the color coded differential energy fluxes are in units of eV/cm$^2$ s sr eV.

Reproduced with permission of the copyright owner. Further reproduction prohibited without permission.

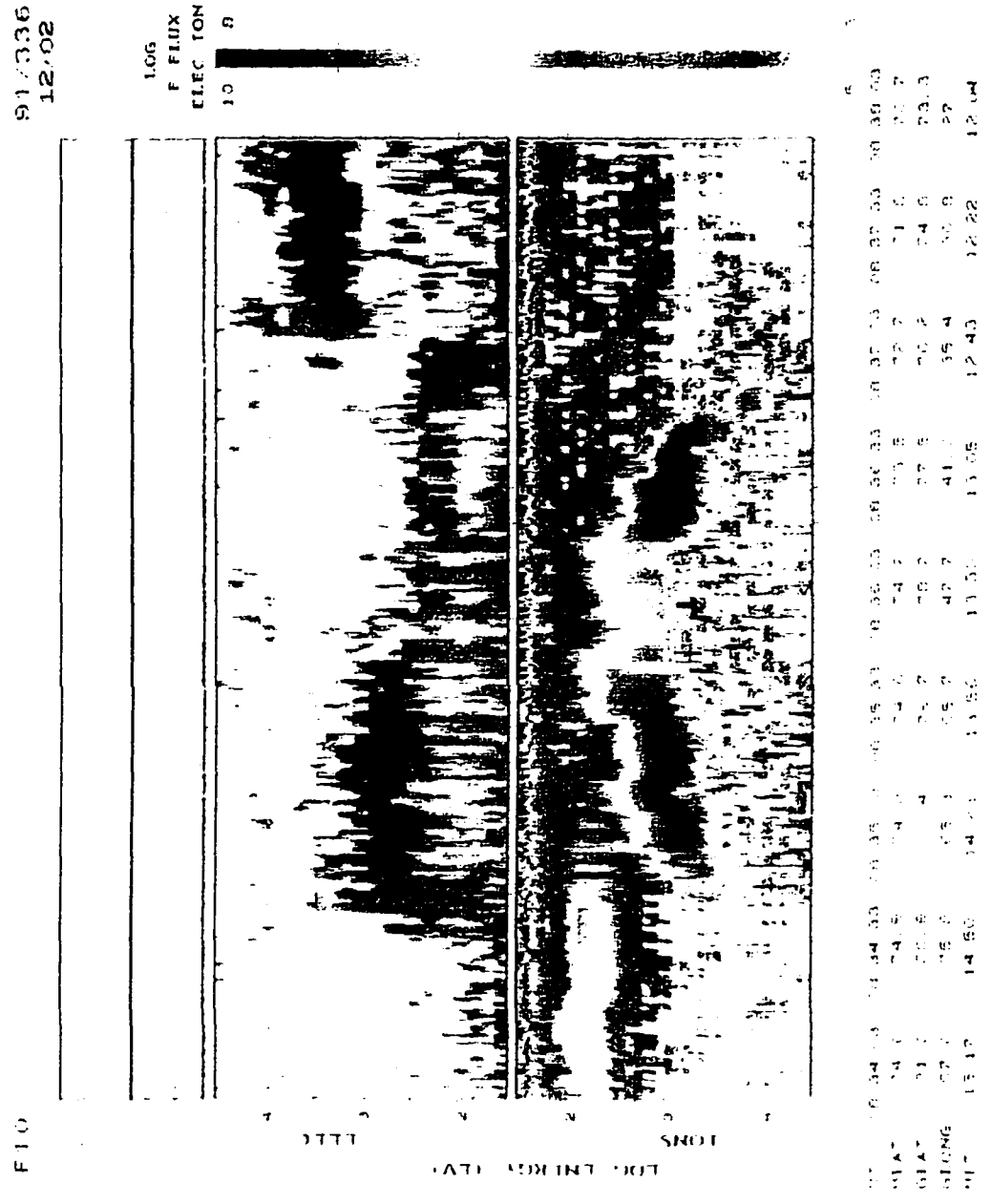

Figure C.2 DMSP F10 Electron and Ion Spectrogram, 2 December 1991. The satellite encountered the northern hemisphere cusp/plasma sheet boundary at approximately 08:37 UT. The plot format and units are the same as Figure C.1.

Reproduced with permission of the copyright owner. Further reproduction prohibited without permission.

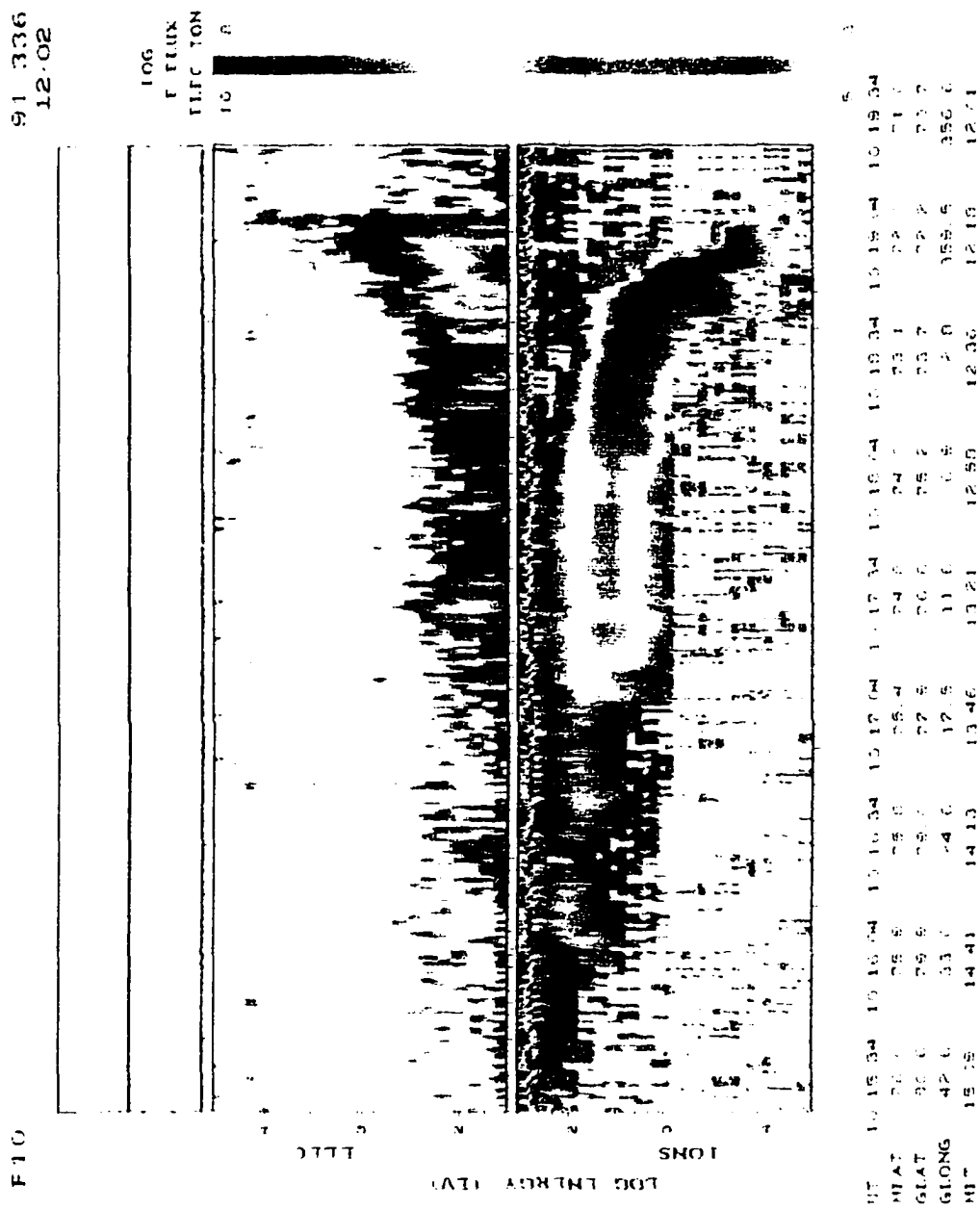

Figure C.3 DMSP F10 Electron and Ion Spectrogram, 2 December 1991. The satellite encountered the northern hemisphere cusp/plasma sheet boundary at approximately 10:19 UT. The plot format and units are the same as Figure C.1.

Reproduced with permission of the copyright owner. Further reproduction prohibited without permission.

# Appendix D Charged Particle Flux Relations

## D.1 Converting Differential Fluxes to Omnidirectional Fluxes

Conversion of differential angular energy fluxes $J(E,\theta,\phi)$ measured by satellites to the omnidirectional integral energy fluxes $J$ required to estimate intensities of emission features using conversion factors of the form

$$I(630.0) = K \;\; kR/ergcm^{-2}s^{-1} \tag{E.1}$$

where $K$ is an energy dependent parameter (c.f., equations (3.40)-(3.42) and (3.46)-(3.47) requires the knowledge of the particle pitch angle distribution.

An energy flux $J(E,\theta,\phi)$ in units of eV/cm$^2$ s sr is converted to a downward hemispherical flux by integrating

$$J(E) = \int\int J(E,\theta,\phi)cos\theta d\omega \;\; erg/cm^2s \tag{E.2}$$

where $d\omega = sin\theta d\theta d\phi$. An isotropic particle distribution is independent of $\theta$ and $\phi$ and the integral yields

$$J(E) = \pi J(e,\theta,\phi) \;\; erg/cm^2s \tag{E.3}$$

while a cosine pitch angle distribution yields

$$J(E) = \frac{2}{3}\pi J(e,\theta,\phi) \;\; erg/cm^2s \tag{E.4}$$

Conversion of the differential angular fluxes into omnidirectional fluxes is only possible if the particle pitch angle distributions are known. The detectors on the DMSP satellites have acceptance half angles of 3° by 4° [P.T. Newell, personal communication, 1995]. Only particle fluxes which are very nearly field aligned are measured and there is no information available in the DMSP records of precipitating particles with pitch angles greater than 4° at 800 km.

Reproduced with permission of the copyright owner. Further reproduction prohibited without permission.

# Appendix E Spectra of Dayside Aurora

## E.1 Survey of Spectral Regions

**Table E.1**
**Published Spectra of Dayside Aurora**

| Wavelength Range (nm) | Notes[1] | Reference |
|---|---|---|
| 53.0 - 150.0 | | *Gentieu et al.*, 1988 |
| 330.0 - 400.0 | | *Sivjee*, 1976 |
| 340.0 - 395.0 | d-n | *Sivjee and Deehr*, 1980 |
| 340.0 - 430.0 | | *Sivjee*, 1983a |
| 368.0 - 381.0 | d-n | *Sivjee*, 1991 |
| 384.0 - 393.0 | | *Sivjee et al.*, 1980 |
| 414.0 - 428.0 | d-n | *Sivjee*, 1983a |
| 419.0 - 428.0 | | *Sivjee and Deehr*, 1980 |
| 480.0 - 570.0 | | *Henriksen et al.*, 1978 |
| 500.0 - 850.0 | | *Gault et al.*, 1991 |
| 519.0 - 524.0 | d-n | *Sivjee and Deehr*, 1980 |
| | | *Sivjee et al.*, 1981 |
| 581.0 - 589.0 | | *Sivjee et al.*, 1980 |
| 600.0 - 700.0 | | *Sivjee and Deehr*, 1980 |
| 630.0 - 690.0 | | *Henriksen et al.*, 1985 |
| 630.0 - 690.0 | d-n | *Sivjee and Deehr*, 1980 |
| 650.0 - 850.0 | d-n | *Sivjee and Deehr*, 1980 |
| 652.0 - 658.0 | | *Sigernes et al.*, 1996 |
| 658.0 - 740.0 | | *Henriksen et al.*, 1984 |
| 685.0 - 740.0 | d-n | *Sivjee*, 1983b |
| 680.0 - 710.0 | d-ng | *Sivjee*, 1983b |
| 770.0 - 850.0 | d-n | *Sivjee and Deehr*, 1980 |
| | | *Sivjee et al.*, 1984 |

[1]Includes comparison between dayside and night aurora (d-n) and dayside aurora and night airglow (d-ng) spectra.

Reproduced with permission of the copyright owner. Further reproduction prohibited without permission.

## References

[Note: References consulted in development of the thesis but not specifically cited in the text are marked by an asterisk.]


Abreu, V.J., and J.H. Yee, Diurnal and seasonal variation of the nighttime OH (8-3) emission at low latitudes, *J. Geophys. Res.*, 94, 11949 - 11957, 1989.

Akasofu, S.-I., Thickness of an active auroral curtain, *J. Atmos. Terr. Physics*, 21, 287 - 288, 1961.

Akasofu, S.-I., *Polar and Magnetospheric Substorms*, Reidel, Dordrecht, 1968.

Akasofu, S.-I., Midday auroras and magnetospheric substorms, *J. Geophys. Res.*, 77, 244 - 247, 1972a.

Akasofu, S.-I., Midday auroras at the South Pole during magnetospheric substorms, *J. Geophys. Res.*, 77, 2303 - 2308, 1972b.

Akasofu, S-I., A study of auroral displays photographed from the DMSP-2 satellite and from Alaska meridian chain of stations, *Space Sci. Rev.*, 16, 617, 1974.

Akasofu, S.-I., Recent progress in studies of DMSP auroral photographs, *Space Sci. Rev.*, 19, 169, 1976.

Akasofu, S.-I., *The Physics of Magnetospheric Substorms*, D. Reidel Pub. Co., Dordrecht, 1977.

Akasofu, S.-I., Energy coupling between the solar wind and the magnetosphere, *Space Sci. Rev.*, 28, 121 - 190, 1981.

Akasofu, S.-I., and S. Chapman, *Solar-Terrestrial Physics*, Oxford at the Clarendon Press, 1972.

Akasofu, S.-I., E.W. Hones, Jr., S.J. Bame, J.R. Asbridge, and A.T.Y. Lui, Magnetotail and boundary layer plasmas at geocentric distance of 18 $R_E$: Vela 5 and 6 observations, *J. Geophys. Res.*, 78, 7257, 1973.

Akasofu, S.-I., and J.R. Kan, Dayside and nightside arc systems, *Geophys. Res. Letters*, 7, 753 - 756, 1980.

Alad'yev, G.A., Modeling the ionosphere in the day-cusp and polar-cap regions during magnetospheric substorms, *Geomagnetism and Aeronomy*, 29, 31 - 35, 1989.

Anderson, K.A., H.K. Harris, and R.J. Paoli, *J. Geophys. Res.*, 70, 1039, 1965.

Andre, D., and W. Baumjohann, Joint two-dimensional observations of ground magnetic and ionospheric electric currents associated with auroral currents. 5. Current system associated with eastward drifting omega bands, *J. Geophys. Res.*, 50, 194.

Antonova, A.E., and V.P. Shabansky, On the structure of the geomagnetic field at large distances from the Earth, *Geomagnetism and Aeronomy*, 8, 801 - 811, 1968.

Aparicio, B., B. Thelin, and R. Lundin, The polar cusp from particle point of view: A statistical study based on Viking data, *J. Geophys. Res.*, 96, 14023 - 14031, 1991.

Asamura, K., and T. Iyemori, Flywheel effect deduced from geomagnetic variation in the polar region, *J. Geomag. Geoelectr.*, 47, 973 - 987, 1995.


Reproduced with permission of the copyright owner. Further reproduction prohibited without permission.

Atkinson, G., F. Creutzberg, R.L. Gattinger, and J.S. Murphree, Interpretation of complicated discrete arc structure and behavior in terms of multiple X lines, *J. Geophys. Res.*, 94, 5292 - 5302, 1989.

Atkinson, G., Mechanism by which merging at X lines causes discrete auroral arcs, *J. Geophys. Res.*, 97, 1337 - 1344, 1992.

Aubry, M.P., C.T. Russell, and M.G. Kivelson, Inward motion of the magnetopause before a substorm, *J. Geophys. Res.*, 75, 7018 - 7031, 1970.

Axford, W.I., The interaction between the solar wind and the earth's magnetosphere, *J. Geophys. Res.*, 67, 3791, 1962.

Axford, W.I., F. Buhler, H.J.A. Chivers, P. Eberhardt, and J. Geiss, Auroral helium precipitation, *J. Geophys. Res.*, 77, 6724 - 6730, 1972.

Axford, W.I., and C.O. Hines, A unifying theory of high-latitude geophysical phenomena and geomagnetic storms, *Canad. J. of Phys.*, 39, 1433 - 1464, 1961.

Baker, D.N., T.I. Pulkkinen, V. Angelopoulos, W. Baumjohann, and R.L. McPherron, Neutral line model of substorms: Past results and present view, *J. Geophys. Res.*, 101, 12975 - 13010, 1996.

Baker, D.N., P. Stauning, E.W. Hones, Jr., P.R. Higbie, and R.D. Belian, Strong electron pitch angle diffusion observed at geostationary orbit, *Geophys. Res. Letters*, 6, 205 - 208, 1979.

Baker, K.B., and S. Wing, A new magnetic coordinate system for conjugate studies at high latitudes, *J. Geophys. Res.*, 94, 9139 - 9143, 1989.

Baluja, K.L. and C.J. Zeippen, M1 and E2 Transition Probabilties for States Within the $2p^4$ Configuration of the O I Isoelectronic Sequence, *J. Phys. B: At. Mol. Opt. Phys.*, 21, 1455 - 1471, 1988.

Bame, S.J., R.C. Anderson, J.R. Asbridge, D.N. Baker, W.C. Feldman, J.T. Gosling, E.W. Hones, Jr., D.J. McComas, and R.D. Zwickl, Plasma regimes in the deep geomagnetic tail: ISEE 3, *Geophys. Res. Letters*, 10, 912 - 915, 1983.

Bame, S.J., A.J. Hundhausen, J.R. Asbridge, and I.B. Strong, Solar wind ion composition, *Phys. Rev. Lett.*, 20, 393, 1968.

Banks, P.M., C.R. Chappell, and A.F. Nagy, A new model for the interaction of auroral electrons with the atmosphere: Spectral degradation, backscatter, optical emission, and ionization, *J. Geophys. Res.*, 79, 1459, 1974.

Baron, M.J., and R.H. Wand, F region ion temperature enhancements resulting from joule heating, *J. Geophys. Res.*, 88, 4114 - 4118, 1983.

Basinska, E.M., W.J. Burke, and M.A. Heinemann, A user's guide to locating flux transfer events in low-altitude satellite measurements: An S3-2 case study, *J. Geophys. Res.*, 94, 6681 - 6691, 1989.

Bates, D.R., Forbidden oxygen and nitrogen lines in the nightglow, *Planet. Space Sci.*, 26, 897 - 912, 1978.

Baumjohannm, W., and G. Haerendel, Dayside convection, viscous interaction and magnetic merging, in *Solar Wind-Magnetosphere Coupling*, edited by Y. Kamide and J.A. Slavin, 415 - 421, Terra Scientific Publishing Company, 1986.

Reproduced with permission of the copyright owner. Further reproduction prohibited without permission.

Berchem, J., and and C.T. Russell, Flux transfer events on the magnetopause: spatial distribution and controlling factors, *J. Geophys. Res.*, 89, 6689 - 6703, 1984.

Berkey, F.T., Observations of pulsating aurora in the day sector auroral zone, *Planet. Space Sci.*, 26, 635 - 650, 1978.

Bewick, A., G.P. Haskell, and R.J. Hynds, Low energy solar protons in the pseudo-trapping region of the magnetosphere, *J. Geophys. Res.*, 78, 597, 1973.

Biermann, L., Kometenschweife und solare korpuskular Strahlung, *Z. Astrophys.*, 29, 274 - 286, 1951.

Biermann, L., Solar corpuscular radiation and the interplanetary gas, *Observatory*, 77, 109 - 110, 1957.

Beard, D.B., and J.Y. Choe, The magnetospheric boundary, in *Correlated Interplanetary and Magnetospheric Observations*, edited by D.E. Page, pp. 97 - 114, D. Reidel, 1974.

Benson, K. B., *Television Engineering Handbook*, McGraw-Hill Book Company, 1986.

Berchem, J., and C.T. Russell, The thickness of the magnetopause current layer: ISEE 1 and 2 Observations, *J. Geophys. Res.*, 87, 2108 - 2114, 1982.

Berchem, J., and C.T. Russell, Flux transfer events on the magnetopause: spatial distribution and controlling factors, *J. Geophys. Res.*, 89, 6689 - 6703, 1984.

Blanchard, G.T., L.R. Lyons, J.C. Samson, F.J. Rich, Locating the polar cap boundary from observations of 6300 Å auroral emissions, *J. Geophys. Res.*, 100, 7855 - 7862, 1995.

Blifford, Jr., I.H., Factors affecting the performance of commericial interference filters, *Applied Optics*, 5, 105 - 111, 1966.

Borovsky, J.E., Auroral arc thicknesses as predicted by various theoris, *J. Geophys. Res.*, 98, 6101 - 6138, 1993.

Borovsky, J.E., R.J. Nemzek, and R.D. Bellian, The occurence rate of magnetospheric-substorm onsets: Random and periodic substorms, *J. Geophys. Res.*, 98, 3807 - 3813, 1993.

Borovsky, J.E., D.M. Suszcynsky, M.I. Buchwald, and H.V. DeHaven, Measuring the thickness of auroral curtains,*Arctic*, 44, 231 - 238, 1991.

Brekke, A., On the evolution in history of the concept of the auroral oval, *EOS*, 65, 45 - 48, 1984.

Brekke, A., and H. Pettersen, Some observations of pulsating aurora at Spitzbergen, *Planet. Space Sci.*, 19, 536 - 540, 1971.

Brewer, H.R., M. Schultz, and A. Eviatar, Origin of drift-periodic echoes in outer-zone electron flux, *J. Geophys. Res.*, 74, 159, 1969.

Brice, N.M., Bulk motion of the magnetosphere, *J. Geophys. Res.*, 72, 5193 - 5211, 1967.

*Broadfoot and Hunten, N2+ emission in twilight, *Planet. Space Sci.*, 14, 1303 - 1319, 1966.

Broadfoot, A.L., and K.R. Kendall, The airglow spectrum, 3100-10000 A, *J. Geophys. Res.*, 73, 426 - 428, 1968.

Bryant, D.A., G.M. Courtier, and G. Bennett, Equatorial modulation of electrons in pulsating aurora, *J. Atmos. Terr. Physics*, 33, 859, 1971.

Buchau, J., J.A. Whalen, and S.-I. Akasofu, On the continuity of the auroral oval, *J. Geophys. Res.*, 75, 7147 - 7160, 1970.

Reproduced with permission of the copyright owner. Further reproduction prohibited without permission.

Buchau, J., G.J. Gassmann, C.P. Pike, R.A. Wagner, and J.A. Whalen, Precipitation patterns in the Arctic ionosphere determined from airborne observations, *Ann. Geophys.*, 28, 443 - 453, 1972.

Buchau, J., B.W. Reinisch, E.J. Weber, and J.G. Moore, Structure and dynamics of the winter polar cap F region, *Radio Science*, 18, 995, 1983.

Buck, R.M., Energetic electron drift motions in the outer dayside magnetosphere–observations and calculations, *EOS Trans. Amer. Geophys. Union*, 56, 628, 1975.

*Buck, R.M., H.I. West, Jr., and R.G. D'Arcy, Jr., Satellite studies of magnetospheric substorms on August 15, 1968: Ogo-5 energetic proton observations-spatial boundaries, J. Geophys. Res., 78, 3103, 1973.

Buhler, F., W.I. Axford, H.J.A. Chivers, and K. Marti, Helium isotopes in an aurora, *J. Geophys. Res.*, 81, 111 - 115, 1976.

Burch, J.L., Rate of erosion of dayside magnetic flux based on a quantitative study of the dependence of polar cusp latitude on the interplanetary field,*Radio Sci.*, 8, 955 - 961, 1973.

Burch, J.L., Effecgts of the interplanetary magnetic field on the auroral oval and plasmasphere, *Space Sci. Rev.*, 23, 449, 1979.

Burch, J.L., P.H. Reiff, R.A. Heelis, J.D. Winningham, W.B. Hanson, C. Gurgiolo, J.D. Menietti, R.A. Hoffman, and J.N. Barfield, Plasma injection and transport in the mid-altitude polar cusp, *Geophys. Res. Letters*, 9, 921 - 924, 1982.

Burch, J.L., P.H. Reiff, J.D. Menietti, R.A. Heelis, W.B. Hanson, D.S. Shawhan, E.G. Shelley, M. Sigiura, and J.D. Winningham, *J. Geophys. Res.*, 1982.

Burch, J.L., Quasi-neutrality in the polar cusp, *Geophys. Res. Letters*, 12, 469 - 472, 1985.

Burch, J.L., P.H. Reiff, J.D. Menietti, R.A. Heelis, W.B. Hanson, D.S. Shawhan, E.G. Shelley, M. Sigiura, D.R. Weimer, and J.D. Winningham, IMF $B_y$ dependent plasma flow and Birkeland currents in the dayside magnetopshere 1. Dynamic Explorer observations, *J. Geophys. Res.*, 90, 1577 - 1593, 1985.

Burke, W.J., D.A. Hardy, and R.P. Vancour, Magnetospheric and high latitude ionospheric electrodynamics, in *Handbook of Space Physics and the Geospace Environment*, edited by A.S. Jursa, ADA 167000, Air Force Geophysics Laboratory, Air Force Systems Command, USAF, 1985.

Burke, W.J., B. Jacobsen, P.E. Sandholt, W.F. Denig, N.C. Maynard, and P.T. Newell, Optical signatures and source of prenoon auroral precipitation, *J. Geophys. Res.*, 98, 11521 - 11529, 1993.

Burlaga, L.F., and J.H. King, Intense interplanetary magnetic fields observed by geocentric spacecraft during 1963-1975, *J. Geophys. Res.*, 84, 6633 - 6640, 1979.

Burnside, R.G., J.W. Meriwether, Jr., and M.R. Torr, Contamination of ground-based measurements of OI (6300 Å) and NI (5200 Å) airglow by OH emissions,*Planet. Space Sci.*, 25, 985 - 988, 1977.

Burrows, J.R., I.B. McDiarmid, and M.D. Wilson, Pitch angles and spectra of particle in the outer zone near noon, in *Earth's Magnetospheric Processes*, edited by B.M. McCormac, pp. 153 - 167, D. Reidel, Hingham, Mass., 1972.

Reproduced with permission of the copyright owner. Further reproduction prohibited without permission.

Bythrow, P.F., B.J. Anderson, T.A. Potemra, L.J. Zanetti, J.D. Winningham, and D.L. Chenette, Filamentary current structures in the postnoon sector: Observations from UARS, *J. Geophys. Res.*, 14917 - 14929, 1994.

Caan, M.N., R.L. McPherron, and C.T. Russell, Substorm and interplanetary magnetic field effects on the geomagnetic tail lobes, *J. Geophys. Res.*, 80, 191, 1975.

Cahill, L.J., and P.G. Amazeen, The boundary of the geomagnetic field, *J. Geophys. Res.*, 68, 1835 - 1843, 1963.

Candidi, M., H.W. Kroehl, and C.-I. Meng, Intensity distribution of dayside polar soft electron precipitation and the IMF, *Planet. Space Sci.*, 31, 489 - 498, 1983.

Carbury, J.F., and C.-I. Meng, Correlation of cusp latitude with $B_z$ and AE(12) using nearly one year's data, *J. Geophys. Res.*, 91, 10047 - 10054, 1986.

Carbury, J.F., and C.-I. Meng, Correlation of cusp width with AE(12) and $B_z$,*Planet. Space Sci.*, 36, 157 - 161, 1988.

Carlheim-Gyllenskiöld, *Observations Faites au Cap Thordsen, Spitzberg, par L'Expédition Suédoise*, L'Académie Royalie des Sciences de Suéde, Volume II., Stockholm, 1887.

Carlson, H.C., and R.B. Torbert, Solar wind ion injections in the morning auroral oval, *J. Geophys. Res.*, 85, 2903, 1980.

Cartwright, D.C., Vibrational populations of the excited states of $N_2$ under auroral conditions, *J. Geophys. Res.*, 83, 517 - 531, 1978.

Chamberlain, J.W., *Physics of the Aurora and Airglow*, Academic Press, New York, 1961.

Chapman, S., History of aurora and airglow, in *Aurora and Airglow*, pp. 15 - 29, edited by B.M. McCormac, Reinhold Pub. Corp., 1967.

Chapman, S., Auroral science, 1600 to 1965 towards its golden age?, in *Atmospheric Emissions*, pp. 11 - 25, B.M. McCormac and A. Omholt, (eds.), Van Nostrand Reinhold Co., 1969.

Chapman, S., and V.C.A. Ferraro, A new theory of magnetic storms, *Terr. Magn. Atmospheric. Elec.*, 36, 77-97, 171-186, 1931.

Chapman, S., and V.C.A. Ferraro, A new theory of magnetic storms, *Terr. Magn. Atmospheric. Elec.*, 37, 147-156, 421-429, 1932.

Chappell, C.R., Recent satelite measurements of the morphology and dynamics of the plasmasphere, *Rev. of Geophys. and Space Phys.*, 10, 951, 1972.

Chappell, C.R., R.C. Olsen, J.L Green, J.F.E. Johnson, and J.H. Waite, Jr., The discovery of nitrogen ions in the Earths's magnetosphere, *Geophys. Res. Letters*, 9, 937 - 940, 1982.

Chernouss, S.A., V.G. Vorob'yev, V.P. Tagiriv, *Polar Geomagnetic Phenomena, Report Summary International Symposium Suzdal*, Nauka Press, Moscow, p. 53, 1986.

Choe, J.Y., and D.B. Beard, The compressed geomagnetic field as a function of dipole tilt, *Planet. Space Sci.*, 22, 595 - 608, 1974.

Christensen, A.B., L.R. Lyons, J.H. Hecht, G.G. Sivjee, R.R. Meier, and D.G. Strickland, *J. Geophys. Res.*, 92, 6163 - 6167, 1987.

Cladis, J.B., and W.E. Francis, Distribution in magnetotail of $O^+$ ions from cusp/cleft ionosphere: A possible substorm trigger, *J. Geophys. Res.*, 97, 123, 1992.

Reproduced with permission of the copyright owner. Further reproduction prohibited without permission.

Clemmons, J.H., C.W. Carlson, and M.H. Boehm, Impulsive ion injections in the morning auroral region, *J. Geophys. Res.*, 100, 12133 - 12149, 1995.

Cogger, L.L., J.S. Murphree, S. Ismail, and C.D. Anger, Characteristics of dayside 5577 Å and 3914 Å aurora, *Geophys. Res. Letters*, 4, 413 - 416, 1977.

Cohen-Tannoudji, C., B. Diu, and F. Laloë, *Quantum Mechanics, Volumes I, II*, Wiley-Interscience Pub., 1977.

Coleman, P.J., Jr., A model of the geomagnetic cavity, *Radio Sci.*, 6, 321, 1971.

Coley, W.R., R.A. Heelis, W.B. Hanson, P.H. Reiff, J.R. Sharber, and J.D. Winningham, Ionospheric convection signatures and magnetic field toplogy, *J. Geophys. Res.*, 92, 12352 - 12364, 1987.

Condon, E.U., *Astrophys. J.*,79, 217, 1934.

Cornwall, J.M., Scattering of energetic trapped electrons by very-low-frequency waves, *J. Geophys. Res.*, 69,1251, 1964.

Cornwall, J.M., Cyclotron instabilities and electromagnetic emissions in the ultra low frequency and very low frequency ranges, *J. Geophys. Res.*, 70, 61, 1965.

Cornwall, J.M., F.V. Coroniti, and R.M. Thorne, Unified theory of SAR arc formation at the plasmapause, *J. Geophys. Res.*, 76, 4428 - 4445, 1971.

Coroniti, F.V., and C.F. Kennel, Auroral micropulsation instability, *J. Geophys. Res.*, 75, 1863 - 1878, 1970a.

Coroniti, F.V., and C.F. Kennel, Electron precipitation pulsations, *J. Geophys. Res.*, 75, 1279 - 1289, 1970b.

Cowley, S.W.H., Comments on the merging of nonantiparallel magnetic fields, *J. Geophys. Res.*, 3455 - 3458, 1976.

Cowley, S.W.H., Plasma populations in a simple open model magnetosphere, *Space Science Reviews*, 26, 217 - 275, 1980.

Cowley, S.W.H., Magnetospheric asymmetries associated with the Y-component of the IMF, *Planet. Space Sci.*, 29, 79, 1981.

Cowley, S.W.H., *Rev. of Geophys.*, 20, 531 - 565, 1982.

Cowley, S.W.H., The impact of recent observations on theoretical understanding of solar wind-magnetosphere interactions, *J. Geomag. Geoelectr.*, 38, 1223 - 1256, 1986.

Cowley, S.W.H., M.P. Freeman, M. Lockwood, and M.F. Smith, The ionospheric signature of flux transfer events, *Proceedings of an International Workshop on Cluster Dayside Polar Cusp, Rep. ESA SP-330*, pp. 105 - 112, Eur. Space Agency, Neuilly, France, 1991.

Cowley, S.W.H., and Z.V. Lewis, Magnetic trapping of energetic particles on open dayside boundary layer flux tubes, *Planet. Space Sci.*, 38, 1343 - 1350, 1990.

Craven, J.D., Temporal variations of electron intensities at low altitudes in the outer radiation zone as observed with satellite Injun 3, *J. Geophys. Res.*, 71, 5643 - 5663, 1966.

Craven, M., and G.B. Burns, High latitude pulsating aurorae, *Geophys. Res. Letters*, 17, 1251 - 1254, 1990.

Crooker, N.U., Explorer 33 entry layer observations, *J. Geophys. Res.*, 82, 515, 1977.

Reproduced with permission of the copyright owner. Further reproduction prohibited without permission.

Crooker, N.U., Reverse convection, *J. Geophys. Res.*, 97, 19363 - 19372, 1992.

Crooker, N.U., G.L. Siscoe, C.T. Russell, and E.J. Smith, Factors controlling degree of correlation between ISEE 1 and ISEE 3 interplanetary magnetic field measurements, *J. Geophys. Res.*, 87, 2224 - 2230, 1982.

Csorba, I.P., *Image Tubes*, Howard W. Sams & Co., Inc., Indianapolis, Indiana, 1985.

Curtis, S.A., W.R. Hoegy, L.H. Brace, N.C. Maynard, M. Suguira, and J.D. Winningham, DE-2 cusp observations: Role of plasma instabilities in topside ionospheric heating and density fluctuations, *Geophys. Res. Letters*, 9, 997 - 1000, 1982.

Daly, P.W., and T.A. Fritz, Trapped electron distributions on open magnetic field lines, *J. Geophys. Res.*, 87, 6081 - 6088, 1982.

Daly, P.W., M.A. Saunders, R.P. Rijnbeek, N. Sckopke, and C.T. Russell, *J. Geophys. Res.*, 89, 3843, 1984.

Dandekar, B.S. and C.P. Pike, The midday, discrete auroral gap, *J. Geophys. Res.*, 83, 4227, 1978.

Dandekar, B.S., Relationship between the IMF, the midday gap, and auroral substorm activity, *J. Geophys. Res.*, 84, 4413, 1979.

Dai, W., and P.R. Woodward, Two-dimensional simulations for the impulsive penetration of a solar wind filament into the magnetosphere, *J. Geophys. Res.*, 99, 8577 - 8584, 1994.

Davidson, G.T., Expected spatial distribution of low-energy protons precipitated in the auroral zones, *J. Geophys. Res.*, 1061 - 1068, 1965.

Davidson, G.T., Pitch angle diffusion in morningside aurora 1. The role of the loss cone in the formation of impulsive bursts of precipitation, *J. Geophys. Res.*, 91, 4413 - 4427, 1986a.

Davidson, G.T., Pitch angle diffusion in morningside aurora 1. The formation of repetitive auroral pulsations, *J. Geophys. Res.*, 91, 4429 - 4436, 1986b.

Davidson, G.T., P.C. Filbert, R.W. Nightingale, W.L. Imhof, J.B. Reagan, and E.C. Whipple, Observations of intense trapped electron fluxes at synchronous altitudes, *J. Geophys. Res.*, 93, 77 - 95, 1988.

Davidson, G.T., and R.D. Sears, Pulsating aurorae: Evidence for flux limiting, *Geophys. Res. Letters*, 7, 185 - 188, 1980.

Davie, R.N., A.L. Vampola, Energy dependence of the average high-latitude cutoff of trapped electrons, *Aerospace Corp.*, REP TR-0066 (5260-20)-5, August, 1969.

Davis, T.N., The application of image orthicon techniques to auroral observation, *Space Sci. Rev.*, 6, 222, 1966.

Davis, T.N, and G.T. Hicks, Television cinemaphotography of auroras and preliminary measurements of auroral velocities, *J. Geophys. Res.*, 69, 1931, 1964.

Deans, A.J., and G.G. Shepherd, Rocket measurements of oxygen and nitrogen emissions in the aurora, *Planet. Space Sci.*, 26, 319 - 333, 1978.

Deehr, C.S., Ground-based optical observations of hydrogen emissions in the auroral substorm, in "Substorms 2, Proceedings of the Second International Conference on Substorms", J.R. Kan, J.D. Craven, and S.-I. Akasofu (eds.), Geophysical Institute, University of Alaska, Fairbanks, Alaska, 1994.

Reproduced with permission of the copyright owner. Further reproduction prohibited without permission.

Deehr, C.S., G.G. Sivjee, A. Egeland, K. Henriksen, P.E. Sandholt, R. Smith, P. Sweeney, C. Duncan, and J. Gilmer, Ground-based observations of F region aurora associated with the magnetospheric cusp, *J. Geophys. Res.*, 85, 2185 - 2192, 1980.

Deehr, C.S., and R.W. Smith, U.S. ground-based space research programs in Svalbard, — *Proceedings of an International Workshop on Cluster Dayside Polar Cusp*, ESA SP-330, 11 - 14, 1991.

DeForest, S.E., and C.E. McIlwain, Plasma coulds in the magnetosphere, *J. Geophys. Res.*, 76, 3587, 1971.

Degen, V., Synthetic spectra for auroral studies: The $N_2$ Vegard-Kaplan band system, *J. Geophys. Res.*, 87, 10541 - 10547, 1982.

Degen, V., Modeling of the $N_2^+$ first negative bands in the sunlit aurora, *Planet. Space Sci.*, 35, 1061 - 1066, 1987.

de la Beaujardiere, O., L.R. Lyons, and E. Friis-Christensen, Sondrestrom radar measurement of the reconnection electric field, *J. Geophys. Res.*, 96, 13907, 1991.

Deng, W., T.L. Killeen, A.G. Burns, R.G. Roble, J.A. Slavin, and L.E. Whorton, The effect of neutral interia on ionospheric currents in the high-latitude thermosphere following a geomagnetic storm, *J. Geophys. Res.*, 98, 7775 - 7790, 1993.

Denig, W.F., W.J. Burke, N.C. Maynard, F.J. Rich, B. Jacobsen, P.E. Sandholt, A. Egeland, S. Leontjev, and V.G. Vorobjev, Ionospheric signatures of dayside magnetopause transients: A case study using satellite and ground measurements, *J. Geophys. Res.*, 98, 5969 - 5980, 1993.

Derblom, H., Observed characteristics of polar cleft $H_\alpha$ and OI emissions,*Planet. Space Sci.*, 23, 1053, 1975.

Dessler, A.J., Length of the magnetospheric tail, *J. Geophys. Res.*, 69, 3913 - 3918, 1964.

Dibon-Smith, R., *Starlist 2000*, John Wiley and Sons, 1992.

Doering, J.P., Absolute differential and integral electron excitation cross sections for atomic oxygen 9. Improved cross section for the $^3P \rightarrow ^1 D$ transition from 4.0 to 30 eV, *J. Geophys. Res.*, 97, 19531 - 19534, 1992.

Doolittle, J.H., S.B. Mende, R.M. Robinson, G.R. Swenson, and C.E. Valladares, An observation of ionospheric convection and auroral arc motion, *J. Geophys. Res.*, 95, 19123 - 19129, 1990.

Duboin, M.L., K. Lassen, and G.G. Shepherd, Observations of horizontal transport effects on high latitude metastable $O(^1D)$ , $N(^2D)$ auroral emissions,*Planet. Space Sci.*, 32, 1407 - 1421, 1984.

Duncan, C.N., and D.J. McEwen, Photometric studies of the postnoon dayside cleft region, *J. Geophys. Res.*, 84, 6533 - 6539, 1979.

Dungey, J.W., Interplanetary magnetic fields and the auroral zone, *Phys. Rev. Letters*, 6, 47, 1961.

Dungey, J.W., *Planet. Space Sci.*, 10, 233, 1965.

Eastman, T.E., and L.A. Frank, Observations of high-speed plasma flow near the Earth's magnetopause: Evidence for reconnection?, *J. Geophys. Res.*, 87, 2187, 1982.

Eastman, T.E., and E.W. Hones, Jr., Characteristics of the magnetospheric boundary layer and magnetopause layer as observed by Imp 6, *J. Geophys. Res.*, 84, 2019 - 2028, 1979.

Reproduced with permission of the copyright owner. Further reproduction prohibited without permission.

Eastman, T.E., E.W. Hones, Jr., S.J. Bame, and J.R. Asbridge, The magnetospheric boundary layer: Site of plasma, momentum and energy transfer from the magnetosheath into the magnetosphere, *Geophys. Res. Letters*, 3, 685, 1976.

Eather, R.H., Radiation from positive particles penetrating the auroral atmosphere, *J. Geophys. Res.*, 71, 4133, 1966.

Eather, R.H., A search for helium emissions in the auroral zone, in *Space Research VIII*, pp. 201 - 209, A.P. Mitra, L.G. Jacchia, and W.S. Newman, (eds.), North-Holland Pub. Co., Amsterdam, 1967.

Eather, R.H., Spectral intensity ratios in proton induced auroras, *J. Geophys. Res.*, 73, 119, 1968.

Eather, R.H., Secondary processes in proton auroras, *J. Geophys. Res.*, 72, 1481, 19767a.

Eather, R.H., Auroral proton precipitation and hydrogen emissions, *Rev. of Geophys.*, 5, 207 - 285, 1967b.

Eather, R.H., Some recent results on the measurement of hydrogren and helium emissions in the auroral zone, *Annal. Geophys.*, 24, 185, 1968.

Eather, R.H., Dayside auroral dynamics, *J. Geophys. Res.*, 89,1695 - 1700, 1984.

Eather, R.H., Polar cusp dynamics, *J. Geophys. Res.*, 90, 1569 - 1576, 1985.

Eather, R.H., Polar cusp dynamics, in *The Polar Cusp*, J.A. Holtet and A. Egeland (eds.), D. Reidel Publishing Company, 149 - 162, 1985.

Eather, R.H., and S.B. Mende, Airborne observations of auroral precipitation patterns, *J. Geophys. Res.*, 76, 1746, 1971.

Eather, R.H., and S.B. Mende, Systematics in auroral energy spectra, *J. Geophys. Res.*, 77, 660, 1972.

Eather, R.H., S.B. Mende, and R.J.R. Judge, Plasma injection at synchronous orbit and spatial and temporal auroral morphology, *J. Geophys. Res.*, 81, 2805 - 2824, 1976.

Eather, R.H, S.B. Mende, and E.J. Weber, Dayside Aurora and Relevance to Substorms Current System and Dayside Merging, *J. Geophys. Res.*, 84, 3339 - 3359, 1979.

Eather, R.H., and D.L. Reasoner, Spectrophotometry of faint light sources with a tilting-filter photometer, *Applied Optics*, 8, 227 - 242, 1969.

Eccles, M.J., M. Elizabeth Sim, K.P. Tritton, *Low Light Level Detectors in Astronomy*, Cambridge University Press, 1983.

Egeland, A., and P.E. Sandholt, Optical signatures of the dayside magnetopause, *EOS*, 73, 475, 1992.

Ekstrom, M.P., (ed.), Digital Image Processing Techniques, Academic Press, Inc., 1984.

Ejiri, M., Trajectory traces of charged particles in the magnetosphere, *J. Geophys. Res.*, 83, 4798 - 4810, 1978.

Ejiri, M., R.A. Hoffman, and P.H. Smith, Energetic particle penetration into the inner magnetosphere, *J. Geophys. Res.*, 85, 653, 1980.

Elphic, R.C., M. Lockwood, S.W.H. Cowley, and P.E.Sandholt, Flux transfer events at the magnetopause and in the ionosphere, *Geophys. Res. Letters*, 17, 2241 - 2244, 1990.

Reproduced with permission of the copyright owner. Further reproduction prohibited without permission.

Elphinstone, R.D., J.S. Murphree, D.J. Hearn, L.L. Cogger, P.T. Newell, and H. Vo, Viking observations of the UV dayside aurora and their relationship to DMSP particle boundary definitions, *Ann. Geophysicae*, 10, 815 - 826, 1992.

Escoubet, C.P., M.F. Smith, S.F. Fung, R.A. Hoffman, and J.M. Bosqued, Electron structures in the cusp/cleft region observed by DE 2 satellite, *J. Geophys. Res.*, 100, 1597 - 1610, 1995.

Etemadi, A., S.W.H. Cowley, and M. Lockwood, The effect of rapid change in ionospheric flow on velocity vectors deduced from radar beamswinging experiments, *J. Atmos. Terr. Physics*, 51, 125, 1989.

Evans, D.S., The characteristics of a persistent auroral arc at high latitude in the 1400 MLT sector, in *The Polar Cusp*, J.A. Holtet and A. Egeland (eds.), D. Reidel Publishing Company, 99 - 109, 1985.

Eviatar, A., and R.A. Wolf, Transfer processes in the magnetopause, *J. Geophys. Res.*, 73, 5561 - 5576, 1968.

*Fairfield, D.H., Bow shock associated waves observed in the far upstream interplanetary medium, J. Geophys. Res., 74, 3541, 1969.

Fairfield, D.H., The ordered magnetic field of the magnetosheath, *J. Geophys. Res.*, 72, 5865 - 5877, 1967.

Fairfield, D.H., Average magnetic field configuration of the outer magnetosphere, *J. Geophys. Res.*, 73, 7329 - 7338, 1968.

Fairfield, D.H., Simultaneous measurements on three satellites and the observation of the geomagnetic tail at 1000 $R_E$, *J. Geophys. Res.*, 73, 6179, 1968.

Fairfield, D.H., On the average configuration of the geomagnetic tail, *J. Geophys. Res.*, 84, 1950 - 1958, 1979.

Fairfield, D.H., An evaluation of the Tsyganenko magnetic field model, *J. Geophys. Res.*, 96, 1481 - 1494, 1991.

Fairfield, D.H., and N.F. Ness, Imp 5 magnetic-field measurements in the high-latitude outer magnetosphere near the noon meridian, *J. Geophys. Res.*, 77, 611 - 623, 1972.

Fairfield, D.H., and J.D. Scudder, Polar rain: Solar coronal electrons in the earth's magnetosphere, *J. Geophys. Res.*, 90, 4055 - 4068, 1985.

Farrugia, C.J., P.E. Sandholt, S.W.H. Cowley, D.J. Southwood, A. Egeland, P. Stauning, R.P. Lepping, A.J. Lazarus, T. Hansen, and E. Friis-Christensen, Reconnection-associated auroral activity stimulated by two types of upstream dynamic pressure variations: Interplanetary magnetic field $B_z \sim 0, B_y << 0$ case, *J. Geophys. Res.*, 100, 21753 - 21772, 1995.

Farrugia, C.J., D.J. Southwood, S.W.H. Cowley, R.P. Rijnbeek, and P.W. Daly, Two-regime flux transfer events, *Planet. Space Sci.*, 35, 737 - 744, 1987.

Fasel, G.J., Dayside poleward moving auroral forms: a statistical study, *J. Geophys. Res.*, 100, 11891 - 11905, 1995.

Fasel, G.J., A mechanism for the multiple brightenings of dayside poleward moving auroral forms, *Geophys. Res. Letters*, 20, 2247, 1994.

Fasel, G.J., J.I. Minow, R.W. Smith, C.S. Deehr, and L.C. Lee, Multiple Brightenings in Dayside Transients, *Geophys. Res. Letters*, 19, 2429 - 2432, 1992.

Reproduced with permission of the copyright owner. Further reproduction prohibited without permission.

Fasel, G.J., L.C. Lee, and R.W. Smith, A mechanism for the brightenings of dayside poleward-moving auroral forms, *Geophys. Res. Letters*, 20, 2247 - 2250, 1993.

Fasel, G.J., J.I. Minow, R.W. Smith, C.S. Deehr, and L.C. Lee, Multiple brightenings of poleward-moving dayside auroral forms, in *Solar Wind Sources of Magnetospheric Ultra-Low- Frequency Waves*, Geophysical Monograph 81, 201 - 211, M.J. Engebretson, K. Takahashi, and M. Scholer, (eds.), American Geophsical Union, 1994a.

Fasel, G.J., J.I. Minow, L.C. Lee, R.W. Smith, and C.S. Deehr, Poleward-moving auroral forms: What do we really know about them?, in *Physical Signatures of Magnetospheric Boundary Layer Processes*, 211 - 226, J.A. Holtet and A. Egeland (eds.), Kluwer Academic Pub., 1994b.

Feldman, P.D., and J.P. Doering, Auroral electrons and the optical emissions of nitrogen, *J. Geophys. Res.*, 80, 2808, 1975.

Feldstein, Y.I., On morphology of auroral and magnetic disturbances at high latitudes, *Geomagnetism and Aeronomy*, 3, 183 - 192, 1963.

Feldstein, Y.I., Some problems concerning the morphology of auroras and magnetic disturbances at high latitudes, *Geomagnetism and Aeronomy*, 2, 183 - 192, 1963.

Feldstein, Y.I., Auroral morphology, I, The location of the auroral zone, *Tellus*, 16, 252 - 257, 1964a.

Feldstein, Y.I., Auroral morphology, II, Auroral and geomagnetic disturbances, *Tellus*, 16, 258 - 267, 1964b.

Feldstein, Y.I., Dynamics of aurora belt and polar geomagnetic disturbances, *Planet. Space Sci.*, 15, 209 - 229, 1967

Feldstein, Y.I., and Yu.I. Galperin, The auroral luminosity structure in the high-latitude upper atmosphere: Its dynamics and relationship to the large-scale structure of the Earth's magnetosphere,*Rev. of Geophys.*, 23, 217 - 275, 1985.

Feldstein, Y.I., and G.V. Starkov, Auroral oval in the IGY and IQSY period, and a ring current in the magnetosphere, *Planet. Space Sci.*, 16, 129, 1968.

Fennell, J.F., P.F. Mizera, and D.R. Croley, Jr., Low energy polar cap electrons during quiet times, *Proc. Int. Conf. Cosmic Rays 14th*, 1267, 1975.

Foster, J.C., and J.R. Burrows, Electron fluxes over the polar cap 1. Intense keV fluxes during poststorm quieting, *J. Geophys. Res.*, 81, 6016 - 6028, 1976.

Foster, J.C., and J.R. Doupnik, Plasma convection in the vicinity of the dayside cleft, *J. Geophys. Res.*, 89, 9107 - 9113, 1984.

Frank, L.A., J.A. Van Allen, and H.K. Hills, A study of charged particles in the earth's outer radiation zone with Explorer 14, *J. Geophys. Res.*, 69, 2171 - 2191, 1964.

Frank, L.A., A survey of electrons $E > 40$ keV beyond 5 Earth radii with Explorer 14, *J. Geophys. Res.*, 70, 1593 - 1626, 1965.

Frank, L.A., Plasma in the Earth's polar magnetosphere, *J. Geophys. Res.*, 76, 5202, 1971.

Frank, L.A., Plasmas in the Earth's magnetotail, *Space Sci. Rev.*, 42, 211 - 240, 1985.

Frank, L.A., and K.L. Ackerson, Observation of charged particle precipitation into the auroral zone, *J. Geophys. Res.*, 76, 3612 - 3643, 1971.

Reproduced with permission of the copyright owner. Further reproduction prohibited without permission.

Frank, L.A., and K.L. Ackerson, Local-time survey of plasma at low altitude over the auroral zones, *J. Geophys. Res.*, 77, 4116, 1972.

Frank, L.A., J.A. Van Allen, and J.D. Craven, Large diurnal variations of geomagnetically trapped and of precipitated electrons observed at low altitudes, *J. Geophys. Res.*, 69, 3155 - 3167, 1964a.

Frank, L.A., J.A. Van Allen, and H.K. Hills, A study of charged particles in the Earth's outer radiation zone with Explorer 14, *J. Geophys. Res.*, 69, 2171 - 2191, 1964b.

Freeman, M.P., J.M. Ruohoniemi, and R.A. Greenwald, The determination of time-stationary two-dimensional convection patterns with single-station radars, *J. Geophys. Res.*, 96, 15735 - 15749, 1991.

Freeman, M.P., and D.J. Southwood, The effect of magnetospheric erosion on mid- and high-latitude ionospheric flows, *Planet. Space Sci.*, 36, 509, 1988.

Frey, H.U., G. Haerendel, D. Knudsen, S. Buchert, and O.H. Bauer, Optical and radar measurements of the motion of auroral arcs, *J. Atmos. Terr. Physics*, 57, 57 - 69, 1996

Friedel, A. Korth, G.D. Reeves, and R.D. Belian, Origin of energetic particle injections at substorm onset as measured by the CCRES spacecraft between 4 and 7 $R_e$ and Los Alamos geostationary satellites, in *Substorms 2, Proceedings of the Second International Conference on Substorms*, edited by J.R. Kan, J.D. Craven, and S.-I Akasofu, pp. 571 - 576, Geophysical Institute, University of Alaska, 1994.

Friis-Christensen, E., and J. Wilhjelm, Polar cap currents for different directions of the interplanetary magnetic field in the Y-Z plane, *J. Geophys. Res.*, 80, 1248 - 1260, 1975.

Friis-Christensen, E., Y. Kamide, A.D. Richmond, and S. Matsushita, Interplanetary magnetic field control of high-latitude electric fields and currents determined from Greenland magnetometer data, *J. Geophys. Res.*, 90, 1325, 1985

Fritz, T.A., High-latitude outer-zone boundary region for $\geq$40-kev electrons during geomagnetically quiet periods, *J. Geophys. Res.*, 73, 7245 - 7255, 1968.

Fritz, T.A., Study of high-latitude, outer-zone boundary region for $\geq$40-kev electrons with satellite Injun 3, *J. Geophys. Res.*, 75, 5387 - 5400, 1970.

Froese Fischer, C., and H.P. Saha, Multiconfiguration Hartree-Fock results with Briet-Pauli corrections for forbidden transitions in the $2p^4$ configuration,*Phys. Rev. A*, 28, 3169, 1983.

Fu, Z.F., and L.C. Lee, Simulation of multiple x-line reconnection at the dayside magnetopause, *Geophys. Res. Letters*, 12, 291 - 294, 1985.

Fuselier, S.A., D.M. Klumpar, and E.G. Shelley, *Geophys. Res. Letters*, 18, 139 - 142, 1991.

Garstang, R.H., Energy levels and transition probabilities in $p^2$ and $p^4$ configurations, *Mon. Not. R. Astron. Soc.*, 111, 115, 1951.

Garstang, R.H., Transition probabilities in auroral lines, in *Airglow and the Aurora*, edited by E.B. Armstrong and A. Dalgarno, 327 - 324, Pergamon, New York, 1956.

Garstang, R.H., Transition probabilities for forbidden lines, in *Planetary Nebulae, IAU Symposium 34*, edited by D.E. Osterbrock and C.R. O'Dell, D. Reidel, Hingham, Mass., 1968.

Gattinger, R.L., F.R. Harris, and A. Vallance Jones, The height, spectrum and mechanism of type-B red aurora and its bearing on the excitation of $O(^1S)$ in aurora, *Planet. Space Sci.*, 33, 207 - 221, 1985.

Reproduced with permission of the copyright owner. Further reproduction prohibited without permission.

Gault, W.A., R.A. Koehler, R. Link, and G.G. Shepherd, Observations of the optical spectrum of the dayside magnetospheric cleft aurora, *Planet. Space Sci.*, 29, 321 - 333, 1981.

Gentieu, E.P., R.W. Eastes, P.D. Feldman, and A.B. Christensen, The ultraviolet spectrum of a dayside aurora: 530 - 1500 Å, *Can. J. Phys*, 67, 82 - 88, 1989.

Gérard, J.-C., and R.G. Roble, Transport of aurorally produced $N(^2D)$ by winds in the high latitude thermosphere, *Planet. Space Sci.*, 30, 1091 - 1105, 1982.

Gloeckler, G., B. Wilken, W. Stüdemann, F.M. Ipavich, D. Hovestadt, D.C. Hamilton, and G. Kremser, First composition measurements of the bulk of the storm-time ring current (1 to 300 keV/e) with AMPTE-CCE, *Geophys. Res. Letters*, 12, 325 - 328, 1985.

Goertz, C.K., E. Nielsen, A. Korth, K.H. Glassmeier, C. Haldoupis, P. Hoeg, and D. Hayward, Observations of a possible ground signature of flux transfer events, *J. Geophys. Res.*, 90, 4069, 1985.

Gonzalez, W.D., and F.S. Mozer, A quantitative model for the potential resulting from reconnection with an arbitrary IMF, *J. Geophys. Res.*, 79, 4186 - 4194, 1974.

Gosling, J.T., J.R. Asbridge, S.J. Bame, W.C. Feldman, G. Paschmann, N. Sckopke, and C.T. Russell, Evidence for quasi-stationary reconnection at the dayside magnetopause, *J. Geophys. Res.*, 2147 - 2158, 1982.

Gosling, J.T., and D.J. McComas, Field line draping about fast coronal mass ejecta: A source of strong out-of-the-ecliptic interplanetary magnetic fields,*Geophys. Res. Letters*, 14, 355 - 358, 1987.

Gosling, J.T., M.F. Thomsen, S.J. Bame, and C.T. Russell, Accelerated plasma flows at the near-tail magnetopause, *J. Geophys. Res.*, 91, 3029, 1986.

Gosling, J.T., M.F. Thomsen, S.J. Bame, R.C. Elphic, and C.T. Russell, Plasma flow reversals at the dayside magnetopause and the origin of asymmetric polar cap convection, *J. Geophys. Res.*, 95, 8073 - 8084, 1990a.

Gosling, J.T., M.F. Thomsen, S.J. Bame, T.G. Onsager, and C.T. Russell, The electron edge of the low latitude boundary layer during accelerated flow events, *Geophys. Res. Letters*, 17, 1833 - 1836, 1990b.

Gosling, J.T., M.F. Thomsen, S.J. Bame, R.C. Elphic, and C.T. Russell, Observations of reconnection of interplanetary and lobe magnetic field lines at the high-latitude magnetopause, *J. Geophys. Res.*, 96, 14097 - 14106, 1991.

Gurnett, D.A., R.R. Anderson, B.T. Tsurutani, E.J. Smith, G. Paschmann, G. Haerendel, S.J. Bame, and C.T. Russell, Plasma wave turbulence at the magnetopause: Observations from ISEE 1 and 2, *J. Geophys. Res.*, 84, 7043, 1979.

Gussenhoven, M.S., Polar rain and the question of direct particle access, in *Electromagnetic Coupling in the Polar Clefts and Caps*, p. 43 - 60, P.E. Sandholt and A. Egeland (eds.), Kluwer Academic Publishers, 1989.

Gussenhoven, M.S., D.A. Hardy, and R.L. Carovillano, Average electron precipitation in the polar cusps, cleft and cap, in *the Polar Cusp*, p 85, J.A. Holtet and A. Egeland (eds.), D. Reidel, 1985.

Gustafsson, G., Y.I. Feldstein, and N.F. Shevnina, The auroral orientation curves for the IQSY, *Planet. Space Sci.*, 17, 1657 - 1666, 1969.

Reproduced with permission of the copyright owner. Further reproduction prohibited without permission.

Haerendel, G., Plasma drifts in the auroral ionosphere derived from barium releases, in *Earth's Magnetospheric Processes*, pp. 246 - 257, B.M. McCormac (ed.), D. Reidel Pub. Co., Dordrecht-Holland, 1972.

Haerendel, G., S. Buchert, C. La Hoz, B. Raaf, and E. Rieger, On the proper motion of auroral arcs, *J. Geophys. Res.*, 98, 6087 - 6099, 1993.

Haerendel, G., B.U. Olipitz, S. Buchert, O.H. Bauer, E. Rieger, and C. La Hoz, Optical and radar observations of auroral arcs with emphasis on small-scale structures, *J. Atmos. Terr. Physics*, 58, 71 - 83, 1996.

Haerendel, G., G. Paschmann, N. Sckopke, H. Rosenbauer, and P.C. Hedgecock, The frontside boundary layer of the magnetosphere and the problem of reconnection, *J. Geophys. Res.*, 83, 3195 - 3216, 1978.

Haerendel, G., and G. Paschmann, Interaction of the solar wind with the dayside magnetosphere, in *Magnetospheric Plasma Physics*, A. Nishida, editor, D. Reidel Publishing Co., 1982.

Hamilton, D.C., G.Gloeckler, F.M. Ipavich, W. Stüdemann, B. Wilken, and G. Kremser, Ring current development during the great geomagnetic storm of February 1986, *J. Geophys. Res.*, 93, 14343 - 14355, 1988.

Hamlin, D.A., R. Karplus, R.C. Vik, and K.M. Watson, Mirror and azimuthal drift frequencies for geomagnetically trapped particles, *J. Geophys. Res.*, 66, 1, 1961.

Hansen, A.M., A. Bahnsen, and N. D'Angelo, The cusp-magnetosheath interface, *J. Geophys. Res.*, 81, 556, 1976.

Hardy, D.A., W.J. Burke, and E. Villalon, Electron dispersion events in the morningside auroral zone and their relationship with VLF emissions, *J. Geophys. Res.*, 95, 6451 - 6466, 1990.

Hargreaves, J.K., and K. Bullough, Mid-latitude VLF emissions and the mechanism of dayside auroral particle precipitation, *Planet. Space Sci.*, 20, 803 - 807, 1972.

Harris III, D.L., The stellar temperature scale and bolometric corrections, in *Basic Astronomical Data*, edited by K.Aa. Strand, University of Chicago Press, 1963.

Hartz, T.R., and N.M. Brice, The general pattern of auroral particle precipitation, *Planet. Space Sci.*, 15, 301 - 329, 1967.

Hays, P.B., and S.K. Atreya, The influence of thermospheric winds on the auroral red line profile of atomic oxygen, *Planet. Space Sci.*, 19, 1225, 1971.

Hedin, A.E., MSIS-86 Thermospheric Model, *J. Geophys. Res.*, 92, 4649, 1987.

Hedin, A.E., N.W. Spencer, and T.L. Killeen, Empirical global model of upper thermosphere winds based on Atmosphere and Dynamics Explorer satellite data, *J. Geophys. Res.*, 93, 9959 - 9978, 1988.

Heikkila, W.J., Is there an electrostatic field tangential to the dayside magnetopause and neutral line?, *Geophys. Res. Letters*, 2, 154 - 157, 1975.

Heikkila, W.J., Impulsive plasma transport through the magnetopause, *Geophys. Res. Letters*, 9, 159, 1982.

Heikkila, W.J., and J.D. Winningham, Penetration of magnetosheath plasma to low altitudes through the dayside magnetospheric cusps, *J. Geophys. Res.*, 76, 883 - 891, 1971.

Heikkila, W.J., J.D. Winningham, R.H. Eather, and S.-I. Akasofu, Auroral emissions and particle precipitation in the noon sector, *J. Geophys. Res.*, 77, 4100 - 4115, 1972.

Reproduced with permission of the copyright owner. Further reproduction prohibited without permission.

Heelis, R.A., The effects of interplanetary magnetic field orientation on dayside high latitude ionospheric convection, *J. Geophys. Res.*, 89, 2873 - 2880, 1984.

Heelis, R.A., P.H. Reiff, J.D. Winningham, and W.B. Hanson, Ionospheric convection signatures observed by DE 2 during northward interplanetary magnetic field, *J. Geophys. Res.*, 91, 5817 - 5830, 1986.

Heelis, R.A., J.D. Winningham, W.B. Hanson, and J.L. Burch, The relationships between high-latitude convection reversals and the energetic particle morphology observed by Atmosphere Explorer, *J. Geophys. Res.*, 85, 3315, 1980.

Heikkila, W.J., J.D. Winningham, R.H. Eather, and S.-I. Akasofu, Auroral emissions and particle precipitation in the noon sector, *J. Geophys. Res.*, 77, 4100 - 4115, 1972.

Henriksen, K., and A. Egeland, The interpretation of the auroral green line, *Eos*, 69, 721, 733-734, 1988.

Henriksen, K., N.I. Fedorova, G.F. Totunova, C.S.Deehr, G.J. Romick, and G.G. Sivjee, Hydrogen emissions in the polar cleft, *J. Atmos. Terr. Physics*, 47, 1051 - 1056, 1985.

Henriksen, K., B. Holback, and G. Witt, Variations in the auroral spectrum at the latitude of the polar cleft,*J. Geophys. (Zeitschrift für Geophysik)*, 44, 401 - 414, 1978.

Henriksen, K., K. Stamnes, C.S. Deehr, and G.G. Sivjee, The HeI 3889 Å line in polar cleft spectra, in *The Polar Cusp*, 127 - 135, J.A. Holtet and A. Egeland (eds.), D. Reidel Pub. Co., 1985.

Heppner, J.P., and N.C. Maynard, *J. Geophys. Res.*, 92, 4467 - 4489, 1987.

Hernandez, G., Analytical Description of a Fabry-Perot Spectrometer. 3: Off axis behavior and interference filters, *Applied Optics*, 13, 2654 - 2661, 1974a.

Hernandez, G., Contamination of the $OI(^3P_2 - ^1D_2)$ emission line by the (9-3) band of $OHX^2II$ in high-resolution measurements of the night sky, *J. Geophys. Res.*, 79, 1119 - 1123, 1974b.

Hernandez, G., F.G. McCormac, and R.W. Smith, Austral thermospheric wind circulation and interplanetary magnetic field orientation, *J. Geophys. Res.*, 96, 5777 - 5783, 1991.

Hill, T.W., and A.J. Dessler, Plasma motions in planetary magnetosphere, *Science*, 252, 410 - 415, 1991.

Hoffman, R.A., and F.W. Berko, Primary electron influx to dayside auroral oval, *J. Geophys. Res.*, 76, 2967 - 2976, 1971.

Hoffman, R.A., and J.L. Burch, Electron precipitation patterns and substorm morphology, *J. Geophys. Res.*, 78, 2867, 1973.

Holzer, R.E., T.A. Farley, R.K. Burton, and M.C. Chapman, A correlated study of ELF waves and electron precipitation on Ogo 6, *J. Geophys. Res.*, 79, 1007, 1974.

Holzer, R.E., and J.A. Slavin, Magnetic flux transfer associated with expansions and contractions of the dayside magnetosphere, *J. Geophys. Res.*, 83, 3831 - 3839, 1978.

Holzworth, R.H., and C.-I. Meng, Mathematical representation of the auroral oval, *Geophys. Res. Letters*, 2, 377 380, 1975.

Hones, E.W., Jr., J.R. Asbridge, S.J. Bame, M.D. Montgomery, S. Singer, and S.-I. Akasofu, Measurements of magnetotail plasma flow made with Vela 4B, *J. Geophys. Res.*, 77, 5503, 1972.

Reproduced with permission of the copyright owner. Further reproduction prohibited without permission.

Horwitz, J.L., and S.-I. Akasofu, The response of the dayside aurora to sharp northward and southward transition of the interplanetary magnetic field and to magnetospheric substorms, *J. Geophys. Res.*, 82, 2723 - 2734, 1977.

Horwitz, J.L., and M. Lockwood, The cleft ion fountain: A two-dimensional kinetic model, *J. Geophys. Res.*, 90, 9749 - 9762, 1985.

Hunten, D.M., Some photometric observations of auroral spectra, *J. Atmos. Terr. Physics*, 7, 141, 1955.

Hunten, D.M., An automatic auroral recorder, *J. Opt. Soc. Am.*, 46, 578, 1956.

Hunten, D.M., and M.B. McElroy, Quenching of metastable states of atomic and molecular oxygen and nitrogen, *Rev. of Geophys.*, 4, 303 - 328, 1966.

Iglesias, G.E., and R.R. Vondrak, Atmospheric spreading of protons in auroral arcs, *J. Geophys. Res.*, 79, 280 - 282, 1974.

Imhof, W.L., R.R. Anderson, J.B. Reagan, and E.E. Gaines, Coordinated measurements of slot region electron precipitation by plasmaspheric wave bands, *J. Geophys. Res.*, 87, 4418 - 4426, 1982.

Imhof, W.L., R.M. Robinson, H.L. Collin, J.R. Wygant, and R.R. Anderson, Simultaneous measurements of waves and precipitating electrons near the equator in the outer radiation belt, *J. Geophys. Res.*, 99, 2415 - 2427, 1994.

Intriligator, D.S., J.H. Wolfe, D.D. McKibben, and H.R. Collard, Preliminary comparison of solar wind plasma observations in the geomagnetospheric wake at 1000 and 500 Earth radii,*Planet. Space Sci.*, 17, 321, 1969.

Intriligator, D.S., H.R. Collard, J.D. Mihalov, O.L. Vaisberg, and J.H. Wolfe, Evidence for earth magnetospheric tail associated phenomena at $3,100R_E$,*Geophys. Res. Letters*, 6, 585, 1979.

Ip, W.-H., and S.-P. Jin, A 2D numerical study jof recurrent driven reconnection processes at the magnetopause, *Geophys. Res. Letters*, 18, 1497 - 1500, 1991.

Jack, T.M., and T.J. Hallinan, Measurement of auroral rays from the space shuttle, *J. Geophys. Res.*, 99, 8865 - 8872, 1994.

Jackson, J.D., *Classical Electrodynamics*, p. 251 - 253, John Wiley & Sons, 1975.

Jacobsen, B., P.E. Sandholt, W.J. Burke, W.F. Denig, and N.C. Maynard, Optical signatures of prenoon auroral precipitation: Sources and responses to solar wind variations, *J. Geophys. Res.*, 100, 8003 - 8012, 1995.

Jacobsen, B., P.E. Sandholt, B. Lybekk, and A. Egeland, Transient auroral events near midday: relationship with solar wind/magnetosheath plasma and magnetic field conditions, *J. Geophys. Res.*, 96, 1327 - 1336, 1991. Jain, A.K., *Fundamentals of Digital Image Processing*, Prentice Hall, 1989.

Johnstone, A.D., The spreading of a proton beam by the atmosphere, *Planet. Space Sci.*, 20, 292 - 295, 1972.

Johnson, F., Gross character of the geomagnetic field in the solar wind, *J. Geophys. Res.*, 65, 3049, 1961.

Johnson, R.G., Energetic ion composition in the Earth's magnetosphere, *Rev. Geophys. Space Phys.*, 17, 696, 1979.

Reproduced with permission of the copyright owner. Further reproduction prohibited without permission.

Johnson, R.G., (ed), *Energetic ion composition in the Earth's magnetosphere*, Terra Scientific Pub. Co., Tokyo, 1983.

Jørgensen, T.S., E. Friis-Christensen, and J. Wilhjelm, Interplanetary magnetic-field direction and high latitude ionospheric currents, *J. Geophys. Res.*, 77, 1976 - 1977, 1972.

Jähne, B, *Digital Image Processing, Applications, Concepts, Algorithms, and Scientific Applications*, Springer-Verlag, 1991.

Kaila, K.U., An iterative method for calculating the altitudes and positions of auroras along the arc, *Planet. Space Sci.*, 35, 245 - 258, 1987.

Kan, J., A theory of patchy and intermittent reconnections for magnetospheric flux transfer events, *J. Geophys. Res.*, 93, 5613 - 5623, 1988.

Karlson, K.A., M. Oieroset, J. Moen, and P.E. Sandholt, A statistical study of flux transfer event signatures in the dayside aurora: The IMF $B_y$-related prenoon-postnoon asymmetry, *J. Geophys. Res.*, 101, 59 - 68, 1996.

Kaufmann, R.L., and A. Konradi, Speed and thickness of the magnetopause, *J. Geophys. Res.*, 78, 6549 - 6568, 1973.

Kelley, M.C., J.A. Starr, and F.S. Mozer, Relationship between magnetospheric electric fields and the motion of auroral forms, *J. Geophys. Res.*, 76, 5269 - 5277, 1971.

Kellogg, P.J., Flow of plasma around the earth, *J. Geophys. Res.*, 67, 3805, 1962.

Kennell, C.F., and H.E. Petschek, Limit on stably trapped particle fluxes, *J. Geophys. Res.*, 71, 1 - 28, 1966.

Kernahan, J.A., and P.H-L. Pang, Experimental Determination of Absolute A Coefficients for 'Forbidden' Atomic Oxygen Lines, *Can. J. Phys.*, 53, 455 - 458, 1975.

Kessel, R.L., S.-H. Chen, J.L. Green, S.F. Fung, S.A. Boardsen, L.C. Tan, T.E. Eastman, J.D. Craven, and L.A. Frank, Evidence of high-latitude reconnecting during northward IMF: Hawkeye observations, *Geophys. Res. Letters*, 23, 583 - 586, 1996.

Khorosheva, O.V., The space and time-distribution of auroras and their relationship with high-latitude geomagnetic disturbances, *Geomagnetism and Aeronomy*, 1, 695, 1961.

Killeen, T.L., and R.G. Roble, An analysis of the high-latitude thermosphere wind pattern calculated by a thermospheric general circulation model 1. Momentum forcing, *J. Geophys. Res.*, 89, 7509 - 7522, 1984.

Killeen, T.L., P.B. Hays, G.R. Carignan, R.A. Heelis, W.B. Hanson, N.W. Spencer, and L.H. Brace, Ion-neutral coupling in the the high-latitude F region: Evaluation of ion heating terms from Dynamics Explorer 2, *J. Geophys. Res.*, 89, 7495 - 7508, 1984.

Killeen, T.L., P.B. Hays, N.W. Spencer, and L.E. Warton, Neutral winds in the polar thermosphere as measured from dunamics explorer, *Geophys. Res. Letters*, 9, 957 - 960, 1982.

Kim, J.S., and Volkman, R.A., Thickness of zenithal auroral arc over Fort Churchill, Canada, *J. Geophys. Res.*, 68, 3187 - 3190, 1963.

Kim, J.S., and Volkman, R.A., Thickness of zenithal auroral arc over Alaska, *J. Atmos. Terr. Physics*, 27, 321 - 328, 1965.

Kirchhoff, V.W.J.H., Theory of the atmospheric sodium layer: A review, *Can. J. Phys.*, 64, 1664 - 1672, 1986.

Reproduced with permission of the copyright owner. Further reproduction prohibited without permission.

Klumpar, D.M., and S.A. Fuselier, A series of flux transfer events in the dayside magnetosphere, in *Physics of Space Plasmas, SPI Conference Proceedings and Reprint Series, Number 10*, 301 - 313, T. Chang, G.B. Crew, and J.R. Jasperse, (eds.), Scientific Pub., Inc., Cambridge, Massachusetts, 1990.

Kofman, W., and V.B. Wickwar, Very high electron temperatures in the daytime F region at Sondrestrom, *Geophys. Res. Letters*, 1, 919 - 922, 1984.

Kokubun, S., R.L. McPherron, and C.T. Russell, *J. Geophys. Res.*, 82, 74, 1977.

Kozyra, J.U., C.E. Valladares, H.C. Carlson, M.J. Buonsanto, and D.W. Slater, A theoretical study of the seasonal and solar cycle variations of stable aurora red arcs, *J. Geophys. Res.*, 95, 12219 - 12234, 1990.

Krall, N.A., A.W. Trivelpiece, *Principles of Plasma Physics*, McGraw-Hill Book Company, 1973.

Krassovsky, V.I., N.N. Shefov, and V.I. Yarin, Atlas of the airglow spectrum 3000-12400 Å, *Planet. Space Sci.*, 9, 883 - 915, 1962.

Kremser, G., and R. Lundin, Average spatial distributions of energetic particles in the midaltitude cusp/cleft region observed by Viking, *J. Geophys. Res.*, 95, 5753 - 5766, 1990.

Kuo, H., C.T. Russell, and G. Le, Statistical studies of flux transfer events, *J. Geophys. Res.*, 100, 3513 - 3519, 1995.

Kvifte, G.J., and H. Petersen, *Planet. Space Sci.*, 17, 1599, 1969.

Lanchester, B.S., and M.H. Rees, Field-aligned current reversals and fine structure in a dayside auroral arc,*Planet. Space Sci.*, 35, 759 - 768, 1987.

Lassen, K., Polar cap aurora, in *Aurora and Airglow*, B.M. McCormac (ed.), pp. 453 - 464, Rheinhold, New York, 1967.

Lassen, K., Polar cap emissions, in *Atmospheric Emissions*, B.M. McCormac and A. Omholt (eds.), Van Nostrand Reinhold Co., 1969.

Lassen, K., The position of the auroral oval over Greenland and Spitzbergen, *Phys. Norv.*, 4, 171 - 175, 1970.

Lassen, K., Relation of the plasma sheet to the nighttime auroral oval, *J. Geophys. Res.*, 79, 3857 - 3858, 1974.

Lassen, K., The quiet-time pattern of auroral arcs as a consequence of magnetospheric convection, *Geophys. Res. Letters*, 6, 777 - 780, 1979.

Lassen, K., and C. Danielsen, Quiet time pattern of auroral arcs for different directions of the interplanetary magnetic field in the Y-Z plane, *J. Geophys. Res.*, 83, 5277 - 5284, 1978.

Lanzerotti, L.J., L.C. Lee, C.G. Maclennan, A. Wolfe, and L.V. Medford, Possible evidence of flux transfer events in the polar ionosphere, *Geophys. Res. Letters*, 13, 1089, 1986.

Lee, L.C., Magnetic flux transfer at the Earth's magnetopause, in *Solar Wind-Magnetosphere Coupling*, edited by Y. Kamide and J.A. Slavin, 297 - 314, Terra Scientific Pub. Co., Tokyo, 1986.

Lee, L.C., A review of magnetic reconnection: MHD models, in *Physics of the Magnetopause*, Geophysical Monograph 90, pp. 139 - 153, P. Song, B.U.Ö. Sonnerup, (eds.), American Geophysical Union, Washington, D.C., 1995.

Reproduced with permission of the copyright owner. Further reproduction prohibited without permission.

Lee, L.C., and Z.F. Fu, A theory of magnetic flux transfer at the earth's magnetosphere, *Geophys. Res. Letters*, 12, 105 - 108, 1985.

Lee, L.C., and Z.F. Fu, Multiple X line reconnection, 1, A criterion for the transition froma single X line to a multiple X line reconnection, *Geophys. Res. Letters*, 91, 6807, 1986.

Lee, L.C., J.R. Johnson, and Z.W. Ma, Kinetic Alfvén waves as a source of plasma transport at the dayside magnetopause, *J. Geophys. Res.*, 99, 17405 - 17411, 1994.

Lee, L.C., Z.W. Ma, Z.F. Fu, and A. Otto, Topology of magentic flux ropes and formation of fossil flux transfer events and boundary layer plasmas, *J. Geophys. Res.*, 98, 3943, 1993.

Lee, L.C., and and C.Q. Wei, Interaction of solar wind with the magnetopause-boundary layer and generation of magnetic impulse events,*J. Atmos. Terr. Physics*, 55, 967 - 978, 1993

Lemaire, J., Impulsive penetration of filamentary plasma elements into the magnetospheres of the Earth and Jupiter, *Planet. Space Sci.*, 25, 887, 1977.

Lemaire, J., and M. Roth, Penetration of solar wind plasma elements into the magnetosphere, *J. Atmos. Terr. Phys.*, 40, 331, 1978.

Lemaire, J., M.J. Rycroft, and M. Roth, Control of impulsive penetration of solar wind irregularities into the magnetosphere by the interplanetary magnetic field direction, *Planet. Space Sci.*, 27, 47, 1979.

Leontyev, S.V., G.V. Starkov, V.G. Vorobjev, V.L. Zverev, Ya.I. Feldstein, Dayside Aurorae and Their Relation to Other Geophysical Phenomena, *Planet. Space Sci.*, 40, 621 - 639, 1992.

Levy, R.H., H.E. Petschek, and G.L. Siscoe, Aerodynamic aspects of the magnetospheric flow, *AIAA J.*, 2, 2065, 1964.

Lin, C.S., and R.A. Hoffman, Fluctuations of inverted V electron fluxes, *J. Geophys. Res.*, 84, 6547, 1979.

Lin, C.S., and R.A. Hoffman, Narrow bursts of intense electron precipitation fluxes within inverted-V events, *Geophys. Res. Letters*, 9, 211, 1982.

Lind, D.L., J. Geiss, and W. Stettler, Solar and terrestrial noble gases in magnetospheric precipitation, *J. Geophys. Res.*, 84, 6435, 1979.

Link, R., J.C. McConnell, and G.G. Shepherd, A self consistent evaluation of the rate constants for the production of the OI 6300 Å airglow, *Planet. Space Sci.*, 29, 589, 1981.

Link, R., J.C. McConnell, and G.G. Shepherd, An analysis of the spatial distribution of dayside cleft optical emissions, *J. Geophys. Res.*, 88, 10145, 1983.

Link, R., and P.K. Swaminathan, $N(^2D)+O_2$: A source of thermospheric 6300 Å emission?, *Planet. Space Sci.*, 40, 699 - 705, 1992.

Lissberger, P.H., Properties of all-dielectric interference filters. I. A new method of calculation, *J. of the Opt. Soc. of America*, 49, 121 - 125, 1959.

Lissberger, P.H., and W.L. Wilcock, Properties of all-dielectric interference filters. II. Filters in parallel beams of light incident obliquely and in convergent beams, *J. of the Opt. Soc. of America*, 49, 126 - 130, 1959.

Lockwood, M., The excitation of ionospheric convection, *J. Atmos. Terr. Physics*, 53, 177 - 199, 1991.

Reproduced with permission of the copyright owner. Further reproduction prohibited without permission.

Lockwood, M., Incoherent scatter radar measurements of the cusp, in *Proceedings of the Cluster Workshop on Cluster Dayside Polar Cusp*, ESA SP-330, pp. 57 - 65, European Space Agency, 1991.

Lockwood, M., Ground-based and satellite observations of the cusp: Evidence for pulsed magnetopause reconnection, in *Physics of the Magnetopause*, Geophysical Monograph 90, P. Song, B.U.Ö. Sonnerup, and M. Thomsen (eds.), American Geophysical Union, Washington, D.C., 1995.

Lockwood, M., The case for transient magnetopause reconnection, *EOS, Trans., AGU*, 77, 246-247, 249, 1996.

Lockwood, M., H.C. Carlson, P.E. Sandholt, Implications of the altitude of the 630-nm dayside auroral emissions, *J. Geophys. Res.*, 98, 15571 - 15587, 1993a.

Lockwood, M., M.O. Chandler, J.L. Horwitz, J.H. Waite, Jr., T.E. Moore, and C.R. Chappell, The cleft ion fountain, *J. Geophys. Res.*, 90, 9736 - 9748, 1985.

Lockwood, M., and S.W.H. Cowley, Observations at the magnetopause and in the auroral ionosphere of momentrum transfer from the solar wind, *Adv. Space Res.*, 8, 281, 1988.

Lockwood, M., Ionospheric signatures of pulsed magnetopause reconnection, in *Physical Signatures of Magnetospheric Boundary Layer Processes*, 229 - 243, J.A. Holtet and A. Egeland (eds.), Kluwer Academic Publishers, 1994.

Lockwood, M. and S.W.H. Cowley, Comment on "Ionospheric Signatures of Daysidee Magnetopause Transients: A Case Study Using Satellite and Ground Measurements" by Denig et al., *J. Geophys. Res.*, 99, 4253 - 4255, 1994.

Lockwood, M., S.W.H. Cowley, and M.P. Freeman, The excitation of ionospheric convection, *J. Geophys. Res.*, 95, 7961, 1990c.

Lockwood, M., S.W.H. Cowley, H. Todd, D.M. Willis, and C.R. Clauer, Ion flows and heating at a contracting polar-cap boundary, *Planet. Space Sci.*, 36, 1229 - 1253, 1988.

Lockwood, M., S.W.H. Cowley, P.E. Sandholt, and R.P. Lepping, The ionospheric signatures of flux transfer events and solar wind dynamic pressure changes, *J. Geophys. Res.*, 95, 17113 - 17135, 1990a.

Lockwood, M., and C.J. Davis, Ana analysis of the accuracy of magnetopause reconnection rate variations deduced from cusp ion dispersion characteristics, *Ann. Geophysicae*, 14, 149 - 161, 1996.

Lockwood, M., C.J. Davis, M.F. Smith, T.G. Onsager, and W.F. Denig, Location and characteristics of the reconnection X line deduced from low-altitude satellite and ground-based observations 2. Defense Meteorological Satellite Program and European inchoherent scatter data, *J. Geophys. Res.*, 100, 21803 - 21813, 1995.

Lockwood, M., W.F. Denig, A.D. Farmer, V.N. Davda, S.W.H. Cowley, and H. Lühr, Ionospheric signatures of pulsed reconnection at the Earth's magnetopause, *Nature*, 361, 424 - 427, 1993b.

Lockwood, M., J. Moen, S.W.H. Cowley, A.D. Farmer, U.P. Løvhaug, H. Lühr, and V.N. Davda, Variability of dayside convection and motions of the cusp/cleft aurora, *Geophys. Res. Letters*, 20, 1011 - 1014, 1993c.

Reproduced with permission of the copyright owner. Further reproduction prohibited without permission.

Lockwood, M., T.G. Onsager, C.J. Davis, M.F. Smith, and W.F. Denig, The characteristics of the magnetopause reconnection X line deduced from low-altitude satellite observations of cusp ions, *Geophys. Res. Letters*, 21, 2757, 1994. (Also see Correction, *Geophys. Res. Letters*, 22, 867, 1995).

Lockwood, M., P.E. Sandholt, and S.W.H. Cowley, Dayside auroral activity and magnetic flux transfer from the solar wind, *Geophys. Res. Letters*, 16, 33-36, 1989a.

Lockwood, M., P.E. Sandholt, S.W.H. Cowley, and T. Oguti, Interplanetary magnetic field control of dayside auroral activity and the transfer of momentum across the dayside magnetopause, *Planet. Space Sci.*, 37, 1347 - 1365, 1989b.

Lockwood, M, P.E. Sandholt, A.D. Farmer, S.W.H Cowley, B. Lybekk, and V.N. Davda, Auroral and plasma flow transients at magnetic noon, *Planet. Space Sci.*, 38, 973 - 993, 1990b.

Lockwood, M., and M.F. Smith, Low altitude signatures of the cusp and flux transfer events, *Geophys. Res. Letters*, 16, 879, 1989.

Lockwood, M., and M.F. Smith, The variation of reconnection rate at the dayside magnetopause and cusp ion precipitation, *J. Geophys. Res.*, 97, 14841 - 14847, 1992.

Lockwood, M., and M.F. Smith, Comment on "Mapping the dayside ionosphere to the magnetosphere according to particle precipitation characteristics" by Newell and Meng, *Geophys. Res. Letters*, 20, 1739 - 1740, 1993.

Lockwood, M., and M.F. Smith, Low and middle altitude cusp particle signatures for general magnetopause reconnection rate variations: 1. Theory, *J. Geophys. Res.*, 99, 8531 - 8553, 1994.

Lockwood, M, and M.N. Wild, On the quasi-periodic nature of magnetopause flux transfer events, *J. Geophys. Res.*, 98, 5935 - 5940, 1993.

Lofthus, A. and P.H. Krupenie, The spectrum of molecular nitrogen, *J. Phys. and Chem. Reference Data*, 6, 113 - 307, 1977.

Loomis, E., On the geographical distribution of aurora in the northern hemisphere, *Amer. J. Sci. Arts.*, 30, 89, 1860.

Loral Fairchild Imaging Sensors, *1991 Loral Fairchild CCD Imaging Databook*, Milpitas, California, 1991.

LLoyd, J.W.F., L.J. Nardone, B.L. Cochrun, and S.M. Silverman, Rocket optical studies of daytime auroras, in *Space Research VIII*, pp. 185 - 194, A.P. Mitra, L.G. Jacchia, W.S. Newman, (eds.), North-Holland Pub. Co., Amsterdam, 1967.

Lorentzen, D.A., C.S. Deehr, J.I. Minow, R.W. Smith, H.C. Stenbaek-Nielsen, F. Sigernes, R.L. Arnoldy, and K. Lynch, SCIFER–Dayside auroral signatures of magnetospheric energetic electrons, *Geophys. Res. Letters*, 23, 1885 - 1888, 1996.

Lui, A.T.Y., P. Perreault, S.-I. Akasofu, and C.D. Anger, The diffuse aurora, *Planet. Space Sci.*, 21, 857 - 861, 1973.

Lui, A.T.Y., and D.G. Sibeck, Dayside auroral activities and their implications for impulsive entry processes in the dayside magnetosphere, *J. Atmos. Terr. Physics*, 53, 219 - 229, 1991.

Lui, A.T.Y., D. Venkatesan, and J.S. Murphree, Auroral bright spots on the dayside oval, *J. Geophys. Res.*, 94, 5515 - 5522, 1989.

Reproduced with permission of the copyright owner. Further reproduction prohibited without permission.

Lummerzheim, D., M.H. Rees, and G.J. Romick, The application of spectroscopic studies of the aurora to thermospheric netural composition, *Planet. Space Sci.*, 38, 67 - 78, 1990.

Lu, G., L.R. Lyons, P.H. Reiff, W.F. Denig, O. de la Beaugardiére, H.W. Kroehl, P.T. Newell, F.J. Rich, H. Opgenoorth, M.A.L. Persson, J.M. Rhohoniemi, E. Friis-christensen, L. Tomlinson, R. Morris, G. Burns, A. McEwin, Characteristics of ionospheric convection and field-aligned current in the dayside cusp region, *J. Geophys. Res.*, 100, 11845 - 11861, 1995.

Lui, A.T.Y., P. Perreault, and S.-I. Akasofu, The diffuse aurora, *Planet. Space Sci.*, 21, 857, 1973.

Lui, A.T.Y., and D.G. Sibeck, Dayside auroral activities and their implications for impulsive entry processes in the dayside magnetosphere, *J. Atmos. Terr. Physics*, 53, 219 - 229, 1991.

Lui, W.W., Ambipolar limit of electron precipitation, *Geophys. Res. Letters*, 20, 343 - 346, 1993.

Lundin, R., On the magnetospheric boundary layer and solar wind energy transfer into the magnetosphere, *Space Sci. Rev.*, 48, 263 - 320, 1988.

Lundin, R. and D.S. Evans, Boundary layer plasmas as a source for high-latitude, early afternoon, auroral arcs, *Planet. Space Sci.*, 33, 1389, 1985.

Lundin, R., B. Hultqvist, N. Pissarenko, and A. Zackarov, The plasma mantle: composition and other characteristics observed by means of the Prognoz-7 satellite, *Space Sci. Rev.*, 31, 247 - 345, 1982.

Lyons, L.R., Plasma processes in the Earth's radiation belts, in *Solar System Plasma Physics, Volume III*, pp. 137 - 163, edited by L.J. Lanzerotti, C.F. Kennel, and E.N. Parker, North-Holland Pub. Co., 1979.

Lyons, L.R., Substorms: Fundamental observational features, distinction from other disturbances, and external triggering, *J. Geophys. Res.*, 101, 13011 - 13025, 1996.

Lyons, L.R., and J.F. Fennel, Characteristics of auroral precipitation on the morning side, *J. Geophys. Res.*, 91, 11225, 1986.

Lyons, L.R., T.L. Killeen, and R.L. Waltersheid, The neutral "flywheel" as a source of quiet-time, polar cap currents, *Geophys. Res. Letters*, 12, 101 - 104, 1985.

Lyons, L.R., M. Schultz, D.C. Pridmore-Brown, and J.L. Roeder, Low-latitude boundary layer near noon: An open field line model, *J. Geophys. Res.*, 99, 17367 - 17377, 1994.

Lyons, L.R., and R.M. Thorne, Equilibrium structure of radiation belt electrons, *J. Geophys. Res.*, 78, 2142 - 2149, 1973.

Lyons, L.R., R.M. Thorne, and C.F. Kennel, Pitch angle diffusion of radiation belt electrons within the plasmasphere, *J. Geophys. Res.*, 77, 3455, 1972.

Lyons, L.R., A.L. Vampola, and T.W. Speiser, *J. Geophys. Res.*, 92, 6417, 1987.

Lyons, L.R., and D.J. Williams, The quiet time structure of energetic (35 - 560 keV) radiation belt electrons, *J. Geophys. Res.*, 80, 943, 1975a.

Lyons, L.R., and D.J. Williams, The storm and post storm evolution of energetic (35 - 560 keV) radiation belt electrons, *J. Geophys. Res.*, 80, 3985, 1975b.

Lyons, L.R., and D.J. Williams, *Quantitative Aspects of Magnetospheric Physics*, D. Reidel Pub. Co., Dordrecht, 1984.

Reproduced with permission of the copyright owner. Further reproduction prohibited without permission.

Ma, Z.W., J.G. Hawkins, and L.C. Lee, A simulation study of impulsive penetration of solar wind irregularities into the magnetosphere at the dayside magnetopause, *J. Geophys. Res.*, 96, 15751 - 15765, 1991.

Macleod, H.A., *Thin-Film Optical Filters*, Macmillan Publishing Company, New York, 1986.

Maeda, K., N.K. Bewtra, and P.H. Smith, Ring current electron trajectories associated with VLF emissions, *J. Geophys. Res.*, 83, 4339 - 4346, 1978.

Maezawa, K., Dependence of the magnetopause position on the southward interplanetary magnetic field, *Planet. Space Sci.*, 22, 1443 - 1453, 1974.

Maezawa, K., Magnetotail boundary motion associated with geomagnetic substorms, *J. Geophys. Res.*, 80, 3543, 1975.

Maggs, J.E., Thicknesses of auroral forms measured in the magnetic zenith over College, Alaska, *PhD Thesis*, University of Alaska, College, Alaska, 1967.

Maggs, J.E., and T.N. Davis, Measurements of the thicknesses of auroral structures,*Planet. Space Sci.*, 16, 205 - 209, 1968.

Mansurov, S.M., New evidence of a relationship between magnetic fields in space and on Earth, *Geomagnetism and Aeronomy*, 9, (Engl. Trans.), 622 - 623, 1969.

Mantas, G.P., and J.C.G. Walker, The penetration of soft electrons into the ionosphere,*Planet. Space Sci.*, 24, 409 - 423, 1976.

Maurits, S.A., and B.J. Watkins, UAF Eulerian model of the polar ionosphere, in *Solar-Terrestrial Energy Program: Handbook of Models*, edited by R.W. Schunk, pp. 95 - 121, Center for Atmospheric and Space Sciences, Utah State University, 1996.

Mayaud, P.N., *Derivation, Meaning, and Use of Geomagnetic Indices*, Geophysical Monograph 22, American Geophysical Union, Washington, D.C., 1980.

Maynard, N.C., W.J. Burke, W.F. Denig, and E.M. Basinska, Signatures and sources of electric fields and particles at dayside high latitudes, in *Physical Signatures of Manetospheric Boundary Layer Processes*, 59 - 72, J.A. Holtet and and A. Egeland (eds.), Kluwer Academic Publishers, 1994.

Maynard, N.C., J.P. Heppner, and A. Egeland, Intense, variable electric fields at ionospheric altitudes in the high latitude regions as observed by DE-2, *Geophys. Res. Letters*, 9, 981 - 984, 1982.

Maynard, N.C. et al., Magnetospheric boundary dynamics: DE 1 and DE 2 observations near the magnetopause and cusp, *J. Geophys. Res.*, 96, 3505, 1991.

McCormac, F.G., T.L. Killeen, B. Nardi, and R.W. Smith, How close are ground-based Fabry-Perot thermospheric wind and temperature measurements to exospheric values? A simulation study,*Planet. Space Sci.*, 35, 1255 - 1265, 1987.

McCormac, F.G., and R.W. Smith, The influence of the interplanetary magnetic field Y component on ion and neutral motions in the polar thermosphere, *Geophys. Res. Letters*, 9, 935 - 938, 1984.

McDiarmid, I.B., and J.R. Burrows, Temporal variations of outer radiation zone electron intensities at 1000 km, *Can. J. Phys.*, 44, 1361 - 1379, 1966.

McDiarmid, I.B., and J.R. Burrows, Local time asymmetries in the high-latitude boundary of the outer radiation zone for the different electron energies, *Can. J. Phys.*, 46, 49, 1968.

Reproduced with permission of the copyright owner. Further reproduction prohibited without permission.

McDiarmid, I.B., J.R. Burrows, and E.E.Budzinski, Average characteristics of magnetospheric electrons (150 eV to 200 keV) at 1400 km, *J. Geophys. Res.*, 80, 73 - 79, 1975.

McDiarmid, I.B., J.R. Burrows, and E.E.Budzinski, Particle properties in the day side cleft, *J. Geophys. Res.*, 81, 221 - 226, 1976.

McEwen, D.J., and P. Venkatarangan, Electron flux and auroral intensity measurements in situ, *Geophys. Res. Letters*, 5, 1051 - 1054, 1978.

McEwen, D.J., and D.A. Bryant, Optical-particle characteristics of pulsating aurora, *J. Atmos. Terr. Physics*, 40, 871, 1978.

McHarg, M.G., The morphology and electrodynamics of the boreal polar winter cusp, *PhD Thesis*, University of Alaska Fairbanks, Fairbanks, Alaska, 1993.

McHenry, M.A., and C.R. Clauer, Modeled ground magnetic signatures of flux transfer events, *J. Geophys. Res.*, 92, 11231 - 11240, 1987.

McIlwain, C.E., Coordinates for mapping the distribution of magnetically trapped particles, *J. Geophys. Res.*, 66, 3681, 1961.

McPherron, R.L., C.T. Russell, and M.P. Aubry, Satellite studies of magnetospheric substorms on August 15, 1968, 9. Phenomenological model for substorms, *J. Geophys. Res.*, 78, 3131 - 3149, 1973.

Mead, G.D., Deformation of the geomagnetic field by the solar wind, *J. Geophys. Res.*, 69, 1181 - 1195, 1964.

Meier, R.R., D.J. Strickland, J.H. Hecht, and A.B. Christensen, Deducing composition and incident electron spectra from ground-based auroral optical measurements: A study of auroral red line processes, *J. Geophys. Res.*, 94, 13541 - 13552, 1989.

Mende, S.B., J.H. Doolittle, R.M. Robinson, R.R. Vondrak, and F.J. Rich, Plasma drifts associated with a system of sun-aligned arcs in the polar cap, *J. Geophys. Res.*, 93, 256 - 264, 1988.

Mende, S.B., and R.H. Eather, The spatial extent of aurorae in O(5577) and $N_2^+$(4278) emissions, *Planet. Space Sci.*, 19, 49 - 58, 1971.

Mende, S.B., R.H. Eather, M.H. Rees, R.R. Vondrak, and R.M. Robinson, Optical mapping of ionospheric conductance, *J. Geophys. Res.*, 89, 1755 - 1763, 1984.

Meng, C.-I., Electron precipitation in the midday auroral oval, *J. Geophys. Res.*, 86, 2149 - 2174, 1981.

Meng, C.-I., Case studies of storm time variation of the polar cusp, *J. Geophys. Res.*, 88, 137, 1983.

Meng, C.-I., Space borne optical remote sensing of midday auroral oval and different precipitation regions, in *Physical Signatures of Magnetospheric Boundary Layer Processes*, J.A. Holtet and A. Egeland, (eds.), 157 - 172, Kluwer Academic Pub., 1994.

Meng, C.-I., and S.-I. Akasofu, Electron precipitation equatorward of the midday oval and the mantle aurora in the midday sector, *Planet. Space Sci.*, 31, 889, 1983.

Meng, C.-I., S.-I. Akasofu, K.A. Anderson, Dawn-dusk gradient of the precipitation of low-energy electrons over the polar cap and its relation to the interplanetary magnetic field, *J. Geophys. Res.*, 82, 5271 - 5275, 1977.

Meng, C.-I., and K.A. Anderson, A layer of energetic electrons (>40 keV) near the magnetopause, *J. Geophys. Res.*, 75, 1827, 1970.

Reproduced with permission of the copyright owner. Further reproduction prohibited without permission.

Meng, C.-I., R.H. Holzworth, and S.-I. Akasofu, Auroral circle–delineating the poleward boundary of the quiet auroral belt, *J. Geophys. Res.*, 82, 164 - 172, 1977.

Meng, C.-I. and R. Lundin, Auroral morphology of the midday oval, *J. Geophys. Res.*, 91, 1572 - 1584, 1986.

Menietti, J.D., and J.L. Burch, Spatial extent of the plasma injection region in the cusp-magnetosheath interface, *J. Geophys. Res.*, 93, 105 - 113, 1988.

Meyer, J.A., D.W. Setser, and D.H. Stedman, Excitation of the auroral green line of atomic oxygen ($^1S - ^1D$) by $N_2(A^3\Sigma_n^+$, *Astrophys. J.*, 157, 1023 - 1025, 1969.

Meyer, J.A., D.W. Setser, and D.H. Stedman, Energy transfer reactions of $N_2(^3\Sigma_n^+$, 2, Quenching and emission by oxygen and nitrogen atoms, *J. Phys. Chem.*, 74, 2238, 1970.

Min, Q., A self-consistent time varying auroral model, *PhD Thesis*, University of Alaska Fairbanks, Fairbanks, Alaska, 1993.

Minow, J.I., R.W. Smith, W.F. Denig, and P.T. Newell, Dayside Auroral Dynamics During Reconfigureation of the Auroral Oval, in *Physical Signatures of Magnetospheric Boundary Layer Processes,* A. Egeland, J. Holtet, and P.E. Sandholt, (eds.), 201 - 210, Kluwer Academic Publishers, 1994.

Mishin, V.M., T.I. Saifudinova, and I.A. Zhulin, Two zones of precipitating energetic particles, *J. Geophys. Res.*, 75, 797 - 806, 1970a.

Mishin, V.M., V.P. Samsonov, T.I. Saifudinova, and V.A. Kurilov, Main zones of corpuscular invasions into ionosphere, — *Invest. Geomagn. Aeron. Solar Phys.* (in Russian), no. 11, 3 - 23, 1970b.

Mitchell, D.G., F. Kutchko, D.J. Williams, T. Eastman, L.A. Frank, and C.T. Russell, An extended study of the low-latitude boundary layer on the dawn and dusk flanks of themagnetosphere, *J. Geophys. Res.*, 92, 7394, 1987.

Mizera, P.F., and J.F. Fennell, Satellite observations of polar, magnetotail lobe, and interplanetary electrons at low energies, *Rev. Geophys.*, 16, 147 - 153, 1978.

Moen, J., M. Lockwood, P.E. Sandholt, U.P. Løvhaug, W.F. Denig, A.P. van Eyken, and A. Egeland, Variability of dayside high-latitude convection associated with a sequence of auroral transients, *J. Atmos. Terr. Physics*, 58,85 - 96, 1994.

Moen, J., W.J. Burke, and P.E. Sandholt, A rotating, midday auroral event with northward interplanetary magnetic field, *J. Geophys. Res.*, 98, 13731 - 13739, 1993.

Moen, J., P.E. Sandholt, M. Lockwood, A. Egeland, and K. Fukui, Multiple, discrete arcs on sunward convection field lines in the 14-15 MLT region, *J. Geophys. Res.*, 99, 6113 - 6123, 1994.

Moen, J., D. Evans, H.C. Carlson, and M. Lockwood, Dayside moving auroral transients related to LLBL dynamics, *Geophys. Res. Letters*, 23, 3247 - 3250, 1996.

Moore, T.E., and D.S. Evans, Distribution of energetic positive ion species above a diffuse midnight aurora, *J. Geophys. Res.*, 84, 6443 - 6450, 1979.

Moore, T.E., R.L. Arnoldy, J. Feynman, and D.A. Hardy, Propagating substorm injection fronts, *J. Geophys. Res.*, 86, 6713 - 6726, 1981.

Morfill, G., and M. Scholer, Study of the magnetosphere using energetic solar particles,*Space Sci. Rev.*, 15, 267, 1973.

Reproduced with permission of the copyright owner. Further reproduction prohibited without permission.

Moses, J.J., G.L. Siscoe, R.A. Heelis, and J.D. Winningham, A model for multiple throat structures in the polar cap flow netry region, *J. Geophys. Res.*, 93, 9785 - 9790, 1988.

Mozer, F.S., Electric fields and plasma convection in the plasmasphere, *Rev. Geophys. Space Phys.*, 11, 755, 1973.

Murphree, J.S., L.L. Cogger, and C.D. Anger, Characteristics of the instantaneous auroral oval in the 1200-1800 MLT sector, *J. Geophys. Res.*, 86, 7657, 1981.

Murphree, J.S., L.L. Cogger, C.D. Anger, S. Ismail, and G.G. Shepherd, Large scale 6300Å, 5577Å, 3914Å dayside auroral morphology, *Geophys. Res. Letters*, 239 - 242, 1980.

Murphree, J.S., R.D. Elphinstone, D. Hearn, and L.L. Cogger, Large-scale high-latitude dayside auroral emissions, *J. Geophys. Res.*, 95, 2345 - 2354, 1990.

Nakamura, M., T. Terasawa, H. Kawano, M. Fujimoto, M. Hirahara, T. Mukai, S. Machida, Y. Saito, S. Kokubun, T. Yamamoto, and K. Tsuruda, Leakage ions from the LLBL to MSBL: Confirmation of reconnection events at the daysiee magnetopause, *J. Geomag. Geoelectr.*, 48, 65 - 70, 1996.

Nemzek, R.J., R. Nakamura, D.N. Baker, R.D. Belian, D.J. McComas, M.F. Thomsen, and T. Yamamoto, The relationship between pulsating auroras observed from the ground and energetic electrons and plasma density measured at geosynchronous orbit, *J. Geophys. Res.*, 100, 23935 - 23944, 1995.

Ness, N.F., Advances in particles and field research in the satellite era, *Rev. of Geophys.*, 3, 521 - 570, 1965.

Ness, N.F., C.S. Scearce, and J.B. Seek, Initial results of the IMP 1 magnetic field experiment, *J. Geophys. Res.*, 69, 3531 - 3569, 1964.

Ness, N.F., C.S. Scearce, J.B. Seek, and J.M. Wilcox, Summary of results from IMP 1 magnetic field experiment,*Space Res.*, 6, 581 - 628, 1966.

Neugebauer, M., and C. Snyder, The mission of Mariner 2; Preliminary observations, solar plasma experiments,*Science*, 138, 1095, 1962.

Neugebauer, M., and C.W. Snyder, Mariner 2 observations of the solar wind, 1, Average properties, *J. Geophys. Res.*, 71, 4469, 1966.

Newell, P.T., Comment on "Low-altitude signatures of the cusp and flux transfer events" by Lockwood and Smith, *Geophys. Res. Letters*, 17, 303 - 304, 1990.

Newell, P.T., W.J. Burke, C.-I. Meng, E.R. Sanchez, and M.R. Greenspan, Identification and observations of the plasma mantle at low altitude, *J. Geophys. Res.*, 96, 35 - 45, 1991a.

Newell, P.T., W.J. Burke, E.R. Sanchez, C.-I. Meng, M.R. Greenspan, and C.R. Clauer, The low-latitude boundary layer and the boundary plasma sheet at low altitude: Prenoon precipitation regions and convection reversal boundaries, *J. Geophys. Res.*, 96, 21013 - 21023, 1991b.

Newell, P.T., and C.-I. Meng, Cusp Width and $B_z$: Observations and a Conceptual Model, *J. Geophys. Res.*, 92, 13673 - 13678, 1987.

Newell, P.T., and C.-I. Meng, The cusp and the cleft/boundary layer: Low-altitude identification and statistical local time variation, *J. Geophys. Res.*, 93, 14549 - 14556, 1988.

Newell, P.T., and C.-I. Meng, Ion acceleration at the equatorward edge of the cusp: Low altitude observations of patchy merging, *Geophys. Res. Letters*, 18, 1829 - 1832, 1991.

Reproduced with permission of the copyright owner. Further reproduction prohibited without permission.

Newell, P.T., and C.-I. Meng, Ion acceleration at the equatorward edge of the cusp: Low altitude observations of patchy merging, *Geophys. Res. Letters*, 10, 1829, 1991.

Newell, P.T., and C.-I. Meng, Mapping the dayside ionosphere to the magnetosphere according to particle precipitation characteristics, *Geophys. Res. Letters*, 19, 609, 1992.

Newell, P.T., and C.-L Meng, Reply, *Geophys. Res. Letters*, 20, 1741 - 1742, 1993.

Newell, P.T., and C.-L Meng, Magnetopause dynamics as inferred from plasma observations on low-altitude satellites, in *Physics of the Magnetopause*, Geophysical Monograph 90, 407 - 416, P. Song, B.O.Ö. Sonnerup, and M.F. Thomsen (eds.), American Geophysical Union, 1995.

Newell, P.T., C.-I. Meng, and R.E. Huffman, Determining the source region of auroral emissions in the prenoon oval using coordinated Polar BEAR UV-imaging and DMSP particle measurements, *J. Geophys. Res.*, 97, 12245 - 12252, 1992. Newell, P.T., C.-I. Meng, D.G. Sibeck, and R. Lepping, Some low-altitude cusp dependencies on the interplanetary magnetic field, *J. Geophys. Res.*, 94, 8921, 1989.

Newell, P.T. and D.G. Sibeck, $B_y$ Fluctuations in the Magnetosheath and Azimuthal Flow Velocity Transients in the Dayside Ionosphere, *Geophys. Res. Letters*, 20, 1719 - 1722, 1993a.

Newell, P.T., and D.G. Sibeck, Upper limits on the contribution of flux transfer events to ionospheric convection, *Geophys. Res. Letters*, 20, 2829 - 2832, 1993b.

Newell, P.T., and D.G. Sibeck, The case for quasi-steady models in describing the physics of dayside merging, *EOS, Trans., AGU*, 77, 246, 249, 1996.

Newell, P.T., S. Wing, C.I. Meng, and V. Sigillito, The auroral oval position, structures, and intensity of precipitation from 1984 onward: An automated on-line data base, *J. Geophys. Res.*, 96, 5877 - 5882, 1991c.

Newell, P.T., K.M. Lyons, and C.-I. Meng, A large survey of electron acceleration events, *J. Geophys. Res.*, 101, 2599 - 2614, 1966.

Nicholls, R.W., Aeronomically important transition probability data, *Can. J. Chem.*, 47, 1847, 1969.

Niciejewski, R.J., T.L. Killeen, and Y. Won, Observations of neutral winds in the polar cap during northward IMF, *J. Atmos. Terr. Physics*, 56, 285 - 295, 1994.

Nishida, A., Formation of a plasmapause, or magnetospheric plasma knee, by combined action of magnetospheric convection and escape from the tail, *J. Geophys. Res.*, 71, 5669 - 5679, 1966.

Nishida, A., Can random reconnection on the magnetopause produce the low latitude boundary layer?, *Geophys. Res. Letters*, 16, 227 - 230, 1989.

Nishida, A., Ionospheric signatures of random reconnection on the dayside magnetopause, *J. Atmos. Terr. Physics*, 53, 213 - 217, 1991.

Nishida, A. The GEOTAIL Mission,*Geophys. Res. Letters*, 21, 2871 - 2873, 1994.

Northrup, T.G., *The Adiabatic Motion of Charged Particles*, Interscience Publishers, 1963.

Oieroset, M., H. Luhr, J.Moen, T. Moretto, and P.E. Sandholt, Dyamical auroral morphology in relation to ionospheric plsma convection and geomagnetic activity: Signatures of magnetopause X line dynamics and flux transfer events, *J. Geophys. Res.*, 101 , 13275 - 13292, 1996.

Reproduced with permission of the copyright owner. Further reproduction prohibited without permission.

Ogilvie, K.W., and R.J. Fitzenreiter, The Kelvin-Helmholtz instability at the magnetopause and inner boundary layer surface, *J. Geophys. Res.*, 94, 15113 - 15123, 1989.

Oguti, T., S. Kokubun, K. Hayashi, K. Tsuruda, S. Machida, T. Kitamura, O. Saka, and T. Watanabe, An auroral torch structure as an activity center of pulsating auroras, *Can. J. Phys.*, 59, 1056, 1981.

Oguti, T., T. Yamamoto, K. Hayashi, S. Kokubun, A. Egeland, and J.A. Holtet, Dayside Auroral Activity and Related Magnetic Impulses in the Polar Cusp Region, *J. Geomag. Geoelectr.*, 40, 387 - 408, 1988.

Okano, S., and J.S. Kim, Observations of a SAR-arc associated with an isolated magnetic substorm, *Planet. Space Sci.*, 35, 475 - 482, 1987.

Oliven, M.N., and D.A. Gurnett, Microburst phenomena, 3, An association between microbursts and VLF chorus, *J. Geophys. Res.*, 73, 2355, 1968.

Olson, W.P., and K.A. Pfitzer, A quantitative model of the magnetospheric magnetic field, *J. Geophys. Res.*, 79, 3739 - 3748, 1974.

Omholt, A., Studies on the excitation of aurora borealis, 1, The hydrogen lines, *Geophys. Publ.*, 20, 1 - 40, 1959.

Omholt, A., The time delay of the red [OI] lines in the aurora, *Planet. Space Sci.*, 2, 246 - 248, 1960.

Ono, T., and T. Hirasawa, An apparent lifetime of auroral 630.0 nm (OI) emissions, *J. Geomag. Geoelectr.*, 44, 91 - 108, 1992.

Onsager, T.G., and R.C. Elphic, Us magnetic reconnection intrinsically transient or steady-state? The Earth's magnetopause as a laboratory, *EOS, Trans., AGU*, 77, 241, 245, 249, 1996.

Onsager, T.G., C.A. Kletzing, J.B. Austin, and H. MacKiernan, Model of magnetosheath plasma in the magnetosphere: Cusp and mantle particles at low-altitudes, *Geophys. Res. Letters*, 20, 479 - 482, 1993.

Opgenoorth, H.J., J. Oksman, K.U. Kaila, E. Nielsen, and W. Baumjohann, Characteristics of eastward drifting omega bands in the morning sector of auroral oval, *J. Geophys. Res.*, 88, 9171, 1983.

Otto, A., and U. Arendt, Numerical simulation of flux transfer events at the magnetopause: Electron dynamics, *Adv. Space Res.*, 11, 129 - 132, 1991.

Owen, C.J., and S.W.H. Cowley, Heikkila's mechanism for impulsive plasma transport through the magnetopause: A reexamination, *J. Geophys. Res.*, 96, 5565 - 5574, 1991.

Palmer, I.D., and E.W. Hones, Jr., Characteristics of energetic electrons in the vicinity of the magnetospheric boundary layer at Vela orbit, *jgr*, 83, 2584, 1978.

Parker, E.N., Dynamics of the interplanetary gas and magnetic fields, *Astrophysics J.*, 128, 664 - 676, 1958.

Parker, E.N., Disturbances of the geomagnetic field by the solar wind, in *Physics of Geomagnetic Phenomena, Volume II*, edited by S. Matsushita and W.H. Campbell, Academic Press, New York, 1967.

Parks, G.K., and J.R. Winckler, Acceleration of energetic electrons observed at the synchronous altitude and the auroral zone, *J. Geophys. Res.*, 73, 5786, 1968.

Reproduced with permission of the copyright owner. Further reproduction prohibited without permission.

Parks, G.K., and J.R. Winckler, Simultaneous observations of 5- to 15-second period modulated energetic electron fluxes at the synchronous altitude and the auroral zone, *J. Geophys. Res.*, 74, 4003, 1969.

Paschmann, G., The Earth's magnetopause, in *Geomagnetism, Volume 4*, J.A. Jacobs, (ed.), Academic Press, 1991.

Paschmann, G., G. Haerendel, N. Sckopke, H. Rosenbauer, and P.C. Hedgecock, Plasma and magnetic field characteristics of the distant polar cusp near local noon: The entry layer, *J. Geophys. Res.*, 81, 2883 - 2889, 1976.

Paschmann, G., N. Sckopke, G. Haerendel, I. Papamastorakis, S.J. Bame, J.R. Asbridge, J.T. Gosling, E.W. Hones, and E.R. Tech, ISEE plasma observations near the subsolar magnetopause, *Space Sci. Rev.*, 22, 717, 1978.

Paschmann, G., B.U.Ö. Sonnerup, I. Papamastorakis, N. Sckopke, G. Haerendel, S.J. Bame, J.R. Asbridge, J.T. Gosling, C.T. Russell, and R.C. Elphic, Plasma acceleration at the Earth's magnetopause: Evidence for reconnection, *Nature*, 282, 243, 1979.

Pasternack, S.,*Astrophys. J.*, 92, 126, 1940.

Pereira, M.C. Kelley, D. Rees, I.S. Mikkelsen, T.S. Jørgensen, and T.J. Fuller-Rowell, Observations of neutral wind profiles between 115- and 175-km altitude in the dayside auroral oval, *J. Geophys. Res.*, 85, 2935 - 2940, 1980.

Peterson, R.N., and G.G. Shepherd, Ground-based photometric observations of the magnetospheric dayside cleft,*Geophys. Res. Letters*, 1, 231 - 234, 1974.

Peterson, W.K., J.P. Doering, T.A. Potemra, R.W. McEntire, and C.O. Bostrom, Conjugate photoelectron fluxes observed on Atmosphere Explorer C, *Geophys. Res. Letters*, 4, 109 - 112, 1977.

Peterson, W.K., E.G. Shelley, G. Haerendel, and G. Paschmann, Energetic ion composition in the subsolar magnetopause and boundary layer, *J. Geophys. Res.*, 87, 2139, 1982.

Peterson, W.K., E.G. Shelley, R.D. Sharp, R.G. Johnson, J. Geiss, and H. Rosenbauer, $H^+$ and $He^{++}$ in the dawnside magnetosheath, *Geophys. Res. Letters*, 6, 667, 1979.

Petrinec, S.P., and C.T. Russell, External and internal influences on the size of the dayside terrestrial magnetosphere, *Geophys. Res. Letters*, 20, 339 - 342, 1993.

Pfitzer, K.A., and J.R. Winckler, Density correlations and substorm electron drift effects in the outer radiation belt measured with by OGO 3 and ATS 1 satellites, *J. Geophys. Res.*, 74, 5005, 1969.

Phillips, J.L., S.J. Bame, R.C. Elphic, J.T. Gosling, M.F. Thomsen, and T.G. Onsager, Well-resolved observations by ISEE 2 of ion dispersion in the magnetospheric cusp, *J. Geophys. Res.*, 98, 13429 - 13440, 1993.

Pike, C.P., C.-I. Meng, S.-I. Akasofu, and J.A. Whalen, Observed correlations between interplanetary field variables and the dynamics of the auroral oval and the high-latitude ionosphere, *J. Geophys. Res.*, 79, 5129, 1974.

Pinnock, M., et al., Observations of an enhanced convection channel in the cusp ionosphere, *J. Geophys. Res.*, 98, 3767, 1993.

Pollack, S.A., Angular dependence of transmission characteristics of interference filters and application to a tunable flourometer, *App. Opt.*, 5, 1749 - 1756, 1966.

Reproduced with permission of the copyright owner. Further reproduction prohibited without permission.

Potter, W.E., Rocket measurements of auroral electric and magnetic fields, *J. Geophys. Res.*, 75, 5415 - 5431, 1970.

Press, W.H., B.P. Flannery, S.A. Teukolsky, and W.T. Vetterling, *Numerical Recipes: The Art of Scientific Computing*, Cambridge University Press, New York, 1986.

Pudovkin, M.I., S.A. Zaitseva, P.E. Sandholt, and A. Egeland, Dynamics of aurorae in the cusp region and characteristics of magnetic reconnection at the magnetopause, *Planet. Space Sci.*, 879 - 887, 1992.

Quantex Corporation, *Quantex DS-50 Digital Video Processor: Installation, Operation, and Maintenance Manual*, (Rev. 0, 9/81), Sunnyvale, California, 1981.

Radio Corporation of America, *RCA-7967 Image Orthicon*, 7967 5-63, Harrison, New Jersey, 1963.

Rairden, R.L., and S.B. Mende, Properties of 6300-Å auroral emissions at South Pole, *J. Geophys. Res.*, 94, 1402 - 1416, 1989.

Reasoner, D.L., Auroral helium precipitation, *Rev. Geophys. Space Phys.*, 11, 169, 1973.

Reasoner, D.L., R.H. Eather, and B.J. O'Brien, Detection of alpha particles in auroral phenomena, *J. Geophys. Res.*, 73, 4185 - 4198, 1968.

Redington, R.W., The Image Orthicon, in *Photoelectronic Imaging Devices, Volume 2, Devices and Their Evaluation*, L.M. Biberman and S. Nudelman, editors, Plenum Press, 1971.

Rees, M.H., Excitation of high altitude red auroral arcs, *Planet. Space Sci.*, 8, 59, 1961.

Rees, M.H., *Physics and Chemistry of the Upper Atmosphere*, Cambridge University Press, Cambridge, 1989.

Rees, M.H., and R.A. Jones, Time dependent studies of the aurora-II. Spectroscopic morphology, *Planet. Space Sci.*, 21, 1213 - 1235, 1973.

Rees, M.H., and D. Luckey, Auroral emission energy derived from ratios of spectroscopic emissions, 1, Model computations, *J. Geophys. Res.*, 79, 5181, 1974.

Rees, M.H., D. Lummerzheim, R.G. Roble, J.D. Winningham, J.D. Craven, and L.A. Frank, Auroral energy deposition rate, characteristic electron energy, and ionospheric parameters derived from Dynamics Explorer 1 images, *J. Geophys. Res.*, 93, 12841 - 12860, 1988.

Rees, M.H., and R.A. Jones, Time dependent studies of the aurora, 2, Spectroscopic morphology, *Planet. Space Sci.*, 21, 1213, 1973.

Rees, M.H., and R.G. Roble, Observations and theory of the formation of stable auroral red arcs, *Rev. of Geophys. and Space Phys.*, 13, 201 - 242, 1975.

Rees, M.H. and R.G. Roble, Excitation of $O(^1D)$ atoms in aurorae and emission of the [OI] 6300 A line, *Can. J. Phys.*, 64, 1608 - 1613, 1986.

Rees, M.H, J.C.G. Walker, and A. Dalgarno, Auroral excitation of the forbidden lines of atomic oxygen, *Planet. Space Sci.*, 15, 1097, 1967.

Reeves, G.D., R.D. Belian, and T.A. Fritz, Numerical tracing of energetic particle drifts in a model magnetosphere, *J. Geophys. Res.*, 96, 13997 - 14008, 1991.

Reeves, G.D., T.A. Fritz, T.E. Cayton, and R.D. Belian, Multi-satellite measurements of the substorm injection region, *Geophys. Res. Letters*, 17, 2015 - 2018, 1990.

Reproduced with permission of the copyright owner. Further reproduction prohibited without permission.

Reeves, G.D., G. Kettmann, T.A. Fritz, and R.D. Belian, Further investigation of the CDAW 7 substorm using geosynchronous particle data: Multiple injections and their implications, *J. Geophys. Res.*, 97, 6417 - 6428, 1992.

Reiff, P.H., and J.L. Burch, IMF $B_y$-dependent plasma flow and birkeland currents in the dayside magnetosphere 2. A global model for northward and southward IMF, *J. Geophys. Res.*, 90, 1595 - 1609, 1985.

Reiff, P.H., J.L. Burch, R.A. Heelis, Dayside auroral arcs and convection, *Geophys. Res. Letters*, 5, 391 - 394, 1978.

Reiff, P.H., J.L. Burch, and T.W. Hill, Cusp proton signatures and the interplanetary magnetic field, *J. Geophys. Res.*, 85, 5997 - 6005, 1980.

Reiff, P.H., T.W. Hill, and J.L. Burch, Solar wind plasma injection at the dayside magnetopause cusp, *J. Geophys. Res.*, 82, 479 - 491, 1977.

Reiff, P.H., and J.G. Luhmann, Solar wind control of the polar-cap voltage, in *Solar Wind-Magnetosphere Coupling*, edited by Y. Kamide and J.A. Slavin, 453 - 476, Terra Scientific Publishing Company, 1986.

Reiff, P.H., R.W. Spiro, and T.W. Hill, Dependence of polar cap potential drop on interplanetary parameters, *J. Geophys. Res.*, 86, 7639 - 7648, 1981.

Richmond, A.D. and Y. Kamide, Mapping Electrodynamic Features of the High- Latitude Ionosphere From Localized Observations: Technique, *J. Geophys. Res.93*, 5741-5749, 1988.

Riehl, K., and D.A. Hardy, Average characteristics of the polar rain and their relationship to the solar wind and the interplanetary magnetic field, *J. Geophys. Res.*, 91, 1557 - 1571, 1986.

Rijnbeek, R.P., S.W.H. Cowley, D.J. Southwood, and C.T. Russell, A survey of dayside flux transfer events observed by ISEE 1 and 2 magnetometers, *J. Geophys. Res.*, 89, 786 - 800, 1984.

Roach, F.E., Photometric observation of the airglow, *Annals of the Inter. Geophys. Year*, 4, 115-138, 1957.

Roach, F.E., Photometric observation of the airglow during the IQSY, *in Annals of the IQSY, Volume 1. Geophysical Measurements: Techniques, Observational Schedules and Treatment of Data*, C.M. Minnis, editor, MIT Press, 145 - 166, 1968.

Roach, F.E., and J.L. Gordon, *The Light of the Night Sky*, D. Reidel Publishing Company, 1973.

Roach, F.E., and J.R. Roach, Stable 6300 Å auroral arcs in mid-latitudes, *Planet. Space Sci.*, 1963, 523 - 545, 1963.

Rodger, A.S., S.B. Mende, T.J. Rosenberg, and K.B. Baker, Simultaneous optical and HF radar observations of the ionospheric cusp, *Geophys. Res. Letters*, 22, 2145 - 2048, 1995.

Roeder, J.L., and L.R. Lyons, Energetic and magnetosheath energy particle signatures of the low-latitude boundary layer at low atitudes near noon, *J. Geophys. Res.*, 97, 13817 - 13828, 1992.

Roederer, J.G., A proposal for trapped particle flux mapping in the outer magnetosphere, *NASA-GSFC preprint X-640-66-313*, 1966.

Roederer, J.L., On the adiabatic motion of energetic particles in a model magnetosphere, *J. Geophys. Res.*, 72, 981 - 992, 1967.

Roederer, J.G., Quantitative models of the magnetosphere, *Rev. of Geophysics*, 7, 77 - 96, 1969.

Reproduced with permission of the copyright owner. Further reproduction prohibited without permission.

Roederer, J.G., *Dynamics of Geomagnetically Trapped Radiation*, Springer-Verlag, Heidelberg, 1970.

Roelof, E.C., and D.G. Sibeck, Magnetopause shape as a bivariate function of interplanetary magnetic field $B_z$ and solar wind dynamic pressure, *J. Geophys. Res.*, 98, 21421 - 21450, 1993.

Romick, G.J., The determination of the spatial distribution of auroral luminosity, *PhD Thesis*, University of Alaska, 1964.

Romick, G.J., The detection and study of the visible spectrum of the aurora and airglow, *Methods for Atm. Radiometry*, 91, 63, 1976.

Romick, G.J., and A.E. Belon, The spatial variation of auroral luminosity–I. The behaviour of synthetic model auroras, *Planet. Space Sci.*, 15, 475 - 493, 1967a

Romick, G.J., and A.E. Belon, The spatial variation of auroral luminosity–II. Determination of volume emission rate profiles, *Planet. Space Sci.*, 15, 1695 - 1716, 1967b.

Romick, G.J., A.E. Belon, and W.J. Stringer, Photometric measurements of H-beta in the aurora,*Planet. Space Sci.*, 22, 725 - 733, 1974.

Romick, G.J., and N.B. Brown, Midday auroral observations in the oval, cusp, region, and polar cap, *J. Geophys. Res.*, 76, 8420 - 8424, 1971.

Rose, A., P.K. Weimer, H.B. Law, The Image Orthicon–A sensitive television pickup tube, *Proceedings of the I.R.E. and Waves and Electrons*, 424 - 432, 1946.

Rosenbauer, H., H. Grunwaldt, M.D. Montgomery, G. Paschmann, and N. Schopke, Heos 2 plasma observations in the distant polar magnetosphere: The plasma mantle, *J. Geophys. Res.*, 80, 2723, 1975.

Rosenberg, T.A., R.A. Helliwell, and J.P. Katsufrakis, Electron precipitation associated with discrete very low frequency emissions, *J. Geophys. Res.*, 76, 8445, 1971.

*Rosenfield, A., and A.C. Kak, *Digital Picture Processing*, Academic Press, 1976.

Rossberg, L., Undisturbed trapping boundary for energetic electrons at low altitudes, *J. Geophys. Res.*, 83, 4307 - 4317, 1978.

Rostoker, G., Triggering of expansion phase intensifications of magnetospheric substorms by northward turnings of the interplanetary magnetic field, *J. Geophys. Res.*, 88, 6981, 1983.

Roth, M., On impulsive penetration of solar wind plasmoids into the geomagnetic cavity, *Planet. Space Sci.*, 40, 193, 1992.

Roth, M., Impulsive transport of solar wind into the magnetosphere, in *Physics of the Magnetopause*, P. Song, B.U.Ö . Sonnerup, and M.F. Thomsen (eds.), pp. 343 - 348, American Geophysical Union, 1995.

Rudland, A., Discrete auroral structures in the cusp/cleft ionosphere: A statistical study based on meridian scanning photometer data, *Thesis*, University of Oslo, Oslo, Norway, 1991.

Rusch, D.W., J.-C. Gérard, and W.E. Sharp, The reaction of $N(^2D)$ with $O_2$ as a source of $O(^1D)$ atoms in aurorae, *Geophys. Res. Letters*, 5, 1043 - 1046, 1978.

Russell, C.T., The structure of the magnetopause, in *Physics of the Magnetopause*, P. Song, B.U.Ö . Sonnerup, and M.F. Thomsen (eds.), pp. 81 - 98, American Geophysical Union, 1995.

Reproduced with permission of the copyright owner. Further reproduction prohibited without permission.

Russell, C.T., J. Berchem, and J. Luhmann, On the source region of flux transfer events, *Adv. Space Res.*, 5, 363, 1985.

Russell, C.T., and R.C. Elphic, Initial ISEE magnetometer results: Magnetopause observations, *Space Sci. Rev.*, 22, 681 - 715, 1978.

Russell, C.T., and R.C. Elphic, ISEE observations of flux transfer events at the dayside magnetopause, *Geophys. Res. Letters*, 6, 33 - 36, 1979.

Russell, C.T., G.L. Siscoe, and E.J. Smith, Comparision of ISEE-1 and -3 interplanetary magnetic field observations, *Geophys. Res. Letters*, 7, 381 - 384, 1980.

Samson, J.C., and K.L. Yeung, Some generalizations on the method of superimposed epoch analysis, *Planet. Space Sci.*, 34, 1133, 1986.

Sanchez, E.R., C.-I. Meng, and P.T. Newell, Observations of solar wind penetration into the Earth's magnetosphere: The plasma mantle, *Johns Hopkins APL Technical Digest*, 11, 272 - 278, 1990.

Sandford, B.P., Aurora and airglow intensity variations with time and magnetic activity at sourthern high latitudes,*J. Atmos. Terr. Physics*, 26, 749, 1964.

Sandford, B.P., Variations of auroral emissions with time, magnetic activity, and the solar cycle, *J. Atmos. Terr. Phys.*, 30, 1921, 1968.

Sandholt, P.E., IMF control of polar cusp and cleft auroras, *Adv. Space Sci.*, 10, (9)21 - (9)34, 1988a.

Sandholt, P.E., Polar cusp electrodynamics–a case study, in *Modeling Magnetospheric Plasma*, Geophysical Monograph 44, 191 - 195, T.E. Moore, J.H. Waite, Jr., (eds.), American Geophysical Union, 1988b. Sandholt, P.E., Electrodynamics of the polar cusp ionosphere: A case study, *J. Geophys. Res.*, 94, 6713 - 6722, 1989a.

Sandholt, P.E., Midday auroral breakup, *J. Geomag. Geoelectr.*, 41, 371, 1989b.

Sandholt, P.E., Electrodynamics of the polar cusp ionosphere: A case study, *J. Geophys. Res.*, 94, 6713 - 6722, 1989c.

Sandholt, P.E., Dayside auroral activity and magnetospheric boundary layer phemomenon, *J. Geomag. Geoelectr.*, 42, 711 - 726, 1990.

Sandholt, P.E., Auroral electrodynamics at the cusp/cleft pleward boundary during northward interplanetary magnetic field, *Geophys. Res. Letters*, 18, 805 - 808, 1991

Sandholt, P.E., Magnetopause plasma transients: signatures in the auroral ionosphere,*J. Atmos. Terr. Physics*, 55, 1699 - 1715, 1993.

Sandholt, P.E., C.S. Deehr, A. Egeland, B. Lybekk, R. Viereck, and G.J. Romick, Signatures in the dayside aurora of plasma transfer from the magnetosheath, *J. Geophys. Res.*, 91, 10063 - 10079, 1986a.

Sandholt, P.E., and A. Egeland, Auroral and magnetic variations in the polar cusp and cleft–signatures of magnetopause boundary-layer dynamics, *Astrophys. and Space Sci.*, 144, 171 - 199, 1988.

Sandholt, P.E., A. Egeland, K. Henriksen, R. Smith, and P. Sweeney, Optical measurements of a nightside poleward expanding aurora, *J. Atmos. Terr. Physics*, 44, 71 - 79, 1982.

Sandholt, P.E., A. Egeland, J.A. Holtet, B. Lybekk, K. Svenes, S. Åsheim, and C.S. Deehr, Large- and small-scale dynamics of the polar cusp, *J. Geophys. Res.*, 90, 4407 - 4414, 1985.

Reproduced with permission of the copyright owner. Further reproduction prohibited without permission.

Sandholt, P.E., A. Egeland, and B. Lybekk, On the spatial relationship between auroral emissions and magnetic signatures of plasma convection in the midday polar cusp and cap ionosphere during negative and positive IMF $B_z$: A case study, *J. Geophys. Res.*, 91, 12108 - 12112, 1986b.

Sandholt, P.E., A. Egeland, B. Lybekk, C.S. Deehr, G.G. Sivjee, and G.J. Romick, Effects of interplanetary magnetic field and magnetospheric substorm variations of the dayside aurora, *Planet. Space Sci.*, 31, 1345 - 1362, 1983.

Sandholt, P.E., C.J. Farrugia, L.F. Burlaga, J.A. Holtet, J. Moen, B. Lybekk, B. Jacobsen, D. Opsvik, A. Egeland, R. Lepping, A.J. Lazarus, T. Hansen, A. Brekke, and E. Friis-Christensen, Cusp/cleft auroral activity in relation to solar wind dynamic pressure, interplanetary magnetic field $B_z$ and $B_y$, *J. Geophys. Res.*, 99, 17323 - 17342, 1994.

Sandholt, P.E., K. Henriksen, C.S. Deehr, G.G. Sivjee, G.J. Romick, and A. Egeland, Dayside cusp auroral morphology related to nightside magnetic activity, *J. Geophys. Res.*, 85, 4132 - 4138, 1980.

Sandholt, P.E., B. Jacobsen, B. Lybekk, A. Egeland, C.-I. Meng, P.T. Newell, F.J. Rich, and E.J. Weber, Polar cleft structure and dynamics in the prenoon sector, *Adv. Space Res.*, 8, 59 - 64, 1988.

Sandholt, P.E., B. Jacobsen, B. Lybekk, A. Egeland, C.-I. Meng, P.T. Newell, F.J. Rich, and E.J. Weber, Structure and dynamics in the polar cleft: Coordinated satellite and ground-based observations in the prenoon sector, *J. Geophys. Res.*, 94, 8928 - 8942, 1989a.

Sandholt, P.E., and M. Lockwood, Periodic auroral events at the high-latitude convection reversal in the 16 MLT region, *Geophys. Res. Letters*, 17, 1877 - 1880, 1990.

Sandholt, P.E., M. Lockwood, B. Lybekk, and A.D. Farmer, Auroral bright spot sequence near 1400 MLT: Coordinated optical and on drift observations, *J. Geophys. Res.*, 95, 21095 - 21109, 1990a.

Sandholt, P.E., M. Lockwood, T. Oguti, S.W.H. Cowley, K.S.C. Freeman, B. Lybekk, A. Egeland, and D.M. Willis, Midday auroral breakup events and related energy and momentum transfer from the magnetosheath, *J. Geophys. Res.*, 95, 1039 - 1060, 1990b.

Sandholt, P.E., B.Lybekk, A. Egeland, R. Nakamura, and T. Oguti, Midday auroral breakup,*J. Geomag. Geoelectr.*, 41, 371 - 387, 1989b.

Sandholt, P.E., J. Moen, and D. Opsvik, Periodic auroral events at the midday polar cap boundary: Implications for solar wind-magnetosphere coupling, *Geophys. Res. Letters*, 19, 1223 - 1226, 1992a.

Sandholt, P.E., M. Lockwood, W.F. Denig, R.C. Elphic, and S. Leontjev, Dynamical auroral structure in the vicinity of the polar cusp: Multipoint observations during southward and northward IMF, *Ann. Geophys.*, 10, 483 - 497, 1992b.

Sandholt, P.E., J. Moen, A. Rudland, D. Opsvik, W.F. Denig, and T. Hansen, Auroral event sequences at the dayside polar cap boundary for positive and negative interplanetary magnetic field $B_y$, *J. Geophys. Res.*, 98, 7737 - 7755, 1993.

Sandholt, P.E., and P.T. Newell, Ground and satellite observations of an auroral event at the cusp/cleft equatorward boundary, *J. Geophys. Res.*, 97, 8685 - 8691, 1992.

Saunders, M.A., The polar cusp ionosphere: a window on solar wind-magnetosphere coupling, *Antarctic Science*, 1, 193 - 203, 1989.

Reproduced with permission of the copyright owner. Further reproduction prohibited without permission.

Saunders, M.A., Magnetosheath, magnetopause, and low latitude boundary layer research, 1987 - 1989, *jatp*, 52, 1107 - 1121, 1990.

Saunders, M.A., C.T. Russell, and N. Sckipke, A dual-satellite study of the spatial properties of FTE's, in *Magnetic Reconnection in Space and Laboratory Plasmas*, (edited by E.W. Hones, Jr.), pp. 145 - 152, American Geophysical Union, Washington, D.C., 1984a.

Saunders, M.A., C.T. Russell, and N. Schopke, Flux transfer events: Scale size and interior structure, *Geophys. Res. Letters*, 11, 131 - 134, 1984b.

Savoini, P., M. Scholer, and M. Fujimoto, Two-dimensional hygrid simulations of impulsive plasma penetration through a tangential discontinuity, *J. Geophys. Res.*, 99, 19377 - 19391, 1994.

Sergeev, V.A., Polar cap and cusp boundaries at day and night, *J. Geomag. Geoelectr.*, 42, 683 - 695, 1990.

Schindler, K., On the role of irregularities in plasma entry into the magnetosphere, *J. Geophys. Res.*, 84, 7257 - 7266, 1979.

Scholer, M., Magnetic flux transfer at the magnetopuase based on single x line bursty reconnection, *Geophys. Res. Letters*, 15, 291 - 294, 1993.

Scholer, M., P.W. Daly, G. Paschmann, and T.A. Fritz, Field line topology determined by energetic particles during a possible magnetopause reconnection event, *J. Geophys. Res.*, 87, 6073 - 6080, 1982a.

Scholer, M., D. Hovestadt, F.M. Ipavich, and G. Gloeckler, Energetic protons, alpha particles, and electrons in magnetic flux transfer events, *J. Geophys. Res.*, 87, 2169 - 2175, 1982b.

Scholer, M., F.M. Ipavich, G. Gloeckler, D. Hovestadt, and B. Klecker, Leakage of magnetospheric ions into the magnetosheath along reconnected field lines at the dayside magnetopause, *J. Geophys. Res.*, 86, 1299 - 1304, 1981.

Scholer, M., and G. Morfill, *Planet. Space Sci.*, 20, 1051, 1972.

Schulz, M., Interplanetary sector structure and the heliomagnetic equator, *Astrophys. Space Sci.*, 24, 371, 1973.

Schulz, M., The Magnetosphere, in *Geomagnetism, Volume 4*, 87 - 293, edited by J.A. Jacobs, Academic Press Limited, 1991.

Sckopke, N., and G. Paschmann, The Plasma mantle: A survey of magnetotail boundary observations, *J. Atmos. Terr. Physics*, 40, 261 - 278, 1978.

Sckopke, N., G. Paschmann, H. Rosenbauer, and D.H. Fairfield, Influence of the interplanetary magnetic field on the occurrence and thickness of the plasma mantle, *J. Geophys. Res.*, 81, 2687 - 2691, 1976.

Sckopke et al., in Magnetospheric Boundary Layers, B. Battrick (ed.), ESA, Paris, SP-148, p 37., 1979.

Sears, R.D., Intensity correlations of the 4278-Å $N_2^+$(0-1) first negative band and 5875-Å emissions in auroras, *J. Geophys. Res.*, 80, 215 - 218, 1975.

Sergeev, V.A., Polar cap and cusp boundaries at day and night, *J. Geomag. Geoelectr.*, 42, 683 - 695, 1990.

Shabansky, V.P. Some processes in the magnetosphere, *Space Sci. Rev.*, 12, 299 - 418, 1971.

Sharp, W.E., and P.B. Hays, Low-energy auroral electrons, *J. Geophys. Res.*, 79, 4319, 1974.

Reproduced with permission of the copyright owner. Further reproduction prohibited without permission.

Sharp, R.D., R.G. Johnson, and E.G. Shelley, Satellite measurements of auroral alpha particles, *J. Geophys. Res.*, 79, 5167 - 5170, 1974.

Sharp, W.E., M.H. Rees, and A.I. Stewart, Coordinated rocket and satellite measurements of an auroral event, 2, The rocket observations and analysis, *J. Geophys. Res.*, 84, 1977, 1979.

Shefov, N.N., Intensities of some twilight and night airglow emissions (translated title). In *Spectral, Electrophotometrical, and Radar Researches of Aurora and Airglow*, No. 1, 25 - 29, Publ. House, Academy of Sciences, Moscow, 1959.

Shelley, E.G., R.G. Johnson, and R.D. Sharp, Satellite observations of energetic heavy ions during a geomagnetic storm, *J. Geophys. Res.* , 77, 6104, 1972.

Shelley, E.G., R.D. Sharp, and R.G. Johnson, $He^{++}$ and $H^{+}$ flux measurements in the day side cusp: Estimate of convection electric field, *J. Geophys. Res.*, 81, 2362 - 2370, 1976.

Shemansky, D.E., $N_2$ Vegard-Kaplan system in absorption, *J. Chem Phys.*, 51, 689, 1969.

Shemansky, D.E., and A. Vallance Jones, Type-B red aurora; the $O_2^+$ first negative system and the $N_2$ first positive system, *Planet. Space Sci.*, 16, 1115 - 1130, 1968.

Shepherd, G.G., Dayside cleft aurora and its ionospheric effects, *Rev. of Geophys. and Space Phys.*, 17, 2017 - 2033, 1979.

Shepherd, G.G., J.F. Pieau, F. Creutzberg, A.G. McNamara, J.-C. Gerard, D.J. McEwen, B. Delana, and J.H. Whitteker, Rocket and ground-based measurements of the dayside magnetospheric cleft from Cape Perry, N.W.T.,*Geophys. Res. Letters*, 3, 69 - 72, 1976a.

Shepherd, G.G., and F.W. Thirkettle, Magnetospheric dayside cusp: A topside view of its 6300-Angstrom atomic oxygen emission,*Science*, 180, 737, 1973.

Shepherd, G.G., F.W. Thirkettle, and C.D. Anger, Topside optical view of the dayside cleft aurora,*plss*, 24, 937, 1976b.

Shepherd, G.G., J.H. Whitteker, J.D. Winningham, J.H. Hoffman, E.J. Maier, L.H. Brace, J.R. Burrows, and L.L. Cogger, The topside magnetospheric cleft ionosphere observed from the ISIS 2 spacecraft, *J. Geophys. Res.*, 81, 6092, 1976b.

Shepherd, G.G., J.D. Winningham, F.E. Bunn, and F.W. Thirkettle, An empirical determination of the production efficiency for auroral 6300-Å emission by energetic electrons, *J. Geophys. Res.*, 85, 715 - 721, 1980.

Shi, Y., C.C. Wu, and L.C. Lee, A study of multiple x line reconnection at the dayside magnetopause, *Geophys. Res. Letters*, 15, 295 - 298, 1988.

Shi, Y., C.C. Wu, and L.C. Lee, Magnetic field reconnection patterns at the dayside magnetopause: An MHD simulation study, *J. Geophys. Res.*, 96, 17627 - 17650, 1991.

Shyn, T.W., S.Y. Cho, and W.E. Sharp, Differential excitation cross section of atomic oxygen by electron impact: $(^3P - ^1S)$ transition, *J. Geophys. Res.*, 91, 13751 - 13754, 1986.

Shyn, T.W., and W.E. Sharp, Differential excitation cross section of atomic oxygen by electron impact: $(^3P - ^1D)$ transition, *J. Geophys. Res.*, 91, 1691 - 1697, 1986.

Sibeck, D.G., and R.W. McEntire, Multiple satellite observations of leakage of particles from the magnetosphere, *Adv. Space Res.*, 8, 201 - 216, 1988.

Sibeck, D.G., R.W. McEntire, S.M. Krimigis, and D.N. Baker, The magnetosphere as a sufficient source for upstream ions on November 1, 1984, *J. Geophys. Res.*, 93, 14328 - 14342, 1988.

Reproduced with permission of the copyright owner. Further reproduction prohibited without permission.

Sibeck, D.G., and R.W. McEntire, Multiple satellite observations of leakage of particle from the magnetosphere, *Adv. Space Res.*, 8, 201 - 216, 1988.

Sibeck, D.G., R.W. McEntire, A.T.Y. Lui, and S.M. Krimigis, A statistical study of ion [itch-angle distributions, in *Magnetotail Physics*, edited by A.T.Y. Lui, pp. 225 - 229, Johns Hopkins Press, Baltimore, 1987a.

Sibeck, D.G., R.W. McEntire, A.T.Y. Lui, R.E. Lopez, and S.M. Krimigis, Magnetic field drift shell splitting: Cause of unusual dayside particle pitch angle distributions during storms and substorms, *J. Geophys. Res.*, 92, 13485 - 13497, 1987a.

Sibeck, D.G., R.W. McEntire, A.T.Y. Lui, R.E. Lopez, S.M. Krimigis, R.B. Decker, L.J. Zanetti, and T.A. Potemra, Energetic magnetospheric ions at the dayside magnetopause: Leakage or merging?, *J. Geophys. Res.*, 92, 12097, 1987b.

Sibeck, D.G., and P.T. Newell, Concerning the location of magnetopause merging, in *Physical Signatures of Magnetospheric Boundary Layer Processes*, 263 - 273, J.A. Holtet and A. Egeland, (eds.), Kluwer Academic Pub., 1994.

Sigernes, F., G. Fasel, C.S. Deehr, R.W. Smith, D.A. Lorentzen, L.T. Wetjen, and K. Henriksen, Proton aurora on the dayside, *Geomagnetism and Aeronomy*, (Eng. Trans.), 34, 637 - 640, 1995.

Sigernes, F., G. Fasel, J. Minow, C.S. Deehr, R.W. Smith, D.A. Lorentzen, L.T. Wetjen, and K. Henriksen, Calculations and ground-based observations of pulsed proton events in the dayside aurora, *J. Atmos. Terr. Physics*, 58, 1281 - 1291, 1996.

Sigernes, F, J. Moen, M. Oieroset, B. Lybekk, J. Holtet, D. Lorentzen, C. Deehr, and R. Smith, SCIFER-Height measurements of the midmorning aurora, *Geophys. Res. Letters*, 23, 1889 - 1892, 1996.

Sivjee, G.G., Differences in near-UV (~3400-4300 A) optical emissions from midday cusp and night-time auroras, *J. Geophys. Res.*, 88, 435, 1983a.

Sivjee, G.G., Atomic nitrogen abundance in polar upper thermosphere, *Geophys. Res. Letters*, 10, 349, 1983b.

Sivjee, G.G., [OII($^2D \rightarrow ^4S$)] 3726-3729 Å emissions from the high altitude mid-day cusp auroras, *Planet. Space Sci.*, 39, 777 - 784, 1991.

Sivjee, G.G., A.B. Christensen, K. Henriksen, and A.E. Belon, OI 7774 A and 8446 A emissions from night-side and midday cusp auroras, *Ann. Geophys.*, 2, 463 - 466, 1984.

Sivjee, G.G., and C.S. Deehr, Difference in polar atmospheric optical emissions between mid-day and night-time auroras, in *Exploration of the Polar Upper Atmosphere*, 199 - 207, C.S. Deehr and J.A. Holtet (eds.), D. Reidel Pub. Co., 1980.

Sivjee, G.G., C.S. Deehr, and K. Henriksen, Difference in quenching of $N(^2D^0_{3/2})$ and $N(^2D^0_{5/2})$ by atomic oxygen, *J. Geophys. Res.*, 86, 1581 - 1584, 1981.

Sivjee, G.G., K. Henriksen, and C.S. Deehr, Orthohelium emissions at 3889 and 5876 Å in the polar upper atmosphere, *J. Geophys. Res.*, 85, 6043 - 6046, 1980.

Sivjee, G.G., and B. Hultqvist, Particle and optical measurements in the magnetic noon sector of the auroral oval, *Planet. Space Sci.*, 23, 1597, 1975.

Sivjee, G.G., G.J. Romick, C.S. Deehr, Optical signatures of some magnetospheric processes on the dayside, *Geophys. Res. Letters*, 9, 676 - 679, 1982.

Reproduced with permission of the copyright owner. Further reproduction prohibited without permission.

Slavin, J.A., B.T. Tsurutani, E.J Smith, D.E. Jones, and D.G. Sibeck, Average configuration of the distant (< 220*Re*) magnetotail: Initial ISEE-3 magnetic field results, *Geophys. Res. Letters*, 10, 973 - 976, 1983.

Smart, W.M., *Textbook on Spherical Astronomy*, sixth edition (revised by R.M. Green), Cambridge Press, 1977.

Smith, E.J., Interplanetary magnetic fields,*Rev. Geophys. Space Phys.*, 17, 610 - 623, 1979.

Smith, M.F., Transient dayside reconnection and its effects on the ionosphere, in *Physical Signatures of Magnetospheric Boundary Layer Processes*, pp. 275 - 289, J.A. Holtet and A. Egeland (eds.), Kluwer Academic Pub., 1994.

Smith, P.H., and R.A. Hoffman, Ring current particle distribution during the magnetic storms of Dec. 16-18, 1971, *J. Geophys. Res.*, 78, 4731, 1973.

Smith, M.F., and M. Lockwood, The pulsating cusp, *Geophys. Res. Letters*, 17, 1069 - 1072, 1990.

Smith, M.F., M. Lockwood, and S.W.H. Cowley, The statistical cusp: A flux transfer event model, *Planet. Space Sci.*, 40, 1251 - 1268, 1992.

Smith, M.F., and D.J. Rodgers, *J. Geophys. Res.*, 95, 11617 - 11624, 1991.

Smith, P.H., N.K. Bewtra, and R.A. Hoffman, Motions of charged particles in the magnetosphere under the influence of a time-varying large scale convection electric field, in *Quantitative Modeling of Magnetospheric Processes*, Geophysical Monograph 21, W.P. Olson, (ed.), pp. 513 - 535, American Geophysical Union, Washington, D.C., 1979.

Smith, P.H., and R.A. Hoffman, Direct observations in the dusk hours of the characteristics of the storm time ring current particles during the beginning of magnetic storms, *J. Geophys. Res.*, 79, 966, 1974.

Smith, R.W., Dayside aurora and magnetopause processes, in *Physical Signatures of Magnetospheric Boundary Layer Processes*, A. Egeland, J. Holtet, and P.E. Sandholt, (eds.), 141 - 155, Kluwer Academic Publishers, 1994.

Smith, R.W., K. Henriksen, C.S. Deehr, D. Rees, F.G. McCormac, and G.G. Sivjee, Thermospheric winds in the cusp: Dependence of the latitude of the cusp, *Planet. Space Sci.*, 33, 305 - 313, 1985.

Smith, R.W., and P.J. Sweeney, Winds in the thermosphere of the northern winter polar cap, *Nature*, 284, 437 - 438, 1980.

Smith, R.W., D. Rees, F.G. McCormac, and P. Charleton, Two station observations of thermospheric winds in the auroral zone and the polar cap, *J. Atmos. Terr. Phys.*, 48, 97 - 105, 1986.

Snyder, A.L., J. Buchau, and S.-I. Akasofu, Formation of auroral patches in the midday sector during a substorm, *Planet. Space Sci.*, 20, 1116 - 1119, 1972.

Solomon, S.C., Optical aeronomy, *Rev. of Geophys., Supplement, U.S. National Report to International Union of Geodesy and Geophysics 1987-1990*, 1089 - 1109, 1991.

Solomon, S.C., P.B. Hays, and V.J. Abreu, The auroral 6300 Å emission: Observations and modeling, *J. Geophys. Res.*, 93, 9867 - 9882, 1988.

Sonnerup, B.U.Ö., Reconnection of magnetic fields, in *Solar Terrestrial Physics: Present and Future*, D.M. Butler and K. Papadopoulos (eds.), Reference Publ. 1120, NASA, Washington, D.C., 1984.

Reproduced with permission of the copyright owner. Further reproduction prohibited without permission.

Sonnerup, B.U.Ö., G. Paschmann, I. Papamastorakis, N. Sckopke, G. Haerendel, S.J. Bame, J.R. Asbridge, J.T. Gosling, and C.T. Russell, Evidence for magnetic field reconnection at the Earth's magnetopause, *J. Geophys. Res.*, 86, 10049 - 10067, 1981.

Southwood, D.J., Theoretical aspects of ionosphere-magnetosphere solar wind coupling, in *Physics of the Ionosphere-Magnetosphere, Adv. Space Res.*, 5, 7 - 14, 1985.

Southwood, D.J., The ionospheric signature of flux transfer events, — J. Geophys. Res., 92, 3207 - 3213, 1987.

Southwood, D.J., Magnetopause coupling processes and ionospheric responses: a theoretical perspective, *Phil. Trans. R. Soc. Lond.*, 328, 79 - 92, 1989.

Southwood, D.J., C.J. Farrugia, and M.A. Saunders, What are flux transfer events?, *Planet. Space Sci.*, 36, 503, 1988.

Southwood, D.J., M.A. Saunders, M.W. Dunlop, W.A.C. Mier-Jedrzejowicz, and R.P. Rijnbeek, A survey of flux transfer events recorded by by UKS spacecraft magnetometer, *Planet. Space Sci.*, 34, 1349 - 1359, 1986.

Sparrow, J.G., E.P. Ney, G.B. Burnett, and J.W. Stoddart, *J. Geophys. Res.*, 73, 857, 1968.

Spreiter, J.R., and S.S. Stahara, A new predictive model for determining solar wind-terrestrial planet interactons, *J. Geophys. Res.*, 85, 6769 - 6777, 1980.

Spreiter, J.R., A.L. Summers, and A.Y. Alksne, Hydromagnetic flow around the magnetosphere, *Planet. Space Sci.*, 14, 223 - 253, 1966.

Spreiter, J.R., and A.Y. Alksne, Plasma flow around the magnetosphere, in *Magnetospheric Physics*, edited by D.J. Williams and G.B. Mead, pp. 11 - 50, American Geophysical Union, 1969.

Stamnes, K., M.H. Rees, B.A. Emery, and R.G. Roble, Modelling of cusp auroras: The relative impact of solar EUV radiation and soft electron precipitation, in *The Polar Cusp*, J.A. Holtet and A. Egeland (eds.), D. Reidel Publishing Company, 137 - 147, 1985.

Starkov, G.B., Auroral altitudes in the polar cap,*Geomagnetism and Aeronomy*, 8, 28, (Engl. Trans.), 1968.

Stasiewicz, K., Polar cusp topology and position as a function of interplanetary magnetic field and magnetic activity: Comparison of a model with viking and other observations, *J. Geophys. Res.*, 96, 15789 - 15800, 1991.

Steele, D.P., and D.J. McEwen, Electron auroral excitation efficiencies and intensity ratios, *J. Geophys. Res.*, 95, 10321 - 10336, 1990. Strickland, D.J., R.R. Meier, J.H. Hecht, and A.B. Christensen, Deducing composition andincident electron spectra from ground-based auroral optical measurements: Theory and model results, *J. Geophys. Res.*, 94, 13527 - 13539, 1989.

Stoffregen, W., Transient emissions on the wavelength of *HeI*, 5876 Å recorded during auroral break-up, *Planet. Space Sci.*, 17, 1927, 1969.

Stoffregen, W., and H. Derblom, Life-time of the atomic oxygen 6300 A line in the auroral spectrum, *Nature*, 185, 28 - 29, 1960.

Stone, E.C., The physical significance and application of $L$, $B_0$, and $R_0$ to geomagnetically trapped particles, *J. Geophys. Res.*, 68, 4157 - 4166, 1963.

Störmer, C., *The Polar Aurora*, Oxford University Press, Oxford, 1955.

Reproduced with permission of the copyright owner. Further reproduction prohibited without permission.

Stringer, W.J., The relationship of auroral hydrogen emissions to auroral morphology,—*PhD Thesis*, University of Alaska, Fairbanks, Alaska, 1971.

Stringer, W.J., and A.E. Belon, The morphology of the IQSY auroral oval. 2. Auroral alignment in and near the auroral oval. *J. Geophys. Res.*, 72, 4423 - 4429, 1967.

Stringer, W.J., and A.E. Belon, The morphology of the IQSY auroral oval. 1. Interpretation of isoauroral diagrams, *J. Geophys. Res.*, 72, 4415 - 4421, 1967a.

Svalgaard, L., Interplanetary magnetic sector structure 1926-1971, *J. Geophys. Res.*, 77, 4027 - 4033, 1972.

Svalgaard, L., Polar cap magnetic variations and their relationship with the interplanetary magnetic sector structure, *J. Geophys. Res.*, 78, 2064 - 2078, 1973.

Swift, D.W., Simulation of the ejection of plasma from the polar ionosphere, *J. Geophys. Res.*, 95, 12103 - 12118, 1990.

Swings, P., The spectra of the night sky and the aurora, in *The Atmospheres of the Earth and Planets*, 159, G.P. Kuiper (ed.), The Univ. of Chicago Press, 1949.

Sørass, F., G. Gustaffson, H. Borg, Field line topology in the dayside cusp region inferred from low altitude particle observations, *Planet. Space Sci.*, 28, 525 - 533, 1980.

Tagirov, V.R., Auroral torch structures: results of optical observations, *J. Atmos. Terr. Physics*, 55, 1775 - 1787, 1993.

Taylor, H.E., and E.W. Hones, Jr., Adiabatic motion of auroral particles in a model of the electric and magnetic fields surrounding the earth, *J. Geophys. Res.*, 70, 3605 - 3628, 1965.

Taylor, W.W.L., and D.A. Gurnett, The morphology of VLF emissions observed with the Injun 3 satellite, *J. Geophys. Res.*, 73, 5615 - 5626, 1968.

Thomas, B.T., and E.J. Smith, The Parker spiral configuration of the interplanetary magnetic field between 1 and 8.5 AU, *J. Geophys. Res.*, 85, 6861 - 6867, 1980.

Thomas, V.A., and D. Winske, Kinetic simulations of the Kelvin-Helmholtz instability at the magnetopause, *J. Geophys. Res.*, 98, 11425 - 11438, 1993.

Thomsen, M.F., J.A. Stansberry, S.J. Bame, S.A. Fuselier, and J.T. Gosling, Ion and electron velocity distributions within flux transfer events, *J. Geophys. Res.*, 92, 12127 - 12136, 1987.

Thorne, R.M., and B.T. Tsurutani, Wave-particle interactions in the magnetopause boundary layer, in *Physics of Space Plasmas*, SPI Conference Proceedings and Reprint Series, Number 10, pp. 119 - 150, Scientific Publishers, Inc., Cambridge, Massachusetts, 1990.

Titheridge, J.E., Ionospheric heating beneath the magnetospheric cleft, *J. Geophys. Res.*, 81, 3221 - 3226, 1976.

Todd, H., B.J.I. Bromage, S.W.H. Cowley, M. Lockwood, A.P. van Eyken, and D.M. Willis, EISCAT observations of bursts of rapid flow in the high latitude dayside ionosphere, *Geophys. Res. Letters*, 13, 909, 1986.

Torbert, R.B., and C.W. Carlson, Evidence for parallel electric field particle acceleration in the dayside auroral oval, *J. Geophys. Res.*, 85, 2909 - 2914, 1980.

Reproduced with permission of the copyright owner. Further reproduction prohibited without permission.

Torbert, R.B., C.A. Cattell, F.S. Mozer, and C.-I. Meng, The boundary of the polar cap and its relation to electric fields, field-aligned currents, and auroral particle precipitation, in *Physics of Auroral Arc Formation*, Geophysical Monograph 25, pp. 143 - 153, S.-I. Akasofu and J.R. Kan, (eds.), American Geophysical Union, Washington, D.C., 1981.

Torr, M.R., and D.G. Torr, The role of metastable species in the thermosphere, *Rev. Geophys.*, 20, 91 - 144, 1982.

Trefall, H., and D.J. Williams, Time structure of postmidnight energetic electron precipitation and the limit of stable trapping, *J. Geophys. Res.*, 84, 2725 - 2735, 1979.

Tsurutani, B.T., and E.J. Smith, Two types of magnetospheric ELF chorus and their substorm dependences, *J. Geophys. Res.*, 82, 5112, 1977.

Tsurutani, B.T., E.J. Smith, R.M. Thorne, R.R. Anderson, D.A. Gurnett, G.K. Parks, C.S. Lin, and C.T. Russell, Wave-particle interactions at the magnetopause: Contributions to the dayside aurora, *Geophys. Res. Letters*, 8, 183 - 186, 1981.

Tsyganenko, N.A., Global quantitative models of the geomagnetic field in the cislunar magnetosphere for different disturbance levels, *Planet. Space Sci.*, 35, 1347, 1987.

Tsyganenko, N.A., A magnetospheric magnetic field model with a warped tail current sheet, *Planet. Space Sci.*, 37, 5 - 20, 1989.

Tsyganenko, N.A., and A.V. Usmanov, Determination of the magnetospheric current system parameters and development of experimental geomagnetic field models based on data from IMP and HEOS satellites, *Planet. Space Sci.*, 30, 985, 1982.

Vaisberg, O.L., Auroral spectroelectrophotometry of the emission $N_2$, $N_2^+$, $OI$, $NII$, results if researches of the program of the IGY, Pub. House Acad. Sci. U.S.S.R., *Polar Aurora and Night Airglow*, 8, 43, 1962.

Valladares, C.E., Su. Basu, R.J. Niciejewski, and R.E. Sheehan, Simultaneous radar and satellite observations of the polar cusp/cleft at Sondre Stromfjord, in *Electromagnetic Coupling in the Polar Clefts and Caps*, pp. 285 - 298, P.E. Sandholt and A. Egeland (eds.), Kluwer Academic Pub., 1989.

Vallance-Jones, A., *Aurora*, D. Reidel Pub. Co., 1974.

Vallance-Jones, A., and R.L. Gattinger, Auroral spectroscopy and its application to the characterization of primary particle fluxes, *J. Geomag. Geoelectr.*, 42, 1385 - 1410, 1990.

Vallance-Jones, A., R.L. Gattinger, P.Shih, J.W. Meriwether, V.B. Wickwar, and J. Kelly, Optical and radar characterization of a short-lived auroral event at high latitude, *J. Geophys. Res.*, 92, 4575 - 4589, 1987.

Vampola, A.L., Access of solar electrons to closed field lines, *J. Geophys. Res.*, 76, 36 - 43, 1971.

Vampola, A.L., The effect of strong pitch angle scattering on the location of the outer-zone electron boundary as observed by low-altitude satellites, *J. Geophys. Res.*, 82, 2289 - 2294, 1977.

Van Allen, J.A.,, The geomagnetically trapped corpuscular radiation, *J. Geophys. Res.*, 64, 1683 - 1689, 1959.

Van Allen, J.A., J.F. Fennell, and N.F. Ness, Asymmetric access of energetic solar protons to the earth's north and south polar caps, *J. Geophys. Res.*, 76, 4262 , 1971.

Van Zyl, B., M.W. Gealy, and H. Neumann, Prediction of photon yields for proton aurorae in an $N_2$ atmosphere, *J. Geophys. Res.*, 89, 1701 - 1710, 1984.

Reproduced with permission of the copyright owner. Further reproduction prohibited without permission.

Vasyliunas, V.M., Theoretical models of magnetic field line merging, 1, *Revs. Geophys. Space Phys.*, 13, 303, 1975.

Vasyliunas, V.M., in *Proceedings of Magnetospheric Boundary Layers Conference*, (ESA SP-148), p. 387, Alpbach, Austria, 1979.

Vaughan, S.O., and J.P. Doering, Absolute experimental differential and integral electron excitation cross sections for atomic oxygen 2. The ($^3P \rightarrow ^3S^0$) transition (1304Å) from 16.5 to 200 eV with comparison to atomic hydrogen, *J. Geophys. Res.*, 91, 13755 - 13760, 1986.

Viereck, R.A., A review of mesospheric dynamics and chemistry, *Rev. of Geophys.*, 29, pt.2, 1132 - 1142, 1991.

Vernov, S.N., and A.E. Chudakov, Investigation of cosmic radiation and of the terrestrial corpulscular radiation by means of rockets and satellites, *Uspekhi Fizicheskikh Nauk*, 70, 585 - 619, 1960.

Vernov, S.N, P.V. Vakulov, S.N. Kuznetsov, Yu. I. Logachev, E.N. Sosnovets, and V.G. Stolpovsky, Boundary of the outer radiation belt and unstable radiation zone, *Geomagnetism and Aeronomy*, (Engl. Trans.), 7, 335 - 339, 1967.

Vlaskov, V.A., and K. Henriksen, Vibrational temperature and excess vibrational energy of molecular nitrogen in the ground state derived from $N_2^+$ emission bands in aurora,*Planet. Space Sci.*, 33, 141 - 145, 1985.

Vo, H.B., and S. Murphree, A study of dayside auroral bright spots seen by the Viking imager, *J. Geophys. Res.*, 100, 3649 - 3655, 1995.

Voight, G.H., A three dimensional, analytical magnetospheric model with defined magnetopause, *Z. Geophys.*, 38, 319 - 346, 1972.

Vorobjev, V.G., G. Gustafasson, G.V. Starkov, Y.I. Feldstein, and N.F. Shernina, Dynamics of day and night aurora during substorms, *Planet. Space Sci.*, 23, 269 - 278, 1975.

Vorobyev, V.G., and V.A. Turyanskiy, Unique behavioral features of the [OI] λ6300 Å and λ5577 Å emissions in daytime auroras,*Geomagnetism and Aeronomy*, 23, 780 - 783, 1983.

Vorobyev, V.G., V.R. Tagirov, and S.A. Chernous, Relative postions of the zones of soft precipitation and auroral pulsations in the daytime polar region, *Geomagnetism and Aeronomy*, 24, 284 - 286, 1984.

Vorobyev, V.B., V.L. Zverev, and S.V. Leontyev, Structure of the auroral luminosity in the midday sector, *Geomag. and Aeron.*, 28, 214 - 217, 1988.

Waite, J.H., Jr., T. Nagai, J.F.E. Johnson, C.R. Chappell, J.L. Burch, T.L. Killeen, P.B. Hays, G.R. Carignan, W.K. Peterson, and E.G. Shelley, Escape of suprathermal $O^+$ ions in the polar cap, *J. Geophys. Res.*, 90, 1619, 1985.

Walt, M., *Introduction to Geomagnetically Trapped Radiation*, Cambridge University Press, 1994.

Walthour, D.W., B.U.Ö . Sonnerup, G. Paschmann, H. Lühr, D. Klumpar, and T. Potemra, Remote sensing of two dimensional magnetopause structures, *J. Geophys. Res.*, 98, 1489 - 1504, 1994.

Weber, E.J., J. Buchau, J.G. Moore, J.R. Sharber, R.C. Livingston, J.D. Winningham, and B. Reinisch, F layer ionization patches in the polar cap, *J. Geophys. Res.*, 89, 1683 - 1694, 1984.

Reproduced with permission of the copyright owner. Further reproduction prohibited without permission.

Watermann, J., D. Lummerzheim, O. de la Beaujardiere, P.T. Newell, and F.J. Rich, Ionospheric footprint of magnetosheathlike particle precipitation observed by an incoherent scatter radar, *J. Geophys. Res.*, 99, 3855 - 3867, 1994a.

Watermann, J., O. de la Beaujardiere, D. Lummerzheim, J. Woch, P.T. Newell, T.A. Potemra, F.J. Rich, and M. Shapshak, The dynamic cusp at low altitudes: A case study utilizing Viking, DMSP-F7, and Sondrestrom incoherent scatter radar observations, *Ann. Geophys.*, 12, 1144 - 1157, 1994b.

Wegener, K.,Das Polarlicht in Spitzbergen nach photogrammetrischen Messungen 1912-1913, in *Das Deutsche Observatorium in Spitzbergen, Beobachtungen and Ergebnisse, I*, edited by H. Hergesell, Strassburg, 1914.

Wei, C.Q., and L.C. Lee, Ground magnetic signatures ofmoving elongated plasma clouds, *J. Geophys. Res.*, 95, 2405, 1990.

Wei, C.Q., and L.C. Lee, Coupling of magnetopause-boundary layer to the polar ionosphere, *J. Geophys. Res.*, 98, 5707, 1993.

Wei, C.Q., L.C. Lee, and A.L. LaBelle-Hamer, A simulation study of the vortex structure in the low-latitude boundary layer, *J. Geophys. Res.*, 95, 20793 - 20807, 1990.

Weiss, L.A., P.H. Reiff, E.J. Weber, H.C. Carlson, M. Lockwood, and W.K. Peterson, Flow-aligned jets in the magnetospheric cusp: Results from the Geospace Environment Modelling Pilot program, *J. Geophys. Res.*, 100, 7649 - 7659, 1995.

Wentworth, R.C., *Lifetimes of geomagnetically trapped particles determined by Coulomb scattering*, PhD Thesis, University of Maryland, 1960.

West, H.I., Jr., The signatures of the various regions of the outer magnetosphere in the pitch angle distributions of energetic particles, in *Quantitative Modelling of Magnetospheric Processes*, Geophysical Monograph 21, pp. 150 - 179, W.P. Olson (ed.), American Geophysical Union, Washington, D.C., 1979.

West, H.I., Jr., R.M. Buck, and J.R. Walton, Electron pitch angle distributions throughout the magnetosphere as observed on Ogo 5, *J. Geophys. Res.*, 78, 1064 - 1081, 1973.

West, H.I., Jr., R.M. Buck, and J.R. Walton, Shadowing of electron azimuth-drift motions near the noon magnetopause, *Nature Physical Science*, 240, 6 -7, 1972.

Westcott, E.M., J.D. Stolarik, and J.P. Heppner, Electric fields in the vicinity of auroral forms from motions of barium vapor releases, *J. Geophys. Res.*, 74, 3469 - 3487, 1969.

Whalen, B.A., D.W. Green, and I.B. McDiarmid, Observations of ionospheric ion flow and related convective electric fields in and near an auroral arc, *J. Geophys. Res.*, 79, 2835 2842, 1974.

Whalen, B.A., and I.B. McDiarmid, Direct measurement of auroral alpha particles, *J. Geophys. Res.*, 73, 2307, 1968.

Whalen, B.A., and I.B. McDiarmid, Further low energy auroral ion composition measurements, *J. Geophys. Res.*, 77, 1306, 1972.

Whalen, J.A., J.R. Miller, and I.B. McDiarmid, Energetic particle measurements in a pulsating aurora, *J. Geophys. Res.*, 76, 978, 1971.

Whalen, J.A., and C.P. Pike, F-Layer and 6300-A measurements in the day sector of the auroral oval, *J. Geophys. Res.*, 78, 3848 - 3856, 1972.

Reproduced with permission of the copyright owner. Further reproduction prohibited without permission.

Wickwar, V.B., and W. Kofman, Dayside red auroras at very high latitudes: The importance of thermal excitation, *Geophys. Res. Letters*, 9, 923 - 926, 1984.

Wilcox, J.M., and N.F. Ness, Quasi-stationary corotating structure of the interplanetary medium, *J. Geophys. Res.*, 70, 5793 - 5805, 1965.

Williams, D.J., Ring current composition and sources: An update, *Planet. Space Sci.*, 29, 1195 - 1203, 1981.

Williams, D.J., and A.M. Smith, Daytime trapped electron intensities at high latitudes at 1100 kilometers, *J. Geophys. Res.*, 70, 541 - 556, 1965.

Williams, D.J., J.F. Arens, and L.J. Lanzerotti, Observations of trapped electrons at low and high altitudes, *J. Geophys. Res.*, 73, 5673 - 5696, 1968.

Williams, D.J., T.A. Fritz, B. Wilken, and E. Keppler, An energetic particle perspective of the magnetopause, *J. Geophys. Res.*, 84, 6385 - 6396, 1979.

Williams, D.J., D.G. Mitchell, T.E. Eastman, and L.A. Frank, Energetic particle observations in the low-latitude boundary layer, *J. Geophys. Res.*, 90, 5097, 1985.

Williams, D.J., and G.D. Mead, Night-side magnetospheric configuration as obtained from trapped electrons at 1100 kilometers, *J. Geophys. Res.*, 70, 3017 - 3029, 1965.

Willis, D.M., M. Lockwood, S.W.H. Cowley, H. Rishbeth, A.P. van Eyken, B.J.I. Bromage, P.R. Smith, and S.R. Crothers, A survey of simultaneous observations of the high latitude ionosphere and interplanetary magnetic field with EISCAT and AMPTE-UKS, *J. Atmos. Terr. Physics*, 48, 987, 1986.

Williams, D.J., and G.D. Mead, Night-side magnetospheric configuration as obtained from trapped electrons at 1100 kilometers, *J. Geophys. Res.*, 70, 3017 - 3029, 1965.

Winningham,J.D., Characteristics of magnetosheath plasma observed at low altitudes in the day-side magnetospheric cusps, in *Earth's Magnetospheric Processes*, pp. 68-80, B.M. McCormac (ed.), D. Reidel Pub. Co., 1972.

Winningham, J.D., and W.J. Heikkila, Polar cap auroral electron fluxes observed with ISIS 1, *J. Geophys. Res.*, 79, 949 , 1974.

Winningham, J.D., S.-I. Akasofu, F. Yasuhara, and W.J. Heikkila, Simultaneous observations of auroras from the South Pole Station and of precipitating electrons by Isis 1, *J. Geophys. Res.*, 78, 6579 - 6584, 1973.

Winningham, J.D., F. Yasuhara, S.-I. Akasofu, and W.J. Heikkila, The latitudinal morphology of 10-eV to 10-keV electron fluxes during magnetically quiet and disturbed times in the 2100 to 0300 MLT sector, *J. Geophys. Res.*, 80, 3148, 1975.

Wing, S., P.T. Newell, and T.G. Onsager, Modeling the entry of magnetosheath electrons into the dayside ionosphere, *J. Geophys. Res.*, 101, 13155 - 13167, 1996.

Winglee, R.M., J.D. Menietti, and C.S. Lin, Magnetosheath-ionospheric plasma interactions in the cusp/cleft 2. Mesoscale particle simulations, *J. Geophys. Res.*, 98, 19331 - 19347, 1993.

Wolfe, A., L.J. Lanzerotti, and C.G. Maclennan, Dependence of hydromagnetic energy spectra on solar wind velocity and interplanetary magnetic field direction, *J. Geophys. Res.*, 85, 114 - 118, 1980.

Wolfe, J.H., R.W. Silva, D.D. McKibben, and R.H. Mason, Preliminary observations of a geomagnetic wake at 1000 Earth radii, *J. Geophys. Res.*, 72, 4577, 1967.

Reproduced with permission of the copyright owner. Further reproduction prohibited without permission.

Wolfe, J.H., R.W. Silva, and M.A. Myers, Observations of the solar wind during the flight of IMP 1, *J. Geophys. Res.*, 71, 1319 - 1340, 1966.

Wu, C.C., R.J. Walker, and J.M. Dawson, A three dimensional MHD model of the Earth's magnetosphere,*Geophys. Res. Letters*, 8, 523 - 526, 1981.

Wu, Q., T.L. Killeen, W. Deng, A.G. Burns, J.D. Winningham, N.W. Spencer, R.A. Heelis, and W.B. Hanson, Dynamics Explorer 2 satellite observations and satellite track model calculations in the cusp/cleft region, *J. Geophys. Res.*, 101, 5329 - 5342, 1996.

Wygant, J.R., R.B. Torbert, and F.S. Mozer, Comparison of S3-3 polar cap potential drops with the interplanetary magnetic field and models of magnetopause reconnection, *J. Geophys. Res.*, 88, 5727 - 5735, 1983.

Xu, D., M.G. Kivelson, R.J. Walker, P.T. Newell, and C.-I. Meng, Interplanetary magnetic field control of mantle precipitation and associated field-aligned currents, *J. Geophys. Res.*, 100, 1837 - 1846, 1995.

Yagodkina, O.I., V.G. Vorobjev, and S.V. Leontiev, Pulsating aurora and geomagnetic pulsations in the daytime high-latitude region, *Planet. Space Sci.*, 38, 149 - 159, 1990.

Yagodkina, O.I., V.G. Vorobjev, and S.V. Leontiev, Structure of pulsating polar aurorae in the day sector and their morphological characteristics, *Geomagnetism and Aeronomy (Eng. edition)*, 29, 368 - 372, 1989.

Yagodkina, O.I., V.G. Vorobjev, and S.V. Leontiev, P.E. Sandholt, and A. Egeland, Bursts of geomagnetic fulsations and their relationship with dayside auroral forms, *Planet. Space Sci.*, 40, 1303 - 1309, 1992.

Yamamoto, T., On the temporal fluctuations ofpulsating auroral luminosity, *J. Geophys. Res.*, 93, 897 - 911, 1988.

Yamamoto, T., K. Shiokawa, and S. Kokubun, Magnetic field structures of the magnetotail as observed by GEOTAIL, *Geophys. Res. Letters*, 21, 2875 - 2878, 1994a.

Yamamoto, T., A. Matsuoka, K. Tsuruda, H. Hayakawa, A. Nishida, M. Nakamura, and S. Kokubun, Dense plasmas in the distant magnetotail as observed by GEOTAIL, *Geophys. Res. Letters*, 21, 2879 - 2882, 1994b.

Yamanouchi, T., and H. Horie,*Phys. Soc. Jap.*, 7, 52, 1952.

Yamauchi, M., and R. Lundin, Classification of large-scale and meso-scale ion dispersion patterns observed by Viking over the cusp-mantle region, in *Physical Signatures of Magnetospheric Boundary Layer Processes*, A. Egeland, J. Holtet, and P.E. Sandholt, (eds.), 99 - 109, Kluwer Academic Publishers, 1994.

Yeager, D.M., and L.A. Frank, Low-energy electron intensities at large distances over the earth's polar cap, *J. Geophys. Res.*, 81, 3966 - 3976, 1976.

Yee, J.H., and V.J. Abreu, Mesospheric 5577Å green line and atmospheric motions–Atmospheric Explorer satellite observations, *Planet. Space Sci.*, 35, 1389 - 1395, 1987.

Yeoman, T.K., N. Matting, J.M. Ruohoniemi, M. Lester, and M. Pinnock, An assessment of the L shell fitting beam-swinging technique for measuring ionospheric E region irregularity drift patterns, *J. Geophys. Res.*, 97, 14885 - 14896, 1992.

Young, D.T., J. Geiss, H. Balsiger, P. Eberhardt, A. Ghielmetti, and H. Rosenbauer, Discovery of $He^{++}$ and $O^{++}$ ions of terrestrial origin in the outer magnetosphere, *Geophys. Res. Letters*, 4, 561, 1977.

Reproduced with permission of the copyright owner. Further reproduction prohibited without permission.

Zaitzeva, S.A., and M.I. Pudovkin, On the longitudinal extent of the polar cusp,*Planet. Space Sci.*, 24, 518 - 519, 1976.

Zanetti, L.J., T.A. Potemra, J.P. Doering, J.S. Lee, and R.A. Hoffman, Magnetic field-aligned electron distributions in the dayside cusp, *J. Geophys. Res.*, 86, 8957 - 8970, 1981.

Zhu, L., and J.R. Kan, Ground magnetic signatures of multiple field-aligned current sheets in flux transfer events, *J. Geophys. Res.*, 94, 6655 - 6664, 1989.

Zwan, B.J., and R.A. Wolf, Depletion of solar wind plasma near a planetary boundary, *J. Geophys. Res.*, 81, 1636, 1976.

Zwickl, R.D., J.R. Asbridge, S.J. Bame, W.C. Feldman, J.T. Gosling, and E.J. Smith, Plasma properties of driver gas following interplanetary shocks observed by ISEE-3, in *Solar Wind Five*, edited by M. Neugebauer, Rep NASA CP-2280, p. 711, 1983.

Reproduced with permission of the copyright owner. Further reproduction prohibited without permission.